PSFC/RR-05-3

DKE: a fast numerical solver for the 3-D relativistic bounce-averaged electron Drift Kinetic Equation

***Joan Decker*[1] *and Y Peysson*[2]**

Association EURATOM-CEA sur la Fusion
CEA-Cadarache, F-13108 Saint Paul-lez-Durance, France

Plasma Science and Fusion Center
Massachusetts Institute of Technology, Cambridge, MA 02139, USA

March 2, 2005

[1]Email: jodecker@alum.mit.edu
[2]Email: yves.peysson@cea.fr

DKE: a fast numerical solver for the 3-D relativistic bounce-averaged electron Drift Kinetic Equation

Joan Decker[1] and Y Peysson[2]

Association EURATOM-CEA sur la Fusion
CEA-Cadarache, F-13108 Saint Paul-lez-Durance, France

Plasma Science and Fusion Center
Massachussetts Institute of Technology, Cambridge, MA 02139, USA

March 2, 2005

[1]Email: jodecker@alum.mit.edu
[2]Email: yves.peysson@cea.fr

Abstract

A new original code for solving the 3-D relativistic and bounce-averaged electron drift kinetic equation is presented. It designed for the current drive problem in tokamak with an arbitrary magnetic equilibrium. This tool allows self-consistent calculations of the bootstrap current in presence of other external current sources. RF current drive for arbitrary type of waves may be used. Several moments of the electron distribution function are determined, like the exact and effective fractions of trapped electrons, the plasma current, absorbed RF power, runaway and magnetic ripple loss rates and non-thermal bremsstrahlung. Advanced numerical techniques have been used to make it the first fully implicit (reverse time) 3-D solver, particularly well designed for implementation in a chain of code for realistic current drive calculations in high β_p plasmas. All the details of the physics background and the numerical scheme are presented, as well a some examples to illustrate main code capabilities. Several important numerical points are addressed concerning code stability and potential numerical and physical limitations.

Contents

1 Introduction **4**

2 Tokamak geometry and particle dynamic **7**
2.1 Coordinate system 7
2.1.1 Momentum Space 7
2.1.2 Configuration Space 7
2.2 Particle motion 11
2.2.1 Arbitrary configuration 11
2.2.2 Circular configuration 18

3 Kinetic description of electrons **22**
3.1 Boltzman equation; Gyro- and Wave-averaging 22
3.2 Guiding-Center Drifts and Drift-Kinetic Equation 25
3.2.1 Drift Velocity from the Conservation of Canonical Momentum . . . 26
3.2.2 Drift Velocity from the Expression of Single Particle Drift 28
3.2.3 Case of Circular concentric flux-surfaces 29
3.2.4 Steady-State Drift-Kinetic Equation 30
3.3 Small drift approximation 30
3.3.1 Small Drift Ordering 32
3.4 Low collision limit and bounce averaging 32
3.4.1 Fokker-Planck Equation 32
3.4.2 Drift-Kinetic Equation 33
3.5 Flux conservative representation 35
3.5.1 General formulation 35
3.5.2 Dynamics in Momentum Space 39
3.5.3 Dynamics in Configuration Space 41
3.5.4 Bounce-averaged flux calculation 43
3.5.5 Up to first order term: the Drift Kinetic equation 44
3.6 Moments of the distribution function 47
3.6.1 Flux-surface Averaging 47
3.6.2 Density 49
3.6.3 Current Density 51
3.6.4 Power Density Associated with a Flux 56
3.6.5 Stream Function for Momentum Space fluxes 59

3.6.6 Ohmic electric field . . . 63
3.6.7 Fraction of trapped electrons . . . 64
3.6.8 Runaway loss rate . . . 68
3.6.9 Magnetic ripple losses . . . 69
3.6.10 Non-thermal bremsstrahlung . . . 72

4 Detailed description of physical processes 80
4.1 Collisions . . . 80
4.1.1 Linearized collision operator . . . 80
4.1.2 Electron-electron collision operators . . . 82
4.1.3 Electron-ion collision operators . . . 87
4.1.4 Bounce Averaged Fokker-Planck Equation . . . 89
4.1.5 Bounce Averaged Drift Kinetic Equation . . . 92
4.2 Ohmic electric field . . . 95
4.2.1 Conservative Form for the Ohmic Electric Field Operator . . . 97
4.2.2 Bounce Averaged Fokker-Planck Equation . . . 97
4.2.3 Bounce Averaged Drift Kinetic Equation . . . 99
4.3 Radio frequency waves . . . 100
4.3.1 Conservative formulation of the RF wave operator . . . 100
4.3.2 RF Diffusion coefficient for a Plane Wave . . . 106
4.3.3 Integration in k-space . . . 106
4.3.4 Incident Energy Flow Density . . . 110
4.3.5 Narrow Beam Approximation . . . 111
4.3.6 Normalized Diffusion Coefficient . . . 113
4.3.7 Bounce Averaged Fokker-Planck Equation . . . 114
4.3.8 Bounce Averaged Drift-Kinetic Equation . . . 116
4.3.9 Modeling of RF Waves . . . 118

5 Numerical calculations 121
5.1 Bounce integrals . . . 121
5.2 Grid definitions . . . 123
5.2.1 Momentum space . . . 124
5.2.2 Configuration space . . . 125
5.2.3 Time grid definition . . . 126
5.3 Discretization procedure . . . 127
5.3.1 Zero order term: Fokker-Planck equation . . . 127
5.3.2 First order term: Drift kinetic equation . . . 129
5.4 Zero order term: the Fokker-Planck equation . . . 130
5.4.1 Momentum dynamics . . . 130
5.4.2 Spatial dynamics . . . 138
5.4.3 Grid interpolation . . . 140
5.4.4 Discrete description of physical processes . . . 157
5.4.5 Collisions . . . 157
5.4.6 Ohmic electric field . . . 166
5.5 Up to first order term: the Drift Kinetic equation . . . 169

5.5.1 Grid interpolation . . . 169
5.5.2 Momentum dynamics . . . 176
5.5.3 Discrete description of physical processes . . . 185
5.6 Initial solution . . . 188
5.6.1 Zero order term: the Fokker-Planck equation . . . 188
5.6.2 Up to first order term: the Drift Kinetic equation . . . 189
5.7 Boundary conditions . . . 196
5.7.1 Zero order term: the Fokker-Planck equation . . . 196
5.7.2 Up to first order term: the Drift Kinetic equation . . . 217
5.8 Moments of the Distribution Function . . . 221
5.8.1 Flux discretization for moment calculations . . . 221
5.8.2 Numerical integrals for moment calculations . . . 224

6 Algorithm 229
6.1 Matrix representation . . . 229
6.1.1 Zero order term: the Fokker-Planck equation . . . 229
6.1.2 Up to first order term: the Drift Kinetic equation . . . 231
6.2 Inversion procedure . . . 233
6.2.1 Incomplete matrix factorization . . . 233
6.2.2 Zero order term: the Fokker-Planck equation . . . 238
6.2.3 Up to first order term: the Drift Kinetic equation . . . 242
6.3 Normalization and definitions . . . 242
6.3.1 Temperature and density . . . 242
6.3.2 Time . . . 244
6.3.3 Momentum, velocity, and kinetic energy . . . 244
6.3.4 Maxwellian electron momentum distribution . . . 245
6.3.5 Poloidal flux coordinate . . . 246
6.3.6 Drift kinetic coefficient . . . 247
6.3.7 Momentum convection and diffusion . . . 247
6.3.8 Radial convection and diffusion . . . 248
6.3.9 Fluxes . . . 250
6.3.10 Current density . . . 251
6.3.11 Power density . . . 251
6.3.12 Electron runaway rate . . . 251
6.3.13 Electron magnetic ripple loss rate . . . 252
6.3.14 Units . . . 253

7 Examples 254
7.1 Ohmic conductivity . . . 255
7.2 Runaway losses . . . 258
7.3 Lower Hybrid Current drive . . . 261
7.4 Electron Cyclotron Current drive . . . 273
7.4.1 Introduction . . . 273
7.4.2 Grid size effects . . . 273

7.4.3 Electron trapping effects . . . 275
7.4.4 Momentum-space dynamics . . . 278
7.4.5 Coupling to propagation models . . . 278
7.4.6 Conclusion . . . 280
7.5 Fast electron radial transport . . . 280
7.6 Fast electron magnetic ripple losses . . . 289
7.7 Maxwellian bootstrap current . . . 294

8 Conclusion 306

9 Acknowledgements 309

A Curvilinear Coordinate Systems 310
A.1 General Case (u^1, u^2, u^3) . . . 310
A.1.1 Vector Algebra . . . 310
A.1.2 Tensor Algebra . . . 315
A.2 Configuration space . . . 315
A.2.1 System (R, Z, ϕ) . . . 315
A.2.2 System (r, θ, ϕ) . . . 318
A.2.3 System (ψ, s, ϕ) . . . 321
A.2.4 System (ψ, θ, ϕ) . . . 325
A.3 Momentum Space . . . 328
A.3.1 System $\left(p_\parallel, p_\perp, \varphi\right)$ . . . 328
A.3.2 System (p, ξ, φ) . . . 331

B Calculation of Bounce Coefficients for Circular Concentric FS 335
B.1 Calculation of $\lambda(\xi_0)$ . . . 335
B.1.1 Series Expansion . . . 335
B.1.2 Calculation of the Integrals J_{2m} . . . 336
B.1.3 Truncated Expression . . . 338
B.2 Calculation of s^* . . . 338
B.3 Calculation of $\{\Psi\}$ . . . 340
B.4 Calculation of Δ_b . . . 340

C Effective trapped fraction for Circular Concentric FS 342

D Cold Plasma Model for RF Waves 349
D.1 Cold Plasma Model . . . 349
D.1.1 Wave Equation and Dispersion Tensor . . . 349
D.1.2 Dispersion Relation . . . 350
D.1.3 Polarization components . . . 351
D.1.4 Power flow . . . 352
D.1.5 Conclusion . . . 352
D.2 Lower Hybrid Current Drive . . . 352
D.2.1 Electrostatic Dispersion Relation . . . 352
D.2.2 Cold Plasma Limit . . . 353

D.2.3 Lower Hybrid Waves . . . 353
D.2.4 Polarization . . . 354
D.2.5 Determination of $\Theta_{\mathbf{k}}^{b,\mathrm{LH}}$ . . . 355
D.2.6 Determination of $\mathbf{\Phi}_{bP}^{\mathrm{LH}}$ . . . 355
D.2.7 Determination of $\mathbf{\Phi}_{bT}^{\mathrm{LH}}$ . . . 356
D.2.8 LH Diffusion Coefficient . . . 358
D.3 Electron Cyclotron Current Drive . . . 360
D.3.1 Polarization . . . 361
D.3.2 Determination of $\Theta_{\mathbf{k}}^{b,\mathrm{EC}}$ . . . 361
D.3.3 Determination of $\mathbf{\Phi}_{b}^{\mathrm{EC}}$ in the low density limit. . . . 363
D.3.4 EC Diffusion Coefficient . . . 363

E Alternative discrete cross-derivatives coefficients **367**

F MatLab File List **378**

List of Figures

2.1 Coordinates systems $\left(p_{\parallel}, p_{\perp}, \varphi\right)$ and $(p, \xi, \varphi)$for momentum dynamics 8
2.2 Coordinates system (R, Z, ϕ). 9
2.3 Coordinates system (r, θ, ϕ). 9
2.4 Coordinates system (ψ, s, ϕ). 10
2.5 Guiding center velocity definition 11

3.1 Domain in configuration space where magnetic ripple well takes place for Tore Supra tokamak 70
3.2 Directions of incident electron and emitted photon with respect to the local magnetic field direction 74

5.1 Grid definition for the momentum dynamics 124
5.2 Chang and Cooper weightingfunction 150
5.3 Lower Hybrid boundary problem 204
5.4 Trapped domain and related flux connections 207
5.5 Momentum flux connections for grid point 1 in the trapped region 208
5.6 Momentum flux connections for grid point 4 in the counter-passing region . 209
5.7 Heuristic magnetic ripple modeling. The trapped/supertrapped boundary varies as well as the collision detrapping threshold are both functions of the radial location 211
5.8 Trapping and detrapping process induced by radial transport 215
5.9 Trapped domain for the first order distribution g 219

6.1 Qualitative shape of matrix $\widehat{\mathbb{B}}$ for the Fokker-Planck equation 231
6.2 Qualitative shape of matrix $\widehat{\mathbb{G}}$ for the drift kinetic equation 233
6.3 Typical arrangement of non-zero matrix coefficients in the first 2000 columns and rows in matrix $\widehat{\mathbb{N}}$ corresponding to the Fokker-Planck equation 235
6.4 Values of the non-zero matrix coefficients after diagonal preconditionning for matrix $\widehat{\mathbb{N}}'$ corresponding to the Fokker-Planck equation. Dot points correspond to pitch-angle process at constant p, while full line for slowing-down process at constant ξ_0. By definition values of all coefficients on the main diagonal are one 235
6.5 Matrix factorization principle. Dashed areas correspond to non-zero coefficients. 236

6.6 Reduction of the non-zero elements for the $\widehat{\mathbb{L}}$ and $\widehat{\mathbb{U}}$ matrices, by increasing δ_{lu}. Values of δ_{lu} are indicated on the top of each subfigure. For $\delta_{lu} = 10^{-2}$, the inversion becomes instable. 238
6.7 Memory storage requirement reduction by increasing the δ_{lu} parameter, for the Lower Hybrid current drive problem. The rate of convergence towards the steady state solution is given, using the biconjugate gradients stabilized method to solve the system of linear equations. Here only a local analysis is considered at a given radial position 239

7.1 Normalized Ohmic resistivity as function of the inverse aspect ratio ϵ 257
7.2 Contour plot of the electron distribution function at $\epsilon = 0.31623$ 259
7.3 Contour plot of the stream lines at $\epsilon = 0.31623$ 259
7.4 Electron distribution function averaged over the perpendicular momentum direction at $\epsilon = 0.31623$. Parallel and perpendicular temperatures of the electron distribution function are also shown 260
7.5 Normalized Ohmic runaway rate as function of the inverse aspect ratio ϵ . . 261
7.6 Variations of the Lower Hybrid current and power densities, ratio between the RF and collision absorbed power density, and the current drive efficiency with the grid size. Here uniform pitch-angle and momentum grids are considered. Detailed aspect of the simulation are given in the text . . . 263
7.7 Variations of the memory storage requirement and the time elapsed for kinetic calculations with the grid size. Here uniform pitch-angle and momentum grids are considered. Detailed aspect of the simulation are given in the text 264
7.8 Variation of the current drive efficiency with the upper mometum limit of the integration domain 265
7.9 Variation of the current drive efficiency with the main ion charge in the plasma 266
7.10 Variation of the current drive efficiency with the amplitude of the quasilinear diffusion coefficient for the Lower Hybrid current drive problem 268
7.11 Contour plot of the electron distribution function for $D_{LH} = 10$ 268
7.12 Contour plot of the electron distribution function for $D_{LH} = 2$ 269
7.13 Contour plot of the electron stream function for $D_{LH} = 2$ 269
7.14 Contour plot of the electron distribution function at $\epsilon = 0.31623$ 271
7.15 Contour plot of the Lower Hybrid quasilinear diffusion coefficient at $\epsilon = 0.31623$ 272
7.16 Electron distribution function averaged over the perpendicular momentum direction at $\epsilon = 0.31623$. The perpendicular and parallel temperatures are also shown 272
7.17 ECCD in DIII-D ($\rho = 0.1$, $D_{\mathrm{EC}} = 0.15$, $N_{\|} = 0.3$, $Y = 0.98$). Output density (a), normalized current density (b), normalized absorbed power density (c), normalized current drive efficiency (d), ratio of power absorbed to power lost on collisions (e), as a function of grid size ($n_p = n_\xi$). 274

7.18 ECCD in DIII-D ($\rho = 0.1,\ D_{\rm EC} = 0.15,\ N_{\|} = 0.3,\ Y = 0.98$). Output density (a), normalized current density (b), normalized absorbed power density (c), normalized current drive efficiency (d), ratio of power absorbed to power lost on collisions (e), as a function of momentum grid limit $p_{\max}$ ($n_p = 10 p_{\max},\ n_\xi = 100$). 276
7.19 ECCD in DIII-D ($D_{\rm EC} = 0.15,\ N_{\|} = 0.3,\ Y = 0.98$). Output density (a), normalized current density (b), normalized absorbed power density (c), normalized current drive efficiency (d), ratio of power absorbed to power lost on collisions (e), as a function of the inverse aspect ratio $\epsilon = r/R_p$; temperatures, densities and $Z_{\rm eff}$ are kept constant across the plasma. 277
7.20 ECCD in DIII-D ($\rho = 0.1,\ D_{\rm EC} = 0.15,\ N_{\|} = 0.3,\ Y = 0.98$). 2D electron distribution function (a), parallel distribution function (b) and perpendicular temperature (c); blue thin lines represent $f_{\rm init}$, red thick lines represent f_0, and green dashed contours represent $D_{\rm EC}$. 279
7.21 ECCD in DIII-D ($\theta_b = 0,\ P_{\rm EC} = 1$ MW, $N_{\|} = 0.3,\ f_{\rm EC} = 110$ MHz). Current and power densities deposition profiles. 3D calculation with $n_p = n_\xi = 100, n_\psi = 26$. 280
7.22 Radial grid for 3-D JET current drive simulation. Circles correspond to the normalized poloidal flux coordinate ψ, while crosses correspond to normalized radius ρ 281
7.23 Pitch-angle grid for 3-D JET current drive simulation. 282
7.24 Momentum grid for 3-D JET current drive simulation. 282
7.25 Momentum grid step for 3-D JET current drive simulation. Circles correspond to the flux grid, while stars to the distribution function half-grid . . 283
7.26 Ion and electron temperature and density profiles, and effective charge profile used for calculating the JET magnetic equilibrium with HELENA. Here hydrogen and tritium densities are zero (pure deuterium plasma) . The poloidal flux coordinate ψ as function of the normalized radius ρ in the equatorial mid-plane corresponds to the magnetic equilibrium code output . 283
7.27 $2-D$ contour plot of the poloidal magnetic flux surfaces as calculated for JET tokamak by the code HELENA 284
7.28 Momentum dependence of the relativistic Maxwellian distribution function at $\rho \simeq 0.36$, and relation between velocity v and momentum p. The deviation from the main diagonal indicates that above $p = 4$, relativistic effects become important 285
7.29 $2-D$ contour plot in momentum space of the Lower Hybrid quasilinear diffusion cofficient at $\rho \simeq 0.36$. The relativistic curvature of the lower bound of the resonance domain avoid intersection with the region of trapped electrons. The two full straight lines correspond to trapped/passing boundaries at that radial position 286
7.30 On the left side, $2-D$ contour plot of the radial diffusion rate at $\rho \simeq 0.36$. The velocity threshold corresponds to a kinetic energy of 35 keV approximately in the $MKSA$ units. On the right side, the velocity dependence of $D_\psi^{(0)}$ at $\xi_0 = 1$ 286

7.31 Relative particle conservation of the drift kinetic code for the $3-D$ JET Lower Hybrid current drive simulation 287
7.32 Flux surface averaged power density profiles for collision, RF and Ohmic electric field absorption for the $3-D$ JET Lower Hybrid current drive simulation. 288
7.33 Flux surface averaged current density profiles for the $3-D$ JET Lower Hybrid current drive simulation. 288
7.34 $2-D$ contour plot of the electron distribution function at $\rho \simeq 0.36$ for JET Lower Hybrid current drive 289
7.35 Electron distribution function averaged over the perpendicular momentum direction at $\rho \simeq 0.36$ for JET Lower Hybrid current drive. The perpendicular and parallel temperatures are also shown 290
7.36 $2-D$ contour plot of the electron distribution function at $\rho \simeq 0.78$ for JET Lower Hybrid current drive 290
7.37 Electron distribution function averaged over the perpendicular momentum direction at $\rho \simeq 0.78$ for JET Lower Hybrid current drive. The perpendicular and parallel temperatures are also shown 291
7.38 Ion and electron temperature and density profiles, and effective charge profile used for calculating the Tore Supra magnetic equilibrium with HELENA. Here hydrogen and tritium densities are zero (pure deuterium plasma) . The poloidal flux coordinate ψ as function of the normalized radius ρ in the equatorial mid-plane corresponds to the magnetic equilibrium code output 292
7.39 $2-D$ contour plot of the poloidal magnetic flux surfaces as calculated for Tore Supra tokamak by the code HELENA 292
7.40 Flux surface averaged current density profiles for the $3-D$ Tore Supra Lower Hybrid current drive simulation. 293
7.41 Magnetic ripple loss rate profile for Tore Supra tokamak in Lower Hybrid-current drive regime, as calculated by two different methods (see the text for more details) 293
7.42 $2-D$ contour plot of the electron distribution function at $\rho \simeq 0.44$ for Tore Supra Lower Hybrid current drive 294
7.43 Electron distribution function averaged over the perpendicular momentum direction at $\rho \simeq 0.44$ for Tore Supra Lower Hybrid current drive. The perpendicular and parallel temperatures are also shown 295
7.44 Bootstrap current profile given in the Lorentz model limit by the drift kinetic code and different analytical formulaes 298
7.45 Effective trapped fraction as given by the by the drift kinetic code in the Lorentz limit and by coefficient L_{31} from analytical expression (see the text for more details) 298
7.46 Exact trapped fraction as given by the by the drift kinetic code in the Lorentz limit and by analytical expression (see the text for more details) . . 299
7.47 Pitch-angle dependence of $\widetilde{f}^{(0)}$ and $g^{(0)}$ at $\rho \simeq 0.4354$, as given by the drift kinetic code and analytical expressions, for the Lorentz model limit 299

7.48 First order distribution $F_{\|0}^{(1)}$ averaged over the perpendicular momentum direction $p_\perp$ as fonction of $p_\|$ at $\rho \simeq 0.4354$, as given by the drift kinetic code and analytical expressions, for the Lorentz model limit 300
7.49 Contour plot of $\widetilde{f}^{(0)}$ at $\rho \simeq 0.4354$, as given by the drift kinetic code for the Lorentz model limit 301
7.50 Contour plot of $g^{(0)}$ at $\rho \simeq 0.4354$, as given by the drift kinetic code for the Lorentz model limit 301
7.51 Bootstrap current profile given by the drift kinetic code for the Tore Supra magnetic configuration and different corresponding analytical formulas (see the text for more details) 302
7.52 Effective trapped fraction as given by the by the drift kinetic code and the HELENA magnetic equilbrium code for the tokamak Tore Supra 302
7.53 Exact trapped fraction as given by the by the drift kinetic code for the tokamak Tore Supra 303
7.54 Pitch-angle dependence of $\widetilde{f}^{(0)}$ and $g^{(0)}$ at $\rho \simeq 0.4354$, as given by the drift kinetic code for the tokamak Tore Supra 303
7.55 First order distribution $F_{\|0}^{(1)}$ averaged over the perpendicular momentum direction $p_\perp$ as fonction of $p_\|$ at $\rho \simeq 0.4354$, as given by the drift kinetic code for the tokamak Tore Supra 304
7.56 Contour plot of $\widetilde{f}^{(0)}$ at $\rho \simeq 0.4354$, as given by the drift kinetic code for the tokamak Tore Supra 304
7.57 Contour plot of $g^{(0)}$ at $\rho \simeq 0.4354$, as given by the drift kinetic code for the tokamak Tore Supra 305

B.1 Bounce averaging coefficient λ 339

C.1 Bootstrap current coefficient κ as a function of the highest terms M and N kept in the series. 347
C.2 Bootstrap current coefficient κ as a function of the highest terms M and N kept in the series, for $M = N$ 348

List of Tables

7.1 Ohmic conductivity as function of the e-e collision model 256
7.2 Ohmic conductivity as function of the effective charge using the linearized e-e collision model 256
7.3 Runaway rate as function of the effective charge using the Maxwellian e-e collision model 258
7.4 Lower Hybrid current drive efficiencies η_{LH} in a pure hydrogen plasma from various $2-D$ relativistic Fokker-Planck codes 267
7.5 Lower Hybrid current drive efficiencies $(A \cdot m/W)$ in a pure hydrogen plasma from various $2-D$ relativistic Fokker-Planck codes 267

Chapter 1

Introduction

The determination of the electron distribution function has a crucial importance in the tokamak plasma physics, since the toroidal current density profile that is mainly driven by electrons is intimately linked to the magnetic equilibrium and confinement performances [1]. Therefore, accurate and realistic calculations must be carried out, with the additional requirement of an optimized numerical approach, in order to reduce as much as possible both memory storage and computer time consumptions. The latter point is especially important, since kinetic calculations must be incorporated in a chain of codes for self-consistent determination of all plasma properties [2].

In this document, an extensive presentation of the fast solver for the linearized electron drift kinetic is presented. This is a completely new tool based on previous numerical developments [3], that is designed for realistic calculations of the electron distribution function in the plasma region where the weak collision banana regime holds. It incorporates the major physical ingredients that must be taken into account for describing the corresponding physics in a fusion reactor, namely relativistic corrections, trapped particle effects, arbitrary magnetic equilibrium for high β_p regimes. For this purpose, both zero and first order kinetic equations with respect to the small drift approximation are solved, which allows to determine self-consistently boostrap current with any type of external current source (RF, Ohmic,...) at any point of the momentum space, and not only at the trapped-passing boundary as done in a previous attempt [4]. Basically, the code gives access to the neoclassical physics dominated by collisions between charged particles, for non-Maxwellian electron distribution functions. Therefore, it is particularly well suited for accurate current drive estimates in advanced tokamak regimes, including ITER, where locally, bootstrap current may strongly interplay with external current sources (ITB, edge pedestal in H-mode...)

Besides these physical properties, the code offer also the possibility to incorporate any type of fast electron radial transport (collision, turbulence or wave induced), which may be a key ingredient for the local control of plasma properties [5]. Written in a fully conservative form, the code naturally conserve the electron density, but also momentum for the current drive problem, keeping first order term of the Legendre polynomial expansion of the Beliaev-Budker collision operator [6]. As usual, several useful moments of the electron distribution function are calculated, namely the current density, the absorbed power, the fraction of trapped electrons, the magnetic ripple losses [7] and the bremsstrahlung

emission [8].

Advanced numerical techniques have been used, so that memory storage requirement can be strongly reduced, while keeping fast convergence rate. For this purpose the electron Drift Kinetic equation is solved by the standard finite difference technique, which has proven so far to be the fastest numerical approach among all possible alternative techniques. Furthermore, this method is particularly well suited when large discontinuities of the diffusion or convection rates have to be considered, a case that occurs frequently when kinetic and ray-tracing calculations are coupled.

Since in most cases, the steady-state solution is seeked with respect to the largest time scale (collision or fast electron radial transport)[1], the appropriate technique is the well known upwind time differencing, corresponding to the fully implicit time scheme, whose characteristic is to be almost unconditionally stable with respect to the time step value Δt. Nevertheless, the code offers also the possibility to investigate time dependent problems, with the usual Crank-Nicholson time differencing, which enables accurate time evolution.

The bounce-averaged Drift Kinetic equation is basically a $3-D$ problem, $2-D$ in momentum space (slowing down, pitch-angle) et $1-D$ in configuration space (radial dimension). Up to now, in order to reduce memory storage requirements, the numerical time scheme was based on the operator splitting technique, where both momentum and spatial dynamics evolved separately. If this approach turns out to be very fruitful, it has the drawback to slow down considerably the convergence towards the steady state solution, since only small time steps may be used for numericaly stable convergence. Therefore, the advantage to use fully implicit time scheme for each sub-space in hindered by this strong limitation, especially when radial transport of fast electrons must be taken into account. In order to avoid this problem, a fully implicit time scheme is considered, where both momentum and spatial dynamics are simultaneaously considered, so that no limitation occurs on the time step, which may be several order of magnitude larger than the collision reference time. However, this method requires a new technique for matrix inversion, in order to keep memory storage at an acceptable level. Indeed, with usual mesh sizes, the standard LU matrix factorization techniques does not hold anymore since matrices requirement may reach several giga-Bytes. An alternative approach is therefore absolutely necessary.

This critical point has been addressed by using advanced inversion techniques, based on incomplete LU factorization with drop tolerance. Since most of the off-diagonal coefficients of the matrices L and U are very small, one may take advantage to remove them so that the sparsity of the matrices can be greatly enhanced. Memory storage requirements can be therefore reduced drastically by one or two orders of magnitude with this pruning method, depending upon the initial matrix preconditioning, while only coefficients that are relevant of the physics problem here addressed are kept. Furthermore, computer time consumption can be also reduced, since the number of non-zero coefficients is considerably reduced. This method is similar to the strongly implicit method used for factorizing nine diagonal matrices [9], except that in this case, no restriction takes place regarding the number of diagonals. However, to take full benefit of this approach, the non-zero elements

[1]The energy transport time scale is usually on order on magnitude larger than the largest characteristic time for current drive calculations, except in tokamaks of small size, where time ordering here considered in the model must be likely revisited

of the matrix which is inverted must lie predominantly along diagonals. Therefore, it may be applied for solving the zero and first order bounce-averaged Fokker-Planck equations, whose structures are well suited for this purpose, though coefficients arrangement can be complex, owing to the radial dependence of the internal trapped-passing boundary in momentum space, especialy when transport in configuration space has to be considered.

This approach has been very successfuly implemented for the electron Drift Kinetic problem in tokamaks, using the MatLab language, which provides a built-in function for incomplete LU factorization with drop tolerance, and several very efficient iterative inversion tools, like the Conjugate Gradient Squared method for solving the system of linear equations. It is important to recall that this method is also available in FORTRAN programming language[2], under the package name SPARSEKIT that has also parallel processing capabilities [10]. Moreover, the very compact MatLab programming syntax allows to design the code structure in an original way, using multidimensional objects that describe simultaneously momentum and configuration space dynamics, but also wave-particle interaction. This makes the code particularly robust and easy to maintain.

In the document, the physics and numerics issues of the code are detailed, and an extensive discussion of the underlying assumptions is presented. A specific attention is paid to derive matrix coefficients in a fully consistent manner, a crucial issue especially for an accurate and robust estimate of the current drive efficiency for the various methods used in tokamaks. Some examples are shown to illustrate code performances, though still numerous possibilities remain to be investigated but are beyond the purpose of this document.

Aside from present day code capabilities, it is important to notice that the new numerical approach, here used, gives access to new physics domains that have never been studied accurately like wave-induce radial transport [11]. Furthermore, since the algorithm used is fast and stable, possible extensions to $4-D$ problems may be foreseen like in the plateau collision regime (current drive at the very plasma edge), as well as studies of the difficult problem of electrons that are locally trapped at different spatial positions, like in stellarator. In addition the code may be extended quite in a straightforward manner to the multi-species problem, taking into account for example of the non-linear damping of the α-particles produced by fusion reactions on the electron population. However, the ion physics requires to perform orbit-averaging instead of bounce-averaging, because of the large banana width of some particles, a challenging issue for kinetic solver based on a finite difference technique. Such a requirement is crucial for describing torque induced by waves. Nevertheless, beside this difficulty, the code is already fully designed to take benefit from parallel processing, if the dynamics of various species must be studied. In particular, non-uniform momentum and pitch-angle grids are already implemented, so that refined calculations can be performed for the ions at low velocity, while accurate ones up to relativistic energies may be considered for the electrons.

[2]Useful informations are available on the website of Pr. Yousef Saad at the following internet address http://www-users.cs.umn.edu/~saad/

Chapter 2

Tokamak geometry and particle dynamic

2.1 Coordinate system

General and specific properties of curvilinear coordinate systems are detailed in Appendix A. In this work, vectors are written in bold characters, like $\mathbf{v}$, except unit vectors, which are covered with a hat, like $\widehat{v}$.

2.1.1 Momentum Space

Because we consider gyro-averaged kinetic equations, it is important to use coordinates with rotational symmetry in order to reduce the dimensionality of the problem. Two different momentum space coordinates system are considered here:

- First, the cylindrical coordinate system $\left(p_{\parallel}, p_{\perp}, \varphi\right)$, where $p_{\parallel}$ is the component of the momentum along the magnetic field, and $p_{\perp}$ is the component perpendicular and φ is the gyro-angle. This system is defined in (A.212) and shown in Fig. 2.1. The cylindrical coordinate system is the natural system for wave-particle interaction, or also the effect of the electric field.

- Second, the spherical coordinate system (p, ξ, φ), where $p$is the magnitude of the momentum, and ξ is the cosine of the pitch-angle. This system is defined in (A.247) and shown in Fig. 2.1 as well. The spherical coordinate system is the natural system for collisions. It is the primary system, used in the Drift Kinetic code, for an accurate description of collisions.

2.1.2 Configuration Space

The particular toroidal geometry of tokamaks requires to use specific coordinates, in order to make use of symmetry properties such as axisymmetry, and takes into account the flux-surface magnetic configuration. Three different configuration space coordinates systems are considered here:

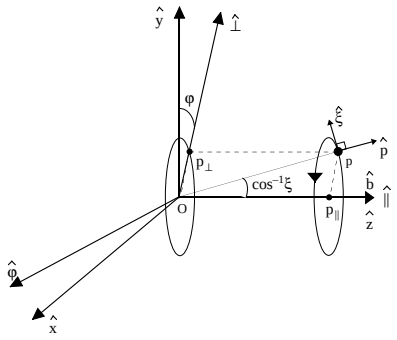

cmcm

Figure 2.1: Coordinates systems $\left(p_{\parallel}, p_{\perp}, \varphi\right)$ and $(p, \xi, \varphi)$for momentum dynamics

- First, the toroidal coordinate system (R, Z, ϕ), where R is the distance from the axis of the torus, and Z the distance along this axis . This coordinates system and the corresponding local orthogonal basis vectors $\left(\widehat{R}, \widehat{Z}, \widehat{\phi}\right)$ are defined in (A.61) and shown in Fig. 2.2. This coordinate system conserves the largest generality in the magnetic geometry.

- Second, the poloidal (polar) coordinate system (r, θ, ϕ) assumes the existence of a toroidal axis at constant position (R_p, Z_p) which is typically the plasma magnetic axis, corresponding to the position of an extremum of the poloidal magnetic flux ψ (which can be arbitrarily chosen as $\psi = 0$). This coordinates system and the corresponding local orthogonal basis vectors $\left(\widehat{r}, \widehat{\theta}, \widehat{\phi}\right)$ are defined in (A.94) and shown in Fig. 2.3.

- Third, the flux coordinate system (ψ, s, ϕ) is the natural system when we describe particles which are confined to a given flux surface ψ. This coordinates system and the corresponding local orthogonal basis vectors $\left(\widehat{\psi}, \widehat{s}, \widehat{\phi}\right)$ are defined in (A.136) and shown in Fig. 2.4. The vector $\widehat{\psi}$ is perpendicular to the flux surface, while $\widehat{s}$ is parallel to the surface, and included in the poloidal plane. The distance s is the length along the poloidal magnetic field lines. We can choose its origin as being at the position of minimum B-field amplitude within a flux-surface.

$$B\left(\psi, s \equiv 0\right) = \min_{s} \left\{B\left(\psi, s\right)\right\} = B_0\left(\psi\right) \tag{2.1}$$

Note that from now on, and all along this paper, the subscript 0 refers to quantities evaluated at the position of minimum B-field on a given flux-surface. The direction

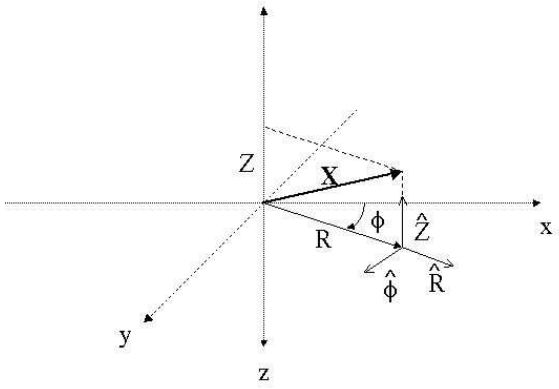

cmcm

Figure 2.2: Coordinates system (R, Z, ϕ).

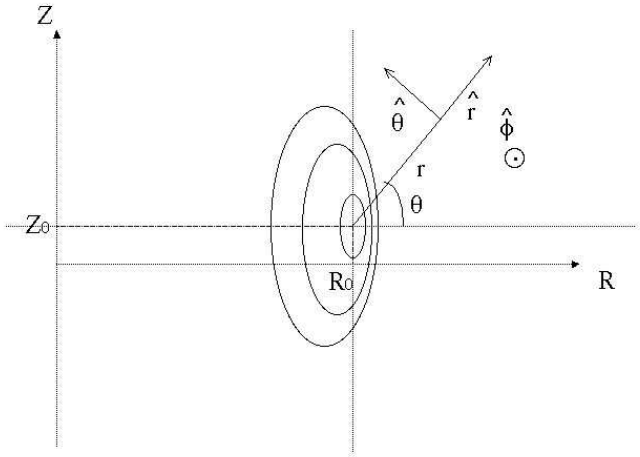

cmcm

Figure 2.3: Coordinates system (r, θ, ϕ).

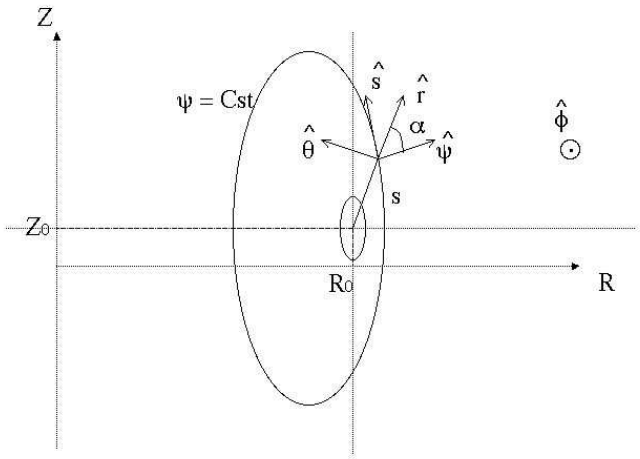

cmcm

Figure 2.4: Coordinates system (ψ, s, ϕ).

of evolution of s is counter-clockwise and the limits $s_{\min}(\psi)$ and $s_{\max}(\psi)$ are set at the position of maximum magnetic field

$$B(\psi, s \equiv s_{\min}) = B(\psi, s \equiv s_{\max}) = \max\{B(\psi, s)\} = B_{\max}(\psi) \tag{2.2}$$

- The system (ψ, θ, ϕ) is an alternative to the previous system, which is used to implement numerically the calculation of the bounce coefficients. One advantage is that the θ grid is now independent of ψ, which simplifies the numerical calculations. On the other hand, the contravariant vectors $\nabla\psi$ and $\nabla\theta$ are not orthogonal, and therefore are not respectively colinear with the covariant vectors $\partial\mathbf{X}/\partial\psi$ and $\partial\mathbf{X}/\partial\theta$. The properties of this curvilinear system are detailed in Appendix A. We also define, for geometrical purposes, a flux-function $\rho(\psi)$ which coincides with the normalized radius on the horizontal Low Field Side (LFS) mid-plane. Indeed, in an axisymmetric system, using the functions $R(\psi, \theta)$ and $Z(\psi, \theta)$, we define $\rho(\psi)$ as

$$\rho(\psi) = \frac{R(\psi, 0) - R_p}{R_{\max} - R_p} \tag{2.3}$$

with $0 \leq \rho \leq 1$ by construction, and where $R_{\max} = R(\psi_{\max}, 0)$ is the value of R on the separatrix as it crosses the mid-plane. Here $a_p = R_{\max} - R_p$ is defined arbitrarily as the plasma minor radius since this definition merges with the exact one for circular concentric flux-surfaces. The $2 - D$ outputs from the axisymmetric equilibrium code HELENA are given on the (ψ, θ) grid [12]. The system (ψ, θ, ϕ) will be used from now on.

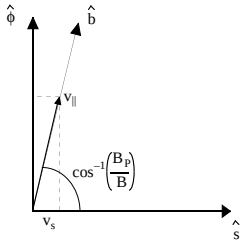

cmcm

Figure 2.5: Guiding center velocity definition

2.2 Particle motion

2.2.1 Arbitrary configuration

Transit or Bounce Time

Normalized Expression The transit, or bounce time, is defined as the time for a passing particle to complete a full orbit in the poloidal plane, and for a trapped particle to complete half a bounce period. Note that this is possible only in the approximation of zero banana width. Otherwise, the bounce motion would be no longer symmetric in the forth and back motions, and both would need to be accounted for. We define then

$$\tau_b(\psi) = \int_{s_{\min}}^{s_{\max}} \frac{ds}{|v_s|} = \int_{s_{\min}}^{s_{\max}} \frac{ds}{|v_{\|}|} \frac{B}{B_P} \tag{2.4}$$

where v_s is the guiding center velocity along the poloidal field lines, and $v_{\|}$ is its velocity parallel to the magnetic field. B is the magnitude of the magnetic field, while B_P is the magnitude of its poloidal component as shown in Fig. 2.5. The limits $s_{\min}$ and $s_{\max}$ are defined in (2.2) for passing electrons, and are the positions, along the field lines, of turning points for trapped electrons.

The differential arc length ds along the poloidal field line is generally expressed in curvilinear coordinates $\left(u^1, u^2, u^3\right)$ as (A.13)

$$ds = \sqrt{g_{ij} du^i du^j} \tag{2.5}$$

where the g_{ij} are the metric coefficients, defined in (A.12). In the (ψ, θ, ϕ) coordinates, the variations $d\psi$ and $d\phi$ are essentially zero along the poloidal field line. As a consequence, (2.5) becomes

$$ds = \sqrt{g_{22}} d\theta \tag{2.6}$$

The velocity and momentum are related through the relativistic factor $\gamma(p)$ introduced in Sec. 6.3.3, and therefore, we have

$$\frac{v_{\parallel}}{v} \simeq \frac{p_{\parallel}}{p} = \xi \tag{2.7}$$

in the weak relativistic regime of tokamak plasmas, where the pitch-angle cosine ξ is defined in (A.247)

We get

$$\tau_b(\psi) = \frac{2\pi}{v|\xi_0|} \int_{\theta_{\min}}^{\theta_{\max}} \frac{d\theta}{2\pi} \sqrt{g_{22}} \frac{\xi_0}{\xi} \frac{B}{B_P} \tag{2.8}$$

where ξ_0 is the pitch angle cosine at the position θ_0 of minimum B-field

$$\theta_0 \equiv \theta(B = B_0(\psi)) \tag{2.9}$$

and the limits $\theta_{\min}$ and $\theta_{\max}$ will be calculated in the next subsection.

The bounce time can be normalized as such:

$$\tau_b(\psi, \xi_0) = \frac{2\pi R_p \widetilde{q}(\psi)}{v|\xi_0|} \lambda(\psi, \xi_0) \tag{2.10}$$

with

$$\lambda(\psi, \xi_0) = \frac{1}{\widetilde{q}(\psi)} \int_{\theta_{\min}}^{\theta_{\max}} \frac{d\theta}{2\pi} \frac{\sqrt{g_{22}}}{R_p} \frac{\xi_0}{\xi} \frac{B}{B_P} \tag{2.11}$$

and

$$\widetilde{q}(\psi) \equiv \int_0^{2\pi} \frac{d\theta}{2\pi} \frac{\sqrt{g_{22}}}{R_p} \frac{B}{B_P} \tag{2.12}$$

The bounce time is normalized to the transit time of particles with parallel momentum only, such that $\lambda(\psi, \pm 1) = 1$.

The covariant metric element g_{22} is given by (A.10)-(A.12), which is in the (ψ, θ, ϕ) system becomes (A.192)

$$g_{22} = |J\nabla\psi \times \nabla\phi|^2 = \frac{r}{\left|\widehat{\psi} \cdot \widehat{r}\right|} \tag{2.13}$$

Consequently, the normalized bounce time takes the form

$$\lambda(\psi, \xi_0) = \frac{1}{\widetilde{q}(\psi)} \int_{\theta_{\min}}^{\theta_{\max}} \frac{d\theta}{2\pi} \frac{1}{\left|\widehat{\psi} \cdot \widehat{r}\right|} \frac{r}{R_p} \frac{B}{B_P} \frac{\xi_0}{\xi} \tag{2.14}$$

with

$$\widetilde{q}(\psi) = \int_0^{2\pi} \frac{d\theta}{2\pi} \frac{1}{\left|\widehat{\psi} \cdot \widehat{r}\right|} \frac{r}{R_p} \frac{B}{B_P} \tag{2.15}$$

Particle Motion in the Magnetic Field The particle motion along the magnetic field lines exhibits one constant of the motion, the energy (or the total momentum p), and an adiabatic invariant, the magnetic moment μ. They are given by the equations

$$p^2 = p_\perp^2 + p_\parallel^2 \tag{2.16}$$

$$\mu = \frac{p_\perp^2}{2m_e B} \tag{2.17}$$

such that, as a function of the moment component $\left(p_{\parallel 0}, p_{\perp 0}\right)$ at the location θ_0 of minimum B-field, we have

$$p_\perp^2 + p_\parallel^2 = p_{\perp 0}^2 + p_{\parallel 0}^2 \tag{2.18}$$

$$\frac{p_\perp^2}{B\left(\psi,\theta\right)} = \frac{p_{\perp 0}^2}{B_0\left(\psi\right)} \tag{2.19}$$

Using the transformation (A.250-A.251) from $\left(p_\parallel, p_\perp\right)$ to (p, ξ), the system (2.18-2.19) becomes

$$p^2 = p_0^2 \tag{2.20}$$

$$\frac{1-\xi^2}{B\left(\psi,\theta\right)} = \frac{1-\xi_0^2}{B_0\left(\psi\right)} \tag{2.21}$$

We get an expression for ξ as a function of ξ_0:

$$\xi\left(\psi,\theta,\xi_0\right) = \sigma\sqrt{1-\Psi\left(\psi,\theta\right)\left(1-\xi_0^2\right)} \tag{2.22}$$

where $\sigma = sign\left(\xi_0\right) = sign\left(v_\parallel\right)$, and $\Psi\left(\psi,\theta\right)$ is the ratio of the total magnetic field B to its minimum value B_0

$$\Psi\left(\psi,\theta\right) \equiv \frac{B\left(\psi,\theta\right)}{B_0\left(\psi\right)} \tag{2.23}$$

The trapping condition is given by $|\xi_0| < \xi_{0T}\left(\psi\right)$, where $\xi_{0T}\left(\psi\right)$ is the pitch angle, defined at the minimum $B_0\left(\psi\right)$ on a given flux-surface, such that the parallel velocity of the particle vanishes at the maximum $B_{\max}\left(\psi\right)$. An expression for $\xi_{0T}\left(\psi\right)$ can then be obtained from (2.22): setting $\xi\left(\xi_{0T}, B = B_{\max}\left(\psi\right)\right) = 0$, we get

$$\xi_{0T}^2\left(\psi\right) = 1 - \frac{B_0\left(\psi\right)}{B_{\max}\left(\psi\right)} \tag{2.24}$$

The turning points are

$$\theta_{\min}\left(\psi,\xi_0\right) = \left| \begin{array}{ll} -\pi & \text{for passing particles} \\ \theta_{T\,\min} & \text{for trapped particles} \end{array} \right. \tag{2.25}$$

$$\theta_{\max}\left(\psi,\xi_0\right) = \left| \begin{array}{ll} \pi & \text{for passing particles} \\ \theta_{T\,\max} & \text{for trapped particles} \end{array} \right. \tag{2.26}$$

We can determine the turning angles $\theta_{T\min}(\psi,\xi_0)$ and $\theta_{T\max}(\psi,\xi_0)$ as the position where $\xi(\psi,\theta,\xi_0)=0$. At this position, we have $B=B_b(\psi,\xi_0)$, where $B_b(\psi,\xi_0)$ is then given by (2.22)

$$B_b(\psi,\xi_0)=\frac{B_0(\psi)}{1-\xi_0^2} \tag{2.27}$$

so that

$$\theta_{T\min}(\psi,\xi_0)=\theta\left(B=B_b\,|\theta<\theta_0\right)\ [2\pi] \tag{2.28}$$

$$\theta_{T\max}(\psi,\xi_0)=\theta\left(B=B_b\,|\theta>\theta_0\right)\ [2\pi] \tag{2.29}$$

where θ_0 is given by (2.9).

Calculation of $\lambda(\psi,\xi_0)$ From the Output Data of Equilibrium Codes The numerical calculation of $\lambda(\psi,\xi_0)$ can be carried from the output of any magnetic equilibrium code. In the kinetic code here considered, we use HELENA for magnetic flux surface calculations [12], since it is used in the the CRONOS tokamak simulation package [2].

Data are assumed to be the parametrization of the flux-surfaces $R(\psi,\theta)$ and $Z(\psi,\theta)$, and the three components of the magnetic field $B_R(\psi,\theta)$, $B_Z(\psi,\theta)$ and $B_\phi(\psi,\theta)$. From these components we derive directly the toroidal and poloidal components of the field, as well as the total field:

$$\begin{aligned} B_T(\psi,\theta)&=|B_\phi(\psi,\theta)|\\ B_P(\psi,\theta)&=\sqrt{B_R^2(\psi,\theta)+B_Z^2(\psi,\theta)}\\ B(\psi,\theta)&=\sqrt{B_T^2(\psi,\theta)+B_P^2(\psi,\theta)} \end{aligned} \tag{2.30}$$

and also

$$R_p=R(0,\theta) \tag{2.31}$$

$$Z_p=Z(0,\theta) \tag{2.32}$$

We also have an expression for r

$$r(\psi,\theta)=\sqrt{\left(R(\psi,\theta)-R_p\right)^2+\left(Z(\psi,\theta)-Z_p\right)^2} \tag{2.33}$$

and, using relation

$$\begin{aligned} \widehat{r}&=\left(\widehat{r}\cdot\widehat{R}\right)\widehat{R}+\left(\widehat{r}\cdot\widehat{Z}\right)\widehat{Z}\\ &=\left(\frac{R(\psi,\theta)-R_p}{r}\right)\widehat{R}+\left(\frac{Z(\psi,\theta)-Z_p}{r}\right)\widehat{Z} \end{aligned} \tag{2.34}$$

that can be easily deduced from vector relation in Fig. 2.2, we get an expression for the scalar product

$$\widehat{\psi}\cdot\widehat{r}=\frac{\left(\nabla\psi\cdot\widehat{R}\right)\left(R(\psi,\theta)-R_p\right)+\left(\nabla\psi\cdot\widehat{Z}\right)\left(Z(\psi,\theta)-Z_p\right)}{r\,|\nabla\psi|} \tag{2.35}$$

In a toroidal axisymmetric geometry, the magnetic field can be expressed generally as

$$\mathbf{B} = I(\psi)\nabla\phi + \nabla\psi \times \nabla\phi \tag{2.36}$$

so that

$$B_T = |I(\psi)|\,|\nabla\phi| = \frac{|I(\psi)|}{R} \tag{2.37}$$

$$B_P = |\nabla\psi|\,|\nabla\phi| = \frac{|\nabla\psi|}{R} \tag{2.38}$$

We also have

$$\mathbf{B}_T = I(\psi)\nabla\phi = B_\phi\widehat{\phi} \tag{2.39}$$

$$\mathbf{B}_P = \nabla\psi \times \nabla\phi = -B_P\widehat{s} \tag{2.40}$$

and therefore

$$\nabla\phi \times \mathbf{B}_P = \nabla\phi \times (\nabla\psi \times \nabla\phi) = |\nabla\phi|^2\nabla\psi \tag{2.41}$$

so that

$$\nabla\psi = \frac{\nabla\phi \times \mathbf{B}_P}{|\nabla\phi|^2} = R\widehat{\phi} \times \mathbf{B}_P \tag{2.42}$$

and we have the projections

$$\left(\nabla\psi \cdot \widehat{R}\right) = R\widehat{R} \cdot \widehat{\phi} \times \mathbf{B}_P = -RB_Z \tag{2.43}$$

$$\left(\nabla\psi \cdot \widehat{Z}\right) = R\widehat{Z} \cdot \widehat{\phi} \times \mathbf{B}_P = RB_R \tag{2.44}$$

Finally, the expressions for the normalized bounce time λ and $\widetilde{q}$ that are used in numerical calculations are

$$\lambda(\psi, \xi_0) = \frac{1}{\widetilde{q}(\psi)} \int_{\theta_{\min}}^{\theta_{\max}} \frac{d\theta}{2\pi} \frac{B\left[(R-R_p)^2 + (Z-Z_p)^2\right]}{R_p\,|B_R(Z-Z_p) - B_Z(R-R_p)|} \frac{\xi_0}{\xi} \tag{2.45}$$

with

$$\widetilde{q}(\psi) = \int_0^{2\pi} \frac{d\theta}{2\pi} \frac{B\left[(R-R_p)^2 + (Z-Z_p)^2\right]}{R_p\,|B_R(Z-Z_p) - B_Z(R-R_p)|} \tag{2.46}$$

where R, Z, B_R, B_Z and B are functions of (ψ, θ), and ξ is a function of (ψ, θ, ξ_0) given by (2.22).

Safety Factor $q(\psi)$ The (averaged) safety factor q is defined in Ref. [13] in a general way as

$$q(\psi) = \frac{I(\psi)}{4\pi^2} \frac{\delta V}{\delta\psi} \left\langle R^{-2} \right\rangle \tag{2.47}$$

where V is the volume enclosed by a flux-surface and $\langle\ \rangle$ denotes the flux-surface average.

It can be expressed as

$$q(\psi) = I(\psi) \int_0^{2\pi} \frac{d\theta}{2\pi} \int_0^{2\pi} \frac{d\phi}{2\pi} \frac{J}{R^2} \tag{2.48}$$

where the Jacobian J is given by (A.195)

$$\begin{aligned} J &= |\nabla\psi \times \nabla\theta \cdot \nabla\phi|^{-1} \\ &= \frac{Rr}{|\nabla\psi| \left|\widehat{\psi} \cdot \widehat{r}\right|} \\ &= \frac{r}{B_P} \frac{1}{\left|\widehat{\psi} \cdot \widehat{r}\right|} \end{aligned} \tag{2.49}$$

where (2.40) is used

We obtain

$$q(\psi) = I(\psi) \int_0^{2\pi} \frac{d\theta}{2\pi} \frac{1}{\left|\widehat{\psi} \cdot \widehat{r}\right|} \frac{r}{B_P R^2} \tag{2.50}$$

and, using (2.36), we finally have

$$q(\psi) = \int_0^{2\pi} \frac{d\theta}{2\pi} \frac{1}{\left|\widehat{\psi} \cdot \widehat{r}\right|} \frac{r}{R} \frac{B_T}{B_P} \tag{2.51}$$

The expression of $q(\psi)$ and its relation to $\widetilde{q}(\psi)$ in the simplified case of circular concentric flux-surfaces will be addressed in sub-section 2.2.2.

Using (2.33) and (2.35), we find the expression

$$q(\psi) = \int_0^{2\pi} \frac{d\theta}{2\pi} \frac{\left[(R - R_p)^2 + (Z - Z_p)^2\right] B_T}{R\left|B_R(Z - Z_p) - B_Z(R - R_p)\right|} \tag{2.52}$$

that is convenient for the numerical evaluation.

Toroidal Extent of Banana Orbits

We are interested in calculating the toroidal extent of banana orbits, that is, the toroidal angle corresponding to the path done by a trapped particle between two turning points. It is given by

$$\Delta\phi = \phi_{\max} - \phi_{\min} = \int_{\phi_{\min}}^{\phi_{\max}} d\phi \tag{2.53}$$

and can be expressed as a function of the length element dl along the path, using (A.198)

$$\Delta\phi = \int_{l(\phi_{\min})}^{l(\phi_{\max})} dl(\phi) \frac{d\phi}{dl(\phi)} = \int_{l(\phi_{\min})}^{l(\phi_{\max})} \frac{dl(\phi)}{R} \tag{2.54}$$

The poloidal and toroidal elements are related through the local angle of the magnetic field,

$$\frac{dl\left(\phi\right)}{dl\left(\theta\right)}=\frac{B_T}{B_P} \tag{2.55}$$

so that

$$\Delta\phi=\int_{l(\phi_{\min})}^{l(\phi_{\max})}dl\left(\phi\right)\frac{d\phi}{dl\left(\phi\right)}=\int_{l(\theta_{\min})}^{l(\theta_{\max})}\frac{1}{R}\frac{B_T}{B_P}dl\left(\theta\right) \tag{2.56}$$

Using (A.197), we get

$$\Delta\phi=\int_{\theta_{\min}}^{\theta_{\max}}d\theta\,\frac{1}{\left|\widehat{\psi}\cdot\widehat{r}\right|}\frac{r}{R}\frac{B_T}{B_P} \tag{2.57}$$

Defining the integral

$$q_T\left(\psi,\xi_0\right)=\int_{\theta_{\min}}^{\theta_{\max}}\frac{d\theta}{2\pi}\,\frac{1}{\left|\widehat{\psi}\cdot\widehat{r}\right|}\frac{r}{R}\frac{B_T}{B_P} \tag{2.58}$$

we find that the toroidal extent of banana orbits is

$$\frac{\Delta\phi}{2\pi}=q_T\left(\psi,\xi_0\right) \tag{2.59}$$

Note that at the trapped/passing limit, we have

$$\lim_{\xi_0\to\xi_{0T}}\frac{\Delta\phi}{2\pi}=q_T\left(\psi,\xi_{0T}\right)=q\left(\psi\right) \tag{2.60}$$

Therefore, we retrieve the interpretation of the safety factors, which is the number of toroidal rotations $\Delta\phi/2\pi$ for one poloidal rotation.

Bounce Average

In order to reduce the dimension of kinetic equations, it is important to define an average over the poloidal motion, which anihilates the term that accounts for the time evolution of the variations of the distribution function along the field lines. The natural average is

$$\left\{\mathcal{A}\right\}=\frac{1}{\tau_b}\left[\frac{1}{2}\sum_{\sigma}\right]_T\int_{s_{\min}}^{s_{\max}}\frac{ds}{|v_s|}\mathcal{A} \tag{2.61}$$

where the sum over σ applies to trapped particles only.

It can be rewritten in terms of the normalized bounce time λ using expression (2.11)

$$\left\{\mathcal{A}\right\}=\frac{1}{\lambda\widetilde{q}}\left[\frac{1}{2}\sum_{\sigma}\right]_T\int_{\theta_{\min}}^{\theta_{\max}}\frac{d\theta}{2\pi}\frac{\sqrt{g_{22}}}{R_p}\frac{B}{B_P}\frac{\xi_0}{\xi}\mathcal{A} \tag{2.62}$$

or

$$\left\{\mathcal{A}\right\}=\frac{1}{\lambda\widetilde{q}}\left[\frac{1}{2}\sum_{\sigma}\right]_T\int_{\theta_{\min}}^{\theta_{\max}}\frac{d\theta}{2\pi}\frac{1}{\left|\widehat{\psi}\cdot\widehat{r}\right|}\frac{r}{R_p}\frac{B}{B_P}\frac{\xi_0}{\xi}\mathcal{A} \tag{2.63}$$

using relation (2.13).

Another expression uses the output data from equilibrium codes. Following the work in the previous section, we find

$$\{\mathcal{A}\} = \frac{1}{\lambda \widetilde{q}} \left[\frac{1}{2}\sum_{\sigma}\right]_T \int_{\theta_{\min}}^{\theta_{\max}} \frac{d\theta}{2\pi} \frac{B\left[(R-R_p)^2 + (Z-Z_p)^2\right]}{R_p \left|B_R\left(Z-Z_p\right) - B_Z\left(R-R_p\right)\right|} \frac{\xi_0}{\xi}\mathcal{A} \tag{2.64}$$

or explicitely

$$\{\mathcal{A}\} = \left[\int_{\theta_{\min}}^{\theta_{\max}} \frac{d\theta}{2\pi} \frac{B\left[(R-R_p)^2 + (Z-Z_p)^2\right]}{R_p \left|B_R\left(Z-Z_p\right) - B_Z\left(R-R_p\right)\right|} \frac{\xi_0}{\xi}\right]^{-1} \times \left[\frac{1}{2}\sum_{\sigma}\right]_T \int_{\theta_{\min}}^{\theta_{\max}} \frac{d\theta}{2\pi} \frac{B\left[(R-R_p)^2 + (Z-Z_p)^2\right]}{R_p \left|B_R\left(Z-Z_p\right) - B_Z\left(R-R_p\right)\right|} \frac{\xi_0}{\xi}\mathcal{A} \tag{2.65}$$

The bounce averaging of momentum-space operators in the kinetic equations leads to a set of coefficients that all have a similar structure, denoted $\lambda_{k,l,m}$ and $\overline{\lambda}_{k,l,m}$, which are define as

$$\left\{\left(\frac{\xi\left(\psi,\theta,\xi_0\right)}{\xi_0}\right)^k \Psi^l\left(\psi,\theta\right)\left(\frac{R_0\left(\psi\right)}{R\left(\psi,\theta\right)}\right)^m\right\} = \frac{\lambda_{k,l,m}\left(\psi,\xi_0\right)}{\lambda\left(\psi,\xi_0\right)} \tag{2.66}$$

and

$$\sigma\left\{\sigma\left(\frac{\xi\left(\psi,\theta,\xi_0\right)}{\xi_0}\right)^k \Psi^l\left(\psi,\theta\right)\left(\frac{R_0\left(\psi\right)}{R\left(\psi,\theta\right)}\right)^m\right\} = \frac{\overline{\lambda}_{k,l,m}\left(\psi,\xi_0\right)}{\lambda\left(\psi,\xi_0\right)} \tag{2.67}$$

where

$$R_0\left(\psi\right) \equiv R\left(\psi,\theta_0\right) \tag{2.68}$$

Note that by definition, $\lambda_{0,0,0} = \lambda$. In addition,

$$\overline{\lambda}_{k,l,m} = \left| \begin{array}{ll} \lambda_{k,l,m} & \text{for passing particles} \\ 0 & \text{for trapped particles} \end{array} \right. \tag{2.69}$$

2.2.2 Circular configuration

Parametrization of the Flux-Surfaces

In this case, we have $\psi = \psi\left(r\right)$ and therefore it is easier to work in the (r,θ,ϕ) coordinate to account for the symmetry in the problem. The normalized radius is

$$\rho\left(\psi\right) = \frac{r}{a_p} \tag{2.70}$$

We have now

$$\widehat{\psi} = \widehat{r} \tag{2.71}$$

so that (A.113)

$$\sqrt{g_{22}} = r \tag{2.72}$$

Magnetic Field

The toroidal field is

$$B_T(r,\theta) = \frac{|I(r)|}{R(r,\theta)} \tag{2.73}$$

and the poloidal field is

$$B_P(r,\theta) = \frac{|\nabla\psi(r)|}{R(r,\theta)} \tag{2.74}$$

where

$$|\nabla\psi(r)| = \left|\frac{d\psi(r)}{dr}\right| = \frac{1}{a_p}\left|\frac{d\psi(\rho)}{d\rho}\right| \tag{2.75}$$

is now only a function of r or ρ.

The total field is then

$$B(r,\theta) = \frac{\sqrt{I^2(r) + |\nabla\psi(r)|^2}}{R(r,\theta)} \tag{2.76}$$

and can be written as

$$B(r,\theta) = B_0(r)\frac{R_0}{R(r,\theta)} \tag{2.77}$$

with

$$B_0(r) = \frac{\sqrt{I^2(r) + |\nabla\psi(r)|^2}}{R_0} \tag{2.78}$$

Consequently, we ratio of magnetic fields Ψ as defined in (2.23) becomes

$$\Psi(r,\theta) = \frac{R_0}{R(r,\theta)} \tag{2.79}$$

and

$$\frac{B}{B_P} = \frac{\sqrt{I^2(r) + |\nabla\psi(r)|^2}}{|\nabla\psi(r)|} = \sqrt{1 + \frac{I^2(r)}{|\nabla\psi(r)|^2}} \tag{2.80}$$

is a function of r only.

Safety factor

The safety factor given by expression (2.51) becomes

$$q(r) = \int_0^{2\pi}\frac{d\theta}{2\pi}\frac{r}{R}\frac{B_T}{B_P} = \frac{r}{R_p}\frac{B_T}{B_P}\int_0^{2\pi}\frac{d\theta}{2\pi}\frac{R_p}{R} \tag{2.81}$$

The averaged value of R_p/R is evaluated in (B.27). It gives

$$\int_0^{2\pi}\frac{d\theta}{2\pi}\frac{R_p}{R} = \frac{1}{\sqrt{1-(r/R_p)^2}} \tag{2.82}$$

so that

$$q(\psi) = \frac{1}{\sqrt{1-(r/R_p)^2}} \frac{r}{R_p} \frac{B_T}{B_P} \tag{2.83}$$

Note that in the factor $\sqrt{1-(r/R_p)^2}$ is usually neglected, which is valid only in the large aspect ratio approximation, i.e. when the inverse aspect ratio ϵ defined as

$$\epsilon = \frac{r}{R_p} \tag{2.84}$$

is much less than unity.

Particle Motion

Using relation (A.95),

$$R(r,\theta) = R_p + r\cos\theta \tag{2.85}$$

and recalling that the minimum B-field B_0 corresponds to the poloidal angle value in that case

$$\theta_0 = 0 \tag{2.86}$$

we find

$$R_{\min}(r) = R_p - r = R_p(1-\epsilon) \tag{2.87}$$

$$R_{\max}(r) = R_p + r = R_p(1+\epsilon) = R_0(r) \tag{2.88}$$

Therefore, the expression (2.79) becomes

$$\Psi(\rho,\theta) = \frac{1+\epsilon}{1+\epsilon\cos\theta} \tag{2.89}$$

and using relation (2.77)

$$B_{\max}(r) = B_0(r)\frac{1+\epsilon}{1-\epsilon} \tag{2.90}$$

expression (2.24) is

$$\xi_{0T}^2(r) = \frac{2\epsilon}{1+\epsilon} \tag{2.91}$$

The pitch-angle cosine ξ is then given by combining relations (2.22) and (2.89)

$$\xi(r,\theta,\xi_0) = \sigma\sqrt{1-\frac{1+\epsilon}{1+\epsilon\cos\theta}\left(1-\xi_0^2\right)} \tag{2.92}$$

and the the turning angles are obtained from expression (2.27), or in the present notation

$$B(r,\theta_T) = B_b(r,\xi_0) = \frac{B_0(r)}{1-\xi_0^2} \tag{2.93}$$

Using relation (2.89), one obtains

$$B_0(r)\frac{1+\epsilon}{1+\epsilon\cos\theta_T} = \frac{B_0(r)}{1-\xi_0^2} \tag{2.94}$$

and then

$$\xi_0^2 = 1 - \frac{1 + \epsilon \cos\theta_T}{1+\epsilon} = \frac{\epsilon\,(1 - \cos\theta_T)}{1+\epsilon} \tag{2.95}$$

so that

$$\theta_T = \arccos\left[1 - \frac{2\xi_0^2}{\xi_{0T}^2}\right] \tag{2.96}$$

and finally by symmetry

$$\begin{aligned} \theta_{T\,\min} &= -\theta_T \\ \theta_{T\,\max} &= \theta_T \end{aligned} \tag{2.97}$$

Bounce Time

Using (2.72), the normalized bounce time reduces to

$$\lambda\,(r, \xi_0) = \frac{\epsilon}{\widetilde{q}} \int_{\theta_{\min}}^{\theta_{\max}} \frac{d\theta}{2\pi} \frac{\xi_0}{\xi} \frac{B}{B_P} \tag{2.98}$$

with, using definition (2.15)

$$\widetilde{q}\,(r) = \epsilon \int_0^{2\pi} \frac{d\theta}{2\pi} \frac{B}{B_P} \tag{2.99}$$

Because B/B_P only a function of r, as seen in (2.80), and can be taken out of the integrals, we get finally

$$\lambda\,(r, \xi_0) = \int_{\theta_{\min}}^{\theta_{\max}} \frac{d\theta}{2\pi} \frac{\xi_0}{\xi} \tag{2.100}$$

This integral can be performed analytically in a series expansion whose coefficients are calculated in (B.1). Note that in the case where $B_T \gg B_P$ and in the large aspect ratio approximation $\epsilon \ll 1$, we have $\widetilde{q}\,(r) \to q\,(r)$, which explains the notations, and the introduction of pseudo safety factor like $\widetilde{q}$. Other new definitions of pseudo safety factors will be introduced throughout the next sections, based on similar arguments.

Chapter 3

Kinetic description of electrons

3.1 Boltzman equation; Gyro- and Wave-averaging

In the kinetic description, electrons are described by a distribution function $f(\mathbf{r},\mathbf{p},t)$, which gives the density in phase space of particles with a momentum $\mathbf{p}$ at a position $\mathbf{r}$ and at time t. The particle conservation equation in phase space is the Boltzmann equation

$$\frac{\partial f}{\partial t}+\mathbf{v}\cdot\nabla_{\mathbf{r}}f+q_e\left[\mathbf{E}(\mathbf{r},t)+\mathbf{v}\times\mathbf{B}(\mathbf{r},t)\right]\cdot\nabla_{\mathbf{p}}f=\left.\frac{\partial f}{\partial t}\right|_{\mathrm{C}} \tag{3.1}$$

where

$$\left.\frac{\partial f}{\partial t}\right|_{\mathrm{C}}\equiv C(f) \tag{3.2}$$

is the collision operator. The fields $\mathbf{E}(\mathbf{r},t)$ and $\mathbf{B}(\mathbf{r},t)$ are assumed to consist of time-independent macroscopic fields $\overline{\mathbf{E}}(\mathbf{r})$ and $\overline{\mathbf{B}}(\mathbf{r})$ and fields associated with plane waves.

$$\mathbf{E}(\mathbf{r},t) = \overline{\mathbf{E}}(\mathbf{r})+\int\widetilde{\mathbf{E}}_{\mathbf{k}}e^{i(\mathbf{k}\cdot\mathbf{r}-\omega t)}d\mathbf{k} \tag{3.3}$$

$$\mathbf{B}(\mathbf{r},t) = \overline{\mathbf{B}}(\mathbf{r})+\int\widetilde{\mathbf{B}}_{\mathbf{k}}e^{i(\mathbf{k}\cdot\mathbf{r}-\omega t)}d\mathbf{k} \tag{3.4}$$

Because we are interested in solving the kinetic equation on the bounce and collisional time scales, we need to average over the faster time scales, which are the gyromotion and the wave oscillation.

Performing a time-averaging $\int_0^{2\pi/\omega}dt$ of the equation (3.1) removes the fast wave time scale from the equation, to give

$$\begin{aligned}&\frac{\partial\overline{f}}{\partial t}+\mathbf{v}\cdot\nabla_{\mathbf{r}}\overline{f}+q_e\left[\overline{\mathbf{E}}(\mathbf{r})+\mathbf{v}\times\overline{\mathbf{B}}(\mathbf{r})\right]\cdot\nabla_{\mathbf{p}}\overline{f}\\ =\;&\left.\frac{\partial\overline{f}}{\partial t}\right|_{\mathrm{C}}-\int_0^{2\pi/\omega}dt\sum_k\left(q_e\left[\widetilde{\mathbf{E}}_k+\mathbf{v}\times\widetilde{\mathbf{B}}_k\right]\cdot\nabla_{\mathbf{p}}f\right)\end{aligned} \tag{3.5}$$

where

$$\overline{f} = \int_0^{2\pi/\omega} dt\ f \tag{3.6}$$

is the wave-period averaged distribution function. The time derivative in the first term of (3.5) implicitely refers to times longer than the wave period ω.

Under the assumption of a strong magnetic field, such that the gyrofrequency Ω_e

$$\Omega_e = \frac{q_e \overline{B}}{\gamma m_e} \tag{3.7}$$

is much larger than both the collisional frequency and the bounce frequency, we can expand the distribution function

$$\overline{f} = \overline{f}_0 + \overline{f}_1 + \overline{f}_2 + \cdots \tag{3.8}$$

with a small parameter

$$\delta \sim \frac{\omega_b}{\Omega_e} \sim \frac{\nu_c}{\Omega_e} \tag{3.9}$$

The zero order equation becomes

$$q_e \mathbf{v} \times \overline{\mathbf{B}}\left(\mathbf{r}\right) \cdot \nabla_{\mathbf{p}} \overline{f}_0 = 0 \tag{3.10}$$

We have, in the $\left(p_\parallel, p_\perp, \varphi\right)$ space defined in Appendix A,

$$\mathbf{v} = \frac{\mathbf{p}}{\gamma\left(p_\parallel, p_\perp\right) m_e} \tag{3.11}$$

with the momentum being given by relation (A.214)

$$\mathbf{p} = p_\parallel \widehat{\parallel} + p_\perp \widehat{\perp} \tag{3.12}$$

and the gradient by expression (A.239)

$$\nabla_{\mathbf{p}} \overline{f} = \frac{\partial \overline{f}}{\partial p_\parallel} \widehat{\parallel} + \frac{\partial \overline{f}}{\partial p_\perp} \widehat{\perp} + \frac{1}{p_\perp} \frac{\partial \overline{f}}{\partial \varphi} \widehat{\varphi} \tag{3.13}$$

In this system, by definition,

$$\overline{\mathbf{B}}\left(\mathbf{r}\right) = \overline{B}\left(\mathbf{r}\right) \widehat{\parallel} \tag{3.14}$$

so that the gyromotion operator becomes

$$\begin{aligned} q_e \mathbf{v} \times \overline{\mathbf{B}}\left(\mathbf{r}\right) \cdot \nabla_{\mathbf{p}} &= \Omega_e \left(\mathbf{p} \times \widehat{\parallel}\right) \cdot \nabla_{\mathbf{p}} \overline{f} \\ &= -\Omega_e \frac{\partial}{\partial \varphi} \end{aligned} \tag{3.15}$$

The equation (3.10) becomes consequently

$$\frac{\partial \overline{f}_0}{\partial \varphi} = 0 \tag{3.16}$$

and therefore $\overline{f}_0$ is independent of φ. The first order equation is

$$\begin{aligned} & \frac{\partial \overline{f}_0}{\partial t} + \mathbf{v} \cdot \nabla_{\mathbf{r}} \overline{f}_0 + q_e \overline{\mathbf{E}}(\mathbf{r}) \cdot \nabla_{\mathbf{p}} \overline{f}_0 + q_e \mathbf{v} \times \overline{\mathbf{B}}(\mathbf{r}) \cdot \nabla_{\mathbf{p}} \overline{f}_1 \\ = & \left. \frac{\partial \overline{f}_0}{\partial t} \right|_{\mathrm{C}} - \int_0^{2\pi/\omega} dt \sum_k \left(q_e \left[\widetilde{\mathbf{E}}_k + \mathbf{v} \times \widetilde{\mathbf{B}}_k \right] \cdot \nabla_{\mathbf{p}} f \right) \end{aligned} \tag{3.17}$$

The last term in the equation (3.17) has been calculated by Lerche for a uniform plasma, in the form of a quasilinear operator $\mathcal{Q}\left(\overline{f}\right)$. We can rewrite

$$\mathcal{C}\left(\overline{f}_0\right) = \left. \frac{\partial \overline{f}_0}{\partial t} \right|_{\mathrm{C}} \tag{3.18}$$

$$\mathcal{Q}\left(\overline{f}_0\right) = - \int_0^{2\pi/\omega} dt \sum_k \left(q_e \left[\widetilde{\mathbf{E}}_k + \mathbf{v} \times \widetilde{\mathbf{B}}_k \right] \cdot \nabla_{\mathbf{p}} f \right) \tag{3.19}$$

Performing the gyro-averaging $\int_0^{2\pi} d\varphi$ on the kinetic equation (3.17), we find, using (3.16), that

$$\int_0^{2\pi} d\varphi \, \frac{\partial \widetilde{f}_0}{\partial t} = \frac{\partial \widetilde{f}_0}{\partial t} \tag{3.20}$$

and

$$\int_0^{2\pi} d\varphi \, \mathbf{v} \cdot \nabla_{\mathbf{r}} \overline{f}_0 = \int_0^{2\pi} (d\varphi \, \mathbf{v}) \cdot \nabla_{\mathbf{r}} \overline{f}_0 = \mathbf{v}_{\mathrm{gc}} \cdot \nabla_{\mathbf{r}} \overline{f}_0 \tag{3.21}$$

where $\mathbf{v}_{\mathrm{gc}}$ is the electron velocity along the guiding center.

Concerning the electric field, we decompose the gradient in momentum space using (3.13)

$$\int_0^{2\pi} d\varphi \, q_e \overline{\mathbf{E}}(\mathbf{r}) \cdot \nabla_{\mathbf{p}} \overline{f}_0 = q_e \overline{\mathbf{E}}(\mathbf{r}) \cdot \int_0^{2\pi} d\varphi \left[\frac{\partial \overline{f}_0}{\partial p_\parallel} \widehat{\parallel} + \frac{\partial \overline{f}_0}{\partial p_\perp} \widehat{\perp} + \frac{1}{p_\perp} \frac{\partial \overline{f}_0}{\partial \varphi} \widehat{\varphi} \right] \tag{3.22}$$

$$\begin{aligned} = \; & q_e \frac{\partial \overline{f}_0}{\partial p_\parallel} \overline{\mathbf{E}}(\mathbf{r}) \cdot \widehat{\parallel} \\ & + q_e \frac{\partial \overline{f}_0}{\partial p_\perp} \overline{\mathbf{E}}(\mathbf{r}) \cdot \int_0^{2\pi} d\varphi \widehat{\perp} \\ & + \frac{q_e}{p_\perp} \overline{\mathbf{E}}(\mathbf{r}) \cdot \int_0^{2\pi} d\varphi \frac{\partial \overline{f}_0}{\partial \varphi} \widehat{\varphi} \end{aligned} \tag{3.23}$$

and, using

$$\int_0^{2\pi} d\varphi \widehat{\perp} = 0 \tag{3.24}$$

$$\int_0^{2\pi} d\varphi \frac{\partial \overline{f}_0}{\partial \varphi} \widehat{\varphi} = -\overline{f}_0 \int_0^{2\pi} d\varphi \frac{\partial \widehat{\varphi}}{\partial \varphi} = \overline{f}_0 \int_0^{2\pi} d\varphi \widehat{\perp} = 0 \tag{3.25}$$

we obtain

$$\int_0^{2\pi} d\varphi \, q_e \overline{\mathbf{E}}(\mathbf{r}) \cdot \nabla_{\mathbf{p}} \overline{f}_0 = q_e \overline{E}_\parallel(\mathbf{r}) \frac{\partial \overline{f}_0}{\partial p_\parallel} \tag{3.26}$$

The gyromotion term is averaged to zero

$$\int_0^{2\pi} d\varphi \; q_e \mathbf{v} \times \overline{\mathbf{B}}\left(\mathbf{r}\right) \cdot \nabla_{\mathbf{p}} \overline{f}_1 = -\Omega_e \int_0^{2\pi} d\varphi \; \frac{\partial \overline{f}_1}{\partial \varphi} = 0 \tag{3.27}$$

so that we get finally

$$\frac{\partial \widetilde{f}_0}{\partial t} + \mathbf{v}_{\mathrm{gc}} \cdot \nabla_{\mathbf{r}} \widetilde{f}_0 + q_e \overline{E}_{\parallel} \frac{\partial}{\partial p_{\parallel}} \left(\mathbf{r}\right) \widetilde{f}_0 = \mathcal{C}\left(\widetilde{f}_0\right) + \mathcal{Q}\left(\widetilde{f}_0\right) \tag{3.28}$$

This equation is called electron drift-kinetic equation. Renaming the guiding-center distribution function $\overline{f}_0 = f\left(\mathbf{r}, p_{\parallel}, p_{\perp}, t\right)$, $\mathbf{E}\left(\mathbf{r}\right) = \overline{\mathbf{E}}\left(\mathbf{r}\right)$ and $\mathbf{B}\left(\mathbf{r}\right) = \overline{\mathbf{B}}\left(\mathbf{r}\right)$, we get

$$\frac{\partial f}{\partial t} + \mathbf{v}_{\mathrm{gc}} \cdot \nabla f = \mathcal{C}\left(f\right) + \mathcal{Q}\left(f\right) + \mathcal{E}\left(f\right) \tag{3.29}$$

where we define an electric field operator

$$\mathcal{E}\left(f\right) = -q_e E_{\parallel}\left(\mathbf{r}\right) \frac{\partial}{\partial p_{\parallel}} f \tag{3.30}$$

Implicitely, the time scale here considered is so that $t \gg \left(2\pi/\omega, 2\pi/\Omega_e\right)$.

3.2 Guiding-Center Drifts and Drift-Kinetic Equation

As shown in previous section, for axisymmetric plasmas, the electron drift kinetic equation may be expressed in the general form

$$\frac{\partial f}{\partial t} + \mathbf{v}_{\mathrm{gc}} \cdot \nabla f = \mathcal{C}\left(f\right) + \mathcal{Q}\left(f\right) + \mathcal{E}\left(f\right) \tag{3.31}$$

where $f = f\left(p, \xi, \psi, \theta, t\right)$ is the guiding-center distribution function.

In tokamaks, it can be shown that the guiding center velocity $\mathbf{v}_{\mathrm{gc}}$ may be decomposed into a fast parallel motion along the field lines, and a vertical drift velocity $\mathbf{v}_D$ across the magnetic flux surfaces

$$\mathbf{v}_{\mathrm{gc}} = v_{\parallel} \widehat{b} + \mathbf{v}_D \tag{3.32}$$

From the general expression (2.36) of the magnetic field $\mathbf{B}$,

$$\mathbf{B} = I\left(\psi\right) \nabla\phi + \nabla\psi \times \nabla\phi \tag{3.33}$$

one obtains in the (ψ, s, ϕ) coordinates system,

$$\mathbf{B} = \frac{I\left(\psi\right)}{R} \widehat{\phi} - \frac{\left|\nabla\psi\right|}{R} \widehat{s} \tag{3.34}$$

As shown in Appendix A, the gradient in (ψ, s, ϕ) coordinates is

$$\nabla = \nabla\psi \frac{\partial}{\partial\psi} + \nabla s \frac{\partial}{\partial s} + \nabla\phi \frac{\partial}{\partial\phi} = \nabla\psi \frac{\partial}{\partial\psi} + \widehat{s} \frac{\partial}{\partial s} + \frac{\widehat{\phi}}{R} \frac{\partial}{\partial\phi} \tag{3.35}$$

and recalling that the constants of the motion are the total energy (or momentum $\mathbf{p}$) as defined in (2.16) and the magnetic moment μ as given by relation (2.17), following conservations laws

$$\frac{\partial \mu}{\partial s} = 0 \tag{3.36}$$

$$\frac{\partial}{\partial s}\left[p_{\parallel}^2 + 2\mu B m_e\right] = 0 \tag{3.37}$$

are satisfied.

3.2.1 Drift Velocity from the Conservation of Canonical Momentum

The toroidal canonical momentum is also a constant of the motion because of axisymmetry. It is expressed as

$$P_\phi = R\left[\gamma m_e v_\phi + q_e A_\phi\right] \tag{3.38}$$

where A_ϕ is the toroidal component of the vector potential. From the relation

$$\mathbf{B} = \nabla \times \mathbf{A} \tag{3.39}$$

and the expression (A.171) of a rotational in (ψ, s, ϕ) coordinates, we get

$$\begin{aligned}
\mathbf{B} \;=\; & \left[\frac{1}{R}\frac{\partial}{\partial s}\left(RA_\phi\right) - \frac{1}{R}\frac{\partial}{\partial \phi}\left(A_s\right)\right]\widehat{\psi} \\
& + \left[\frac{1}{R}\frac{\partial}{\partial \phi}\left(A_\psi\right) - \frac{|\nabla\psi|}{R}\frac{\partial}{\partial \psi}\left(RA_\phi\right)\right]\widehat{s} \\
& + \left[|\nabla\psi|\frac{\partial}{\partial \psi}\left(A_s\right) - |\nabla\psi|\frac{\partial}{\partial s}\left(\frac{A_\psi}{|\nabla\psi|}\right)\right]\widehat{\phi}
\end{aligned} \tag{3.40}$$

with

$$A_\psi = \mathbf{A}\cdot\widehat{\psi} \tag{3.41}$$

$$A_s = \mathbf{A}\cdot\widehat{s} \tag{3.42}$$

$$A_\phi = \mathbf{A}\cdot\widehat{\phi} \tag{3.43}$$

In axisymmetric plasma, this reduces to

$$\begin{aligned}
\mathbf{B} \;=\; & \frac{1}{R}\frac{\partial}{\partial s}\left(RA_\phi\right)\widehat{\psi} \\
& - \frac{|\nabla\psi|}{R}\frac{\partial}{\partial \psi}\left(RA_\phi\right)\widehat{s} \\
& + \left[|\nabla\psi|\frac{\partial}{\partial \psi}\left(A_s\right) - |\nabla\psi|\frac{\partial}{\partial s}\left(\frac{A_\psi}{|\nabla\psi|}\right)\right]\widehat{\phi}
\end{aligned} \tag{3.44}$$

so that

$$B_s = -\frac{|\nabla\psi|}{R}\frac{\partial}{\partial \psi}\left(RA_\phi\right) \tag{3.45}$$

In addition, we know from expression (3.34) that

$$B_s = -\frac{|\nabla\psi|}{R} \tag{3.46}$$

so that be obtain

$$\frac{\partial RA_\phi}{\partial\psi} = 1 \tag{3.47}$$

Because the toroidal canonical momentum is a constant of the motion, we have

$$\mathbf{v}_{\rm gc}\cdot\nabla P_\phi = 0 \tag{3.48}$$

which can be decomposed into

$$\mathbf{v}_{\rm gc}\cdot\nabla\left(R\gamma m_e v_\phi\right) + \mathbf{v}_{\rm gc}\cdot\nabla\left(q_e RA_\phi\right) = 0 \tag{3.49}$$

Using relation (A.169), we get

$$\mathbf{v}_{\rm gc}\cdot\nabla\left(q_e RA_\phi\right) = \mathbf{v}_{\rm gc}\cdot\left[\nabla\psi\frac{\partial}{\partial\psi} + \widehat{s}\frac{\partial}{\partial s} + \frac{\widehat{\phi}}{R}\frac{\partial}{\partial\phi}\right]\left(q_e RA_\phi\right) \tag{3.50}$$

which in axisymmetric systems gives

$$\mathbf{v}_{\rm gc}\cdot\nabla\left(q_e A_\phi\right) = q_e\mathbf{v}_{\rm gc}\cdot\left[\nabla\psi\frac{\partial RA_\phi}{\partial\psi} + \widehat{s}\frac{\partial RA_\phi}{\partial s}\right] \tag{3.51}$$

Since $B_\psi = 0$, we have from relation (3.44) $\partial\left(RA_\phi\right)/\partial s = 0$ and therefore, using expression (3.47),

$$\mathbf{v}_{\rm gc}\cdot\nabla\left(q_e A_\phi\right) = q_e\mathbf{v}_{\rm gc}\cdot\nabla\psi \tag{3.52}$$

The only velocity accross the flux-surfaces is the drift velocity we are looking for, so that we get, using relation (3.32)

$$\mathbf{v}_{\rm gc}\cdot\nabla\left(q_e A_\phi\right) = q_e\mathbf{v}_D\cdot\nabla\psi \tag{3.53}$$

and the equation (3.49) becomes

$$q_e\mathbf{v}_D\cdot\nabla\psi = -\mathbf{v}_{\rm gc}\cdot\nabla\left(R\gamma m_e v_\phi\right) \tag{3.54}$$

Assuming a priori that $\left|v_\parallel\right| \gg |\mathbf{v}_D|$, a condition that holds in tokamaks, this equation reduces to

$$\begin{aligned}\mathbf{v}_D\cdot\nabla\psi &= -\frac{1}{q_e}\frac{v_\parallel}{B}\mathbf{B}\cdot\nabla\left(R\gamma m_e v_\phi\right)\\ &= -\frac{v_\parallel}{\Omega_e}\mathbf{B}\cdot\nabla\left(Rv_\phi\right)\end{aligned} \tag{3.55}$$

where we used that $\partial\gamma/\partial s = 0$ because of the conservation of energy.

The toroidal velocity is related to the parallel velocity by

$$v_\phi = \frac{B_\phi}{B}v_\parallel = \frac{I\left(\psi\right)}{RB}v_\parallel \tag{3.56}$$

so that

$$Rv_\phi = \frac{I(\psi)}{B} v_\parallel \tag{3.57}$$

Since $I(\psi)$ is a flux function, it can be taken out of the gradient, so that

$$\mathbf{v}_D \cdot \nabla\psi = -\frac{v_\parallel}{\Omega_e} I(\psi)\, \mathbf{B} \cdot \nabla\left(\frac{v_\parallel}{B}\right) \tag{3.58}$$

3.2.2 Drift Velocity from the Expression of Single Particle Drift

The guiding-center drift velocity due to the magnetic field gradient and curvature is

$$\mathbf{v}_D = \frac{1}{\Omega_e}\left(v_\parallel^2 + \frac{v_\perp^2}{2}\right)\frac{\mathbf{B}\times\nabla B}{B^2} \tag{3.59}$$

and its component perpendicular to the flux-surface can be written as

$$\mathbf{v}_D \cdot \nabla\psi = \frac{1}{\Omega_e}\left(v_\parallel^2 + \frac{v_\perp^2}{2}\right)\frac{1}{B^2}\nabla\psi \times \mathbf{B}\cdot\nabla B \tag{3.60}$$

Inserting the expression (3.34) of the magnetic field, we find

$$\mathbf{v}_D \cdot \nabla\psi = -\frac{1}{\Omega_e}\left(v_\parallel^2 + \frac{v_\perp^2}{2}\right)\frac{|\nabla\psi|}{B^2 R}\left[I(\psi)\,\widehat{s} + |\nabla\psi|\,\widehat{\phi}\right]\cdot\nabla B \tag{3.61}$$

Using (3.35), the equation (3.61) becomes

$$\mathbf{v}_D \cdot \nabla\psi = -\frac{1}{\Omega_e}\left(v_\parallel^2 + \frac{v_\perp^2}{2}\right)\frac{|\nabla\psi|}{B^2 R}\left[I(\psi)\frac{\partial B}{\partial s} + \frac{|\nabla\psi|}{R}\frac{\partial B}{\partial\phi}\right] \tag{3.62}$$

Under the assumption of axisymmetry, we are left with

$$\mathbf{v}_D \cdot \nabla\psi = -\frac{1}{\Omega_e}\left(v_\parallel^2 + \frac{v_\perp^2}{2}\right)\frac{|\nabla\psi|\, I(\psi)}{B^2 R}\frac{\partial B}{\partial s} \tag{3.63}$$

With the definition (2.17) of the magnetic moment μ, we rewrite

$$\mathbf{v}_D \cdot \nabla\psi = -\frac{1}{\Omega_e}\frac{|\nabla\psi|\, I(\psi)}{B^2 R}\left(v_\parallel^2 + \frac{\mu B}{m_e}\right)\frac{\partial B}{\partial s} \tag{3.64}$$

We have, using the conservation of magnetic momentum (3.36),

$$\left(v_\parallel^2 + \frac{\mu B}{m_e}\right)\frac{\partial B}{\partial s} = v_\parallel^2\frac{\partial B}{\partial s} + B\frac{\partial}{\partial s}\left(\frac{\mu B}{m_e}\right) \tag{3.65}$$

Using the conservation of energy (3.37), we get

$$\begin{aligned}\left(v_\parallel^2 + \frac{\mu B}{m_e}\right)\frac{\partial B}{\partial s} &= v_\parallel^2\frac{\partial B}{\partial s} - B\frac{\partial}{\partial s}\left(\frac{v_\parallel^2}{2}\right) &(3.66)\\ &= -v_\parallel\left[B\frac{\partial v_\parallel}{\partial s} - v_\parallel\frac{\partial B}{\partial s}\right] &(3.67)\\ &= -v_\parallel B^2\frac{\partial}{\partial s}\left(\frac{v_\parallel}{B}\right) &(3.68)\end{aligned}$$

and finally, the equation (3.64) becomes

$$\mathbf{v}_D \cdot \nabla\psi = \frac{v_\parallel}{\Omega_e} I(\psi) \frac{|\nabla\psi|}{R} \frac{\partial}{\partial s}\left(\frac{v_\parallel}{B}\right) \tag{3.69}$$

In addition,

$$\begin{aligned} \mathbf{B}\cdot\nabla &= I(\psi)\nabla\phi\cdot\nabla + \nabla\psi\times\nabla\phi\cdot\nabla \\ &= \frac{I(\psi)}{R}\frac{\partial}{\partial\phi} - \frac{|\nabla\psi|}{R}\frac{\partial}{\partial s} \end{aligned} \tag{3.70}$$

and, using axisymmetry,

$$\mathbf{B}\cdot\nabla = -\frac{|\nabla\psi|}{R}\frac{\partial}{\partial s} \tag{3.71}$$

so that we can rewrite (3.69) as

$$\mathbf{v}_D \cdot \nabla\psi = -\frac{v_\parallel}{\Omega_e} I(\psi)\, \mathbf{B}\cdot\nabla\left(\frac{v_\parallel}{B}\right) \tag{3.72}$$

expression which is the same as (3.58).

3.2.3 Case of Circular concentric flux-surfaces

In this case, $\psi = \psi(r)$ and therefore

$$\nabla\psi = \psi'(r)\,\widehat{r} \tag{3.73}$$

and

$$v_{Dr} = \mathbf{v}_D\cdot\widehat{r} = \frac{\mathbf{v}_D\cdot\nabla\psi}{\psi'} \tag{3.74}$$

which gives

$$v_{Dr} = -\frac{v_\parallel}{\Omega_e}\frac{I(\psi)}{\psi'}\mathbf{B}\cdot\nabla\left(\frac{v_\parallel}{B}\right) \tag{3.75}$$

In addition,

$$\mathbf{B}\cdot\nabla = -\frac{|\nabla\psi|}{R}\frac{\partial}{\partial s} = -\frac{|\psi'|}{R}\frac{\partial}{\partial s} \tag{3.76}$$

and, because

$$\widehat{s}\cdot\widehat{\theta} = \widehat{\psi}\cdot\widehat{r} = \sigma_\psi \tag{3.77}$$

we find

$$\frac{\partial}{\partial s} = \frac{\sigma_\psi}{r}\frac{\partial}{\partial\theta} \tag{3.78}$$

and

$$\mathbf{B}\cdot\nabla = -\frac{\psi'}{Rr}\frac{\partial}{\partial\theta} \tag{3.79}$$

so that finally

$$v_{Dr} = \frac{v_\parallel}{\Omega_e}\frac{I(\psi)}{Rr}\frac{\partial}{\partial\theta}\left(\frac{v_\parallel}{B}\right) = \frac{v_\parallel}{r}\frac{I(\psi)}{RB}\frac{\partial}{\partial\theta}\left(\frac{v_\parallel}{\Omega}\right) \tag{3.80}$$

When the toroidal field dominates, $B \simeq I(\psi)/R$ and

$$v_{Dr} \simeq \frac{v_\parallel}{r}\frac{\partial}{\partial\theta}\left(\frac{v_\parallel}{\Omega}\right) \tag{3.81}$$

3.2.4 Steady-State Drift-Kinetic Equation

Using expressions (3.31), (3.32) and (3.58) or (3.72), we obtain in steady-state

$$v_{\parallel}\widehat{b}\cdot\nabla f-\frac{v_{\parallel}}{\Omega_e}I\left(\psi\right)\mathbf{B}\cdot\nabla\left(\frac{v_{\parallel}}{B}\right)\frac{\partial f}{\partial\psi}=\mathcal{C}\left(f\right)+\mathcal{Q}\left(f\right)+\mathcal{E}\left(f\right) \tag{3.82}$$

which can be rewritten as

$$v_s\frac{\partial f}{\partial s}+\frac{v_{\parallel}}{\Omega_e}I\left(\psi\right)\frac{\left|\nabla\psi\right|}{R}\frac{\partial}{\partial s}\left(\frac{v_{\parallel}}{B}\right)\frac{\partial f}{\partial\psi}=\mathcal{C}\left(f\right)+\mathcal{Q}\left(f\right)+\mathcal{E}\left(f\right) \tag{3.83}$$

with

$$v_s=v_{\parallel}\left(\widehat{b}\cdot\widehat{s}\right) \tag{3.84}$$

3.3 Small drift approximation

We recall the electron drift kinetic equation may be expressed as

$$v_s\frac{\partial f}{\partial s}+\frac{v_{\parallel}}{\Omega}I\left(\psi\right)\frac{\left|\nabla\psi\right|}{R}\frac{\partial}{\partial s}\left(\frac{v_{\parallel}}{B}\right)\frac{\partial f}{\partial\psi}=\mathcal{C}\left(f\right)+\mathcal{Q}\left(f\right)+\mathcal{E}\left(f\right) \tag{3.85}$$

Each of these terms corresponds to a time evolution, and is therefore associated with a time-scale:

- *Motion along magnetic field lines.* The time scale here is the bounce time τ_b for trapped electrons, or the transit time τ_t for circulating ones, which can be deduced directly from expression (2.10). For circulating electrons

$$\tau_t=\frac{2\pi R_p\widetilde{q}}{v\left|\xi_0\right|}\sim\frac{2\pi qR_p}{v_{Te}} \tag{3.86}$$

  taking $\lambda\sim 1$ in that case, and $q\simeq\widetilde{q}$ that is valid circular plasma cross-sections, and $v\left|\xi_0\right|=v_{\parallel}\simeq v_{Te}$ for thermal electrons. Since $v_{\parallel}\leq\sqrt{\epsilon}v_{\perp}\simeq\sqrt{\epsilon}v_{Te}$ for trapped electrons, as the consequence of the magnetic moment conservation, it turns out that τ_b may be deduced directly from τ_t

$$\tau_b=\frac{2\pi R_p\widetilde{q}}{v\left|\xi_0\right|}\sim\frac{2\pi qR_p}{\sqrt{\epsilon}v_{Te}} \tag{3.87}$$

  Consequently, $\tau_b\geq\tau_t$, since $\epsilon\leq 1$, a result which is the consequence of the progressive slowing down of the parallel velocity as far as the electron approaches the turning point.

- *Vertical drift across magnetic field lines.* The time scale here is the drift time τ_d, which corresponds to the time for an electron to drift across the plasma. It is then given by

$$\tau_d=\int_0^{\psi_a}d\psi\frac{\Omega_e}{v_{\parallel}I\left(\psi\right)}\frac{R}{\left|\nabla\psi\right|}\left[\frac{\partial}{\partial s}\left(\frac{v_{\parallel}}{B}\right)\right]^{-1} \tag{3.88}$$

using expression 3.69 for the radial component $\mathbf{v}_D \cdot \nabla\psi$ of the drift velocity $\mathbf{v}_D$ as defined in 3.59. Using relation $I(\psi)$ as defined in (2.37), and the fact that $d\psi/|\nabla\psi| = dr$ for circular concentric plasma cross-sections,

$$\tau_d \simeq \frac{\Omega_e}{v_{Te}^2} \int_0^{a_p} \frac{dr}{B_T} \left[\frac{\partial}{\partial s} \left(\frac{1}{B} \right) \right]^{-1} \tag{3.89}$$

and since in that magnetic configuration $\partial/\partial s \sim 2\pi/R_p$, ones obtains finally

$$\tau_d \simeq 2\pi \frac{\Omega_e}{v_{Te}^2} R_p \int_0^{a_p} \frac{B}{B_T} dr \tag{3.90}$$

or

$$\tau_d \simeq 2\pi \frac{\Omega_e}{v_{Te}^2} R_p a_p \tag{3.91}$$

Consequently, the small drift parameter δ_d is defined as the ratio

$$\delta_d \equiv \frac{\tau_t}{\tau_d} \sim q \frac{\rho_L}{a_p} \sim \frac{\rho_L}{a_p} \tag{3.92}$$

where the thermal Larmor radius $\rho_L = v_{Te}/\Omega_e$ has been introduced.

- *Collisions.* The Fokker-Planck theory considers the cumulative effect of many small-angle collisions in calculating the rate of change of a particle distribution. From this theory, the characteristic time scale τ_c corresponds for Coulomb collisons to deflect an electron's path by a significant angle, on the order of $\pi/2$. This is the electron thermal collision time τ_c whose expression is

$$\tau_c = \nu_c^{-1} = \frac{4\pi\varepsilon_0 m_e^2 v_{Te}^3}{q_e^4 n_e \ln\Lambda} \tag{3.93}$$

where $\ln\Lambda$ is the well known Coulomb logarithm, a slowly varying function of the plasma temperature and density. The collision time scale τ_c holds for circulating electrons.

For trapped ones, it is more physical to consider an alternate collision time scale determined not by the time for deflection of the path by $\pi/2$, but by the time needed for the electron to be deflected so that it is no longer on a trapped orbit. In the limit $\epsilon \ll 1$, we can approximate the change of the pitch angle necessary to make trapped particles become untrapped

$$\Delta\xi_0 \sim \xi_{0T} \simeq \sqrt{\frac{2\epsilon}{1+\epsilon}} \sim \sqrt{\epsilon} \tag{3.94}$$

Because the small-angle collisions produce a random-walk change in the pitch-angle ξ_0, the *effective* collision time for detrapping $\tau_c^{eff.}$ or τ_{dt} is approximately deduced from relation

$$\nu_c^{eff.} \sim \frac{\nu_c}{\Delta\xi_0^2} \sim \frac{\nu_c}{\epsilon} \tag{3.95}$$

and

$$\tau_{dt} = \tau_c^{eff.} \sim \epsilon\tau_c \tag{3.96}$$

- *Constant electric field acceleration.* From the relation (3.30), it is straightforward to estimate that the time scale associated to constant electric field acceleration is

$$\tau_e \sim \frac{m_e v_{Te}}{|q_e| E_\parallel} \sim \tau_c \frac{|E_D|}{E_\parallel} \tag{3.97}$$

  where the well known Dreicer field E_D

$$E_D = \nu_c \frac{m_e v_{Te}}{q_e} \tag{3.98}$$

  is introduced. Here only circulating particle are concerned.

- *Quasilinear diffusion.* In a similar approach,

$$\tau_{ql} \sim \frac{(m_e v_{Te})^2}{D_{ql}} \sim \tau_c \frac{D_{ql}^\dagger}{D_{ql}} \tag{3.99}$$

  where $D_{ql}^\dagger = \nu_c (m_e v_{Te})^2$.

3.3.1 Small Drift Ordering

In the small drift expansion $\delta_d \ll 1$, where the small parameter is defined by relation (3.92)

$$f = f_0 + f_1 + \cdots \tag{3.100}$$

the first order equation is

$$v_s \frac{\partial f_0}{\partial s} = \mathcal{C}(f_0) + \mathcal{Q}(f_0) + \mathcal{E}(f_0) \tag{3.101}$$

which is usually referred to as the Fokker-Planck equation.

The second order equation is

$$v_s \frac{\partial f_1}{\partial s} + \frac{v_\parallel}{\Omega_e} I(\psi) \frac{|\nabla \psi|}{R} \frac{\partial}{\partial s} \left(\frac{v_\parallel}{B} \right) \frac{\partial f_0}{\partial \psi} = \mathcal{C}(f_1) + \mathcal{Q}(f_1) + \mathcal{E}(f_1) \tag{3.102}$$

which is referred to as the electron Drift Kinetic equation.

3.4 Low collision limit and bounce averaging

3.4.1 Fokker-Planck Equation

The Fokker-Planck Equation is

$$v_s \frac{\partial f_0}{\partial s} = \mathcal{C}(f_0) + \mathcal{Q}(f_0) + \mathcal{E}(f_0) \tag{3.103}$$

In the low collision regime, which is characterized by the condition

$$\nu^* \equiv \frac{\tau_b}{\tau_{dt}} \ll 1 \tag{3.104}$$

where $\tau_{dt} = \epsilon\tau_c$ is the collision detrapping time, as defined in the previous section, it is assumed that electrons circulating or trapped are able to complete their orbit in a time too short for collisions to deflect them from their orbit. As a consequence, the dominant term in the Fokker-Planck equation is simply

$$v_s \frac{\partial f_0}{\partial s} = 0 \tag{3.105}$$

so that f_0 is constant along the field lines.

Then, performing a bounce-averaging, we have

$$\begin{aligned} \left\{ v_s \frac{\partial f_0}{\partial s} \right\} &= \frac{1}{\tau_b} \left[\frac{1}{2} \sum_\sigma \right]_T \int_{s_{\min}}^{s_{\max}} \frac{ds}{|v_s|} v_s \frac{\partial f_0}{\partial s} \\ &= \frac{1}{\tau_b} \left[\frac{1}{2} \sum_\sigma \right]_T \sigma \left[f_0 \right]_{s_{\min}}^{s_{\max}} \end{aligned} \tag{3.106}$$

For passing particles, the positions $s_{\min}$ and $s_{\max}$ coincide, so that $[f_0]_{s_{\min}}^{s_{\max}} = 0$ and the term vanishes. For trapped particles, the term also vanishes because of the sum over $\sigma = \pm 1$, since, by definition, $v_\parallel = 0$ at the turning points $s_{\min}$ and $s_{\max}$, and consequently f_0 is independent of the sign of σ.

Therefore, the bounce-averaged Fokker-Planck equation becomes

$$\{\mathcal{C}(f_0)\} + \{\mathcal{Q}(f_0)\} + \{\mathcal{E}(f_0)\} = 0 \tag{3.107}$$

with f_0 constant along the field lines.

3.4.2 Drift-Kinetic Equation

The drift kinetic equation is

$$v_s \frac{\partial f_1}{\partial s} + \frac{v_\parallel}{\Omega_e} I(\psi) \frac{|\nabla\psi|}{R} \frac{\partial}{\partial s} \left(\frac{v_\parallel}{B} \right) \frac{\partial f_0}{\partial \psi} = \mathcal{C}(f_1) + \mathcal{Q}(f_1) + \mathcal{E}(f_1) \tag{3.108}$$

In the low collisiona regime $\nu^* \ll 1$, the dominant term is

$$v_s \frac{\partial f_1}{\partial s} + \frac{v_\parallel}{\Omega_e} I(\psi) \frac{|\nabla\psi|}{R} \frac{\partial}{\partial s} \left(\frac{v_\parallel}{B} \right) \frac{\partial f_0}{\partial \psi} = 0 \tag{3.109}$$

which gives

$$f_1 = \widetilde{f} + g \tag{3.110}$$

where

$$\widetilde{f} = -\int ds \frac{v_\parallel}{v_s \Omega_e} I(\psi) B_P \frac{\partial}{\partial s} \left(\frac{v_\parallel}{B} \right) \frac{\partial f_0}{\partial \psi} \tag{3.111}$$

and g is a constant function along the field lines. Noting that

$$\widehat{b} \cdot \widehat{s} = -\frac{B_P}{B} \tag{3.112}$$

we get

$$\begin{aligned}\widetilde{f} &= \int ds \frac{1}{\Omega_e} I(\psi) B \frac{\partial}{\partial s}\left(\frac{v_\parallel}{B}\right)\frac{\partial f_0}{\partial \psi} \\ &= \frac{\gamma m_e I(\psi)}{q_e}\frac{\partial f_0}{\partial \psi}\int ds \frac{\partial}{\partial s}\left(\frac{v_\parallel}{B}\right) \\ &= \frac{v_\parallel}{\Omega_e} I(\psi)\frac{\partial f_0}{\partial \psi}\end{aligned} \tag{3.113}$$

where we used the fact that $\partial f_0/\partial s = 0$.

Then, performing a bounce-averaging, we find again, using the same argument as in (3.106), that

$$\left\{ v_s \frac{\partial f_1}{\partial s} \right\} = 0 \tag{3.114}$$

In addition, we have

$$\begin{aligned}&\left\{ \frac{v_\parallel}{\Omega_e} I(\psi)\frac{|\nabla\psi|}{R}\frac{\partial}{\partial s}\left(\frac{v_\parallel}{B}\right)\frac{\partial f_0}{\partial \psi}\right\} \\ &= \frac{1}{\tau_b}\left[\frac{1}{2}\sum_\sigma\right]_T \int_{s_{\min}}^{s_{\max}} \frac{ds}{|v_s|}\frac{v_\parallel}{\Omega_e} I(\psi)\frac{|\nabla\psi|}{R}\frac{\partial}{\partial s}\left(\frac{v_\parallel}{B}\right)\frac{\partial f_0}{\partial \psi} \\ &= \frac{1}{\tau_b}\frac{\gamma m_e I(\psi)}{q_e}\frac{\partial f_0}{\partial \psi}\left[\frac{1}{2}\sum_\sigma\right]_T \sigma \int_{s_{\min}}^{s_{\max}} ds \frac{\partial}{\partial s}\left(\frac{v_\parallel}{B}\right) \\ &= \frac{1}{\tau_b}\frac{\gamma m_e I(\psi)}{q_e}\frac{\partial f_0}{\partial \psi}\left[\frac{1}{2}\sum_\sigma\right]_T \sigma \left[\frac{v_\parallel}{B}\right]_{s_{\min}}^{s_{\max}}\end{aligned} \tag{3.115}$$

Again, for passing particles, the positions $s_{\min}$ and $s_{\max}$ coincide, so that $\left[v_\parallel/B\right]_{s_{\min}}^{s_{\max}} = 0$ and the term vanishes. For trapped particles, the term also vanishes because $v_\parallel \to 0$ at the turning points $s_{\min}$ and $s_{\max}$.

Consequently, we find that the bounce-averaged drift kinetic equation becomes

$$\{\mathcal{C}(f_1)\} + \{\mathcal{Q}(f_1)\} + \{\mathcal{E}(f_1)\} = 0 \tag{3.116}$$

where .

$$f_1 = \widetilde{f} + g \tag{3.117}$$

$$\widetilde{f} = \frac{v_\parallel}{\Omega_e} I(\psi)\frac{\partial f_0}{\partial \psi} \tag{3.118}$$

and g is then given by

$$\{\mathcal{C}(g)\} + \{\mathcal{Q}(g)\} + \{\mathcal{E}(g)\} = -\left\{\mathcal{C}\left(\widetilde{f}\right)\right\} - \left\{\mathcal{Q}\left(\widetilde{f}\right)\right\} - \left\{\mathcal{E}\left(\widetilde{f}\right)\right\} \tag{3.119}$$

using the fact that all operators are linear.

3.5 Flux conservative representation

3.5.1 General formulation

The starting point of the flux conservative representation is the conservation of the total number of particles in the plasma,

$$N = \int \cdots \int f\left(\mathbf{X}, P\right) d^3\mathbf{X} d^3\mathbf{P} \tag{3.120}$$

where $\mathbf{X}$ and $\mathbf{P}$ are respectively coordinates in configuration and momentum spaces. According to the systems which are used in the calculations, $\mathbf{X} = (\psi, \theta, \phi)$ and $\mathbf{P} = (p, \xi, \varphi)$,

$$\begin{cases} d^3\mathbf{X} = \frac{Rr}{|\nabla\psi|\left|\widehat{\psi}\cdot\widehat{r}\right|} d\psi d\theta d\phi \\ d^3\mathbf{P} = p^2 dp d\xi d\varphi \end{cases} \tag{3.121}$$

as shown in Appendix A, one obtains

$$N = \int \cdots \int f\left(\psi, \theta, \phi, p, \xi, \varphi\right) \frac{Rr}{|\nabla\psi|\left|\widehat{\psi}\cdot\widehat{r}\right|} p^2 d\psi d\theta d\phi dp d\xi d\varphi \tag{3.122}$$

Using the transformation

$$\frac{1-\xi^2}{B\left(\psi,\theta\right)} = \frac{1-\xi_0^2}{B_0\left(\psi\right)} \tag{3.123}$$

that results from conservation of the magnetic moment and energy,

$$N = \int \cdots \int f\left(\psi, \theta, \phi, p, \xi, \varphi\right) \frac{Rr}{|\nabla\psi|\left|\widehat{\psi}\cdot\widehat{r}\right|} p^2 \frac{\xi_0}{\xi} \frac{B\left(\psi,\theta\right)}{B_0\left(\psi\right)} d\psi d\theta d\phi dp d\xi_0 d\varphi \tag{3.124}$$

because $\xi d\xi / B\left(\psi,\theta\right) = \xi_0 d\xi_0 / B_0\left(\psi\right)$. Since at the zero order, f_0 is constant along a magnetic field line, $f_0 = f_0^{(0)}$ is independent of the poloidal angle θ, where $f_0^{(0)}$ is the bounce averaged distribution function. Hence

$$\begin{aligned} N &= \iiint f_0^{(0)}\left(\psi, p, \xi_0\right) p^2 d\psi dp d\xi_0 \times \\ &\quad \int_{\theta_{\min}}^{\theta_{\max}} \frac{Rr}{|\nabla\psi|\left|\widehat{\psi}\cdot\widehat{r}\right|} \frac{\xi_0}{\xi} \frac{B\left(\psi,\theta\right)}{B_0\left(\psi\right)} d\theta \int_0^{2\pi} d\phi \int_0^{2\pi} d\varphi \\ &= 4\pi^2 \iiint f_0^{(0)}\left(\psi, p, \xi_0\right) \frac{1}{B_0\left(\psi\right)} p^2 d\psi dp d\xi_0 \times \\ &\quad \int_{\theta_{\min}}^{\theta_{\max}} \frac{Rr}{|\nabla\psi|\left|\widehat{\psi}\cdot\widehat{r}\right|} \frac{\xi_0}{\xi} B\left(\psi,\theta\right) d\theta \end{aligned} \tag{3.125}$$

taking into account, in addition, of the toroidal aximmetry, and cylindrical symmetry of the distribution along the magnetic field line direction. Here, $\theta_{\min}$ and $\theta_{\max}$ depends of the particle trajectory in the configuration space, wether they are passing or trapped.

From plasma equilibrium, since

$$\frac{|\nabla\psi|}{R} = B_P \tag{3.126}$$

where B_P is the poloidal magnetic field,

$$\int_{\theta_{\min}}^{\theta_{\max}} \frac{Rr}{|\nabla\psi|\left|\widehat{\psi}\cdot\widehat{r}\right|}\frac{\xi_0}{\xi}B\left(\psi,\theta\right)d\theta = \int_{\theta_{\min}}^{\theta_{\max}} \frac{r}{\left|\widehat{\psi}\cdot\widehat{r}\right|}\frac{\xi_0}{\xi}\frac{B}{B_P}d\theta = 2\pi\lambda\left(\psi,\xi_0\right)\widetilde{q}\left(\psi\right) \tag{3.127}$$

Here, appears, as expected the normalized bounce time $\lambda\left(\psi,\xi_0\right)$ and the factor $\widetilde{q}\left(\psi\right)$ introduced in Sec. 2.2.1, which in conjunction with $B_0\left(\psi\right)$ characterizes the local shape of magnetic flux surface. Hence,

$$N = 8\pi^3 \iiint f_0^{(0)}\left(\psi,p,\xi_0\right)\frac{\widetilde{q}\left(\psi\right)}{B_0\left(\psi\right)}\lambda\left(\psi,\xi_0\right)p^2 d\psi dp d\xi_0 \tag{3.128}$$

From this expression, the Jacobian J of the coordinate system (ψ,p,ξ_0) may be simply defined as,

$$J = J_\psi J_p J_{\xi_0} = \frac{\widetilde{q}\left(\psi\right)}{B_0\left(\psi\right)}\lambda\left(\psi,\xi_0\right)p^2 \tag{3.129}$$

where

$$\begin{cases} J_\psi = \widetilde{q}\left(\psi\right)/B_0\left(\psi\right) \\ J_p = p^2 \\ J_{\xi_0} = \lambda\left(\psi,\xi_0\right) \end{cases} \tag{3.130}$$

and the generic conservative form of the kinetic equation may be immediatly deduced

$$\frac{\partial f_0^{(0)}}{\partial t} + \nabla_{(\psi,p,\xi_0)}\cdot\mathbf{S}^{(0)} = 0 \tag{3.131}$$

where the phase space flux $\mathbf{S}^{(0)}$ at $B = B_{\min}$ is decomposed into a diffusive and a convective part

$$\mathbf{S}^{(0)} = -\mathbb{D}^{(0)}\nabla f_0^{(0)} + \mathbf{F}^{(0)} f_0^{(0)} \tag{3.132}$$

in the mean field theory. Here, $\mathbb{D}^{(0)}$ and $\mathbf{F}^{(0)}$ are respectively the diffusion tensor and convection vector in phase space. They can be expressed generally as

$$\mathbb{D}^{(0)} = \begin{pmatrix} D_{\psi\psi}^{(0)} & D_{\psi p}^{(0)} & D_{\psi\xi}^{(0)} \\ D_{p\psi}^{(0)} & D_{pp}^{(0)} & D_{p\xi}^{(0)} \\ D_{\xi\psi}^{(0)} & D_{\xi p}^{(0)} & D_{\xi\xi}^{(0)} \end{pmatrix} \tag{3.133}$$

and

$$\mathbf{F}^{(0)} = \begin{pmatrix} F_p^{(0)} \\ F_\xi^{(0)} \\ F_\psi^{(0)} \end{pmatrix} \tag{3.134}$$

where each element is function of (ψ, p, ξ_0). Here the gradient vector in the reduced (ψ, p, ξ_0) space is

$$\nabla = \begin{pmatrix} \nabla_\psi = |\nabla\psi|\, \partial/\partial\psi \\ \nabla_p = \partial/\partial p \\ \nabla_{\xi_0} = -\frac{\sqrt{1-\xi_0^2}}{p}\partial/\partial\xi_0 \end{pmatrix} \tag{3.135}$$

so, following calculations given in Appendix A,

$$\begin{aligned} \nabla_{(\psi,p,\xi_0)} \cdot \mathbf{S}^{(0)} \left(f_0^{(0)}\right) &= \frac{1}{J}\frac{\partial}{\partial p}\left(J\mathbf{S}^{(0)} \cdot \mathbf{e}^p\right) + \frac{1}{J}\frac{\partial}{\partial \xi_0}\left(J\mathbf{S}^{(0)} \cdot \mathbf{e}^\xi\right) + \frac{1}{J}\frac{\partial}{\partial \psi}\left(J\mathbf{S}^{(0)} \cdot \mathbf{e}^\psi\right) \\ &= \frac{1}{J}\frac{\partial}{\partial p}\left(J\mathbf{S}^{(0)} \cdot \widehat{p}\right) - \frac{1}{J}\frac{1}{p}\frac{\partial}{\partial \xi_0}\left(\sqrt{1-\xi_0^2}J\mathbf{S}^{(0)} \cdot \widehat{\xi}\right) \\ &\quad + \frac{1}{J}\frac{\partial}{\partial \psi}\left(J\left|\nabla\psi\right|_0 \mathbf{S}^{(0)} \cdot \widehat{\psi}\right) \\ &= \frac{1}{p^2}\frac{\partial}{\partial p}\left(p^2\mathbf{S}_p^{(0)}\right) - \frac{1}{\lambda\left(\psi,\xi_0\right)}\frac{1}{p}\frac{\partial}{\partial \xi_0}\left(\sqrt{1-\xi_0^2}\lambda\left(\psi,\xi_0\right)\mathbf{S}_\xi^{(0)}\right) \\ &\quad + \frac{B_0\left(\psi\right)}{\lambda\left(\psi,\xi_0\right)\widetilde{q}\left(\psi\right)}\frac{\partial}{\partial \psi}\left(\frac{\widetilde{q}\left(\psi\right)}{B_0\left(\psi\right)}\lambda\left(\psi,\xi_0\right)\left|\nabla\psi\right|_0 \mathbf{S}_\psi^{(0)}\right) \end{aligned} \tag{3.136}$$

where $|\nabla\psi|_0$ is taken on the magnetic flux surface where B is minimum, i.e., $B = B_0$. The first two terms correspond to the usual dynamics in momentum space at a given spatial position ψ, while the third one is associated to spatial transport at fixed p and ξ_0. It is interesting to note that spatial transport is not independent of the momentum dynamics through the parameter $\lambda\left(\psi,\xi_0\right)$. It corrects the spatial transport from the particle dynamics along the magnetic field line, since most particles tend to spend more time far from $B = B_0$. In the limit of strongly passing particles, $\lambda\left(\psi,\xi_0\right) \simeq 1$, and the spatial term becomes independent of ξ_0.

It is interesting to cross-check the conservative nature of the transport equation is well ensured by performing the integral

$$\iiint \left[\frac{\partial f_0^{(0)}}{\partial t} + \nabla_{(\psi,p,\xi_0)} \cdot \mathbf{S}^{(0)}\right] J dp d\xi_0 d\psi = 0 \tag{3.137}$$

or

$$\frac{\partial N}{\partial t} + \iiint \nabla_{(\psi,p,\xi_0)} \cdot \mathbf{S}^{(0)} J dp d\xi_0 d\psi = 0 \tag{3.138}$$

Indeed, in that case, the variation of the total number of particles $\partial N/\partial t$ as a function of time depends only from boundary conditions.

$$\iiint \nabla_{(\psi,p,\xi_0)} \cdot \mathbf{S}^{(0)} J dp d\xi_0 d\psi = \mathcal{I}_p - \mathcal{I}_{\xi_0} + \mathcal{I}_\psi \tag{3.139}$$

where

$$\mathcal{I}_p = \iiint \frac{1}{p^2}\frac{\partial}{\partial p}\left(p^2\mathbf{S}_p^{(0)}\right) J dp d\xi_0 d\psi \tag{3.140}$$

$$\mathcal{I}_{\xi_0} = \iiint \frac{1}{\lambda\left(\psi,\xi_0\right)}\frac{1}{p}\frac{\partial}{\partial \xi_0}\left(\sqrt{1-\xi_0^2}\lambda\left(\psi,\xi_0\right)\mathbf{S}_\xi^{(0)}\right) J dp d\xi_0 d\psi \tag{3.141}$$

$$\mathcal{I}_\psi = \iiint \frac{B_0(\psi)}{\lambda(\psi,\xi_0)\,\widetilde{q}(\psi)} \frac{\partial}{\partial\psi}\left(\frac{\widetilde{q}(\psi)}{B_0(\psi)}\lambda(\psi,\xi_0)\,|\nabla\psi|\,\mathbf{S}_\psi^{(0)}\right) J dp d\xi_0 d\psi \tag{3.142}$$

For $\mathcal{I}_p$,

$$\begin{aligned}
&\iiint \frac{1}{p^2}\frac{\partial}{\partial p}\left(p^2\mathbf{S}_p^{(0)}\right) J dp d\xi_0 d\psi \\
&= \iint \left[p^2\mathbf{S}_p^{(0)}\right]_0^{p_{\max}} \frac{\widetilde{q}(\psi)}{B_0(\psi)}\lambda(\psi,\xi_0)\,d\xi_0 d\psi \\
&= p_{\max}^2 \iint \mathbf{S}_p^{(0)}(p_{\max})\,\frac{\widetilde{q}(\psi)}{B_0(\psi)}\lambda(\psi,\xi_0)\,d\xi_0 d\psi
\end{aligned} \tag{3.143}$$

and assuming that $\lim_{p\to\infty} p^2\mathbf{S}_p^{(0)} = 0$, one finds $\mathcal{I}_p = 0$. This condition is generally well fullfiled, except in strong runaway regimes, where above the Dreicer limit characterized by critical momentum p_D, electrons gain energy up to very high energies, that are usually well beyond the domain of integration addressed in numerical calculations for the current drive problem. However, in this case, $\mathcal{I}_p$ is given by $\mathbf{S}_p^{(0)}$ at $p_{\max}$, where $p_{\max}$ corresponds to the boundary of the momentum domain of integration. Its conservative nature is well ensured, since $\partial N/\partial t$ only depends of this parameter for p.

The integration of ξ_0 leads to

$$\begin{aligned}
\mathcal{I}_{\xi_0} &= \iiint \frac{1}{\lambda(\psi,\xi_0)}\frac{1}{p}\frac{\partial}{\partial\xi_0}\left(\sqrt{1-\xi_0^2}\lambda(\psi,\xi_0)\,\mathbf{S}_\xi^{(0)}\right) J dp d\xi_0 d\psi \\
&= \iint \left[\sqrt{1-\xi_0^2}\lambda(\psi,\xi_0)\,\mathbf{S}_\xi^{(0)}\right]_{-1}^{+1} \frac{\widetilde{q}(\psi)}{B_0(\psi)} p dp d\psi \\
&= 0
\end{aligned} \tag{3.144}$$

which indicates that pitch-angle scattering never contributes to variations of N, and therefore the conservative nature of this term in the transport equation is also well demonstrated.

Finally,

$$\begin{aligned}
\mathcal{I}_\psi &= \iiint \frac{B_0(\psi)}{\lambda(\psi,\xi_0)\,\widetilde{q}(\psi)} \frac{\partial}{\partial\psi}\left(\frac{\widetilde{q}(\psi)}{B_0(\psi)}\lambda(\psi,\xi_0)\,|\nabla\psi|\,\mathbf{S}_\psi^{(0)}\right) J dp d\xi_0 d\psi \\
&= \iint \left[\frac{\widetilde{q}(\psi)}{B_{\min}(\psi)}\lambda(\psi,\xi_0)\,|\nabla\psi|\,\mathbf{S}_\psi^{(0)}\right]_0^{\psi_a} p^2 dp d\xi_0 \\
&= \frac{\widetilde{q}(\psi_a)}{B_0(\psi_a)}\,|\nabla\psi|_{\psi_a} \iint \lambda(\psi_a,\xi_0)\,\mathbf{S}_\psi^{(0)}(\psi_a)\,p^2 dp d\xi_0
\end{aligned} \tag{3.145}$$

which only depends of edge values at ψ_a since $|\nabla\psi|_0 = R_0 B_{P0} = 0$ at $\psi = 0$ when no particle is injected at the plasma center. Here, B_{P0} is the poloidal magnetic field where B is minimum. If $\mathbf{S}_\psi^{(0)}(\psi_a) = 0$, $\mathcal{I}_\psi = 0$, and the total number of particles is conserved in the discharge.

It is important to notice that the magnetic moment is intrinsically conserved in the equations, in particular for the radial transport part, through the pitch-angle dependence of the normalized bounce time λ. Therefore, spatial transport is valid not only for circulating particles satisfying $p_\parallel/p_\perp \gg 1$, but also for highly trapped electrons, i.e. when $p_\parallel/p_\perp \ll 1$.

3.5.2 Dynamics in Momentum Space

Momentum space operator It is possible to recover the general bounce averaged transport equation in momentum space by another independent approach. Here, the momentum space dynamics of the kinetic equation is be expressed in conservative form as a flux divergence that may expressed according to the (A.57) introduced in Appendix A

$$\nabla_{\mathbf{p}} \cdot \mathbf{S}_{\mathbf{p}} = \frac{1}{J_{\mathbf{p}}} \frac{\partial}{\partial p^i} \left(J_{\mathbf{p}} S^i_{\mathbf{p}} \right) \tag{3.146}$$

where $J_{\mathbf{p}}$ is the momentum space Jacobian associated with the momentum space coordinate system (p, ξ, φ), described in (A.247). Since the spherical system has the natural symmetry of collisions, the momentum space Jacobian is (A.269)

$$J_{\mathbf{p}} = p^2 \tag{3.147}$$

so that, taking into account that the kinetic equation is gyroaveraged and therefore the coordinate φ disappears, the following expression for the divergence (A.278) is obtained

$$\nabla_{\mathbf{p}} \cdot \mathbf{S}_{\mathbf{p}} = \frac{1}{p^2} \frac{\partial}{\partial p} \left(p^2 S_p \right) - \frac{1}{p} \frac{\partial}{\partial \xi} \left(\sqrt{1 - \xi^2} S_\xi \right) \tag{3.148}$$

where by definition

$$S_p = \mathbf{S}_{\mathbf{p}} \cdot \widehat{p} \tag{3.149}$$

$$S_\xi = \mathbf{S}_{\mathbf{p}} \cdot \widehat{\xi} \tag{3.150}$$

In the mean-field theory, the momentum space fluxes may be expressed as the sum of diffusive and convective parts,

$$\mathbf{S}_{\mathbf{p}} = -\mathbb{D}_{\mathbf{p}} \nabla_{\mathbf{p}} \mho + \mathbf{F}_{\mathbf{p}} \mho \tag{3.151}$$

with

$$\mathbb{D}_{\mathbf{p}} = \begin{pmatrix} D_{pp} & D_{p\xi} \\ D_{\xi p} & D_{\xi\xi} \end{pmatrix} \tag{3.152}$$

$$\mathbf{F}_{\mathbf{p}} = \begin{pmatrix} F_p \\ F_\xi \end{pmatrix} \tag{3.153}$$

The gradient vector $\nabla_{\mathbf{p}}$ in the reduced coordinates system (p, ξ) in given by (A.277)

$$\nabla_{\mathbf{p}} = \begin{pmatrix} \nabla_p \\ \nabla_\xi \end{pmatrix} \tag{3.154}$$

with

$$\nabla_p = \frac{\partial}{\partial p} \tag{3.155}$$

$$\nabla_\xi = -\frac{\sqrt{1 - \xi^2}}{p} \frac{\partial}{\partial \xi} \tag{3.156}$$

so that

$$S_p = -D_{pp}\frac{\partial f}{\partial p} + \frac{\sqrt{1-\xi^2}}{p}D_{p\xi}\frac{\partial f}{\partial \xi} + F_p f \tag{3.157}$$

and

$$S_\xi = -D_{\xi p}\frac{\partial f}{\partial p} + \frac{\sqrt{1-\xi^2}}{p}D_{\xi\xi}\frac{\partial f}{\partial \xi} + F_\xi f \tag{3.158}$$

Bounce-averaged operator The bounce averaged operator is

$$\{\nabla_{\mathbf{p}}\cdot\mathbf{S}_{\mathbf{p}}\} = \left\{\frac{1}{p^2}\frac{\partial}{\partial p}\left(p^2 S_p\right)\right\} - \left\{\frac{1}{p}\frac{\partial}{\partial \xi}\left(\sqrt{1-\xi^2}S_\xi\right)\right\} \tag{3.159}$$

where the bounce averaging operation is defined in (2.62)

$$\{\mathcal{A}\} = \frac{1}{\lambda\widetilde{q}}\left[\frac{1}{2}\sum_\sigma\right]_T \int_{\theta_{\min}}^{\theta_{\max}} \frac{d\theta}{2\pi}\frac{1}{\left|\widehat{\psi}\cdot\widehat{r}\right|}\frac{r}{R_p}\frac{B}{B_P}\frac{\xi_0}{\xi}\mathcal{A} \tag{3.160}$$

and ξ is given along the trajectory by

$$\xi\left(\psi,\theta,\xi_0\right) = \sigma\sqrt{1-\Psi\left(\psi,\theta\right)\left(1-\xi_0^2\right)} \tag{3.161}$$

with

$$\Psi\left(\psi,\theta\right) = \frac{B\left(\psi,\theta\right)}{B_0\left(\psi\right)} \tag{3.162}$$

as shown in Sec.2.2.1.

We find from (3.161) that in momentum space

$$\xi d\xi = \Psi\xi_0 d\xi_0 \tag{3.163}$$

and we also get

$$\left(1-\xi^2\right) = \Psi\left(1-\xi_0^2\right) \tag{3.164}$$

Then, keeping in mind that $|\xi_0| = \sigma\xi_0$ is independent of σ, we can transform as follows,

$$\begin{aligned}
&\left\{\frac{1}{p}\frac{\partial}{\partial \xi}\left(\sqrt{1-\xi^2}S_\xi\right)\right\} \\
&= \frac{1}{\lambda\widetilde{q}}\left[\frac{1}{2}\sum_\sigma\right]_T \int_{\theta_{\min}}^{\theta_{\max}} \frac{d\theta}{2\pi}\frac{1}{\left|\widehat{\psi}\cdot\widehat{r}\right|}\frac{r}{R_p}\frac{B}{B_P}\frac{\xi_0}{\xi}\frac{1}{p}\frac{\partial}{\partial \xi}\left(\sqrt{1-\xi^2}S_\xi\right) \\
&= \frac{1}{\lambda p}\frac{\partial}{\partial \sigma\xi_0}\frac{1}{\widetilde{q}}\left[\frac{1}{2}\sum_\sigma\right]_T \int_{\theta_{\min}}^{\theta_{\max}} \frac{d\theta}{2\pi}\frac{1}{\left|\widehat{\psi}\cdot\widehat{r}\right|}\frac{r}{R_p}\frac{B}{B_P}\frac{\sigma}{\Psi}\left(\sqrt{1-\xi^2}S_\xi\right) \\
&= \frac{1}{\lambda p}\frac{\partial}{\partial \xi_0}\sqrt{1-\xi_0^2}\sigma\frac{1}{\widetilde{q}}\left[\frac{1}{2}\sum_\sigma\right]_T \int_{\theta_{\min}}^{\theta_{\max}} \frac{d\theta}{2\pi}\frac{1}{\left|\widehat{\psi}\cdot\widehat{r}\right|}\frac{r}{R_p}\frac{B}{B_P}\frac{\sigma}{\sqrt{\Psi}}\left(S_\xi\right) \\
&= \frac{1}{\lambda p}\frac{\partial}{\partial \xi_0}\sqrt{1-\xi_0^2}\lambda\sigma\left\{\frac{\sigma\xi}{\sqrt{\Psi}\xi_0}S_\xi\right\}
\end{aligned} \tag{3.165}$$

using relation $\xi d\xi = \Psi \xi_0 d\xi_0$ that is deduced from expression (3.161).

Finally, we can rewrite the equation (3.159) in a conservative form as

$$\{\nabla_{\mathbf{p}} \cdot \mathbf{S}_{\mathbf{p}}\} = \frac{1}{p^2}\frac{\partial}{\partial p}\left(p^2 S_p^{(0)}\right) - \frac{1}{\lambda p}\frac{\partial}{\partial \xi_0}\left(\sqrt{1-\xi_0^2}\lambda S_{\xi_0}^{(0)}\right) \tag{3.166}$$

where the following components are defined

$$S_p^{(0)} = \{S_p\} \tag{3.167}$$

and

$$S_{\xi_0}^{(0)} = \sigma\left\{\frac{\sigma\xi}{\sqrt{\Psi}\xi_0} S_\xi\right\} \tag{3.168}$$

Here, expression (3.166) is completely equivalent to the momentum transport equation deduced from particle conservation. However, this equivalence may be used only because the bounce-averaged operator is local, and does not depends of ψ.

3.5.3 Dynamics in Configuration Space

Configuration space operator The operator that describes the spatial transport is given by relation

$$\left.\frac{\partial f_0^{(0)}}{\partial t}\right|_{\mathbf{r}} = \frac{B_0(\psi)}{\lambda(\psi,\xi_0)\,\widetilde{q}(\psi)}\frac{\partial}{\partial\psi}\left(\frac{\widetilde{q}(\psi)}{B_0(\psi)}\lambda(\psi,\xi_0)\left|\nabla\psi\right|_0 \mathbf{S}_\psi^{(0)}\right) \tag{3.169}$$

and since $B_P = |\nabla\psi|/R$, it may be rewritten in the form

$$\left.\frac{\partial f_0^{(0)}}{\partial t}\right|_{\mathbf{r}} = \frac{B_0(\psi)}{\lambda(\psi,\xi_0)\,\widetilde{q}(\psi)}\frac{\partial}{\partial\psi}\left(R_0(\psi)\,\widetilde{q}(\psi)\,\frac{B_{P0}(\psi)}{B_0(\psi)}\lambda(\psi,\xi_0)\,\mathbf{S}_\psi^{(0)}\right) \tag{3.170}$$

where R_0 and B_{P0} are taken at the poloidal location where the magnetic field is minimum $B = B_0$. Much in the same way,

$$\begin{aligned}
\mathbf{S}_\psi^{(0)} &= -D_{\psi\psi}^{(0)}\nabla_\psi f_0^{(0)} + F_\psi^{(0)} f_0^{(0)} \\
&= -D_{\psi\psi}^{(0)}\left|\nabla\psi\right|_0 \frac{\partial f_0^{(0)}}{\partial\psi} + F_\psi^{(0)} f_0^{(0)} \\
&= -D_{\psi\psi}^{(0)} R_0(\psi)\, B_{P0}(\psi)\,\frac{\partial f_0^{(0)}}{\partial\psi} + F_\psi^{(0)} f_0^{(0)}
\end{aligned} \tag{3.171}$$

where the diffusion cross-terms $D_{p\psi}^{(0)}$, $D_{\psi p}^{(0)}, D_{\xi\psi}^{(0)}$ and $D_{\psi\xi}^{(0)}$ between momentum and configuration spaces have been neglected.

Case of circular concentric flux-surfaces In that case, $\widehat{\psi} = \widehat{r}$, and by definition $D^{(0)}_{\psi\psi} = D^{(0)}_{rr}$, $F^{(0)}_{\psi} = F^{(0)}_{r}$, since ψ is here just a label. Therefore, using relation $|\nabla\psi|_0 \, \partial/\partial\psi = \partial/\partial r$,

$$\begin{aligned}
\mathbf{S}^{(0)}_{\psi} &= -D^{(0)}_{\psi\psi}\nabla_{\psi} f^{(0)}_0 + F^{(0)}_{\psi} f^{(0)}_0 \\
&= -D^{(0)}_{\psi\psi}\,|\nabla\psi|_0 \frac{\partial f^{(0)}_0}{\partial\psi} + F^{(0)}_{\psi} f^{(0)}_0 \\
&= -D^{(0)}_{rr}\frac{\partial f^{(0)}_0}{\partial r} + F^{(0)}_{r} f^{(0)}_0 \\
&= \mathbf{S}^{(0)}_{r}
\end{aligned} \tag{3.172}$$

Furthermore, since

$$\widetilde{q}\,(r) = \frac{r}{R_p}\frac{B_0}{B_{P0}} \tag{3.173}$$

one obtains,

$$\begin{aligned}
\left.\frac{\partial f^{(0)}_0}{\partial t}\right|^{circ.}_{\mathbf{r}} &= \frac{R_p B_{P0}}{\lambda\,(r,\xi_0)\,r}\frac{\partial}{\partial\psi}\left(\frac{R_0}{R_p} r\lambda\,(r,\xi_0)\,\mathbf{S}^{(0)}_{r}\right) \\
&= \frac{|\nabla\psi|_0}{\lambda\,(r,\xi_0)\,R_0 r}\frac{\partial}{\partial\psi}\left(R_0 r\lambda\,(r,\xi_0)\,\mathbf{S}^{(0)}_{r}\right) \\
&= \frac{1}{\lambda\,(r,\xi_0)\,R_0 r}\frac{\partial}{\partial r}\left(R_0 r\lambda\,(r,\xi_0)\,\mathbf{S}^{(0)}_{r}\right)
\end{aligned} \tag{3.174}$$

Note that R_0 may not be here simplified, since it is a function of r, which corresponds to the toroidal configuration. Dynamics in momentum and configuration spaces are also not decoupled, the normalized bounce time $\lambda\,(r,\xi_0)$ being on both sides of the radial derivative. Only for strongly circulating electrons,

$$\lim_{|\xi_0|\to 1}\left.\frac{\partial f^{(0)}_0}{\partial t}\right|^{circ.}_{\mathbf{r}} = \frac{1}{rR_0}\frac{\partial}{\partial r}\left(rR_0\mathbf{S}^{(0)}_{r}\right) \tag{3.175}$$

since $\lim_{|\xi_0|\to 1}\lambda\,(r,\xi_0) = 1$, and the usual cylindrical conservative expression of the radial transport

$$\lim_{|\xi_0|\to 1}\left.\frac{\partial f^{(0)}_0}{\partial t}\right|^{circ.}_{\mathbf{r}} = \frac{1}{r}\frac{\partial}{\partial r}\left(r\mathbf{S}^{(0)}_{r}\right) \tag{3.176}$$

is only found in the case $\epsilon \ll 1$, i.e. when $R_0 \approx R_p$.

3.5.4 Bounce-averaged flux calculation

Zero order term: the Fokker-Planck equation

The bounce averaged Fokker-Planck equation is is given in the conservative form by relation (3.166), with the bounce-averaged fluxes (3.167) and (3.168)

$$S_p^{(0)} = \{S_p\} \tag{3.177}$$

$$S_{\xi_0}^{(0)} = \sigma \left\{ \frac{\sigma\xi}{\sqrt{\Psi}\xi_0} S_\xi \right\} \tag{3.178}$$

Because f_0 is constant along a magnetic field line, we have $f_0(p,\xi) = f_0^{(0)}(p,\xi_0)$ which is independent of θ and σ. Using the following identities

$$-\left\{ D_{pp} \frac{\partial f_0}{\partial p} \right\} = -\{D_{pp}\} \frac{\partial f_0^{(0)}}{\partial p} \tag{3.179}$$

$$\left\{ D_{p\xi} \frac{\sqrt{1-\xi^2}}{p} \frac{\partial f_0}{\partial \xi} \right\} = \frac{\sqrt{1-\xi_0^2}}{p} \left\{ \frac{\sigma\xi}{\sqrt{\Psi}\xi_0} D_{p\xi} \right\} \frac{\partial f_0^{(0)}}{\sigma \partial \xi_0} \tag{3.180}$$

$$\{F_p f_0\} = \{F_p\} f_0^{(0)} \tag{3.181}$$

$$-\sigma \left\{ \frac{\sigma\xi}{\sqrt{\Psi}\xi_0} D_{\xi p} \frac{\partial f_0}{\partial p} \right\} = -\sigma \left\{ \frac{\sigma\xi}{\sqrt{\Psi}\xi_0} D_{\xi p} \right\} \frac{\partial f_0^{(0)}}{\partial p} \tag{3.182}$$

$$\sigma \left\{ \frac{\sigma\xi}{\sqrt{\Psi}\xi_0} D_{\xi\xi} \frac{\sqrt{1-\xi^2}}{p} \frac{\partial f_0}{\partial \xi} \right\} = \frac{\sqrt{1-\xi_0^2}}{p} \sigma \left\{ \frac{\xi^2}{\Psi\xi_0^2} D_{\xi\xi} \right\} \frac{\partial f_0^{(0)}}{\sigma \partial \xi_0} \tag{3.183}$$

$$\sigma \left\{ \frac{\sigma\xi}{\sqrt{\Psi}\xi_0} F_\xi f_0 \right\} = \sigma \left\{ \frac{\sigma\xi}{\sqrt{\Psi}\xi_0} F_\xi \right\} f_0^{(0)} \tag{3.184}$$

we can rewrite

$$\mathbf{S}_{\mathbf{p}}^{(0)} = -\mathbb{D}_{\mathbf{p}}^{(\not\leftarrow)} \cdot \nabla_{\shortmid,\xi\not\leftarrow} \mho_{\not\leftarrow}^{(\not\leftarrow)} + \mathbf{F}_{\mathbf{p}}^{(\not\leftarrow)} \mho_{\not\leftarrow}^{(\not\leftarrow)} \tag{3.185}$$

where the bounce averaged flux is decomposed into

$$\mathbf{S}_{\mathbf{p}}^{(0)} = \begin{pmatrix} S_p^{(0)} \\ S_{\xi_0}^{(0)} \end{pmatrix} \tag{3.186}$$

with

$$S_p^{(0)} = -D_{pp}^{(0)} \frac{\partial f_0^{(0)}}{\partial p} + \frac{\sqrt{1-\xi_0^2}}{p} D_{p\xi}^{(0)} \frac{\partial f_0^{(0)}}{\partial \xi_0} + F_p^{(0)} f_0^{(0)} \tag{3.187}$$

$$S_{\xi_0}^{(0)} = -D_{\xi p}^{(0)} \frac{\partial f_0^{(0)}}{\partial p} + \frac{\sqrt{1-\xi_0^2}}{p} D_{\xi\xi}^{(0)} \frac{\partial f_0^{(0)}}{\partial \xi_0} + F_\xi^{(0)} f_0^{(0)} \tag{3.188}$$

by defining the diffusion components

$$D_{pp}^{(0)} = \{D_{pp}\} \tag{3.189}$$

$$D_{p\xi}^{(0)} = \sigma \left\{ \frac{\sigma\xi}{\sqrt{\Psi}\xi_0} D_{p\xi} \right\} \tag{3.190}$$

$$D_{\xi p}^{(0)} = \sigma \left\{ \frac{\sigma\xi}{\sqrt{\Psi}\xi_0} D_{\xi p} \right\} \tag{3.191}$$

$$D_{\xi\xi}^{(0)} = \left\{ \frac{\xi^2}{\Psi\xi_0^2} D_{\xi\xi} \right\} \tag{3.192}$$

and the convection components

$$F_{p}^{(0)} = \{F_{p}\} \tag{3.193}$$

$$F_{\xi}^{(0)} = \sigma \left\{ \frac{\sigma\xi}{\sqrt{\Psi}\xi_0} F_{\xi} \right\} \tag{3.194}$$

where the gradient vector in the reduced (p, ξ_0) momentum space is

$$\nabla_{p,\xi_0} = \begin{pmatrix} \nabla_p \\ \nabla_{\xi_0} \end{pmatrix} \tag{3.195}$$

with

$$\nabla_p = \frac{\partial}{\partial p} \tag{3.196}$$

$$\nabla_{\xi_0} = \frac{-\sqrt{1-\xi_0^2}}{p} \frac{\partial}{\partial \xi_0} \tag{3.197}$$

3.5.5 Up to first order term: the Drift Kinetic equation

In the first-order drift kinetic equation, the momentum space operator

$$\nabla_{\mathbf{p}} \cdot \mathbf{S}_{\mathbf{p}} (f_1) \tag{3.198}$$

where the fluxes are expressed as (3.151) may be decomposed as

$$\nabla_{\mathbf{p}} \cdot \mathbf{S}_{\mathbf{p}} (f_1) = \nabla_{\mathbf{p}} \cdot \mathbf{S}_{\mathbf{p}} \left(\widetilde{f} \right) + \nabla_{\mathbf{p}} \cdot \mathbf{S}_{\mathbf{p}} (g) \tag{3.199}$$

According to (3.166), we can express the bounce-averaged operator as

$$\left\{ J_{\mathbf{p}} \nabla_{\mathbf{p}} \cdot \mathbf{S}_{\mathbf{p}} \left(\widetilde{f} \right) \right\} = \frac{\partial}{\partial p} \left(p^2 \widetilde{S}_p^{(0)} \right) - \frac{p}{\lambda} \frac{\partial}{\partial \xi_0} \left(\sqrt{1-\xi_0^2} \lambda \widetilde{S}_{\xi_0}^{(0)} \right) \tag{3.200}$$

$$\{ J_{\mathbf{p}} \nabla_{\mathbf{p}} \cdot \mathbf{S}_{\mathbf{p}} (g) \} = \frac{\partial}{\partial p} \left(p^2 S_p^{(0)} \right) - \frac{p}{\lambda} \frac{\partial}{\partial \xi_0} \left(\sqrt{1-\xi_0^2} \lambda S_{\xi_0}^{(0)} \right) \tag{3.201}$$

where we need to evaluate the bounce-averaged fluxes (3.167) and (3.168) for $\widetilde{f}$ and g respectively

$$\widetilde{S}_p^{(0)} = \left\{ S_p \left(\widetilde{f} \right) \right\} \tag{3.202}$$

$$\widetilde{S}_{\xi_0}^{(0)} = \sigma \left\{ \frac{\sigma \xi}{\sqrt{\Psi} \xi_0} S_\xi \left(\widetilde{f} \right) \right\} \tag{3.203}$$

and

$$S_p^{(0)} = \{ S_p (g) \} \tag{3.204}$$

$$S_{\xi_0}^{(0)} = \sigma \left\{ \frac{\sigma \xi}{\sqrt{\Psi} \xi_0} S_\xi (g) \right\} \tag{3.205}$$

Because g is constant along a field line, we have $g(p, \xi) = g^{(0)}(p, \xi_0)$which is independent of θ and σ. Therefore, the fluxes for g have exactly the same expression as for f_0 in the zero-order equation described in section. This is why the same notation in (3.201) is used, while the fluxes associated with $\widetilde{f}$ are noted $\widetilde{S}$.

Indeed, $\widetilde{f}$ has an explicit dependence upon θ, which can be isolated as follows:

$$\widetilde{f}(\psi, \theta, p, \xi) = \frac{\xi(\psi, \theta, \xi_0)}{\Psi(\psi, \theta) \xi_0} \widetilde{f}^{(0)}(\psi, p, \xi_0) \tag{3.206}$$

with

$$\widetilde{f}^{(0)}(\psi, p, \xi_0) = \frac{p \xi_0 I(\psi)}{q_e B_0(\psi)} \frac{\partial f_0^{(0)}(\psi, p, \xi_0)}{\partial \psi} \tag{3.207}$$

We can note that $\widetilde{f}^{(0)}$ is antisymmetric in the trapped region, since $f_0^{(0)}$ is symmetric and ξ_0 is, of course, antisymmetric. As a result, only $\sigma \widetilde{f}^{(0)}$ can be taken out of the bounce

averaging operator. Taking the bounce-average of each term, we find

$$\left\{-D_{pp}\frac{\partial\widetilde{f}}{\partial p}\right\} = -\sigma\left\{\sigma\frac{\xi}{\Psi\xi_0}D_{pp}\right\}\frac{\partial\widetilde{f}^{(0)}}{\partial p} \tag{3.208}$$

$$\left\{D_{p\xi}\frac{\sqrt{1-\xi^2}}{p}\frac{\partial\widetilde{f}}{\partial\xi}\right\} = \frac{\sqrt{1-\xi_0^2}}{p}\left\{\frac{\xi^2}{\Psi^{3/2}\xi_0^2}D_{p\xi}\right\}\frac{\partial\widetilde{f}^{(0)}}{\partial\xi_0} + \frac{\sqrt{1-\xi_0^2}}{p}\sigma\left\{\sigma\frac{\Psi-1}{\Psi^{3/2}\xi_0^3}D_{p\xi}\right\}\widetilde{f}^{(0)} \tag{3.209}$$

$$\left\{F_p\widetilde{f}\right\} = \sigma\left\{\sigma\frac{\xi}{\Psi\xi_0}F_p\right\}\widetilde{f}^{(0)} \tag{3.210}$$

$$-\sigma\left\{\frac{\sigma\xi}{\sqrt{\Psi}\xi_0}D_{\xi p}\frac{\partial\widetilde{f}}{\partial p}\right\} = -\left\{\frac{\xi^2}{\Psi^{3/2}\xi_0^2}D_{\xi p}\right\}\frac{\partial\widetilde{f}^{(0)}}{\partial p} \tag{3.211}$$

$$\sigma\left\{\frac{\sigma\xi}{\sqrt{\Psi}\xi_0}D_{\xi\xi}\frac{\sqrt{1-\xi^2}}{p}\frac{\partial\widetilde{f}}{\partial\xi}\right\} = \frac{\sqrt{1-\xi_0^2}}{p}\sigma\left\{\frac{\sigma\xi^3}{\Psi^2\xi_0^3}D_{\xi\xi}\right\}\frac{\partial\widetilde{f}^{(0)}}{\partial\xi_0} + \frac{\sqrt{1-\xi_0^2}}{p}\left\{\frac{\xi\left(\Psi-1\right)}{\Psi^2\xi_0^4}D_{\xi\xi}\right\}\widetilde{f}^{(0)} \tag{3.212}$$

$$\sigma\left\{\frac{\sigma\xi}{\sqrt{\Psi}\xi_0}F_\xi\widetilde{f}\right\} = \left\{\frac{\xi^2}{\Psi^{3/2}\xi_0^2}F_\xi\right\}\widetilde{f}^{(0)} \tag{3.213}$$

where the following relation is used

$$\begin{aligned}\frac{\partial}{\partial\xi_0}\frac{\xi}{\xi_0} &= \sigma\frac{\partial}{\partial\left|\xi_0\right|}\frac{\sqrt{1-\Psi\left(1-\left|\xi_0\right|^2\right)}}{\left|\xi_0\right|}\\ &= \sigma\frac{\Psi\xi_0^2-\xi^2}{\left|\xi\right|\xi_0^2}\\ &= \sigma\frac{\Psi-1}{\left|\xi\right|\xi_0^2}\end{aligned} \tag{3.214}$$

We can therefore rewrite

$$\widetilde{\mathbf{S}}_{\mathbf{p}}^{(0)}\left(\widetilde{f}^{(0)}\right) = -\widetilde{\mathbb{D}}_{\mathbf{p}}^{(0)}\cdot\nabla_{p,\xi_0}\widetilde{f}^{(0)} + \widetilde{\mathbf{F}}_{\mathbf{p}}^{(0)}\widetilde{f}^{(0)}$$

where the bounce averaged flux is decomposed into

$$\mathbf{S}_{\mathbf{p}}^{(0)} = \begin{pmatrix} S_p^{(0)} \\ S_{\xi_0}^{(0)} \end{pmatrix} \tag{3.215}$$

with

$$\widetilde{S}_p^{(0)} = -\widetilde{D}_{pp}^{(0)}\frac{\partial\widetilde{f}^{(0)}}{\partial p} + \frac{\sqrt{1-\xi_0^2}}{p}\widetilde{D}_{p\xi}^{(0)}\frac{\partial\widetilde{f}^{(0)}}{\partial\xi_0} + \widetilde{F}_p^{(0)}\widetilde{f}^{(0)} \tag{3.216}$$

$$\widetilde{S}_{\xi_0}^{(0)} = -\widetilde{D}_{\xi p}^{(0)}\frac{\partial\widetilde{f}^{(0)}}{\partial p} + \frac{\sqrt{1-\xi_0^2}}{p}\widetilde{D}_{\xi\xi}^{(0)}\frac{\partial\widetilde{f}^{(0)}}{\partial\xi_0} + \widetilde{F}_\xi^{(0)}\widetilde{f}^{(0)} \tag{3.217}$$

by defining the diffusion components

$$\widetilde{D}_{pp}^{(0)} = \sigma \left\{ \sigma \frac{\xi}{\Psi \xi_0} D_{pp} \right\} \tag{3.218}$$

$$\widetilde{D}_{p\xi}^{(0)} = \left\{ \frac{\xi^2}{\Psi^{3/2} \xi_0^2} D_{p\xi} \right\} \tag{3.219}$$

$$\widetilde{D}_{\xi p}^{(0)} = \left\{ \frac{\xi^2}{\Psi^{3/2} \xi_0^2} D_{\xi p} \right\} \tag{3.220}$$

$$\widetilde{D}_{\xi\xi}^{(0)} = \sigma \left\{ \frac{\sigma \xi^3}{\Psi^2 \xi_0^3} D_{\xi\xi} \right\} \tag{3.221}$$

and the convection components

$$\widetilde{F}_{p}^{(0)} = \sigma \left\{ \sigma \frac{\xi}{\Psi \xi_0} F_p \right\} + \frac{\sqrt{1-\xi_0^2}}{p \xi_0^3} \left\{ \frac{(\Psi - 1)}{\Psi^{3/2}} D_{p\xi} \right\} \tag{3.222}$$

$$\widetilde{F}_{\xi}^{(0)} = \left\{ \frac{\xi^2}{\Psi^{3/2} \xi_0^2} F_\xi \right\} + \frac{\sqrt{1-\xi_0^2}}{p \xi_0^3} \sigma \left\{ \frac{\sigma \xi \left(\Psi - 1\right)}{\xi_0 \Psi^2} D_{\xi\xi} \right\} \tag{3.223}$$

where we use the fact that $\sigma \xi_0^3$ may be taken out of the bounce averaged operator, since ξ_0^3 is an odd function of ξ_0. The gradient vector in the reduced (p, ξ_0) momentum space is

$$\nabla_{p,\xi_0} = \begin{pmatrix} \nabla_p \\ \nabla_{\xi_0} \end{pmatrix} \tag{3.224}$$

with

$$\nabla_p = \frac{\partial}{\partial p} \tag{3.225}$$

$$\nabla_{\xi_0} = \frac{-\sqrt{1-\xi_0^2}}{p} \frac{\partial}{\partial \xi_0} \tag{3.226}$$

3.6 Moments of the distribution function

3.6.1 Flux-surface Averaging

Surface densities

We consider the flux-surface averaging of a surface quantity, such as a flux of a current, generally noted $\mathbf{\Gamma}\left(\psi, \theta\right)$. It is defined as the averaged flux of $\mathbf{\Gamma}$ through the infinitesimal poloidal surface $dS\left(\psi\right)$

$$\left\langle \Gamma \right\rangle_S \left(\psi\right) = \frac{\int_{dS(\psi)} \mathbf{dS} \cdot \mathbf{\Gamma}\left(\psi, \theta\right)}{\int_{dS(\psi)} dS} \tag{3.227}$$

In the (ψ, θ, ϕ) system, the differential poloidal surface element is given by (A.201) as introduced in Appendix A

$$\mathbf{dS} = \frac{r}{\left|\nabla \psi\right| \left|\widehat{\psi} \cdot \widehat{r}\right|} d\psi d\theta \widehat{\phi} \tag{3.228}$$

so that the infinitesimal poloidal surface element $dS_p(\psi)$ is

$$\int_{dS_p(\psi)} dS = \int_{dS_p(\psi)} \frac{r}{|\nabla\psi| \left|\widehat{\psi}\cdot\widehat{r}\right|} d\psi d\theta = d\psi \int_0^{2\pi} d\theta \frac{r}{|\nabla\psi| \left|\widehat{\psi}\cdot\widehat{r}\right|} \tag{3.229}$$

and the flux-surface averaged flux in the toroidal direction is

$$\langle\Gamma\rangle_\phi(\psi) = \left(\frac{dS_p}{d\psi}\right)^{-1} \int_0^{2\pi} d\theta \frac{r}{|\nabla\psi| \left|\widehat{\psi}\cdot\widehat{r}\right|} \left[\widehat{\phi}\cdot\mathbf{\Gamma}(\psi,\theta)\right] \tag{3.230}$$

with

$$\frac{dS_p(\psi)}{d\psi} = \int_0^{2\pi} d\theta \frac{r}{|\nabla\psi| \left|\widehat{\psi}\cdot\widehat{r}\right|} \tag{3.231}$$

$$= \int_0^{2\pi} d\theta \frac{1}{\left|\widehat{\psi}\cdot\widehat{r}\right|} \frac{r}{R} \frac{1}{B_P} \tag{3.232}$$

Defining the new pseudo saftey factor $\overline{q}$ as

$$\overline{q}(\psi) \equiv \int_0^{2\pi} \frac{d\theta}{2\pi} \frac{1}{\left|\widehat{\psi}\cdot\widehat{r}\right|} \frac{r}{R} \frac{B_0(\psi)}{B_P} \tag{3.233}$$

we get

$$\frac{dS_p(\psi)}{d\psi} = \frac{2\pi\overline{q}(\psi)}{B_0(\psi)} \tag{3.234}$$

and

$$\langle\Gamma\rangle_\phi(\psi) = \frac{1}{\overline{q}(\psi)} \int_0^{2\pi} \frac{d\theta}{2\pi} \frac{1}{\left|\widehat{\psi}\cdot\widehat{r}\right|} \frac{r}{R} \frac{B_0(\psi)}{B_P} \left[\widehat{\phi}\cdot\mathbf{\Gamma}(\psi,\theta)\right] \tag{3.235}$$

Volume densities

We consider the flux-surface averaging of a volume quantity, such as a power density, generally noted $\mathbf{\Phi}(\psi,\theta)$. It is defined as the average value of $\mathbf{\Phi}$ within the infinitesimal volume $dV(\psi)$

$$\langle\mathbf{\Phi}\rangle_V(\psi) = \frac{\iint_{dV(\psi)} \mathbf{\Phi}(\psi,\theta)\, dV}{\iint_{dV(\psi)} dV} \tag{3.236}$$

In the (ψ,θ,ϕ) system, the differential volume element is given by (A.202) as introduced in Appendix A

$$dV = \frac{Rr}{|\nabla\psi| \left|\widehat{\psi}\cdot\widehat{r}\right|} d\psi d\theta d\phi \tag{3.237}$$

so that the infinitesimal volume element $dV(\psi)$ of a flux-surface is

$$\iint_{dV(\psi)} dV = \iint_{dV(\psi)} \frac{Rr}{|\nabla\psi| \left|\widehat{\psi}\cdot\widehat{r}\right|} d\psi d\theta d\phi = d\psi \int_0^{2\pi} d\theta \int_0^{2\pi} d\phi \frac{Rr}{|\nabla\psi| \left|\widehat{\psi}\cdot\widehat{r}\right|} \tag{3.238}$$

and the flux-surface averaged quantity in the toroidal direction is

$$\langle \mathbf{\Phi} \rangle_V (\psi) = \left(\frac{dV}{d\psi} \right)^{-1} \int_0^{2\pi} d\theta \int_0^{2\pi} d\phi \frac{Rr}{|\nabla \psi| \left| \widehat{\psi} \cdot \widehat{r} \right|} \mathbf{\Phi} (\psi, \theta) \tag{3.239}$$

with

$$\frac{dV(\psi)}{d\psi} = \int_0^{2\pi} d\theta \int_0^{2\pi} d\phi \frac{Rr}{|\nabla \psi| \left| \widehat{\psi} \cdot \widehat{r} \right|} \tag{3.240}$$

$$= \int_0^{2\pi} d\theta \int_0^{2\pi} d\phi \frac{r}{\left| \widehat{\psi} \cdot \widehat{r} \right|} \frac{1}{B_P} \tag{3.241}$$

Under the assumption of axisymmetry, we get

$$\frac{dV(\psi)}{d\psi} = 4\pi^2 \int_0^{2\pi} \frac{d\theta}{2\pi} \frac{r}{\left| \widehat{\psi} \cdot \widehat{r} \right|} \frac{1}{B_P} \tag{3.242}$$

$$= \frac{4\pi^2 R_0}{B_0(\psi)} \int_0^{2\pi} \frac{d\theta}{2\pi} \frac{1}{\left| \widehat{\psi} \cdot \widehat{r} \right|} \frac{r}{R_p} \frac{B_0(\psi)}{B_P} \tag{3.243}$$

Defining the new pseudo saftey factor $\widehat{q}$ as

$$\widehat{q}(\psi) \equiv \int_0^{2\pi} \frac{d\theta}{2\pi} \frac{1}{\left| \widehat{\psi} \cdot \widehat{r} \right|} \frac{r}{R_p} \frac{B_0(\psi)}{B_P} \tag{3.244}$$

we get

$$\frac{dV(\psi)}{d\psi} = \frac{4\pi^2 R_p \widehat{q}(\psi)}{B_0(\psi)} \tag{3.245}$$

and finally

$$\langle \mathbf{\Phi} \rangle_V (\psi) = \frac{1}{\widehat{q}(\psi)} \int_0^{2\pi} \frac{d\theta}{2\pi} \frac{1}{\left| \widehat{\psi} \cdot \widehat{r} \right|} \frac{r}{R_p} \frac{B_0(\psi)}{B_P} \mathbf{\Phi} (\psi, \theta) \tag{3.246}$$

3.6.2 Density

Definition

The electron density $n_e(\psi, \theta)$ is given by the relation

$$n_e(\psi, \theta) = 2\pi \int_{-1}^{+1} d\xi \int_0^{\infty} p^2 dp \; f(p, \xi, \psi, \theta) \tag{3.247}$$

Using the general expression (3.246) of the flux-surface averaging of a volumic quantity

$$\begin{aligned}\langle n_e\rangle_V(\psi) &= \frac{1}{\widehat{q}}\int_0^{2\pi}\frac{d\theta}{2\pi}\frac{1}{\left|\widehat{\psi}\,.\,\widehat{r}\right|}\frac{r}{R_p}\frac{B_0}{B_P}n_e(\psi,\theta)\\ &= \frac{2\pi}{\widehat{q}}\int_0^{\infty}p^2dp\int_0^{2\pi}\frac{d\theta}{2\pi}\frac{1}{\left|\widehat{\psi}\,.\,\widehat{r}\right|}\frac{r}{R_p}\frac{B_0}{B_P}\int_{-1}^{+1}d\xi\; f(\psi,\theta,p,\xi)\\ &= \frac{2\pi}{\widehat{q}}\int_0^{\infty}p^2dp\int_0^{2\pi}\frac{d\theta}{2\pi}\frac{1}{\left|\widehat{\psi}\,.\,\widehat{r}\right|}\frac{r}{R_p}\frac{B_0}{B_P}\int_{-1}^{+1}\left[\frac{1}{2}\sum_{\sigma=\pm1}\right]_T d\xi\; f(\psi,\theta,p,\xi)\end{aligned} \tag{3.248}$$

where the trapping condition evaluated at the location θ is given by

$$|\xi| < \xi_T = \sqrt{1-\frac{B(\psi,\theta)}{B_0(\psi)}} \tag{3.249}$$

Using $\xi d\xi = \Psi\xi_0 d\xi_0$ with the condition (3.270) on ξ_0

$$|\xi_0| \geq \sqrt{1-\frac{1}{\Psi(\psi,\theta)}} \tag{3.250}$$

one get

$$\int_{-1}^{+1}\left[\frac{1}{2}\sum_{\sigma=\pm1}\right]_T d\xi = \int_{-1}^{+1}\left[\frac{1}{2}\sum_{\sigma=\pm1}\right]_T \Psi(\psi,\theta)\frac{\xi_0}{\xi}H\left(|\xi_0|-\sqrt{1-\frac{1}{\Psi(\psi,\theta)}}\right)d\xi_0 \tag{3.251}$$

where H is the usual Heaviside function which is defined as $H(x)=1$ for $x>0$, and $H(x)=0$ elsewhere.

Note that the condition (3.250) is equivalent to

$$\theta_{\min}(\psi,\xi_0) \leq \theta \leq \theta_{\max}(\psi,\xi_0) \tag{3.252}$$

so that, the integrals over θ and ξ_0 may be permuted,

$$\begin{aligned}\langle n_e\rangle_V(\psi) = \frac{2\pi}{\widehat{q}}\int_0^{\infty}p^2dp\int_{-1}^{+1}d\xi_0\times\\ \left[\frac{1}{2}\sum_{\sigma=\pm1}\right]_T\int_{\theta_{\min}}^{\theta_{\max}}\frac{d\theta}{2\pi}\frac{1}{\left|\widehat{\psi}\,.\,\widehat{r}\right|}\frac{r}{R_p}\frac{B}{B_P}\frac{\xi_0}{\xi}f(\psi,\theta,p,\xi_0)\end{aligned} \tag{3.253}$$

where the bounce-averaging of the distribution appears naturally. Therefore, expression (3.371) can be rewriten in the simple form

$$\langle n_e\rangle_V(\psi) = 2\pi\frac{\widetilde{q}}{\widehat{q}}\int_0^{\infty}p^2dp\int_{-1}^{+1}d\xi_0\lambda\left\{f(\psi,\theta,p,\xi_0)\right\} \tag{3.254}$$

Fokker-Planck Equation

For the zero order distribution function, since f_0 is constant along a field line,

$$f_0\left(\psi,\theta,p,\xi\right)=f_0^{(0)}\left(\psi,p,\xi_0\right) \tag{3.255}$$

one obtains

$$\langle n_e\rangle_V^0\left(\psi\right)=2\pi\frac{\widetilde{q}}{\widehat{q}}\int_0^\infty p^2dp\int_{-1}^{+1}d\xi_0\lambda f_0^{(0)}\left(\psi,p,\xi_0\right) \tag{3.256}$$

Drift Kinetic Equation

When we consider the first order distribution function, we have $f_1=\widetilde{f}+g$, where g is constant along a field line, and therefore its contribution $\langle n_e\rangle_V^1\left(\psi\right)$ has the same expression as for f_0. However, $\widetilde{f}$ has an explicit dependence upon θ, which is given by (3.206)

$$\widetilde{f}(\psi,\theta,p,\xi)=\frac{\xi(\psi,\theta,\xi_0)}{\Psi(\psi,\theta)\xi_0}\widetilde{f}^{(0)}(\psi,p,\xi_0) \tag{3.257}$$

Therefore, the flux-surface averaged density contribution of $\widetilde{f}$ is

$$\langle\widetilde{n}_e\rangle_V^1\left(\psi\right)=2\pi\frac{\widetilde{q}}{\widehat{q}}\int_0^\infty p^2dp\int_{-1}^{+1}d\xi_0\lambda\left\{\frac{\xi}{\Psi(\psi,\theta)\xi_0}\right\}\widetilde{f}^{(0)}(\psi,p,\xi_0) \tag{3.258}$$

$$=2\pi\frac{\widetilde{q}}{\widehat{q}}\int_0^\infty p^2dp\int_{-1}^{+1}d\xi_0\overline{\lambda}_{1,-1,0}\widetilde{f}^{(0)}(\psi,p,\xi_0) \tag{3.259}$$

where

$$\overline{\lambda}_{1,-1,0}=\sigma\left\{\sigma\frac{\xi}{\Psi(\psi,\theta)\xi_0}\right\}\lambda \tag{3.260}$$

according to the notation in Sec. 2.2.1, since $\widetilde{f}^{(0)}$ is antisymmetric in the trapped region.

Since $\widetilde{f}^{(0)}$ and g have no definite symmetry properties, both can contribute to the density and

$$\langle n_e\rangle_V\left(\psi\right)=\langle n_e\rangle_V^0\left(\psi\right)+\langle n_e\rangle_V^1\left(\psi\right)+\langle\widetilde{n}_e\rangle_V^1\left(\psi\right) \tag{3.261}$$

3.6.3 Current Density

Definition

The density of current carried by electrons is given by

$$\mathbf{J}\left(\mathbf{x}\right)=q_e\iiint d^3p\,\mathbf{v}f\left(\mathbf{x},\mathbf{p}\right) \tag{3.262}$$

so that the parallel current density is

$$J_\parallel\left(\mathbf{x}\right)=q_e\iiint d^3p\,v_\parallel f\left(\mathbf{x},\mathbf{p}\right) \tag{3.263}$$

which becomes in (ψ,θ,p,ξ) phase space

$$J_\parallel\left(\psi,\theta\right)=2\pi q_e\int_0^\infty p^2dp\int_{-1}^{1}d\xi\,\frac{p\xi}{\gamma m}f\left(\psi,\theta,p,\xi\right) \tag{3.264}$$

Flux-Surface Averaging

We are usually interested in the flux-surface averaged current density in the toroidal direction. It is generally given by (3.230)

$$\begin{aligned}\left\langle J_{\parallel}\right\rangle_{\phi}(\psi) &= \frac{1}{\overline{q}}\int_0^{2\pi}\frac{d\theta}{2\pi}\frac{1}{\left|\widehat{\psi}\,.\,\widehat{r}\right|}\frac{r}{R}\frac{B_0}{B_P}J_{\parallel}(\psi,\theta)\left[\widehat{\phi}\cdot\widehat{b}\right] \\ &= \frac{1}{\overline{q}}\int_0^{2\pi}\frac{d\theta}{2\pi}\frac{1}{\left|\widehat{\psi}\,.\,\widehat{r}\right|}\frac{r}{R}\frac{B_0}{B_P}J_{\parallel}(\psi,\theta)\frac{B_T}{B}\end{aligned} \tag{3.265}$$

and finally, using (2.23)

$$\left\langle J_{\parallel}\right\rangle_{\phi}(\psi) = \frac{1}{\overline{q}}\int_0^{2\pi}\frac{d\theta}{2\pi}\frac{1}{\left|\widehat{\psi}\,.\,\widehat{r}\right|}\frac{r}{R}\frac{B_T}{B_P}\frac{J_{\parallel}(\psi,\theta)}{\Psi(\psi,\theta)} \tag{3.266}$$

Fokker-Planck Equation

When we consider only the zero order distribution function, we have that f_0 is constant along a field line, so that

$$f_0(\psi,\theta,p,\xi) = f_0^{(0)}(\psi,p,\xi_0) \tag{3.267}$$

where

$$\xi_0 = \sigma\sqrt{1-\frac{1}{\Psi(\psi,\theta)}\left(1-\xi^2\right)} \tag{3.268}$$

Consequently, we find

$$\begin{aligned}J_{\parallel}^0(\psi,\theta) &= 2\pi q_e\int_0^{\infty}p^2dp\int_{-1}^{1}d\xi\,\frac{p\xi}{\gamma m_e}f_0(\psi,\theta,p,\xi) \\ &= 2\pi q_e\int_0^{\infty}p^2dp\int_{-1}^{1}d\xi\,\frac{p\xi}{\gamma m_e}f_0^{(0)}(\psi,p,\xi_0) \\ &= 2\pi q_e\int_0^{\infty}p^2dp\int_{-1}^{1}d\xi_0\Psi(\psi,\theta)\times \\ &H\left(|\xi_0|-\sqrt{1-\frac{1}{\Psi(\psi,\theta)}}\right)\frac{p\xi_0}{\gamma m_e}f_0^{(0)}(\psi,p,\xi_0)\end{aligned} \tag{3.269}$$

where the condition

$$|\xi_0| \geq \sqrt{1-\frac{1}{\Psi(\psi,\theta)}} \tag{3.270}$$

results from the equation (3.268) and means that only the particle who reach the position θ must be considered. Note that the integrand in the equation (3.269) is odd in ξ_0 for trapped electrons, since $f_0^{(0)}$ is symmetric in the trapped region. As a consequence, the contribution from trapped electrons vanishes, and (3.269) can be rewritten as

$$J_{\parallel}^0(\psi,\theta) = 2\pi q_e\int_0^{\infty}p^2dp\int_{-1}^{1}d\xi_0\Psi(\psi,\theta)\,H\left(|\xi_0|-\xi_{0T}\right)\frac{p\xi_0}{\gamma m_e}f_0^{(0)}(\psi,p,\xi_0) \tag{3.271}$$

Therefore, the flux-surface averaged current density

$$\left\langle J_{\parallel}\right\rangle_{\phi}^{0}(\psi)=\frac{1}{\overline{q}}\int_{0}^{2\pi}\frac{d\theta}{2\pi}\frac{1}{\left|\widehat{\psi}\,.\,\widehat{r}\right|}\frac{r}{R}\frac{B_{T}}{B_{P}}\frac{J_{\parallel}^{0}(\psi,\theta)}{\Psi(\psi,\theta)} \tag{3.272}$$

becomes

$$\begin{aligned}\left\langle J_{\parallel}\right\rangle_{\phi}^{0}(\psi)=\frac{2\pi q_{e}}{m_{e}}\int_{0}^{\infty}dp\,\frac{p^{3}}{\gamma}\frac{1}{\overline{q}}\int_{0}^{2\pi}\frac{d\theta}{2\pi}\frac{1}{\left|\widehat{\psi}\,.\,\widehat{r}\right|}\frac{r}{R}\frac{B_{T}}{B_{P}}\frac{1}{\Psi(\psi,\theta)}\times\\ \int_{-1}^{1}d\xi_{0}\Psi(\psi,\theta)\,H\left(|\xi_{0}|-\xi_{0T}\right)\,\xi_{0}f_{0}^{(0)}(\psi,p,\xi_{0})\end{aligned} \tag{3.273}$$

The integrals over θ and ξ_0 can be permuted

$$\begin{aligned}\left\langle J_{\parallel}\right\rangle_{\phi}^{0}(\psi)=\frac{2\pi q_{e}}{m_{e}}\int_{0}^{\infty}dp\,\frac{p^{3}}{\gamma}\int_{-1}^{1}d\xi_{0}\,H\left(|\xi_{0}|-\xi_{0T}\right)\,\xi_{0}f_{0}^{(0)}(\psi,p,\xi_{0})\times\\ \frac{1}{\overline{q}}\int_{0}^{2\pi}\frac{d\theta}{2\pi}\frac{1}{\left|\widehat{\psi}\,.\,\widehat{r}\right|}\frac{r}{R}\frac{B_{T}}{B_{P}}\end{aligned} \tag{3.274}$$

We recognize the expression of the safety factor (2.51) so that

$$\left\langle J_{\parallel}\right\rangle_{\phi}^{0}(\psi)=\frac{2\pi q_{e}}{m_{e}}\frac{q}{\overline{q}}\int_{0}^{\infty}dp\,\frac{p^{3}}{\gamma}\int_{-1}^{1}d\xi_{0}\,H\left(|\xi_{0}|-\xi_{0T}\right)\,\xi_{0}f_{0}^{(0)}(\psi,p,\xi_{0}) \tag{3.275}$$

Case of circular concentric flux-surfaces In that case, we showed in (2.83) that the safety factor is

$$q(r)=\frac{\epsilon}{\sqrt{1-\epsilon^{2}}}\frac{B_{T}}{B_{P}} \tag{3.276}$$

with $\epsilon=r/R_{p}$ the inverse aspect ratio.

In addition, $\overline{q}(r)$ becomes

$$\begin{aligned}\overline{q}(r)&=\int_{0}^{2\pi}\frac{d\theta}{2\pi}\frac{r}{R_{p}}\frac{B_{0}}{B_{P}}\\&=\int_{0}^{2\pi}\frac{d\theta}{2\pi}\frac{r}{R_{p}}\frac{B_{0}}{B}\frac{B}{B_{P}}\\&=\epsilon\frac{B}{B_{P}}\frac{R_{p}}{R_{0}}\\&=\frac{\epsilon}{1+\epsilon}\frac{B}{B_{P}}\end{aligned} \tag{3.277}$$

since $R=R_{p}+r\cos\theta$, and $B_{0}/B=R/R_{0}$. We have then

$$\frac{q(r)}{\overline{q}(r)}=\sqrt{\frac{1+\epsilon}{1-\epsilon}}\frac{B_{T}}{B} \tag{3.278}$$

In the case when $B_{T}\gg B_{P}$, we retrieve the bounce-averaged coefficient s^{*} and in the large aspect ratio limit $\epsilon\ll1$,

$$\lim_{\epsilon\to0}\frac{q(r)}{\overline{q}(r)}=(1+\epsilon)\frac{B_{T}}{B} \tag{3.279}$$

Drift Kinetic Equation

When we consider the first order distribution function, we have $f_1 = \widetilde{f} + g$, where g is constant along a field line, and therefore its contribution has the same expression as for f_0. However, $\widetilde{f}$ has an explicit dependence upon θ, which is given by (3.206)

$$\widetilde{f}(\psi,\theta,p,\xi) = \frac{\xi(\psi,\theta,\xi_0)}{\Psi(\psi,\theta)\xi_0}\widetilde{f}^{(0)}(\psi,p,\xi_0) \tag{3.280}$$

where

$$\xi_0 = \sigma\sqrt{1-\frac{1}{\Psi\left(\psi,\theta\right)}\left(1-\xi^2\right)} \tag{3.281}$$

Consequently, we find

$$\begin{aligned}\widetilde{J}_{\parallel}^{1}\left(\psi,\theta\right) &= 2\pi q_e\int_0^\infty p^2dp\int_{-1}^{1}d\xi\ \frac{p\xi}{\gamma m_e}\widetilde{f}\left(\psi,\theta,p,\xi\right)\\ &= 2\pi q_e\int_0^\infty p^2dp\int_{-1}^{1}d\xi\ \frac{p\xi}{\gamma m_e}\frac{\xi}{\Psi(\psi,\theta)\xi_0}\widetilde{f}^{(0)}(\psi,p,\xi_0)\\ &= 2\pi q_e\int_0^\infty p^2dp\int_{-1}^{1}d\xi_0\frac{\xi}{\xi_0}\times\\ &H\left(|\xi_0|-\sqrt{1-\frac{1}{\Psi\left(\psi,\theta\right)}}\right)\ \frac{p\xi_0}{\gamma m_e}\widetilde{f}^{(0)}\left(\psi,p,\xi_0\right)\end{aligned} \tag{3.282}$$

where again the condition

$$|\xi_0| \geq \sqrt{1-\frac{1}{\Psi\left(\psi,\theta\right)}} \tag{3.283}$$

results from the equation (3.268) and means that only the particle who reach the poloidal position θ must be considered.

Therefore, the flux-surface averaged current density contribution from $\widetilde{f}$

$$\left\langle\widetilde{J}_{\parallel}\right\rangle_{\phi}^{1}(\psi) = \frac{1}{\overline{q}}\int_0^{2\pi}\frac{d\theta}{2\pi}\frac{1}{\left|\widehat{\psi}\cdot\widehat{r}\right|}\frac{r}{R}\frac{B_T}{B_P}\frac{\widetilde{J}_{\parallel}^{1}\left(\psi,\theta\right)}{\Psi\left(\psi,\theta\right)} \tag{3.284}$$

becomes

$$\begin{aligned}\left\langle\widetilde{J}_{\parallel}\right\rangle_{\phi}^{1}(\psi) = \frac{2\pi q_e}{m}\int_0^\infty dp\ \frac{p^3}{\gamma}\frac{1}{\overline{q}}\int_0^{2\pi}\frac{d\theta}{2\pi}\frac{1}{\left|\widehat{\psi}\cdot\widehat{r}\right|}\frac{r}{R}\frac{B_T}{B_P}\frac{1}{\Psi\left(\psi,\theta\right)}\times\\ \int_{-1}^{1}d\xi_0\frac{\xi}{\xi_0}H\left(|\xi_0|-\sqrt{1-\frac{1}{\Psi\left(\psi,\theta\right)}}\right)\ \xi_0\widetilde{f}^{(0)}\left(\psi,p,\xi_0\right)\end{aligned} \tag{3.285}$$

Note that the condition (3.283) is equivalent to

$$\theta_{\min}\left(\psi,\xi_0\right) \leq \theta \leq \theta_{\max}\left(\psi,\xi_0\right) \tag{3.286}$$

so that, permuting the integrals over θ and ξ_0, we find

$$\left\langle \widetilde{J}_{\parallel} \right\rangle_{\phi}^{1}(\psi) = \frac{2\pi q_e}{m_e} \int_0^{\infty} dp\, \frac{p^3}{\gamma} \int_{-1}^{1} d\xi_0\, \xi_0 \widetilde{f}^{(0)}(\psi, p, \xi_0) \frac{1}{\overline{q}} \int_{\theta_{\min}}^{\theta_{\max}} \frac{d\theta}{2\pi} \frac{1}{\left| \widehat{\psi} \cdot \widehat{r} \right|} \frac{r}{R} \frac{B_T}{B_P} \frac{1}{\Psi(\psi, \theta)} \frac{\xi}{\xi_0} \tag{3.287}$$

We have then

$$\frac{r}{R} \frac{B_T}{B_P} \frac{1}{\Psi(\psi, \theta)} = \frac{R_p I(\psi)}{R_0^2 B_0} \frac{r}{R_p} \frac{B}{B_P} \frac{R_0^2}{R^2} \Psi^{-2}(\psi, \theta) \tag{3.288}$$

Then, noting the the integrand in (3.287) is independent of σ , so that the sum over σ for trapped particles can be added, we obtain

$$\left\langle \widetilde{J}_{\parallel} \right\rangle_{\phi}^{1}(\psi) = \frac{2\pi q_e}{m_e} \int_0^{\infty} dp\, \frac{p^3}{\gamma} \int_{-1}^{1} d\xi_0\, \xi_0 \widetilde{f}^{(0)}(\psi, p, \xi_0) \frac{1}{\overline{q}} \frac{R_p I(\psi)}{R_0^2 B_0} \times \left[\frac{1}{2} \sum_{\sigma} \right]_T \int_{\theta_{\min}}^{\theta_{\max}} \frac{d\theta}{2\pi} \frac{1}{\left| \widehat{\psi} \cdot \widehat{r} \right|} \frac{r}{R_p} \frac{B}{B_P} \frac{\xi_0}{\xi} \left[\frac{R_0}{R} \right]^2 \Psi^{-2}(\psi, \theta) \left[\frac{\xi}{\xi_0} \right]^2 \tag{3.289}$$

We recognize the expression of a bounce coefficients defined by the general relation (2.66) in Sec. 2.2.1, so that we get finally

$$\left\langle \widetilde{J}_{\parallel} \right\rangle_{\phi}^{1}(\psi) = \frac{2\pi q_e}{m_e} \frac{\widetilde{q}}{\overline{q}} \frac{R_p}{R_0} \frac{B_{T0}}{B_0} \int_0^{\infty} dp\, \frac{p^3}{\gamma} \int_{-1}^{1} d\xi_0\, \lambda_{2,-2,2} \xi_0 \widetilde{f}^{(0)}(\psi, p, \xi_0) \tag{3.290}$$

with

$$\lambda_{2,-2,2} = \lambda \left\{ \left(\frac{\xi}{\xi_0} \right)^2 \Psi^{-2} \left(\frac{R_0}{R} \right)^2 \right\} \tag{3.291}$$

Case of circular concentric flux-surfaces In that case, we showed in (2.99) that $\widetilde{q}$ is

$$\widetilde{q}(r) = \epsilon \frac{B}{B_P} \tag{3.292}$$

with $\epsilon = r/R_p$ the inverse aspect ratio.

In addition, $\overline{q}(r)$ is

$$\overline{q}(r) = \frac{\epsilon}{1+\epsilon} \frac{B}{B_P} \tag{3.293}$$

and since

$$R_0 = R_p(1+\epsilon) \tag{3.294}$$

we have then

$$\frac{\widetilde{q}}{\overline{q}} \frac{R_p}{R_0} \frac{B_{T0}}{B_0} = \frac{B_{T0}}{B_0} \simeq 1 \tag{3.295}$$

in the limit $B_P \ll B$.

Also, in this case,

$$\Psi(\psi,\theta) = \frac{R_0}{R} \tag{3.296}$$

so that

$$\lambda_{2,-2,2} = \lambda_{2,0,0} = \lambda\left\{\frac{\xi^2}{\xi_0^2}\right\} = \widetilde{s}^* \tag{3.297}$$

using notations used in previous publications. The exact expression of $\widetilde{s}^*$ in terms of a series expansion is given in relation (4.130).

3.6.4 Power Density Associated with a Flux

Definition

The kinetic energy associated with a relativistic electron of momentum p is

$$E_c = m_e c^2(\gamma - 1) \tag{3.298}$$

Then, the local energy density of electrons is

$$\varepsilon(\mathbf{x}) = \int d^3p\ m_e c^2(\gamma-1) f(\mathbf{x},\mathbf{p}) \tag{3.299}$$

The density of power absorbed through the process $\mathcal{O}$, $P_{abs}^{\mathcal{O}}$, is

$$P_{abs}^{\mathcal{O}}(\mathbf{x}) = \left.\frac{\partial\varepsilon}{\partial t}\right|_{\mathcal{O}} = \int d^3p\ m_e c^2\,(\gamma-1)\left.\frac{\partial f(\mathbf{x},\ \mathbf{p})}{\partial t}\right|_{\mathcal{O}} \tag{3.300}$$

When the operator is described in conservative form, as the divergence of a flux

$$\left.\frac{\partial f}{\partial t}\right|_{\mathcal{O}} = -\nabla_{\ \mathbf{p}}\cdot\mathbf{S}_{\mathbf{p}}^{\mathcal{O}} = -\frac{1}{p^2}\frac{\partial}{\partial p}\left(p^2 S_p^{\mathcal{O}}\right) + \frac{1}{p}\frac{\partial}{\partial\xi}\left(\sqrt{1-\xi^2}S_\xi^{\mathcal{O}}\right) \tag{3.301}$$

then the power density becomes

$$P_{abs}^{\mathcal{O}} = -2\pi m_e c^2\int_0^\infty p^2dp\ (\gamma-1)\int_{-1}^{+1}d\xi\left[\frac{1}{p^2}\frac{\partial}{\partial p}\left(p^2S_p^{\mathcal{O}}\right) - \frac{1}{p}\frac{\partial}{\partial\xi}\left(\sqrt{1-\xi^2}S_\xi^{\mathcal{O}}\right)\right] \tag{3.302}$$

The integration of the $S_\xi^{\mathcal{O}}$ term gives no contribution, since the particle energy is function of p only

$$\int_{-1}^{+1}d\xi\ \frac{\partial}{\partial\xi}\left(\sqrt{1-\xi^2}S_\xi^{\mathcal{O}}\right) = \left[\sqrt{1-\xi^2}S_\xi^{\mathcal{O}}\right]_{-1}^{+1} = 0 \tag{3.303}$$

and the equation (3.302) reduces to

$$P_{abs}^{\mathcal{O}} = -2\pi m_e c^2\int_{-1}^{+1}d\xi\int_0^\infty(\gamma-1)\frac{\partial}{\partial p}\left(p^2S_p^{\mathcal{O}}\right)dp \tag{3.304}$$

Integrating by parts, we get

$$P_{abs}^{\mathcal{O}} = -2\pi m_e c^2 \int_{-1}^{+1} d\xi \left(\left[(\gamma - 1)\, p^2 S_p^{\mathcal{O}} \right]_0^{\infty} - \int_0^{\infty} \frac{d\gamma}{dp} p^2 S_p^{\mathcal{O}} dp \right) \tag{3.305}$$

Assuming that $\lim_{p\to\infty} p^2 S_p^{\mathcal{O}} = 0$, and using

$$\frac{d\gamma}{dp} = \frac{p}{\gamma m_e^2 c^2} \tag{3.306}$$

the equation (3.305) reduces to

$$P_{abs}^{\mathcal{O}}(\psi, \theta) = 2\pi \int_{-1}^{+1} d\xi \int_0^{\infty} dp\, \frac{p^3}{\gamma m_e} S_p^{\mathcal{O}} \tag{3.307}$$

Flux-Surface Averaging

Starting from the general expression of the flux-surface averaging of a volume quantity (3.246), the flux-surface averaged power density $\left\langle P_{abs}^{\mathcal{O}} \right\rangle_V (\psi)$ is

$$\left\langle P_{abs}^{\mathcal{O}} \right\rangle_V (\psi) = \frac{1}{\widehat{q}} \int_0^{2\pi} \frac{d\theta}{2\pi} \frac{1}{\left| \widehat{\psi} \,.\, \widehat{r} \right|} \frac{r}{R_p} \frac{B_0}{B_P} P_{abs}^{\mathcal{O}}(\psi, \theta) \tag{3.308}$$

which becomes

$$\left\langle P_{abs}^{\mathcal{O}} \right\rangle_V (\psi) = 2\pi \int_0^{\infty} dp\, \frac{p^3}{\gamma m_e} \frac{1}{\widehat{q}} \int_0^{2\pi} \frac{d\theta}{2\pi} \frac{1}{\left| \widehat{\psi} \,.\, \widehat{r} \right|} \frac{r}{R_p} \frac{B_0}{B_P} \int_{-1}^{+1} d\xi\; S_p^{\mathcal{O}} \tag{3.309}$$

The sum over σ for trapped electrons can be added, using

$$\begin{aligned}
\int_{-1}^{1} d\xi \left[\frac{1}{2} \sum_{\sigma=\pm 1} \right]_T S_p^{\mathcal{O}} &= \int_{-1}^{-\xi_T} d\xi S_p^{\mathcal{O}} + \int_{\xi_T}^{1} d\xi S_p^{\mathcal{O}} + \frac{1}{2} \int_{-\xi_T}^{\xi_T} d\xi \sum_{\sigma=\pm 1} S_p^{\mathcal{O}} \\
&= \int_{-1}^{-\xi_T} d\xi S_p^{\mathcal{O}} + \int_{\xi_T}^{1} d\xi S_p^{\mathcal{O}} + \frac{1}{2} \int_{-\xi_T}^{\xi_T} d\xi \left[S_p^{\mathcal{O}}(\xi) + S_p^{\mathcal{O}}(-\xi) \right] \\
&= \int_{-1}^{-\xi_T} d\xi S_p^{\mathcal{O}} + \int_{\xi_T}^{1} d\xi S_p^{\mathcal{O}} + \int_{-\xi_T}^{\xi_T} d\xi S_p^{\mathcal{O}}(\xi) \\
&= \int_{-1}^{1} d\xi S_p^{\mathcal{O}}
\end{aligned} \tag{3.310}$$

where the trapping condition evaluated at the poloidal location θ is

$$|\xi| < \xi_T = \sqrt{1 - \frac{B(\psi, \theta)}{B_{\max}(\psi)}} \tag{3.311}$$

Using $\xi d\xi = \Psi \xi_0 d\xi_0$ with the condition (3.270) on ξ_0

$$|\xi_0| \geq \sqrt{1 - \frac{1}{\Psi(\psi, \theta)}} \tag{3.312}$$

we get that

$$\int_{-1}^{+1} d\xi = \int_{-1}^{+1} d\xi_0 \, \frac{\Psi(\psi,\theta)\,\xi_0}{\xi} H\left(|\xi_0| - \sqrt{1 - \frac{1}{\Psi(\psi,\theta)}}\right) \tag{3.313}$$

Note that the condition (3.312) is equivalent to

$$\theta_{\min}(\psi,\xi_0) \leq \theta \leq \theta_{\max}(\psi,\xi_0) \tag{3.314}$$

so that, permuting the integrals over θ and ξ_0, we find

$$\left\langle P_{abs}^{\mathcal{O}} \right\rangle_V (\psi) = 2\pi \int_0^{\infty} dp \, \frac{p^3}{\gamma m_e} \int_{-1}^{+1} d\xi_0 \tag{3.315}$$

$$\frac{1}{\widehat{q}} \left[\frac{1}{2} \sum_{\sigma=\pm 1}\right]_T \int_{\theta_{\min}}^{\theta_{\max}} \frac{d\theta}{2\pi} \frac{1}{\left|\widehat{\psi} \,.\, \widehat{r}\right|} \frac{r}{R_p} \frac{B}{B_P} \frac{\xi_0}{\xi} S_p^{\mathcal{O}} \tag{3.316}$$

We see that the bounce-averaging of the fluxes appears naturally, so that we can rewrite

$$\left\langle P_{abs}^{\mathcal{O}} \right\rangle_V (\psi) = 2\pi \frac{\widetilde{q}}{\widehat{q}} \int_0^{\infty} dp \, \frac{p^3}{\gamma m_e} \int_{-1}^{+1} d\xi_0 \lambda \left\{ S_p^{\mathcal{O}} \right\} \tag{3.317}$$

Using the definition (3.167), we observe that the flux-surface averaged power density is calculated using the momentum flux component of the bounce-averaged kinetic equation:

$$\left\langle P_{abs}^{\mathcal{O}} \right\rangle_V (\psi) = 2\pi \frac{\widetilde{q}}{\widehat{q}} \int_0^{\infty} dp \, \frac{p^3}{\gamma m_e} \int_{-1}^{+1} d\xi_0 \lambda S_p^{(0)\mathcal{O}} \tag{3.318}$$

Case of circular concentric flux-surfaces In that case, we showed in (3.292) that the coefficient $\widetilde{q}$ is

$$\widetilde{q}(r) = \epsilon \frac{B}{B_P} \tag{3.319}$$

with $\epsilon = r/R_p$.

In addition, $\widehat{q}(r)$ becomes

$$\begin{aligned} \widehat{q}(r) &= \int_0^{2\pi} \frac{d\theta}{2\pi} \frac{r}{R_p} \frac{B_0}{B_P} \\ &= \epsilon \frac{B}{B_P} \int_0^{2\pi} \frac{d\theta}{2\pi} \frac{B_0}{B} \\ &= \epsilon \frac{B}{B_P} \int_0^{2\pi} \frac{d\theta}{2\pi} \frac{R}{R_0} \\ &= \frac{\epsilon}{1+\epsilon} \frac{B}{B_P} \end{aligned} \tag{3.320}$$

using the simple relation $B/B_0 = R_0/R$ and $R_0 = R_p(1+\epsilon)$.

We have then

$$\frac{\widetilde{q}(\psi)}{\widehat{q}(\psi)} = 1 + \epsilon \tag{3.321}$$

Fokker-Planck Equation

The Fokker-Planck equation (3.107) solves for the zero-order distribution function f_0. The density of power transfered to f_0 through the momentum-space mechanism $\mathcal{O}$ is then

$$\left\langle P_{abs}^{\mathcal{O}} \right\rangle_V^0 (\psi) = 2\pi \frac{\widetilde{q}}{\widehat{q}} \int_0^\infty dp \, \frac{p^3}{\gamma m_e} \int_{-1}^{+1} d\xi_0 \lambda S_p^{(0)\mathcal{O}} (f_0) \tag{3.322}$$

where $S_p^{(0)\mathcal{O}} (f_0)$ is given by (3.187)

$$S_p^{(0)\mathcal{O}} (f_0) = -D_{pp}^{(0)\mathcal{O}} \frac{\partial f_0^{(0)}}{\partial p} + \frac{\sqrt{1-\xi_0^2}}{p} D_{p\xi}^{(0)\mathcal{O}} \frac{\partial f_0^{(0)}}{\partial \xi_0} + F_p^{(0)\mathcal{O}} f_0^{(0)} \tag{3.323}$$

The momentum-space diffusion and convection elements $D_{pp}^{(0)\mathcal{O}}$, $D_{p\xi}^{(0)\mathcal{O}}$ and $F_p^{(0)\mathcal{O}}$ associated with a particular mechanism $\mathcal{O}$ are calculated in chapter 4.

Drift Kinetic Equation

The Fokker-Planck equation (6.1) solves for the first-order distribution function $f_1 = \widetilde{f} + g$ (3.117). The densities of power transfered to $\widetilde{f}$ and g through the momentum-space mechanism $\mathcal{O}$ are then respectively

$$\left\langle \widetilde{P}_{abs}^{\mathcal{O}} \right\rangle_V^1 (\psi) = 2\pi \frac{\widetilde{q}}{\widehat{q}} \int_0^\infty dp \, \frac{p^3}{\gamma m_e} \int_{-1}^{+1} d\xi_0 \lambda \widetilde{S}_p^{(0)\mathcal{O}} \left(\widetilde{f} \right) \tag{3.324}$$

$$\left\langle P_{abs}^{\mathcal{O}} \right\rangle_V^1 (\psi) = 2\pi \frac{\widetilde{q}}{\widehat{q}} \int_0^\infty dp \, \frac{p^3}{\gamma m_e} \int_{-1}^{+1} d\xi_0 \lambda S_p^{(0)\mathcal{O}} (g) \tag{3.325}$$

where $\widetilde{S}_p^{(0)\mathcal{O}} \left(\widetilde{f} \right)$ and $S_p^{(0)\mathcal{O}} (g)$ are given by (3.187) and (3.216)

$$\widetilde{S}_p^{(0)} \left(\widetilde{f} \right) = -\widetilde{D}_{pp}^{(0)} \frac{\partial \widetilde{f}^{(0)}}{\partial p} + \frac{\sqrt{1-\xi_0^2}}{p} \widetilde{D}_{p\xi}^{(0)} \frac{\partial \widetilde{f}^{(0)}}{\partial \xi_0} + \widetilde{F}_p^{(0)} \widetilde{f}^{(0)} \tag{3.326}$$

$$S_p^{(0)\mathcal{O}} (g) = -D_{pp}^{(0)\mathcal{O}} \frac{\partial g^{(0)}}{\partial p} + \frac{\sqrt{1-\xi_0^2}}{p} D_{p\xi}^{(0)\mathcal{O}} \frac{\partial g^{(0)}}{\partial \xi_0} + F_p^{(0)\mathcal{O}} g^{(0)} \tag{3.327}$$

The momentum-space diffusion and convection elements $D_{pp}^{(0)\mathcal{O}}$, $D_{p\xi}^{(0)\mathcal{O}}$, $F_p^{(0)\mathcal{O}}$, $\widetilde{D}_{pp}^{(0)}$, $\widetilde{D}_{p\xi}^{(0)}$ and $\widetilde{F}_p^{(0)}$ associated with a particular mechanism $\mathcal{O}$ are calculated in chapter 4.

3.6.5 Stream Function for Momentum Space fluxes

When transport in configuration space is ignored, and a steady-state regime is assumed to be reached, the Fokker-Planck equation reduces to the conservative equation (3.146)

$$\nabla_{\mathbf{p}} \cdot \mathbf{S}_{\mathbf{p}} = 0 \tag{3.328}$$

Because $\mathbf{S}_{\mathbf{p}}$ is a divergence-free field vector, it can be expressed as the curl of a stream function

$$\mathbf{S}_{\mathbf{p}} = \nabla \times \mathbf{T}_{\mathbf{p}} \tag{3.329}$$

The expression of a curl in momentum space (p, ξ, φ) is given by relation (A.279) in Appendix A

$$S_p = \frac{1}{p}\frac{\partial}{\partial \xi}\left(\sqrt{1-\xi^2}T_\varphi\right) + \frac{1}{p\sqrt{1-\xi^2}}\frac{\partial T_\xi}{\partial \varphi} \tag{3.330}$$

$$S_\xi = \frac{1}{p}\frac{\partial}{\partial p}\left(pT_\varphi\right) - \frac{1}{p\sqrt{1-\xi^2}}\frac{\partial T_p}{\partial \varphi} \tag{3.331}$$

$$S_\varphi = -\frac{1}{p}\frac{\partial}{\partial p}\left(pT_\xi\right) - \frac{\sqrt{1-\xi^2}}{p}\frac{\partial T_p}{\partial \xi} \tag{3.332}$$

Because $S_\varphi = 0$, we can choose $T_\xi = T_p = 0$, which leads to

$$S_p = \frac{1}{p}\frac{\partial}{\partial \xi}\left(\sqrt{1-\xi^2}T_\varphi\right) \tag{3.333}$$

$$S_\xi = \frac{1}{p}\frac{\partial}{\partial p}\left(pT_\varphi\right) \tag{3.334}$$

and we can rewrite

$$\mathbf{S_p} = \nabla \times T_\varphi \widehat{\varphi} \tag{3.335}$$

In order to give a physical meaning to $T_\varphi(p, \xi, \psi)$, we define formally

$$T_\varphi(\psi, p, \xi) = K(\psi, p, \xi)\, A(\psi, p, \xi) \tag{3.336}$$

where the function $A(p, \xi)$ is such that the flux of electrons between two contours A_1 and A_2 is equal to $n_e(\psi)\ (A_2 - A_1)$. Lets consider a path γ_{12} between the contours A_1 and A_2. The total flux of electrons through this path, which is in fact a surface, given the rotational symmetry in φ, is given by

$$\begin{aligned}\Gamma_{12} &= \iint_{S_{12}} dS\ \mathbf{S_p}\cdot\widehat{n} \\ &= \iint_{S_{12}} d\mathbf{S}\cdot\nabla\times T_\varphi\widehat{\varphi} \\ &= \oint_{C_{12}} T_\varphi\, d\mathbf{l}\cdot\widehat{\varphi}\end{aligned} \tag{3.337}$$

By rotational symmetry in φ, and using (A.272), we get

$$\Gamma_{12} = 2\pi p_2\sqrt{1-\xi_2^2}T_{\varphi 2}\ - 2\pi p_1\sqrt{1-\xi_1^2}T_{\varphi 1} \tag{3.338}$$

If we define

$$K(\psi, p, \xi) \equiv \frac{n_e(\psi)}{2\pi p\sqrt{1-\xi^2}} \tag{3.339}$$

we obtain

$$\Gamma_{12} = n_e(\psi)\,(A_2\ - A_1) \tag{3.340}$$

and therefore the total flux between the contours A_1 and A_2 is equal to $n_e(\psi)\ (A_2 - A_1)$. We call $A(\psi, p, \xi)$ the stream function, and we get finally

$$S_p = \frac{n_e(\psi)}{2\pi p^2}\frac{\partial A}{\partial \xi} \tag{3.341}$$

$$S_\xi = \frac{n_e(\psi)}{2\pi p\sqrt{1-\xi^2}}\frac{\partial A}{\partial p} \tag{3.342}$$

Since there are no fluxes across the internal boundaries in the momentum space, this boundary coincide with a contour A, and therefore we can arbitrarily set this value to 0:

$$A(0, \xi) = A(p, \pm 1) = 0 \tag{3.343}$$

Then A can be calculated by any of the integrals

$$A(\psi, p, \xi) = \frac{2\pi p^2}{n_e(\psi)}\int_{-1}^{\xi} d\xi\ S_p = \frac{2\pi p^2}{n_e(\psi)}\int_{1}^{\xi} d\xi'\ S_p \tag{3.344}$$

or

$$A(\psi, p, \xi) = \frac{2\pi\sqrt{1-\xi^2}}{n_e(\psi)}\int_0^p p'dp'\ S_\xi \tag{3.345}$$

However, $A(\psi, p, \xi)$ remains a function of ξ, which depends upon θ. Starting from the bounce-averaged fluxes, it is interesting to compute a function $A^{(0)}(\psi, p, \xi_0)$, such that

$$\begin{aligned} A^{(0)}(0, \xi_0) &= \overline{A}(p, \pm 1) = 0 \\ S_p^{(0)} &= \frac{n_e(\psi)}{2\pi p^2}\frac{\partial A^{(0)}}{\partial \xi_0} \\ S_\xi^{(0)} &= \frac{n_e(\psi)}{2\pi p\sqrt{1-\xi_0^2}}\frac{\partial A^{(0)}}{\partial p} \end{aligned} \tag{3.346}$$

We first need to demonstrate the existence of such a function. Starting from $S_p^{(0)}$,

$$\begin{aligned}
A^{(0)}(\psi,p,\xi_0) &= \frac{2\pi p^2}{n_e(\psi)}\int_{-1}^{\xi_0} d\xi_0' \ \{S_p\} \\
&= \frac{2\pi p^2}{n_e(\psi)}\int_{-1}^{\xi_0} d\xi_0' \ \frac{1}{\lambda\widetilde{q}}\left[\frac{1}{2}\sum_\sigma\right]_T \int_{\theta_{\min}}^{\theta_{\max}} \frac{d\theta}{2\pi}\frac{1}{\left|\widehat{\psi}\cdot\widehat{r}\right|}\frac{r}{R_p}\frac{B}{B_P}\frac{\xi_0'}{\xi'}S_p \\
&= \int_{-1}^{\xi_0} d\xi_0' \ \frac{1}{\lambda\widetilde{q}}\left[\frac{1}{2}\sum_\sigma\right]_T \int_0^{2\pi} \frac{d\theta}{2\pi}H(B_b-B)\frac{1}{\left|\widehat{\psi}\cdot\widehat{r}\right|}\frac{r}{R_p}\frac{B}{B_P}\frac{\xi_0'}{\xi'}\frac{\partial A}{\partial\xi'} \\
&= \frac{\sigma}{\lambda\widetilde{q}}\left[\frac{1}{2}\sum_\sigma\right]_T \int_0^{2\pi}\frac{d\theta}{2\pi}\frac{1}{\left|\widehat{\psi}\cdot\widehat{r}\right|}\frac{r}{R_p}\frac{B}{B_P} \\
&\qquad \int_{-1}^{\xi_0} d\xi_0' H\left(|\xi_0|-\sqrt{1-\frac{1}{\Psi}}\right)\sigma\frac{\xi_0'}{\xi'}\frac{\partial A}{\partial\xi'} \\
&= \frac{\sigma}{\lambda\widetilde{q}}\left[\frac{1}{2}\sum_\sigma\right]_T \int_0^{2\pi}\frac{d\theta}{2\pi}\frac{1}{\left|\widehat{\psi}\cdot\widehat{r}\right|}\frac{r}{R_p}\frac{B}{B_P}\frac{\sigma}{\Psi}\int_{-1}^{\xi} d\xi'\frac{\partial A}{\partial\xi'} \\
&= \frac{\sigma}{\lambda\widetilde{q}}\left[\frac{1}{2}\sum_\sigma\right]_T \int_0^{2\pi}\frac{d\theta}{2\pi}\frac{1}{\left|\widehat{\psi}\cdot\widehat{r}\right|}\frac{r}{R_p}\frac{B_0}{B_P}\sigma A \\
&= \sigma\frac{\widehat{q}}{\lambda\widetilde{q}}\left[\frac{1}{2}\sum_\sigma\right]_T \langle\sigma A\rangle_V
\end{aligned} \tag{3.347}$$

where we used

$$\theta_{\min}\le\theta\le\theta_{\max}\Leftrightarrow B\le B_b\Leftrightarrow\sqrt{1-\frac{1}{\Psi}}\le|\xi_0| \tag{3.348}$$

Now, starting from $S_\xi^{(0)}$, we have

$$\begin{aligned}
A^{(0)}(\psi,p,\xi_0) &= \frac{2\pi\sqrt{1-\xi_0^2}}{n_e(\psi)}\int_0^p p'dp'\;\sigma\left\{\frac{\sigma\xi}{\sqrt{\Psi}\xi_0}S_\xi\right\}\\
&= \frac{2\pi\sqrt{1-\xi_0^2}}{n_e(\psi)}\int_0^p p'dp'\;\sigma\frac{1}{\lambda\widetilde{q}}\left[\frac{1}{2}\sum_\sigma\right]_T\int_{\theta_{\min}}^{\theta_{\max}}\frac{d\theta}{2\pi}\frac{1}{\left|\widehat{\psi}\cdot\widehat{r}\right|}\frac{r}{R_p}\frac{B}{B_P}\frac{\sigma}{\sqrt{\Psi}}S_\xi\\
&= \int_0^p dp'\;\sigma\frac{1}{\lambda\widetilde{q}}\left[\frac{1}{2}\sum_\sigma\right]_T\int_{\theta_{\min}}^{\theta_{\max}}\frac{d\theta}{2\pi}\frac{1}{\left|\widehat{\psi}\cdot\widehat{r}\right|}\frac{r}{R_p}\frac{B}{B_P}\frac{\sigma}{\sqrt{\Psi}}\frac{\sqrt{1-\xi_0^2}}{\sqrt{1-\xi^2}}\frac{\partial A}{\partial p'}\\
&= \frac{\sigma}{\lambda\widetilde{q}}\left[\frac{1}{2}\sum_\sigma\right]_T\int_{\theta_{\min}}^{\theta_{\max}}\frac{d\theta}{2\pi}\frac{1}{\left|\widehat{\psi}\cdot\widehat{r}\right|}\frac{r}{R_p}\frac{B}{B_P}\frac{\sigma}{\Psi}\int_0^p dp'\frac{\partial A}{\partial p'}\\
&= \frac{\sigma}{\lambda\widetilde{q}}\left[\frac{1}{2}\sum_\sigma\right]_T\int_{\theta_{\min}}^{\theta_{\max}}\frac{d\theta}{2\pi}\frac{1}{\left|\widehat{\psi}\cdot\widehat{r}\right|}\frac{r}{R_p}\frac{B_0}{B_P}\sigma A\\
&= \sigma\frac{\widehat{q}}{\lambda\widetilde{q}}\left[\frac{1}{2}\sum_\sigma\right]_T\langle\sigma A\rangle_V
\end{aligned}\tag{3.349}$$

and we find the same function $A^{(0)}$. The existence of a function $A^{(0)}$ verifying (3.346) is therefore demonstrated. We need now to demonstrate that $A^{(0)}$ verifying (3.346) leads to the bounce-averaged Fokker-Planck equation (3.166):

$$\begin{aligned}
\{\nabla_{\mathbf{p}}\cdot\mathbf{S}_{\mathbf{p}}\} &= \frac{1}{p^2}\frac{\partial}{\partial p}\left(p^2S_p^{(0)}\right)-\frac{1}{\lambda p}\frac{\partial}{\partial\xi_0}\left(\sqrt{1-\xi_0^2}\lambda S_{\xi_0}^{(0)}\right)\\
&= \frac{1}{p^2}\frac{\partial}{\partial p}\left(p^2\frac{n_e(\psi)}{2\pi p^2}\frac{\partial A^{(0)}}{\partial\xi_0}\right)-\frac{1}{\lambda p}\frac{\partial}{\partial\xi_0}\left(\sqrt{1-\xi_0^2}\lambda\frac{n_e(\psi)}{2\pi p\sqrt{1-\xi_0^2}}\frac{\partial A^{(0)}}{\partial p}\right)\\
&= \frac{1}{\lambda p^2}\frac{\partial^2}{\partial p\xi_0}\left[\frac{\lambda n_e(\psi)A^{(0)}}{2\pi}\right]-\frac{1}{\lambda p^2}\frac{\partial^2}{\partial\xi_0\partial p}\left[\frac{\lambda n_e(\psi)A^{(0)}}{2\pi}\right]\\
&= 0
\end{aligned}\tag{3.350}$$

In conclusion, a stream function verifying

$$A^{(0)}(0,\xi_0)=\overline{A}(p,\pm1)=0\tag{3.351}$$

has been found which leads to the bounce-averaged Fokker-Planck equation and which can be calculated from the bounce-averaged fluxes by either

$$A^{(0)}(\psi,p,\xi_0)=\frac{2\pi p^2}{n_e(\psi)}\int_{-1}^{\xi_0}d\xi_0'\;S_p^{(0)}=\frac{2\pi p^2}{n_e(\psi)}\int_1^{\xi_0}d\xi_0'\;S_p^{(0)}\tag{3.352}$$

or

$$A^{(0)}(\psi,p,\xi_0)=\frac{2\pi\sqrt{1-\xi_0^2}}{n_e(\psi)}\int_0^p p'dp'\;S_\xi^{(0)}\tag{3.353}$$

relations.

3.6.6 Ohmic electric field

The electrical conductivity of the plasma σ_e is defined as the ratio of the flux averaged current density $\left\langle J_{\parallel}\right\rangle_{\phi}^{0}$ to the flux surface averaged parallel Ohmic electric field $\left\langle E_{\parallel}\right\rangle_{\phi}$,

$$\sigma_e = \frac{\left\langle J_{\parallel}\right\rangle_{\phi}^{0}}{\left\langle E_{\parallel}\right\rangle_{\phi}} \tag{3.354}$$

By definition,

$$\begin{aligned}\left\langle E_{\parallel}\right\rangle_{\phi}(\psi) &= \frac{1}{\overline{q}(\psi)}\int_0^{2\pi}\frac{d\theta}{2\pi}\frac{1}{\left|\widehat{\psi}\,.\,\widehat{r}\right|}\frac{r}{R}\frac{B_0}{B_P}E_{\parallel}(\psi,\theta)\left[\widehat{\phi}\cdot\widehat{b}\right]\\ &= \frac{1}{\overline{q}(\psi)}\int_0^{2\pi}\frac{d\theta}{2\pi}\frac{1}{\left|\widehat{\psi}\,.\,\widehat{r}\right|}\frac{r}{R}\frac{B_0(\psi)}{B_P}E_{\parallel}(\psi,\theta)\frac{B_T}{B}\\ &= \frac{1}{\overline{q}(\psi)}\int_0^{2\pi}\frac{d\theta}{2\pi}\frac{1}{\left|\widehat{\psi}\,.\,\widehat{r}\right|}\frac{r}{R}\frac{B_T}{B_P}\frac{E_{\parallel}(\psi,\theta)}{\Psi(\psi,\theta)}\end{aligned} \tag{3.355}$$

Using

$$E_{\parallel}(\psi,\theta) = \frac{1}{\Psi(\psi,\theta)}\frac{R_0^2}{R^2}E_{\parallel 0}(\psi) \tag{3.356}$$

where $E_{\parallel 0}(\psi)$ is the value at the minimum magnetic field B_0, one obtains

$$\begin{aligned}\left\langle E_{\parallel}\right\rangle_{\phi}(\psi) &= \frac{1}{\overline{q}}\int_0^{2\pi}\frac{d\theta}{2\pi}\frac{1}{\left|\widehat{\psi}\,.\,\widehat{r}\right|}\frac{r}{R}\frac{B_T}{B_P}\frac{E_{\parallel 0}(\psi)}{\Psi^2(\psi,\theta)}\frac{R_0^2}{R^2}\\ &= E_{\parallel 0}(\psi)\frac{1}{\overline{q}}\int_0^{2\pi}\frac{d\theta}{2\pi}\frac{1}{\left|\widehat{\psi}\,.\,\widehat{r}\right|}\frac{r}{R}\frac{B_T}{B_P}\frac{1}{\Psi^2(\psi,\theta)}\frac{R_0^2}{R^2}\end{aligned} \tag{3.357}$$

or

$$\begin{aligned}\left\langle E_{\parallel}\right\rangle_{\phi}(\psi) &= E_{\parallel 0}(\psi)\frac{1}{\overline{q}}\frac{R_p}{R_0}\int_0^{2\pi}\frac{d\theta}{2\pi}\frac{1}{\left|\widehat{\psi}\,.\,\widehat{r}\right|}\frac{r}{R_p}\frac{B}{B_P}\frac{\xi_0}{\xi}\left[\frac{\xi}{\xi_0}\frac{B_T}{B}\frac{1}{\Psi^2(\psi,\theta)}\frac{R_0^3}{R^3}\right]\\ &= E_{\parallel 0}(\psi)\frac{1}{\overline{q}(\psi)}\frac{R_p}{R_0}\int_0^{2\pi}\frac{d\theta}{2\pi}\frac{1}{\left|\widehat{\psi}\,.\,\widehat{r}\right|}\frac{r}{R_p}\frac{B}{B_P}\frac{\xi_0}{\xi}\times\\ &\left[\frac{\xi}{\xi_0}\frac{B_T}{B_{T0}}\frac{B_{T0}}{B_0}\frac{B_0}{B}\frac{1}{\Psi^2(\psi,\theta)}\frac{R_0^3}{R^3}\right]\\ &= E_{\parallel 0}(\psi)\frac{1}{\overline{q}}\frac{B_{T0}}{B_0}\frac{R_p}{R_0}\int_0^{2\pi}\frac{d\theta}{2\pi}\frac{1}{\left|\widehat{\psi}\,.\,\widehat{r}\right|}\frac{r}{R_p}\frac{B}{B_P}\frac{\xi_0}{\xi}\left[\frac{\xi}{\xi_0}\frac{1}{\Psi^3(\psi,\theta)}\frac{R_0^4}{R^4}\right]\\ &= E_{\parallel 0}(\psi)\frac{\widetilde{q}}{\overline{q}}\frac{R_p}{R_0}\frac{B_{T0}}{B_0}\lambda\sigma\left\{\sigma\frac{\xi}{\xi_0}\frac{1}{\Psi^3(\psi,\theta)}\frac{R_0^4}{R^4}\right\}\\ &= E_{\parallel 0}(\psi)\frac{\widetilde{q}}{\overline{q}}\frac{R_p}{R_0}\frac{B_{T0}}{B_0}\overline{\lambda}_{1,-3,4}\end{aligned} \tag{3.358}$$

Case of circular concentric flux-surfaces In that case,

$$\frac{\widetilde{q}(r)}{\overline{q}(r)} = 1 + \epsilon \tag{3.359}$$

and since $R_p/R_0 = 1/(1+\epsilon)$,

$$\begin{aligned} \left\langle E_{\parallel} \right\rangle_{\phi}(r) &= \frac{B_T}{B}\overline{\lambda}_{1,-1,2} E_{\parallel 0}(r) \\ &= \frac{B_T}{B}\overline{\lambda}_{1,1,0} E_{\parallel 0}(r) \end{aligned} \tag{3.360}$$

using relation $\Psi(r,\theta) = R/R_0$. Therefore,

$$\left\langle E_{\parallel} \right\rangle_{\phi}(r) = \frac{B_T}{B}\sqrt{\frac{1+\epsilon}{1-\epsilon}} E_{\parallel 0}(r) \tag{3.361}$$

as $\overline{\lambda}_{1,-1,2} = \sqrt{\frac{1+\epsilon}{1-\epsilon}}$ for circular concentric flux-surfaces. Moreover, in this limit,

$$\sigma_e = \frac{\left\langle J_{\parallel} \right\rangle_{\phi}^{(0)}}{\left\langle E_{\parallel} \right\rangle_{\phi}} = \frac{J_{\parallel}^{(0)}}{E_{\parallel 0}} \tag{3.362}$$

since

$$\left\langle J_{\parallel} \right\rangle_{\phi}^{(0)}(\psi,\theta) = \frac{B_T}{B}\sqrt{\frac{1+\epsilon}{1-\epsilon}} J_{\parallel}^{(0)} \tag{3.363}$$

with

$$J_{\parallel}^{(0)} = \frac{2\pi q_e}{m_e}\int_0^{\infty} p^2 dp \int_{-1}^{1} d\xi_0 H\left(|\xi_0| - \xi_{0T}\right) \frac{p\xi_0}{\gamma m} f_0^{(0)}(\psi, p, \xi_0) \tag{3.364}$$

In that case, the neo-classical conductivity can be either calculated from flux surface averaged quantity, or local values at $B = B_0$.

3.6.7 Fraction of trapped electrons

The ratio between the number of trapped and passing electrons is an important quantity in the neoclassical transport theory, since the parallel viscosity responsible for reduction of the Ohmic conductivity and the bootstrap current level are both roughly proportional to this parameter. Therefore, under the influence of RF waves, its large variation will indicate unambiguously that significant macroscopic changes are to be expected on the current generation and the power absorption due to neoclassical effects. We could expect to encounter such circomstances especially when wave-particle interaction takes place in the near vicinity of the trapped-passing boundary.

The starting point of the calculations is the determination of the flux averaged density $\langle n_e \rangle$. According to the definition of the electron momentum distribution function f, the local electron density $n_e(\psi,\theta)$ is given by the relation

$$n_e(\psi,\theta) = 2\pi \int_{-1}^{+1} d\xi \int_0^{\infty} p^2 dp\; f(\psi,\theta,p,\xi) \tag{3.365}$$

Using the general expression (3.246) of the flux-surface averaging of a volumic quantity

$$\begin{aligned}\langle n_e\rangle_V(\psi) &= \frac{1}{\widehat{q}}\int_0^{2\pi}\frac{d\theta}{2\pi}\frac{1}{\left|\widehat{\psi}\,.\,\widehat{r}\right|}\frac{r}{R_p}\frac{B_0}{B_P}n_e(\psi,\theta)\\ &= \frac{2\pi}{\widehat{q}}\int_0^{\infty}p^2dp\int_0^{2\pi}\frac{d\theta}{2\pi}\frac{1}{\left|\widehat{\psi}\,.\,\widehat{r}\right|}\frac{r}{R_p}\frac{B_0(\psi)}{B_P}\int_{-1}^{+1}d\xi\ f(\psi,\theta,p,\xi)\\ &= \frac{2\pi}{\widehat{q}}\int_0^{\infty}p^2dp\int_0^{2\pi}\frac{d\theta}{2\pi}\frac{1}{\left|\widehat{\psi}\,.\,\widehat{r}\right|}\frac{r}{R_p}\frac{B_0(\psi)}{B_P}\times\\ &\int_{-1}^{+1}\left[\frac{1}{2}\sum_{\sigma=\pm1}\right]_T d\xi\ f(\psi,\theta,p,\xi)\end{aligned} \tag{3.366}$$

where the trapping condition evaluated at the location θ is given by

$$|\xi|<\xi_T=\sqrt{1-\frac{B(\psi,\theta)}{B_{\max}(\psi)}} \tag{3.367}$$

Using $\xi d\xi=\Psi\xi_0 d\xi_0$ with the condition (3.270) on ξ_0

$$|\xi_0|\geq\sqrt{1-\frac{1}{\Psi(\psi,\theta)}} \tag{3.368}$$

one get

$$\int_{-1}^{+1}\left[\frac{1}{2}\sum_{\sigma=\pm1}\right]_T d\xi=\int_{-1}^{+1}\left[\frac{1}{2}\sum_{\sigma=\pm1}\right]_T\Psi(\psi,\theta)\frac{\xi_0}{\xi}H\left(|\xi_0|-\sqrt{1-\frac{1}{\Psi(\psi,\theta)}}\right)d\xi_0 \tag{3.369}$$

Note that the condition (3.368) is equivalent to

$$\theta_{\min}(\psi,\xi_0)\leq\theta\leq\theta_{\max}(\psi,\xi_0) \tag{3.370}$$

so that, the integrals over θ and ξ_0 may be permuted,

$$\begin{aligned}\langle n_e\rangle_V(\psi) = \frac{2\pi}{\widehat{q}}\int_0^{\infty}p^2dp\ \int_{-1}^{+1}d\xi_0\times\\ \left[\frac{1}{2}\sum_{\sigma=\pm1}\right]_T\int_{\theta_{\min}}^{\theta_{\max}}\frac{d\theta}{2\pi}\frac{1}{\left|\widehat{\psi}\,.\,\widehat{r}\right|}\frac{r}{R_p}\frac{B}{B_P}\frac{\xi_0}{\xi}f(\psi,\theta,p,\xi_0)\end{aligned} \tag{3.371}$$

where the bounce-averaging of the distribution appears naturally. Therefore, expression (3.371) can be rewriten in the simple form

$$\langle n_e\rangle_V(\psi)=2\pi\frac{\widetilde{q}}{\widehat{q}}\int_0^{\infty}p^2dp\ \int_{-1}^{+1}d\xi_0\lambda\left\{f(\psi,\theta,p,\xi_0)\right\} \tag{3.372}$$

and the exact trapped fraction $\mathcal{F}_t$ is given by the ratio

$$\mathcal{F}_t(\psi) = \frac{\int_0^\infty p^2 dp \int_{-\xi_{0T}}^{+\xi_{0T}} \lambda \{f\} d\xi_0}{\int_0^\infty p^2 dp \int_{-1}^{+1} \lambda \{f\} d\xi_0} \tag{3.373}$$

where λ is the normalized bounce time 2.11.

Since, $\{f\} \simeq f_0^{(0)} + \widetilde{f}^{(0)} + g^{(0)}$,

$$\mathcal{F}_t(\psi) = \frac{\int_0^\infty p^2 dp \int_{-\xi_{0T}}^{+\xi_{0T}} \lambda \left[f_0^{(0)} + g^{(0)}\right] d\xi_0}{\int_0^\infty p^2 dp \int_{-1}^{+1} \lambda \left[f_0^{(0)} + \widetilde{f}^{(0)} + g^{(0)}\right] d\xi_0} \tag{3.374}$$

taking into account that $\widetilde{f}^{(0)}$ is an odd function of ξ_0 in the trapped region.

When $f_0^{(0)} = f_{0M}^{(0)} = f_M$ is a Maxwellian distribution on the magnetic flux surface ψ,

$$\mathcal{F}_t^M(\psi) = \frac{\int_0^\infty p^2 dp \int_{-\xi_{0T}}^{+\xi_{0T}} \lambda f_{0M}^{(0)} d\xi_0}{\int_0^\infty p^2 dp \int_{-1}^{+1} \lambda \left[f_{0M}^{(0)} + g_M^{(0)}\right] d\xi_0} \tag{3.375}$$

taking into account that $g_M^{(0)} = 0$ for trapped electrons. Neglecting the contribution of $g_M^{(0)}$, the zero order trapped fraction $\mathcal{F}_{t0}^M$ is given by

$$\mathcal{F}_{t0}^M(\psi) = \frac{\int_0^\infty p^2 dp \int_{-\xi_{0T}(\psi)}^{+\xi_{0T}(\psi)} \lambda f_{0M}^{(0)}(p,\psi) d\xi_0}{\int_0^\infty p^2 dp \int_{-1}^{+1} \lambda f_{0M}^{(0)}(p,\psi) d\xi_0} \tag{3.376}$$

which reduces to

$$\mathcal{F}_{t0}^M(\psi) = \frac{\int_{-\xi_{0T}(\psi)}^{+\xi_{0T}(\psi)} \lambda d\xi_0}{\int_{-1}^{+1} \lambda d\xi_0} = \frac{\int_0^{+\xi_{0T}(\psi)} \lambda d\xi_0}{\int_0^{+1} \lambda d\xi_0} \tag{3.377}$$

In this limit, $\mathcal{F}_{t0}^M$ is only a function of the geometrical magnetic configuration, while is the general case, $\mathcal{F}_t$ is a fully kinetic quantity.

Case of circular concentric flux-surfaces In that case, the normalized bounce time is simply

$$\lambda(\xi_0) = \int_{\theta_{\min}}^{\theta_{\max}} \frac{d\theta}{2\pi} \frac{\xi_0}{\xi} \simeq \frac{2}{\pi} \left[J_0(\xi_0, \xi_{0T}) - \frac{1}{2}\xi_{0T}^2 J_2(\xi_0, \xi_{0T})\right] \tag{3.378}$$

which may be expanded up to the second order with an excellent accuracy as shown in Appendix B.1. Here,

$$\xi_{0T} = \sqrt{\frac{2\epsilon}{1+\epsilon}} \tag{3.379}$$

with $\epsilon = r/R_p$ the usual inverse aspect ratio.

It is interesting to estimate the parametric dependence of $\mathcal{F}_{t0}^M$ for $\epsilon \ll 1$. For trapped particles,

$$\lambda(\xi_0) \simeq \frac{2}{\pi} \frac{|\xi_0|}{\xi_{0T}} \left[K\left(\frac{\xi_0^2}{\xi_{0T}^2}\right) - \frac{1}{2}\xi_{0T}^2 \left[K\left(\frac{\xi_0^2}{\xi_{0T}^2}\right) - E\left(\frac{\xi_0^2}{\xi_{0T}^2}\right)\right]\right] \tag{3.380}$$

where $K(x)$ and $E(x)$ are complete elliptic integrals of the first and second kind. Hence,

$$\int_0^{+\xi_{0T}(\psi)} \lambda(\xi_0)\, d\xi_0 = \frac{2\sqrt{2}}{\pi}\sqrt{\epsilon}\int_0^1 x\left[K(x) - \epsilon\left(K(x) - E(x)\right)\right] dx \tag{3.381}$$

Using the recurrence relation

$$n^2\int_0^1 x^n K(x)\, dx = (n-1)^2\int_0^1 x^{n-2}K(x)\, dx + 1 \tag{3.382}$$

and since

$$\int_0^1 xE(x)\, dx = 2/3 \tag{3.383}$$

according to formulaes (6.147) and (6.132) in Ref. [14],

$$\lim_{\epsilon\to 0}\int_0^{+\xi_{0T}(\psi)} \lambda(\xi_0)\, d\xi_0 \simeq \frac{2\sqrt{2}}{\pi}\sqrt{\epsilon}\,(1-\epsilon/3) \tag{3.384}$$

For circulating electrons,

$$\lambda(\xi_0) \simeq \frac{2}{\pi}\left[K\left(\frac{\xi_{0T}^2}{\xi_0^2}\right) - \frac{1}{2}\xi_0^2\left[K\left(\frac{\xi_{0T}^2}{\xi_0^2}\right) - E\left(\frac{\xi_{0T}^2}{\xi_0^2}\right)\right]\right] \tag{3.385}$$

and

$$\int_{+\xi_{0T}(\psi)}^1 \lambda(\xi_0)\, d\xi_0 = \frac{2\sqrt{2}}{\pi}\sqrt{\epsilon}\int_{\sqrt{2\epsilon}}^1 \left(\frac{K(x)}{x^2} + \epsilon\frac{K(x) - E(x)}{x^4}\right) dx \tag{3.386}$$

From the relation

$$\int \frac{K(x)}{x^2}dx = -\frac{E(x)}{x} \tag{3.387}$$

which is given by formula (5.112.9) of Ref. [14],

$$\begin{aligned}\int_{+\xi_{0T}(\psi)}^1 \lambda(\xi_0)\, d\xi_0 &= \frac{2\sqrt{2}}{\pi}\sqrt{\epsilon}\left(\frac{E\left(\sqrt{2\epsilon}\right)}{\sqrt{2\epsilon}} - 1\right) + \frac{2\sqrt{2}}{\pi}\epsilon\sqrt{\epsilon}\int_{\sqrt{2\epsilon}}^1 \frac{K(x) - E(x)}{x^4}dx \\ &\simeq 1 - \frac{2\sqrt{2}}{\pi}\sqrt{\epsilon} + \frac{2\sqrt{2}}{\pi}\epsilon\sqrt{\epsilon}\int_{\sqrt{2\epsilon}}^1 \frac{K(x) - E(x)}{x^4}dx\end{aligned} \tag{3.388}$$

and using the indefinite integrals

$$\int \frac{K(x) - E(x)}{x}dx = -E(x) \tag{3.389}$$

and

$$\int \frac{E(x)}{x^4}dx = \frac{1}{9x^3}\left[2(x^2-2)E(x) + \left(1-x^2\right)K(x)\right] \tag{3.390}$$

according to formulaes (5.113.1) and (5.112.12) in Ref. [14],

$$\lim_{\delta\to 0}\delta^3\int_\delta^1 \frac{K(x) - E(x)}{x^4}dx = -\frac{\delta^3}{3} + \frac{K(\delta) - E(\delta)}{3}\left(1-\delta^2\right) + \frac{\delta^2}{3}E(\delta) \simeq \frac{\pi}{4}\delta^2 \tag{3.391}$$

so that up to the first order term,

$$\int_0^1 \lambda\left(\xi_0\right) d\xi_0 \simeq 1 + \frac{\epsilon}{2} \tag{3.392}$$

Consequently,

$$\lim_{\epsilon \to 0} \mathcal{F}_{t0}^{M}\left(\psi\right) \simeq \frac{2\sqrt{2}}{\pi}\sqrt{\epsilon} \simeq 0.9\sqrt{\epsilon} \tag{3.393}$$

and the $\sqrt{\epsilon}$ dependence in the limit $\epsilon \ll 1$ is well recovered, as expected from an intuitive explanation.

It is worth noting that this result is well recovered by a simple Monte-Carlo technique, where the poloidal angle θ is taken to be a uniform random variable between 0 and 2π, as well as ξ between -1 and 1. Using the relation (2.22) which translates ξ to ξ_0 at the minimum B value, and considering that the particle is trapped when $|\xi_0| \leq \xi_{0T}$, the fraction of trapped particle found numerically is exactly $\mathcal{F}_{t0}^{M}\left(\psi\right)$, while the distribution scales like $\lambda\left(\xi_0\right)$.

It is important to precise that $\mathcal{F}_{t0}^{M}$ is not the "*effective*" trapped fraction $\mathcal{F}_{t}^{eff.}$ given by the well known relation

$$\mathcal{F}_{t}^{eff.}\left(\psi\right) = 1 - \frac{3}{4}\left\langle h^2 \right\rangle \int_0^1 \frac{x dx}{\left\langle \sqrt{1 - xh} \right\rangle} \tag{3.394}$$

found repeatedly in the litterature for the bootstrap current or the neoclassical conductivity, where $h = B/B_{max}$ and B_{max} is the maximum value of the magnetic field B along the particle trajectory. This quantity results from the reduction of the conductivity due to trapped particles, or the onset of the bootstrap current. Its expression with notations used in the text is determined from the bootstrap current calculations with the Lorentz collision operator, as shown Sec.5.6.2. It is important to notice that $\mathcal{F}_{t}^{eff.}$ is in principle not a fraction of trapped electrons, and in addition there is no demonstration that $\mathcal{F}_{t}^{eff.} \leq 1$ is always satisfied for all magnetic configurations, as mentioned clearly in Ref. [15]. In fact the denomination "*effective*" trapped fraction $\mathcal{F}_{t}^{eff.}$ is quite confusing, since it applies only for Maxwellian regime, and is not established as a kinetic quantity like $\mathcal{F}_{t0}^{M}$. This point is especially important when non-Maxwellian distributions are considered for evaluating the bootstrap current. Consequently, $\mathcal{F}_{t}^{eff.}$ must not be used in such regimes, but only $\mathcal{F}_t$ as an true physical sense for comparisons between different regimes.

3.6.8 Runaway loss rate

When the Ohmic electric field exceeds the Dreicer level, a fraction of the electron population run away. The total number of electrons is therefore no more conserved, since the flux $S_p \neq 0$ at $p = p_{\max}$, on the boundary of the integration domain. The runaway loss rate Γ_R is given by the relation

$$\Gamma_R\left(\psi, \theta\right) = \iint \mathbf{S_p}\left(\psi, p_{\max}, \xi\right) \cdot d\mathbf{S}\left(p_{\max}\right) \tag{3.395}$$

where element of surface $d\mathbf{S}(p) = p2d\xi d\varphi\widehat{p}$ according to the Appendix A. Therefore, since $\int d\varphi = 2\pi$ by symmetry, one obtains immediately

$$\Gamma_R(\psi,\theta) = 2\pi p_{\max}^2 \int_{-1}^{+1} S_p(\psi, p_{\max}, \xi)\, d\xi \tag{3.396}$$

Since all quantities are calculated at the spatial location where B is minimum, one have by definition in a straightforward manner

$$\Gamma_R^{(0)}(\psi) = 2\pi p_{\max}^2 \int_{-1}^{+1} S_p^{(0)}(\psi, p_{\max}, \xi_0)\, \lambda(\psi,\xi_0)\, d\xi_0 \tag{3.397}$$

where $S_p^{(0)}(\psi, p_{\max}, \xi_0)$ results from the solution of the bounce-averaged Fokker-Planck equation. The term $\lambda(\psi,\xi_0)$ arises from the Jacobian J_ξ.

The flux-surface averaged runaway rate $\langle\Gamma_R\rangle_V$ is given by the relation

$$\langle\Gamma_R\rangle_V(\psi) = \frac{2\pi}{\widehat{q}} p_{\max}^2 \int_0^{2\pi} \frac{d\theta}{2\pi} \frac{1}{\left|\widehat{\psi}\,.\,\widehat{r}\right|} \frac{r}{R_p} \frac{B_0(\psi)}{B_P} \int_{-1}^{+1} S_p(\psi, p_{\max}, \xi_0)\, d\xi \tag{3.398}$$

and since

$$\int_{-1}^{+1} d\xi = \int_{-1}^{+1} \Psi(\psi,\theta) \frac{\xi_0}{\xi} H\left(|\xi_0| - \sqrt{1 - \frac{1}{\Psi(\psi,\theta)}}\right) d\xi_0 \tag{3.399}$$

one obtains

$$\begin{aligned}
\langle\Gamma_R\rangle_V(\psi) &= \frac{2\pi}{\widehat{q}} p_{\max}^2 \int_{-1}^{+1} d\xi_0 \left[\frac{1}{2}\sum_\sigma\right]_T \int_{\theta_{\min}}^{\theta_{\max}} \frac{d\theta}{2\pi} \frac{1}{\left|\widehat{\psi}\,.\,\widehat{r}\right|} \frac{r}{R_p} \frac{B}{B_P} \frac{\xi_0}{\xi} S_p(\psi, p_{\max}, \xi_0) \\
&= \frac{2\pi}{\widehat{q}} p_{\max}^2 \int_{-1}^{+1} \{S_p(\psi, p_{\max}, \xi)\}\, \lambda(\psi,\xi_0)\, \widetilde{q}(\psi)\, d\xi_0 \\
&= \frac{\widetilde{q}}{\widehat{q}} 2\pi p_{\max}^2 \int_{-1}^{+1} \lambda(\psi,\xi_0)\, S_p^{(0)}(\psi, p_{\max}, \xi_0)\, d\xi_0
\end{aligned} \tag{3.400}$$

3.6.9 Magnetic ripple losses

Though magnetic ripple losses is a full $4-D$ problem, it can be considered in a simple manner by defining a super-trapped volume $V_{ST}^{\mathbf{p}}$ in momentum space,

$$V_{ST}^{\mathbf{p}}(\psi) = 2\pi \int_0^\infty p^2 dp \int_{-1}^{+1} H(p - p_c)\left(1 - H\left(|\xi_0| - \xi_{0ST}\right)\right) d\xi_0 \tag{3.401}$$

in which particle escape the plasma. A low energy, it is bounded by the collision de-trapping when $p \le p_c$, while the pitch-angle dependence results from the condition that only electrons whose banana tip enter the bad confinement region characterized by the well known criterion $\alpha^* \le 1$ are trapped in the magnetic well, in an irreversible manner. As shown in Fig. 3.1, even if this is a rather crude modeling, it captures most of the salient features of the physics. Therefore, all trapped electrons which in addition fullfils

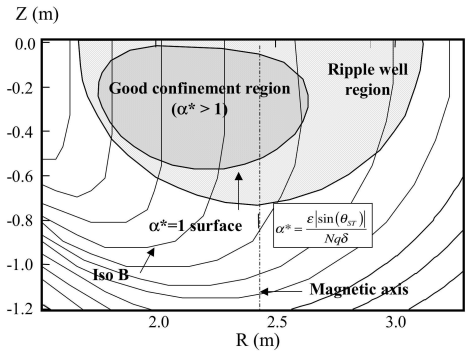

cmcm

Figure 3.1: Domain in configuration space where magnetic ripple well takes place for Tore Supra tokamak

the condition $p_{\|}/p \leq \xi_{0ST}$ are super-trapped. Here, ξ_{0ST} is deduced from the intersection between the poloidal extend of the banana and the good confinement domain $\alpha^* \geq 1$ on a given flux surface [7]. The pitch-angle threshold ξ_{0ST} depends therefore of the radial position ψ and close to the edge,

$$\lim_{\psi \to \psi_a} \xi_{0ST} = \xi_{0T} \tag{3.402}$$

which indicates that all trapped electrons are expected to escape the magnetic configuration. Furthermore, it is assumed that electrons, once in this magnetic well, do not contribute anymore to the overall momentum dynamics, which is obviously a very crude approximation.

An heuristic description of this process may be obtained by introducing a Krook term restricted to the volume $V_{ST}^{\mathbf{P}}$ in the Fokker-Planck equation

$$\left.\frac{\partial f_0^{(0)}}{\partial t}\right|_{} = \nu_{d_{ST}} f_0^{(0)}\left(\psi, p, \xi_0\right) H\left(p - p_c\right)\left(1 - H\left(|\xi_0| - \xi_{0ST}\right)\right) \tag{3.403}$$

where $\nu_{d_{ST}}^{-1}$ is the drifting time taken by super-trapped electrons for leaving the plasma. In order to reproduce the fact that super-trapped electrons are decoupled from the momentum dynamics, a simple method is to force $\nu_{d_{ST}}^{-1} \ll \tau_b$. Without detailed knowledge of the local dynamics, $\nu_{d_{ST}}$ is taken constant in $V_{ST}^{\mathbf{P}}$, which is obviously a coarse approximation. However, in the limit $\nu_{d_{ST}}^{-1} \ll \tau_b$, the shape of the distribution function becomes independent of $\nu_{d_{ST}}$, since by definition $f_0^{(0)}\left(\psi, p, \xi_0\right) \simeq 0$ in the super-trapped domain.

Obviously, when a Krook term is introduced, the Fokker-Planck equation is no more conservative, since a fraction of fast electrons is definitively leaving the plasma . Assuming the particle loss rate is small, a steady-state solution may be found, provided some external source of electron is added, in order to keep the density locally constant. This important point is discussed in Sec.5.7.1. The new form of the bounce-averaged Fokker-Planck equation is

$$\frac{\partial f_0^{(0)}}{\partial t} + \nabla_{(\psi,p,\xi_0)} \cdot \mathbf{S}^{(0)} + \nu_{d_{ST}} f_0^{(0)} H\left(p - p_c\right)\left(1 - H\left(|\xi_0| - \xi_{0ST}\right)\right) = 0 \tag{3.404}$$

and in this stationnary limit $\lim_{t\to\infty} \partial f_0^{(0)}/\partial t = 0$,

$$\nabla_{(\psi,p,\xi_0)} \cdot \mathbf{S}^{(0)} = -\nu_{d_{ST}} f_0^{(0)} H\left(p - p_c\right)\left(1 - H\left(|\xi_0| - \xi_{0ST}\right)\right) \tag{3.405}$$

Losses are assumed to be mainly local, since they occur on a very short time scale as compared to the fast electron transport one. Therefore, only the momentum dynamics is considered, and integrating equation (3.405), one obtains

$$\begin{aligned} &\iiint_{V_{ST}^{\mathbf{p}}} \nabla_{(p,\xi_0)} \cdot \mathbf{S}_{\mathbf{p}}^{(0)} J_p J_{\xi_0} dp d\xi_0 d\varphi \\ &= -\iiint_{V_{ST}^{\mathbf{p}}} \nu_{d_{ST}} f_0^{(0)} H\left(p - p_c\right)\left(1 - H\left(|\xi_0| - \xi_{0ST}\right)\right) J_p J_{\xi_0} dp d\xi_0 d\varphi \end{aligned} \tag{3.406}$$

where J_p and J_{ξ_0} are the Jacobians as defined in Sec. 3.5.1. The magnetic ripple loss rate $\Gamma_{ST}^{(0)}(\psi)$ on the B_0 axis is simply given by

$$\Gamma_{ST}^{(0)}(\psi) = \iiint_{V_{ST}^{\mathbf{p}}} \nu_{d_{ST}} f_0^{(0)} H\left(p - p_c\right)\left(1 - H\left(|\xi_0| - \xi_{0ST}\right)\right) J dp d\xi_0 d\varphi \tag{3.407}$$

or

$$\Gamma_{ST}^{(0)}(\psi) = 2\pi \int_{p_c}^{p_{\max}} p^2 dp \int_{-\xi_{0ST}}^{+\xi_{0ST}} \nu_{d_{ST}} f_0^{(0)} \lambda\left(\psi, \xi_0\right) d\xi_0 \tag{3.408}$$

since $\int d\varphi = 2\pi$.

An equivalent form can be deduced from the flux of particle leaving the integration domain,

$$\begin{aligned} \Gamma_{ST}^{(0)}(\psi) &= \iiint_{V_{ST}^{\mathbf{p}}} \nabla_{(p,\xi_0)} \cdot \mathbf{S}_{\mathbf{p}}^{(0)} J_p J_{\xi_0} dp d\xi_0 d\varphi \\ &= \iint_{S_{ST}^{\mathbf{p}}} \mathbf{S}_{\mathbf{p}}^{(0)} \cdot d\mathbf{S} \end{aligned} \tag{3.409}$$

using the Green-Ostrogradsky theorem, where $S_{ST}^{\mathbf{p}}$ is the surface that encloses volume $V_{ST}^{\mathbf{p}}$. as shown in Fig. 3.1, $S_{ST}^{\mathbf{p}}$ may be split into two terms corresponding to coordinate surfaces

$$S_{ST}^{\mathbf{p}} = S_{ST,p}^{\mathbf{p}} + S_{ST,\xi}^{\mathbf{p}} \tag{3.410}$$

where $S^{\mathbf{p}}_{ST,p}$ is the surface at constant p, while $S^{\mathbf{p}}_{ST,\xi_0}$ is the surface at constant ξ_0 . Therefore, for the surface $S^{\mathbf{p}}_{ST,p}$,

$$\mathbf{S}^{(0)}_{\mathbf{p}} \cdot d\mathbf{S}\Big|_{S^{\mathbf{p}}_{ST,p}} = S^{(0)}_p p^2 \lambda\left(\psi,\xi_0\right) d\xi_0 d\varphi \tag{3.411}$$

$$\mathbf{S}^{(0)}_{\mathbf{p}} \cdot d\mathbf{S}\Big| S^{\mathbf{p}}_{ST,\xi_0} = -\, S^{(0)}_{\xi_0} p\lambda\left(\psi,\xi_0\right) \sqrt{1-\xi_0^2}\, dp d\varphi \tag{3.412}$$

according to the differential relations in Appendix A. One obtains finaly

$$\Gamma^{(0)}_{ST}\left(\psi\right) = 2\pi p_c^2 \int_{-\xi_{0ST}}^{+\xi_{0ST}} \lambda\left(\psi,\xi_0\right) S^{(0)}_p d\xi_0 + 4\pi\lambda\left(\psi,+\xi_{0ST}\right)\sqrt{1-\xi_{0ST}^2}\int_{p_c}^{p_{\max}} p S^{(0)}_{\xi_0} dp \tag{3.413}$$

since the flux $S^{(0)}_{\xi_0}$ is a symmetric function of ξ_0.

3.6.10 Non-thermal bremsstrahlung

Several other moments of the electron distribution function may be calculated, mainly for diagnosing purposes of the plasma performances. In most cases, the local value of the distribution function f must be determined not only at different plasma radius, but also at various poloidal positions. In that case, the problem is $4-D$, since its shape is function also of the poloidal position on a given flux surface ψ. A good example is the calculation of the non-thermal bremsstrahlung [8], which requires the exact shape of the distribution function f at each plasma position along the lines-of-sight, as well as the local angle between the magnetic field line direction $\widehat{s}$ and the direction of observation $\widehat{d}$.

The number of counts N_{E_0} that is recorded by a photon detection system in the energy range $E_0 \pm \Delta E$ between times $t_{\min}$ and $t_{\max}$ is given by the integral

$$N_{E_0} = \int_{t_{\min}}^{t_{\max}} dt \int_{E_0-\Delta E}^{E_0+\Delta E} \frac{dN_E\left(t,E\right)}{dtdE} dE \tag{3.414}$$

where $dN_E\left(t\right)/dtdE$ is the measured photon energy spectrum. Its relation to the effective photon energy spectrum $dN_k\left(t\right)/dkdt$ emitted by the plasma in the direction of the detector may be expressed as

$$\frac{dN_E\left(t,E\right)}{dtdE} = \int_0^{\infty} \eta_A\left(k\right)\left(1-\eta_D\left(k\right)\right) G\left(k,E\right) \frac{dN_k\left(t,k\right)}{dtdk} dk \tag{3.415}$$

where $G\left(k,E\right)$ is the normalized instrumental response function,

$$\int_0^{\infty} G\left(k,E\right) dk = 1 \tag{3.416}$$

which gives the overall broadening of the energy spectrum, $\eta_A\left(k\right)$ the fraction of photons that transmitted rather than being absorbed by various objects along the line-of-sight between the plasma and the detector, and finally, $1-\eta_D\left(k\right)$ the fraction that are effectively stopped inside the active part of the photon detector. For most detection systems, $G\left(k,E\right)$ is a complicated function, that is usualy determined experimentaly with monoenergetic

photon sources. It incorporates the photoelectric conversion process that may be usualy modeled by a Gaussian shape around the photon energy k whose half-width depends of the type of detector, and the Compton scattering by electrons, which can be approximately described by a Fermi-like function[1].

Since the plasma is an extended source of photons, all contributions inside the volume ΔV viewing the detector with a solid angle $\Delta\Omega$ must be added

$$\frac{dN_k\left(t,k\right)}{dtdk}=\int_{\Delta V(k)}dV\int_{\Delta\Omega(k)}\frac{dN_k\left(t,k,\mathbf{X},\widehat{b}\cdot\widehat{d}\right)}{dtdkdVd\Omega}d\Omega \tag{3.417}$$

taking into account that photon plasma emissivity depends not only of the plasma position $\mathbf{X}$ (inhomogeneity) but also of the angle $\widehat{b}\cdot\widehat{d}$ between the directions of the magnetic field line $\widehat{b}_{\mathbf{X}}$ and the line-of-sight $\widehat{d}$ at $\mathbf{X}$ (anisotropy that results from relativistic effects). In principle, both $\Delta V\left(k\right)$ and $\Delta\Omega\left(k\right)$ are functions of the photon energy, because of the partial transparency of the collimating aperture with k. However, the design of the diaphragm is usualy optimized so that this effect can be neglected.

In the limit where the aperture of the diaphragm is small, so that variation of the photon emissivity transverse to the line-of-sight may be neglected in the field of observation, $dN_k\left(t,k\right)/dtdk$ may be approximated by the simple sum

$$\frac{dN_k\left(t,k\right)}{dtdk}\simeq\int_{l_{\min}}^{l_{\max}}\mathcal{G}_{\mathcal{D}}\frac{dn_k\left(t,k,\mathbf{X},\widehat{b}\cdot\widehat{d}\right)}{dtdkd\Omega}dl \tag{3.418}$$

where $L_c=l_{c\max}-l_{c\min}$ is the chord length in the plasma, and $\mathcal{G}_{\mathcal{D}}$ is a geometrical factor that is independent of the position l_c along the line-of-sight[2]. Here, $n_k=dN_k/dV$ is the photon density. By definition, the determination of $dN_k\left(t,k\right)/dtdk$ requires to evaluate $\mathbf{X}$ and $\widehat{\iota}_{\mathbf{X}}\cdot\widehat{d}$ as a function of l for a given magnetic equilibrium. Since magnetic flux surfaces are nested in tokamaks inside the separatrix, the calculation requires the determination of $\psi\left(l_c\right)$, $\theta\left(l_c\right)$ and $\widehat{b}\cdot\widehat{d}=\cos\theta_d\left(l_c\right)$.

In the appropriate range of energy, the photon density energy spectrum results from the bremsstrahlung process only[3]. It is the sum of two contributions, one arising from

[1]The broadening that results of Compton scattering depends not only of the types of atoms of which is made the detector, but also its shape. It is usually given by Monte-carlo codes that describe the instrumental configuration in a realistic manner

[2]It can be shown that the geometrical factor $\mathcal{G}_{\mathcal{D}}$ may be roughly expressed as

$$\mathcal{G}_{\mathcal{D}}\simeq\frac{s_Ds_d}{l_{Dd}}$$

where s_d and s_D are the surfaces of the diaphragm and the detector perpendicular to the line-of-sight, and l_{Dd} is the distance between the intersections of s_d and s_D with the chord axis.

[3]This is the well known free-free radiation process which predominates for photon energies k much larger than the fundamental Rydberg state Z^2I_H of the heaviest impurity in the plasma, where $I_H\simeq13.6eV$ is the fundamental Rydberg state of hydrogen. For the carbon, $Z=6$ and the condition is $k\gg0.5keV$, while for iron with $Z=26$, it is $k\gg9keV$. At lower energies, one must therefore consider the free-bound radiation process.

electron-ion interactions, the other resulting from electron self-collisions

$$\frac{dn_k\left(t,k,\mathbf{X},\widehat{b}\cdot\widehat{d}\right)}{dtdkd\Omega}=\sum_s\frac{dn_k^{ei}\left(t,k,\mathbf{X},\widehat{b}\cdot\widehat{d},Z_s\right)}{dtdkd\Omega}+\frac{dn_k^{ee}\left(t,k,\mathbf{X},\widehat{b}\cdot\widehat{d}\right)}{dtdkd\Omega} \tag{3.419}$$

which are related to the respective bremsstrahlung differential cross-sections $d\sigma_{ei}/dtdkd\Omega$ and $d\sigma_{ee}/dtdkd\Omega$ by the relations

$$\frac{dn_k^{ei}\left(t,k,\mathbf{X},\widehat{b}\cdot\widehat{d},Z_s\right)}{dtdkd\Omega}=n_s\left(t,\psi\right)\iiint d^3\mathbf{p}\frac{d\sigma_{ei}\left(k,p,\widehat{k}\cdot\widehat{p},Z_s\right)}{dtdkd\Omega}vf\left(t,\mathbf{X},\mathbf{P}\right) \tag{3.420}$$

$$\frac{dn_k^{ee}\left(t,k,\mathbf{X},\widehat{b}\cdot\widehat{d}\right)}{dtdkd\Omega}=n_e\left(t,\psi\right)\iiint d^3\mathbf{p}\frac{d\sigma_{ee}\left(k,p,\widehat{k}\cdot\widehat{p}\right)}{dtdkd\Omega}vf\left(t,\mathbf{X},\mathbf{P}\right) \tag{3.421}$$

where Z_s is the number of protons for the impurity of type s[4], whose density on the flux surface ψ at time t is $n_s\left(t,\psi\right)$. The velovity v is the velocity of test partcles, in accordance with the definition of the cross-sections. Here $\cos\chi=\widehat{k}\cdot\widehat{p}$ is the cosine of the angle between directions of the incident electron of momentum p and the emitted photon of energy k. If one defines the angles $\xi=\cos\theta_e=\widehat{b}\cdot\widehat{p}$ and $\cos\theta_d=\widehat{b}\cdot\widehat{d}$, the angle relation between χ, θ_e and θ_d is

$$\cos\chi=\cos\theta_e\cos\theta_d+\sin\theta_e\sin\theta_d\cos\varphi \tag{3.422}$$

as shown in Fig. 3.2.

It is possible to take advantage of the azimuthal symmetry of the distribution function around the field line direction as well as the relations between angles χ, θ_e and θ_d using projection on Legendre polynomials, in order to reduce the required number of integrations. The numerical accuracy for the determination of $dn_k/dtdkd\Omega$ may be then greatly enhanced, while the computational time strongly reduced. Let define the series for a function $h\left(x\right)$

$$h\left(x\right)=\sum_{l=0}^{\infty}\left(m+1/2\right)h^{(m)}P_l\left(x\right) \tag{3.423}$$

where coefficients $h^{(m)}$

$$h^{(m)}=\int_{-1}^{+1}h\left(x\right)P_m\left(x\right)dx \tag{3.424}$$

and P_m is the Legendre polynomial of degree m.

[4]For a plasma with a single fully ionized impurity, the fast electron bremsstrahlung may be determined using the effective charge Z_{eff}, from which $n_s\left(\psi\right)$ may be evaluated, as shown in Sec. ***. However, when heavy impurities partially ionized are present in the plasma, their densities $n_s\left(\psi\right)=\sum_{s'}n_{ss'}\left(\psi\right)$ must be determined from an impurity transport code, which gives the contribution of all different states. Indeed, when kinetic energies of the fast electrons are much larger than the fundamental Rydberg state, only the charge state of the nucleus must be considered for the bremsstrahlung calculations, since screening effects with bounded electrons is negligible.

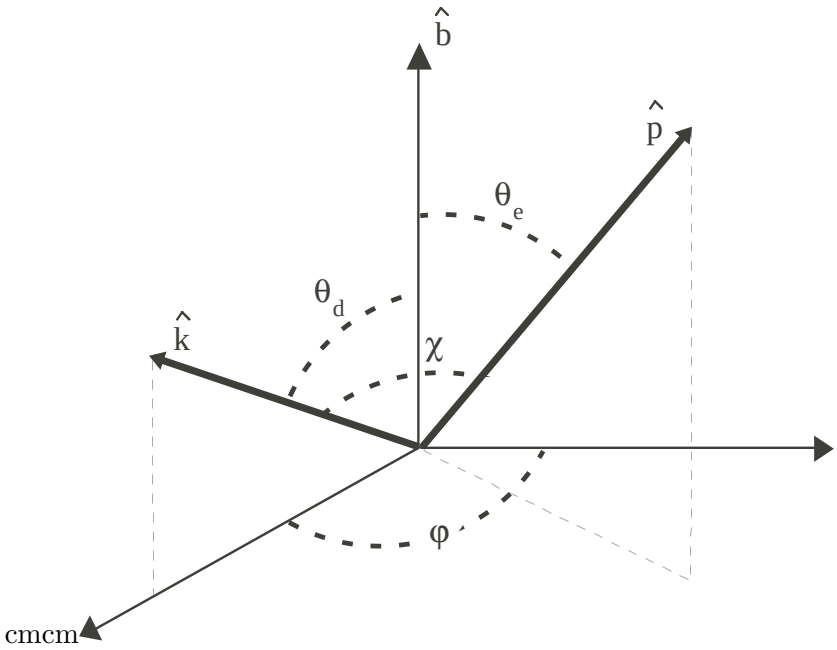

Figure 3.2: Directions of incident electron and emitted photon with respect to the local magnetic field direction

Applying the Legendre polynomial series to differential cross-sections $d\sigma^{ei}/dtdkd\Omega$ and $d\sigma^{ee}/dtdkd\Omega$ and to $f\left(t,\mathbf{X},p,\xi\right)$,

$$\frac{dn_k^{ei}\left(t,k,\mathbf{X},\widehat{b}\cdot\widehat{d},Z_s\right)}{dtdkd\Omega}=n_s\left(t,\psi\right)\int_0^\infty vp^2dp\int_0^{2\pi}d\varphi\int_{-1}^{+1}d\xi\times$$
$$\sum_{m=0}^{\infty}\sum_{m'=0}^{\infty}\left(m+1/2\right)\left(m'+1/2\right)\frac{d\sigma_{ei}^{(m)}\left(k,p,Z_s\right)}{dtdkd\Omega}\times$$
$$f^{(m)}\left(t,\mathbf{X},p\right)P_m\left(\cos\chi\right)P_{m'}\left(\xi\right) \tag{3.425}$$

where

$$\frac{d\sigma_{ei}^{(m)}\left(k,p,Z_s\right)}{dtdkd\Omega}=\int_{-1}^{+1}\frac{d\sigma_{ei}^{(m)}\left(k,p,\widehat{k}\cdot\widehat{p},Z_s\right)}{dtdkd\Omega}P_m\left(\widehat{k}\cdot\widehat{p}\right)d\left(\cos\chi\right) \tag{3.426}$$

and

$$f^{(m')}\left(t,\mathbf{X},p\right)=\int_{-1}^{+1}f\left(t,\mathbf{X},p,\xi\right)P_{m'}\left(\xi\right)d\xi \tag{3.427}$$

one obtains

$$\frac{dn_k^{ei}\left(t,k,\mathbf{X},\widehat{b}\cdot\widehat{d},Z_s\right)}{dtdkd\Omega}=n_s\left(t,\psi\right)\int_0^\infty vp^2dp\sum_{m=0}^{\infty}\sum_{m'=0}^{\infty}\left(m+1/2\right)\left(m'+1/2\right)\times$$
$$\frac{d\sigma_{ei}^{(m)}\left(k,p,Z_s\right)}{dtdkd\Omega}f^{(m')}\left(t,\mathbf{X},p\right)\times$$
$$\int_0^{2\pi}d\varphi\int_{-1}^{+1}d\xi P_m\left(\cos\chi\right)P_{m'}\left(\xi\right) \tag{3.428}$$

Using the well known sum relation for the Legendre polynomials that holds for angle relation between χ, θ_e and θ_d,

$$P_m\left(\cos\chi\right)=P_m\left(\cos\theta_d\right)P_l\left(\xi\right)+2\sum_{n=m}^{n=m}\frac{(m-n)!}{(m+n)!}P_m^n\left(\cos\theta_d\right)P_m^n\left(\xi\right)\cos\left(n\varphi\right) \tag{3.429}$$

where $P_m^n\left(x\right)$ is the associated Legendre function of degree m and order n, expression (3.428) becomes

$$\frac{dn_k^{ei}\left(t,k,\mathbf{X},\widehat{b}\cdot\widehat{d},Z_s\right)}{dtdkd\Omega}=n_s\left(t,\psi\right)\int_0^\infty vp^2dp\sum_{m=0}^{\infty}\sum_{m'=0}^{\infty}\left(m+1/2\right)\left(m'+1/2\right)\times$$
$$\frac{d\sigma_{ei}^{(m)}\left(k,p,Z_s\right)}{dtdkd\Omega}f^{(m')}\left(t,\mathbf{X},p\right)\int_0^{2\pi}d\varphi\times$$
$$\int_{-1}^{+1}P_m\left(\cos\theta_d\right)P_m\left(\xi\right)P_{m'}\left(\xi\right)d\xi \tag{3.430}$$

since

$$2\int_0^{2\pi}d\varphi\int_{-1}^{+1}\sum_{n=m}^{n=m}\frac{(m-n)!}{(m+n)!}P_m^n\left(\cos\theta_d\right)P_m^n\left(\xi\right)\cos\left(n\varphi\right)d\xi=0 \tag{3.431}$$

after permutation of integrals over ξ and φ. Using finally the orthogonality relation

$$\int_{-1}^{+1}P_m\left(x\right)P_{m'}\left(x\right)dx=\frac{\delta_{mm'}}{m+1/2} \tag{3.432}$$

where $\delta_{mm'}$ is the Kronecker symbol, one obtains the simple relation

$$\frac{dn_k^{ei}\left(t,k,\mathbf{X},\widehat{b}\cdot\widehat{d},Z_s\right)}{dtdkd\Omega}=2\pi n_s\left(t,\psi\right)\int_0^\infty vp^2dp\sum_{m=0}^{\infty}\left(m+1/2\right)\times$$
$$\frac{d\sigma_{ei}^{(m)}\left(k,p,Z_s\right)}{dtdkd\Omega}f^{(m)}\left(t,\mathbf{X},p\right)P_m\left(\widehat{b}\cdot\widehat{d}\right) \tag{3.433}$$

or

$$\frac{dn_k^{ei}\left(t,k,\mathbf{X},\widehat{b}\cdot\widehat{d},Z_s\right)}{dtdkd\Omega}=2\pi n_s\left(t,\psi\right)\sum_{m=0}^{\infty}\left(m+1/2\right)\times$$
$$P_m\left(\widehat{b}\cdot\widehat{d}\right)\int_0^\infty vp^2\frac{d\sigma_{ei}^{(m)}\left(k,p,Z_s\right)}{dtdkd\Omega}f^{(m)}\left(t,\mathbf{X},p\right)dp \tag{3.434}$$

A similar expression may be obtained for the e-e bremsstrahlung, and the total bremsstrahlung is then

$$\frac{dn_k\left(t,k,\mathbf{X},\widehat{b}\cdot\widehat{d}\right)}{dtdkd\Omega}=\sum_{m=0}^{\infty}\left(m+1/2\right)I_B^{(m)}\left(t,\mathbf{X},p,k\right)P_m\left(\widehat{b}\cdot\widehat{d}\right) \tag{3.435}$$

where the bremsstrahlung function $I_B^{(m)}\left(t,\mathbf{X},p,k\right)$ is

$$I_B^{(m)}\left(t,\mathbf{X},p,k\right)=2\pi\int_0^{\infty}vp^2f^{(m)}\left(t,\mathbf{X},p\right)\left[\sum_s n_s\left(t,\mathbf{X}\right)\frac{d\sigma_{ei}^{(m)}\left(k,p,Z_s\right)}{dtdkd\Omega}\,dp\right.$$
$$\left.+n_e\left(t,\mathbf{X}\right)\frac{d\sigma_{ee}^{(m)}\left(k,p\right)}{dtdkd\Omega}\right]dp \tag{3.436}$$

and the densitites $n_s\left(t,\mathbf{X}\right)=n_s\left(t,\psi\right)$ and $n_e\left(t,\mathbf{X}\right)=n_e\left(t,\psi\right)$ are considered to be uniform on a magnetic flux surface ψ.

With this formulation, bremsstrahlung emission may be determined for any direction of observation with the same numerical accuracy. Indeed, the projection of the distribution function and the differential cross-sections over the Legendre polynomial basis is equivalent to determine their value for all azimuthal directions. It is then only necessary to select the interesting direction that is given by the local $\widehat{b}\cdot\widehat{d}$ value, which depends of the local instrumental arrangement, but also of the magnetic equilibrium. This formulation is particularly convenient when the instrument is made of different chords with different orientations. It is not only important for tangential observation of the plasma, but also for perpendicular ones, since $\widehat{b}\cdot\widehat{d}$ evolves with ψ as a consequence of the local magnetic shear. Moreover, this method offer the advantage to evaluate $d\sigma_{ei}^{(m)}\left(k,p,Z_s\right)/dtdkd\Omega$ and $d\sigma_{ee}^{(m)}\left(k,p,Z_s\right)/dtdkd\Omega$ only once for various distribution functions, a procedure which may save considerably computer time consumption when the distribution function and the plasma equilibrium, i.e. $\widehat{b}\cdot\widehat{d}$ evolves with the time t.

From expression (3.435), it is also possible to extract interesting local quantities about the bremsstrahlung, like the mean radiation level in all directions of the configuration space $dn_k^{4\pi}\left(t,k,\mathbf{X}\right)/dtdkd\Omega$

$$\frac{dn_k^{4\pi}\left(t,k,\mathbf{X}\right)}{dtdkd\Omega}=\frac{1}{4\pi}\int\frac{dn_k\left(t,k,\mathbf{X},\cos\theta_d\right)}{dtdkd\Omega}d\Omega$$
$$=\frac{1}{4\pi}\int_0^{\pi}d\theta_d\int_{-\pi}^{\pi}\sin\theta_d d\varphi_d\frac{dn_k\left(t,k,\mathbf{X},\cos\theta_d\right)}{dtdkd\Omega} \tag{3.437}$$
$$=\frac{1}{2}\int_{-1}^{1}d\xi_d\frac{dn_k\left(t,k,\mathbf{X},\xi_d\right)}{dtdkd\Omega} \tag{3.438}$$
$$=\frac{1}{2}\sum_{m=0}^{\infty}\left(m+1/2\right)I_B^{(m)}\left(t,\mathbf{X},p,k\right)\int_{-1}^{1}d\xi_d P_m\left(\xi_d\right) \tag{3.439}$$

and since $P_0\left(x\right)=1$, using the orthogonality relation (3.432), one obtains

$$\frac{dn_k^{4\pi}\left(t,k,\mathbf{X}\right)}{dtdkd\Omega}=\frac{1}{2}I_B^{(m=0)}\left(t,\mathbf{X},p,k\right) \tag{3.440}$$

Much in the same way, the local anisotropy of the photon emission $R_B(t,k,\mathbf{X})$ may be evaluated from the ratio between the forward emission corresponding to $\cos\theta_d = 1$ and the perpendicular one corresponding to $\cos\theta_d = 0$.

The determination of $I_B^{(m)}(t,\mathbf{X},p,k)$ requires to evaluate the projection of the electron distribution function given by the electron drift kinetic equation, at all $\mathbf{X}$ positions.[5] Since the magnetic configuration is a toroidaly symmetric, only the radial ψ and poloidal θ positions are necessary, and therefore $f(t,\mathbf{X},p,\xi) = f(t,\psi,\theta,p,\xi)$. Since $f^{(m)}(t,\mathbf{X},p)$ is a linear function of $f(t,\psi,\theta,p,\xi)$, it may be split into the three contributions, namely

$$\begin{aligned} f^{(m)}(t,\mathbf{X},p) &= f_0^{(m)}(t,\mathbf{X},p) + f_1^{(m)}(t,\mathbf{X},p) \\ &= f_0^{(m)}(t,\mathbf{X},p) + \widetilde{f}^{(m)}(t,\mathbf{X},p) + g^{(m)}(t,\mathbf{X},p) \end{aligned} \tag{3.441}$$

where $f_0^{(m)}(t,\mathbf{X},p)$ are the Legendre coefficients for the zero order distribution function f_0, while $f_1^{(m)}(t,\mathbf{X},p)$ correspond to the first order distribution function f_1.

Like for other moments of the distribution function, starting from the angular relation

$$\xi_0 = \sigma\sqrt{1 - \frac{1}{\Psi(\psi,\theta)}\left(1-\xi^2\right)} \tag{3.442}$$

and using the relation $\xi d\xi = \Psi(\psi,\theta)\,\xi_0 d\xi_0$, one obtains for the zero order distribution function $f_0^{(0)}$

$$\begin{aligned} f_0^{(m)}(t,\mathbf{X},p) &= \int_{-1}^{+1} f_0(t,\psi,\theta,p,\xi)\,P_m(\xi)\,d\xi \\ &= \Psi(\psi,\theta)\int_{-1}^{+1} f_0^{(0)}(t,\psi,p,\xi_0)\,\frac{\xi_0}{\xi}\times \\ &\quad H\left(|\xi_0| - \sqrt{1-\frac{1}{\Psi(\psi,\theta)}}\right) P_m(\xi)\,d\xi_0 \end{aligned} \tag{3.443}$$

since f_0 is constant along a magnetic field line, i.e. $f_0(t,\psi,\theta,p,\xi) = f_0^{(0)}(t,\psi,p,\xi_0)$. Here the Heaviside function H indicates that only electrons who reach the poloidal position θ must be considered. By expanding part of the integrand in (3.443) as a series of Legendre polynomials, according to the relation

$$\frac{\xi_0}{\xi}H\left(|\xi_0| - \sqrt{1-\frac{1}{\Psi(\psi,\theta)}}\right)P_l(\xi) = \sum_{m'=0}^{\infty}\left(m'+1/2\right)c_m^{(m')}(\psi,\theta)\,P_{m'}(\xi_0) \tag{3.444}$$

with

$$c_m^{(m')}(\psi,\theta) = \int_{-1}^{+1}\frac{\xi_0}{\xi}H\left(|\xi_0| - \sqrt{1-\frac{1}{\Psi(\psi,\theta)}}\right)P_m(\xi)\,P_{m'}(\xi_0)\,d\xi_0 \tag{3.445}$$

[5] In presence of magnetic ripple, the local field line direction $\widehat{b}$ must be carefuly taken into account when the direction of observation does not lie exactly in a poloidal cross-section of the plasma.

one obtains finaly

$$f_0^{(m)}(t,\mathbf{X},p)=\Psi(\psi,\theta)\sum_{m'=0}^{\infty}\left(m'+1/2\right)c_m^{(m')}(\psi,\theta)\int_{-1}^{+1}f_0^{(0)}(t,\psi,p,\xi_0)\,P_{m'}(\xi_0)\,d\xi_0 \tag{3.446}$$

or

$$f_0^{(m)}(t,\mathbf{X},p)=\Psi(\psi,\theta)\sum_{m'=0}^{\infty}\left(m'+1/2\right)c_m^{(m')}(\psi,\theta)\,f_0^{(0)(m')}(t,\psi,p) \tag{3.447}$$

where

$$f_0^{(0)(m')}(t,\psi,p)=\int_{-1}^{+1}f_0^{(0)}(t,\psi,p,\xi_0)\,P_{m'}(\xi_0)\,d\xi_0 \tag{3.448}$$

For the first order distribution function, $f_1=\widetilde{f}+g$, since g is constant is constant along a field line, its contribution is the same as for f_0. Because $\widetilde{f}$ has an explicit dependence upon θ, which is given by relation (3.280),

$$\begin{aligned}\widetilde{f}^{(m)}(t,\mathbf{X},p)&=\int_{-1}^{+1}\widetilde{f}\,(t,\psi,\theta,p,\xi)\,P_m(\xi)\,d\xi\\&=\int_{-1}^{+1}\widetilde{f}^{(0)}(t,\psi,p,\xi_0)\,H\left(|\xi_0|-\sqrt{1-\frac{1}{\Psi(\psi,\theta)}}\right)P_m(\xi)\,d\xi_0\end{aligned} \tag{3.449}$$

If

$$H\left(|\xi_0|-\sqrt{1-\frac{1}{\Psi(\psi,\theta)}}\right)P_m(\xi)=\sum_{m'=0}^{\infty}\left(m'+1/2\right)\widetilde{c}_m^{(m')}(\psi,\theta)\,P_{m'}(\xi_0) \tag{3.450}$$

with

$$\widetilde{c}_m^{(m')}(\psi,\theta)=\int_{-1}^{+1}H\left(|\xi_0|-\sqrt{1-\frac{1}{\Psi(\psi,\theta)}}\right)P_m(\xi)\,P_{m'}(\xi_0)\,d\xi_0 \tag{3.451}$$

then expression (3.449) becomes

$$\widetilde{f}^{(m)}(t,\mathbf{X},p)=\sum_{m'=0}^{\infty}\left(m'+1/2\right)\widetilde{c}_m^{(m')}(\psi,\theta)\int_{-1}^{+1}\widetilde{f}^{(0)}(t,\psi,p,\xi_0)\,P_{m'}(\xi_0)\,d\xi_0 \tag{3.452}$$

Since

$$\widetilde{f}^{(0)(m')}(t,\psi,p)=\int_{-1}^{+1}\widetilde{f}^{(0)}(t,\psi,p,\xi_0)\,P_{m'}(\xi_0)\,d\xi_0 \tag{3.453}$$

one obtains finaly

$$\widetilde{f}^{(m)}(t,\mathbf{X},p)=\sum_{m'=0}^{\infty}\left(m'+1/2\right)\widetilde{c}_m^{(m')}(\psi,\theta)\,\widetilde{f}^{(0)(m')}(t,\psi,p) \tag{3.454}$$

It is interesting to notice that the determination of the $f^{(m)}(t, \mathbf{X}, p)$ does not require the explicit evaluation of the distribution function $f(t, \mathbf{X}, p, \xi)$ at all poloidal positions, and only its value at $B_{\min}$ is needed for the $4-D$ problem that is represented by the bremsstrahlung. This result which is a direct consequence of the weak collisional or "banana" regime, is very important for the numerical evaluation. Indeed, all the physics of the trapped-passing electrons is incorporated in the coefficients $f^{(m)}(t, \mathbf{X}, p)$, while the contribution arising from magnetic field line helicity is independently described by $\cos\theta_d = \widehat{b} \cdot \widehat{d}$.

Chapter 4

Detailed description of physical processes

4.1 Collisions

4.1.1 Linearized collision operator

The collision operator used in the calculations may be expressed as

$$\mathcal{C}(f) = \sum_s \sum_{s'} C(f, f_{ss'}) + C(f, f) \tag{4.1}$$

where $\sum_s \sum_{s'} C(f, f_{ss'})$ describe interactions between electrons and ions of species s in the ionization state s' and $C(f, f)$ is the self-collision contribution, as discussed in Ref. [16]. For the electron-ion collisions, it is considered that $f_{ss'}$ is a Maxwellian distribution function, the corresponding temperature being $T_{ss'}$. In the application of the code here foreseen, including RF heating and current drive, collisions dominate thermal particles, and therefore the distribution function f may be expanded about the Maxwellian f_M according to the relation

$$f \simeq f_M + \delta f \tag{4.2}$$

The self-collision operator $C(f, f)$ may be consequently approximated by its linearized form

$$C(f, f) \simeq C(f, f_M) + C(f_M, f) \tag{4.3}$$

where the the relation $C(f_M, f_M) = 0$ has been used, and terms of order δf^2 have been ignored. It can be shown that the operator $C(f, f_M)$ may be computed as $C(f, f_{ss'})$ and expressed in a conservative form

$$\sum_s \sum_{s'} C(f, f_{ss'}) + C(f, f_M) \rightarrow \nabla_{\mathbf{p}} \cdot \mathbf{S}_{\mathbf{p}}(f) \tag{4.4}$$

where component S_p and S_ξ of the flux $\mathbf{S_p}$ are

$$S_p = -D_{pp}\frac{\partial f_0}{\partial p} + \frac{\sqrt{1-\xi^2}}{p}D_{p\xi}\frac{\partial f_0}{\partial \xi} + F_p f_0 \tag{4.5}$$

$$S_\xi = -D_{\xi p}\frac{\partial f_0}{\partial p} + \frac{\sqrt{1-\xi^2}}{p}D_{\xi\xi}\frac{\partial f_0}{\partial \xi} + F_\xi f_0 \tag{4.6}$$

In the standard notations,

$$\begin{cases} D_{pp} = A(\psi, p) \\ D_{p\xi} = 0 \\ D_{\xi p} = 0 \\ D_{\xi\xi} = B_t(\psi, p) \end{cases} \tag{4.7}$$

and

$$\begin{cases} F_p = F(\psi, p) \\ F_\xi = 0 \end{cases} \tag{4.8}$$

The term $C(f_M, f)$ requires is specific treatment. By expanding f as a sum of Legendre harmonics according to the relation

$$f(t, \mathbf{X}, p, \xi) = \sum_{m=0}^{\infty} (m + 1/2) f^{(m)}(t, \mathbf{X}, p) P_m(\xi) \tag{4.9}$$

with

$$f^{(m)}(t, \mathbf{X}, p) = \int_{-1}^{+1} f(t, \mathbf{X}, p, \xi) P_m(\xi) d\xi \tag{4.10}$$

one obtains

$$C(f_M, f) = \sum_{m=0}^{\infty} (m + 1/2) C\left(f_M, f^{(m)}(t, \mathbf{X}, p) P_m(\xi)\right) \tag{4.11}$$

By definition, $f^{(m=0)}(t, \mathbf{X}, p) \simeq f_M$ and, since $P_0(\xi) = 1$,

$$C\left(f_M, f^{(m=0)}(t, \mathbf{X}, p) P_0(\xi)\right) \simeq C(f_M, f_M) = 0,$$

The first non-zero term in the series is then kept, so that

$$C(f_M, f) \simeq C\left(f_M, \frac{3}{2}\xi f^{(m=1)}(t, \mathbf{X}, p)\right) \tag{4.12}$$

since $P_1(\xi) = \xi$. By construction the linearized electron-electron collision operator conserves momentum, but not energy, so there is no need to introduce an energy loss term in the kinetic equation. Since $f^{(m=1)}$ is an integral of f, the term $C(f_M, f)$ introduce a non-linear dependence in the Fokker-Planck or drift kinetic equation. However, even if it is crucial for the current drive problem, including the determination of the boostrap current level, this non-linearity remains weak, so that the rate of convergence towards the solution of the kinetic equation is not significantly affected, even if this term is treated

explicitely, regarding the time scheme. For the calculations, the notation used in Ref. [17] is considered, and

$$\begin{aligned} C\left(f_M, \frac{3}{2}\xi f^{(m=1)}(t,\mathbf{X},p)\right) &= -\frac{3}{2}\xi\mathcal{I}\left(f_M, f^{(m=1)}(t,\mathbf{X},p)\right) \\ &= -\frac{3}{2}\xi\mathcal{I}(t,\mathbf{X},p) \end{aligned} \tag{4.13}$$

In the code, it is possible to choose different collision models for simulations. Most of them have been implemented for benchmarking, the only realistic one being the Belaiev-Budker relativistic collision operator.

4.1.2 Electron-electron collision operators

Belaiev-Budker relativistic collision model

In the calculations, the Belaiev-Budker collision operator is used for weakly relativistic plasmas. This operator ranges from non-relativistic to fully relativistic limits and is therefore very well suited for studying the heating and current drive problems. Its recent formulation in terms of Rosenbluth-like potential has open the possibility to use it in numerical calculations (Ref.[6]). Following the work done in Ref. [17], coefficients $A^{ee}(\psi,p)$, $F^{ee}(\psi,p)$ and $B_t^{ee}(\psi,p)$ are

$$A^{ee}(\psi,p) = \frac{F_1(\psi,p) + F_2(\psi,p)}{v}\overline{T}_e(\psi) \tag{4.14}$$

and

$$F^{ee}(\psi,p) = F_1(\psi,p) + F_2(\psi,p) \tag{4.15}$$

Here,

$$F_1(\psi,p) = \frac{4\pi}{v^2}F_{11}(\psi,p) + \frac{4\pi}{p^2}F_{12}(\psi,p) \tag{4.16}$$

$$F_2(\psi,p) = \frac{4\pi}{v}\left(1 - \frac{\gamma\zeta}{z}\right)F_{21}(\psi,p) \tag{4.17}$$

$$F_{11}(\psi,p) = \int_0^p p'v' f_M\left(\psi,p'\right)dp' \tag{4.18}$$

$$F_{12}(\psi,p) = \int_0^p p'v'\left(1 - \frac{\gamma'\zeta'}{z'}\right)f_M\left(\psi,p'\right)dp' \tag{4.19}$$

$$F_{21}(\psi,p) = \int_p^\infty p' f_M\left(\psi,p'\right)dp' \tag{4.20}$$

Much in the same way, the expression of coefficient B_t^{ee} is

$$B_t^{ee}(\psi,p) = B_{t1}(\psi,p) + B_{t2}(\psi,p) \tag{4.21}$$

with

$$B_{t1}(\psi,p) = 4\pi\sum_{n=1}^{5} B_{t1}^{[n]}(\psi,p) \tag{4.22}$$

and

$$B_{t2}(\psi,p)=4\pi\sum_{n=1}^{5}B_{t2}^{[n]}(\psi,p) \tag{4.23}$$

where

$$B_{t1}^{[1]}(\psi,p)=\frac{1}{2v}\int_0^p p'^2 f_M\left(\psi,p'\right)dp' \tag{4.24}$$

$$B_{t1}^{[2]}(\psi,p)=-\frac{1}{6vp^2}\int_0^p p'^4 f_M\left(\psi,p'\right)dp' \tag{4.25}$$

$$B_{t1}^{[3]}(\psi,p)=\frac{1}{8\gamma^2z^2}\int_0^p p'^2\frac{J_1(p')}{\gamma'}f_M\left(\psi,p'\right)dp' \tag{4.26}$$

$$B_{t1}^{[4]}(\psi,p)=-\frac{1}{4z_{i+1/2}^2}\int_0^p p'^2\frac{J_2(p')}{\gamma'}f_M\left(\psi,p'\right)dp' \tag{4.27}$$

$$B_{t1}^{[5]}(\psi,p)=-\frac{1}{4\gamma_{i+1/2}^2}\int_0^p \frac{p'^2}{\gamma'}\left(\gamma'-\frac{\zeta'}{z'}\right)f_M\left(\psi,p'\right)dp' \tag{4.28}$$

and

$$B_{t2}^{[1]}(\psi,p)=\frac{1}{2}\int_p^\infty \frac{p'^2}{v'}f_M\left(\psi,p'\right)dp' \tag{4.29}$$

$$B_{t2}^{[2]}(\psi,p)=-\frac{\gamma^2}{6}\int_p^\infty \frac{p'^2}{\gamma'^2v'}f_M dp' \tag{4.30}$$

$$B_{t2}^{[3]}(\psi,p)=\frac{J_1(p)}{8\gamma z^2}\int_p^\infty \frac{p'^2}{v'}\frac{1}{\gamma'^2}f_M\left(\psi,p'\right)dp' \tag{4.31}$$

$$B_{t2}^{[4]}(\psi,p)=-\frac{\gamma J_2(p)}{4z^2}\int_p^\infty \frac{p'^2}{v'}\frac{1}{\gamma'^2}f_M\left(\psi,p'\right)dp' \tag{4.32}$$

$$B_{t2}^{[5]}(\psi,p)=-\frac{1}{4\gamma p^2}\left(\gamma-\frac{\zeta}{z}\right)\int_p^\infty p'^2v' f_M\left(\psi,p'\right)dp' \tag{4.33}$$

Here,

$$J_1(p)=-3\gamma+\zeta\left(\frac{3}{z}+2z\right) \tag{4.34}$$

$$J_2(p)=\gamma+\frac{\zeta}{z}-\frac{2}{3}\gamma z^2 \tag{4.35}$$

with

$$z=\beta_{th}^{\dagger 2}p \tag{4.36}$$

$$\gamma=\sqrt{1+z^2} \tag{4.37}$$

$$\zeta=\sinh^{-1}z \tag{4.38}$$

and $f_M(\psi,p)$is the weakly relativistic Maxwellian distribution function given in Sec.6.3.4.

The first order Legendre correction of the collision operator $\mathcal{I}(t,\mathbf{X},p)$ is expressed as

$$\mathcal{I}\left(f_{M,},f^{(m=1)}\left(\psi,p\right)\right)$$
$$=\frac{4\pi}{\gamma}f^{(m=1)}\left(\psi,p\right)+\frac{1}{p^2}\mathcal{I}_1\left(f_{M,},f_0^{(m=1)}\left(\psi,p\right)\right)+p\mathcal{I}_2\left(f_{M,},f_0^{(m=1)}\left(\psi,p\right)\right) \quad (4.39)$$

where

$$\mathcal{I}_1\left(f_{M,},f_0^{(m=1)}\left(\psi,p\right)\right)=\sum_{n=1}^{10}\mathcal{I}_1^{[n]}\left(\psi,p\right) \quad (4.40)$$

and

$$\mathcal{I}_2\left(f_{M,},f_0^{(0)(m=1)}\left(\psi,p\right)\right)=\sum_{n=1}^{7}\mathcal{I}_2^{[n]}\left(\psi,p\right) \quad (4.41)$$

The set of coefficients $\mathcal{I}_1^{[n]}\left(\psi,p\right)$ is

$$\mathcal{I}_1^{[1]}\left(\psi,p\right)=\frac{1}{3\overline{T}_{e,l+1/2}}\int_0^p\frac{p'^3}{\gamma'}f_0^{(m=1)}\left(\psi,p\right)dp' \quad (4.42)$$

$$\mathcal{I}_1^{[2]}\left(\psi,p\right)=-\frac{2\gamma_{i+1/2}}{3\overline{T}_{e,l+1/2}}\int_0^p p'^3f_0^{(m=1)}\left(\psi,p\right)dp' \quad (4.43)$$

$$\mathcal{I}_1^{[3]}\left(\psi,p\right)=\frac{\gamma_{i+1/2}}{5\overline{T}_{e,l+1/2}^2}\int_0^p\frac{p'^5}{\gamma'}f_0^{(m=1)}\left(\psi,p\right)dp' \quad (4.44)$$

$$\mathcal{I}_1^{[4]}\left(\psi,p\right)=\int_0^p\frac{p'}{\gamma'}\left(\gamma'-\frac{\zeta'}{z'}\right)f_0^{(m=1)}dp' \quad (4.45)$$

$$\mathcal{I}_1^{[5]}\left(\psi,p\right)=-\frac{\gamma_{i+1/2}}{\overline{T}_{e,l+1/2}}\int_0^p\frac{p'^3}{\gamma'}\frac{J_2\left(p'\right)}{z'^2}f_0^{(m=1)}\left(\psi,p\right)dp' \quad (4.46)$$

$$\mathcal{I}_1^{[6]}\left(\psi,p\right)=\frac{\gamma p^2-5\overline{T}_e\left(\psi\right)}{6\overline{T}_e^2\left(\psi\right)}\int_0^p\frac{p'^3}{\gamma'}\left(1+\frac{3}{z'^2}-\frac{3\gamma'\zeta'}{z'^3}\right)f_0^{(m=1)}\left(\psi,p\right)dp' \quad (4.47)$$

$$\mathcal{I}_1^{[7]}\left(\psi,p\right)=\frac{\gamma}{2\beta_{th}^{\dagger 2}\overline{T}_e^2\left(\psi\right)}\int_0^p\frac{p'^3}{\gamma'}\frac{J_3\left(p'\right)}{z'}f_0^{(m=1)}\left(\psi,p\right)dp' \quad (4.48)$$

$$\mathcal{I}_1^{[8]}\left(\psi,p\right)=\frac{\gamma}{2\overline{T}_e\left(\psi\right)}\int_0^p\frac{p'^3}{\gamma'}\frac{J_1\left(p'\right)}{z'^2}f_0^{(m=1)}\left(\psi,p\right)dp' \quad (4.49)$$

$$\mathcal{I}_1^{[9]}\left(\psi,p\right)=\frac{p^2}{\overline{T}_e\left(\psi\right)}\int_0^p\frac{p'}{\gamma'}\left(\frac{\gamma'\zeta'}{z'}-1\right)f_0^{(m=1)}\left(\psi,p\right)dp' \quad (4.50)$$

$$\mathcal{I}_1^{[10]}\left(\psi,p\right)=-\frac{\gamma^2}{12\beta_{th}^{\dagger 2}\overline{T}_e^2\left(\psi\right)}\int_0^p\frac{p'^3}{\gamma'}\frac{J_4\left(\psi\right)}{z'}f_0^{(m=1)}\left(\psi,p\right)dp' \quad (4.51)$$

and the coefficients $\mathcal{I}_2^{[n]}\left(\psi,p\right)$ are

$$\mathcal{I}_2^{[1]}(\psi,p)=\frac{1}{3\overline{T}_e(\psi)}\int_p^\infty\frac{1}{\gamma'}f_0^{(m=1)}(\psi,p)\,dp' \tag{4.52}$$

$$\mathcal{I}_2^{[2]}(\psi,p)=\left(-\frac{2\gamma}{3\overline{T}_e(\psi)}+\frac{p^2}{5\overline{T}_e^2(\psi)}\right)\int_p^\infty f_0^{(m=1)}(\psi,p)\,dp' \tag{4.53}$$

$$\mathcal{I}_2^{[3]}(\psi,p)=\left(\gamma-\frac{\zeta}{z}\right)\frac{1}{p^2}\int_p^\infty\frac{1}{\gamma'}f_0^{(m=1)}(\psi,p)\,dp' \tag{4.54}$$

$$\mathcal{I}_2^{[4]}(\psi,p)=-\frac{J_2(p)}{z^2\overline{T}_e(\psi)}\int_p^\infty f_0^{(m=1)}(\psi,p)\,dp' \tag{4.55}$$

$$\mathcal{I}_2^{[5]}(\psi,p)=\left(1+\frac{3}{z^2}-\frac{3\gamma\zeta}{z^3}\right)\frac{1}{6\overline{T}_e^2(\psi)}\int_p^\infty\left(\frac{\gamma\prime p'^2-5\overline{T}_e(\psi)}{\gamma'}\right)f_0^{(m=1)}(\psi,p)\,dp' \tag{4.56}$$

$$\mathcal{I}_2^{[6]}(\psi,p)=\left(\frac{J_3(p)}{2z\beta_{th}^{\dagger 2}\overline{T}_e^2(\psi)}+\frac{J_1(p)}{2z^2\overline{T}_e(\psi)}-\frac{J_4(p)}{12z\beta_{th}^{\dagger 2}\overline{T}_e^2(\psi)}\right)\int_p^\infty f_0^{(m=1)}(\psi,p)\,dp' \tag{4.57}$$

$$\mathcal{I}_2^{[7]}(\psi,p)=\frac{1}{p^2\overline{T}_e(\psi)}\left(\frac{\gamma\zeta}{z}-1\right)\int_p^\infty\frac{p'^2}{\gamma'}f_0^{(m=1)}(\psi,p)\,dp' \tag{4.58}$$

where

$$J_3(p)=-\frac{3\gamma\zeta}{z}+\frac{3}{z}+z-\frac{2}{5}z^3 \tag{4.59}$$

$$J_4(p)=\gamma\zeta\left(\frac{15}{z^2}+6\right)-\frac{15}{z}+11z \tag{4.60}$$

Relativistic Maxwellian background

The relativistic Maxwellian limit corresponds to that case where the first order Legendre correction for momentum conservation is neglected, but nevertheless using the Beliaev-Budker formulation for coefficients $A^{ee}(\psi,p)$, $F^{ee}(\psi,p)$ and $B_t^{ee}(\psi,p)$. This is an academic case that allows only fruitful comparison with some theorerical works for code benchmarking.

Non-relativistic Maxwellian background

The non-relativistic collision operator with a Maxwellian background is extensively discussed in Ref. [16]. It is an interesting model, since analytical evaluation of the collision integrals may be performed. Its validity is restricted to the limit $\gamma\ll 1$, where γ is the Lorentz factor defined is Sec.6.3.3. . In that case $v=p$ is the unit system here employed. Using the standard notations

$$A^{ee}(\psi,p)=\frac{\overline{n}_e(\psi)}{2vu_\psi^2}\left[erf(u_\psi)-u_\psi erf'(u_\psi)\right] \tag{4.61}$$

$$F^{ee}(\psi,p)=\frac{\overline{n}_e(\psi)}{v^2}\left[erf(u_\psi)-u_\psi erf'(u_\psi)\right] \tag{4.62}$$

and

$$B_t^{ee}(\psi,p) = \frac{\overline{n}_e(\psi)}{4vu_\psi^2}\left[\left(2u_\psi^2-1\right)erf(u_\psi) + u_\psi erf'(u_\psi)\right] \tag{4.63}$$

where

$$u_\psi = \frac{v}{2\overline{n}_e(\psi)} \tag{4.64}$$

$$erf(x) = \frac{2}{\sqrt{\pi}}\int_0^x \exp\left(-y^2\right)dy \tag{4.65}$$

is the well know error function defined in Refs [14] and [18] , and its derivative

$$erf'(x) = \frac{2}{\sqrt{\pi}}\exp\left(-x^2\right) \tag{4.66}$$

The relation

$$\frac{F^{ee}(\psi,p)}{A^{ee}(\psi,p)} = v \tag{4.67}$$

which ensures that the Maxwellian is the correct solution when collisions is the only physical process. In that limit, self-collisions are neglected.

High-velocity limit

Though the high velocity limit corresponds to a restricted range of application regarding the full collision operator, it can contribute to useful comparisons with some theoretical calculations, as shown in Ref. [16]. Therefore, this possibility has been implemented in the code. In that case, expressions of the coefficients are greatly simplified,

$$A^{ee}(\psi,p) = \frac{1}{v^3}\overline{n}_e(\psi)\,\overline{T}_e(\psi) \tag{4.68}$$

and

$$F^{ee}(\psi,p) = \frac{1}{v^2}\overline{n}_e(\psi) \tag{4.69}$$

while

$$B_t^{ee}(\psi,p) = \frac{1}{2v}\overline{n}_e(\psi) - \frac{1}{2v^3}\overline{n}_e(\psi)\,\overline{T}_e(\psi) \tag{4.70}$$

In that limit, self-collisions are neglected.

Non-relativistic Lorentz model

This case corresponds to the limit where only pitch-angle scattering of electrons on massive ions with $\overline{T}_{ss'}(\psi) = 0$, with large $Z_{ss'}$. Consequently, large simplifications may be performed, and

$$A^{ee}(\psi,p) = F^{ee}(\psi,p) = B_t^{ee}(\psi,p) = 0 \tag{4.71}$$

This simple model is very interesting since analytical expressions may be obtained in this limit, which allow accurate code benchmarking, especially for the bootstrap current problem in arbitrary magnetic configuration. Obviously, self-collisions are neglected by definition.

4.1.3 Electron-ion collision operators

Non-relativistic Maxwellian background

Since ions mass is much larger than electron ones, their dynamics is almost non-relativistic. Consequently, electron-ion collisions may be described in this limit considering a Maxwellian ion background. Expressions for arbirary type of ions is also given in Ref. [16] and their validities are also restricted to the limit $\gamma \ll 1$, where γ is the Lorentz factor defined is Sec.6.3.3. . In that case $v = p$ is the unit system here employed. Using the standard notations

$$A^{ei}(\psi, p) = \frac{1}{2v} \sum_s \sum_{s'} \frac{1}{u_\psi^{ss'2}} \left[erf\left(u_\psi^{ss'}\right) - u_\psi erf'\left(u_\psi^{ss'}\right) \right] Z_{ss'}^2 \overline{n}_{ss'}(\psi) \tag{4.72}$$

$$F^{ei}(\psi, p) = \frac{1}{v^2} \sum_s \sum_{s'} \left[erf\left(u_\psi^{ss'}\right) - u_\psi^{ss'} erf'\left(u_\psi^{ss'}\right) \right] Z_{ss'}^2 \frac{\overline{n}_{ss'}(\psi)}{\overline{m}_s} \tag{4.73}$$

and

$$B_t^{ei}(\psi, p) = \frac{1}{4v} \sum_s \sum_{s'} \frac{1}{u_\psi^{ss'2}} \left[\left(2u_\psi^{ss'2} - 1\right) erf\left(u_\psi^{ss'}\right) + u_\psi^{ss'} erf'\left(u_\psi^{ss'}\right) \right] Z_{ss'}^2 \overline{n}_{ss'}(\psi) \tag{4.74}$$

where

$$u_\psi^{ss'} = \frac{v}{2v_{th,ss'}^\dagger} = \frac{v}{2\sqrt{\overline{T}_{ss'}(\psi)/\overline{m}_s}}$$

Here, $v_{th,ss'}^\dagger$ is the thermal velocity of species s in ionization state s', while $erf(x)$ and $erf'(x)$ have the same expressions as for the electron-electron collision term. Here again

$$\frac{F^{ei}(\psi, p)}{A^{ei}(\psi, p)} = v \frac{\left(\sum_s \sum_{s'} Z_{ss'}^2 \frac{\overline{n}_{ss'}(\psi)\overline{T}_{ss'}(\psi)}{\overline{m}_s} \right)}{\sum_s \sum_{s'} Z_{ss'}^2 \frac{\overline{n}_{ss'}(\psi)}{\overline{m}_s}} \tag{4.75}$$

which ensures that the Maxwellian is the correct solution when electron-ion collisions is the only physical process. However, when electron -electron and electron-ion are both considered, the low velocity limit has a different v dependence,

$$\frac{F(\psi, p)}{A(\psi, p)} = \frac{F^{ee}(\psi, p) + F^{ei}(\psi, p)}{A^{ee}(\psi, p) + A^{ei}(\psi, p)} \nsim v \tag{4.76}$$

except when equipartition between electrons and all ion species is satisfied, i.e. when $\overline{T}_{ss'} = \overline{T}_e$. In principle, the lack of equipartition lead to a non-Maxwellian behaviour of the electrons close to $v = 0$, a problem that require a multi-species Fokker-Planck code.

High-velocity limit

For most current drive studies like for the Lower Hybrid wave where the resonance condition is far from the thermal bulk, it is reasonable to consider the high velocity limit of the electron-ion collision operator. Corresponding coefficients $A^{ei}(\psi,p)$, $F^{ei}(\psi,p)$ and $B_t^{ei}(\psi,p)$ are

$$A^{ei}(\psi,p) = \frac{1}{v^3}\sum_s\sum_{s'} Z_{ss'}^2 \frac{\overline{n}_{ss'}(\psi)\,\overline{T}_{ss'}(\psi)}{\overline{m}_s} \tag{4.77}$$

$$F^{ei}(\psi,p) = \frac{1}{v^2}\sum_s\sum_{s'} Z_{ss'}^2 \frac{\overline{n}_{ss'}(\psi)}{\overline{m}_s} \tag{4.78}$$

and

$$B_t^{ei}(\psi,p) = \frac{1}{2v}\sum_s\sum_{s'} Z_{ss'}^2 \overline{n}_{ss'}(\psi)\left(1-\frac{1}{v^2}\frac{\overline{T}_{ss'}(\psi)}{\overline{m}_s}\right) \tag{4.79}$$

where the double sum $\sum_s\sum_{s'}$ takes into account of all ions species s in ionization state s'. Here, $\overline{n}_{ss'}(\psi)$ is the normalized ion density at ψ, as introduced in Sec. 6.3.1, and $\overline{m}_s$ is the ion rest mass normalized to the electron rest mass m_e.

Above expressions are valid in the limit $v \gg v_{th,ss'}^{\dagger}$ a reasonable assumption, since $\overline{m}_s \gg 1$. The collision operator has however the nice property that

$$\frac{F^{ei}(\psi,p)}{A^{ei}(\psi,p)} \propto v \tag{4.80}$$

which ensures that the Maxwellian is the solution close to $v \simeq 0$. It is used in Ref. [17] in conjunction with the Belaiev-Budker electron-electron collision operator, but in the code, its use is now restricted to the case when the high-velocity limit of the electron-electron collision operator is employed, for consistency between collision models.

Non-relativistic Lorentz model

Since only pitch-angle electron scattering on massive ions with $\overline{T}_{ss'}(\psi) = 0$, with large $Z_{ss'}$ is considered in this model, by definition

$$A^{ei}(\psi,p) = F^{ei}(\psi,p) = 0 \tag{4.81}$$

while

$$B_t^{ei}(\psi,p) = 1/2 \tag{4.82}$$

The solutions of the Fokker-Planck and the drift kinetic equations is independent in this limit of the B_t^{ei} value. Here the standard value 1/2 is chosen as used in several publications.

4.1.4 Bounce Averaged Fokker-Planck Equation

Flux conservative term

In the Fokker-Planck equation, the diffusion and convection elements are bounce-averaged according to the expressions (3.189)-(3.194), which gives, using (4.7)-(4.8),

$$D_{pp}^{\mathrm{C}(0)} = \{A(\psi,p)\} \tag{4.83}$$
$$D_{p\xi}^{\mathrm{C}(0)} = 0 \tag{4.84}$$
$$D_{\xi p}^{\mathrm{C}(0)} = 0 \tag{4.85}$$
$$D_{\xi\xi}^{\mathrm{C}(0)} = \left\{ \frac{\xi^2}{\Psi\xi_0^2} B(\psi,p) \right\} \tag{4.86}$$

and the convection components

$$F_{p}^{\mathrm{C}(0)} = -\{F(\psi,p)\} \tag{4.87}$$
$$F_{\xi}^{\mathrm{C}(0)} = 0 \tag{4.88}$$

and therefore

$$D_{pp}^{\mathrm{C}(0)} = A^{(0)}(\psi,p) \tag{4.89}$$
$$D_{p\xi}^{\mathrm{C}(0)} = 0 \tag{4.90}$$
$$D_{\xi p}^{\mathrm{C}(0)} = 0 \tag{4.91}$$
$$D_{\xi\xi}^{\mathrm{C}(0)} = \frac{\lambda_{2,-1,0}}{\lambda} B_t^{(0)}(\psi,p) \tag{4.92}$$

and

$$F_{p}^{\mathrm{C}(0)} = -F^{(0)}(\psi,p) \tag{4.93}$$
$$F_{\xi}^{\mathrm{C}(0)} = 0 \tag{4.94}$$

Here, coefficients $A^{(0)}(p,\psi)$, $B_t^{(0)}(p,\psi)$ and $F^{(0)}(p,\psi)$ are determined at the location where $B = B_0$ on the magnetic flux surface. However, since A, B_t and F are only functions of the density and temperature that are flux surface quantities as shown in Sec. 4.1, their respective values are consequently independent of the poloidal position and therefore, $A^{(0)} = A$, $B_t^{(0)} = B_t$ and $F^{(0)} = F$. The bounce coefficient $\lambda_{2,-1,0}$ is defined as (2.66)

$$\lambda_{2,-1,0} = \lambda \left\{ \frac{\xi^2}{\Psi\xi_0^2} \right\} \tag{4.95}$$

For reference to the litterature ([19]), note that we could also perform the following transformation

$$\begin{aligned}\left\{\frac{\xi^2}{\Psi\xi_0^2}\right\} &= \left\{\frac{1-\Psi\left(1-\xi_0^2\right)}{\Psi\xi_0^2}\right\} \\ &= \left\{1-\frac{1}{\xi_0^2}\left(1-\frac{1}{\Psi}\right)\right\} \\ &= 1-\frac{\Delta_b}{\xi_0^2} \end{aligned} \tag{4.96}$$

with

$$\Delta_b \equiv \left\{1-\frac{1}{\Psi}\right\} \tag{4.97}$$

The evaluation of Δ_b for circular concentric flux surfaces in given in Appendix B.1.

First order Legendre correction

Concerning the term that ensures momentum conservation in the collision operator, one must evaluate

$$\left\{C\left(f_M, \frac{3}{2}\xi f_0^{(m=1)}\right)\right\} = -\frac{3}{2}\left\{\xi\mathcal{I}\left(f_M, f_0^{(m=1)}\right)\right\} \tag{4.98}$$

Making the substitution $\Psi\xi_0 d\xi_0 = \xi d\xi$ in the integral $f_0^{(m=1)} = \int_{-1}^{+1} \xi f_0\left(p,\xi,\psi,\theta\right) d\xi$, one obtains

$$f_0^{(m=1)}\left(p,\xi,\psi,\theta\right) = \int_{-1}^{-\sqrt{1-1/\Psi}} \Psi\xi_0 f_0^{(0)}\left(p,\xi_0,\psi\right) d\xi_0 + \int_{\sqrt{1-1/\Psi}}^{+1} \Psi\xi_0 f_0^{(0)}\left(p,\xi_0,\psi\right) d\xi_0 \tag{4.99}$$

where the limits of integration come from the relation $\xi\left(\psi,\theta,\xi_0\right) = \sigma\sqrt{1-\Psi\left(\psi,\theta\right)\left(1-\xi_0^2\right)}$. Since $f_0^{(0)}$ is symmetric in the region of the phase space $\xi_0 \in \left(-\sqrt{1-1/\Psi}, \sqrt{1-1/\Psi}\right)$which corresponds to trapped orbits,

$$\int_{-\sqrt{1-1/\Psi}}^{+\sqrt{1-1/\Psi}} \Psi\xi_0 f_0^{(0)}\left(p,\xi_0,\psi\right) d\xi_0 = 0 \tag{4.100}$$

one get

$$\begin{aligned} f_0^{(m=1)}\left(p,\xi,\psi,\theta\right) &= \int_{-1}^{+1} \Psi\xi_0 f_0^{(0)}\left(p,\xi_0,\psi\right) d\xi_0 \\ &= \Psi\int_{-1}^{+1} \xi_0 f_0^{(0)}\left(p,\xi_0,\psi\right) d\xi_0 \\ &= \Psi f_0^{(0)(m=1)}\left(p,\xi_0,\psi\right) \end{aligned} \tag{4.101}$$

where $f_0^{(0)(m=1)}(p,\xi_0,\psi)$is the Legendre integral evaluated at $B_0 = B(\psi,\theta_0)$, independent of θ. Since the operator $\mathcal{I}$ is linear,

$$\begin{aligned}\frac{3}{2}\left\{\xi\mathcal{I}\left(f_{0M},f_0^{(m=1)}\right)\right\} &= \frac{3}{2}\left\{\xi\Psi\right\}\mathcal{I}\left(f_M,f_0^{(0)(m=1)}\right)\\ &= \sigma\left\{\sigma\frac{\xi}{\xi_0}\Psi\right\}\frac{3}{2}\xi_0\mathcal{I}\left(f_M,f_0^{(0)(m=1)}\right)\\ &= \frac{\overline{\lambda}_{1,1,0}}{\lambda}\frac{3}{2}\xi_0\mathcal{I}\left(f_M,f_0^{(0)(m=1)}\right)\end{aligned} \tag{4.102}$$

and consequently

$$\begin{aligned}\left\{C\left(f_M,\frac{3}{2}\xi f_0^{(m=1)}\right)\right\} &= C^{(0)}\left(f_M,f_0^{(0)(m=1)}\right)\\ &= -\frac{\overline{\lambda}_{1,1,0}}{\lambda}\frac{3}{2}\xi_0\mathcal{I}\left(f_M,f_0^{(0)(m=1)}\right)\end{aligned} \tag{4.103}$$

Expression of $\overline{\lambda}_{1,1,0}$ This coefficient is expressed as

$$\overline{\lambda}_{1,1,0} = \frac{\sigma}{\widetilde{q}}\left[\frac{1}{2}\sum_{\sigma}\right]_T\int_{\theta_{\min}}^{\theta_{\max}}\frac{d\theta}{2\pi}\frac{1}{\left|\widehat{\psi}\,.\,\widehat{r}\right|}\frac{r}{R_p}\frac{B}{B_P}\sigma\Psi \tag{4.104}$$

Since the integral is odd in σ, the sum over trapped particles vanishes, $\overline{\lambda}_{1,1,0}=0$ for trapped electrons, and $\overline{\lambda}_{1,1,0}=\overline{\lambda}^P_{1,1,0}\neq 0$ for circulating ones. Hence

$$\begin{aligned}\overline{\lambda}^P_{1,1,0} &= \frac{1}{\widetilde{q}}\int_0^{2\pi}\frac{d\theta}{2\pi}\frac{1}{\left|\widehat{\psi}\,.\,\widehat{r}\right|}\frac{r}{R_p}\frac{B}{B_P}\Psi\\ &= \frac{1}{\widetilde{q}}\int_0^{2\pi}\frac{d\theta}{2\pi}\frac{1}{\left|\widehat{\psi}\,.\,\widehat{r}\right|}\frac{r}{R_p}\frac{B^2}{B_PB_0}\end{aligned} \tag{4.105}$$

Case of circular concentric flux-surfaces In this case, $\epsilon = r/R_p$, $\widehat{\psi}\cdot\widehat{r}=1$ and since the ratio B/B_P is a function of r only

$$\begin{aligned}\overline{\lambda}^P_{1,1,0} &= \frac{1}{\widetilde{q}}\frac{B}{B_P}\epsilon\int_0^{2\pi}\frac{d\theta}{2\pi}\frac{1+\epsilon}{1+\epsilon\cos\theta}\\ &= \int_0^{2\pi}\frac{d\theta}{2\pi}\frac{1+\epsilon}{1+\epsilon\cos\theta}\\ &= s^*\end{aligned} \tag{4.106}$$

using the relation $\widetilde{q}B_P/B=\epsilon$. The integral s^*, according to the old notations found in the litterature ([19]),

$$s^* = \int_0^{2\pi}\frac{d\theta}{2\pi}\frac{1+\epsilon}{1+\epsilon\cos\theta} \tag{4.107}$$

can be performed analytically, as shown in Appendix B.1, and

$$\overline{\lambda}^{P}_{1,1,0} = \sqrt{\frac{1+\epsilon}{1-\epsilon}} \tag{4.108}$$

Moreover, in this limit, $\overline{\lambda}^{P}_{1,1,0} = \overline{\lambda}^{P}_{1,-1,2}$, as shown in Sec.4.2.2.

4.1.5 Bounce Averaged Drift Kinetic Equation

Flux conservative term

In the first order drift kinetic equation, the diffusion and convection flux elements related to $\widetilde{f}$ are bounce-averaged according to the expressions (3.218)-(3.223), which gives, using (4.7)-(4.8),

$$\begin{aligned}
\widetilde{D}^{\mathrm{C}(0)}_{pp} &= \sigma\left\{\sigma\frac{\xi}{\Psi\xi_0}A\left(\psi,p\right)\right\} \\
\widetilde{D}^{\mathrm{C}(0)}_{p\xi} &= 0 \\
\widetilde{D}^{\mathrm{C}(0)}_{\xi p} &= 0 \\
\widetilde{D}^{\mathrm{C}(0)}_{\xi\xi} &= \sigma\left\{\frac{\sigma\xi^3}{\Psi^2\xi_0^3}B_t\left(\psi,p\right)\right\}
\end{aligned} \tag{4.109}$$

and the convection components

$$\begin{aligned}
\widetilde{F}^{\mathrm{C}(0)}_{p} &= -\sigma\left\{\sigma\frac{\xi}{\Psi\xi_0}F\left(\psi,p\right)\right\} \\
\widetilde{F}^{\mathrm{C}(0)}_{\xi} &= \frac{\sqrt{1-\xi_0^2}}{p\xi_0^3}\sigma\left\{\frac{\sigma\xi\left(\Psi-1\right)}{\xi_0\Psi^2}B_t\left(\psi,p\right)\right\}
\end{aligned} \tag{4.110}$$

and therefore

$$\begin{aligned}
\widetilde{D}^{\mathrm{C}(0)}_{pp} &= \frac{\overline{\lambda}_{1,-1,0}}{\lambda}A\left(\psi,p\right) \\
\widetilde{D}^{\mathrm{C}(0)}_{p\xi} &= 0 \\
\widetilde{D}^{\mathrm{C}(0)}_{\xi p} &= 0 \\
\widetilde{D}^{\mathrm{C}(0)}_{\xi\xi} &= \frac{\overline{\lambda}_{3,-2,0}}{\lambda}B_t\left(\psi,p\right)
\end{aligned} \tag{4.111}$$

and

$$\begin{aligned}
\widetilde{F}^{\mathrm{C}(0)}_{p} &= -\frac{\overline{\lambda}_{1,-1}}{\lambda}F(p) \\
\widetilde{F}^{\mathrm{C}(0)}_{\xi} &= \frac{\sqrt{1-\xi_0^2}}{p\xi_0^3}\frac{\left(\overline{\lambda}_{1,-1,0}-\overline{\lambda}_{1,-2,0}\right)}{\lambda}B_t\left(\psi,p\right)
\end{aligned} \tag{4.112}$$

The following bounce coefficients are defined (2.66)

$$\overline{\lambda}_{1,-1,0} = \lambda\sigma\left\{\frac{\sigma\xi}{\Psi\xi_0}\right\} \tag{4.113}$$

$$\overline{\lambda}_{3,-2,0} = \lambda\sigma\left\{\frac{\sigma\xi^3}{\Psi^2\xi_0^3}\right\} \tag{4.114}$$

$$\overline{\lambda}_{1,-2,0} = \lambda\sigma\left\{\frac{\sigma\xi}{\Psi^2\xi_0}\right\} \tag{4.115}$$

We also have the following relation, by expanding ξ^2

$$\overline{\lambda}_{3,-2,0} = \frac{\overline{\lambda}_{1,-2,0} - \left(1-\xi_0^2\right)\overline{\lambda}_{1,-1,0}}{\xi_0^2} \tag{4.116}$$

First order Legendre correction

Concerning the term that ensures momentum conservation in the collision operator, one must evaluate

$$\left\{C\left(f_M, \frac{3}{2}\xi\widetilde{f}\right)\right\} = -\frac{3}{2}\left\{\xi\mathcal{I}\left(f_M, \widetilde{f}^{(m=1)}\right)\right\} \tag{4.117}$$

Making like for the Fokker-Planck term the substitution $\Psi\xi_0 d\xi_0 = \xi d\xi$ in the integral $\widetilde{f}^{(m=1)} = \int_{-1}^{+1}\xi\widetilde{f}\left(p,\xi,\psi,\theta\right)d\xi$, one obtains

$$\begin{aligned}\widetilde{f}^{(m=1)}\left(p,\xi,\psi,\theta\right) = & \int_{-1}^{-\sqrt{1-1/\Psi}}\Psi\xi_0\left(\frac{\xi}{\Psi\xi_0}\right)\widetilde{f}^{(0)}\left(p,\xi_0,\psi\right)d\xi_0 \\ & + \int_{\sqrt{1-1/\Psi}}^{+1}\Psi\xi_0\left(\frac{\xi}{\Psi\xi_0}\right)\widetilde{f}^{(0)}\left(p,\xi_0,\psi\right)d\xi_0\end{aligned} \tag{4.118}$$

which becomes

$$\widetilde{f}^{(m=1)}\left(p,\xi,\psi,\theta\right) = \int_{-1}^{1}H\left(|\xi_0|-\xi_{0T}\right)\xi\widetilde{f}^{(0)}\left(p,\xi_0,\psi\right)d\xi_0 \tag{4.119}$$

Then,

$$\frac{3}{2}\left\{\xi\mathcal{I}\left(f_M,\widetilde{f}^{(m=1)}\right)\right\} = \frac{3}{2}\mathcal{I}\left(f_M,\left\{\xi\widetilde{f}^{(m=1)}\right\}\right) \tag{4.120}$$

since f_M and $\mathcal{I}$ are independent of θ. It is therefore necessary to evaluate

$$\begin{aligned}\left\{\xi\widetilde{f}^{(m=1)}\right\} &= \frac{1}{\lambda\widetilde{q}}\left[\frac{1}{2}\sum_{\sigma}\right]_T\int_{\theta_{\min}}^{\theta_{\max}}\frac{d\theta}{2\pi}\frac{1}{\left|\widehat{\psi}\,.\,\widehat{r}\right|}\frac{r}{R_p}\frac{B}{B_P}\frac{\xi_0}{\xi}\xi\widetilde{f}^{(m=1)} \\ &= \frac{1}{\lambda\widetilde{q}}\left[\frac{1}{2}\sum_{\sigma}\right]_T\int_{\theta_{\min}}^{\theta_{\max}}\frac{d\theta}{2\pi}\frac{1}{\left|\widehat{\psi}\,.\,\widehat{r}\right|}\frac{r}{R_p}\frac{B}{B_P}\xi_0\widetilde{f}^{(m=1)} \\ &= \frac{\xi_0}{\lambda\widetilde{q}}H\left(|\xi_0|-\xi_{0T}\right)\int_0^{2\pi}\frac{d\theta}{2\pi}\frac{1}{\left|\widehat{\psi}\,.\,\widehat{r}\right|}\frac{r}{R_p}\frac{B}{B_P}\widetilde{f}^{(m=1)}\end{aligned} \tag{4.121}$$

since $\widetilde{f}^{(m=1)}$ is independent of σ because of the integration over ξ_0, while $\left[\frac{1}{2}\sum_\sigma\right]_T \xi_0 = 0$ for trapped orbits. Hence,

$$\begin{aligned}
&\left\{\xi \widetilde{f}^{(m=1)}\right\} \\
&= \frac{\xi_0}{\lambda\widetilde{q}} H\left(|\xi_0| - \xi_{0T}\right) \int_0^{2\pi} \frac{d\theta}{2\pi} \frac{1}{\left|\widehat{\psi}\,.\,\widehat{r}\right|} \frac{r}{R_p} \frac{B}{B_P} \left[\frac{3}{2}\int_{-1}^{1} H\left(|\xi_0| - \xi_{0T}\right) \xi \widetilde{f}^{(0)} d\xi_0\right] \\
&= \frac{\xi_0}{\lambda} H\left(|\xi_0| - \xi_{0T}\right) \int_{-1}^{1} H\left(|\xi_0| - \xi_{0T}\right) \widetilde{f}^{(0)} d\xi_0 \left[\frac{1}{\widetilde{q}} \int_0^{2\pi} \frac{d\theta}{2\pi} \frac{1}{\left|\widehat{\psi}\,.\,\widehat{r}\right|} \frac{r}{R_p} \frac{B}{B_P} \xi\right] \\
&= \frac{\xi_0}{\lambda} H\left(|\xi_0| - \xi_{0T}\right) \int_{-1}^{1} H\left(|\xi_0| - \xi_{0T}\right) \widetilde{f}^{(0)} \xi_0 \lambda d\xi_0 \left[\frac{1}{\lambda\widetilde{q}} \int_0^{2\pi} \frac{d\theta}{2\pi} \frac{1}{\left|\widehat{\psi}\,.\,\widehat{r}\right|} \frac{r}{R_p} \frac{B}{B_P} \frac{\xi_0}{\xi} \frac{\xi^2}{\xi_0^2}\right] \\
&= \frac{\xi_0}{\lambda} H\left(|\xi_0| - \xi_{0T}\right) \int_{-1}^{1} \xi_0 H\left(|\xi_0| - \xi_{0T}\right) \widetilde{f}^{(0)} \lambda \left\{\frac{\xi^2}{\xi_0^2}\right\} d\xi_0 \\
&= \frac{\xi_0}{\lambda} H\left(|\xi_0| - \xi_{0T}\right) \int_{-1}^{1} \xi_0 H\left(|\xi_0| - \xi_{0T}\right) \widetilde{f}^{(0)} \lambda_{2,0,0} d\xi_0
\end{aligned} \tag{4.122}$$

Defining

$$\begin{aligned}
\widetilde{f}^{(0)(m=1)} &\equiv \int_{-1}^{1} \xi_0 H\left(|\xi_0| - \xi_{0T}\right) \widetilde{f}^{(0)} \lambda_{2,0,0} d\xi_0 \\
&= \int_{-1}^{1} \xi_0 \widetilde{f}^{(0)} \overline{\lambda}_{2,0,0} d\xi_0
\end{aligned} \tag{4.123}$$

one obtains

$$\begin{aligned}
\left\{C\left(f_M, \frac{3}{2}\xi \widetilde{f}^{(m=1)}\right)\right\} &= \widetilde{C}^{(0)}\left(f_M, \frac{3}{2}\xi_0 \widetilde{f}^{(0)(m=1)}\right) \\
&= \frac{3}{2}\frac{\xi_0}{\lambda} H\left(|\xi_0| - \xi_{0T}\right) \mathcal{I}\left(f_{0M}, \widetilde{f}^{(0)(m=1)}\right)
\end{aligned} \tag{4.124}$$

Case of circular concentric flux-surfaces

Note that in the case of circular concentric flux-surfaces, we can find analytical expressions for the bounce coefficients

$$\begin{aligned}
\overline{\lambda}_{1,-1,0} &= H(|\xi_0| - \xi_{0T}) \int_0^{2\pi} \frac{d\theta}{2\pi} \frac{1}{\Psi} \\
&= \frac{1}{(1+\epsilon)} H(|\xi_0| - \xi_{0T}) \int_0^{\pi} \frac{d\theta}{\pi} \left(1 + \epsilon\cos\theta\right) \\
&= \frac{1}{(1+\epsilon)} H(|\xi_0| - \xi_{0T})
\end{aligned} \tag{4.125}$$

$$\begin{aligned}\overline{\lambda}_{1,-2,0} &= H(|\xi_0|-\xi_{0T})\int_0^{2\pi}\frac{d\theta}{2\pi}\frac{1}{\Psi^2}\\ &= \frac{H(|\xi_0|-\xi_{0T})}{(1+\epsilon)^2}\int_0^{\pi}\frac{d\theta}{\pi}\left(1+\epsilon\cos\theta\right)^2\\ &= \frac{H(|\xi_0|-\xi_{0T})}{(1+\epsilon)^2}\left(1+\frac{\epsilon^2}{2}\right)\end{aligned} \tag{4.126}$$

so that

$$\overline{\lambda}_{3,-2,0} = \frac{H(|\xi_0|-\xi_{0T})}{(1+\epsilon)\,\xi_0^2}\left(\xi_0^2-\frac{\epsilon\,(1-\epsilon/2)}{(1+\epsilon)}\right) \tag{4.127}$$

Furthermore,

$$\begin{aligned}\overline{\lambda}_{2,0,0} &= H(|\xi_0|-\xi_{0T})\int_0^{2\pi}\frac{d\theta}{2\pi}\frac{\xi}{\xi_0}\\ &= H(|\xi_0|-\xi_{0T})\int_0^{2\pi}\frac{d\theta}{2\pi}\frac{\xi_0}{\xi}\frac{\xi^2}{\xi_0^2}\\ &= H(|\xi_0|-\xi_{0T})\int_0^{2\pi}\frac{d\theta}{2\pi}\frac{\xi_0}{\xi}\frac{1-\Psi\left(1-\xi_0^2\right)}{\xi_0^2}\\ &= H(|\xi_0|-\xi_{0T})\frac{\lambda}{\xi_0^2}\left[1-\left(1-\xi_0^2\right)\{\Psi\}\right]\end{aligned} \tag{4.128}$$

and using the expression of $\{\Psi\}$ given in Appendix B.1,

$$\{\Psi\} = \frac{1}{\lambda}\frac{2}{\pi}\sum_{m=0}^{\infty}\widetilde{\chi}_m\xi_{0T}^{2m}J_{2m} \tag{4.129}$$

where J_{2m} is expressed in terms of complete elliptic integrals of the first and second kind, and $\widetilde{\chi}_m$ is given by the recurrence relation $\widetilde{\chi}_m = \frac{2m-1}{2m}\widetilde{\chi}_{m-1}$ with $\widetilde{\chi}_0 = 1$,

$$\overline{\lambda}_{2,0,0} = \frac{2}{\pi}H(|\xi_0|-\xi_{0T})\sum_{m=0}^{\infty}\left[\chi_m-\widetilde{\chi}_m\left(1-\xi_0^2\right)\right]\frac{\xi_{0T}^{2m}}{\xi_0^2}J_{2m} \tag{4.130}$$

Here χ_m is defined in Appendix B.1. The series expansion is converging less rapidly than for $\lambda_{0,0,0} = \lambda$, therefore, at least first three terms have to be kept for accurate calculations, so that the truncated expression is

$$\overline{\lambda}_{2,0,0} \simeq \frac{2}{\pi}H(|\xi_0|-\xi_{0T})\left[J_0+\left(\frac{1}{2}-\frac{1}{\xi_0^2}\right)\xi_{0T}^2J_2+\left(\frac{3}{8}-\frac{1}{2\xi_0^2}\right)\xi_{0T}^4J_4\right] \tag{4.131}$$

4.2 Ohmic electric field

The generation of Ohmic current is based on the concept of transformer, where the plasma torus is the secondary circuit. An electric field is induced by the temporal variation $\partial\psi/\partial t$ of the poloidal flux generated by the primary circuit. The induced current density is then calculated by Ohm's law, $\mathbf{J} = \sigma_\Omega\mathbf{E}$, where σ_Ω is the electric conductivity calculated by

accounting for the Coulomb interaction between the strongly magnetized components of the plasma. Using Faraday's law,

$$\frac{\partial \mathbf{B}}{\partial t} = -\nabla \times \mathbf{E}$$

We consider the surface $S(\psi, \theta)$ which is a truncated cone delimited by two circles being C_1, the magnetic axis, and $C_2(\psi, \theta)$, the toroidal line at position (ψ, θ). Applying the integral formula to Faraday's law, we have

$$\iint_{S(\psi,\theta)} \mathbf{dS} \cdot \frac{\partial \mathbf{B}}{\partial t} = -\iint_{S(\psi,\theta)} \mathbf{dS} \cdot \nabla \times \mathbf{E} = -\oint_{C(\psi,\theta)} \mathbf{dl} \cdot \mathbf{E} \tag{4.132}$$

The poloidal flux is given by

$$\psi = \frac{1}{2\pi} \iint_{S(\psi,\theta)} dS B_P = \frac{1}{2\pi} \iint_{S(\psi,\theta)} \mathbf{dS} \cdot \mathbf{B} \tag{4.133}$$

so that we get

$$2\pi \frac{\partial \psi}{\partial t} = \oint_{C_1} \mathbf{dl} \cdot \mathbf{E} - \oint_{C_2(\psi,\theta)} \mathbf{dl} \cdot \mathbf{E} \tag{4.134}$$

$$= \int_0^{2\pi} R_p d\phi E_{\phi 0} - \int_0^{2\pi} R(\psi, \theta) d\phi E_\phi(\psi, \theta) \tag{4.135}$$

where R_p is the major radius on axis and $E_{\phi p}$ is the electric field on axis. Using axisymmetry, this becomes

$$\frac{\partial \psi}{\partial t} = R_p E_{\phi p} - R(\psi, \theta) E_\phi(\psi, \theta) \tag{4.136}$$

and therefore

$$R E_\phi = R_p E_{\phi p} - \frac{\partial \psi}{\partial t} \tag{4.137}$$

and RE_ϕ is only a function of ψ. We can therefore rewrite

$$E_\phi(\psi, \theta) = E_{\phi 0} \frac{R_0}{R} \tag{4.138}$$

where R_0 is the major radius taken at the the poloidal position θ_0 where the magnetic field $\mathbf{B}$ is minimum on a flux-surface.By definition,

$$E_{\|0}(\psi) = E_\|(\psi, \theta_0) \tag{4.139}$$

The electric field along the field line can then be obtained by projection, which gives

$$E_\| = \left(\widehat{b} \cdot \widehat{\phi}\right) E_\phi = \frac{B_T}{B} E_\phi \tag{4.140}$$

so that we get

$$\frac{B}{B_T} E_\| = \frac{B_0}{B_{T0}} E_{\|0} \frac{R_0}{R} \tag{4.141}$$

and then

$$E_\| = \frac{B_T}{B_{T0}} \frac{B_0}{B} \frac{R_0}{R} E_{\|0}(\psi) = \frac{1}{\Psi} \frac{R_0^2}{R^2} E_{\|0}(\psi) \tag{4.142}$$

with $\Psi = B/B_0$ as defined in Sec. 2.2.1.

4.2.1 Conservative Form for the Ohmic Electric Field Operator

The effect of the electric fied $E_\parallel$ can be expressed in a conservative form as $\mathcal{E}(f_0) = \nabla_{\mathbf{p}} \cdot \mathbf{S}^{\mathrm{E}}$, where the flux in momentum space is easily expressed in cylindrical coordinates $\left(p_\parallel, p_\perp\right)$ as

$$\mathbf{S}^{\mathrm{E}}_{(p_\parallel, p_\perp)} = \begin{pmatrix} S^E_{p_\parallel} \\ S^E_{p_\perp} \end{pmatrix} \tag{4.143}$$

with

$$S^{\mathrm{E}}_{p_\parallel} = q_e E_\parallel f_0 \tag{4.144}$$
$$S^{\mathrm{E}}_{p_\perp} = 0 \tag{4.145}$$

where q_e is the electronic charge.

The transformation from cylindrical to spherical coordinates is given by

$$\mathbf{S}^{\mathrm{E}}_{(p,\xi)} = \mathcal{R}^{-1} \mathbf{S}^{\mathrm{E}}_{(p_\parallel, p_\perp)} \tag{4.146}$$

where $\mathcal{R}$ is the rotational matrix

$$\mathcal{R} = \begin{pmatrix} \xi & -\sqrt{1-\xi^2} \\ \sqrt{1-\xi^2} & \xi \end{pmatrix}$$

Using $\mathcal{R}^{-1} = {}^t\mathcal{R}$ we find

$$S^{\mathrm{E}}_p = \xi S^{\mathrm{E}}_{p_\parallel} \tag{4.147}$$
$$S^{\mathrm{E}}_\xi = -\sqrt{1-\xi^2} S^{\mathrm{E}}_{p_\parallel} \tag{4.148}$$

and $\mathbf{S}^{\mathrm{E}}$ countains a convective part only

$$\mathbf{S}^{\mathrm{E}} = \mathbf{F}^{\mathrm{E}}_{\mathbf{p}} f_0 \tag{4.149}$$

with

$$F^{\mathrm{E}}_p = q_e \xi E_\parallel$$
$$F^{\mathrm{E}}_\xi = -q_e \sqrt{1-\xi^2} E_\parallel$$

4.2.2 Bounce Averaged Fokker-Planck Equation

In the Fokker-Planck equation, the diffusion and convection elements are bounce-averaged according to the expressions (3.189)-(3.194), which gives, using (4.149),

$$\mathbb{D}^{\mathrm{E}(0)}_{\mathbf{p}} = 0 \tag{4.150}$$

and the convection components

$$F^{\mathrm{E}(0)}_p = \left\{ q_e \xi E_\parallel \right\} \tag{4.151}$$
$$F^{\mathrm{E}(0)}_\xi = -\sigma \left\{ \frac{\sigma \xi}{\sqrt{\Psi} \xi_0} q_e \sqrt{1-\xi^2} E_\parallel \right\} \tag{4.152}$$

Since the poloidal dependence of the electric field on a flux-surface is given by ()

$$E_{\|}\left(\psi,\theta\right)=\frac{1}{\Psi\left(\psi,\theta\right)}\frac{R_0^2}{R^2}E_{\|0}\left(\psi\right) \tag{4.153}$$

we find

$$F_p^{\mathrm{E}(0)} = \frac{\overline{\lambda}_{1,-1,2}}{\lambda}q_e\xi_0 E_{\|0}\left(\psi\right) \tag{4.154}$$

$$F_\xi^{\mathrm{E}(0)} = -\frac{\overline{\lambda}_{1,-1,2}}{\lambda}q_e\sqrt{1-\xi_0^2}E_{\|0}\left(\psi\right) \tag{4.155}$$

where we defined the bounce averaged coefficient (2.66)

$$\overline{\lambda}_{1,-1,2}=\lambda\sigma\left\{\sigma\frac{\xi}{\xi_0}\frac{1}{\Psi\left(\psi,\theta\right)}\frac{R_0^2}{R^2}\right\} \tag{4.156}$$

Expression of $\overline{\lambda}_{1,-1,2}$

The coefficient $\overline{\lambda}_{1,-1,2}$, which is known as s^* in the old notation found in the litterature ([19]), is expressed as

$$\overline{\lambda}_{1,-1,2}=\frac{\sigma}{\widetilde{q}}\left[\frac{1}{2}\sum_\sigma\right]_T\int_{\theta_{\min}}^{\theta_{\max}}\frac{d\theta}{2\pi}\frac{1}{\left|\widehat{\psi}\,.\,\widehat{r}\right|}\frac{r}{R_p}\frac{B}{B_P}\sigma\frac{1}{\Psi\left(\psi,\theta\right)}\frac{R_0^2}{R^2} \tag{4.157}$$

Since the integral is odd in σ, the sum over trapped particles vanishes, and we have

$$\overline{\lambda}_{1,-1,2}=\left|\begin{array}{ll}0 & \text{for trapped particles}\\ \lambda_{1,-1,2}^P & \text{for passing particles}\end{array}\right. \tag{4.158}$$

$$\begin{aligned}\lambda_{1,-1,2}^P &= \frac{1}{\widetilde{q}}\int_0^{2\pi}\frac{d\theta}{2\pi}\frac{1}{\left|\widehat{\psi}\,.\,\widehat{r}\right|}\frac{r}{R_p}\frac{B}{B_P}\frac{1}{\Psi\left(\psi,\theta\right)}\frac{R_0^2}{R^2}\\ &= \frac{1}{\widetilde{q}}\frac{R_0}{R_p}\int_0^{2\pi}\frac{d\theta}{2\pi}\frac{1}{\left|\widehat{\psi}\,.\,\widehat{r}\right|}\frac{r}{R}\frac{B_0}{B_P}\frac{R_0}{R}\\ &= \frac{1}{\widetilde{q}}\frac{R_0}{R_p}\frac{B_0}{B_{T0}}\int_0^{2\pi}\frac{d\theta}{2\pi}\frac{1}{\left|\widehat{\psi}\,.\,\widehat{r}\right|}\frac{r}{R}\frac{B_{T0}}{B_P}\frac{R_0}{R}\\ &= \frac{1}{\widetilde{q}}\frac{R_0}{R_p}\frac{B_0}{B_{T0}}\int_0^{2\pi}\frac{d\theta}{2\pi}\frac{1}{\left|\widehat{\psi}\,.\,\widehat{r}\right|}\frac{r}{R}\frac{B_T}{B_P}\\ &= \frac{q}{\widetilde{q}}\frac{R_0}{R_p}\frac{B_0}{B_{T0}}\end{aligned} \tag{4.159}$$

Case of circular concentric flux-surfaces

Since in the case of circular concentric flux-surfaces, we have

$$\widetilde{q} = \frac{r}{R_p}\frac{B}{B_P} \tag{4.160}$$

$$q = \frac{r}{R_p}\frac{B_T}{B_P}\int_0^{2\pi}\frac{d\theta}{2\pi}\frac{R_p}{R} \tag{4.161}$$

so that

$$\lambda^P_{1,-1,2} = \int_0^{2\pi}\frac{d\theta}{2\pi}\frac{R_0}{R} = \int_0^{2\pi}\frac{d\theta}{2\pi}\frac{1+\epsilon}{1+\epsilon\cos\theta} \tag{4.162}$$

This integral can then be performed analytically, as shown in Sec. B.1, at formula (B.27), which gives

$$\lambda^P_{1,-1,2} = \sqrt{\frac{1+\epsilon}{1-\epsilon}} \tag{4.163}$$

4.2.3 Bounce Averaged Drift Kinetic Equation

In the first order Drift-Kinetic equation, the diffusion and convection flux elements related to $\widetilde{f}$ are bounce-averaged according to the expressions (3.218)-(3.223), which gives, using (4.149),

$$\widetilde{\mathbb{D}}^{\mathrm{E}(0)}_{\mathbf{p}} = 0 \tag{4.164}$$

and the convection components

$$\widetilde{F}^{\mathrm{E}(0)}_p = \sigma\left\{\sigma\frac{\xi}{\Psi\xi_0}q_e\xi E_\parallel\right\} \tag{4.165}$$

$$\widetilde{F}^{\mathrm{E}(0)}_\xi = -\left\{\frac{\xi^2}{\Psi^{3/2}\xi_0^2}q_e\sqrt{1-\xi^2}E_\parallel\right\} \tag{4.166}$$

Since the poloidal dependence of the electric field on a flux-surface is given by relation (4.142)

$$E_\parallel(\psi,\theta) = \frac{1}{\Psi(\psi,\theta)}\frac{R_0^2}{R^2}E_{\parallel 0}(\psi) \tag{4.167}$$

we find

$$\widetilde{F}^{\mathrm{E}(0)}_p = \frac{\overline{\lambda}_{2,-2,2}}{\lambda}q_e\xi_0 E_{\parallel 0}(\psi) \tag{4.168}$$

$$\widetilde{F}^{\mathrm{E}(0)}_\xi = -\frac{\overline{\lambda}_{2,-2,2}}{\lambda}q_e\sqrt{1-\xi_0^2}E_{\parallel 0}(\psi)$$

where we defined the bounce averaged coefficient (2.66)

$$\overline{\lambda}_{2,-2,2} = \lambda\left\{\frac{\xi^2}{\xi_0^2}\frac{1}{\Psi^2}\frac{R_0^2}{R^2}\right\} \tag{4.169}$$

4.3 Radio frequency waves

The volume-averaged quasilinear diffusion operator for radiofrequency waves in an infinite uniform plasma was first developped by Kennel and Engelmann [20]. The relativistic treatment was performed by Lerche [21], who proposes the following operator

$$Q(f) = -\frac{e^2}{(2\pi)^3} \lim_{V\to\infty} \frac{1}{V} \sum_{n=-\infty}^{\infty} \iiint d^3k \left[\left(P_\parallel^* E_{\mathbf{k},\parallel}^* J_n + \left[P_\perp^* - \frac{1}{p_\perp} \left(\frac{k_\parallel v_\parallel}{\omega^*} - 1 \right) \right] E_{\mathbf{k},\perp}^* \right) \cdot \frac{i}{\left[n\Omega + k_\parallel v_\parallel - \omega \right]} \left(E_{\mathbf{k},\parallel} J_n P_\parallel + E_{\mathbf{k},\perp} P_\perp \right) f \right] \tag{4.170}$$

with

$$P_\parallel = \frac{\partial}{\partial p_\parallel} - \frac{n\Omega}{\omega v_\perp} \left(v_\perp \frac{\partial}{\partial p_\parallel} - v_\parallel \frac{\partial}{\partial p_\perp} \right) \tag{4.171}$$

$$P_\perp = \frac{\partial}{\partial p_\perp} + \frac{k_\parallel}{\omega} \left(v_\perp \frac{\partial}{\partial p_\parallel} - v_\parallel \frac{\partial}{\partial p_\perp} \right) \tag{4.172}$$

$$E_{\mathbf{k},\perp} = \frac{1}{\sqrt{2}} \left(E_{\mathbf{k},-} e^{i\alpha} J_{n+1} + E_{\mathbf{k},+} e^{-i\alpha} J_{n-1} \right) \tag{4.173}$$

The electric field is assumed to be monochromatic at the frequency ω, and is decomposed into its Fourier components

$$\mathbf{E}(\mathbf{x}, t) = \iiint \frac{d^3k}{(2\pi)^3} e^{i\mathbf{k}\cdot\mathbf{x} - i\omega t} \mathbf{E}_\mathbf{k}(\mathbf{k}) \tag{4.174}$$

which are projected on the rotating field frame

$$E_{\mathbf{k},\pm} = \frac{1}{\sqrt{2}} \left(E_{\mathbf{k},x} \pm i E_{\mathbf{k},y} \right) \tag{4.175}$$

$$E_{\mathbf{k},\parallel} = E_{\mathbf{k},z} \tag{4.176}$$

The wave vector is expressed in cylindrical coordinates as

$$\begin{aligned} k_x &= k_\perp \cos\alpha \\ k_y &= k_\perp \sin\alpha \\ k_z &= k_\parallel \end{aligned} \tag{4.177}$$

and the argument of the Bessel functions is $k_\perp v_\perp / \Omega$. The relativistic cyclotron frequency is

$$\Omega = \frac{q_e B}{\gamma m_e} \tag{4.178}$$

4.3.1 Conservative formulation of the RF wave operator

In order to incorporate the RF wave physics in the Fokker-Planck or Drift Kinetic solvers, the operator (4.170) must be cast in a conservative form.

Spherical coordinates representation

The transformation from cylindrical to spherical momentum derivatives is given by

$$\frac{\partial}{\partial p_\parallel} = \frac{\partial p}{\partial p_\parallel}\frac{\partial}{\partial p} + \frac{\partial \xi}{\partial p_\parallel}\frac{\partial}{\partial \xi} \tag{4.179}$$

$$\frac{\partial}{\partial p_\perp} = \frac{\partial p}{\partial p_\perp}\frac{\partial}{\partial p} + \frac{\partial \xi}{\partial p_\perp}\frac{\partial}{\partial \xi} \tag{4.180}$$

Since

$$p = \sqrt{p_\parallel^2 + p_\perp^2} \tag{4.181}$$

$$\xi = \frac{p_\parallel}{\sqrt{p_\parallel^2 + p_\perp^2}} \tag{4.182}$$

one obtains

$$\frac{\partial p}{\partial p_\parallel} = \xi \tag{4.183}$$

$$\frac{\partial p}{\partial p_\perp} = \sqrt{1-\xi^2} \tag{4.184}$$

$$\frac{\partial \xi}{\partial p_\parallel} = \frac{1-\xi^2}{p} \tag{4.185}$$

$$\frac{\partial \xi}{\partial p_\perp} = -\frac{\xi\sqrt{1-\xi^2}}{p} \tag{4.186}$$

Hence rewritting (4.171-4.172) in cylindrical coordinates using (4.179-4.180)

$$P_\parallel = \xi\frac{\partial}{\partial p} + \frac{1}{p}\left(1-\xi^2-\frac{n\Omega}{\omega}\right)\frac{\partial}{\partial \xi} \tag{4.187}$$

$$P_\perp = \sqrt{1-\xi^2}\frac{\partial}{\partial p} - \frac{\sqrt{1-\xi^2}}{p\xi}\left(\xi^2 - \frac{k_\parallel v_\parallel}{\omega}\right)\frac{\partial}{\partial \xi} \tag{4.188}$$

In order to permute derivatives and the integral in expression (4.170) and obtain a conservative formulation, one must express both $P_\parallel$ and $P_\perp$ in terms of the derivatives associated with the divergence of a flux: $1/p^2\,(\partial/\partial p)\,p^2$ and $-1/p\,(\partial/\partial \xi)$.

Since

$$\xi\frac{\partial}{\partial p} = \frac{1}{p^2}\frac{\partial}{\partial p}p^2\xi - \frac{2\xi}{p} \tag{4.189}$$

$$\sqrt{1-\xi^2}\frac{\partial}{\partial p} = \frac{1}{p^2}\frac{\partial}{\partial p}p^2\sqrt{1-\xi^2} - \frac{2\sqrt{1-\xi^2}}{p} \tag{4.190}$$

and

$$\frac{1}{p}\left(1-\xi^2-\frac{n\Omega}{\omega}\right)\frac{\partial}{\partial\xi}=-\frac{1}{p}\frac{\partial}{\partial\xi}\left(-1+\xi^2+\frac{n\Omega}{\omega}\right)+\frac{2\xi}{p} \tag{4.191}$$

$$-\frac{\sqrt{1-\xi^2}}{p\xi}\left(\xi^2-\frac{k_\parallel v_\parallel}{\omega}\right)\frac{\partial}{\partial\xi}=-\frac{1}{p}\frac{\partial}{\partial\xi}\frac{\sqrt{1-\xi^2}}{\xi}\left(\xi^2-\frac{k_\parallel v_\parallel}{\omega}\right)+\frac{1}{p_\perp}\left(\frac{k_\parallel v_\parallel}{\omega}-1\right)+\frac{2\sqrt{1-\xi^2}}{p} \tag{4.192}$$

the operators in (4.170) can be expressed in a divergence form

$$P_\parallel=\frac{1}{p^2}\frac{\partial}{\partial p}p^2\xi-\frac{1}{p}\frac{\partial}{\partial\xi}\left(-1+\xi^2+\frac{n\Omega}{\omega}\right) \tag{4.193}$$

$$P_\perp-\frac{1}{p_\perp}\left(\frac{k_\parallel v_\parallel}{\omega}-1\right)=\frac{1}{p^2}\frac{\partial}{\partial p}p^2\sqrt{1-\xi^2}-\frac{1}{p}\frac{\partial}{\partial\xi}\frac{\sqrt{1-\xi^2}}{\xi}\left(\xi^2-\frac{k_\parallel v_\parallel}{\omega}\right) \tag{4.194}$$

so that (4.170) can be rewritten as

$$Q\left(f\right)=-\nabla\cdot S^{\mathrm{RF}}=-\frac{1}{p^2}\frac{\partial}{\partial p}\left(p^2S_p^{\mathrm{RF}}\right)+\frac{1}{p}\frac{\partial}{\partial\xi}\left(\sqrt{1-\xi^2}S_\xi^{\mathrm{RF}}\right) \tag{4.195}$$

with

$$S_p^{\mathrm{RF}}=\lim_{V\to\infty}\frac{e^2}{\left(2\pi\right)^3}\frac{1}{V}\sum_{n=-\infty}^{\infty}\iiint d^3k\left[\left(\xi E_{\mathbf{k},\parallel}^*J_n+\sqrt{1-\xi^2}E_{\mathbf{k},\perp}^*\right)\cdot\frac{i}{\left[n\Omega+k_\parallel v_\parallel-\omega\right]}\left(E_{\mathbf{k},\parallel}J_nP_\parallel+E_{\mathbf{k},\perp}P_\perp\right)f\right] \tag{4.196}$$

$$S_\xi^{\mathrm{RF}}=\lim_{V\to\infty}\frac{e^2}{\left(2\pi\right)^3}\frac{1}{V}\sum_{n=-\infty}^{\infty}\iiint d^3k\left[\left(\frac{-1}{\sqrt{1-\xi^2}}\left(1-\xi^2-\frac{n\Omega}{\omega^*}\right)E_{\mathbf{k},\parallel}^*J_n+\frac{1}{\xi}\left(\xi^2-\frac{k_\parallel v_\parallel}{\omega^*}\right)E_{\mathbf{k},\perp}^*\right)\cdot\frac{i}{\left[n\Omega+k_\parallel v_\parallel-\omega\right]}\left(E_{\mathbf{k},\parallel}J_nP_\parallel+E_{\mathbf{k},\perp}P_\perp\right)f\right] \tag{4.197}$$

Considering the above expressions of the fluxes and the operators (4.187-4.188), RF-induced fluxes are purely diffusive, and therefore they are expressed as

$$\mathbf{S}^{\mathrm{RF}}=-\mathbb{D}^{\mathrm{RF}}\cdot\nabla_{\mathbf{p}}f \tag{4.198}$$

with

$$\mathbb{D}^{\mathrm{RF}}=\begin{pmatrix}D_{pp}^{\mathrm{RF}} & D_{p\xi}^{\mathrm{RF}}\\ D_{\xi p}^{\mathrm{RF}} & D_{\xi\xi}^{\mathrm{RF}}\end{pmatrix} \tag{4.199}$$

Hence, using the expression of the gradient in spherical coordinates,

$$S_p^{\mathrm{RF}} = -D_{pp}^{\mathrm{RF}} \frac{\partial f}{\partial p} + D_{p\xi}^{\mathrm{RF}} \frac{\sqrt{1-\xi^2}}{p} \frac{\partial f}{\partial \xi} \tag{4.200}$$

$$S_\xi^{\mathrm{RF}} = -D_{\xi p}^{\mathrm{RF}} \frac{\partial f}{\partial p} + D_{\xi\xi}^{\mathrm{RF}} \frac{\sqrt{1-\xi^2}}{p} \frac{\partial f}{\partial \xi} \tag{4.201}$$

with

$$\begin{aligned} D_{pp}^{\mathrm{RF}} = &- \lim_{V\to\infty} \frac{e^2}{(2\pi)^3} \frac{1}{V} \sum_{n=-\infty}^{\infty} \iiint d^3k \left[\left(\xi E_{\mathbf{k},\parallel}^* J_n + \sqrt{1-\xi^2} E_{\mathbf{k},\perp}^* \right) \right. \\ &\left. \cdot \frac{i}{\left[n\Omega + k_\parallel v_\parallel - \omega \right]} \left(\xi E_{\mathbf{k},\parallel} J_n + \sqrt{1-\xi^2} E_{\mathbf{k},\perp} \right) \right] \end{aligned} \tag{4.202}$$

$$\begin{aligned} D_{p\xi}^{\mathrm{RF}} = &\lim_{V\to\infty} \frac{e^2}{(2\pi)^3} \frac{1}{V} \sum_{n=-\infty}^{\infty} \iiint d^3k \left[\left(\xi E_{\mathbf{k},\parallel}^* J_n + \sqrt{1-\xi^2} E_{\mathbf{k},\perp}^* \right) \right. \\ &\left. \cdot \frac{i}{\left[n\Omega + k_\parallel v_\parallel - \omega \right]} \left(\frac{1}{\sqrt{1-\xi^2}} \left(1 - \xi^2 - \frac{n\Omega}{\omega} \right) E_{\mathbf{k},\parallel} J_n - \frac{1}{\xi} \left(\xi^2 - \frac{k_\parallel v_\parallel}{\omega} \right) E_{\mathbf{k},\perp} \right) \right] \end{aligned} \tag{4.203}$$

$$\begin{aligned} D_{\xi p}^{\mathrm{RF}} = &- \lim_{V\to\infty} \frac{e^2}{(2\pi)^3} \frac{1}{V} \sum_{n=-\infty}^{\infty} \iiint d^3k \\ &\left[\left(\frac{-1}{\sqrt{1-\xi^2}} \left(1 - \xi^2 - \frac{n\Omega}{\omega^*} \right) E_{\mathbf{k},\parallel}^* J_n + \frac{1}{\xi} \left(\xi^2 - \frac{k_\parallel v_\parallel}{\omega^*} \right) E_{\mathbf{k},\perp}^* \right) \right. \\ &\left. \cdot \frac{i}{\left[n\Omega + k_\parallel v_\parallel - \omega \right]} \left(E_{\mathbf{k},\parallel} J_n \xi + E_{\mathbf{k},\perp} \sqrt{1-\xi^2} \right) \right] \end{aligned} \tag{4.204}$$

$$\begin{aligned} D_{\xi\xi}^{\mathrm{RF}} = &\lim_{V\to\infty} \frac{e^2}{(2\pi)^3} \frac{1}{V} \sum_{n=-\infty}^{\infty} \iiint d^3k \\ &\left[\left(\frac{-1}{\sqrt{1-\xi^2}} \left(1 - \xi^2 - \frac{n\Omega}{\omega^*} \right) E_{\mathbf{k},\parallel}^* J_n + \frac{1}{\xi} \left(\xi^2 - \frac{k_\parallel v_\parallel}{\omega^*} \right) E_{\mathbf{k},\perp}^* \right) \right. \\ &\left. \cdot \frac{i}{\left[n\Omega + k_\parallel v_\parallel - \omega \right]} \left(\frac{1}{\sqrt{1-\xi^2}} \left(1 - \xi^2 - \frac{n\Omega}{\omega} \right) E_{\mathbf{k},\parallel} J_n - \frac{1}{\xi} \left(\xi^2 - \frac{k_\parallel v_\parallel}{\omega} \right) E_{\mathbf{k},\perp} \right) \right] \end{aligned} \tag{4.205}$$

In the limit of a resonant diffusion,

$$\frac{1}{\left[n\Omega + k_\parallel v_\parallel - \omega \right]} \to i\pi\delta \left(\omega - k_\parallel v_\parallel - n\Omega \right) \tag{4.206}$$

and using the resonance condition

$$k_\parallel v_\parallel = \omega - n\Omega \tag{4.207}$$

RF diffusion coefficients may be expressed in a simple form

$$D_{pp}^{\mathrm{RF}} = \sum_{n=-\infty}^{\infty} \left(1-\xi^2\right) D_n^{\mathrm{RF}}\left(p,\xi\right) \tag{4.208}$$

$$D_{p\xi}^{\mathrm{RF}} = \sum_{n=-\infty}^{\infty} -\frac{\sqrt{1-\xi^2}}{\xi}\left(1-\xi^2-\frac{n\Omega}{\omega}\right) D_n^{\mathrm{RF}}\left(p,\xi\right) \tag{4.209}$$

$$D_{\xi p}^{\mathrm{RF}} = \sum_{n=-\infty}^{\infty} -\frac{\sqrt{1-\xi^2}}{\xi}\left(1-\xi^2-\frac{n\Omega}{\omega}\right) D_n^{\mathrm{RF}}\left(p,\xi\right) \tag{4.210}$$

$$D_{\xi\xi}^{\mathrm{RF}} = \sum_{n=-\infty}^{\infty} \frac{1}{\xi^2}\left(1-\xi^2-\frac{n\Omega}{\omega}\right)^2 D_n^{\mathrm{RF}}\left(p,\xi\right) \tag{4.211}$$

where we define a diffusion coefficient

$$D_n^{\mathrm{RF}}\left(p,\xi\right) = \lim_{V\to\infty}\frac{\pi e^2}{V}\iiint\frac{d^3k}{\left(2\pi\right)^3}\delta\left(\omega-k_\parallel v_\parallel-n\Omega\right)\left|E_{\mathbf{k},\perp}+\frac{\xi}{\sqrt{1-\xi^2}}E_{\mathbf{k},\parallel}J_n\right|^2 \tag{4.212}$$

Using (4.173), we can define

$$\begin{aligned} D_{\mathbf{k}}^{(n)} = e^2\Bigg|&\frac{1}{\sqrt{2}}E_{\mathbf{k},+}e^{-i\alpha}J_{n-1}\left(\frac{k_\perp v_\perp}{\Omega}\right)+\frac{1}{\sqrt{2}}E_{\mathbf{k},-}e^{+i\alpha}J_{n+1}\left(\frac{k_\perp v_\perp}{\Omega}\right)\\ &+\frac{p_\parallel}{p_\perp}E_{\mathbf{k},\parallel}J_n\left(\frac{k_\perp v_\perp}{\Omega}\right)\Bigg|^2 \end{aligned} \tag{4.213}$$

so that (4.212) becomes

$$D_n^{\mathrm{RF}}(p,\xi) = \lim_{V\to\infty}\frac{\pi}{V}\int\frac{d^3k}{\left(2\pi\right)^3}D_{\mathbf{k}}^{(n)}\delta(\omega-k_\parallel v_\parallel-n\Omega) \tag{4.214}$$

If rays are gathered in RF beams of different frequencies ω_b, diffusion coefficients are sums of each contribution ower all hamonics n , leading to the expression

$$D_{pp}^{\mathrm{RF}} = \sum_{n=-\infty}^{+\infty}\sum_b(1-\xi^2)D_{b,n}^{\mathrm{RF}}(p,\xi) \tag{4.215}$$

$$D_{p\xi}^{\mathrm{RF}} = \sum_{n=-\infty}^{+\infty}\sum_b -\frac{\sqrt{1-\xi^2}}{\xi}\left[1-\xi^2-\frac{n\Omega}{\omega_b}\right]D_{b,n}^{\mathrm{RF}}(p,\xi) \tag{4.216}$$

$$D_{\xi p}^{\mathrm{RF}} = \sum_{n=-\infty}^{+\infty}\sum_b -\frac{\sqrt{1-\xi^2}}{\xi}\left[1-\xi^2-\frac{n\Omega}{\omega_b}\right]D_{b,n}^{\mathrm{RF}}(p,\xi) \tag{4.217}$$

$$D_{\xi\xi}^{\mathrm{RF}} = \sum_{n=-\infty}^{+\infty}\sum_b \frac{1}{\xi^2}\left[1-\xi^2-\frac{n\Omega}{\omega_b}\right]^2 D_{b,n}^{\mathrm{RF}}(p,\xi) \tag{4.218}$$

where

$$D_{n,b}^{\mathrm{RF}}(p,\xi) = \lim_{V\to\infty}\frac{\pi}{V}\int\frac{d^3k}{\left(2\pi\right)^3}D_{\mathbf{k}}^{b,(n)}\delta(\omega_b-k_\parallel v_\parallel-n\Omega) \tag{4.219}$$

and $D_{\mathbf{k}}^{b,(n)}$ accounts for the polarization and the intensity of the RF wave. It is given by

$$D_{\mathbf{k}}^{b,(n)} = e^2 \left| \frac{1}{\sqrt{2}} E_{\mathbf{k},b,+} e^{-i\alpha} J_{n-1}\left(\frac{k_{b\perp} v_\perp}{\Omega}\right) + \frac{1}{\sqrt{2}} E_{\mathbf{k},b,-} e^{+i\alpha} J_{n+1}\left(\frac{k_{b\perp} v_\perp}{\Omega}\right) + \frac{p_\parallel}{p_\perp} E_{\mathbf{k},b,\parallel} J_n\left(\frac{k_{b\perp} v_\perp}{\Omega}\right) \right|^2 \tag{4.220}$$

Cylindrical coordinates representation

The Fokker-Planck equation is usually solved numerically in spherical coordinates, because of the spherical symmetry of the collisional operator. Therefore, in this coordinate system, the numerical problem is well-conditionned, ensuring stable convergence towards the solution. However, in many case the RF quasilinear operator has a more cylindrical symmetry, and it could be useful to derive its expression in this coordinate system, in order to get a more physical insight of the wave-particle interaction. Starting from the general expression of the flux divergence in cylindrical coordinates,

$$\nabla_p \cdot \mathbf{S} = \frac{1}{p_\perp} \frac{\partial}{\partial p_\perp} \left(p_\perp S_\perp\right) + \frac{\partial}{\partial p_\parallel} \left(S_\parallel\right) \tag{4.221}$$

and taking into account of the diffusive nature of the wave-particle interaction,

$$\mathbf{S}^{\mathrm{RF}} = -\mathbb{D}^{\mathrm{RF}} \cdot \nabla f = - \begin{pmatrix} D_{\perp\perp} & D_{\perp\parallel} \\ D_{\parallel\perp} & D_{\parallel\parallel} \end{pmatrix} \cdot \begin{pmatrix} \partial f/\partial p_\perp \\ \partial f/\partial p_\parallel \end{pmatrix} \tag{4.222}$$

where the cylindrical tensor elements are related to the spherical ones by

$$\begin{pmatrix} D_{\perp\perp} \\ D_{\perp\parallel} \\ D_{\parallel\perp} \\ D_{\parallel\parallel} \end{pmatrix} = \begin{pmatrix} \left(1-\xi^2\right) & \xi\sqrt{1-\xi^2} & \xi\sqrt{1-\xi^2} & \xi^2 \\ \xi\sqrt{1-\xi^2} & -\left(1-\xi^2\right) & \xi^2 & -\xi\sqrt{1-\xi^2} \\ \xi\sqrt{1-\xi^2} & \xi^2 & -\left(1-\xi^2\right) & -\xi\sqrt{1-\xi^2} \\ \xi^2 & -\xi\sqrt{1-\xi^2} & -\xi\sqrt{1-\xi^2} & \left(1-\xi^2\right) \end{pmatrix} \cdot \begin{pmatrix} D_{pp} \\ D_{p\xi} \\ D_{\xi p} \\ D_{\xi\xi} \end{pmatrix} \tag{4.223}$$

Applying this transformation, one obtains,

$$D_{\perp\perp}^{\mathrm{RF}} = \sum_{n=-\infty}^{+\infty} \sum_b \left[\frac{n\Omega}{\omega_b}\right]^2 D_{b,n}^{\mathrm{RF}}(p,\xi) \tag{4.224}$$

$$D_{\perp\parallel}^{\mathrm{RF}} = \sum_{n=-\infty}^{+\infty} \sum_b \frac{\sqrt{1-\xi^2}}{\xi} \frac{n\Omega}{\omega_b} \left[1 - \frac{n\Omega}{\omega_b}\right] D_{b,n}^{\mathrm{RF}}(p,\xi) \tag{4.225}$$

$$D_{\parallel\perp}^{\mathrm{RF}} = \sum_{n=-\infty}^{+\infty} \sum_b \frac{\sqrt{1-\xi^2}}{\xi} \frac{n\Omega}{\omega_b} \left[1 - \frac{n\Omega}{\omega_b}\right] D_{b,n}^{\mathrm{RF}}(p,\xi) \tag{4.226}$$

$$D_{\parallel\parallel}^{\mathrm{RF}} = \sum_{n=-\infty}^{+\infty} \sum_b \frac{\left(1-\xi^2\right)}{\xi^2} \left[1 - \frac{n\Omega}{\omega_b}\right]^2 D_{b,n}^{\mathrm{RF}}(p,\xi) \tag{4.227}$$

For $n = 0$ (which corresponds to the Lower Hybrid wave) the quasilinear diffusion is strictly along the parallel direction (i.e. magnetic field line). Also, at a cyclotron harmonic, where $\omega_b = n\Omega$, the diffusion is only perpendicular, when relativistic corrections are not considered.

4.3.2 RF Diffusion coefficient for a Plane Wave

4.3.3 Integration in k-space

The quasilinear diffusion coefficient (4.212), describing the interaction of the electrons with a given beam b at an harmonic n, is rewritten as

$$D_{b,n}^{\mathrm{RF}}(p,\xi) = \lim_{V\to\infty} \frac{e^2\pi}{V} \iiint \frac{d^3k}{(2\pi)^3} \left|\mathbf{E}_{b\mathbf{k}}\right|^2 \left|\Theta_{\mathbf{k}}^{b,(n)}\right|^2 \delta\left(\omega_b - k_\parallel v_\parallel - n\Omega\right) \tag{4.228}$$

where,

$$\begin{aligned}\Theta_{\mathbf{k}}^{b,(n)} = &\frac{1}{\sqrt{2}} e_{b\mathbf{k},+} e^{-i\alpha} J_{n-1}\left(\frac{k_\perp v_\perp}{\Omega}\right) + \frac{1}{\sqrt{2}} e_{b\mathbf{k},-} e^{+i\alpha} J_{n+1}\left(\frac{k_\perp v_\perp}{\Omega}\right) \\ &+ \frac{p_\parallel}{p_\perp} e_{b\mathbf{k},\parallel} J_n\left(\frac{k_\perp v_\perp}{\Omega}\right)\end{aligned} \tag{4.229}$$

Here, the polarization vector in Fourier space

$$\mathbf{e}_{b\mathbf{k}} = \frac{\mathbf{E}_{b\mathbf{k}}}{\left|\mathbf{E}_{b\mathbf{k}}\right|} \tag{4.230}$$

is introduced, whose components in the rotating field frame are

$$\begin{aligned} e_{b\mathbf{k},+} &= \frac{E_{b\mathbf{k},+}}{\left|\mathbf{E}_{b\mathbf{k}}\right|} = \frac{E_{b\mathbf{k},x} + iE_{b\mathbf{k},y}}{\sqrt{2}\left|\mathbf{E}_{b\mathbf{k}}\right|} \\ e_{b\mathbf{k},-} &= \frac{E_{b\mathbf{k},-}}{\left|\mathbf{E}_{b\mathbf{k}}\right|} = \frac{E_{b\mathbf{k},x} - iE_{b\mathbf{k},y}}{\sqrt{2}\left|\mathbf{E}_{b\mathbf{k}}\right|} \\ e_{b\mathbf{k},\parallel} &= \frac{E_{b\mathbf{k},\parallel}}{\left|\mathbf{E}_{b\mathbf{k}}\right|} = \frac{E_{b\mathbf{k},z}}{\left|\mathbf{E}_{b\mathbf{k}}\right|} \end{aligned} \tag{4.231}$$

The electric field associated with a given ray is described by a plane wave, with given frequency ω_b and wave number $\mathbf{k}_b$:

$$\mathbf{E}_b\left(\mathbf{x},t\right) = \mathrm{Re}\left[\mathbf{E}_{b0} e^{i(\mathbf{k}_b\cdot\mathbf{x}-\omega_b t)}\right] = \mathrm{Re}\left[\widetilde{\mathbf{E}}_b\right] \tag{4.232}$$

$$= \frac{1}{2}\left[\mathbf{E}_{b0} e^{i(\mathbf{k}_b\cdot\mathbf{x}-\omega_b t)} + \mathbf{E}_{b0}^* e^{-i(\mathbf{k}_b\cdot\mathbf{x}-\omega_b t)}\right] \tag{4.233}$$

so that

$$\begin{aligned}\mathbf{E}_{b\mathbf{k}}\left(\mathbf{k},t\right) &\equiv \iiint d^3x\; e^{-i\mathbf{k}\cdot\mathbf{x}} \mathbf{E}_b\left(\mathbf{x},t\right) \\ &= \frac{1}{2}\left[\mathbf{E}_{b0} e^{-i\omega_b t} \iiint d^3x\; e^{i(\mathbf{k}_b-\mathbf{k})\cdot\mathbf{x}} + \mathbf{E}_{b0}^* e^{i\omega_b t} \iiint d^3x\; e^{i(\mathbf{k}_b+\mathbf{k})\cdot\mathbf{x}}\right] \\ &= \frac{1}{2}\left[\mathbf{E}_{b0} e^{-i\omega_b t}\delta\left(\mathbf{k}_b-\mathbf{k}\right) + \mathbf{E}_{b0}^* e^{i\omega_b t}\delta\left(\mathbf{k}_b+\mathbf{k}\right)\right]\end{aligned} \tag{4.234}$$

The electric field is the sum of two contributions with different frequencies

$$\mathbf{E}^{+}_{b\mathbf{k}}(\mathbf{k}) = \frac{1}{2}\mathbf{E}_{b0}\delta(\mathbf{k}_b - \mathbf{k}) \text{ with } \omega = \omega_b \tag{4.235}$$

$$\mathbf{E}^{-}_{b\mathbf{k}}(\mathbf{k}) = \frac{1}{2}\mathbf{E}^{*}_{b0}\delta(\mathbf{k}_b + \mathbf{k}) \text{ with } \omega = -\omega_b \tag{4.236}$$

Therefore the QL diffusion tensor (4.199) is the sum of these two contributions:

$$\mathbb{D}^{\mathrm{RF}} = \mathbb{D}^{\mathrm{RF}+} + \mathbb{D}^{\mathrm{RF}-} \tag{4.237}$$

associated with the diffusion coefficients

$$D^{\mathrm{RF}+}_{b,n}(p,\xi) = \lim_{V\to\infty}\frac{e^2\pi}{V}\iiint\frac{d^3k}{(2\pi)^3}\left|\frac{1}{2}\mathbf{E}_{b0}\delta(\mathbf{k}_b-\mathbf{k})\right|^2\left|\Theta^{b^+,n}_{\mathbf{k}}\right|^2\delta\left(\omega_b - k_\parallel v_\parallel - n\Omega\right) \tag{4.238}$$

$$D^{\mathrm{RF}-}_{b,n}(p,\xi) = \lim_{V\to\infty}\frac{e^2\pi}{V}\iiint\frac{d^3k}{(2\pi)^3}\left|\frac{1}{2}\mathbf{E}^{*}_{b0}\delta(\mathbf{k}_b+\mathbf{k})\right|^2\left|\Theta^{b^-,n}_{\mathbf{k}}\right|^2\delta\left(-\omega_b - k_\parallel v_\parallel - n\Omega\right)$$

with, using (4.229)

$$\begin{aligned}\Theta^{b+,(n)}_{\mathbf{k}} &= \frac{1}{\sqrt{2}}e_{b^+\mathbf{k},+}e^{-i\alpha}J_{n-1}\left(\frac{k_\perp v_\perp}{\Omega}\right) + \frac{1}{\sqrt{2}}e_{b^+\mathbf{k},-}e^{+i\alpha}J_{n+1}\left(\frac{k_\perp v_\perp}{\Omega}\right)\\ &\quad + \frac{p_\parallel}{p_\perp}e_{b^+\mathbf{k},\parallel}J_n\left(\frac{k_\perp v_\perp}{\Omega}\right)\\ \Theta^{b-,(n)}_{\mathbf{k}} &= \frac{1}{\sqrt{2}}e_{b^-\mathbf{k},+}e^{-i\alpha}J_{n-1}\left(\frac{k_\perp v_\perp}{\Omega}\right) + \frac{1}{\sqrt{2}}e_{b^-\mathbf{k},-}e^{+i\alpha}J_{n+1}\left(\frac{k_\perp v_\perp}{\Omega}\right)\\ &\quad + \frac{p_\parallel}{p_\perp}e_{b^-\mathbf{k},\parallel}J_n\left(\frac{k_\perp v_\perp}{\Omega}\right)\end{aligned} \tag{4.239}$$

The polarization components (4.231) are

$$\begin{aligned}e_{b^+\mathbf{k},+} &= \frac{E_{b0,x}+iE_{b0,y}}{\sqrt{2}\,|\mathbf{E}_{b0}|} = e_{b0,+}\\ e_{b^+\mathbf{k},-} &= \frac{E_{b0,x}-iE_{b0,y}}{\sqrt{2}\,|\mathbf{E}_{b0}|} = e_{b0,-}\\ e_{b^+\mathbf{k},\parallel} &= \frac{E_{b0,z}}{|\mathbf{E}_{b0}|} = e_{b0,\parallel}\end{aligned} \tag{4.240}$$

and

$$\begin{aligned}e_{b^-\mathbf{k},+} &= \frac{E^*_{b0,x}+iE^*_{b0,y}}{\sqrt{2}\,|\mathbf{E}_{b0}|} = e^*_{b0,-}\\ e_{b^-\mathbf{k},-} &= \frac{E^*_{b0,x}-iE^*_{b0,y}}{\sqrt{2}\,|\mathbf{E}_{b0}|} = e^*_{b0,+}\\ e_{b^-\mathbf{k},\parallel} &= \frac{E^*_{b0,z}}{|\mathbf{E}_{b0}|} = e^*_{b0,\parallel}\end{aligned} \tag{4.241}$$

Expressing the condition $\mathbf{k} = \pm\mathbf{k}_b$ from the first delta function in (4.238), we find

$$D_{b,n}^{\mathrm{RF}+}(p,\xi) = \lim_{V\to\infty} \frac{e^2\pi}{4V}\frac{1}{|v_\parallel|}\iiint \frac{d^3k}{(2\pi)^3}\,|\mathbf{E}_{b0}|^2\,\delta^2\left(\mathbf{k}_b-\mathbf{k}\right)\left|\Theta_{\mathbf{k}}^{b+,n}\right|^2\delta\left(k_{b\parallel}-\frac{\omega_b-n\Omega}{v_\parallel}\right) \tag{4.242}$$

$$D_{b,n}^{\mathrm{RF}-}(p,\xi) = \lim_{V\to\infty} \frac{e^2\pi}{4V}\frac{1}{|v_\parallel|}\iiint \frac{d^3k}{(2\pi)^3}\,|\mathbf{E}_{b0}^*|^2\,\delta^2\left(\mathbf{k}_b+\mathbf{k}\right)\left|\Theta_{\mathbf{k}}^{b-,n}\right|^2\delta\left(k_{b\parallel}-\frac{\omega_b+n\Omega}{v_\parallel}\right)$$

with now (4.239) being

$$\begin{aligned}\Theta_{\mathbf{k}}^{b+,(n)} &= \frac{1}{\sqrt{2}}e_{b0,+}e^{-i\alpha_b}J_{n-1}\left(\frac{k_{b\perp}v_\perp}{\Omega}\right)+\frac{1}{\sqrt{2}}e_{b0,-}e^{+i\alpha_b}J_{n+1}\left(\frac{k_{b\perp}v_\perp}{\Omega}\right)\\ &\quad+\frac{p_\parallel}{p_\perp}e_{b0,\parallel}J_n\left(\frac{k_{b\perp}v_\perp}{\Omega}\right)\end{aligned} \tag{4.243}$$

$$\begin{aligned}\Theta_{\mathbf{k}}^{b-,(n)} &= \frac{1}{\sqrt{2}}e_{b0,-}^*e^{-i(\alpha_b+\pi)}J_{n-1}\left(\frac{k_{b\perp}v_\perp}{\Omega}\right)+\frac{1}{\sqrt{2}}e_{b0,+}^*e^{+i(\alpha_b+\pi)}J_{n+1}\left(\frac{k_{b\perp}v_\perp}{\Omega}\right)\\ &\quad+\frac{p_\parallel}{p_\perp}e_{b0,\parallel}^*J_n\left(\frac{k_{b\perp}v_\perp}{\Omega}\right)\\ &= -\frac{1}{\sqrt{2}}e_{b0,-}^*e^{-i\alpha_b}J_{n-1}\left(\frac{k_{b\perp}v_\perp}{\Omega}\right)-\frac{1}{\sqrt{2}}e_{b0,+}^*e^{+i\alpha_b}J_{n+1}\left(\frac{k_{b\perp}v_\perp}{\Omega}\right)\\ &\quad+\frac{p_\parallel}{p_\perp}e_{b0,\parallel}^*J_n\left(\frac{k_{b\perp}v_\perp}{\Omega}\right)\end{aligned} \tag{4.244}$$

where we used the fact that $\mathbf{k}_b$ is transformed into $-\mathbf{k}_b$ by changing $k_{b\parallel}$ to $-k_{b\parallel}$ and α_b to $\alpha_b+\pi$.

Using the properties of the Bessel functions, and defining $n' = -n$,

$$\begin{aligned}J_{n+1} &= (-1)^{n+1}\,J_{n'-1}\\ J_{n-1} &= (-1)^{n-1}\,J_{n'+1}\\ J_n &= (-1)^n\,J_{n'}\end{aligned} \tag{4.245}$$

so that (4.244) becomes

$$\begin{aligned}\Theta_{\mathbf{k}}^{b-,(n)} &= (-1)^n\left[\frac{1}{\sqrt{2}}e_{b0,-}^*e^{-i\alpha_b}J_{n'+1}\left(\frac{k_{b\perp}v_\perp}{\Omega}\right)+\frac{1}{\sqrt{2}}e_{b0,+}^*e^{+i\alpha_b}J_{n'-1}\left(\frac{k_{b\perp}v_\perp}{\Omega}\right)\right.\\ &\quad\left.+\frac{p_\parallel}{p_\perp}e_{b0,\parallel}^*J_{n'}\left(\frac{k_{b\perp}v_\perp}{\Omega}\right)\right] \qquad (4.246)\\ &= (-1)^n\left(\Theta_{\mathbf{k}}^{b+,(n)'}\right)^* \qquad (4.247)\end{aligned}$$

and the diffusion coefficients become

$$D_{b,n}^{\mathrm{RF}+}(p,\xi) = \lim_{V\to\infty} \frac{e^2\pi}{4V}\frac{1}{|v_\parallel|}\left|\Theta_{\mathbf{k}}^{b,(n)}\right|^2|\mathbf{E}_{b0}|^2\,\delta\left(k_{b\parallel}-\frac{\omega_b-n\Omega}{v_\parallel}\right)\iiint\frac{d^3k}{(2\pi)^3}\delta^2\left(\mathbf{k}_b-\mathbf{k}\right) \tag{4.248}$$

$$D_{b,n}^{\mathrm{RF}-}(p,\xi) = \lim_{V\to\infty} \frac{e^2\pi}{4V}\frac{1}{|v_\parallel|}\left|\Theta_{\mathbf{k}}^{b,(n)'}\right|^2|\mathbf{E}_{b0}|^2\,\delta\left(k_{b\parallel}-\frac{\omega_b-n'\Omega}{v_\parallel}\right)\iiint\frac{d^3k}{(2\pi)^3}\delta^2\left(\mathbf{k}_b+\mathbf{k}\right)$$

Using Parseval's theorem,

$$\lim_{V\to\infty}\frac{1}{V}\iiint\frac{d^3k}{(2\pi)^3}\delta^2\left(\mathbf{k}_b-\mathbf{k}\right)=\lim_{V\to\infty}\frac{1}{V}\iiint d^3x=1$$
$$\lim_{V\to\infty}\frac{1}{V}\iiint\frac{d^3k}{(2\pi)^3}\delta^2\left(\mathbf{k}_b+\mathbf{k}\right)=\lim_{V\to\infty}\frac{1}{V}\iiint d^3x=1 \tag{4.249}$$

one obtains

$$D_{b,n}^{\mathrm{RF}+}(p,\xi)=e^2\pi\frac{1}{\left|v_\parallel\right|}\frac{\left|\mathbf{E}_{b0}\right|^2}{4}\left|\Theta_{\mathbf{k}}^{b,(n)}\right|^2\delta\left(k_{b\parallel}-\frac{\omega_b-n\Omega}{v_\parallel}\right) \tag{4.250}$$

$$D_{b,n}^{\mathrm{RF}-}(p,\xi)=e^2\pi\frac{1}{\left|v_\parallel\right|}\frac{\left|\mathbf{E}_{b0}\right|^2}{4}\left|\Theta_{\mathbf{k}}^{b,(n)'}\right|^2\delta\left(k_{b\parallel}-\frac{\omega_b-n'\Omega}{v_\parallel}\right) \tag{4.251}$$

In the expression (4.216-4.218) for $\mathbb{D}^{\mathrm{RF}-}$ tensor elements, we subsitute

$$\left[1-\xi^2-\frac{n\Omega}{-\omega_b}\right]=\left[1-\xi^2-\frac{n'\Omega}{\omega_b}\right] \tag{4.252}$$

Then, by redefining $n'\to n$ in the sum over all harmonics for $\mathbb{D}^{\mathrm{RF}-}$, we can combine the two contributions of $\mathbb{D}^{\mathrm{RF}+}$ and $\mathbb{D}^{\mathrm{RF}-}$, and finally we obtain an expression with one diffusion coefficient:

$$\begin{aligned}D_{b,n}^{\mathrm{RF}}(p,\xi)&=e^2\pi\frac{1}{\left|v_\parallel\right|}\frac{\left|\mathbf{E}_{b0}\right|^2}{2}\left|\Theta_{\mathbf{k}}^{b,(n)}\right|^2\delta\left(k_{b\parallel}-\frac{\omega_b-n\Omega}{v_\parallel}\right)\\&=e^2\pi\frac{1}{\left|v_\parallel\right|}\frac{\left|\mathbf{E}_{b0}\right|^2}{2}\left|\Theta_{\mathbf{k}}^{b,(n)}\right|^2\frac{c}{\omega_b}\delta\left(N_{b\parallel}-N_{\parallel\mathrm{res}}\right)\end{aligned} \tag{4.253}$$

with (4.243)

$$\Theta_{\mathbf{k}}^{b,(n)}=\frac{1}{\sqrt{2}}e_{b0,+}e^{-i\alpha_b}J_{n-1}\left(\frac{k_{b\perp}v_\perp}{\Omega}\right)+\frac{1}{\sqrt{2}}e_{b0,-}e^{+i\alpha_b}J_{n+1}\left(\frac{k_{b\perp}v_\perp}{\Omega}\right)+\frac{p_\parallel}{p_\perp}e_{b0,\parallel}J_n\left(\frac{k_{b\perp}v_\perp}{\Omega}\right) \tag{4.254}$$

$$N_{b\parallel}=\frac{k_{b\parallel}c}{\omega_b} \tag{4.255}$$

$$\begin{aligned}N_{\parallel\mathrm{res}}&=\frac{c}{v_\parallel}\left(1-\frac{n\Omega}{\omega_b}\right)\\&=\frac{1}{\beta_{Te}}\frac{p_{Te}}{p_\parallel}\left(\gamma-\frac{n'\omega_{ce}}{\omega_b}\right)\end{aligned} \tag{4.256}$$

where

$$\Omega=\frac{q_eB}{\gamma m_e}=\frac{-\omega_{ce}}{\gamma}\text{ with }\omega_{ce}=\frac{eB}{m_e} \tag{4.257}$$

$$n'=-n \tag{4.258}$$

$$\beta_{Te}=\frac{p_{Te}}{m_ec}=\frac{v_{Te}}{c}=\sqrt{\frac{kT_e}{m_ec^2}} \tag{4.259}$$

4.3.4 Incident Energy Flow Density

Relation to the Electric Field

The time-averaged energy flow density in the beam is in general given by

$$\overline{s}_b = \mathbf{P}_b + \mathbf{T}_b \tag{4.260}$$

where

$$\mathbf{P}_b = \frac{1}{2}\mathrm{Re}\left[\widetilde{\mathbf{E}}_b \times \widetilde{\mathbf{H}}_b^*\right] \tag{4.261}$$

is the flow of the electromagnetic energy or Poynting vector, and

$$\mathbf{T}_b = -\frac{\epsilon_0 \omega_b}{4}\widetilde{\mathbf{E}}_b^* \cdot \frac{\partial \mathbb{K}^{\mathbb{H}}}{\partial \mathbf{k}} \cdot \widetilde{\mathbf{E}}_b \tag{4.262}$$

is the kinetic energy flow density where $\mathbb{K}^{\mathbb{H}}$ is the Hermitian part of the dielectric tensor.

$\widetilde{\mathbf{E}}_b$ is the complex form of the electric field (4.232)

$$\widetilde{\mathbf{E}}_b = \mathbf{E}_{b0} e^{i\mathbf{k}_b \cdot \mathbf{x} - i\omega_b t} \tag{4.263}$$

and the magnetic field $\widetilde{\mathbf{H}}_b$ is given by

$$\widetilde{\mathbf{H}}_b = \frac{\mathbf{k}_b \times \widetilde{\mathbf{E}}_b}{\mu_0 \omega_b} = \frac{\mathbf{N}_b \times \widetilde{\mathbf{E}}_b}{\mu_0 c} \tag{4.264}$$

using the relation $\mathbf{N}_b = \mathbf{k}_b \omega_b / c$.

The energy flow density (4.260) can be formally rewritten as

$$\overline{s}_b = \frac{\epsilon_0 c}{2} \left|\mathbf{E}_{b0}\right|^2 \mathbf{\Phi}_b \tag{4.265}$$

where $\mathbf{\Phi}_b$ is a non dimensional vector defined as

$$\mathbf{\Phi}_b = \mathbf{\Phi}_{bP} + \mathbf{\Phi}_{bT} \tag{4.266}$$

with

$$\mathbf{\Phi}_{bP} = \frac{\mu_0 c}{\left|\mathbf{E}_{b0}\right|^2}\mathrm{Re}\left[\widetilde{\mathbf{E}}_b \times \widetilde{\mathbf{H}}_b^*\right] \tag{4.267}$$

and

$$\mathbf{\Phi}_{bT} = -\frac{1}{2}\mathbf{e}_b^* \cdot \frac{\partial \mathbb{K}^{\mathbb{H}}}{\partial \mathbf{N}} \cdot \mathbf{e}_b \tag{4.268}$$

Using (4.264), we obtain

$$\begin{aligned} \mathbf{\Phi}_{bP} &= \mathrm{Re}\left[\mathbf{e}_b \times (\mathbf{N}_b \times \mathbf{e}_b^*)\right] \\ &= \mathrm{Re}\left[\mathbf{N}_b - (\mathbf{N}_b \cdot \mathbf{e}_b)\,\mathbf{e}_b^*\right] \end{aligned} \tag{4.269}$$

In vacuum, $\mathbf{\Phi}_b = \widehat{k}$, unit vector in the direction of propagation, and $\mathbf{\Phi}_{bT} = 0$. Here,

$$\mathbf{e}_b = \frac{\mathbf{E}_{b0}}{\left|\mathbf{E}_{b0}\right|} \tag{4.270}$$

is the polarization vector. The incident power flux on a flux-surface is therefore given by

$$\overline{\mathbf{s}}_{b\mathrm{inc}} = \frac{\epsilon_0 c}{2} \left|\mathbf{E}_{b0}\right|^2 \left|\mathbf{\Phi}_b \cdot \widehat{\psi}\right| \tag{4.271}$$

where $\widehat{\psi}$ is the local vector normal to the flux-surface.

Relation to the ray trajectories

The energy flows in the direction of the group velocity, noted $\widehat{g}$

$$\widehat{g}_b = \frac{\mathbf{\Phi}_b}{|\mathbf{\Phi}_b|} \tag{4.272}$$

In ray-tracing calculations, this is the direction of the ray trajectories, which are parametrized by $(\psi_b(s), \theta_b(s), \phi_b(s))$ where s is the distance along the ray. Therefore $\widehat{g}_b$ can be determined from ray-tracing calculations or any other wave propagation model, and we have

$$\overline{\mathbf{s}}_{b\text{inc}} = \frac{\epsilon_0 c}{2} |\mathbf{E}_{b0}|^2 |\mathbf{\Phi}_b| \left|\widehat{g}_b \cdot \widehat{\psi}\right| \tag{4.273}$$

In DKE calculations, flux-surfaces are discretized on a grid $\psi_{l+1/2}$ and have a finite volume (). In consequence, the factor $\left|\widehat{g}_b \cdot \widehat{\psi}\right|$ must be "integrated" along the ray trajectory within this volume. We therefore define an incidence factor

$$f_{\text{inc},b}^{l+1/2} = \frac{1}{\Delta l_{l+1/2}^{\theta_b}} \int_{\psi_{l+1/2} \mp \Delta\psi_{l+1/2}/2}^{\psi_{l+1/2} \pm \Delta\psi_{l+1/2}/2} ds \tag{4.274}$$

where the $\pm$ sign accounts for the fact that the ray may be locally directed either inward or outward, and where $\Delta l_{l+1/2}^{\theta_b}$ is the local thickness of the flux-surface.

$$\Delta l_{l+1/2}^{\theta_b} = \frac{\Delta\psi_{l+1/2}}{|\nabla\psi|_{l+1/2}^{\theta_b}} = \frac{\Delta\psi_{l+1/2}}{R_{l+1/2}^{\theta_b} B_{P,l+1/2}^{\theta_b}} \tag{4.275}$$

The factor $f_{\text{inc},b}^{l+1/2}$ can be numerically calculated from the equilibrium and ray-tracing data. In the limit of an infinitely thin flux-surface, we have

$$f_{\text{inc},b}^{l+1/2} \to \left|\widehat{g}_b \cdot \widehat{\psi}\right|^{-1} \tag{4.276}$$

We therefore substitute

$$\overline{\mathbf{s}}_{b\text{inc}} = \frac{\epsilon_0 c}{2} |\mathbf{E}_{b0}|^2 \frac{|\mathbf{\Phi}_b|}{f_{\text{inc},b}^{l+1/2}} \tag{4.277}$$

4.3.5 Narrow Beam Approximation

Let consider a ray which crosses the flux surface at the respective poloidal locations θ_b. Here, it is assumed that all electrons interact with the beam, whatever its toroidal location, because of the axisymmetry. Therefore, calculations are only valid for circulating electrons, except for those localized on low n order rational q-surfaces, since their trajectories are exactly periodic in configuration space. Consequently, either they may never crosses the beam or if they cross it, the quasilinear assumption might likely fail, since some correlations could remain between two momentum kicks. However, the total weight of these electrons is marginal, and their contribution to RF power absorption and current generation is

simply neglected. It is important to recal that trapped particle interaction with RF wave is not addressed in this code for similar arguments. For all particles whose trajectory is periodic, a specific treatment of the quasilinear interaction is necessary, which is at this stage beyond the scope of this development.

If we assume that the extension of the beam power on the flux-surface is very small in the poloidal directions, we can approximate

$$\bar{\mathbf{s}}_{b\text{inc}} \simeq \frac{P_{b,\text{inc}}}{\mathcal{A}_b}\delta\left(\theta-\theta_b\right) \tag{4.278}$$

This assumption is in contradication with the plane-wave decomposition of the RF beam, since plane waves are essentially present in the entire configuration space. However, it is assumed that plane waves interfere destructively everywhere except in the beam region, which can be limited to a narrow poloidal and toroidal extention. By definition, $\mathcal{A}_b$ is determined so that $P_{b,\text{inc}}$ is the total incident power on the flux-surface

$$\iint dS\,\bar{\mathbf{s}}_{b\text{inc}} = P_{b,\text{inc}} \tag{4.279}$$

which gives in the system (ψ,θ,ϕ) , using (A.199)

$$1 = \int_0^{2\pi} d\phi \int_0^{2\pi} \frac{rR}{\mathcal{A}_b\left|\widehat{\psi}\cdot\widehat{r}\right|}\delta\left(\theta-\theta_b\right)d\theta \tag{4.280}$$

Hence,

$$\mathcal{A}_b = \frac{2\pi rR}{\left|\widehat{\psi}\cdot\widehat{r}\right|} \tag{4.281}$$

and the incident power flux is simply

$$\bar{\mathbf{s}}_{b\text{inc}} = \frac{P_{b,\text{inc}}}{2\pi rR}\left|\widehat{\psi}\cdot\widehat{r}\right|\delta\left(\theta-\theta_b\right) \tag{4.282}$$

Using (4.277) and (4.282),

$$\frac{\left|\mathbf{E}_{b0}\right|^2}{2} = \frac{1}{\epsilon_0 c}\frac{1}{2\pi rR}\left|\widehat{\psi}\cdot\widehat{r}\right|\frac{f_{\text{inc},b}^{l+1/2}}{\left|\mathbf{\Phi}_b\right|}\delta\left(\theta-\theta_b\right)P_{b,\text{inc}} \tag{4.283}$$

For concentric circular flux surfaces, $\widehat{\psi}=\widehat{r}$, then $\left|\widehat{\psi}\cdot\widehat{r}\right|=1$. We obtain

$$\frac{\left|\mathbf{E}_{b0}\right|^2}{2} = \frac{1}{\epsilon_0 c}\frac{1}{2\pi rR_p}\frac{\Psi}{\Psi_p}\frac{f_{\text{inc},b}^{l+1/2}}{\left|\mathbf{\Phi}_b\right|}\delta\left(\theta-\theta_b\right)P_{b,\text{ inc}} \tag{4.284}$$

where $\Psi_p\left(r\right)=\Psi_p\left(r,\pi/2\right)=1+\epsilon$.

4.3.6 Normalized Diffusion Coefficient

The diffusion coefficient is usually normalized to the collisional diffusion coefficient $\nu_e p_{Te}^2$, thus defining

$$\overline{D}_{b,n}^{\mathrm{RF}}(p,\xi) \equiv \frac{D_{b,n}^{\mathrm{RF}}(p,\xi)}{\nu_e p_{Te}^2} \tag{4.285}$$

with

$$\nu_e = \frac{e^4 n_e \ln\Lambda}{4\pi\epsilon_0^2 m_e^2 v_{Te}^3} \tag{4.286}$$

Using (4.253) and (4.283), the diffusion coefficient (4.285) becomes

$$\overline{D}_{b,n}^{\mathrm{RF}}(p,\xi) = \overline{D}_{b,n,0}^{\mathrm{RF}} \left|\Theta_{\mathbf{k}}^{b,(n)}\right|^2 \frac{\gamma p_{Te}}{p\,|\xi|} \delta\left(N_{b\|} - N_{\|\mathrm{res}}\right) 2\pi\delta\left(\theta - \theta_b\right) \tag{4.287}$$

with

$$\begin{aligned}\overline{D}_{b,n,0}^{\mathrm{RF}} &= \frac{1}{\nu_e p_{Te}^2} \frac{1}{v_{Te}} \frac{\pi}{\omega_b} \frac{e^2}{\epsilon_0} \frac{1}{4\pi^2 r R} \left|\widehat{\psi}\cdot\widehat{r}\right| \frac{f_{\mathrm{inc},b}^{l+1/2}}{|\mathbf{\Phi}_b|} P_{b,\mathrm{inc}} \\ &= \frac{1}{rR} \frac{1}{m_e \ln\Lambda} \frac{1}{\omega_b \omega_{pe}^2} \left|\widehat{\psi}\cdot\widehat{r}\right| \frac{f_{\mathrm{inc},b}^{l+1/2}}{|\mathbf{\Phi}_b|} P_{b,\mathrm{inc}}\end{aligned} \tag{4.288}$$

where ω_{pe} is the electron plasma frequency

$$\omega_{pe} = \sqrt{\frac{e^2 n_e}{\epsilon_0 m_e}} \tag{4.289}$$

We also recall the expressions (4.254), (4.256) and (4.266-4.269)

$$\Theta_{\mathbf{k}}^{b,(n)} = \frac{1}{\sqrt{2}} e_{b0,+} e^{-i\alpha_b} J_{n-1}\left(\frac{k_{b\perp} v_\perp}{\Omega}\right) + \frac{1}{\sqrt{2}} e_{b0,-} e^{+i\alpha_b} J_{n+1}\left(\frac{k_{b\perp} v_\perp}{\Omega}\right) + \frac{p_\|}{p_\perp} e_{b0,\|} J_n\left(\frac{k_{b\perp} v_\perp}{\Omega}\right) \tag{4.290}$$

$$N_{\|\mathrm{res}} = \frac{c}{v_\|}\left(1 - \frac{n\Omega}{\omega_b}\right) = \frac{1}{\beta_{Te}} \frac{p_{Te}}{p_\|}\left(\gamma - \frac{n'\omega_{ce}}{\omega_b}\right) \tag{4.291}$$

$$\mathbf{\Phi}_b = \mathbf{\Phi}_{bP} + \mathbf{\Phi}_{bT} \tag{4.292}$$

$$\mathbf{\Phi}_{bP} = \mathrm{Re}\left[\mathbf{N}_b - \left(\mathbf{N}_b\cdot\mathbf{e}_b\right)\mathbf{e}_b^*\right] \tag{4.293}$$

$$\mathbf{\Phi}_{bT} = -\frac{1}{2}\mathbf{e}_b^* \cdot \frac{\partial \mathbb{K}^{\mathbb{H}}}{\partial \mathbf{N}} \cdot \mathbf{e}_b \tag{4.294}$$

For concentric circular flux surfaces,

$$\overline{D}_{b,n,0}^{\mathrm{RF}} = \frac{1}{rR_p} \frac{\Psi}{\Psi_p} \frac{1}{m_e \ln\Lambda} \frac{1}{\omega_b \omega_{pe}^2} \frac{f_{\mathrm{inc},b}^{l+1/2}}{|\mathbf{\Phi}_b|} P_{b,\mathrm{inc}} \tag{4.295}$$

4.3.7 Bounce Averaged Fokker-Planck Equation

In the Fokker-Planck equation, the diffusion and convection elements are bounce-averaged according to the expressions (3.189) and (3.194), which gives, using (4.215-4.218)

$$D_{pp}^{\mathrm{RF}(0)} = \left\{ \sum_{n=-\infty}^{+\infty} \sum_{b} (1-\xi^2) D_{b,n}^{\mathrm{RF}}(p,\xi) \right\} \tag{4.296}$$

$$D_{p\xi}^{\mathrm{RF}(0)} = \sigma \left\{ \frac{\sigma\xi}{\sqrt{\Psi}\xi_0} \sum_{n=-\infty}^{+\infty} \sum_{b} -\frac{\sqrt{1-\xi^2}}{\xi} \left[1-\xi^2 - \frac{n\Omega}{\omega_b} \right] D_{b,n}^{\mathrm{RF}}(p,\xi) \right\}$$

$$D_{\xi p}^{\mathrm{RF}(0)} = \sigma \left\{ \frac{\sigma\xi}{\sqrt{\Psi}\xi_0} \sum_{n=-\infty}^{+\infty} \sum_{b} -\frac{\sqrt{1-\xi^2}}{\xi} \left[1-\xi^2 - \frac{n\Omega}{\omega_b} \right] D_{b,n}^{\mathrm{RF}}(p,\xi) \right\}$$

$$D_{\xi\xi}^{\mathrm{RF}(0)} = \left\{ \frac{\xi^2}{\Psi\xi_0^2} \sum_{n=-\infty}^{+\infty} \sum_{b} \frac{1}{\xi^2} \left[1-\xi^2 - \frac{n\Omega}{\omega_b} \right]^2 D_{b,n}^{\mathrm{RF}}(p,\xi) \right\}$$

where ()

$$\{\mathcal{O}\} = \frac{1}{\lambda \widetilde{q}} \left[\frac{1}{2} \sum_{\sigma} \right]_T \int_{\theta_{\min}}^{\theta_{\max}} \frac{d\theta}{2\pi} \frac{1}{\left| \widehat{\psi} \,.\, \widehat{r} \right|} \frac{r}{R_p} \frac{B}{B_P} \frac{\xi_0}{\xi} \mathcal{O} \tag{4.297}$$

Since $1-\xi^2 = \Psi\left(1-\xi_0^2\right)$,

$$D_{pp}^{\mathrm{RF}(0)} = \sum_{n=-\infty}^{+\infty} \sum_{b} (1-\xi_0^2) D_{b,n}^{\mathrm{RF}(0)}(p,\xi_0) \tag{4.298}$$

$$D_{p\xi}^{\mathrm{RF}(0)} = \sum_{n=-\infty}^{+\infty} \sum_{b} -\frac{\sqrt{1-\xi_0^2}}{\xi_0} \left[1-\xi_0^2 - \frac{n\Omega_0}{\omega_b} \right] D_{b,n}^{\mathrm{RF}(0)}(p,\xi_0)$$

$$D_{\xi p}^{\mathrm{RF}(0)} = \sum_{n=-\infty}^{+\infty} \sum_{b} -\frac{\sqrt{1-\xi_0^2}}{\xi_0} \left[1-\xi_0^2 - \frac{n\Omega_0}{\omega_b} \right] D_{b,n}^{\mathrm{RF}(0)}(p,\xi_0)$$

$$D_{\xi\xi}^{\mathrm{RF}(0)} = \sum_{n=-\infty}^{+\infty} \sum_{b} \frac{1}{\xi_0^2} \left[1-\xi_0^2 - \frac{n\Omega_0}{\omega_b} \right]^2 D_{b,n}^{\mathrm{RF}(0)}(p,\xi_0)$$

where

$$D_{b,n}^{\mathrm{RF}(0)}(p,\xi_0) = \left\{ \Psi D_{b,n}^{\mathrm{RF}}(p,\xi) \right\} \tag{4.299}$$

and Ω_0 is the cyclotron frequency taken at the minimum B value, according to the relation

$$\Omega_0 = \frac{eB_0}{\gamma m_e} = -\frac{\omega_{ce,0}}{\gamma} = \frac{\Omega}{\Psi} \tag{4.300}$$

with

$$\omega_{ce,0} = \frac{eB_0}{m_e} \tag{4.301}$$

Therefore, only the bounce averaged diffusion coefficient $D_{b,n}^{\mathrm{RF}(0)}(p,\xi_0)$ has to be calculated for the different types of RF waves, keeping the same formalism. It is determined by inserting expression (4.287) into (4.299),

$$\overline{D}_{b,n}^{\mathrm{RF}(0)}(p,\xi_0)=\left\{\Psi\overline{D}_{b,n,0}^{\mathrm{RF}}\left|\Theta_{\mathbf{k}}^{b,(n)}\right|^2\frac{\gamma p_{Te}}{p\left|\xi\right|}\delta\left(N_{\|b}-N_{\|\mathrm{res}}\right)2\pi\delta\left(\theta-\theta_b\right)\right\} \tag{4.302}$$

which gives

$$\overline{D}_{b,n}^{\mathrm{RF}(0)}(p,\xi_0)=\frac{\gamma p_{Te}}{p\left|\xi_0\right|}\left\{\frac{\xi_0}{\xi}\Psi\overline{D}_{b,n,0}^{\mathrm{RF}}\left|\Theta_{\mathbf{k}}^{b,(n)}\right|^2 2\pi\delta\left(\theta-\theta_b\right)\delta\left(N_{b\|}-N_{\|\mathrm{res}}\right)\right\} \tag{4.303}$$

We perform the poloidal integration

$$\begin{aligned}&\left\{\frac{\xi_0}{\xi}\Psi\overline{D}_{b,n,0}^{\mathrm{RF}}\left|\Theta_{\mathbf{k}}^{b,(n)}\right|^2 2\pi\delta\left(\theta-\theta_b\right)\delta\left(N_{b\|}-N_{\|\mathrm{res}}\right)\right\}\\&=\frac{1}{\lambda\widetilde{q}}\left[\frac{1}{2}\sum_{\sigma}\right]_T\int_{\theta_{\min}}^{\theta_{\max}}d\theta\frac{1}{\left|\widehat{\psi}\cdot\widehat{r}\right|}\frac{r}{R_p}\frac{B}{B_P}\frac{\xi_0^2}{\xi^2}\Psi\overline{D}_{b,n,0}^{\mathrm{RF}}\left|\Theta_{\mathbf{k}}^{b,(n)}\right|^2\delta\left(\theta-\theta_b\right)\delta\left(N_{b\|}-N_{\|\mathrm{res}}\right)\end{aligned} \tag{4.304}$$

$$=\frac{1}{\lambda\widetilde{q}}\frac{r_{\theta_b}}{R_p}\frac{B^{\theta_b}}{B_P^{\theta_b}}\frac{\xi_0^2}{\xi_{\theta_b}^2}\Psi_{\theta_b}\overline{D}_{b,n,0}^{\mathrm{RF},\theta_b}H\left(\theta_b-\theta_{\min}\right)H\left(\theta_{\max}-\theta_b\right)\left[\frac{1}{2}\sum_{\sigma}\right]_T\delta\left(N_{b\|}-N_{\|\mathrm{res}}^{\theta_b}\right)\left|\Theta_{\mathbf{k},\theta_b}^{b,(n)}\right|^2 \tag{4.305}$$

with

$$\widehat{\psi}_{\theta_b}=\widehat{\psi}(\psi,\theta_b) \tag{4.306}$$

$$r_{\theta_b}=r\left(\psi,\theta_b\right) \tag{4.307}$$

$$R_{\theta_b}=R\left(\psi,\theta_b\right) \tag{4.308}$$

$$B^{\theta_b}=B\left(\psi,\theta_b\right) \tag{4.309}$$

$$B_P^{\theta_b}=B_P\left(\psi,\theta_b\right) \tag{4.310}$$

$$\Psi_{\theta_b}=\frac{B\left(\psi,\theta_b\right)}{B_0\left(\psi\right)}=\frac{B^{\theta_b}}{B_0} \tag{4.311}$$

$$\xi_{\theta_b}=\xi\left(\psi,\theta_b,\xi_0\right)=\sigma\sqrt{1-\Psi_{\theta_b}\left(1-\xi_0^2\right)} \tag{4.312}$$

and where $H\left(x\right)$ is the usual Heaviside step function

Therefore,

$$\begin{aligned}\overline{D}_{b,n}^{\mathrm{RF}(0)}(p,\xi_0)=&\frac{\gamma p_{Te}}{p\left|\xi_0\right|}\frac{1}{\lambda\widetilde{q}}\frac{r_{\theta_b}}{R_p}\frac{B^{\theta_b}}{B_P^{\theta_b}}\frac{\xi_0^2}{\xi_{\theta_b}^2}\Psi_{\theta_b}\overline{D}_{b,n,0}^{\mathrm{RF},\theta_b}\times\\&H\left(\theta_b-\theta_{\min}\right)H\left(\theta_{\max}-\theta_b\right)\left[\frac{1}{2}\sum_{\sigma}\right]_T\delta\left(N_{b\|}-N_{\|\mathrm{res}}^{\theta_b}\right)\left|\Theta_{\mathbf{k},\theta_b}^{b,(n)}\right|^2\end{aligned} \tag{4.313}$$

where we define, using (4.290), (4.291) and (4.288),

$$\Theta_{\mathbf{k},\theta_b}^{b,(n)}=\frac{1}{\sqrt{2}}e_{b0,+}e^{-i\alpha_b}J_{n-1}\left(z_b^{\theta_b}\right)+\frac{1}{\sqrt{2}}e_{b0,-}e^{+i\alpha_b}J_{n+1}\left(z_b^{\theta_b}\right)+\frac{\xi_{\theta_b}}{\sqrt{\Psi_{\theta_b}\left(1-\xi_0^2\right)}}e_{b0,\|}J_n\left(z_b^{\theta_b}\right) \tag{4.314}$$

$$N_{\|\mathrm{res}}^{\theta_b} = \frac{1}{\beta_{Te}} \frac{p_{Te}}{p\xi_{\theta_b}} \left(\gamma - \frac{n' \Psi_{\theta_b} \omega_{ce,0}}{\omega_b} \right) \tag{4.315}$$

$$\overline{D}_{b,n,0}^{\mathrm{RF},\theta_b} = \frac{1}{r_{\theta_b} R_{\theta_b}} \frac{1}{m_e \ln \Lambda} \frac{1}{\omega_b \omega_{pe}^2} \frac{f_{\mathrm{inc},b}^{l+1/2}}{|\mathbf{\Phi}_b|} P_{b,\mathrm{inc}} \tag{4.316}$$

with

$$\begin{aligned} z_b^{\theta_b} &= \frac{k_{b\perp} v_\perp^{\theta_b}}{\Omega_{\theta_b}} \\ &= -N_{b\perp} \frac{\omega_b}{\omega_{ce}^{\theta_b}} \frac{p}{m_e c} \sqrt{1 - \xi_{\theta_b}^2} \\ &= -N_{b\perp} \frac{\omega_b}{\omega_{ce,0}} \frac{p}{m_e c} \frac{\sqrt{1 - \xi_0^2}}{\sqrt{\Psi_{\theta_b}}} \end{aligned} \tag{4.317}$$

4.3.8 Bounce Averaged Drift-Kinetic Equation

In the Drift Kinetic equation, the diffusion and convection elements are bounce-averaged according to the expressions (3.218) and (3.223), which gives, using (4.215-4.218)

$$\widetilde{D}_{pp}^{\mathrm{RF}(0)} = \sigma \left\{ \frac{\sigma\xi}{\Psi\xi_0} \sum_{n=-\infty}^{+\infty} \sum_b (1 - \xi^2) D_{b,n}^{\mathrm{RF}}(p,\xi) \right\} \tag{4.318}$$

$$\widetilde{D}_{p\xi}^{\mathrm{RF}(0)} = \left\{ \frac{\xi^2}{\Psi^{3/2}\xi_0^2} \sum_{n=-\infty}^{+\infty} \sum_b -\frac{\sqrt{1-\xi^2}}{\xi} \left[1 - \xi^2 - \frac{n\Omega}{\omega_b} \right] D_{b,n}^{\mathrm{RF}}(p,\xi) \right\}$$

$$\widetilde{D}_{\xi p}^{\mathrm{RF}(0)} = \left\{ \frac{\xi^2}{\Psi^{3/2}\xi_0^2} \sum_{n=-\infty}^{+\infty} \sum_b -\frac{\sqrt{1-\xi^2}}{\xi} \left[1 - \xi^2 - \frac{n\Omega}{\omega_b} \right] D_{b,n}^{\mathrm{RF}}(p,\xi) \right\}$$

$$\widetilde{D}_{\xi\xi}^{\mathrm{RF}(0)} = \sigma \left\{ \frac{\sigma\xi^3}{\Psi^2\xi_0^3} \sum_{n=-\infty}^{+\infty} \sum_b \frac{1}{\xi^2} \left[1 - \xi^2 - \frac{n\Omega}{\omega_b} \right]^2 D_{b,n}^{\mathrm{RF}}(p,\xi) \right\}$$

and

$$\widetilde{F}_p^{\mathrm{RF}(0)} = \frac{\sqrt{1-\xi_0^2}}{p\xi_0^3} \left\{ \frac{(\Psi - 1)}{\Psi^{3/2}} \sum_{n=-\infty}^{+\infty} \sum_b -\frac{\sqrt{1-\xi^2}}{\xi} \left[1 - \xi^2 - \frac{n\Omega}{\omega_b} \right] D_{b,n}^{\mathrm{RF}}(p,\xi) \right\} \tag{4.319}$$

$$\widetilde{F}_\xi^{\mathrm{RF}(0)} = \frac{\sqrt{1-\xi_0^2}}{p\xi_0^3} \sigma \left\{ \frac{\sigma\xi\,(\Psi - 1)}{\xi_0 \Psi^2} \sum_{n=-\infty}^{+\infty} \sum_b \frac{1}{\xi^2} \left[1 - \xi^2 - \frac{n\Omega}{\omega_b} \right]^2 D_{b,n}^{\mathrm{RF}}(p,\xi) \right\}$$

where

$$\{\mathcal{O}\} = \frac{1}{\lambda \widetilde{q}} \left[\frac{1}{2} \sum_\sigma \right]_T \int_{\theta_{\min}}^{\theta_{\max}} \frac{d\theta}{2\pi} \frac{1}{\left| \widehat{\psi} \cdot \widehat{r} \right|} \frac{r}{R_p} \frac{B}{B_P} \frac{\xi_0}{\xi} \mathcal{O} \tag{4.320}$$

Since $1-\xi^2 = \Psi\left(1-\xi_0^2\right)$ and $\Omega = \Psi\Omega_0$,

$$\widetilde{D}_{pp}^{\mathrm{RF}(0)} = \sum_{n=-\infty}^{+\infty}\sum_b (1-\xi_0^2)\widetilde{D}_{b,n}^{\mathrm{RF}(0)\mathrm{D}}(p,\xi_0) \tag{4.321}$$

$$\widetilde{D}_{p\xi}^{\mathrm{RF}(0)} = \sum_{n=-\infty}^{+\infty}\sum_b -\frac{\sqrt{1-\xi_0^2}}{\xi_0}\left[1-\xi_0^2-\frac{n\Omega_0}{\omega_b}\right]\widetilde{D}_{b,n}^{\mathrm{RF}(0)\mathrm{D}}(p,\xi_0) \tag{4.322}$$

$$\widetilde{D}_{\xi p}^{\mathrm{RF}(0)} = \sum_{n=-\infty}^{+\infty}\sum_b -\frac{\sqrt{1-\xi_0^2}}{\xi_0}\left[1-\xi_0^2-\frac{n\Omega_0}{\omega_b}\right]\widetilde{D}_{b,n}^{\mathrm{RF}(0)\mathrm{D}}(p,\xi_0) \tag{4.323}$$

$$\widetilde{D}_{\xi\xi}^{\mathrm{RF}(0)} = \sum_{n=-\infty}^{+\infty}\sum_b \frac{1}{\xi_0^2}\left[1-\xi_0^2-\frac{n\Omega_0}{\omega_b}\right]^2\widetilde{D}_{b,n}^{\mathrm{RF}(0)\mathrm{D}}(p,\xi_0) \tag{4.324}$$

$$\widetilde{F}_{p}^{\mathrm{RF}(0)} = \frac{\sqrt{1-\xi_0^2}}{p\xi_0^3}\sum_{n=-\infty}^{+\infty}\sum_b -\frac{\sqrt{1-\xi_0^2}}{\xi_0}\left[1-\xi_0^2-\frac{n\Omega_0}{\omega_b}\right]\widetilde{D}_{b,n}^{\mathrm{RF}(0)\mathrm{F}}(p,\xi_0) \tag{4.325}$$

$$\widetilde{F}_{\xi}^{\mathrm{RF}(0)} = \frac{\sqrt{1-\xi_0^2}}{p\xi_0^3}\sum_{n=-\infty}^{+\infty}\sum_b \frac{1}{\xi_0^2}\left[1-\xi_0^2-\frac{n\Omega_0}{\omega_b}\right]^2\widetilde{D}_{b,n}^{\mathrm{RF}(0)\mathrm{F}}(p,\xi_0)$$

where

$$\widetilde{D}_{b,n}^{\mathrm{RF}(0)\mathrm{D}}(p,\xi_0) = \sigma\left\{\sigma\frac{\xi}{\xi_0}D_{b,n}^{\mathrm{RF}}(p,\xi)\right\} \tag{4.326}$$

$$\widetilde{D}_{b,n}^{\mathrm{RF}(0)\mathrm{F}}(p,\xi_0) = \sigma\left\{\sigma\left(\Psi-1\right)\frac{\xi_0}{\xi}D_{b,n}^{\mathrm{RF}}(p,\xi)\right\}$$

and Ω_0 is the cyclotron frequency taken at the minumum B value, as defined for the Fokker-Planck equation. Therefore, only the two bounce averaged diffusion coefficient $\widetilde{D}_{b,n}^{\mathrm{RF}(0))\mathrm{D}}(p,\xi_0)$ and $\widetilde{D}_{b,n}^{\mathrm{RF}(0)\mathrm{F}}(p,\xi_0)$ have to be calculated for the different types of RF waves, keeping also the same formalism. It is important to recall that only $|\xi_0| = \sigma\xi_0$ can be put outside the $\{\}$ corresponding of the bounce-averaging integral.

These coefficient are determined by inserting expression (4.287) into (4.299),

$$\widetilde{D}_{b,n}^{\mathrm{RF}(0)\mathrm{D}}(p,\xi_0) = \sigma\left\{\sigma\frac{\xi}{\xi_0}\overline{D}_{b,n,0}^{\mathrm{RF}}\left|\Theta_{\mathbf{k}}^{b,(n)}\right|^2\frac{\gamma p_{Te}}{p\,|\xi|}\delta\left(N_{b\|}-N_{\|\mathrm{res}}\right)2\pi\delta\left(\theta-\theta_b\right)\right\} \tag{4.327}$$

$$\widetilde{D}_{b,n}^{\mathrm{RF}(0)\mathrm{F}}(p,\xi_0) = \sigma\left\{\sigma\left(\Psi-1\right)\frac{\xi_0}{\xi}\overline{D}_{b,n,0}^{\mathrm{RF}}\left|\Theta_{\mathbf{k}}^{b,(n)}\right|^2\frac{\gamma p_{Te}}{p\,|\xi|}\delta\left(N_{b\|}-N_{\|\mathrm{res}}\right)2\pi\delta\left(\theta-\theta_b\right)\right\}$$

which gives

$$\widetilde{D}_{b,n}^{\mathrm{RF}(0)\mathrm{D}}(p,\xi_0) = \frac{\gamma p_{Te}}{p\,|\xi_0|}\sigma\left\{\sigma\overline{D}_{b,n,0}^{\mathrm{RF}}\left|\Theta_{\mathbf{k}}^{b,(n)}\right|^2 2\pi\delta\left(\theta-\theta_b\right)\delta\left(N_{b\|}-N_{\|\mathrm{res}}\right)\right\} \tag{4.328}$$

$$\widetilde{D}_{b,n}^{\mathrm{RF}(0)\mathrm{F}}(p,\xi_0) = \frac{\gamma p_{Te}}{p\,|\xi_0|}\sigma\left\{\sigma\left(\Psi-1\right)\frac{\xi_0^2}{\xi^2}\overline{D}_{b,n,0}^{\mathrm{RF}}\left|\Theta_{\mathbf{k}}^{b,(n)}\right|^2 2\pi\delta\left(\theta-\theta_b\right)\delta\left(N_{b\|}-N_{\|\mathrm{res}}\right)\right\}$$

We perform the poloidal integration

$$\begin{aligned}
&\sigma\left\{\sigma\overline{D}^{\mathrm{RF}}_{b,n,0}\left|\Theta^{b,(n)}_{\mathbf{k}}\right|^2 2\pi\delta\left(\theta-\theta_b\right)\delta\left(N_{b\|}-N_{\|\mathrm{res}}\right)\right\}\\
&=\frac{1}{\lambda\widetilde{q}}\sigma\left[\frac{1}{2}\sum_{\sigma}\right]_T\int_{\theta_{\min}}^{\theta_{\max}}d\theta\frac{1}{\left|\widehat{\psi}\cdot\widehat{r}\right|}\frac{r}{R_p}\frac{B}{B_P}\frac{\xi_0}{\xi}\sigma\overline{D}^{\mathrm{RF}}_{b,n,0}\left|\Theta^{b,(n)}_{\mathbf{k}}\right|^2\delta\left(\theta-\theta_b\right)\delta\left(N_{b\|}-N_{\|\mathrm{res}}\right)\\
&=\frac{1}{\lambda\widetilde{q}}\frac{r_{\theta_b}}{R_p}\frac{B^{\theta_b}}{B_P^{\theta_b}}\frac{\xi_0}{\xi_{\theta_b}}\overline{D}^{\mathrm{RF},\theta_b}_{b,n,0}H\left(\theta_b-\theta_{\min}\right)H\left(\theta_{\max}-\theta_b\right)\sigma\left[\frac{1}{2}\sum_{\sigma}\right]_T\sigma\delta\left(N_{b\|}-N^{\theta_b}_{\|\mathrm{res}}\right)\left|\Theta^{b,(n)}_{\mathbf{k},\theta_b}\right|^2
\end{aligned}\tag{4.329}$$

$$\begin{aligned}
&\sigma\left\{\sigma\left(\Psi-1\right)\frac{\xi_0^2}{\xi^2}\overline{D}^{\mathrm{RF}}_{b,n,0}\left|\Theta^{b,(n)}_{\mathbf{k}}\right|^2 2\pi\delta\left(\theta-\theta_b\right)\delta\left(N_{b\|}-N_{\|\mathrm{res}}\right)\right\}\\
&=\frac{1}{\lambda\widetilde{q}}\sigma\left[\frac{1}{2}\sum_{\sigma}\right]_T\int_{\theta_{\min}}^{\theta_{\max}}d\theta\frac{1}{\left|\widehat{\psi}\cdot\widehat{r}\right|}\frac{r}{R_p}\frac{B}{B_P}\left(\Psi-1\right)\frac{\xi_0^3}{\xi^3}\sigma\overline{D}^{\mathrm{RF}}_{b,n,0}\\
&\qquad\times\left|\Theta^{b,(n)}_{\mathbf{k}}\right|^2\delta\left(\theta-\theta_b\right)\delta\left(N_{b\|}-N_{\|\mathrm{res}}\right)\\
&=\frac{1}{\lambda\widetilde{q}}\frac{r_{\theta_b}}{R_p}\frac{B^{\theta_b}}{B_P^{\theta_b}}\left(\Psi^{\theta_b}-1\right)\frac{\xi_0^3}{\xi_{\theta_b}^3}\overline{D}^{\mathrm{RF},\theta_b}_{b,n,0}H\left(\theta_b-\theta_{\min}\right)H\left(\theta_{\max}-\theta_b\right)\\
&\qquad\times\sigma\left[\frac{1}{2}\sum_{\sigma}\right]_T\sigma\delta\left(N_{b\|}-N^{\theta_b}_{\|\mathrm{res}}\right)\left|\Theta^{b,(n)}_{\mathbf{k},\theta_b}\right|^2
\end{aligned}\tag{4.330}$$

where $H\left(x\right)$ is the usual Heaviside step function and $\overline{D}^{\mathrm{RF},\theta_b}_{b,n,0}$ is given by (4.313).

Therefore, we find

$$\begin{aligned}
\widetilde{\overline{D}}^{\mathrm{RF(0)D}}_{b,n}\left(p,\xi_0\right)=&\frac{\gamma p_{Te}}{p\left|\xi_0\right|}\frac{1}{\lambda\widetilde{q}}\frac{r_{\theta_b}}{R_p}\frac{B^{\theta_b}}{B_P^{\theta_b}}\frac{\xi_0}{\xi_{\theta_b}}\overline{D}^{\mathrm{RF},\theta_b}_{b,n,0}\times\\
&H\left(\theta_b-\theta_{\min}\right)H\left(\theta_{\max}-\theta_b\right)\sigma\left[\frac{1}{2}\sum_{\sigma}\right]_T\sigma\delta\left(N_{b\|}-N^{\theta_b}_{\|\mathrm{res}}\right)\left|\Theta^{b,(n)}_{\mathbf{k},\theta_b}\right|^2
\end{aligned}\tag{4.331}$$

$$\begin{aligned}
\widetilde{\overline{D}}^{\mathrm{RF(0)F}}_{b,n}\left(p,\xi_0\right)=&\frac{\gamma p_{Te}}{p\left|\xi_0\right|}\frac{1}{\lambda\widetilde{q}}\frac{r_{\theta_b}}{R_p}\frac{B^{\theta_b}}{B_P^{\theta_b}}\left(\Psi^{\theta_b}-1\right)\frac{\xi_0^3}{\xi_{\theta_b}^3}\overline{D}^{\mathrm{RF},\theta_b}_{b,n,0}\times\\
&H\left(\theta_b-\theta_{\min}\right)H\left(\theta_{\max}-\theta_b\right)\sigma\left[\frac{1}{2}\sum_{\sigma}\right]_T\sigma\delta\left(N_{b\|}-N^{\theta_b}_{\|\mathrm{res}}\right)\left|\Theta^{b,(n)}_{\mathbf{k},\theta_b}\right|^2
\end{aligned}\tag{4.332}$$

4.3.9 Modeling of RF Waves

The quasilinear diffusion coefficients (4.313), (4.331) and (4.332) describe the interaction between electrons and a discrete set (b) of RF plane waves (4.232) with frequencies ω_b.

In addition, we can linearly superpose a discrete set of plane waves with the same frequency but different parallel wave number $k_\parallel$ because of the linearity of the QL operator (4.170) in $\mathbf{k}$. This set of plane waves is typically represented by rays. Each ray is characterized by: the wave frequency ω_b, the poloidal location θ_b, the index of refraction $\mathbf{N}_b$, the polarization vector $\mathbf{e}_b$ and the power flow $\mathbf{\Phi}_b$. In general, the ray propagation path (r_b, θ_b) and the evolution of the index of refraction $\mathbf{N}_b$ are determined by ray-tracing (RT) calculations. When the wave properties are determined by RT calculations, the launched power spectrum in $k_\parallel$ is typically decomposed in an array of rays with different poloidal launching angle and/or $k_\parallel$ power spectrum. This distribution depends on the antenna and other launching parameters. The evolution of each ray is determined separately, by the RT code, and the contributions of each ray to wave-particle interaction are separately accounted for in the sum over b in (4.215-4.218). The separation of these contributions is justified if their $k_\parallel$ power spectrums do not overlap.

We do not address the RT problem in this work. Therefore, we assume that the path $\theta_b(\psi)$ and the parallel index of refraction $N_{b\parallel}$ are determined either by coupling of DKE to a RT code, or by any other propagation model. RT calculations require to calculate the dispersion tensor and solve the dispersion relation, and therefore they can provide input for the remaining wave properties $(N_{b\perp}, \mathbf{e}_b, \mathbf{\Phi}_b)$. However, these properties can also be determined by solving locally the wave equation, once ψ, θ_b and $N_\parallel$ are known. Keeping the calculation of $(N_{b\perp}, \mathbf{e}_b, \mathbf{\Phi}_b)$ within DKE allows us to use a more advanced model - such as the fully relativistic dispersion solver R2D2 - for the evaluation of these important wave properties. A numerical code is required to solve the wave equation, and evaluate the diffusion coefficient (4.313) in the general case. However, it is possible to obtain analytic expressions in some cases, assuming that the waves can be treated in the cold plasma limit. The calculation of $\overline{D}_{b,n}^{\mathrm{RF}(0)}(p, \xi_0)$ in the cold plasma model is performed in Appendix D. In addition, simplified expression and the comparison with operators used in the litterature are given for lower-hybrid (LH) and electron-cyclotron (EC) waves in appendices D.2 and D.3 respectively.

Note that the cold plasma model, if used in the RT calculations, does not account for the wave-particle interaction and the power absorption from the rays. The power absorbed from each ray and deposited on electrons can be evaluated if a hot plasma model is used, but even then, the calculation is not consistent with DKE because quasilinear effects are not accounted for. In order to have a consistency between RT and DKE calculations, the power absorption calculated by DKE must be inserted back in the RT calculations. In the case where rays turn back toward the edge (as it can happen in LHCD), iterations between RT and DKE calculations are necessary to ensure self-consistency.

Modeling of RF $k_\parallel$ spectrum

We consider two different models for the $k_\parallel$ spectrum of a given ray.

Square power spectrum in $k_\parallel$ Here, the power spectrum of a given ray is taken as being constant in $N_\parallel$ between two limits $N_{b\parallel\,\min}$ and $N_{b\parallel\,\max}$. Therefore, we operate the

following transformation

$$\delta\left(N_{\parallel}-N_{\parallel\mathrm{res},b}\right)\rightarrow\frac{1}{\Delta N_{b\parallel}}H\left(N_{\parallel\mathrm{res},b}-N_{b\parallel\,\min}\right)H\left(N_{b\parallel\,\max}-N_{b\parallel\mathrm{res},b}\right) \tag{4.333}$$

where

$$\Delta N_{b\parallel}=N_{b\parallel\,\max}-N_{b\parallel\,\min} \tag{4.334}$$

In this case, the RT calculations and wave equation are solved for the central value.

$$N_{b\parallel,0}=\frac{N_{b\parallel\,\max}+N_{b\parallel\,\min}}{2} \tag{4.335}$$

which is a good approximation only when

$$\frac{\Delta_b N_{\parallel}}{N_{b\parallel,0}}\ll 1 \tag{4.336}$$

For simplification and benchmarking purposes, in LHCD, one can consider only one ray with a square spectrum. Then, the limits $N_{b\parallel\,\min}$ and $N_{b\parallel\,\max}$ are respectively given by the accessibility condition and the condition for strong linear Laudau damping.

Gaussian power spectrum in $k_{\parallel}$ The power spectrum of a given ray can be assumed to have a Gaussian dependence on $N_{\parallel}$, centered around a value $N_{b\parallel,0}$ and with a Gaussian width $\Delta N_{b\parallel}$. Then, we operate the transformation

$$\delta\left(N_{b\parallel}-N_{\parallel\mathrm{res}}\right)\rightarrow\frac{1}{\sqrt{\pi}\Delta N_{b\parallel}}\exp\left[\frac{-\left(N_{\parallel\mathrm{res}}-N_{b\parallel,0}\right)^2}{\Delta N_{b\parallel}^2}\right] \tag{4.337}$$

In this case too, the RT calculations and wave equation are solved for the central value $N_{b\parallel,0}$, which is a good approximation only when

$$\frac{\Delta_b N_{\parallel}}{N_{b\parallel,0}}\ll 1 \tag{4.338}$$

For simplification and benchmarking purposes, in ECCD, one can consider only one ray with a Gaussian spectrum. Then, the wave properties $N_{b\parallel,0}$ and $\Delta N_{b\parallel}$ are determined by the beam characteristics, as described in 4.3.9.

Beam size and power spectrum

If we consider a Gaussian beam of waist d, of negligible diffraction angle, and of negligible dispersion, such that the wave vector is in the direction of the beam, and $N\simeq 1$, we get that by the properties of Fourier transform, the width $\Delta N_{\parallel}$ is related to the beam waist d as

$$\Delta N_{\parallel}=\frac{N_{\perp}}{N}\frac{c}{\omega d} \tag{4.339}$$

This conditions are approximately satisfied for EC beamsif the density is low ($\omega_{pe}\ll\omega$).

Then, and we can verify that for a beam waist of a few centimeters ($d=5$ cm, $f=110$ GHz, $N_{\parallel}\simeq 0.2\rightarrow\Delta N_{\parallel}\simeq 0.01$), the condition (4.338) is satisfied, and there is no nead to decompose the beam spectrum into many rays.

Chapter 5

Numerical calculations

5.1 Bounce integrals

The numerical calculation of bounce coefficients requires an integration over θ which can be expressed symbolically as

$$I(\psi, \xi_0) = \int_{\theta_{\min}}^{\theta_{\max}} \frac{d\theta}{2\pi} F(\psi, \theta, \xi_0; B_R, B_Z, B_\phi, R, Z) \tag{5.1}$$

where B_R, B_Z, B_ϕ, R, Z are functions of (ψ, θ). They are given on a uniform grid of N_θ points in θ

$$\theta_j = \frac{2\pi j}{N_\theta - 1},\ j = 0, 1, \cdots, N_\theta - 1 \tag{5.2}$$

Domain of Integration It is very important to account for the entire bounce path of the particle, including in particular the tip of banana orbits near $\theta_{T\min}$ and $\theta_{T\max}$. The contribution of these banana tips is often larger than the $d\theta = 2\pi/(N_\theta - 1)$ accuracy level, because $F(\theta)$ can become very large near the turning points. This is true for example in the calculation of λ, since $F(\theta) \sim 1/\xi$ and $\xi \to 0$ at the turning points. It is therefore crucial to perform the integration up to $\theta_{T\min}$ and $\theta_{T\max}$. However, these boundaries are defined by (2.28) and (2.29)

$$B(\psi, \theta_T) = B_b(\psi, \xi_0) = \frac{B_0(\psi)}{1 - \xi_0^2} \tag{5.3}$$

which in general do not coincide with a grid points. In order to calculate θ_T, we impose that the values of the data B_R, B_Z, B_ϕ, R, Z in θ_T be obtained by linear interpolation, while the value of $B(\psi, \theta_T)$ is obtained from (2.30).

We consider the magnetic field $B_b(\psi, \xi_0)$ at the turning point $\theta_{T\min}$ to be located between the two (consecutive) values $B_1(\psi, \theta_1)$ and $B_2(\psi, \theta_2)$ on the (ψ, θ) grid. These values are determined from the three components issued by the equilibrium code simply by

$$B_1(\psi, \theta_1) = \sqrt{B_R^2(\psi, \theta_1) + B_Z^2(\psi, \theta_1) + B_\phi^2(\psi, \theta_1)} \tag{5.4}$$

$$B_2(\psi, \theta_2) = \sqrt{B_R^2(\psi, \theta_2) + B_Z^2(\psi, \theta_2) + B_\phi^2(\psi, \theta_2)} \tag{5.5}$$

We choose to define the values of B_R, B_Z and B_ϕ at the location θ_T by linear interpolation:

$$B_i\left(\psi,\theta_T\right)=B_{i1}+\frac{\left(\theta_T-\theta_1\right)}{\left(\theta_2-\theta_1\right)}\left(B_{i2}-B_{i1}\right) \tag{5.6}$$

where $i=R,Z,\phi$. Then, the location θ_T of the turning point can be calculated by requiring that the relation

$$B_b\left(\psi,\xi_0\right)=B\left(\psi,\theta_T\right)=\sqrt{B_R^2\left(\psi,\theta_T\right)+B_Z^2\left(\psi,\theta_T\right)+B_\phi^2\left(\psi,\theta_T\right)} \tag{5.7}$$

be satisfied. This implies

$$B_R^2\left(\psi,\theta_T\right)+B_Z^2\left(\psi,\theta_T\right)+B_\phi^2\left(\psi,\theta_T\right)=B_b^2\left(\psi,\xi_0\right) \tag{5.8}$$

and then

$$\sum_{i=R,Z,\phi}\left[B_{i1}+\frac{\left(\theta_T-\theta_1\right)}{\left(\theta_2-\theta_1\right)}\left(B_{i2}-B_{i1}\right)\right]^2-B_b^2\left(\psi,\xi_0\right)=0 \tag{5.9}$$

Defining

$$\alpha=\frac{\left(\theta_T-\theta_1\right)}{\left(\theta_2-\theta_1\right)} \tag{5.10}$$

we find

$$\left[\sum_{i=R,Z,\phi}\left(B_{i2}-B_{i1}\right)^2\right]\alpha^2+2\left[\sum_{i=R,Z,\phi}B_{i1}\left(B_{i2}-B_{i1}\right)\right]\alpha+\sum_{i=R,Z,\phi}B_{i1}^2-B_b^2\left(\psi,\xi_0\right)=0 \tag{5.11}$$

which solves as

$$\alpha=\frac{\pm\sqrt{\left[\sum_i B_{i1}\left(B_{i2}-B_{i1}\right)\right]^2-\left[\sum_i\left(B_{i2}-B_{i1}\right)^2\right]\left[\sum_i B_{i1}^2-B_b^2\right]}-\sum_i B_{i1}\left(B_{i2}-B_{i1}\right)}{\sum_i\left(B_{i2}-B_{i1}\right)^2} \tag{5.12}$$

We have

$$\begin{aligned}
&\sqrt{\left[\sum_i B_{i1}\left(B_{i2}-B_{i1}\right)\right]^2-\left[\sum_i\left(B_{i2}-B_{i1}\right)^2\right]\left[\sum_i B_{i1}^2-B_b^2\left(\psi,\xi_0\right)\right]}\\
&=\sqrt{\begin{array}{c}\left(B_{R1}B_{R2}+B_{Z1}B_{Z2}+B_{\phi1}B_{\phi2}\right)^2-B_1^2B_2^2\\+\left[B_2^2+B_1^2-2\left(B_{R2}B_{R1}+B_{Z2}B_{Z1}+B_{\phi2}B_{\phi1}\right)\right]B_b^2\left(\psi,\xi_0\right)\end{array}}\\
&=\sqrt{\left(Y-B_b^2\right)^2-\left(B_b^2-B_1^2\right)\left(B_b^2-B_2^2\right)}
\end{aligned} \tag{5.13}$$

with

$$Y=B_{R1}B_{R2}+B_{Z1}B_{Z2}+B_{\phi1}B_{\phi2} \tag{5.14}$$

so that

$$\alpha_b=\frac{\pm\sqrt{\left(Y-B_b^2\right)^2-\left(B_b^2-B_1^2\right)\left(B_b^2-B_2^2\right)}+B_1^2-Y}{B_1^2+B_2^2-2Y} \tag{5.15}$$

and finally

$$\theta_T = \theta_1 + (\theta_2 - \theta_1)\,\frac{\pm\sqrt{\left(Y - B_b^2\right)^2 - \left(B_b^2 - B_1^2\right)\left(B_b^2 - B_2^2\right)} + B_1^2 - Y}{B_1^2 + B_2^2 - 2Y} \tag{5.16}$$

We must choose (numerically) the solution that gives $0 \leq \alpha_b \leq 1$. Note that if the magnetic fields in points 1 and 2 are equal, we have $Y = B_1^2 = B_2^2 = B_b^2$.

Numerical Integration Once the two turning points have been added to the θ grid, now noted $\widetilde{\theta}_j$, $j = 0, 1, 2, \cdots N_\theta + 1$, we define the half grid

$$\overline{\theta}_k = \frac{\left(\widetilde{\theta}_{k+1} + \widetilde{\theta}_k\right)}{2},\ k = 0, 1, 2, \cdots N_\theta \tag{5.17}$$

and calculate the discrete function

$$F_k = F\left(\psi, \overline{\theta}_k, \xi_0; B_{Rk}, B_{Zk}, B_{\phi k}, R_k, Z_k\right) \tag{5.18}$$

where $B_{Rk}, B_{Zk}, B_{\phi k}, R_k, Z_k$ have been calculated on the grid $\overline{\theta}_k$ by linear interpolation, and the step $\overline{d\theta}_k$, defined by

$$\overline{d\theta}_k = \widetilde{\theta}_{k+1} - \widetilde{\theta}_k,\ k = 0, 1, 2, \cdots N_\theta \tag{5.19}$$

so that the integral becomes

$$I\left(\psi, \xi_0\right) = \frac{1}{2\pi}\sum_{k=0}^{N_\theta} \overline{d\theta}_k F_k \tag{5.20}$$

5.2 Grid definitions

The drift kinetic equation may be solved by different numerical techniques. Here one of the most natural approach is described, namely the finite difference method, which is based on the transformation of a differential equation into an algebraic one. The volume $\mathcal{V}$ on which the drift kinetic equation is solved is characterized by three dimensions (ψ, p, ξ_0), and, the time evolution is introduced with the parameter t.

Since the drift kinetic equation is expressed in conservative form, it is natural to define the grids for the flux S grid as the starting point of the numerical calculations.

$$S\left(t_k, \psi_l, p_i, \xi_{0,j}\right) \rightarrow \begin{cases} t_k \in [0, +\infty], k \rightarrow \{0, n_t\} \\ \psi_l \in [0, \psi_a], l \rightarrow \{0, n_\psi\} \\ p_i \in [0, p_{\max}], i \rightarrow \{0, n_p\} \\ \xi_{0,j} \in [-1, 1], j \rightarrow \{0, n_{\xi_0}\} \end{cases} \tag{5.21}$$

This grid system defines a set of cells of non-uniform sizes characterized by index numbers which, by definition, are integers. The distribution function f is represented by its values inside these cells, as shown in Fig.5.1 for the momentum dynamics. With

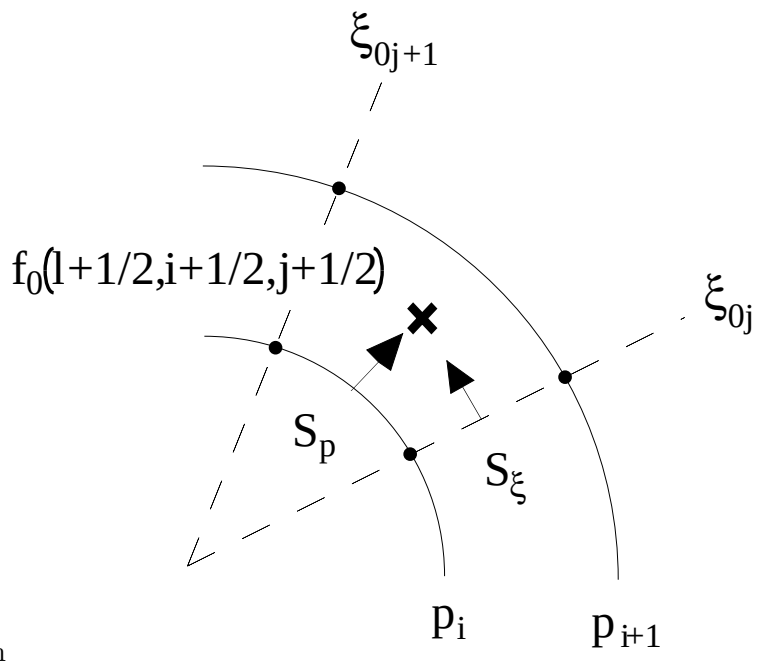

Figure 5.1: Grid definition for the momentum dynamics

this form, the conservative nature of the problem is preserved numerically, avoiding the occurence of spurious numerical fluxes which lead to wrong estimate of the solution.

$$f\left(t_k, \psi_{l+1/2}, p_{i+1/2}, \xi_{0j+1/2}\right) \rightarrow \begin{cases} t_k \in [0, +\infty], k \rightarrow \{0, n_t\} \\ \psi_{l+1/2} \in \left[0 + \frac{\Delta\psi_{1/2}}{2}, a - \frac{\Delta\psi_{n_r-1/2}}{2}\right], l \rightarrow \{0, n_\psi - 1\} \\ p_{i+1/2} \in \left[\frac{\Delta p_{1/2}}{2}, p_{\max} - \frac{\Delta p_{n_p-1/2}}{2}\right], i \rightarrow \{0, n_p - 1\} \\ \xi_{0j+1/2} \in \left[-1 + \frac{\Delta\xi_{0,1/2}}{2}, 1 - \frac{\Delta\xi_{0,n_{\xi_0}-1/2}}{2}\right], j \rightarrow \{0, n_{\xi_0} - 1\} \end{cases} \tag{5.22}$$

5.2.1 Momentum space

Momentum dynamic in p and pitch-angle ξ_0 being independent, the position of $p_{i+1/2}$ in between p_i and p_{i+1}, and of $\xi_{0,j+1/2}$ in between $\xi_{0,j}$ and $\xi_{0,j+1}$ is an arbitrary choice. The most simple and natural one is to place the point where the distribution function f is determined exactly in the middle of the cell,

$$\begin{cases} p_{i+1/2} = \frac{p_i + p_{i+1}}{2} \\ \xi_{j+1/2} = \frac{\xi_{0,j} + \xi_{0,j+1}}{2} \end{cases} \tag{5.23}$$

Then, intervals on the different grids are

$$\begin{cases} \Delta p_{i+1} = p_{i+3/2} - p_{i+1/2} \\ \Delta p_{i+1/2} = p_{i+1} - p_i \\ \Delta p_i = p_{i+1/2} - p_{i-1/2} \\ \Delta \xi_{0,j+1} = \xi_{0,j+3/2} - \xi_{0,j+1/2} \\ \Delta \xi_{0,j+1/2} = \xi_{0,j+1} - \xi_{0,j} \\ \Delta \xi_{0,j} = \xi_{0,j+1/2} - \xi_{0,j-1/2} \end{cases} \tag{5.24}$$

where

$$\begin{aligned} \Delta p_{i+1} &= p_{i+3/2} - p_{i+1/2} \\ &= p_{i+3/2} - p_{i+1} + p_{i+1} - p_{i+1/2} \\ &= \frac{\Delta p_{i+3/2}}{2} + \frac{\Delta p_{i+1/2}}{2} \end{aligned} \tag{5.25}$$

$$\begin{aligned} \Delta \xi_{0,j+1} &= \xi_{0,j+3/2} - \xi_{0,j+1/2} \\ &= \xi_{0,j+3/2} + \xi_{0,j+1} - \xi_{0,j+1} - \xi_{0,j+1/2} \\ &= \frac{\Delta \xi_{0,j+3/2}}{2} + \frac{\Delta \xi_{0,j+1/2}}{2} \end{aligned} \tag{5.26}$$

It is important to note that the need of a non-uniform momentum grid is justified by the $3-D$ approach of the numerical code. Indeed, since all radii are considered at each time step, ans since plasma temperature is usually much lower at the edage than at the plasma center, this requires a finer mesh close to $p = 0$, in order to describe momentum dynamics at all radii with a single p grid. Moreover, this argument holds for the case of multi-species drift kinetic calculations, since ion velocities are much lower than electron ones.

5.2.2 Configuration space

By an appropriate bounce averaging, the number of dimension is reduced to one, i.e. the radial one. As for the dynamics in momentum space, the point where the distribution function f is determined is chosen exactly in the middle of the cell,

$$\psi_{l+1/2} = \frac{\psi_l + \psi_{l+1}}{2} \tag{5.27}$$

and the intervals on the different grids are,

$$\begin{cases} \Delta \psi_{l+1} = \psi_{l+3/2} - \psi_{l+1/2} \\ \Delta \psi_{l+1/2} = \psi_{l+1} - \psi_l \\ \Delta \psi_l = \psi_{l+1/2} - \psi_{l-1/2} \end{cases} \tag{5.28}$$

where

$$\begin{aligned} \Delta \psi_{l+1} &= \psi_{l+3/2} - \psi_{l+1/2} \\ &= \psi_{l+3/2} - \psi_{l+1} + \psi_{l+1} - \psi_{l+1/2} \\ &= \frac{\Delta \psi_{l+3/2}}{2} + \frac{\Delta \psi_{l+1/2}}{2} \end{aligned} \tag{5.29}$$

Link between momentum and configuration grids

When the bounce averaged drift kinetic equation is solved, the distribution function $f^{(0)} \equiv f\left(B = B_0\right)$ is determined by definition at the poloidal angle value where the magnetic field is minimal on a given magnetic flux surface as shown in Sec.2.2.1. It is indeed the only common poloidal point on the magnetic flux surface that is crossed by trajectories of both trapped and circulating electrons. In momentum space, the dynamics of trapped and passing particles is characterized by an interval boundary which is defined by the relation

$$\xi_{0T}^2\left(\psi\right) = 1 - \frac{B_0\left(\psi\right)}{B_{\max}\left(\psi\right)} \tag{5.30}$$

From relation (5.30), it is clear that momentum and radial grids are no more fully independent. In order to achieve calculations with a high numerical accuracy, the pitch-angle flux grid is therefore chosen so that there exists an index number j_l where the following condition is exactly fullfiled[1],

$$\xi_{0T,j_l}^2\left(\psi_l\right) = 1 - \frac{B_0\left(\psi_l\right)}{B_{\max}\left(\psi_l\right)} \tag{5.31}$$

With this definition, the trapped passing boundaries are consistent with both pitch-angle and spatial flux grids. Obviously, the use of a non-uniform pitch-angle flux grid is fully necessary, because of this numerical requirement. Hence, if the number of radial points for the flux grid is arbitrary by definition, the number of points for the pitch-angle grid has a lower limit. It is straightforward to give a rough estimate, in order to evaluate the numerical size of the objects in the code. Let n_ψ being the number of flux grid points, $n_{\xi_0} \geq 6n_\psi + 7$, since at least each trapped passing boundary on the pitch-angle flux grid must be framed by two consecutive neighbors points, on each side, for $\xi_0 > 0$ et $\xi_0 \leq 0$ domains. In addition, accurate calculations must be performed at ξ_0 (3 points) et at $|\xi_0| = 1$ (4 points). Hence, for $n_\psi = 30$, $n_{\xi_0} \geq 187$.

5.2.3 Time grid definition

Time evolution is also projected on a numerical grid,

$$t_k = k\Delta t \tag{5.32}$$

which is taken uniform for two reasons. First, in the numerical approach here considered, the algorithm, as discussed in Sec. 6.1.1, is mainly dedicated to the fast determination of the asymptotic stationary solution $\lim_{t\to+\infty} f\left(\psi, t, p, \xi_0\right) = f^{(\infty)}\left(\psi, p, \xi_0\right)$, and therefore time step values must fulfill the condition $\Delta t \gg 1$. In this limit, the time t used in the iterative procedure because of the weak non-linearities of the collision operator, acts mainly as a regularization parameter, when matrix to be inverted is close to be ill-conditionned. Furthermore, with a non-uniform time grid, matrix must be calculated at each time step, which prevents the use of the very efficient incomplete LU matrix factorization technique,

[1]This choice is possible, since bounce integrals are determined numerically from magnetic equilibrium codes, and therefore, no singularity is encountered.

as discussed in Sec. 6.2.2, a procedure that allows to reduce considerably computer time consumption. Since the code is expected to be incorporate in a chain of codes, in order to obtain self-consistent magnetic equilibrium, wave propagation and kinetic calculations, this is therefore the only choice that can be considered.

5.3 Discretization procedure

5.3.1 Zero order term: Fokker-Planck equation

The starting point of the numerical calculations for the Fokker-Planck equation is the following expression

$$\begin{aligned} & \frac{\partial f_0^{(0)}}{\partial t} + \frac{1}{p^2}\frac{\partial}{\partial p}\left(p^2 \mathbf{S}_p^{(0)}\right) - \frac{1}{\lambda}\frac{1}{p}\frac{\partial}{\partial \xi_0}\left(\sqrt{1-\xi_0^2}\lambda \mathbf{S}_\xi^{(0)}\right) \\ & + \frac{B_0(\psi)}{\lambda(\psi,\xi_0)\,\widetilde{q}(\psi)}\frac{\partial}{\partial \psi}\left(R_0(\psi)\,\widetilde{q}(\psi)\,\frac{B_{P0}(\psi)}{B_0(\psi)}\lambda(\psi,\xi_0)\,\mathbf{S}_\psi^{(0)}\right) \\ = \; & 0 \end{aligned} \tag{5.33}$$

In order to avoid numerical singularities at $p = 0$, it is convenient to multiply all the terms by the partial Jacobian

$$J_\psi J_p = \frac{\widetilde{q}(\psi)}{B_0(\psi)}p^2 \tag{5.34}$$

which leads to the equivalent form

$$\begin{aligned} & \partial\left[\frac{\widetilde{q}(\psi)}{B_0(\psi)}p^2 f_0^{(0)}\right]/\partial t \\ & + \frac{\widetilde{q}(\psi)}{B_0(\psi)}\frac{\partial}{\partial p}\left(p^2 \mathbf{S}_p^{(0)}\right) \\ & - \frac{\widetilde{q}(\psi)}{B_0(\psi)}\frac{p}{\lambda(\psi,\xi_0)}\frac{\partial}{\partial \xi_0}\left(\sqrt{1-\xi_0^2}\lambda(\psi,\xi_0)\,\mathbf{S}_\xi^{(0)}\right) \\ & + \frac{p^2}{\lambda(\psi,\xi_0)}\frac{\partial}{\partial \psi}\left(R_0(\psi)\,\widetilde{q}(\psi)\,\frac{B_{P0}(\psi)}{B_0(\psi)}\lambda(\psi,\xi_0)\,\mathbf{S}_\psi^{(0)}\right) \\ = \; & 0 \end{aligned} \tag{5.35}$$

Using the grid definition defined in Sec.5.2 and applying the backward time discretization, which corresponds to the fully implicit time differencing as discussed in Sec. 6.1.1, the discrete form of the Fokker-planck equation may be expressed as

$$
\begin{aligned}
&\frac{\widetilde{q}_{l+1/2}}{B_{0,l+1/2}} p_{i+1/2}^2 \frac{f_{0,l+1/2,i+1/2,j+1/2}^{(0)(k+1)} - f_{0,l+1/2,i+1/2,j+1/2}^{(0)(k)}}{\Delta t} \\
&+ \frac{\widetilde{q}_{l+1/2}}{B_{0,l+1/2}} \left. \frac{\partial \left(p^2 \mathbf{S}_p^{(0)} \right)}{\partial p} \right|_{l+1/2,i+1/2,j+1/2}^{(k+1)} \\
&- \frac{\widetilde{q}_{l+1/2}}{B_{0,l+1/2}} \frac{p_{i+1/2}}{\lambda^{l+1/2,j+1/2}} \times \\
&\left. \frac{\partial}{\partial \xi_0} \left(\sqrt{1-\xi_0^2} \lambda \mathbf{S}_\xi^{(0)} \right) \right|_{l+1/2,i+1/2,j+1/2}^{(k+1)} \\
&+ \frac{p_{i+1/2}^2}{\lambda^{l+1/2,j+1/2}} \times \\
&\left. \frac{\partial}{\partial \psi} \left(R_0 \widetilde{q} \frac{B_{P0}}{B_0} \lambda \mathbf{S}_\psi^{(0)} \right) \right|_{l+1/2,i+1/2,j+1/2}^{(k+1)} \\
= \;& 0
\end{aligned}
\tag{5.36}
$$

where $\widetilde{q}_{l+1/2} = \widetilde{q}\left(\psi_{l+1/2}\right)$, $B_{0,l+1/2} = B_0\left(\psi_{l+1/2}\right)$ and $\lambda^{l+1/2,j+1/2} = \lambda\left(\psi_{l+1/2}, \xi_{0,j+1/2}\right)$. In a compact form

$$
\begin{aligned}
&\frac{\widetilde{q}_{l+1/2}}{B_{0,l+1/2}} p_{i+1/2}^2 \frac{f_{0,l+1/2,i+1/2,j+1/2}^{(0)(k+1)} - f_{0,l+1/2,i+1/2,j+1/2}^{(0)(k)}}{\Delta t} \\
&+ \left. \frac{\widetilde{q}}{B_0} p^2 \nabla_{\mathbf{p}} \cdot \mathbf{S}_{\mathbf{p}}^{(0)} \right|_{l+1/2,i+1/2,j+1/2}^{(k+1)} \\
&+ \left. \frac{\widetilde{q}}{B_0} p^2 \nabla_{\psi} \cdot \mathbf{S}_{\psi}^{(0)} \right|_{l+1/2,i+1/2,j+1/2}^{(k+1)} \\
= \;& 0
\end{aligned}
\tag{5.37}
$$

where

$$
\begin{aligned}
\left. \frac{\widetilde{q}}{B_0} p^2 \nabla_{\mathbf{p}} \cdot \mathbf{S}_{\mathbf{p}}^{(0)} \right|_{l+1/2,i+1/2,j+1/2}^{(k+1)} = \;& \frac{\widetilde{q}_{l+1/2}}{B_{0,l+1/2}} \left. \frac{\partial \left(p^2 \mathbf{S}_p^{(0)} \right)}{\partial p} \right|_{l+1/2,i+1/2,j+1/2}^{(k+1)} \\
&- \frac{\widetilde{q}_{l+1/2}}{B_{0,l+1/2}} \frac{p_{i+1/2}}{\lambda^{l+1/2,j+1/2}} \times \\
&\left. \frac{\partial}{\partial \xi_0} \left(\sqrt{1-\xi_0^2} \lambda \mathbf{S}_\xi^{(0)} \right) \right|_{l+1/2,i+1/2,j+1/2}^{(k+1)}
\end{aligned}
\tag{5.38}
$$

and

$$\frac{\widetilde{q}}{B_0}p^2\nabla_\psi\cdot\mathbf{S}_\psi^{(0)}\Big|_{l+1/2,i+1/2,j+1/2}^{(k+1)} = \frac{p_{i+1/2}^2}{\lambda^{l+1/2,j+1/2}}\times \frac{\partial}{\partial\psi}\left(R_0\widetilde{q}\frac{B_{P0}}{B_0}\lambda\mathbf{S}_\psi^{(0)}\right)\Big|_{l+1/2,i+1/2,j+1/2}^{(k+1)} \quad (5.39)$$

5.3.2 First order term: Drift kinetic equation

Since the first order drift kinetic equation may be also expressed in a conservative form as for the Fokker-Planck one as shwon in Sec. 3.5.5, a similar formalism may be kept. In that case,

$$\begin{aligned}&\frac{1}{p^2}\frac{\partial}{\partial p}\left(p^2\mathbf{S}_p^{(0)}\right)-\frac{1}{\lambda\left(\psi,\xi_0\right)}\frac{1}{p}\frac{\partial}{\partial\xi_0}\left(\sqrt{1-\xi_0^2}\lambda\left(\psi,\xi_0\right)\mathbf{S}_\xi^{(0)}\right)\\ =\;&\frac{1}{p^2}\frac{\partial}{\partial p}\left(p^2\widetilde{\mathbf{S}}_p^{(0)}\right)-\frac{1}{\lambda\left(\psi,\xi_0\right)}\frac{1}{p}\frac{\partial}{\partial\xi_0}\left(\sqrt{1-\xi_0^2}\lambda\left(\psi,\xi_0\right)\widetilde{\mathbf{S}}_\xi^{(0)}\right)\end{aligned} \quad (5.40)$$

where in the left-hand side, the fluxes concern the function $g^{(0)}\left(\psi,p,\xi_0\right)$ which is to be determined, knowing $\widetilde{\mathbf{S}}_p^{(0)}$ and $\widetilde{\mathbf{S}}_\xi^{(0)}$ from the spatial derivative of $f_0^{(0)}\left(\psi,p,\xi_0\right)$ given by the zero order Fokker-Planck equation. Multiplying also both sides by the partial Jacobian $J_\psi J_p$ defined in Sec. 3.5.1, one obtains

$$\begin{aligned}&\frac{\partial}{\partial p}\left(p^2\mathbf{S}_p^{(0)}\right)-\frac{p}{\lambda\left(\psi,\xi_0\right)}\frac{\partial}{\partial\xi_0}\left(\sqrt{1-\xi_0^2}\lambda\left(\psi,\xi_0\right)\mathbf{S}_\xi^{(0)}\right)\\ =\;&\frac{\partial}{\partial p}\left(p^2\widetilde{\mathbf{S}}_p^{(0)}\right)-\frac{p}{\lambda\left(\psi,\xi_0\right)}\frac{\partial}{\partial\xi_0}\left(\sqrt{1-\xi_0^2}\lambda\left(\psi,\xi_0\right)\widetilde{\mathbf{S}}_\xi^{(0)}\right)\end{aligned} \quad (5.41)$$

and the discrete form of the first order drift kinetic equation is then simply

$$\begin{aligned}&\frac{\partial\left(p^2\mathbf{S}_p^{(0)}\right)}{\partial p}\Big|_{l+1/2,i+1/2,j+1/2}^{(k)}-\frac{p_{i+1/2}}{\lambda^{l+1/2,j+1/2}}\times\\ &\frac{\partial}{\partial\xi_0}\left(\sqrt{1-\xi_0^2}\lambda\mathbf{S}_\xi^{(0)}\right)\Big|_{l+1/2,i+1/2,j+1/2}^{(k)}\\ =\;&\frac{\partial\left(p^2\widetilde{\mathbf{S}}_p^{(0)}\right)}{\partial p}\Big|_{l+1/2,i+1/2,j+1/2}^{(k)}-\frac{p_{i+1/2}}{\lambda^{l+1/2,j+1/2}}\times\\ &\frac{\partial}{\partial\xi_0}\left(\sqrt{1-\xi_0^2}\widetilde{\mathbf{S}}_\xi^{(0)}\right)\Big|_{l+1/2,i+1/2,j+1/2}^{(k)}\end{aligned} \quad (5.42)$$

5.4 Zero order term: the Fokker-Planck equation

5.4.1 Momentum dynamics

In this section, only the electron dynamics in momentum space is discussed, at fixed $\psi_{l+1/2}$. Hence

$$\begin{aligned}\frac{\widetilde{q}}{B_0}p^2\frac{\partial f^{(0)}}{\partial p}\bigg|^{(k+1)}_{l+1/2,i+1/2,j+1/2} &= \frac{\widetilde{q}_{l+1/2}}{B_{0,l+1/2}}\frac{\partial\left(p^2\mathbf{S}_p^{(0)}\right)}{\partial p}\bigg|^{(k+1)}_{l+1/2,i+1/2,j+1/2} \\ &- \frac{\widetilde{q}_{l+1/2}}{B_{0,l+1/2}}\frac{p_{i+1/2}}{\lambda^{l+1/2,j+1/2}}\times \\ &\frac{\partial}{\partial\xi_0}\left(\sqrt{1-\xi_0^2}\lambda\mathbf{S}_\xi^{(0)}\right)\bigg|^{(k+1)}_{l+1/2,i+1/2,j+1/2}\end{aligned} \tag{5.43}$$

where

$$\begin{cases} S_p^{(0)} = -D_{pp}^{(0)}\frac{\partial f_0^{(0)}}{\partial p} + D_{p\xi}^{(0)}\frac{\sqrt{1-\xi_0^2}}{p}\frac{\partial f_0^{(0)}}{\partial\xi_0} + F_p^{(0)}f_0^{(0)} \\ S_\xi^{(0)} = -D_{\xi p}^{(0)}\frac{\partial f_0^{(0)}}{\partial p} + D_{\xi\xi}^{(0)}\frac{\sqrt{1-\xi_0^2}}{p}\frac{\partial f_0^{(0)}}{\partial\xi_0} + F_\xi^{(0)}f_0^{(0)} \end{cases} \tag{5.44}$$

Here, diffusion cross-terms between momentum and configuration spaces are neglected, i.e. $D_{p\psi}^{(0)} = D_{\psi p}^{(0)} = D_{\xi\psi}^{(0)} = D_{\psi\xi}^{(0)} = 0$. By definition, the discretization procedure must preserve the conservative nature of the momentum dynamics, as discussed in Sec. 3.5.1, and therefore, careful attention must be paid how to proceed from Eq. 5.4.1, in particular when diffusion or convection coefficients vary strongly on a grid step. Moreover, boundary conditions on flux grid must be as much as possible naturaly satisfied by the discrete form of the Fokker-Planck equation. Indeed, cross-derivatives never satisfy this condition simultaneously along the momentum and pitch-angle directions, and consequently additional external boundary conditions must be added to enforce this condition.

There are several ways to perform the discretization of the cross-derivatives. Since $D_{p\xi}^{(0)}$ and $D_{\xi p}^{(0)}$ terms do not contribute to the Maxwellian solution when no external perturbation is applied, it is not necessary to perform an interpolation between full and half grids for cross-derivatives in order to ensure a correct numerical flux balance in momentum space. In that case, the usual procedure is simply to center differences, as done in this section. However, there is a much more complex approach, but also more consistent one with respect to the use two grids, one for the fluxes and the other for the distribution, which is also presented in Appendix E. However, because of its complexity, it has not been yet implemented in the code even if this approach is in principle better designed for non-uniform grids with strong localized variations of $D_{p\xi}^{(0)}$ and $D_{\xi p}^{(0)}$.

The starting point of the discretization procedure is the following expressions

$$\begin{aligned}\frac{\partial\left(p^2 S_p^{(0)}\right)}{\partial p} &= \frac{\partial}{\partial p}\left(-p^2 D_{pp}^{(0)}\frac{\partial f_0^{(0)}}{\partial p} + p^2 F_p^{(0)} f_0^{(0)}\right) \\ &+ \sqrt{1-\xi_0^2}\frac{\partial}{\partial p}\left(pD_{p\xi}^{(0)}\right)\frac{\partial f_0^{(0)}}{\partial \xi_0} \\ &+ \sqrt{1-\xi_0^2} pD_{p\xi}^{(0)}\frac{\partial^2 f_0^{(0)}}{\partial p \partial \xi_0}\end{aligned} \tag{5.45}$$

$$\begin{aligned}\frac{\partial\left(\sqrt{1-\xi_0^2}\lambda S_\xi^{(0)}\right)}{\partial \xi_0} &= \frac{\partial}{\partial \xi_0}\left(D_{\xi\xi}^{(0)}\frac{1-\xi_0^2}{p}\lambda\frac{\partial f_0^{(0)}}{\partial \xi_0}\right. \\ &\left.+\sqrt{1-\xi_0^2}\lambda F_\xi^{(0)} f_0^{(0)}\right) \\ &- \frac{\partial}{\partial \xi_0}\left(\sqrt{1-\xi_0^2}\lambda D_{\xi p}^{(0)}\right)\frac{\partial f_0^{(0)}}{\partial p} \\ &- \sqrt{1-\xi_0^2}\lambda D_{\xi p}^{(0)}\frac{\partial^2 f_0^{(0)}}{\partial \xi_0 \partial p}\end{aligned} \tag{5.46}$$

where cross-derivatives terms have been developped directly from analytical formulas, and considered in separately. Here, it is assumed in an implicit manner that derivatives of $pD_{p\xi}^{(0)}$ and $\sqrt{1-\xi_0^2}\lambda D_{\xi p}^{(0)}$ exists.

Hence

$$\frac{\widetilde{q}}{B_0}p^2\frac{\partial f_0^{(0)}}{\partial t}\bigg|_{l+1/2,i+1/2,j+1/2}^{(k+1)} = \frac{\widetilde{q}_{l+1/2}}{B_{0,l+1/2}}\sum_{m=1}^{m=8} T^{[m]} \tag{5.47}$$

with

$$T^{[1]} = \frac{-p_{i+1}^2 D_{pp,l+1/2,i+1,j+1/2}^{(0)}\left.\frac{\partial f_0^{(0)}}{\partial p}\right|_{l+1/2,i+1,j+1/2}^{(k+1)} + p_{i+1}^2 F_{p,l+1/2,i+1,j+1/2}^{(0)} f_{0,l+1/2,i+1,j+1/2}^{(0)(k+1)}}{\Delta p_{i+1/2}} \tag{5.48}$$

$$T^{[2]} = \frac{p_i^2 D_{pp,l+1/2,i,j+1/2}^{(0)}\left.\frac{\partial f_0^{(0)}}{\partial p}\right|_{l+1/2,i,j+1/2}^{(k+1)} - p_i^2 F_{p,l+1/2,i,j+1/2}^{(0)} f_{0,l+1/2,i,j+1/2}^{(0)(k+1)}}{\Delta p_{i+1/2}} \tag{5.49}$$

$$T^{[3]} = +\sqrt{1-\xi_{0,j+1/2}^2}\left.\frac{\partial\left(pD_{p\xi}^{(0)}\right)}{\partial p}\right|_{l+1/2,i+1/2,j+1/2}\left.\frac{\partial f_0^{(0)}}{\partial \xi}\right|_{l+1/2,i+1/2,j+1/2}^{(k+1)} \tag{5.50}$$

$$T^{[4]} = +\sqrt{1-\xi_{0,j+1/2}^2}\, p_{i+1/2} D_{p\xi,l+1/2,i+1/2,j+1/2}^{(0)}\left.\frac{\partial^2 f_0^{(0)}}{\partial p \partial \xi}\right|_{l+1/2,i+1/2,j+1/2}^{(k+1)} \tag{5.51}$$

$$T^{[5]} = -\frac{p_{i+1/2}}{\lambda^{l+1/2,j+1/2}} \left[\frac{D^{(0)}_{\xi\xi,l+1/2,i+1/2,j+1} \left(1-\xi^2_{0,j+1}\right) \lambda^{l+1/2,j+1} \left.\frac{\partial f_0^{(0)}}{\partial \xi}\right|^{(k+1)}_{l+1/2,i+1/2,j+1}}{p_{i+1/2}\Delta\xi_{j+1/2}} \right.$$
$$\left. + \frac{p_{i+1/2}\sqrt{1-\xi^2_{0,j+1}}\lambda^{l+1/2,j+1} F^{(0)}_{\xi,l+1/2,i+1/2,j+1} f^{(0)(k+1)}_{0,l+1/2,i+1/2,j+1}}{\Delta\xi_{j+1/2}} \right] \tag{5.52}$$

$$T^{[6]} = \frac{p_{i+1/2}}{\lambda^{l+1/2,j+1/2}} \left[\frac{D^{(0)}_{\xi\xi,l+1/2,i+1/2,j} \left(1-\xi^2_{0,j}\right) \lambda^{l+1/2,j} \left.\frac{\partial f_0^{(0)}}{\partial \xi}\right|^{(k+1)}_{l+1/2,i+1/2,j}}{p_{i+1/2}\Delta\xi_{j+1/2}} \right.$$
$$\left. + \frac{p_{i+1/2}\sqrt{1-\xi^2_{0,j}}\lambda^{l+1/2,j} F^{(0)}_{\xi,l+1/2,i+1/2,j} f^{(0)(k+1)}_{0,l+1/2,i+1/2,j}}{\Delta\xi_{j+1/2}} \right] \tag{5.53}$$

$$T^{[7]} = \frac{p_{i+1/2}}{\lambda^{l+1/2,j+1/2}} \left.\frac{\partial}{\partial\xi_0}\left(\sqrt{1-\xi_0^2}\lambda D^{(0)}_{\xi p}\right)\right|_{l+1/2,i+1/2,j+1/2} \left.\frac{\partial f_0^{(0)}}{\partial p}\right|^{(k+1)}_{l+1/2,i+1/2,j+1/2} \tag{5.54}$$

$$T^{[8]} = \frac{p_{i+1/2}}{\lambda^{l+1/2,j+1/2}}\sqrt{1-\xi^2_{0,j+1/2}}\lambda^{l+1/2,j+1/2} D^{(0)}_{\xi p,l+1/2,i+1/2,j+1/2} \left.\frac{\partial^2 f_0^{(0)}}{\partial\xi_0\partial p}\right|^{(k+1)}_{l+1/2,i+1/2,j+1/2} \tag{5.55}$$

Discrete expressions of the partial derivatives are,

$$\left.\frac{\partial f_0^{(0)}}{\partial p}\right|^{(k+1)}_{l+1/2,i+1,j+1/2} = \frac{f^{(0)(k+1)}_{0,l+1/2,i+3/2,j+1/2} - f^{(0)(k+1)}_{0,l+1/2,i+1/2,j+1/2}}{\Delta p_{i+1}} \tag{5.56}$$

$$\left.\frac{\partial f_0^{(0)}}{\partial p}\right|^{(k+1)}_{l+1/2,i+1/2,j+1/2} = \frac{f^{(0)(k+1)}_{0,l+1/2,i+3/2,j+1/2} - f^{(0)(k+1)}_{0,l+1/2,i-1/2,j+1/2}}{\Delta p_{i+1} + \Delta p_i} \tag{5.57}$$

$$\left.\frac{\partial f_0^{(0)}}{\partial p}\right|^{(k+1)}_{l+1/2,i,j+1/2} = \frac{f^{(0)(k+1)}_{0,l+1/2,i+1/2,j+1/2} - f^{(0)(k+1)}_{0,l+1/2,i-1/2,j+1/2}}{\Delta p_i} \tag{5.58}$$

$$\left.\frac{\partial f_0^{(0)}}{\partial \xi_0}\right|^{(k+1)}_{l+1/2,i+1/2,j+1} = \frac{f^{(0)(k+1)}_{0,l+1/2,i+1/2,j+3/2} - f^{(0)(k+1)}_{0,l+1/2,i+1/2,j+1/2}}{\Delta\xi_{0,j+1}} \tag{5.59}$$

$$\left.\frac{\partial f_0^{(0)}}{\partial \xi_0}\right|^{(k+1)}_{l+1/2,i+1/2,j+1/2} = \frac{f^{(0)(k+1)}_{0,l+1/2,i+1/2,j+3/2} - f^{(0)(k+1)}_{0,l+1/2,i+1/2,j-1/2}}{\Delta\xi_{0,j+1} + \Delta\xi_{0,j}} \tag{5.60}$$

$$\left.\frac{\partial f_0^{(0)}}{\partial \xi_0}\right|_{l+1/2,i+1/2,j}^{(k+1)} = \frac{f_{0,l+1/2,i+1/2,j+1/2}^{(0)(k+1)} - f_{0,l+1/2,i+1/2,j-1/2}^{(0)(k+1)}}{\Delta\xi_{0,j}} \tag{5.61}$$

and cross-derivatives

$$\begin{aligned}\left.\frac{\partial^2 f_0^{(0)}}{\partial p \partial \xi_0}\right|_{l+1/2,i+1/2,j+1/2}^{(k+1)} &= \left.\frac{\partial^2 f_0^{(0)}}{\partial \xi_0 \partial p}\right|_{l+1/2,i+1/2,j+1/2}^{(k+1)} \\ &= \frac{f_{0,l+1/2,i+3/2,j+3/2}^{(0)(k+1)} + f_{0,l+1/2,i-1/2,j-1/2}^{(0)(k+1)}}{\left(\Delta p_{i+1} + \Delta p_i\right)\left(\Delta\xi_{0,j+1} + \Delta\xi_{0,j}\right)} \\ &- \frac{f_{0,l+1/2,i+3/2,j-1/2}^{(0)(k+1)} + f_{0,l+1/2,i-1/2,j+3/2}^{(0)(k+1)}}{\left(\Delta p_{i+1} + \Delta p_i\right)\left(\Delta\xi_{0,j+1} + \Delta\xi_{0,j}\right)}\end{aligned} \tag{5.62}$$

while other derivatives become in discrete form

$$\left.\frac{\partial\left(pD_{p\xi}^{(0)}\right)}{\partial p}\right|_{l+1/2,i+1/2,j+1/2} = \frac{p_{i+1}D_{p\xi,l+1/2,i+1,j+1/2}^{(0)} - p_i D_{p\xi,l+1/2,i,j+1/2}^{(0)}}{\Delta p_{i+1/2}} \tag{5.63}$$

and

$$\begin{aligned}&\left.\frac{\partial}{\partial\xi_0}\left(\sqrt{1-\xi_0^2}\lambda D_{\xi p}^{(0)}\right)\right|_{l+1/2,i+1/2,j+1/2} \\ &= \frac{\sqrt{1-\xi_{0,j+1}^2}\lambda^{l+1/2,j+1} D_{\xi p,l+1/2,i+1/2,j+1}^{(0)}}{\Delta\xi_{0,j+1/2}} \\ &- \frac{\sqrt{1-\xi_{0,j}^2}\lambda^{l+1/2,j} D_{\xi p,l+1/2,i+1/2,j}^{(0)}}{\Delta\xi_{0,j+1/2}}\end{aligned} \tag{5.64}$$

By definition, cross-derivatives are symmetric. Furthermore, the derivative

$$\frac{\partial}{\partial\xi_0}\left(\sqrt{1-\xi_0^2}\lambda D_{\xi p}^{(0)}\right) \tag{5.65}$$

must be taken on the flux grid in order to fullfil naturally boundary condition at $|\xi_0| = 1$ and avoid to specify $D_{\xi p}^{(0)}$ at this momentum space location. It is a crucial point, especially for the Lower Hybrid and the Ohmic current drive problems, since this domain of the momentum space plays a very important role for the determination of the plasma current level.

Since the distribution function is defined on the half grid, while fluxes on the full grid, it is necessary to interpolate, because in some derivatives, values of $f_0^{(0)}$ are taken on the full grid. In a general way, whatever the detailed value of the weighting factor $\delta^{(0)}$ which will be discussed in the Sec. 5.4.3, one may write for the terms proportional to $D_{pp}^{(0)}$ and $F_p^{(0)}$,

$$\begin{aligned}f_{0,l+1/2,i+1,j+1/2}^{(0)(k+1)} &= \left(1 - \delta_{p,l+1/2,i+1,j+1/2}^{(0)}\right) f_{0,l+1/2,i+3/2,j+1/2}^{(0)(k+1)} \\ &+ \delta_{p,l+1/2,i+1,j+1/2}^{(0)} f_{0,l+1/2,i+1/2,j+1/2}^{(0)(k+1)}\end{aligned} \tag{5.66}$$

$$f^{(0)(k+1)}_{0,l+1/2,i,j+1/2} = \left(1 - \delta^{(0)}_{p,l+1/2,i,j+1/2}\right) f^{(0)(k+1)}_{0,l+1/2,i+1/2,j+1/2} + \delta^{(0)}_{p,l+1/2,i,j+1/2} f^{(0)(k+1)}_{0,l+1/2,i-1/2,j+1/2} \tag{5.67}$$

and for terms proportional to $D^{(0)}_{\xi\xi}$ and $F^{(0)}_{\xi}$

$$f^{(0)(k+1)}_{0,i+1/2,j+1} = \left(1 - \delta^{(0)}_{\xi,l+1/2,i+1/2,j+1}\right) f^{(0)(k+1)}_{0,l+1/2,i+1/2,j+3/2} + \delta^{(0)}_{\xi,l+1/2,i+1/2,j+1} f^{(0)(k+1)}_{0,l+1/2,i+1/2,j+1/2} \tag{5.68}$$

$$f^{(0)(k+1)}_{0,i+1/2,j} = \left(1 - \delta^{(0)}_{\xi,l+1/2,i+1/2,j}\right) f^{(0)(k+1)}_{0,l+1/2,i+1/2,j+1/2} \tag{5.69}$$

$$+ \delta^{(0)}_{\xi,l+1/2,i+1/2,j} f^{(0)(k+1)}_{0,l+1/2,i+1/2,j-1/2} \tag{5.70}$$

Gathering all terms, corresponding matrix coefficients for the zero order Fokker-Planck equation may be expressed as

$$\left.\frac{\widetilde{q}}{B_0} p^2 \frac{\partial f^{(0)}}{\partial p}\right|^{(k+1)}_{l+1/2,i+1/2,j+1/2} = \frac{\widetilde{q}_{l+1/2}}{B_{0,l+1/2}} \sum_{i'=i-1}^{i'=i+1} \sum_{j'=j-1}^{j'=j+1} \overline{\overline{M}}^{(0)}_{p,l+1/2,i'+1/2,j'+1/2} f^{(0)(k+1)}_{0,l+1/2,i'+1/2,j'+1/2} \tag{5.71}$$

where

$$\overline{\overline{M}}^{(0)}_{p,l+1/2,i+3/2,j+3/2} = \frac{p_{i+1/2}}{\Delta p_{i+1} + \Delta p_i} \frac{\sqrt{1 - \xi^2_{0,j+1/2}}}{\Delta\xi_{0,j+1} + \Delta\xi_{0,j}} D^{(0)}_{p\xi,l+1/2,i+1/2,j+1/2} + \frac{p_{i+1/2}}{\Delta p_{i+1} + \Delta p_i} \frac{\sqrt{1 - \xi^2_{0,j+1/2}}}{\Delta\xi_{0,j+1} + \Delta\xi_{0,j}} D^{(0)}_{\xi p,l+1/2,i+1/2,j+1/2} \tag{5.72}$$

$$\begin{aligned}\overline{\overline{M}}^{(0)}_{p,l+1/2,i+1/2,j+3/2} = {} & \frac{p_{i+1}}{\Delta p_{i+1/2}} \frac{\sqrt{1 - \xi^2_{0,j+1/2}}}{\Delta\xi_{0,j+1} + \Delta\xi_{0,j}} D^{(0)}_{p\xi,l+1/2,i+1,j+1/2} \\ & - \frac{p_i}{\Delta p_{i+1/2}} \frac{\sqrt{1 - \xi^2_{0,j+1/2}}}{\Delta\xi_{0,j+1} + \Delta\xi_{0,j}} D^{(0)}_{p\xi,l+1/2,i,j+1/2} \\ & - \frac{1 - \xi^2_{0,j+1}}{\Delta\xi_{0,j+1/2}\Delta\xi_{0,j+1}} \frac{\lambda^{l+1/2,j+1}}{\lambda^{l+1/2,j+1/2}} D^{(0)}_{\xi\xi,l+1/2,i+1/2,j+1} \\ & - p_{i+1/2} \frac{\sqrt{1 - \xi^2_{0,j+1}}}{\Delta\xi_{0,j+1/2}} \left(1 - \delta^{(0)}_{\xi,l+1/2,i+1/2,j+1}\right) \times \\ & \frac{\lambda^{l+1/2,j+1}}{\lambda^{l+1/2,j+1/2}} F^{(0)}_{\xi,l+1/2,i+1/2,j+1}\end{aligned} \tag{5.73}$$

$$\begin{aligned}\overline{\overline{M}}^{(0)}_{p,l+1/2,i-1/2,j+3/2} = &-\frac{p_{i+1/2}}{\Delta p_{i+1}+\Delta p_i}\frac{\sqrt{1-\xi^2_{0,j+1/2}}}{\Delta\xi_{0,j+1}+\Delta\xi_{0,j}}D^{(0)}_{p\xi,l+1/2,i+1/2,j+1/2}\\ &-\frac{p_{i+1/2}}{\Delta p_{i+1}+\Delta p_i}\frac{\sqrt{1-\xi^2_{0,j+1/2}}}{\Delta\xi_{0,j+1}+\Delta\xi_{0,j}}D^{(0)}_{\xi p,l+1/2,i+1/2,j+1/2}\end{aligned} \tag{5.74}$$

$$\begin{aligned}\overline{\overline{M}}^{(0)}_{p,l+1/2,i+3/2,j+1/2} = &-\frac{p^2_{i+1}}{\Delta p_{i+1}\Delta p_{i+1/2}}D^{(0)}_{pp,l+1/2,i+1,j+1/2}\\ &+\frac{p_{i+1/2}}{\Delta p_{i+1}+\Delta p_i}\frac{\sqrt{1-\xi^2_{0,j+1}}}{\Delta\xi_{0,j+1/2}}\times\\ &\frac{\lambda^{l+1/2,j+1}}{\lambda^{l+1/2,j+1/2}}D^{(0)}_{\xi p,l+1/2,i+1/2,j+1}\\ &-\frac{p_{i+1/2}}{\Delta p_{i+1}+\Delta p_i}\frac{\sqrt{1-\xi^2_{0,j}}}{\Delta\xi_{0,j+1/2}}\times\\ &\frac{\lambda^{l+1/2,j}}{\lambda^{l+1/2,j+1/2}}D^{(0)}_{\xi p,l+1/2,i+1/2,j}\\ &+\frac{p^2_{i+1}}{\Delta p_{i+1/2}}\left(1-\delta^{(0)}_{p,l+1/2,i+1,j+1/2}\right)F^{(0)}_{p,l+1/2,i+1,j+1/2}\end{aligned} \tag{5.75}$$

$$\begin{aligned}
\overline{\overline{M}}^{(0)}_{p,i+1/2,j+1/2} = & \frac{p_{i+1}^2}{\Delta p_{i+1/2}\Delta p_{i+1}} D^{(0)}_{pp,l+1/2,i+1,j+1/2} \\
& + \frac{p_{i+1}^2}{\Delta p_{i+1/2}} F_{p,l+1/2,i+1,j+1/2}\delta^{(0)}_{p,l+1/2,i+1,j+1/2} \\
& + \frac{p_i^2}{\Delta p_{i+1/2}\Delta p_i} D^{(0)}_{pp,l+1/2,i,j+1/2} \\
& - \frac{p_i^2}{\Delta p_{i+1/2}} \left(1 - \delta^{(0)}_{p,l+1/2,i,j+1/2}\right) F^{(0)}_{p,l+1/2,i,j+1/2} \\
& + \frac{1-\xi_{0,j+1}^2}{\Delta\xi_{0,j+1/2}\Delta\xi_{0,j+1}} \frac{\lambda^{l+1/2,j+1}}{\lambda^{l+1/2,j+1/2}} D^{(0)}_{\xi\xi,l+1/2,i+1/2,j+1} \\
& - p_{i+1/2} \frac{\sqrt{1-\xi_{0,j+1}^2}}{\Delta\xi_{0,j+1/2}} \delta^{(0)}_{\xi,l+1/2,i+1/2,j+1} \times \\
& \frac{\lambda^{l+1/2,j+1}}{\lambda^{l+1/2,j+1/2}} F^{(0)}_{\xi,l+1/2,i+1/2,j+1} \\
& + \frac{1-\xi_{0,j}^2}{\Delta\xi_{0,j}\Delta\xi_{0,j+1/2}} \frac{\lambda^{l+1/2,j}}{\lambda^{l+1/2,j+1/2}} D^{(0)}_{\xi\xi,l+1/2,i+1/2,j} \\
& + p_{i+1/2} \frac{\sqrt{1-\xi_{0,j}^2}}{\Delta\xi_{0,j+1/2}} \left(1 - \delta^{(0)}_{\xi,l+1/2,i+1/2,j}\right) \times \\
& \frac{\lambda^{l+1/2,j}}{\lambda^{l+1/2,j+1/2}} F^{(0)}_{\xi,l+1/2,i+1/2,j}
\end{aligned} \tag{5.76}$$

$$\begin{aligned}
\overline{\overline{M}}^{(0)}_{p,l+1/2,i-1/2,j+1/2} = & -\frac{p_i^2}{\Delta p_{i+1/2}\Delta p_i} D^{(0)}_{pp,l+1/2,i,j+1/2} \\
& - \frac{p_{i+1/2}}{\Delta p_{i+1} + \Delta p_i} \frac{\sqrt{1-\xi_{0,j+1}^2}}{\Delta\xi_{0,j+1/2}} \times \\
& \frac{\lambda^{l+1/2,j+1}}{\lambda^{l+1/2,j+1/2}} D^{(0)}_{\xi p,l+1/2,i+1/2,j+1} \\
& + \frac{p_{i+1/2}}{\Delta p_{i+1} + \Delta p_i} \frac{\sqrt{1-\xi_{0,j}^2}}{\Delta\xi_{0,j+1/2}} \times \\
& \frac{\lambda^{l+1/2,j}}{\lambda^{l+1/2,j+1/2}} D^{(0)}_{\xi p,l+1/2,i+1/2,j} \\
& - \frac{p_i^2}{\Delta p_{i+1/2}} \delta^{(0)}_{p,i,j+1/2} F^{(0)}_{p,l+1/2,i,j+1/2}
\end{aligned} \tag{5.77}$$

$$\overline{\overline{M}}^{(0)}_{p,l+1/2,i+3/2,j-1/2} = -\frac{p_{i+1/2}}{\Delta p_{i+1}+\Delta p_i}\frac{\sqrt{1-\xi^2_{0,j+1/2}}}{\Delta\xi_{0,j+1}+\Delta\xi_{0,j}}D^{(0)}_{p\xi,l+1/2,i+1/2,j+1/2} - \frac{p_{i+1/2}}{\Delta p_{i+1}+\Delta p_i}\frac{\sqrt{1-\xi^2_{0,j+1/2}}}{\Delta\xi_{0,j+1}+\Delta\xi_{0,j}}D^{(0)}_{\xi p,l+1/2,i+1/2,j+1/2} \tag{5.78}$$

$$\begin{aligned}\overline{\overline{M}}^{(0)}_{p,l+1/2,i+1/2,j-1/2} = &-\frac{p_{i+1}}{\Delta p_{i+1/2}}\frac{\sqrt{1-\xi^2_{0,j+1/2}}}{\Delta\xi_{0,j+1}+\Delta\xi_{0,j}}D^{(0)}_{p\xi,l+1/2,i+1,j+1/2}\\ &+\frac{p_i}{\Delta p_{i+1/2}}\frac{\sqrt{1-\xi^2_{0,j+1/2}}}{\Delta\xi_{0,j+1}+\Delta\xi_{0,j}}D^{(0)}_{p\xi,l+1/2,i,j+1/2}\\ &-\frac{1-\xi^2_{0,j}}{\Delta\xi_{0,j+1/2}\Delta\xi_{0,j}}\frac{\lambda^{l+1/2,j}}{\lambda^{l+1/2,j+1/2}}D^{(0)}_{\xi\xi,l+1/2,i+1/2,j}\\ &+p_{i+1/2}\frac{\sqrt{1-\xi^2_{0,j}}}{\Delta\xi_{0,j+1/2}}\delta^{(0)}_{\xi,l+1/2,i+1/2,j}\times\\ &\frac{\lambda^{l+1/2,j}}{\lambda^{l+1/2,j+1/2}}F^{(0)}_{\xi,l+1/2,i+1/2,j}\end{aligned} \tag{5.79}$$

$$\overline{\overline{M}}^{(0)}_{p,l+1/2,i-1/2,j-1/2} = \frac{p_{i+1/2}}{\Delta p_{i+1}+\Delta p_i}\frac{\sqrt{1-\xi^2_{0,j+1/2}}}{\Delta\xi_{0,j+1}+\Delta\xi_{0,j}}D^{(0)}_{p\xi,l+1/2,i+1/2,j+1/2} + \frac{p_{i+1/2}}{\Delta p_{i+1}+\Delta p_i}\frac{\sqrt{1-\xi^2_{0,j+1/2}}}{\Delta\xi_{0,j+1}+\Delta\xi_{0,j}}D^{(0)}_{\xi p,l+1/2,i+1/2,j+1/2} \tag{5.80}$$

For each coefficient, identical diffusion and convection terms appear, which must be evaluated for all physical processes that take place in the plasma (RF, Ohmic electric field, ...),

$$\overline{\overline{D}}^{(0)}_{p} \rightarrow \begin{cases} D^{(0)}_{pp,l+1/2,i+1,j+1/2}\\ D^{(0)}_{pp,l+1/2,i,j+1/2}\\ D^{(0)}_{p\xi,l+1/2,i+1,j+1/2}\\ D^{(0)}_{\xi p,l+1/2,i+1/2,j+1}\\ D^{(0)}_{p\xi,l+1/2,i+1/2,j+1/2}\\ D^{(0)}_{\xi p,l+1/2,i+1/2,j+1/2}\\ D^{(0)}_{p\xi,l+1/2,i,j+1/2}\\ D^{(0)}_{\xi p,l+1/2,i+1/2,j}\\ D^{(0)}_{\xi\xi,l+1/2,i+1/2,j+1}\\ D^{(0)}_{\xi\xi,l+1/2,i+1/2,j}\end{cases} \tag{5.81}$$

and

$$\overline{\overline{F}}_p^{(0)} \rightarrow \begin{cases} F^{(0)}_{p,l+1/2,i+1,j+1/2} \\ F^{(0)}_{p,l+1/2,i,j+1/2} \\ F^{(0)}_{\xi,l+1/2,i+1/2,j+1} \\ F^{(0)}_{\xi,l+1/2,i+1/2,j} \end{cases} \tag{5.82}$$

5.4.2 Spatial dynamics

In this section, only the electron dynamics in configuration space is discussed, at fixed $p_{i+1/2}$ and $\xi_{0,j+1/2}$,

$$\begin{aligned} & \frac{\widetilde{q}}{B_0} p^2 \frac{\partial f^{(0)}}{\partial \psi}\bigg|^{(k+1)}_{l+1/2,i+1/2,j+1/2} \\ = \; & \frac{p^2_{i+1/2}}{\lambda^{l+1/2,j+1/2}} \times \\ & \frac{\partial}{\partial \psi}\left(R_0 \widetilde{q} \frac{B_{P0}}{B_0} \lambda \mathbf{S}^{(0)}_{\psi} \right)\bigg|^{(k+1)}_{l+1/2,i+1/2,j+1/2} \end{aligned} \tag{5.83}$$

where

$$\mathbf{S}^{(0)}_{\psi} = -D^{(0)}_{\psi\psi} \left|\nabla\psi\right|_0 \frac{\partial f^{(0)}_0}{\partial \psi} + F^{(0)}_{\psi} f^{(0)}_0 \tag{5.84}$$

since cross-terms between momentum and configuration spaces are neglected, i.e. $D^{(0)}_{p\psi} = D^{(0)}_{\psi p} = D^{(0)}_{\xi\psi} = D^{(0)}_{\psi\xi} = 0$.

Therefore,

$$\frac{\widetilde{q}}{B_0} p^2 \frac{\partial f^{(0)}}{\partial \psi}\bigg|^{(k+1)}_{l+1/2,i+1/2,j+1/2} = \frac{p^2_{i+1/2}}{\lambda^{l+1/2,j+1/2}} \sum_{m=1}^{m=4} T^{[m]} \tag{5.85}$$

with

$$\begin{aligned} T^{[1]} \; = \; & -D^{(0)}_{\psi\psi,l+1,i+1/2,j+1/2} \left[R^2_{0,l+1} \widetilde{q}_{l+1} \frac{B^2_{P0,l+1}}{B_{0,l+1}} \lambda^{l+1,j+1/2} \right] \times \\ & \frac{\partial f^{(0)}_0}{\partial \psi}\bigg|^{(k+1)}_{l+1,i+1/2,j+1/2} / \Delta\psi_{l+1/2} \end{aligned} \tag{5.86}$$

$$\begin{aligned} T^{[2]} \; = \; & F^{(0)}_{\psi,l+1,i+1/2,j+1/2} \left[R_{0,l+1} \widetilde{q}_{l+1} \frac{B_{P0,l+1}}{B_{0,l+1}} \lambda^{l+1,j+1/2} \right] \times \\ & f^{(0)(k+1)}_{0,l+1,i+1/2,j+1/2} / \Delta\psi_{l+1/2} \end{aligned} \tag{5.87}$$

$$T^{[3]} = +D^{(0)}_{\psi\psi,l,i+1/2,j+1/2}\left[R^2_{0,l}\widetilde{q}_l\frac{B^2_{P0,l}}{B_{0,l}}\lambda^{l,j+1/2}\right]\times \frac{\partial f^{(0)}_0}{\partial\psi}\bigg|^{(k+1)}_{l,i+1/2,j+1/2}/\Delta\psi_{l+1/2} \tag{5.88}$$

$$T^{[4]} = -F^{(0)}_{\psi,l,i+1/2,j+1/2}\left[R_{0,l}\widetilde{q}_l\frac{B_{P0,l}}{B_{0,l}}\lambda^{l,j+1/2}\right]\times f^{(0)(k+1)}_{0,l,i+1/2,j+1/2}/\Delta\psi_{l+1/2} \tag{5.89}$$

and discrete expressions of the partial derivatives are,

$$\frac{\partial f^{(0)}_0}{\partial\psi}\bigg|^{(k+1)}_{l+1,i+1/2,j+1/2} = \frac{f^{(0)(k+1)}_{0,l+3/2,i+1/2,j+1/2} - f^{(0)(k+1)}_{0,l+1/2,i+1/2,j+1/2}}{\Delta\psi_{l+1}} \tag{5.90}$$

$$\frac{\partial f^{(0)}_0}{\partial\psi}\bigg|^{(k+1)}_{l,i+1/2,j+1/2} = \frac{f^{(0)(k+1)}_{0,l+1/2,i+1/2,j+1/2} - f^{(0)(k+1)}_{0,l-1/2,i+1/2,j+1/2}}{\Delta\psi_{l}} \tag{5.91}$$

As for the dynamics in momentum space, interpolation between full and half grids must be performed, since some values of the distribution function $f^{(0)}_0$ must be determined on the flux grid. Therefore

$$f^{(0)(k+1)}_{0,l+1,i+1/2,j+1/2} = \left(1-\delta^{(0)}_{\psi,l+1,i+1/2,j+1/2}\right)f^{(0)(k+1)}_{0,l+3/2,i+1/2,j+1/2} + \delta^{(0)}_{\psi,l+1,i+1/2,j+1/2}f^{(0)(k+1)}_{0,l+1/2,i+1/2,j+1/2} \tag{5.92}$$

$$f^{(0)(k+1)}_{0,l,i+1/2,j+1/2} = \left(1-\delta^{(0)}_{\psi,l,i+1/2,j+1/2}\right)f^{(0)(k+1)}_{0,l+1/2,i+1/2,j+1/2} + \delta^{(0)}_{\psi,l,i+1/2,j+1/2}f^{(0)(k+1)}_{0,l-1/2,i+1/2,j+1/2} \tag{5.93}$$

Gathering all terms, matrix coefficients for the zero order Fokker-Planck equation, according to the relation,

$$\frac{\widetilde{q}\,(\psi)}{B_0\,(\psi)}p^2\frac{\partial f^{(0)}}{\partial\psi}\bigg|^{(k+1)}_{l+1/2,i+1/2,j+1/2} = \frac{p^2_{i+1/2}}{\lambda^{l+1/2,j+1/2}}\times \sum_{l'=l-1}^{l'=l+1}\overline{\overline{M}}^{(0)}_{\psi,l'+1/2,i+1/2,j+1/2}f^{(0)(k+1)}_{0,l'+1/2,i+1/2,j+1/2} \tag{5.94}$$

are

$$\begin{aligned}\overline{\overline{M}}^{(0)}_{\psi,l+3/2,i+1/2,j+1/2} &= -\frac{\alpha^{(0)}_{l+1,j+1/2}}{\Delta\psi_{l+1/2}\Delta\psi_{l+1}}R_{0,l+1}B_{P0,l+1}D^{(0)}_{\psi\psi,l+1,i+1/2,j+1/2} \\ &\quad +\frac{\alpha^{(0)}_{l+1,j+1/2}}{\Delta\psi_{l+1/2}}F^{(0)}_{\psi,l+1,i+1/2,j+1/2}\left(1-\delta^{(0)}_{\psi,l+1,i+1/2,j+1/2}\right) \quad (5.95)\end{aligned}$$

$$\begin{aligned}\overline{\overline{M}}^{(0)}_{\psi,l+1/2,i+1/2,j+1/2} &= +\frac{\alpha^{(0)}_{l+1,j+1/2}}{\Delta\psi_{l+1/2}\Delta\psi_{l+1}}R_{0,l+1}B_{P0,l+1}D^{(0)}_{\psi\psi,l+1,i+1/2,j+1/2} \\ &\quad +\frac{\alpha^{(0)}_{l+1,j+1/2}}{\Delta\psi_{l+1/2}}F^{(0)}_{\psi,l+1,i+1/2,j+1/2}\delta^{(0)}_{\psi,l+1,i+1/2,j+1/2} \\ &\quad +\frac{\alpha^{(0)}_{l,j+1/2}}{\Delta\psi_{l+1/2}\Delta\psi_{l}}R_{0,l}B_{P0,l}D^{(0)}_{\psi\psi,l,i+1/2,j+1/2} \\ &\quad -\frac{\alpha^{(0)}_{l,j+1/2}}{\Delta\psi_{l+1/2}}F^{(0)}_{\psi,l,i+1/2,j+1/2}\left(1-\delta^{(0)}_{\psi,l,i+1/2,j+1/2}\right) \quad (5.96)\end{aligned}$$

$$\begin{aligned}\overline{\overline{M}}^{(0)}_{\psi,l-1/2,i+1/2,j+1/2} &= -\frac{\alpha^{(0)}_{l,j+1/2}}{\Delta\psi_{l+1/2}\Delta\psi_{l}}R_{0,l}B_{P0,l}D^{(0)}_{\psi\psi,l,i+1/2,j+1/2} \\ &\quad -\frac{\alpha^{(0)}_{l,j+1/2}}{\Delta\psi_{l+1/2}}F^{(0)}_{\psi,l,i+1/2,j+1/2}\delta^{(0)}_{\psi,l,i+1/2,j+1/2} \quad (5.97)\end{aligned}$$

with

$$\alpha^{(0)}_{l,j+1/2} = R_{0,l}\widetilde{q}_l\frac{B_{P0,l}}{B_{0,l}}\lambda^{l,j+1/2} \quad (5.98)$$

$$\alpha^{(0)}_{l+1,j+1/2} = R_{0,l+1}\widetilde{q}_{l+1}\frac{B_{P0,l+1}}{B_{0,l+1}}\lambda^{l+1,j+1/2} \quad (5.99)$$

As expected, spatial transport corresponds to a simple tridiagonal matrix.

5.4.3 Grid interpolation

Momentum grid interpolation The usual method for determining interpolation coefficients $\delta^{(0)}_{p,l+1/2,i+1,j+1/2}$, $\delta^{(0)}_{p,l+1/2,i,j+1/2}$, $\delta^{(0)}_{\xi,l+1/2,i+1/2,j+1}$ and $\delta^{(0)}_{\xi,l+1/2,i+1/2,j}$ so that the distribution function $f^{(0)}_0$ may be estimated on the full grid (flux grid) from its value on the half grid (distribution grid) is to satisfy the constraint that numerically, the stationary solution $\lim_{t\to+\infty} f^{(0)}_0 = f_M$ is an exact Maxwellian whithout any external accelerating mechanism (RF wave or Ohmic electric field). In this case, under the influence of collisional

slowing-down and pitch-angle only, coefficients $D^{(0)}_{p\xi} = D^{(0)}_{\xi p} = 0$, and

$$S^{(0)}_p\Big|^{(\infty)}_{l+1/2,i+1,j+1/2} = -D^{(0)}_{pp,l+1/2,i+1,j+1/2}\frac{f^{(0)(\infty)}_{0,l+1/2,i+3/2,j+1/2} - f^{(0)(\infty)}_{0,l+1/2,i+1/2,j+1/2}}{\Delta p_{i+1}} + F^{(0)}_{p,l+1/2,i+1,j+1/2} f^{(0)(\infty)}_{0,l+1/2,i+1,j+1/2} \quad (5.100)$$

$$S^{(0)}_p\Big|^{(\infty)}_{l+1/2,i,j+1/2} = -D^{(0)}_{pp,l+1/2,i,j+1/2}\frac{f^{(0)(\infty)}_{0,l+1/2,i+1/2,j+1/2} - f^{(0)(\infty)}_{0,l+1/2,i-1/2,j+1/2}}{\Delta p_i} + F^{(0)}_{p,l+1/2,i,j+1/2} f^{(0)(\infty)}_{0,l+1/2,i,j+1/2} \quad (5.101)$$

$$S^{(0)}_\xi\Big|^{(\infty)}_{l+1/2,i+1/2,j+1} = +D^{(0)}_{\xi\xi,l+1/2,i+1/2,j+1}\sqrt{1-\xi^2_{0,j+1}}\frac{f^{(0)(\infty)}_{0,i+1/2,j+3/2} - f^{(0)(\infty)}_{0,i+1/2,j+1/2}}{p_{i+1/2}\Delta\xi_{0,j+1}} + F^{(0)}_{\xi,l+1/2,i+1/2,j+1} f^{(0)(\infty)}_{0,l+1/2,i+1/2,j+1} \quad (5.102)$$

$$S^{(0)}_\xi\Big|^{(\infty)}_{l+1/2,i+1/2,j} = +D^{(0)}_{\xi\xi,l+1/2,i+1/2,j}\sqrt{1-\xi^2_{0,j}}\frac{f^{(0)(\infty)}_{0,i+1/2,j+1/2} - f^{(0)(\infty)}_{0,i+1/2,j-1/2}}{p_{i+1/2}\Delta\xi_{0,j}} + F^{(0)}_{\xi,l+1/2,i+1/2,j} f^{(0)(\infty)}_{0,l+1/2,i+1/2,j} \quad (5.103)$$

or

$$\Delta p_{i+1}\ S^{(0)}_p\Big|^{(\infty)}_{l+1/2,i+1,j+1/2} = -D^{(0)}_{pp,l+1/2,i+1,j+1/2}\left(f^{(0)(\infty)}_{0,l+1/2,i+3/2,j+1/2} - f^{(0)(\infty)}_{0,l+1/2,i+1/2,j+1/2}\right) + \Delta p_{i+1} F^{(0)}_{p,l+1/2,i+1,j+1/2} f^{(0)(\infty)}_{0,l+1/2,i+1,j+1/2} \quad (5.104)$$

$$\Delta p_i\ S^{(0)}_p\Big|^{(\infty)}_{l+1/2,i,j+1/2} = -D^{(0)}_{pp,l+1/2,i,j+1/2}\left(f^{(0)(\infty)}_{0,l+1/2,i+1/2,j+1/2} - f^{(0)(\infty)}_{0,l+1/2,i-1/2,j+1/2}\right) + \Delta p_i F^{(0)}_{p,l+1/2,i,j+1/2} f^{(0)(\infty)}_{0,l+1/2,i,j+1/2} \quad (5.105)$$

$$p_{i+1/2}\Delta\xi_{0,j+1}\ S^{(0)}_\xi\Big|^{(\infty)}_{l+1/2,i+1/2,j+1} = +D^{(0)}_{\xi\xi,l+1/2,i+1/2,j+1}\sqrt{1-\xi^2_{0,j+1}}\times \left(f^{(0)(\infty)}_{0,l+1/2,i+1/2,j+3/2} - f^{(0)(\infty)}_{0,l+1/2,i+1/2,j+1/2}\right) + p_{i+1/2}\Delta\xi_{0,j+1} F^{(0)}_{\xi,l+1/2,i+1/2,j+1} f^{(0)(\infty)}_{0,l+1/2,i+1/2,j+1} \quad (5.106)$$

$$
\begin{aligned}
p_{i+1/2}\Delta\xi_{0,j}\ S_{\xi}^{(0)}\Big|_{l+1/2,i+1/2,j}^{(\infty)} &= +D^{(0)}_{\xi\xi,l+1/2,i+1/2,j}\sqrt{1-\xi_{0,j}^2}\times \\
&\quad \left(f^{(0)(\infty)}_{0,l+1/2,i+1/2,j+1/2}-f^{(0)(\infty)}_{0,l+1/2,i+1/2,j-1/2}\right) \\
&\quad +p_{i+1/2}\Delta\xi_{0,j}F^{(0)}_{\xi,l+1/2,i+1/2,j}f^{(0)(\infty)}_{0,l+1/2,i+1/2,j} \qquad (5.107)
\end{aligned}
$$

Since this constraint corresponds to the relation

$$
\lim_{t\to+\infty}\frac{\partial f_0^{(0)}}{\partial t}=-\nabla_{\mathbf{p}}\mathbf{S}_{\mathbf{p}}^{(0)}=0 \qquad (5.108)
$$

one can deduce,

$$
\begin{aligned}
&\Delta p_{i+1}F^{(0)}_{p,l+1/2,i+1,j+1/2}f^{(0)(\infty)}_{0,l+1/2,i+1,j+1/2} \\
&= D^{(0)}_{pp,l+1/2,i+1,j+1/2}\left(f^{(0)(\infty)}_{0,l+1/2,i+3/2,j+1/2}-f^{(0)(\infty)}_{0,l+1/2,i+1/2,j+1/2}\right) \qquad (5.109)
\end{aligned}
$$

$$
\begin{aligned}
&\Delta p_{i}F^{(0)}_{p,l+1/2,i,j+1/2}f^{(0)(\infty)}_{0,l+1/2,i,j+1/2} \\
&= D^{(0)}_{pp,l+1/2,i,j+1/2}\left(f^{(0)(\infty)}_{0,l+1/2,i+1/2,j+1/2}-f^{(0)(\infty)}_{0,l+1/2,i-1/2,j+1/2}\right) \qquad (5.110)
\end{aligned}
$$

$$
\begin{aligned}
&p_{i+1/2}\Delta\xi_{0,j+1}F^{(0)}_{\xi,l+1/2,i+1/2,j+1}f^{(0)(\infty)}_{0,l+1/2,i+1/2,j+1} \\
&= -D^{(0)}_{\xi\xi,l+1/2,i+1/2,j+1}\sqrt{1-\xi_{0,j+1}^2}\left(f^{(0)(\infty)}_{0,l+1/2,i+1/2,j+3/2}\right. \\
&\qquad \left.-f^{(0)(\infty)}_{0,l+1/2,i+1/2,j+1/2}\right) \qquad (5.111)
\end{aligned}
$$

$$
\begin{aligned}
&p_{i+1/2}\Delta\xi_{0,j}F^{(0)}_{\xi,l+1/2,i+1/2,j}f^{(0)(\infty)}_{0,l+1/2,i+1/2,j} \\
&= -D^{(0)}_{\xi\xi,l+1/2,i+1/2,j}\sqrt{1-\xi_{0,j}^2}\left(f^{(0)(\infty)}_{0,l+1/2,i+1/2,j+1/2}-f^{(0)(\infty)}_{0,l+1/2,i+1/2,j-1/2}\right) \qquad (5.112)
\end{aligned}
$$

and replacing the distribution functions on the full grid by their interpolated values, according to the relations

$$
\begin{aligned}
f^{(0)(k+1)}_{0,l+1/2,i+1,j+1/2} &= \left(1-\delta^{(0)}_{p,l+1/2,i+1,j+1/2}\right)f^{(0)(k+1)}_{0,l+1/2,i+3/2,j+1/2} \\
&\quad +\delta^{(0)}_{p,l+1/2,i+1,j+1/2}f^{(0)(k+1)}_{0,l+1/2,i+1/2,j+1/2} \qquad (5.113)
\end{aligned}
$$

$$
\begin{aligned}
f^{(0)(k+1)}_{0,l+1/2,i,j+1/2} &= \left(1-\delta^{(0)}_{p,l+1/2,i,j+1/2}\right)f^{(0)(k+1)}_{0,l+1/2,i+1/2,j+1/2} \\
&\quad +\delta^{(0)}_{p,l+1/2,i,j+1/2}f^{(0)(k+1)}_{0,l+1/2,i-1/2,j+1/2} \qquad (5.114)
\end{aligned}
$$

and

$$
\begin{aligned}
f^{(0)(k+1)}_{0,i+1/2,j+1} &= \left(1-\delta^{(0)}_{\xi,l+1/2,i+1/2,j+1}\right)f^{(0)(k+1)}_{0,l+1/2,i+1/2,j+3/2} \\
&\quad +\delta^{(0)}_{\xi,l+1/2,i+1/2,j+1}f^{(0)(k+1)}_{0,l+1/2,i+1/2,j+1/2} \qquad (5.115)
\end{aligned}
$$

$$f^{(0)(k+1)}_{0,i+1/2,j} = \left(1-\delta^{(0)}_{\xi,l+1/2,i+1/2,j}\right) f^{(0)(k+1)}_{0,l+1/2,i+1/2,j+1/2} + \delta^{(0)}_{\xi,l+1/2,i+1/2,j} f^{(0)(k+1)}_{0,l+1/2,i+1/2,j-1/2} \tag{5.116}$$

one finds,

$$\begin{aligned} &\Delta p_{i+1} F^{(0)}_{p,l+1/2,i+1,j+1/2} \left[\left(1-\delta^{(0)}_{p,l+1/2,i+1,j+1/2}\right) f^{(0)(k+1)}_{0,l+1/2,i+3/2,j+1/2} \right. \\ &\left. +\delta^{(0)}_{p,l+1/2,i+1,j+1/2} f^{(0)(k+1)}_{0,l+1/2,i+1/2,j+1/2}\right] \\ =\ & D^{(0)}_{pp,l+1/2,i+1,j+1/2}\left(f^{(0)(\infty)}_{0,l+1/2,i+3/2,j+1/2} - f^{(0)(\infty)}_{0,l+1/2,i+1/2,j+1/2}\right) \end{aligned} \tag{5.117}$$

$$\begin{aligned} &\Delta p_{i} F^{(0)}_{p,l+1/2,i,j+1/2} \left[\left(1-\delta^{(0)}_{p,l+1/2,i,j+1/2}\right) f^{(0)(k+1)}_{0,l+1/2,i+1/2,j+1/2} \right. \\ &\left. +\delta^{(0)}_{p,l+1/2,i,j+1/2} f^{(0)(k+1)}_{0,l+1/2,i-1/2,j+1/2}\right] \\ =\ & D^{(0)}_{pp,l+1/2,i,j+1/2}\left(f^{(0)(\infty)}_{0,l+1/2,i+1/2,j+1/2} - f^{(0)(\infty)}_{0,l+1/2,i-1/2,j+1/2}\right) \end{aligned} \tag{5.118}$$

$$\begin{aligned} &p_{i+1/2}\Delta\xi_{0,j+1} F^{(0)}_{\xi,l+1/2,i+1/2,j+1} \left[\left(1-\delta^{(0)}_{\xi,l+1/2,i+1/2,j+1}\right) f^{(0)(k+1)}_{0,l+1/2,i+1/2,j+3/2} \right. \\ &\left. +\delta^{(0)}_{\xi,l+1/2,i+1/2,j+1} f^{(0)(k+1)}_{0,l+1/2,i+1/2,j+1/2}\right] \\ =\ & -D^{(0)}_{\xi\xi,l+1/2,i+1/2,j+1}\sqrt{1-\xi^2_{0,j+1}}\left(f^{(0)(\infty)}_{0,l+1/2,i+1/2,j+3/2} \right. \\ &\left. -f^{(0)(\infty)}_{0,l+1/2,i+1/2,j+1/2}\right) \end{aligned} \tag{5.119}$$

$$\begin{aligned} &p_{i+1/2}\Delta\xi_{0,j} F^{(0)}_{\xi,l+1/2,i+1/2,j} \left[\left(1-\delta^{(0)}_{\xi,l+1/2,i+1/2,j}\right) f^{(0)(k+1)}_{0,l+1/2,i+1/2,j+1/2} \right. \\ &\left. +\delta^{(0)}_{\xi,l+1/2,i+1/2,j} f^{(0)(k+1)}_{0,l+1/2,i+1/2,j-1/2}\right] \\ =\ & -D^{(0)}_{\xi\xi,l+1/2,i+1/2,j}\sqrt{1-\xi^2_{0,j}}\left(f^{(0)(\infty)}_{0,l+1/2,i+1/2,j+1/2} - f^{(0)(\infty)}_{0,l+1/2,i+1/2,j-1/2}\right) \end{aligned} \tag{5.120}$$

Hence, the ratios are

$$\begin{aligned} &\frac{f^{(0)(\infty)}_{0,l+1/2,i+3/2,j+1/2}}{f^{(0)(\infty)}_{0,l+1/2,i+1/2,j+1/2}} \\ =\ & \frac{D^{(0)}_{pp,l+1/2,i+1,j+1/2} + \Delta p_{i+1} F^{(0)}_{p,l+1/2,i+1,j+1/2}\delta^{(0)}_{p,l+1/2,i+1,j+1/2}}{D^{(0)}_{pp,l+1/2,i+1,j+1/2} - \Delta p_{i+1} F^{(0)}_{p,l+1/2,i+1,j+1/2}\left(1-\delta^{(0)}_{p,l+1/2,i+1,j+1/2}\right)} \end{aligned} \tag{5.121}$$

$$\begin{aligned} &\frac{f^{(0)(\infty)}_{0,l+1/2,i+1/2,j+1/2}}{f^{(0)(\infty)}_{0,l+1/2,i-1/2,j+1/2}} \\ =\ & \frac{D^{(0)}_{pp,l+1/2,i,j+1/2} + \Delta p_{i} F^{(0)}_{p,l+1/2,i,j+1/2}\delta^{(0)}_{p,l+1/2,i,j+1/2}}{D^{(0)}_{pp,l+1/2,i,j+1/2} - \Delta p_{i} F^{(0)}_{p,l+1/2,i,j+1/2}\left(1-\delta^{(0)}_{p,l+1/2,i,j+1/2}\right)} \end{aligned} \tag{5.122}$$

$$\frac{\dfrac{f^{(0)(\infty)}_{0,l+1/2,i+1/2,j+3/2}}{f^{(0)(\infty)}_{0,l+1/2,i+1/2,j+1/2}}}{} = \frac{-D^{(0)}_{\xi\xi,l+1/2,i+1/2,j+1}\sqrt{1-\xi^2_{0,j+1}} + p_{i+1/2}\Delta\xi_{0,j+1}F^{(0)}_{\xi,l+1/2,i+1/2,j+1}\delta^{(0)}_{\xi,l+1/2,i+1/2,j+1}}{-D^{(0)}_{\xi\xi,l+1/2,i+1/2,j+1}\sqrt{1-\xi^2_{0,j+1}} - p_{i+1/2}\Delta\xi_{0,j+1}F^{(0)}_{\xi,l+1/2,i+1/2,j+1}\left(1-\delta^{(0)}_{\xi,l+1/2,i+1/2,j+1}\right)} \tag{5.123}$$

$$\frac{\dfrac{f^{(0)(\infty)}_{0,l+1/2,i+1/2,j+1/2}}{f^{(0)(\infty)}_{0,l+1/2,i+1/2,j-1/2}}}{} = \frac{-D^{(0)}_{\xi\xi,l+1/2,i+1/2,j}\sqrt{1-\xi^2_{0,j}} + p_{i+1/2}\Delta\xi_{j}F^{(0)}_{\xi,l+1/2,i+1/2,j}\delta^{(0)}_{\xi,l+1/2,i+1/2,j}}{-D^{(0)}_{\xi\xi,l+1/2,i+1/2,j}\sqrt{1-\xi^2_{0,j}} - p_{i+1/2}\Delta\xi_{0,j}F^{(0)}_{\xi,l+1/2,i+1/2,j}\left(1-\delta^{(0)}_{\xi,l+1/2,i+1/2,j}\right)} \tag{5.124}$$

which may be recast in a compact form

$$\frac{f^{(0)(\infty)}_{0,l+1/2,i+3/2,j+1/2}}{f^{(0)(\infty)}_{0,l+1/2,i+1/2,j+1/2}} = \frac{1-w^{(0)(u)}_{p,l+1/2,i+1,j+1/2}\delta^{(0)}_{p,l+1/2,i+1,j+1/2}}{1+w^{(0)(u)}_{p,l+1/2,i+1,j+1/2}\left(1-\delta^{(0)}_{p,l+1/2,i+1,j+1/2}\right)} \tag{5.125}$$

$$\frac{f^{(0)(\infty)}_{0,l+1/2,i+1/2,j+1/2}}{f^{(0)(\infty)}_{0,l+1/2,i-1/2,j+1/2}} = \frac{1-w^{(0)(u)}_{p,i,j+1/2}\delta^{(0)}_{p,l+1/2,i,j+1/2}}{1+w^{(0)(u)}_{p,l+1/2,i,j+1/2}\left(1-\delta^{(0)}_{p,l+1/2,i,j+1/2}\right)} \tag{5.126}$$

$$\frac{f^{(0)(\infty)}_{0,l+1/2,i+1/2,j+3/2}}{f^{(0)(\infty)}_{0,l+1/2,i+1/2,j+1/2}} = \frac{1-w^{(0)(u)}_{\xi,l+1/2,i+1/2,j+1}\delta^{(0)}_{\xi,l+1/2,i+1/2,j+1}}{1+w^{(u)}_{\xi,l+1/2,i+1/2,j+1}\left(1-\delta^{(0)}_{\xi,l+1/2,i+1/2,j+1}\right)} \tag{5.127}$$

$$\frac{f^{(0)(\infty)}_{0,l+1/2,i+1/2,j+1/2}}{f^{(0)(\infty)}_{0,,l+1/2,i+1/2,j-1/2}} = \frac{1-w^{(0)(u)}_{\xi,l+1/2,i+1/2,j}\delta^{(0)}_{\xi,l+1/2,i+1/2,j}}{1+w^{(0)(u)}_{\xi,l+1/2,i+1/2,j}\left(1-\delta^{(0)}_{\xi,l+1/2,i+1/2,j}\right)} \tag{5.128}$$

with

$$w^{(0)(u)}_{p,l+1/2,i+1,j+1/2} = -\Delta p_{i+1}\frac{F^{(0)}_{p,l+1/2,i+1,j+1/2}}{D^{(0)}_{pp,l+1/2,i+1,j+1/2}} \tag{5.129}$$

$$w^{(0)(u)}_{p,l+1/2,i,j+1/2} = -\Delta p_{i}\frac{F^{(0)}_{p,l+1/2,i,j+1/2}}{D^{(0)}_{pp,l+1/2,i,j+1/2}} \tag{5.130}$$

$$w^{(0)(u)}_{\xi,l+1/2,i+1/2,j+1} = +p_{i+1/2}\frac{\Delta\xi_{0,j+1}}{\sqrt{1-\xi^2_{0,j+1}}}\frac{F^{(0)}_{\xi,l+1/2,i+1/2,j+1}}{D^{(0)}_{\xi\xi,l+1/2,i+1/2,j+1}} \tag{5.131}$$

$$w^{(0)(u)}_{\xi,l+1/2,i+1/2,j} = +p_{i+1/2}\frac{\Delta\xi_{0,j}}{\sqrt{1-\xi^2_{0,j}}}\frac{F^{(0)}_{\xi,l+1/2,i+1/2,j}}{D^{(0)}_{\xi\xi,l+1/2,i/2,j}} \tag{5.132}$$

Furthermore, since $\nabla_{\mathbf{p}}\mathbf{S}^{(0)}_{\mathbf{p}} = 0$, one deduces naturally that

$$-D^{(0)}_{pp}\frac{df^{(0)(\infty)}_0}{dp} + F^{(0)}_p f^{(0)(\infty)}_0 = 0 \tag{5.133}$$

$$+\frac{\sqrt{1-\xi^2_0}}{p}D^{(0)}_{\xi\xi}\frac{df^{(0)(\infty)}_0}{d\xi_0} + F^{(0)}_\xi f^{(0)(\infty)}_0 = 0 \tag{5.134}$$

and since $F^{(0)}_\xi = 0$ for collisions, because of the isotropic nature of pitch-angle scattering

$$\frac{\partial f^{(0)(\infty)}_0}{f^{(\infty)}_0} = \left(\frac{F^{(0)}_p}{D^{(0)}_{pp}}\right)\partial p \tag{5.135}$$

$$\frac{\partial f^{(0)(\infty)}_0}{\partial\xi_0} = 0 \tag{5.136}$$

which indicates that when collisions is the single physical process considered, $f^{(0)(\infty)}_0$ is independent of ξ_0. Therefore, $\partial/\partial p \to d/dp$, and integrating the first equation of (5.135) leads to the relation

$$\ln f^{(0)}_0 = \int\left(\frac{F^{(0)}_p}{D^{(0)}_{pp}}\right)dp + Cte \tag{5.137}$$

Values of $f^{(0)(\infty)}_0$ on the respective half grid positions $(l+1/2, i+3/2, j+1/2)$ and $(l+1/2, i+1/2, j+1/2)$ are then

$$\ln f^{(0)(\infty)}_{0,l+1/2,i+3/2,j+1/2} = \int_0^{p_{i+3/2}}\left(\frac{F^{(0)}_p\left(\psi_{l+1/2},p,\xi_{0,j+1/2}\right)}{D^{(0)}_{pp}\left(\psi_{l+1/2},p,\xi_{0,j+1/2}\right)}\right)dp + Cte \tag{5.138}$$

$$\ln f^{(0)(\infty)}_{0,l+1/2,i+1/2,j+1/2} = \int_0^{p_{i+1/2}}\left(\frac{F^{(0)}_p\left(\psi_{l+1/2},p,\xi_{0,j+1/2}\right)}{D^{(0)}_{pp}\left(\psi_{l+1/2},p,\xi_{0,j+1/2}\right)}\right)dp + Cte \tag{5.139}$$

and ratios are finally easily determined

$$\frac{f^{(0)(\infty)}_{0,l+1/2,i+3/2,j+1/2}}{f^{(0)(\infty)}_{0,l+1/2,i+1/2,j+1/2}} = \exp\left[\int_{p_{i+1/2}}^{p_{i+3/2}}\left(\frac{F^{(0)}_p\left(\psi_{l+1/2},p,\xi_{0,j+1/2}\right)}{D^{(0)}_{pp}\left(\psi_{l+1/2},p,\xi_{0,j+1/2}\right)}\right)dp\right] \tag{5.140}$$

$$\frac{f^{(0)(\infty)}_{0,l+1/2,i+1/2,j+1/2}}{f^{(0)(\infty)}_{0,l+1/2,i-1/2,j+1/2}} = \exp\left[\int_{p_{i-1/2}}^{p_{i13/2}}\left(\frac{F^{(0)}_p\left(\psi_{l+1/2},p,\xi_{0,j+1/2}\right)}{D^{(0)}_{pp}\left(\psi_{l+1/2},p,\xi_{0,j+1/2}\right)}\right)dp\right] \tag{5.141}$$

while, since $f^{(0)(\infty)}_0$ does not depend of ξ_0,

$$\frac{f^{(0)(\infty)}_{0,l+1/2,i+1/2,j+3/2}}{f^{(0)(\infty)}_{0,l+1/2,i+1/2,j+1/2}} = \frac{f^{(0)(\infty)}_{0,l+1/2,i+1/2,j+1/2}}{f^{(0)(\infty)}_{0,l+1/2,i+1/2,j-1/2}} = 1 \tag{5.142}$$

It is then straightforward to evaluate coefficients $\delta^{(0)}_{p,l+1/2,i+1,j+1/2}$ et $\delta^{(0)}_{p,l+1/2,i,j+1/2}$ by the trapezoidal method,

$$\begin{aligned}
&\int_{p_{i+1/2}}^{p_{i+3/2}} \frac{F_p^{(0)}\left(\psi_{l+1/2,}p,\xi_{0,j+1/2}\right)}{D_{pp}^{(0)}\left(\psi_{l+1/2,}p,\xi_{0,j+1/2}\right)}dp \simeq \\
&\frac{1}{2}\frac{F^{(0)}_{p,l+1/2,i+1/2,j+1/2}}{D^{(0)}_{pp,l+1/2,i+1/2,j+1/2}}\frac{\Delta p_{i+1/2}}{2} \\
&+\frac{1}{2}\frac{F^{(0)}_{p,l+1/2,i+1,j+1/2}}{D^{(0)}_{pp,l+1/2,i+1,j+1/2}}\frac{\Delta p_{i+1/2}}{2} \\
&+\frac{1}{2}\frac{F^{(0)}_{p,l+1/2,i+1,j+1/2}}{D^{(0)}_{pp,l+1/2,i+1,j+1/2}}\frac{\Delta p_{i+3/2}}{2} \\
&+\frac{1}{2}\frac{F^{(0)}_{p,l+1/2,i+3/2,j+1/2}}{D^{(0)}_{pp,l+1/2,i+3/2,j+1/2}}\frac{\Delta p_{i+3/2}}{2}
\end{aligned} \tag{5.143}$$

and

$$\begin{aligned}
&\int_{p_{i-1/2}}^{p_{i+1/2}} \frac{F_p^{(0)}\left(\psi_{l+1/2,}p,\xi_{0,j+1/2}\right)}{D_{pp}^{(0)}\left(\psi_{l+1/2,}p,\xi_{0,j+1/2}\right)}dp \simeq \\
&\frac{1}{2}\frac{F^{(0)}_{p,l+1/2,i-1/2,j+1/2}}{D^{(0)}_{pp,l+1/2,i-1/2,j+1/2}}\frac{\Delta p_{i-1/2}}{2} \\
&+\frac{1}{2}\frac{F^{(0)}_{p,l+1/2,i-1/2,j+1/2}}{D^{(0)}_{pp,l+1/2,i-1/2,j+1/2}}\frac{\Delta p_{i-1/2}}{2} \\
&+\frac{1}{2}\frac{F^{(0)}_{p,l+1/2,i,j+1/2}}{D^{(0)}_{pp,l+1/2,i,j+1/2}}\frac{\Delta p_{i+1/2}}{2} \\
&+\frac{1}{2}\frac{F^{(0)}_{p,l+1/2,i+1/2,j+1/2}}{D^{(0)}_{pp,l+1/2,i+1/2,j+1/2}}\frac{\Delta p_{i+1/2}}{2}
\end{aligned} \tag{5.144}$$

then gathering terms $p_{i+3/2}$, p_{i+1} and $p_{i+1/2}$, one obtains

$$\begin{aligned}
&\int_{p_{i+1/2}}^{p_{i+3/2}} \frac{F_p^{(0)}\left(\psi_{l+1/2,}p,\xi_{0,j+1/2}\right)}{D_{pp}^{(0)}\left(\psi_{l+1/2,}p,\xi_{0,j+1/2}\right)}dp \simeq \\
&\frac{1}{2}\frac{F^{(0)}_{p,l+1/2,i+1,j+1/2}}{D^{(0)}_{pp,l+1/2,i+1,j+1/2}}\left(\frac{\Delta p_{i+1/2}}{2}+\frac{\Delta p_{i+3/2}}{2}\right) \\
&+\frac{F^{(0)}_{p,l+1/2,i+1/2,j+1/2}}{D^{(0)}_{pp,l+1/2,i+1/2,j+1/2}}\frac{\Delta p_{i+1/2}}{4} \\
&+\frac{F^{(0)}_{p,l+1/2,i+3/2,j+1/2}}{D^{(0)}_{pp,l+1/2,i+3/2,j+1/2}}\frac{\Delta p_{i+3/2}}{4} \\
=\ &\frac{F^{(0)}_{p,l+1/2,i+1,j+1/2}}{D^{(0)}_{pp,l+1/2,i+1,j+1/2}}\frac{\Delta p_{i+1}}{2} \\
&+\frac{F^{(0)}_{p,l+1/2,i+1/2,j+1/2}}{D^{(0)}_{pp,l+1/2,i+1/2,j+1/2}}\frac{\Delta p_{i+1/2}}{4} \\
&+\frac{F^{(0)}_{p,l+1/2,i+3/2,j+1/2}}{D^{(0)}_{pp,l+1/2,i+3/2,j+1/2}}\frac{\Delta p_{i+3/2}}{4}
\end{aligned} \tag{5.145}$$

or

$$\begin{aligned}
&\int_{p_{i+1/2}}^{p_{i+3/2}} \frac{F_p^{(0)}\left(\psi_{l+1/2,}p,\xi_{0,j+1/2}\right)}{D_{pp}^{(0)}\left(\psi_{l+1/2,}p,\xi_{0,j+1/2}\right)}dp = \\
&\Delta p_{i+1}\frac{F^{(0)}_{p,l+1/2,i+1,j+1/2}}{D^{(0)}_{pp,l+1/2,i+1,j+1/2}} \\
&+\frac{F^{(0)}_{p,l+1/2,i+1/2,j+1/2}}{D^{(0)}_{pp,l+1/2,i+1/2,j+1/2}}\frac{\Delta p_{i+1/2}}{4} \\
&+\frac{F^{(0)}_{p,l+1/2,i+3/2,j+1/2}}{D^{(0)}_{pp,l+1/2,i+3/2,j+1/2}}\frac{\Delta p_{i+3/2}}{4} \\
&-\frac{\Delta p_{i+1}}{2}\frac{F^{(0)}_{p,l+1/2,i+1,j+1/2}}{D^{(0)}_{pp,l+1/2,i+1,j+1/2}}
\end{aligned} \tag{5.146}$$

Since

$$\frac{F^{(0)}_{p,l+1/2,i+1,j+1/2}}{D^{(0)}_{pp,l+1/2,i+1,j+1/2}} = \frac{\Delta p_{i+3/2}}{\Delta p_{i+1/2}+\Delta p_{i+3/2}} \frac{F^{(0)}_{p,l+1/2,i+1/2,j+1/2}}{D^{(0)}_{pp,l+1/2,i+1/2,j+1/2}} + \frac{\Delta p_{i+1/2}}{\Delta p_{i+1/2}+\Delta p_{i+3/2}} \frac{F^{(0)}_{p,l+1/2,i+3/2,j+1/2}}{D^{(0)}_{pp,l+1/2,i+3/2,j+1/2}} \tag{5.147}$$

one obtains

$$\frac{F^{(0)}_{p,l+1/2,i+1,j+1/2}}{D^{(0)}_{pp,l+1/2,i+1,j+1/2}} = \frac{\Delta p_{i+3/2}}{2\Delta p_{i+1}} \frac{F^{(0)}_{p,l+1/2,i+1/2,j+1/2}}{D^{(0)}_{pp,l+1/2,i+1/2,j+1/2}} + \frac{\Delta p_{i+1/2}}{2\Delta p_{i+1}} \frac{F^{(0)}_{p,l+1/2,i+3/2,j+1/2}}{D^{(0)}_{pp,l+1/2,i+3/2,j+1/2}} \tag{5.148}$$

and after gathering all terms

$$\int_{p_{i+1/2}}^{p_{i+3/2}} \frac{F^{(0)}_{p}\left(\psi_{l+1/2,p},\xi_{0,j+1/2}\right)}{D^{(0)}_{pp}\left(\psi_{l+1/2,p},\xi_{0,j+1/2}\right)}dp = \Delta p_{i+1}\frac{F^{(0)}_{p,l+1/2,i+1,j+1/2}}{D^{(0)}_{pp,l+1/2,i+1,j+1/2}} + \frac{\Delta p_{i+3/2}-\Delta p_{i+1/2}}{4}\frac{F^{(0)}_{p,l+1/2,i+3/2,j+1/2}}{D^{(0)}_{pp,l+1/2,i+3/2,j+1/2}} - \frac{\Delta p_{i+3/2}-\Delta p_{i+1/2}}{4}\frac{F^{(0)}_{p,l+1/2,i+1/2,j+1/2}}{D^{(0)}_{pp,l+1/2,i+1/2,j+1/2}} \tag{5.149}$$

Much as the same way, using index conversion $p_{i+3/2} \to p_{i+1/2}$, $p_{i+1} \to p_i$ and $p_{i+1/2} \to p_{i-1/2}$ in the previous relation, one obtains for the second integral,

$$\int_{p_{i-1/2}}^{p_{i+1/2}} \frac{F_p^{(0)}\left(\psi_{l+1/2,}p,\xi_{0,j+1/2}\right)}{D_{pp}^{(0)}\left(\psi_{l+1/2,}p,\xi_{0,j+1/2}\right)}dp \simeq$$
$$\Delta p_i \frac{F^{(0)}_{p,l+1/2,i,j+1/2}}{D^{(0)}_{pp,l+1/2,i,j+1/2}}$$
$$+\frac{\Delta p_{i+1/2}-\Delta p_{i-1/2}}{4}\frac{F^{(0)}_{p,l+1/2,i+1/2,j+1/2}}{D^{(0)}_{pp,l+1/2,i+1/2,j+1/2}}$$
$$-\frac{\Delta p_{i+1/2}-\Delta p_{i-1/2}}{4}\frac{F^{(0)}_{p,l+1/2,i-1/2,j+1/2}}{D^{(0)}_{pp,l+1/2,i-1/2,j+1/2}} \tag{5.150}$$

From the two formulations of the ratios

$$\frac{f^{(0)(\infty)}_{0,l+1/2,i+3/2,j+1/2}}{f^{(0)(\infty)}_{0,l+1/2,i+1/2,j+1/2}} \tag{5.151}$$

one obtains easily

$$\begin{aligned}\delta^{(0)}_{p,l+1/2,i+1,j+1/2} &= \frac{1}{w^{(0)(u)}_{p,l+1/2,i+1,j+1/2}} \\ &\quad -\frac{1}{\exp\left[w^{(0)(u)}_{p,l+1/2,i+1,j+1/2}+w^{(0)(nu)}_{p,l+1/2,i+1,j+1/2}\right]-1}\end{aligned} \tag{5.152}$$

with

$$\begin{aligned}w^{(0)(nu)}_{p,l+1/2,i+1,j+1/2} &= -\frac{\Delta p_{i+3/2}-\Delta p_{i+1/2}}{4}\frac{F^{(0)}_{p,l+1/2,i+3/2,j+1/2}}{D^{(0)}_{pp,l+1/2,i+3/2,j+1/2}} \\ &\quad +\frac{\Delta p_{i+3/2}-\Delta p_{i+1/2}}{4}\frac{F^{(0)}_{p,l+1/2,i+1/2,j+1/2}}{D^{(0)}_{pp,l+1/2,i+1/2,j+1/2}}\end{aligned} \tag{5.153}$$

Much in the same way,

$$\delta^{(0)}_{p,l+1/2,i,j+1/2} = \frac{1}{w^{(0)(u)}_{p,l+1/2,i,j+1/2}} - \frac{1}{\exp\left[w^{(0)(u)}_{p,l+1/2,i,j+1/2}+w^{(0)(nu)}_{p,l+1/2,i,j+1/2}\right]-1} \tag{5.154}$$

with ß

$$\begin{aligned}w^{(0)(nu)}_{p,l+1/2,i,j+1/2} &= -\frac{\Delta p_{i+1/2}-\Delta p_{i-1/2}}{4}\frac{F^{(0)}_{p,l+1/2,i+1/2,j+1/2}}{D^{(0)}_{pp,l+1/2,i+1/2,j+1/2}} \\ &\quad +\frac{\Delta p_{i+1/2}-\Delta p_{i-1/2}}{4}\frac{F^{(0)}_{p,l+1/2,i-1/2,j+1/2}}{D^{(0)}_{pp,l+1/2,i-1/2,j+1/2}}\end{aligned} \tag{5.155}$$

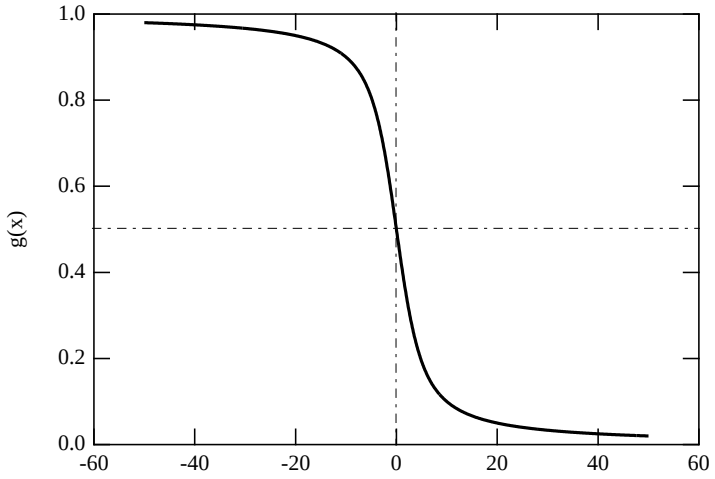

cmcm

Figure 5.2: Chang and Cooper weightingfunction

For a uniform grid, $w^{(0)(nu)}_{p,l+1/2,i,j+1/2} = 0$, and the well known expression of the Chang and Cooper function is recovered,

$$g\left(x\right) = \frac{1}{x} - \frac{1}{e^x - 1} \tag{5.156}$$

with $x = w^{(0)(u)}_p$. In the limit where $x \ll 1$, an expansion of the function gives $g\left(x\right) = 0.5 - x/12 + x^3/720 + \mathrm{O}\left(x^4\right)$ with $\lim_{x\to 0} g\left(x\right) = \frac{1}{2}$, as shwon in Fig.5.2. For a non-uniform grid, a generalized Chang and Cooper function must be introduced, with two arguments

$$g\left(x,y\right) = \frac{1}{x} - \frac{1}{e^{x+y} - 1} \tag{5.157}$$

where the term $y = w^{(0)(nu)}_p$ is zero for the uniform case, as shown in Ref.[22].

With this definition,

$$\frac{f^{(0)(\infty)}_{0,l+1/2,i+3/2,j+1/2}}{f^{(\infty)}_{0,l+1/2,i+1/2,j+1/2}} = \frac{T^{cc}_1}{T^{cc}_2} = \frac{T^{cc}_4}{T^{cc}_5} \tag{5.158}$$

where

$$\begin{aligned} T^{cc}_1 \quad = \quad & 1 - w^{(0)(u)}_{p,l+1/2,i+1,j+1/2} \left[\frac{1}{w^{(0)(u)}_{p,,l+1/2,i+1,j+1/2}} \right. \\ & \left. - \frac{1}{\exp\left[w^{(0)(u)}_{p,l+1/2,i+1,j+1/2} + w^{(0)(nu)}_{p,l+1/2,i+1,j+1/2} \right] - 1} \right] \end{aligned} \tag{5.159}$$

$$T^{cc}_2 = 1 + w^{(0)(u)}_{p,l+1/2,i+1,j+1/2} \left(1 - T^{cc}_3\right) \tag{5.160}$$

and

$$T_3^{cc} = \frac{1}{w^{(0)(u)}_{p,l+1/2,i+1,j+1/2}} - \frac{1}{\exp\left[w^{(0)(u)}_{p,l+1/2,i+1,j+1/2} + w^{(0)(nu)}_{p,l+1/2,i+1,j+1/2}\right] - 1} \tag{5.161}$$

whilewith

$$T_4^{cc} = \frac{w^{(0)(u)}_{p,l+1/2,i+1,j+1/2}}{\exp\left[w^{(0)(u)}_{p,l+1/2,i+1,j+1/2} + w^{(0)(nu)}_{p,l+1/2,i+1,j+1/2}\right] - 1} \tag{5.162}$$

and

$$T_5^{cc} = w^{(0)(u)}_{p,l+1/2,i+1,j+1/2} + \frac{w^{(0)(u)}_{p,l+1/2,i+1,j+1/2}}{\exp\left[w^{(0)(u)}_{p,l+1/2,i+1,j+1/2} + w^{(0)(nu)}_{p,l+1/2,i+1,j+1/2}\right] - 1} \tag{5.163}$$

This expression simplifies and becomes

$$\frac{f^{(0)(\infty)}_{0,l+1/2,i+3/2,j+1/2}}{f^{(0)(\infty)}_{0,l+1/2,i+1/2,j+1/2}} = \exp\left[-w^{(0)(u)}_{p,l+1/2,i+1,j+1/2} - w^{(0)(nu)}_{p,l+1/2,i+1,j+1/2}\right] \tag{5.164}$$

Furthermore, when plasma relaxation by collisions is the single process considered, the relation

$$\frac{F_p^{(0)}\left(\psi, p, \xi_0\right)}{D_{pp}^{(0)}\left(\psi, p, \xi_0\right)} \cong -p \tag{5.165}$$

holds[2], since $f_0^{(0)(\infty)}$ must be Maxwellian f_M, and one finds

$$\frac{f^{(0)(\infty)}_{0,l+1/2,i+3/2,j+1/2}}{f^{(0)(\infty)}_{0,l+1/2,i+1/2,j+1/2}} = \exp\left[-\Delta p_{i+1} p_{i+1} - \frac{\Delta p_{i+3/2} - \Delta p_{i+1/2}}{4}\left(p_{i+3/2} - p_{i+1/2}\right)\right] \tag{5.166}$$

Using identities introduced in Sec. 5.2,

$$\begin{cases} p_{i+3/2} = p_{i+1} + \frac{\Delta p_{i+3/2}}{2} \\ p_{i+1/2} = p_{i+1} - \frac{\Delta p_{i+1/2}}{2} \end{cases} \tag{5.167}$$

it is easy to demonstrate that

$$p_{i+1} = \frac{1}{2}\left(p_{i+3/2} + p_{i+1/2}\right) - \frac{1}{2}\left(\frac{\Delta p_{i+3/2}}{2} - \frac{\Delta p_{i+1/2}}{2}\right) \tag{5.168}$$

and

$$\Delta p_{i+1} = \frac{1}{2}\left(\Delta p_{i+3/2} + \Delta p_{i+1/2}\right) = p_{i+3/2} - p_{i+1/2} \tag{5.169}$$

[2]It is important to note that this condition is not fulfilled in the vicinity of $p = 0$, where electron-ion predominates over electron-electron interactions, if $T_e \neq T_i$. The lack of equipartition makes the dependence of $F_p^{(0)}/D_{pp}^{(0)}$ more complex, either when using a high-velocity limit expression of the $e-i$ collision operator, or a more physical description based on a Maxwellian background.

Finally, since

$$\begin{aligned} & -\Delta p_{i+1} p_{i+1} - \frac{\Delta p_{i+3/2} - \Delta p_{i+1/2}}{4} \left(p_{i+3/2} - p_{i+1/2} \right) \\ = & -\left(p_{i+3/2} - p_{i+1/2} \right) \left[\frac{1}{2} \left(p_{i+3/2} + p_{i+1/2} \right) - \frac{1}{4} \left(\Delta p_{i+3/2} - \Delta p_{i+1/2} \right) \right] \\ & -\frac{\Delta p_{i+3/2} - \Delta p_{i+1/2}}{4} \left(p_{i+3/2} - p_{i+1/2} \right) \\ = & -\frac{1}{2} \left(p_{i+3/2} + p_{i+1/2} \right) \left(p_{i+3/2} - p_{i+1/2} \right) \\ = & -\frac{1}{2} \left(p_{i+3/2}^2 - p_{i+1/2}^2 \right) \end{aligned} \tag{5.170}$$

one obtains the following relation

$$\frac{f^{(0)(\infty)}_{0,l+1/2,i+3/2,j+1/2}}{f^{(0)(\infty)}_{0,l+1/2,i+1/2,j+1/2}} = \exp\left[-\frac{p_{i+3/2}^2 - p_{i+1/2}^2}{2} \right] \tag{5.171}$$

which is exactly corresponding to a numerical Maxwellian distribution function. Hence, numerical errors do not propagate with the weighting here considered.

Finally, for the non-uniform p grid, the final results for interpolation rules are

$$\delta_p^{(0)} \rightarrow \begin{pmatrix} \delta^{(0)}_{p,l+1/2,i+1,j+1/2} \\ \delta^{(0)}_{p,l+1/2,i,j+1/2} \end{pmatrix} \tag{5.172}$$

with

$$\delta^{(0)}_{p,l+1/2,i+1,j+1/2} = \frac{1}{w^{(0)(u)}_{p,l+1/2,i+1,j+1/2}} - \frac{1}{\exp\left[w^{(0)(u)}_{p,l+1/2,i+1,j+1/2} + w^{(0)(nu)}_{p,l+1/2,i+1,j+1/2} \right] - 1} \tag{5.173}$$

and

$$\delta^{(0)}_{p,l+1/2,i,j+1/2} = \frac{1}{w^{(0)(u)}_{p,l+1/2,i,j+1/2}} - \frac{1}{\exp\left[w^{(0)(u)}_{p,l+1/2,i,j+1/2} + w^{(0)(nu)}_{p,l+1/2,i,j+1/2} \right] - 1} \tag{5.174}$$

and where

$$w_p^{(0)(u)} \rightarrow \begin{pmatrix} w^{(0)(u)}_{p,l+1/2,i+1,j+1/2} \\ w^{(0)(u)}_{p,l+1/2,i,j+1/2} \end{pmatrix} \tag{5.175}$$

with

$$w^{(0)(u)}_{p,l+1/2,i+1,j+1/2} = -\Delta p_{i+1} \frac{F^{(0)}_{p,l+1/2,i+1,j+1/2}}{D^{(0)}_{pp,l+1/2,i+1,j+1/2}} \tag{5.176}$$

and

$$w^{(0)(u)}_{p,l+1/2,i,j+1/2} = -\Delta p_{i} \frac{F^{(0)}_{p,l+1/2,i,j+1/2}}{D^{(0)}_{pp,l+1/2,i,j+1/2}} \tag{5.177}$$

Much in the same way,

$$w_p^{(0)(nu)} \rightarrow \begin{pmatrix} w_{p,l+1/2,i+1,j+1/2}^{(0)(nu)} \\ w_{p,i,j+1/2}^{(0)(nu)} \end{pmatrix} \tag{5.178}$$

where

$$w_{p,l+1/2,i+1,j+1/2}^{(0)(nu)} = -\frac{\Delta p_{i+3/2} - \Delta p_{i+1/2}}{4} \left[\frac{F_{p,l+1/2,i+3/2,j+1/2}^{(0)}}{D_{ppl+1/2,i+3/2,j+1/2}^{(0)}} - \frac{F_{pl+1/2,i+1/2,j+1/2}^{(0)}}{D_{ppl+1/2,i+1/2,j+1/2}^{(0)}} \right] \tag{5.179}$$

and

$$w_{p,i,j+1/2}^{(0)(nu)} = -\frac{\Delta p_{i+1/2} - \Delta p_{i-1/2}}{4} \left[\frac{F_{pl+1/2,i+1/2,j+1/2}^{(0)}}{D_{ppl+1/2,i+1/2,j+1/2}^{(0)}} - \frac{F_{pl+1/2,i-1/2,j+1/2}^{(0)}}{D_{ppl+1/2,i-1/2,j+1/2}^{(0)}} \right] \tag{5.180}$$

It is important to note that since only collisions are considered for evaluating interpolating coefficients $\delta_p^{(0)}$, momentum and pitch-angle dynamics are naturally decoupled. Consequently, the ratios $F_p^{(0)}/D_{pp}^{(0)}$ are only functions of p, and it is the reason why they haves similar values at different pitch-angle grid points ξ_0.

By definition, $\delta_p^{(0)}$ must be lower than unity, a condition that is naturaly satisfied for the uniform momentum grid, as shown in Fig.5.2. However, special care must be taken for the non-uniform case, since there is no exact cancellation between $1/x$ and $1/\left(e^{x+y}-1\right)$. In the limit $y < x \ll 1$, it can be easily shown that

$$g\left(x,y\right) \simeq \frac{y}{x\left(x+y\right)} \tag{5.181}$$

and the condition $g\left(x,y\right) \leq 1$ is equivalent to the relation

$$\frac{y/x}{1+y/x} < x \tag{5.182}$$

For a uniform grid, this condition is always fulfilled, since it corresponds to $y = 0$. For the non-uniform case, it is clear that the range of validity of the extended Chang and Cooper function is much more restricted, since y/x is finite. Consequently, if $x \simeq p\Delta p$ is small, y which is proportional to the variation of the grid step as function of p must be significantly smaller which means that the momentum grid is nearly uniform in this region of the phase space. For larger values of x, the condition is easier to satisfy, which indicates that the non-uniformity must be a growing function of the momentum value p, and nearly flat close to $p = 0$.

There are however additional limitations on the choice of the momentum for large p values. Indeed, in this domain, other mechanismes are at play, and the usual technique is to extrapolate calculations carried out for collisions to other accelaration mechanismes (Ohmic electric field, RF waves,...), using the generalized weighting factor based on the simple rule,

$$\left.\frac{F_p^{(0)}}{D_{pp}^{(0)}}\right|_{effective} = \frac{\sum_m F_p^{(0)(m)}}{\sum_m D_{pp}^{(0)(m)}} \tag{5.183}$$

where $\sum_m$ is the sum over all the physical processes m that take place in the plasma. Since the same syntax may be kept, one obtains simply

$$w^{(0)(u)}_{p,l+1/2,i+1,j+1/2} = -\Delta p_{i+1} \left.\frac{F_p^{(0)}}{D_{pp}^{(0)}}\right|^{l+1/2,i+1,j+1/2}_{effective} \tag{5.184}$$

and

$$w^{(0)(u)}_{p,l+1/2,i,j+1/2} = -\Delta p_{i} \left.\frac{F_p^{(0)}}{D_{pp}^{(0)}}\right|^{l+1/2,i,j+1/2}_{effective} \tag{5.185}$$

for the uniform contribution, while for the non-uniform one

$$w^{(0)(nu)}_{p,l+1/2,i+1,j+1/2} = -\frac{\Delta p_{i+3/2} - \Delta p_{i+1/2}}{4} \left[\left.\frac{F_p^{(0)}}{D_{pp}^{(0)}}\right|^{l+1/2,i+3/2,j+1/2}_{effective} - \left.\frac{F_p^{(0)}}{D_{pp}^{(0)}}\right|^{l+1/2,i+1/2,j+1/2}_{effective} \right] \tag{5.186}$$

and

$$w^{(0)(nu)}_{p,l+1/2,i,j+1/2} = -\frac{\Delta p_{i+1/2} - \Delta p_{i-1/2}}{4} \left[\left.\frac{F_p^{(0)}}{D_{pp}^{(0)}}\right|^{l+1/2,i+1/2,j+1/2}_{effective} - \left.\frac{F_p^{(0)}}{D_{pp}^{(0)}}\right|^{l+1/2,i-1/2,j+1/2}_{effective} \right] \tag{5.187}$$

In that case, the interpolating weights exhibit a dependence with ξ_0. This has however a weak importance for the accuracy of the calculations, since in the domain where fluxes are strongly modified since usually $\left.\frac{F_p^{(0)}}{D_{pp}^{(0)}}\right|_{effective} \rightarrow 0$ in presence of RF quasilinear diffusion. The Maxwellian distribution function is consequently no more the solution of the Fokker-Planck equation.

The reason why an effective expression of $F_p^{(0)}/D_{pp}^{(0)}$ is used for evaluating $\delta_p^{(0)}$ where collisions are not the single process is based on the fact that the Chang and Cooper function tends towards $\delta_p^{(0)} \simeq \frac{1}{2}$ for a uniform mesh when $\left.\frac{F_p^{(0)}}{D_{pp}^{(0)}}\right|_{effective}$ increases. In that case, it corresponds exactly to the standard linear interpolation, i.e. the well known arithmetic mean. The interpolation procedure is therefore consistent with the grid, an important characteristic for reducing the rate of convergence.

Unfortunately, such a property is not valid for a non-uniform grid, and the interpolation may be wrong , leading to possible an anomalous behaviour of the code. Consequently, even at larger values of p, only a uniform mesh may provide a consistent solution with the numerical grid in presence of external sources of acceleration. From this analysis, it turns out that the only purpose for using a non-uniform momentum mesh is to establish a link between the fine mesh in the vicinity of $p = 0$, and a coarse grid in the region where other physical mechanismes are at play. Consequently, the momentum mesh is build from the relation

$$\Delta p_i = \frac{\left(\Delta p_{n_p-1} - \Delta p_0\right)}{2} \tanh\left(i - i_{ref}\right) + \frac{\left(\Delta p_{n_p-1} + \Delta p_0\right)}{2} \tag{5.188}$$

with the recurrence relation

$$p_{i+1} = \Delta p_i + p_i \tag{5.189}$$

where $p_0 = 0$, $\Delta p_{n_p-1} = p_{\max}/\left(n_p - 1\right)$ and Δp_0 is an arbitrary value. Here i_{ref} is the index value corresponding to the transition between the fine and the coarse grids. When $\Delta p_0 = \Delta p_{n_p-1}$, the case of an uniform mesh is well recovered, whatever i_{ref}. Here Δp_0 and i_{ref} must be chosen so that the non-uniform part of the momentum grid is far enough from $p = 0$ in order the relation $\delta_p^{(0)} > 1$ is satisfied, but also far from the region where external forces play a role[3].

Finally, $w_p^{(0)(nu)}$ require evaluations of the quantities at the respective grid points $(l + 1/2, i - 1/2, j + 1/2)$ and $(l + 1/2, i + 3/2, j + 1/2)$. The usual method to deal with this problem is shifting indexes, according to the relation

$$(l + 1/2, i + 1/2, j + 1/2) \in \{[1 : n_\psi], [1 : n_p], [1 : n_\xi]\} \tag{5.190}$$

and

$$\begin{cases} (l + 1/2, i - 1/2, j + 1/2) \in \{[1 : n_\psi], [X, 1 : n_p - 1], [1 : n_\xi]\} \\ (l + 1/2, i + 3/2, j + 1/2) \in \{[1 : n_\psi], [2 : n_p, X], [1 : n_\xi]\} \end{cases} \tag{5.191}$$

Hence, all quantities have the same size (n_ψ, n_p, n_ξ), which is crucial for the $3 - D$ matrix representation. Furthermore, boundary conditions are naturally satisfied with this technique, since arbitrary values may be attributed to the variable X at these grid points.

Pitch-angle grid interpolation For the pitch-angle terms, calculation is very simple, and from previous relations, one deduces directly that $w^{(0)}_{\xi,l+1/2,i+1/2,j+1} = w^{(0)}_{\xi,l+1/2,i+1/2,j} = 0$ since $F_\xi^{(0)} = 0$. Therefore, $\delta^{(0)}_{\xi,l+1:2,i+1/2,j+1}$ may be defined in an arbitrary manner. It is important to note that this choice is different from the one described in Ref. [22], where the pitch-angle weighting factors are defined in the same way as for the momentum p. However, it turns out that in presence of RF waves, this leads sometimes to spurious numerical evolutions, while the simple approach here described avoid them.

The most natural way is therefore to perform a linear interpolation, between $f^{(0)(\infty)}_{0,l+1/2,i+1/2,j+3/2}$ and $f^{(0)(\infty)}_{0,l+1/2,i+1/2,j+3/2}$, and also between $f^{(0)(\infty)}_{0,l+1:2,i+1/2,j+1/2}$ and $f^{(0)(\infty)}_{0,l+1/2,i+1/2,j-1/2}$ according to the relations

$$\begin{aligned} f^{(0)(\infty)}_{0,l+1/2,i+1/2,j+1} &= \left(\frac{\Delta\xi_{0,j+1/2}}{\Delta\xi_{0,j+1/2} + \Delta\xi_{0,j+3/2}}\right) f^{(0)(\infty)}_{0,l+1/2,i+1/2,j+3/2} \\ &\quad + \left(\frac{\Delta\xi_{0,j+3/2}}{\Delta\xi_{0,j+1/2} + \Delta\xi_{0,j+3/2}}\right) f^{(0)(\infty)}_{0,l+1/2,i+1/2,j+1/2} \end{aligned} \tag{5.192}$$

$$\begin{aligned} f^{(0)(\infty)}_{0,l+1/2,i+1/2,j} &= \left(\frac{\Delta\xi_{0,j-1/2}}{\Delta\xi_{0,j-1/2} + \Delta\xi_{0,j+1/2}}\right) f^{(0)(\infty)}_{0,l+1/2,i+1/2,j+1/2} \\ &\quad + \left(\frac{\Delta\xi_{0,j+1/2}}{\Delta\xi_{0,j-1/2} + \Delta\xi_{0,j+1/2}}\right) f^{(0)(\infty)}_{0,l+1/2,i+1/2,j-1/2} \end{aligned} \tag{5.193}$$

[3]In the expression for calculating Δp_i, $i - i_{ref}$ may be replaced by $(i - i_{ref})/\Delta i$, where Δi is a free parameter for controlling the sharpness of the transition between the two domains in momentum space. However, $\Delta i = 1$ provides the adequate number of point, of the order of 5, in order to avoid both a large jump, or a too smooth transition that may lead to violation of the condition that $\delta < 1$ for small i values.

Taking into account of the non-uniform grid steps

$$\delta^{(0)}_{\xi,l+1/2,i+1/2,j+1} = \frac{\Delta\xi_{0,j+3/2}}{\Delta\xi_{0,j+1/2}+\Delta\xi_{0,j+3/2}} \tag{5.194}$$

$$\delta^{(0)}_{\xi,l+1/2,i+1/2,j} = \frac{\Delta\xi_{0,j+1/2}}{\Delta\xi_{0,j-1/2}+\Delta\xi_{0,j+1/2}} \tag{5.195}$$

and for a uniform grid, the relation $\delta^{(0)}_{\xi,l+1/2,i+1/2,j+1} = \delta^{(0)}_{\xi,l+1/2,i+1/2,j} = 1/2$ are exactly recovered.

Finally, for the non-uniform pitch-angle grid ξ, the interpolation rules are

$$\delta^{(0)}_{\xi} \rightarrow \left\{ \begin{array}{l} \delta^{(0)}_{\xi,l+1/2,i+1/2,j+1} = \frac{\Delta\xi_{0,j+3/2}}{\Delta\xi_{0,j+1/2}+\Delta\xi_{0,j+3/2}} \\ \delta^{(0)}_{\xi,l+1/2,i+1/2,j} = \frac{\Delta\xi_{0,j+1/2}}{\Delta\xi_{0,j-1/2}+\Delta\xi_{0,j+1/2}} \end{array} \right. \tag{5.196}$$

Furthermore, $\delta^{(0)}_{\xi}$ require evaluations of the quantities at the respective grid points $(l+1/2, i+1/2, j-1/2)$ and $(l+1/2, j+1/2, j+3/2)$. As for the momentum grid interpolation, indexes are shifted,

$$\left\{ \begin{array}{l} (l+1/2, i+1/2, j-1/2) \in \{[1:n_\psi], [1:n_p], [X, 1:n_\xi-1]\} \\ (l+1/2, i+1/2, j+3/2) \in \{[1:n_\psi], [1:n_p], [2:n_\xi, X]\} \end{array} \right. \tag{5.197}$$

Spatial grid interpolation The determination of $\delta^{(0)}_{\psi}$ is based on the same method used for $\delta^{(0)}_{\xi}$, since no specific condition is required for interpolating $f^{(0)}_0$ on the flux grid. A linear interpolation is considered between $f^{(0)(\infty)}_{0,l+3/2,i+1/2,j+1/2}$ and $f^{(0)(\infty)}_{0,l+1/2,i+1/2,j+1/2}$ and also between $f^{(0)(\infty)}_{0,l+1/2,i+1/2,j+1/2}$ and $f^{(0)(\infty)}_{0,l-1/2,i+1/2,j+1/2}$,

$$\begin{aligned} f^{(0)(\infty)}_{0,l+1,i+1/2,j+1/2} &= \left(\frac{\Delta\psi_{l+1/2}}{\Delta\psi_{l+1/2}+\Delta\psi_{l+3/2}}\right) f^{(0)(\infty)}_{0,l+3/2,i+1/2,j+1/2} \\ &\quad + \left(\frac{\Delta\psi_{l+3/2}}{\Delta\psi_{l+1/2}+\Delta\psi_{l+3/2}}\right) f^{(0)(\infty)}_{0,l+1/2,i+1/2,j+1/2} \end{aligned} \tag{5.198}$$

$$\begin{aligned} f^{(0)(\infty)}_{0,l,i+1/2,j+1/2} &= \left(\frac{\Delta\psi_{l-1/2}}{\Delta\psi_{l-1/2}+\Delta\psi_{l+1/2}}\right) f^{(0)(\infty)}_{0,l+1/2,i+1/2,j+1/2} \\ &\quad + \left(\frac{\Delta\psi_{l+1/2}}{\Delta\psi_{l-1/2}+\Delta\psi_{l+1/2}}\right) f^{(0)(\infty)}_{0,l-1/2,i+1/2,j+1/2} \end{aligned} \tag{5.199}$$

taking into account of the non-uniform nature of the grid

$$\delta^{(0)}_{\psi,l+1} = \frac{\Delta\psi_{l+3/2}}{\Delta\psi_{l+1/2}+\Delta\psi_{l+3/2}} \tag{5.200}$$

$$\delta^{(0)}_{\psi,l} = \frac{\Delta\psi_{l+1/2}}{\Delta\psi_{l-1/2}+\Delta\psi_{l+1/2}} \tag{5.201}$$

For a uniform grid the relation $\delta^{(0)}_{\psi,l+1} = \delta^{(0)}_{\psi,l} = 1/2$ is well recovered.

Furthermore, $\delta^{(0)}_{\psi}$ require evaluations of the quantities at the respective grid points $(l-1/2, i+1/2, j+1/2)$ and $(l+3/2, j+1/2, j+1/2)$. As for the momentum grid interpolation, indexes are shifted according to the rule

$$\begin{cases} (l-1/2, i+1/2, j+1/2) \in \{[X, 1:n_\psi - 1], [1:n_p], [1:n_\xi]\} \\ (l+3/2, i+1/2, j+1/2) \in \{[2:n_\psi, X], [1:n_p], [1:n_\xi]\} \end{cases} \tag{5.202}$$

5.4.4 Discrete description of physical processes

5.4.5 Collisions

According to the bounce averaged expression,

$$\overline{\overline{D}}^{C(0)}_{p} \rightarrow \begin{cases} D^{C(0)}_{pp,l+1/2,i+1,j+1/2} = A_{l+1/2,i+1} \\ D^{C(0)}_{pp,l+1/2,i,j+1/2} = A_{l+1/2,i} \\ D^{C(0)}_{p\xi,l+1/2,i+1,j+1/2} = 0 \\ D^{C(0)}_{\xi p,l+1/2,i+1/2,j+1} = 0 \\ D^{C(0)}_{p\xi,l+1/2,i+1/2,j+1/2} = 0 \\ D^{C(0)}_{\xi p,l+1/2,i+1/2,j+1/2} = 0 \\ D^{C(0)}_{p\xi,l+1/2,i,j+1/2} = 0 \\ D^{C(0)}_{\xi p,l+1/2,i+1/2,j} = 0 \\ D^{C(0)}_{\xi\xi,l+1/2,i+1/2,j+1} = \left(\lambda^{l+1/2,j+1}_{2,-1,0}/\lambda^{l+1/2,j+1}\right) B_{t,l+1/2,i+1/2} \\ D^{C(0)}_{\xi\xi,l+1/2,i+1/2,j} = \left(\lambda^{l+1/2,j}_{2,-1,0}/\lambda^{l+1/2,j}\right) B_{t,l+1/2,i+1/2} \end{cases} \tag{5.203}$$

and

$$\overline{\overline{F}}^{C(0)}_{p} \rightarrow \begin{cases} F^{C(0)}_{p,l+1/2,i+1,j+1/2} = -F_{l+1/2,i+1} \\ F^{C(0)}_{p,l+1/2,i,j+1/2} = -F_{l+1/2,i} \\ F^{C(0)}_{\xi,l+1/2,i+1/2,j+1} = 0 \\ F^{C(0)}_{\xi,l+1/2,i+1/2,j} = 0 \end{cases} \tag{5.204}$$

where each coefficient is the sum of the electron-electron and electron-ion interactions.

Electron-electron collision operator

Belaiev-Budker relativistic collision model Here, coefficients corresponding to the Belaiev-Budker collision operator that ranges from non-relativistic to fully relativistic regimes may be expressed as, according to the notation used in Ref.[17],

$$A^{ee}_{l+1/2,i+1/2} = \frac{\left(F_{1,l+1/2,i+1/2} + F_{2,l+1/2,i+1/2}\right)}{v_{i+1/2}} \overline{T}_{e,l+1/2} \tag{5.205}$$

$$F^{ee}_{l+1/2,i+1/2} = F_{1,l+1/2,i+1/2} + F_{2,l+1/2,i+1/2} \tag{5.206}$$

with

$$F_{1,l+1/2,i+1/2} = \frac{4\pi}{v_{i+1/2}^2} F_{11,l+1/2,i+1/2} + \frac{4\pi}{p_{i+1/2}^2} F_{12,l+1/2,i+1/2} \tag{5.207}$$

$$F_{2,l+1/2,i+1/2} = \frac{4\pi}{v_{i+1/2}} \left(1 - \frac{\gamma_{i+1/2}\zeta_{,i+1/2}}{z_{i+1/2}}\right) F_{21,l+1/2,i+1/2} \tag{5.208}$$

Expressions of coefficients $F_{11,l+1/2,i+1/2}$, $F_{12,l+1/2,i+1/2}$ and $F_{21,l+1/2,i+1/2}$ are

$$F_{11,l+1/2,i+1/2} = \int_0^{i+1/2} p'v' f_M\left(\psi_{l+1/2}, p'\right) dp' \tag{5.209}$$

$$F_{12,l+1/2,i+1/2} = \int_0^{i+1/2} p'v' \left(1 - \frac{\gamma'\zeta'}{z'}\right) f_M\left(\psi_{l+1/2}, p'\right) dp' \tag{5.210}$$

$$F_{21,l+1/2,i+1/2} = \int_{i+1/2}^{\infty} p' f_M\left(\psi_{l+1/2}, p'\right) dp' \tag{5.211}$$

Coefficients A^{ee} and F^{ee} must be also calculated on the flux grids and therefore, according to the previous definition,

$$A_{l+1/2,i}^{ee} = \frac{\left(F_{1,l+1/2,i} + F_{2,l+1/2,i}\right)}{v_i} \overline{T}_{e,l+1/2} \tag{5.212}$$

and

$$F_{l+1/2,i}^{ee} = F_{1,l+1/2,i} + F_{2,l+1/2,i} \tag{5.213}$$

where

$$F_{1,l+1/2,i} = \frac{4\pi}{v_i^2} F_{11,l+1/2,i} + \frac{4\pi}{p_i^2} F_{12,l+1/2,i} \tag{5.214}$$

$$F_{2,l+1/2,i} = \frac{4\pi}{v_i} \left(1 - \frac{\gamma_i\zeta_i}{z_i}\right) F_{21,l+1/2,i} \tag{5.215}$$

and

$$F_{11,l+1/2,i} = \int_0^{i} p'v' f_M\left(\psi_{l+1/2}, p'\right) dp' \tag{5.216}$$

$$F_{12,l+1/2,i} = \int_0^{i} p'v' \left(1 - \frac{\gamma'\zeta'}{z'}\right) f_M\left(\psi_{l+1/2}, p'\right) dp' \tag{5.217}$$

$$F_{21,l+1/2,i} = \int_i^{\infty} p' f_M\left(\psi_{l+1/2}, p'\right) dp' \tag{5.218}$$

for the grid points i, while for the grid points $i+1$, one has just to replace i by $i+1$ in the set of above expressions.

Furthermore, the expression of coefficient B_t^{ee} is

$$B_{t,l+1/2,i+1/2}^{ee} = B_{t1,l+1/2,i+1/2} + B_{t2,l+1/2,i+1/2} \tag{5.219}$$

with

$$B_{t1,l+1/2,i+1/2} = 4\pi \sum_{n=1}^{5} B_{t1,l+1/2,i+1/2}^{[n]} \tag{5.220}$$

and

$$B_{t2,l+1/2,i+1/2} = 4\pi \sum_{n=1}^{5} B^{[n]}_{t2,l+1/2,i+1/2} \tag{5.221}$$

where

$$B^{[1]}_{t1,l+1/2,i+1/2} = \frac{1}{2v_{i+1/2}} \int_0^{i+1/2} p'^2 f_M\left(\psi_{l+1/2}, p'\right) dp' \tag{5.222}$$

$$B^{[2]}_{t1,l+1/2,i+1/2} = -\frac{1}{6v_{i+1/2}p^2_{i+1/2}} \int_0^{i+1/2} p'^4 f_M\left(\psi_{l+1/2}, p'\right) dp' \tag{5.223}$$

$$B^{[3]}_{t1,l+1/2,i+1/2} = \frac{1}{8\gamma^2_{i+1/2}z^2_{i+1/2}} \int_0^{i+1/2} p'^2 \frac{J'_1}{\gamma'} f_M\left(\psi_{l+1/2}, p'\right) dp' \tag{5.224}$$

$$B^{[4]}_{t1,l+1/2,i+1/2} = -\frac{1}{4z^2_{i+1/2}} \int_0^{i+1/2} p'^2 \frac{J'_2}{\gamma'} f_M\left(\psi_{l+1/2}, p'\right) dp' \tag{5.225}$$

$$B^{[5]}_{t1,l+1/2,i+1/2} = -\frac{1}{4\gamma^2_{i+1/2}} \int_0^{i+1/2} \frac{p'^2}{\gamma'} \left(\gamma' - \frac{\zeta'}{z'}\right) f_M\left(\psi_{l+1/2}, p'\right) dp' \tag{5.226}$$

and

$$B^{[1]}_{t2,l+1/2,i+1/2} = \frac{1}{2} \int_{i+1/2}^{\infty} \frac{p'^2}{v'} f_M\left(\psi_{l+1/2}, p'\right) dp' \tag{5.227}$$

$$B^{[2]}_{t2,l+1/2,i+1/2} = -\frac{\gamma^2_{i+1/2}}{6} \int_{i+1/2}^{\infty} \frac{p'^2}{\gamma'^2 v'} f_M\left(\psi_{l+1/2}, p'\right) dp' \tag{5.228}$$

$$B^{[3]}_{t2,l+1/2,i+1/2} = \frac{J_{1,i+1/2}}{8\gamma_{i+1/2}z^2_{i+1/2}} \int_{i+1/2}^{\infty} \frac{p'^2}{v'} \frac{1}{\gamma'^2} f_M\left(\psi_{l+1/2}, p'\right) dp' \tag{5.229}$$

$$B^{[4]}_{t2,l+1/2,i+1/2} = -\frac{\gamma_{i+1/2}J_{2,i+1/2}}{4z^2_{i+1/2}} \int_{i+1/2}^{\infty} \frac{p'^2}{v'} \frac{1}{\gamma'^2} f_M\left(\psi_{l+1/2}, p'\right) dp' \tag{5.230}$$

$$B^{[5]}_{t2,l+1/2,i+1/2} = -\frac{1}{4\gamma_{i+1/2}p^2_{i+1/2}} \left(\gamma_{i+1/2} - \frac{\zeta_{i+1/2}}{z_{i+1/2}}\right) \int_{i+1/2}^{\infty} p'^2 v' f_M\left(\psi_{l+1/2}, p'\right) dp' \tag{5.231}$$

Here,

$$J_{1,i+1/2} = -3\gamma_{i+1/2} + \zeta_{i+1/2}\left(\frac{3}{z_{i+1/2}} + 2z_{i+1/2}\right) \tag{5.232}$$

$$J_{2,i+1/2} = \gamma_{i+1/2} + \frac{\zeta_{i+1/2}}{z_{i+1/2}} - \frac{2}{3}\gamma_{i+1/2}z^2_{i+1/2} \tag{5.233}$$

with

$$z_{i+1/2} = \beta^{\dagger 2}_{th} p_{i+1/2} \tag{5.234}$$

$$\gamma_{i+1/2} = \sqrt{1 + z^2_{i+1/2}} \tag{5.235}$$

and

$$\zeta_{i+1/2} = \sinh^{-1} z_{i+1/2} \tag{5.236}$$

Coefficients A, B_t and F for the Beliaev-Budker relativistic collision operator need to calculate accurately integrals of type

$$\begin{cases} \int_0^{p_i} X dp' \\ \int_0^{p_{i+1/2}} X dp' \\ \int_0^{p_{i+1}} X dp' \end{cases} \tag{5.237}$$

which require a special attention in the vicinity of $p = 0$, and also of type,

$$\begin{cases} \int_{p_i}^{\infty} X dp' \\ \int_{p_{i+1/2}}^{\infty} X dp' \\ \int_{p_{i+1}}^{\infty} X dp' \end{cases} \tag{5.238}$$

The goal is to ensure an acceptable numerical accuracy which preserves the conservative nature of the equations to be solved by numerical method, without any use of ad-hoc boundary conditions to compensate spurious particle leak arisinf from an improper flux balance at each grid point. For this purpose, a new momentum grid called "super-grid" is introduced, correponding to a refined mesh. Since no specific condition is required as compared to the links between distribution and flux grids, the momentum super-grid is simply defined as a sum of two different meshes for integrals of type $\int_0^{p_{i+1/2}} X dp'$

$$\begin{cases} p^s_{i'} \in \left[\frac{p_{1/2}}{n^s_p}, p_{1/2}\right[, i' \rightarrow \left\{0, n^s_p - 1\right\} \\ p^s_{i'} \in \left[p_{1/2}, p_{i+1/2}\right] , i' \rightarrow \left\{0, n^s_p - 1\right\} \end{cases} \tag{5.239}$$

one for very fine calculations below $p_{1/2}$, and a second, less refined up to $p_{i+1/2}$. For integrals of type $\int_0^{p_i} X dp'$ and $\int_0^{p_{i+1}} X dp'$, the corresponding super-grids are defined in the same way,

$$\begin{cases} p^s_{i'} \in \left[\frac{p_{1/2}}{n^s_p}, p_1\right] , i' \rightarrow \left\{0, n^s_p - 1\right\} \\ p^s_{i'} \in \left[p_1, p_i\right] , i' \rightarrow \left\{0, n^s_p - 1\right\} \end{cases} \tag{5.240}$$

and

$$\begin{cases} p^s_{i'} \in \left[\frac{p_{1/2}}{n^s_p}, p_1\right] , i' \rightarrow \left\{0, n^s_p - 1\right\} \\ p^s_{i'} \in \left[p_1, p_{i+1}\right] , i' \rightarrow \left\{0, n^s_p - 1\right\} \end{cases} \tag{5.241}$$

It is important to note that p_1 correponds to the second point of the grid p_i while it is the first one for the grid p_{i+1}, so that numerical integration starts at the same momentum value. Much in the same way, integrals of type $\int_{p_i}^{\infty} X dp'$, $\int_{p_{i+1/2}}^{\infty} X dp'$ and $\int_{p_{i+1}}^{\infty} X dp'$ are simply defined on the following super-grids

$$\begin{cases} p^s_{i'} \in \left[p_i, p_{\max} - \Delta p_{n_p}\right] , i' \rightarrow \left\{0, n^s_p - 1\right\} \\ p^s_{i'} \in \left[p_{i+1/2}, p_{\max} - \frac{\Delta p_{n_p - 1/2}}{2}\right] , i' \rightarrow \left\{0, n^s_p - 1\right\} \\ p^s_{i'} \in \left[p_{i+1}, p_{\max}\right] , i' \rightarrow \left\{0, n^s_p - 1\right\} \end{cases} \tag{5.242}$$

All integrals are performed by the trapezoidal method, even if any more accurate technique like the Simpson method may be used in that case. A crucial point is that

integrals exactly end or start at points p_i, $p_{i+1/2}$ or p_{i+1} so that no overlap between $\int_0^{p_{i+1/2}} X dp'$ and $\int_{p_{i+1/2}}^{\infty} X dp'$ can take place. This is especially important to avoid spurious numerical particle leak, that could break the conservative nature of the equations to be solved.

Concerning the first order Legendre correction that ensures momentum conservation, one must calculate

$$\{C\left(f_M, f\right)\} \simeq -\frac{3}{2}\frac{\overline{\lambda}_{1,1,0}}{\lambda}\xi_0 \mathcal{I}\left(f_M, f_0^{(0)(m=1)}\right) \tag{5.243}$$

on the distribution function grid, where

$$f_0^{(0)(m=1)}\left(p, \xi_0, \psi\right) = \int_{-1}^{+1} \xi_0 f_0^{(0)}\left(p, \xi_0, \psi\right) d\xi_0 \tag{5.244}$$

as shown in Sec. 4.1.4.

Therefore, by definition,

$$\{C\left(f_M, f\right)\}^{(k)}_{l+1/2,i+1/2,j+1/2} = -\frac{3}{2}\frac{\overline{\lambda}^{l+1/2,j+1/2}_{1,1,0}}{\lambda^{l+1/2,j+1/2}}\xi_{0,j+1/2}\mathcal{I}\left(f_{M,}, f_0^{(0)(m=1)}\right)^{(k)}_{l+1/2,i+1/2,j+1/2} \tag{5.245}$$

where for the Belaiev-Budker relativistic collision operator,

$$\begin{aligned}
\mathcal{I} \quad & \left(f_{0M,}, f_0^{(0)(m=1)}\right)^{(k)}_{l+1/2,i+1/2,j+1/2} \\
& = \frac{4\pi}{\gamma_{i+1/2}}\left(f^{(0)(k)}_{0,l=1,l+1/2,i+1/2,j+1/2}\right. \\
& + \frac{1}{p_{i+1/2}}\mathcal{I}_1\left(f_{M,}, f_0^{(0)(m=1)}\right)^{(k)}_{l+1/2,i+1/2,j+1/2} \\
& \left. + p_{i+1/2}\mathcal{I}_2\left(f_{M,}, f_0^{(0)(m=1)}\right)^{(k)}_{l+1/2,i+1/2,j+1/2}\right)
\end{aligned} \tag{5.246}$$

with

$$\mathcal{I}_1\left(f_{M,}, f_0^{(0)(m=1)}\right)^{(k)}_{l+1/2,i+1/2,j+1/2} = \sum_{n=1}^{10} \mathcal{I}^{[n](k)}_{1,l+1/2,i+1/2,j+1/2} \tag{5.247}$$

and

$$\mathcal{I}_2\left(f_{M,}, f_0^{(0)(m=1)}\right)^{(k)}_{l+1/2,i+1/2,j+1/2} = \sum_{n=1}^{7} \mathcal{I}^{[n](k)}_{2,l+1/2,i+1/2,j+1/2} \tag{5.248}$$

The set of coefficients $\mathcal{I}_1^{[n]}$ is

$$\mathcal{I}^{[1](k)}_{1,l+1/2,i+1/2,j+1/2} = \frac{1}{3\overline{T}_{e,l+1/2}}\sum_{i'=0}^{i}\frac{p^3_{i'+1/2}}{\gamma_{i'+1/2}} f^{(0)(m=1)(k)}_{0,l+1/2,i'+1/2}\Delta p_{i'+1/2} \tag{5.249}$$

$$\mathcal{I}^{[2](k)}_{1,l+1/2,i+1/2,j+1/2} = -\frac{2\gamma_{i+1/2}}{3\overline{T}_{e,l+1/2}}\sum_{i'=0}^{i} p^3_{i'+1/2} f^{(0)(m=1)(k)}_{0,,l+1/2,i'+1/2}\Delta p_{i'+1/2} \tag{5.250}$$

$$\mathcal{I}^{[3](k)}_{1,l+1/2,i+1/2,j+1/2} = \frac{\gamma_{i+1/2}}{5\overline{T}^2_{e,l+1/2}} \sum_{i'=0}^{i} \frac{p^5_{i'+1/2}}{\gamma_{i'+1/2}} f^{(0)(m=1)(k)}_{0,l+1/2,i'+1/2} \Delta p_{i'+1/2} \tag{5.251}$$

$$\mathcal{I}^{[4](k)}_{1,l+1/2,i+1/2,j+1/2} = \sum_{i'=0}^{i} \frac{p_{i'+1/2}}{\gamma_{i'+1/2}} \left(\gamma_{i'+1/2} - \frac{\zeta_{i'+1/2}}{z_{i'+1/2}} \right) f^{(0)(m=1)(k)}_{0,l+1/2,i'+1/2} \Delta p_{i'+1/2} \tag{5.252}$$

$$\mathcal{I}^{[5](k)}_{1,l+1/2,i+1/2,j+1/2} = -\frac{\gamma_{i+1/2}}{\overline{T}_{e,l+1/2}} \sum_{i'=0}^{i} \frac{p^3_{i'+1/2}}{\gamma_{i'+1/2}} \frac{J_{2,i'+1/2}}{z^2_{i'+1/2}} f^{(0)(m=1)(k)}_{0,l+1/2,i'+1/2} \Delta p_{i'+1/2} \tag{5.253}$$

$$\begin{aligned} \mathcal{I}^{[6](k)}_{1,l+1/2,i+1/2,j+1/2} &= \frac{\gamma_{i+1/2} p^2_{i+1/2} - 5\overline{T}_{e,l+1/2}}{6\overline{T}^2_{e,l+1/2}} \sum_{i'=0}^{i} \frac{p^3_{i'+1/2}}{\gamma_{i'+1/2}} f^{(0)(m=1)(k)}_{0,l+1/2,i'+1/2} \Delta p_{i'+1/2} \\ &\times \left(1 + \frac{3}{z^2_{i'+1/2}} - \frac{3\gamma_{i'+1/2}\zeta_{i'+1/2}}{z^3_{i'+1/2}} \right) \end{aligned} \tag{5.254}$$

$$\mathcal{I}^{[7](k)}_{1,l+1/2,i+1/2,j+1/2} = \frac{\gamma_{i+1/2}}{2\beta^{\dagger 2}_{th}\overline{T}^2_{e,l+1/2}} \sum_{i'=0}^{i} \frac{p^3_{i'+1/2}}{\gamma_{i'+1/2}} \frac{J_{3,i'+1/2}}{z_{i'+1/2}} f^{(0)(m=1)(k)}_{0,l+1/2,i'+1/2} \Delta p_{i'+1/2} \tag{5.255}$$

$$\mathcal{I}^{[8](k)}_{1,l+1/2,i+1/2,j+1/2} = \frac{\gamma_{i+1/2}}{2\overline{T}_{e,l+1/2}} \sum_{i'=0}^{i} \frac{p^3_{i'+1/2}}{\gamma_{i'+1/2}} \frac{J_{1,i'+1/2}}{z^2_{i'+1/2}} f^{(0)(m=1)(k)}_{0,l+1/2,i'+1/2} \Delta p_{i'+1/2} \tag{5.256}$$

$$\mathcal{I}^{[9](k)}_{1,l+1/2,i+1/2,j+1/2} = \frac{p^2_{i+1/2}}{\overline{T}_{e,l+1/2}} \sum_{i'=0}^{i} \frac{p_{i'+1/2}}{\gamma_{i'+1/2}} \left(\frac{\gamma_{i'+1/2}\zeta_{i'+1/2}}{z_{i'+1/2}} - 1 \right) f^{(0)(m=1)(k)}_{0,l+1/2,i'+1/2} \Delta p_{i'+1/2} \tag{5.257}$$

$$\mathcal{I}^{[10](k)}_{1,l+1/2,i+1/2,j+1/2} = -\frac{\gamma^2_{i+1/2}}{12\beta^{\dagger 2}_{th}\overline{T}^2_{e,l+1/2}} \sum_{i'=0}^{i} \frac{p^3_{i'+1/2}}{\gamma_{i'+1/2}} \frac{J_{4,i'+1/2}}{z_{i'+1/2}} f^{(0)(m=1)(k)}_{0,l+1/2,i'+1/2} \Delta p_{i'+1/2} \tag{5.258}$$

and the coefficients $\mathcal{I}^{[n]}_2$ are

$$\mathcal{I}^{[1](k)}_{2,l+1/2,i+1/2,j+1/2} = \frac{1}{3\overline{T}_{e,l+1/2}} \sum_{i'=i}^{n_p-1} \frac{1}{\gamma_{i'+1/2}} f^{(0)(m=1)(k)}_{0,l+1/2,i'+1/2} \Delta p_{i'+1/2} \tag{5.259}$$

$$\mathcal{I}^{2(k)}_{2,l+1/2,i+1/2,j+1/2} = \left(-\frac{2\gamma_{i+1/2}}{3\overline{T}_{e,l+1/2}} + \frac{p^2_{i+1/2}}{5\overline{T}^2_{e,l+1/2}} \right) \sum_{i'=i}^{n_p-1} f^{(0)(m=1)(k)}_{0,l+1/2,i'+1/2} \Delta p_{i'+1/2} \tag{5.260}$$

$$\mathcal{I}^{[3](k)}_{2,l+1/2,i+1/2,j+1/2} = \left(\gamma_{i+1/2} - \frac{\zeta_{i+1/2}}{z_{i+1/2}} \right) \frac{1}{p^2_{i+1/2}} \sum_{i'=i}^{n_p-1} \frac{1}{\gamma_{i'+1/2}} f^{(0)(m=1)(k)}_{0,l+1/2,i'+1/2} \Delta p_{i'+1/2} \tag{5.261}$$

$$\mathcal{I}^{[4](k)}_{2,l+1/2,i+1/2,j+1/2} = -\frac{J_{2,i+1/2}}{z^2_{i+1/2}\overline{T}_{e,l+1/2}} \sum_{i'=i}^{n_p-1} f^{(0)(m=1)(k)}_{0,l+1/2,i'+1/2} \Delta p_{i'+1/2} \tag{5.262}$$

$$\mathcal{I}^{[5](k)}_{2,l+1/2,i+1/2,j+1/2} = \left(1+\frac{3}{z^2_{i+1/2}}-\frac{3\gamma_{i+1/2}\zeta_{i+1/2}}{z^3_{i+1/2}}\right)\frac{1}{6\overline{T}^2_{e,l+1/2}} \times\sum_{i'=i}^{n_p-1}\left(\frac{\gamma_{i'+1/2}p^2_{i'+1/2}-5\overline{T}_{e,l+1/2}}{\gamma_{i'+1/2}}\right)f^{(0)(m=1)(k)}_{0,l+1/2,i'+1/2}\Delta p_{i'+1/2} \tag{5.263}$$

$$\mathcal{I}^{[6](k)}_{2,l+1/2,i+1/2,j+1/2} = \left(\frac{J_{3,i+1/2}}{2z_{i+1/2}\beta^{\dagger 2}_{th}\overline{T}^2_{e,l+1/2}}+\frac{J_{1,i+1/2}}{2z^2_{i+1/2}\overline{T}_{e,l+1/2}} -\frac{J_{4,i+1/2}}{12z_{i+1/2}\beta^{\dagger 2}_{th}\overline{T}^2_{e,l+1/2}}\right)\times\sum_{i'=i}^{n_p-1}f^{(0)(m=1)(k)}_{0,l+1/2,i'+1/2}\Delta p_{i'+1/2} \tag{5.264}$$

$$\mathcal{I}^{[7](k)}_{2,l+1/2,i+1/2,j+1/2} = \frac{1}{p^2_{i+1/2}\overline{T}_{e,l+1/2}}\left(\frac{\gamma_{i+1/2}\zeta_{i+1/2}}{z_{i+1/2}}-1\right) \times\sum_{i'=i}^{n_p-1}\frac{p^2_{i'+1/2}}{\gamma_{i'+1/2}}f^{(0)(m=1)(k)}_{0,l+1/2,i'+1/2}\Delta p_{i'+1/2} \tag{5.265}$$

where

$$J_{3,i+1/2} = -\frac{3\gamma_{i+1/2}\zeta_{i+1/2}}{z_{i+1/2}}+\frac{3}{z_{i+1/2}}+z_{i+1/2}-\frac{2}{5}z^3_{i+1/2} \tag{5.266}$$

$$J_{4,i+1/2} = \gamma_{i+1/2}\zeta_{i+1/2}\left(\frac{15}{z^2_{i+1/2}}+6\right)-\frac{15}{z_{i+1/2}}+11z_{i+1/2} \tag{5.267}$$

and

$$f^{(0)(l=1)(k)}_{0,l+1/2,i+1/2,j+1/2} = \sum_{j'=0}^{n_{\xi_0}-1}\xi_{0,j'+1/2}f^{(0)(k)}_{0,l+1/2,i+1/2,j'+1/2}\Delta\xi_{0,j'+1/2} \tag{5.268}$$

For this case, integrals are simply calculated according to the rule

$$\begin{cases}\int_0^{p_{i+1/2}}X dp' \to \sum_{i'=0}^{i}X_{i'+1/2}\Delta p_{i'+1/2}\\ \int_{p_{i+1/2}}^{\infty}X dp' \to \sum_{i'=i}^{n_p-1}X_{i'+1/2}\Delta p_{i'+1/2}\end{cases} \tag{5.269}$$

so that $f^{(0)(l=1)(k)}_{0,l+1/2,i+1/2,j+1/2}$ must not be interpolated between 0 and $p_{i+1/2}$ for refined calculations as done for coefficients A^{ee}, B^{ee}_t and F^{ee}. Even if by this techniqe, the numerical accuracy is poor in the vicinity of $p=0$, consequences are fairly negligible for the momentum conservation and the current level, since first-order Legendre corrections are weighted by p.

Relativistic Maxwellian background The relativistic Maxwellian background corresponds to that case where the first order Legendre correction for momentum conservation is neglected. Matrix coeffients A^{ee}, B^{ee}_t and F^{ee} determined in the previous section are used.

Non-relativistic Maxwellian background For this case, matrix coefficients are

$$A^{ee}_{l+1/2,i+1/2} = \frac{\overline{n}_{e,l+1/2}}{2v_{i+1/2}u^2_{l+1/2,i+1/2}}\left[erf\left(u_{l+1/2,i+1/2}\right) - u_{l+1/2,i+1/2}erf'\left(u_{l+1/2,i+1/2}\right)\right] \tag{5.270}$$

$$F^{ee}_{l+1/2,i+1/2} = \frac{\overline{n}_{e,l+1/2}}{v^2_{i+1/2}}\left[erf\left(u_{l+1/2,i+1/2}\right) - u_{l+1/2,i+1/2}erf'\left(u_{l+1/2,i+1/2}\right)\right] \tag{5.271}$$

and

$$B^{ee}_{t,l+1/2,i+1/2} = \frac{\overline{n}_{e,l+1/2}}{4v_{i+1/2}u^2_{l+1/2,i+1/2}}\left[\left(2u^2_{l+1/2,i+1/2} - 1\right)erf\left(u_{l+1/2,i+1/2}\right) + u_{l+1/2,i+1/2}erf'\left(u_{l+1/2,i+1/2}\right)\right] \tag{5.272}$$

where

$$u_{l+1/2,i+1/2} = \frac{v_{i+1/2}}{2\overline{n}_{e,l+1/2}} \tag{5.273}$$

For values of the matrix coefficients A^{ee}, B^{ee}_t and F^{ee} on the momentum flux grids, one just has to replace $i+1/2$ by i or $i+1$.

High velocity limit Though the high velocity limit corresponds to a restricted range of application regarding the full collision operator, it can contribute to useful comparisons with some theoretical calculations. Therefore, this possibility has been implemented in the code. In that case, expressions of the coefficients are greatly simplified,

$$A^{ee}_{l+1/2,i+1/2} = \frac{1}{v^3_{i+1/2}}\overline{n}_{e,l+1/2}\overline{T}_{e,l+1/2} \tag{5.274}$$

and

$$F^{ee}_{l+1/2,i+1/2} = \frac{1}{v^2_{i+1/2}}\overline{n}_{e,l+1/2} \tag{5.275}$$

while

$$B^{ee}_{t,l+1/2,i+1/2} = \frac{1}{2v_{i+1/2}}\overline{n}_{e,l+1/2} - \frac{1}{2v^3_{i+1/2}}\overline{n}_{e,l+1/2}\overline{T}_{e,l+1/2} \tag{5.276}$$

Since no integrals appear in the coefficients, the expressions at momentum flux grid points i and $i+1$ can be obtained in a straightforward manner, by just replacing $i+1/2$ by the corresponding index values. In that limit, the first-order Legendre correction is neglected. In the calculations, both electron-electron and electron-ion collision model in the high velocity limit are used for a consistent description of the collisions.

Non-relativistic Lorentz model This very simple case corresponds to

$$A^{ee}_{l+1/2,i+1/2} = F^{ee}_{l+1/2,i+1/2} = B^{ee}_{t,l+1/2,i+1/2} = 0 \tag{5.277}$$

and also on the momentum flux grid points i and $i+1$. Obviously, the first-order Legendre correction is also neglected in that case.

Electron-ion collision operator

Non-relativistic Maxwellian background In that case matrix coefficients are

$$A^{ei}_{l+1/2,i+1/2} = \frac{1}{2v_{i+1/2}} \sum_s \sum_{s'} \frac{1}{u^{ss'2}_{l+1/2,i+1/2}} \left[erf\left(u^{ss'}_{l+1/2,i+1/2}\right) - u_{l+1/2,i+1/2} erf'\left(u^{ss'}_{l+1/2,i+1/2}\right)\right] Z^2_{ss'} \overline{n}_{ss',l+1/2} \tag{5.278}$$

$$F^{ei}_{l+1/2,i+1/2} = \frac{1}{v^2_{i+1/2}} \sum_s \sum_{s'} \left[erf\left(u^{ss'}_{l+1/2,i+1/2}\right) - u^{ss'}_{l+1/2,i+1/2} erf'\left(u^{ss'}_{l+1/2,i+1/2}\right)\right] Z^2_{ss'} \frac{\overline{n}_{ss',l+1/2}}{\overline{m}_s} \tag{5.279}$$

and

$$B^{ei}_{t,l+1/2,i+1/2} = \frac{1}{4v_{i+1/2}} \sum_s \sum_{s'} \frac{1}{u^{ss'2}_{l+1/2,i+1/2}} \left[\left(2u^{ss'2}_{l+1/2,i+1/2} - 1\right) erf\left(u^{ss'}_{l+1/2,i+1/2}\right) + u^{ss'}_{l+1/2,i+1/2} erf'\left(u^{ss'}_{l+1/2,i+1/2}\right)\right] Z^2_{ss'} \overline{n}_{ss',l+1/2} \tag{5.280}$$

where

$$u^{ss'}_{l+1/2,i+1/2} = \frac{v_{i+1/2}}{2v^{\dagger}_{th,ss',l+1/2}} = \frac{v_{i+1/2}}{2\sqrt{\overline{T}_{ss',l+1/2}/\overline{m}_s}}$$

In the case $\overline{T}_{ss',l+1/2} = 0$, to avoid a singularity,

$$A^{ei}_{l+1/2,i+1/2} = B^{ei}_{t,l+1/2,i+1/2} = 0 \tag{5.281}$$

while

$$F^{ei}_{l+1/2,i+1/2} = \frac{1}{v^2_{i+1/2}} \sum_s \sum_{s'} Z^2_{ss'} \frac{\overline{n}_{ss',l+1/2}}{\overline{m}_s} \tag{5.282}$$

since $erf\,(+\infty) = 1$ and $erf'\,(+\infty) = 0$.

Finally, for values of the matrix coefficients A^{ei}, F^{ei} and B^{ei}_t on the momentum flux grids, one just has to replace $i + 1/2$ by i or $i + 1$.

High-velocity limit In this limit, matrix coefficients are

$$A^{ei}_{l+1/2,i+1/2} = \frac{1}{v^3_{i+1/2}} \sum_s \sum_{s'} Z^2_{ss'} \frac{\overline{n}_{ss',l+1/2} \overline{T}_{ss',l+1/2}}{\overline{m}_s} \tag{5.283}$$

$$F^{ei}_{l+1/2,i+1/2} = \frac{1}{v^2_{i+1/2}} \sum_s \sum_{s'} Z^2_{ss'} \frac{\overline{n}_{ss',l+1/2}}{\overline{m}_s} \tag{5.284}$$

The double sum $\sum_s \sum_{s'}$ takes into account of all ions species s in ionization state s'. Here, $\overline{n}_{ss',l+1/2}$ is the normalized ion density at $\psi_{l+1/2}$, as introduced in Sec. 6.3.1, and $\overline{m}_s$ is the ion rest mass normalized to the electron rest mass m_e.

Coefficients A^{ei} and F^{ei} must be also calculated on the flux grids and therefore, according to the previous definition,

$$A^{ei}_{l+1/2,i} = \frac{1}{v_i^3} \sum_s \sum_{s'} Z^2_{ss'} \frac{\overline{n}_{ss',l+1/2} \overline{T}_{ss',l+1/2}}{\overline{m}_s} \tag{5.285}$$

and

$$F^{ei}_{l+1/2,i} = \frac{1}{v_i^2} \sum_s \sum_{s'} Z^2_{ss'} \frac{\overline{n}_{ss',l+1/2}}{\overline{m}_s} \tag{5.286}$$

for the grid points i, while for the grid points $i+1$, one has just to replace i by $i+1$ in the set of above expressions.

Furthermore, the expression of coefficient B^{ei}_l is

$$B^{ei}_{t,l+1/2,i+1/2} = \frac{1}{2v_{i+1/2}} \sum_s \sum_{s'} Z^2_{ss'} \overline{n}_{ss',l+1/2} \left(1 - \frac{1}{v^2_{i+1/2}} \frac{\overline{T}_{ss',l+1/2}}{\overline{m}_s} \right) \tag{5.287}$$

Non-relativistic Lorentz model In that limit

$$A^{ei}_{l+1/2,i+1/2} = F^{ei}_{l+1/2,i+1/2} = 0 \tag{5.288}$$

while

$$B^{ei}_{t,l+1/2,i+1/2} = 1/2 \tag{5.289}$$

A straightforward extrapolation may be done for the momentum flux grid i by $i+1$.

5.4.6 Ohmic electric field

According to the bounce averaged expression,

$$\overline{\overline{D}}^{E(0)}_p \rightarrow \begin{cases} D^{E(0)}_{pp,l+1/2,i+1,j+1/2} = 0 \\ D^{E(0)}_{pp,l+1/2,i,j+1/2} = 0 \\ D^{E(0)}_{p\xi,l+1/2,i+1,j+1/2} = 0 \\ D^{E(0)}_{\xi p,l+1/2,i+1/2,j+1} = 0 \\ D^{E(0)}_{p\xi,l+1/2,i+1/2,j+1/2} = 0 \\ D^{E(0)}_{\xi p,l+1/2,i+1/2,j+1/2} = 0 \\ D^{E(0)}_{p\xi,l+1/2,i,j+1/2} = 0 \\ D^{E(0)}_{\xi p,l+1/2,i+1/2,j} = 0 \\ D^{E(0)}_{\xi\xi,l+1/2,i+1/2,j+1} = 0 \\ D^{E(0)}_{\xi\xi,l+1/2,i+1/2,j} = 0 \end{cases} \tag{5.290}$$

and

$$\overline{\overline{F}}_p^{E(0)} \rightarrow \begin{cases} F^{E(0)}_{p,l+1/2,i+1,j+1/2} = \left(\overline{\lambda}^{l+1/2,j+1/2}_{1,-1,2}/\lambda^{l+1/2,j+1/2}\right)\xi_{0,j+1/2}\overline{E}_{\|0,l+1/2} \\ F^{E(0)}_{p,l+1/2,i,j+1/2} = \left(\overline{\lambda}^{l+1/2,j+1/2}_{1,-1,2}/\lambda^{l+1/2,j+1/2}\right)\xi_{0,j+1/2}\overline{E}_{\|0,l+1/2} \\ F^{E(0)}_{\xi,l+1/2,i+1/2,j+1} = -\left(\overline{\lambda}^{l+1/2,j+1}_{1,-1,2}/\lambda^{l+1/2,j+1}\right)\sqrt{1-\xi^2_{0,j+1}}\overline{E}_{\|0,l+1/2} \\ F^{E(0)}_{\xi,l+1/2,i+1/2,j} = -\left(\overline{\lambda}^{l+1/2,j}_{1,-1,2}/\lambda^{l+1/2,j}\right)\sqrt{1-\xi^2_{0,j}}\overline{E}_{\|0,l+1/2} \end{cases} \tag{5.291}$$

where $\overline{E}_{\|0,l+1/2}$ is the parallel component of the Ohmic electric field along the magnetic field line direction normalized to the Dreicer field taken at the poloidal position where the magnetic field $\mathbf{B}$ is minimum, as explained in Sec.4.2.

It is important to recall that the Ohmic electric field operator has a cylindrical symmetry, while the description of the electron dynamics in momentum space is based on the spherical symmetry of the collision operator. As a consequence, there is a fundamental contradiction for the internal boundary at $p = 0$ where $p^2 S_p = 0$. Indeed, for large values of $\overline{E}_{\|0}$, the maximum of the distribution function $f_0^{(0)}$ is no more at $p = 0$, but may be significantly shifted along the axis $p_\perp = 0$. Since in that extrem case $p^2 S_p \neq 0$ at $p = 0$ while it is naturally enforced to be null by construction with the grid definition, the distribution function has a wrong shape close to $p = 0$ and the conservative scheme is no more preserved. It is also important to note that the external boundary $\partial f_0^{(0)}/\partial\xi_0 = 0$ at $\xi_0 = 0$ is also no more consistent with initial bounce averaged assumptions, which represents also an important failure of the use of the code.

Consequently, in order to avoid a misuse of the code, the range of validity of $\overline{E}_{\|0}$ is restricted so that condition

$$\left|\frac{F_p^{E(0)}}{F_p^{C(0)}}\right| \ll 1 \tag{5.292}$$

is fullfiled at $p/p_{th} = 1$. Using the high-velicity limit of the collision operator, this corresponds roughly to

$$\frac{\overline{E}_{\|0}}{\overline{n}_e} \simeq \overline{E}_{\|0} \ll 1 \tag{5.293}$$

since $\overline{n}_e \simeq 1$ in normalized units, as defined in Sec.6.3.1. Consequently, flux surface averaged value of the Ohmic electric field $\langle\overline{E}\rangle$ should be restricted to 0.05, in Dreicer units. A warning is indicated when this value is exceeded.

Radio-frequency waves

From the expressions given in Sec. 4.3.7, the components of the tensor $\overline{\overline{D}}_p^{\mathrm{RF}(0)}$ are

$$\begin{array}{l}
D^{\mathrm{RF}(0)}_{pp,l+1/2,i+1,j+1/2} = \sum_{n=-\infty}^{+\infty}\sum_b (1-\xi^2_{0,j+1/2})\overline{D}^{\mathrm{RF}(0)}_{b,n,l+1/2,i+1,j+1/2} \\
D^{\mathrm{RF}(0)}_{pp,l+1/2,i,j+1/2} = \sum_{n=-\infty}^{+\infty}\sum_b (1-\xi^2_{0,j+1/2})\overline{D}^{\mathrm{RF}(0)}_{b,n,l+1/2,i,j+1/2} \\
D^{\mathrm{RF}(0)}_{p\xi,l+1/2,i+1,j+1/2} = \sum_{n=-\infty}^{+\infty}\sum_b -\frac{\sqrt{1-\xi^2_{0,j+1/2}}}{\xi_{0,j+1/2}}\left[1-\xi^2_{0,j+1/2}-\frac{n\Omega_{0,l+1/2,i+1}}{\omega_b}\right]\overline{D}^{\mathrm{RF}(0)}_{b,n,l+1/2,i+1,j+1/2} \\
D^{\mathrm{RF}(0)}_{\xi p,l+1/2,i+1/2,j+1} = \sum_{n=-\infty}^{+\infty}\sum_b -\frac{\sqrt{1-\xi^2_{0,j+1}}}{\xi_{0,j+1}}\left[1-\xi^2_{0}-\frac{n\Omega_{0,l+1/2,i+1/2}}{\omega_b}\right]\overline{D}^{\mathrm{RF}(0)}_{b,n,l+1/2,i+1/2,j+1} \\
D^{\mathrm{RF}(0)}_{p\xi,l+1/2,i+1/2,j+1/2} = \sum_{n=-\infty}^{+\infty}\sum_b -\frac{\sqrt{1-\xi^2_{0,j+1/2}}}{\xi_{0,j+1/2}}\left[1-\xi^2_{0}-\frac{n\Omega_{0,l+1/2,i+1/2}}{\omega_b}\right]\overline{D}^{\mathrm{RF}(0)}_{b,n,l+1/2,i+1/2,j+1/2} \\
D^{\mathrm{RF}(0)}_{\xi p,l+1/2,i+1/2,j+1/2} = \sum_{n=-\infty}^{+\infty}\sum_b -\frac{\sqrt{1-\xi^2_{0,j+1/2}}}{\xi_{0,j+1/2}}\left[1-\xi^2_{0}-\frac{n\Omega_{0,l+1/2,i+1/2}}{\omega_b}\right]\overline{D}^{\mathrm{RF}(0)}_{b,n,l+1/2,i+1/2,j+1/2} \\
D^{\mathrm{RF}(0)}_{p\xi,l+1/2,i,j+1/2} = \sum_{n=-\infty}^{+\infty}\sum_b -\frac{\sqrt{1-\xi^2_{0,j+1/2}}}{\xi_{0,j+1/2}}\left[1-\xi^2_{0}-\frac{n\Omega_{0,l+1/2,i}}{\omega_b}\right]\overline{D}^{\mathrm{RF}(0)}_{b,n,l+1/2,i,j+1/2} \\
D^{\mathrm{RF}(0)}_{\xi p,l+1/2,i+1/2,j} = \sum_{n=-\infty}^{+\infty}\sum_b -\frac{\sqrt{1-\xi^2_{0,j}}}{\xi_{0,j}}\left[1-\xi^2_{0,j}-\frac{n\Omega_{0,l+1/2,i+1/2}}{\omega_b}\right]\overline{D}^{\mathrm{RF}(0)}_{b,n,l+1/2,i+1/2,j} \\
D^{\mathrm{RF}(0)}_{\xi\xi,l+1/2,i+1/2,j+1} = \sum_{n=-\infty}^{+\infty}\sum_b \frac{1}{\xi^2_{0,j+1}}\left[1-\xi^2_{0,j}-\frac{n\Omega_{0,l+1/2,i+1/2}}{\omega_b}\right]^2\overline{D}^{\mathrm{RF}(0)}_{b,n,l+1/2,i+1/2,j+1} \\
D^{\mathrm{RF}(0)}_{\xi\xi,l+1/2,i+1/2,j} = \sum_{n=-\infty}^{+\infty}\sum_b \frac{1}{\xi^2_{0,j}}\left[1-\xi^2_{0,j}-\frac{n\Omega_{0,l+1/2,i+1/2}}{\omega_b}\right]^2\overline{D}^{\mathrm{RF}(0)}_{b,n,l+1/2,i+1/2,j}
\end{array} \tag{5.294}$$

and

$$\overline{\overline{F}}_p^{\mathrm{RF}(0)} \rightarrow \begin{cases} F^{\mathrm{RF}(0)}_{p,l+1/2,i+1,j+1/2} = 0 \\ F^{\mathrm{RF}(0)}_{p,l+1/2,i,j+1/2} = 0 \\ F^{\mathrm{RF}(0)}_{\xi,l+1/2,i+1/2,j+1} = 0 \\ F^{\mathrm{RF}(0)}_{\xi,l+1/2,i+1/2,j} = 0 \end{cases} \tag{5.295}$$

where $\Omega_{0,l+1/2,i+1/2}$ is the electron cyclotron frequency taken at the minimum B value

$$\Omega_{0,l+1/2,i+1/2} = \frac{\Omega_{i+1/2}}{\Psi_{l+1/2}} \tag{5.296}$$

Here the dependence of $\Omega_{0,l+1/2,i+1/2}$ with the index i arises from relativistic downshift. The indexes n and b correspond respectively to the wave harmonics and the narrow beam label (for ray-tracing calculations). The discrete expression of the quasilinear diffusion coefficient $\overline{D}^{\mathrm{RF}(0)}_{b,n,l+1/2,i+1/2,j+1/2}$ is

$$\begin{array}{rcl}
\overline{D}^{\mathrm{RF}(0)}_{b,n,l+1/2,i+1/2,j+1/2} & = & \dfrac{\gamma_{i+1/2}p_{Te}}{p_{i+1/2}\left|\xi_{0,j+1/2}\right|}\dfrac{1}{\lambda^{l+1/2,j+1/2}\widetilde{q}_{l+1/2}}\dfrac{r_{\theta_b,l+1/2}}{R_p}\dfrac{B^{\theta_b}_{l+1/2}}{B^{\theta_b}_{P,l+1/2}}\dfrac{\xi^2_{0,j+12}}{\xi^2_{\theta_b,l+1/2,j+1/2}} \\
 & & \times\Psi_{\theta_b,l+1/2}\overline{D}^{\mathrm{RF},\theta_b}_{b,n,0,l+12}H\left(\theta_b-\theta_{\min}\right)H\left(\theta_{\max}-\theta_b\right) \\
 & & \times\left[\dfrac{1}{2}\sum_\sigma\right]_T\delta\left(N_{b\|}-N^{\theta_b}_{\|\mathrm{res},l+1/2,i+1/2,j+1/2}\right)\left|\Theta^{b,(n)}_{\mathbf{k},\theta_b,l+1/2,i+1/2,j+1/2}\right|^2
\end{array} \tag{5.297}$$

where

$$\begin{aligned}\Theta^{b,(n)}_{\mathbf{k},\theta_b,l+1/2,i+1/2,j+1/2} &= \frac{1}{\sqrt{2}} e_{b0,+} e^{-i\alpha_b} J_{n-1}\left(z^{\theta_b}_{b,l+1/2,i+1/2,j+1/2}\right) \\ &+ \frac{1}{\sqrt{2}} e_{b0,-} e^{+i\alpha_b} J_{n+1}\left(z^{\theta_b}_{b,l+1/2,i+1/2,j+1/2}\right) \\ &+ \frac{\xi_{\theta_b,l+1/2}}{\sqrt{\Psi_{\theta_b,l+1/2}\left(1-\xi^2_{0,j+1/2}\right)}} e_{b0,\parallel} J_n\left(z^{\theta_b}_{b,l+1/2,i+1/2,j+1/2}\right)\end{aligned} \tag{5.298}$$

$$N^{\theta_b}_{\parallel\mathrm{res},l+1/2,i+1/2,j+1/2} = \frac{1}{\beta_{Te}} \frac{p_{Te}}{p_{i+1/2}\xi_{\theta_b,l+1/2}} \left(\gamma_{i+1/2} - \frac{n' \Psi_{\theta_b,l+1/2}\omega_{ce,0}}{\omega_b}\right) \tag{5.299}$$

$$\overline{D}^{\mathrm{RF},\theta_b}_{b,n,0,l+1/2} = \frac{1}{r_{\theta_b,l+1/2} R_{\theta_b,l+1/2}} \frac{1}{m_e \ln\Lambda_{l+1/2}} \frac{1}{\omega_b \omega^2_{pe,l+1/2}} \frac{f^{l+1/2}_{\mathrm{inc},b}}{|\mathbf{\Phi}_b|} P_{b,\mathrm{inc}} \tag{5.300}$$

with

$$z^{\theta_b}_{b,l+1/2,i+1/2,j+1/2} = -N_{b\perp} \frac{\omega_b}{\omega_{ce,0,l+1/2}} \frac{p_{i+1/2}}{m_e c} \frac{\sqrt{1-\xi^2_{0,j+1/2}}}{\sqrt{\Psi_{\theta_b,l+1/2}}} \tag{5.301}$$

and

$$\widehat{\psi}_{\theta_b,l+1/2} = \widehat{\psi}(\psi_{l+1/2},\theta_b) \tag{5.302}$$

$$r_{\theta_b,l+1/2} = r\left(\psi_{l+1/2},\theta_b\right) \tag{5.303}$$

$$R_{\theta_b,l+1/2} = R\left(\psi_{l+1/2},\theta_b\right) \tag{5.304}$$

$$B^{\theta_b}_{l+1/2} = B\left(\psi_{l+1/2},\theta_b\right) \tag{5.305}$$

$$B^{\theta_b}_{P,l+1/2} = B_P\left(\psi_{l+1/2},\theta_b\right) \tag{5.306}$$

$$\Psi_{\theta_b,l+1/2} = \frac{B\left(\psi_{l+1/2},\theta_b\right)}{B_0\left(\psi_{l+1/2}\right)} = \frac{B^{\theta_b}_{l+1/2}}{B_{0,l+1/2}} \tag{5.307}$$

$$\xi_{\theta_b,l+1/2,j+1/2} = \xi\left(\psi_{l+1/2},\theta_b,\xi_{0,j+1/2}\right) = \sigma\sqrt{1-\Psi_{\theta_b,l+1/2}\left(1-\xi^2_{0,j+1/2}\right)} \tag{5.308}$$

All coefficients corresponding to different indexes may be obtained readily by performing the adequate index transformation, $i+1/2 \to (i,i+1)$ and $j+1/2 \to (j,j+1)$

5.5 Up to first order term: the Drift Kinetic equation

5.5.1 Grid interpolation

Spatial grid interpolation for gradient calculation The first order drift kinetic equation requires to calculate $\widetilde{f}^{(0)}$ defined as

$$\widetilde{f}^{(0)}(p,\xi_0,\psi) = \frac{p\xi_0 I(\psi)}{q_e B_0(\psi)} \frac{\partial f^{(0)}_0(p,\xi_0,\psi)}{\partial\psi} \tag{5.309}$$

where $|I(\psi)| = RB_T$. Here all quantities are determined on the poloidal position where the magnetic field $\mathbf{B}$ is minimum.

The spatial grid being non-uniform, radial derivative requires a specific treatment, for an accurate determination. Let ψ_-, ψ et ψ_+ the three neighbor radial positions where are calculated the distribution function $f_0^{(0)}$ with $\Delta\psi_- = \psi_- - \psi$, $\Delta\psi_+ = \psi_+ - \psi$ and $\Delta\psi = \psi_+ - \psi_-$. A parabolic interpolation of the form $y = a\psi^2 + b\psi + c$ is used for calculating the radial derivative $dy/d\psi = 2a\psi + b$. The coefficients a, b and c being determined by values y_-, y and y_+ at grid points ψ_-, ψ and ψ_+, one can easily show that

$$\left.\frac{dy}{d\psi}\right|_\psi = \frac{1}{\det V}\left(-\Delta\psi_+^2 y_- + \Delta\psi\left(\Delta\psi_+ + \Delta\psi_-\right)y + \Delta\psi_-^2 y_+\right) \tag{5.310}$$

where $\overline{\overline{V}}$ is a Van der Monde matrix of order 3,

$$\overline{\overline{V}} = \begin{bmatrix} 1 & \psi_- & \psi_-^2 \\ 1 & \psi & \psi^2 \\ 1 & \psi_+ & \psi_+^2 \end{bmatrix} \tag{5.311}$$

whose determinant is simply

$$\det V = -\Delta\psi_-\Delta\psi\Delta\psi_+ \tag{5.312}$$

Therefore

$$\left.\frac{dy}{d\psi}\right|_r = \frac{\Delta\psi_+}{\Delta\psi\Delta\psi_-}y_- - \frac{\left(\Delta\psi_+ + \Delta\psi_-\right)}{\Delta\psi_+\Delta\psi_-}y - \frac{\Delta\psi_-}{\Delta\psi\Delta\psi_+}y_+ \tag{5.313}$$

and applying this result for $\widetilde{f}^{(0)}$,

$$\begin{aligned}
\widetilde{f}^{(0)(k+1)}_{l+1/2,i+1/2,j+1/2} &= \frac{p_{i+1/2}\xi_{0,j+1/2}I_{l+1/2}}{q_e B_{0,l+1/2}} \times \\
&\left[\frac{\left(\psi_{l+3/2} - \psi_{l+1/2}\right)}{\left(\psi_{l+3/2} - \psi_{l-1/2}\right)\left(\psi_{l-1/2} - \psi_{l+1/2}\right)} f^{(0)(k+1)}_{0,l-1/2,i+1/2,j+1/2}\right. \\
&- \frac{\left(\psi_{l+3/2} - 2\psi_{l+1/2} + \psi_{l-1/2}\right)}{\left(\psi_{l+3/2} - \psi_{l+1/2}\right)\left(\psi_{l-1/2} - \psi_{l+1/2}\right)} f^{(0)(k+1)}_{0,l+1/2,i+1/2,j+1/2} \\
&\left. - \frac{\left(\psi_{l-1/2} - \psi_{l+1/2}\right)}{\left(\psi_{l+3/2} - \psi_{l-1/2}\right)\left(\psi_{l+3/2} - \psi_{l+1/2}\right)} f^{(0)(k+1)}_{0,l+3/2,i+1/2,j+1/2}\right]
\end{aligned} \tag{5.314}$$

where $I_{l+1/2} = I\left(\psi_{l+1/2}\right)$. In a compact form,

$$\begin{aligned}
\widetilde{f}^{(0)(k+1)}_{l+1/2,i+1/2,j+1/2} &= \frac{p_{i+1/2}\xi_{0,j+1/2}I_{l+1/2}}{q_e B_{0,l+1/2}} \times \\
&\left[\alpha^-_{l+1/2} f^{(0)(k+1)}_{0,l-1/2,i+1/2,j+1/2} + \alpha^0_{l+1/2} f^{(0)(k+1)}_{0,l+1/2,i+1/2,j+1/2}\right. \\
&\left. + \alpha^+_{l+1/2} f^{(0)(k+1)}_{0,l+3/2,i+1/2,j+1/2}\right]
\end{aligned} \tag{5.315}$$

where coefficients are

$$\alpha^{-}_{l+1/2} = \frac{\left(\psi_{l+3/2} - \psi_{l+1/2}\right)}{\left(\psi_{l+3/2} - \psi_{l-1/2}\right)\left(\psi_{l-1/2} - \psi_{l+1/2}\right)} \tag{5.316}$$

$$\alpha^{0}_{l+1/2} = -\frac{\left(\psi_{l+3/2} - 2\psi_{l+1/2} + \psi_{l-1/2}\right)}{\left(\psi_{l+3/2} - \psi_{l+1/2}\right)\left(\psi_{l-1/2} - \psi_{l+1/2}\right)} \tag{5.317}$$

and

$$\alpha^{+}_{l+1/2} = -\frac{\left(\psi_{l-1/2} - \psi_{l+1/2}\right)}{\left(\psi_{l+3/2} - \psi_{l-1/2}\right)\left(\psi_{l+3/2} - \psi_{l+1/2}\right)} \tag{5.318}$$

Momentum grid interpolation As indicated in Sec. 3.5.5, it is possible to keep the conservative form for the first-order drift kinetic equation. The main advantage is that the numerical differencing technique already used for the zero-order Fokker-Planck equation may be also employed for determining the numerical solution of this equation. The determination of the momentum $\left.\frac{\partial\left(p^2\widetilde{\mathbf{S}}_p^{(0)}\right)}{\partial p}\right|^{(k)}_{l+1/2,i+1/2,j+1/2}$ and pitch-angle $\left.\frac{\partial}{\partial\xi_0}\left(\sqrt{1-\xi_0^2}\lambda\widetilde{\mathbf{S}}_\xi^{(0)}\right)\right|^{(k)}_{l+1/2,i+1/2,j+1/2}$ derivatives requires, as for $f_0^{(0)}$, interpolation techniques in order to evaluate $\widetilde{f}^{(0)}$ on flux grid at the radial position $l+1/2$. By analogy, one have to determine $\widetilde{f}^{(0)}$ on the following grid points

$$\widetilde{f}^{(0)(k+1)}_{l+1/2,i+1,j+1/2} = \frac{p_{i+1}\xi_{0,j+1/2}I_{l+1/2}}{q_e B_{0,l+1/2}}\left.\frac{\partial f_0^{(0)}}{\partial\psi}\right|^{(k+1)}_{l+1/2,i+1,j+1/2} \tag{5.319}$$

$$\widetilde{f}^{(0)(k+1)}_{l+1/2,i,j+1/2} = \frac{p_i\xi_{0,j+1/2}I_{l+1/2}}{q_e B_{0,l+1/2}}\left.\frac{\partial f_0^{(0)}}{\partial\psi}\right|^{(k+1)}_{l+1/2,i,j+1/2} \tag{5.320}$$

$$\widetilde{f}^{(0)(k+1)}_{l+1/2,i+1/2,j+1} = \frac{p_{i+1/2}\xi_{0,j+1}I_{l+1/2}}{q_e B_{0,l+1/2}}\left.\frac{\partial f_0^{(0)}}{\partial\psi}\right|^{(k+1)}_{l+1/2,i+1/2,j+1} \tag{5.321}$$

and

$$\widetilde{f}^{(0)(k+1)}_{l+1/2,i+1/2,j} = \frac{p_{i+1/2}\xi_{0,j}I_{l+1/2}}{q_e B_{0,l+1/2}}\left.\frac{\partial f_0^{(0)}}{\partial\psi}\right|^{(k+1)}_{l+1/2,i+1/2,j} \tag{5.322}$$

Using the weighting factors $\delta_p^{(0)}$ introduced for $f_0^{(0)}$, as shown in Sec. 5.4.3 which both

are functions of ψ, one obtains for the grid point $(l+1/2, i+1, j+1/2)$

$$\begin{aligned}
\left.\frac{\partial f_0^{(0)}}{\partial \psi}\right|^{(k+1)}_{l+1/2,i+1,j+1/2} &= \alpha^-_{l+1/2} f^{(0)(k+1)}_{0,l-1/2,i+1,j+1/2} + \alpha^0_{l+1/2} f^{(0)(k+1)}_{0,l+1/2,i+1,j+1/2} \\
&\quad + \alpha^+_{l+1/2} f^{(0)(k+1)}_{0,l+3/2,i+1,j+1/2} \\
&= \alpha^-_{l+1/2}\left(1-\delta^{(0)}_{p,l-1/2,i+1,j+1/2}\right) f^{(0)(k+1)}_{0,l-1/2,i+3/2,j+1/2} \\
&\quad + \alpha^-_{l+1/2}\delta^{(0)}_{p,l-1/2,i+1,j+1/2} f^{(0)(k+1)}_{0,l-1/2,i+1/2,j+1/2} \\
&\quad + \alpha^0_{l+1/2}\left(1-\delta^{(0)}_{p,l+1/2,i+1,j+1/2}\right) f^{(0)(k+1)}_{0,l+1/2,i+3/2,j+1/2} \\
&\quad + \alpha^0_{l+1/2}\delta^{(0)}_{p,l+1/2,i+1,j+1/2} f^{(0)(k+1)}_{0,l+1/2,i+1/2,j+1/2} \\
&\quad + \alpha^+_{l+1/2}\left(1-\delta^{(0)}_{p,l+3/2,i+1,j+1/2}\right) f^{(0)(k+1)}_{0,l+3/2,i+3/2,j+1/2} \\
&\quad + \alpha^+_{l+1/2}\delta^{(0)}_{p,l+3/2,i+1,j+1/2} f^{(0)(k+1)}_{0,l+3/2,i+1/2,j+1/2}
\end{aligned} \tag{5.323}$$

and

$$\begin{aligned}
\widetilde{f}^{(0)(k+1)}_{l+1/2,i+1,j+1/2} &= \frac{p_{i+1}\xi_{0,j+1/2}I_{l+1/2}}{q_e B_{0,l+1/2}}\alpha^-_{l+1/2}\left(1-\delta^{(0)}_{p,l-1/2,i+1,j+1/2}\right) f^{(0)(k+1)}_{0,l-1/2,i+3/2,j+1/2} \\
&\quad + \frac{p_{i+1}\xi_{0,j+1/2}I_{l+1/2}}{q_e B_{0,l+1/2}}\alpha^-_{l+1/2}\delta^{(0)}_{p,l-1/2,i+1,j+1/2} f^{(0)(k+1)}_{0,l-1/2,i+1/2,j+1/2} \\
&\quad + \frac{p_{i+1}\xi_{0,j+1/2}I_{l+1/2}}{q_e B_{0,l+1/2}}\alpha^0_{l+1/2}\left(1-\delta^{(0)}_{p,l+1/2,i+1,j+1/2}\right) f^{(0)(k+1)}_{0,l+1/2,i+3/2,j+1/2} \\
&\quad + \frac{p_{i+1}\xi_{0,j+1/2}I_{l+1/2}}{q_e B_{0,l+1/2}}\alpha^0_{l+1/2}\delta^{(0)}_{p,l+1/2,i+1,j+1/2} f^{(0)(k+1)}_{0,l+1/2,i+1/2,j+1/2} \\
&\quad + \frac{p_{i+1}\xi_{0,j+1/2}I_{l+1/2}}{q_e B_{0,l+1/2}}\alpha^+_{l+1/2}\left(1-\delta^{(0)}_{p,l+3/2,i+1,j+1/2}\right) f^{(0)(k+1)}_{0,l+3/2,i+3/2,j+1/2} \\
&\quad + \frac{p_{i+1}\xi_{0,j+1/2}I_{l+1/2}}{q_e B_{0,l+1/2}}\alpha^+_{l+1/2}\delta^{(0)}_{p,l+3/2,i+1,j+1/2} f^{(0)(k+1)}_{0,l+3/2,i+1/2,j+1/2}
\end{aligned} \tag{5.324}$$

which becomes

$$\begin{aligned}
\widetilde{f}^{(0)(k+1)}_{l+1/2,i+1,j+1/2} &= \frac{p_{i+1}}{p_{i+3/2}}\frac{p_{i+3/2}\xi_{0,j+1/2}I_{l+1/2}}{q_eB_{0,l+1/2}}\alpha^-_{l+1/2}\times \\
&\left(1-\delta^{(0)}_{p,l-1/2,i+1,j+1/2}\right)f^{(0)(k+1)}_{0,l-1/2,i+3/2,j+1/2} \\
&+\frac{p_{i+1}}{p_{i+3/2}}\frac{p_{i+3/2}\xi_{0,j+1/2}I_{l+1/2}}{q_eB_{0,l+1/2}}\alpha^0_{l+1/2}\times \\
&\left(1-\delta^{(0)}_{p,l+1/2,i+1,j+1/2}\right)f^{(0)(k+1)}_{0,l+1/2,i+3/2,j+1/2} \\
&+\frac{p_{i+1}}{p_{i+3/2}}\frac{p_{i+3/2}\xi_{0,j+1/2}I_{l+1/2}}{q_eB_{0,l+1/2}}\alpha^+_{l+1/2}\times \\
&\left(1-\delta^{(0)}_{p,l+3/2,i+1,j+1/2}\right)f^{(0)(k+1)}_{0,l+3/2,i+3/2,j+1/2} \\
&+\frac{p_{i+1}}{p_{i+1/2}}\frac{p_{i+1/2}\xi_{0,j+1/2}I_{l+1/2}}{q_eB_{0,l+1/2}}\alpha^-_{l+1/2}\times \\
&\delta^{(0)}_{p,l-1/2,i+1,j+1/2}f^{(0)(k+1)}_{0,l-1/2,i+1/2,j+1/2} \\
&+\frac{p_{i+1}}{p_{i+1/2}}\frac{p_{i+1/2}\xi_{0,j+1/2}I_{l+1/2}}{q_eB_{0,l+1/2}}\alpha^0_{l+1/2}\times \\
&\delta^{(0)}_{p,l+1/2,i+1,j+1/2}f^{(0)(k+1)}_{0,l+1/2,i+1/2,j+1/2} \\
&+\frac{p_{i+1}}{p_{i+1/2}}\frac{p_{i+1/2}\xi_{0,j+1/2}I_{l+1/2}}{q_eB_{0,l+1/2}}\alpha^+_{l+1/2}\times \\
&\delta^{(0)}_{p,l+3/2,i+1,j+1/2}f^{(0)(k+1)}_{0,l+3/2,i+1/2,j+1/2}
\end{aligned} \tag{5.325}$$

or

$$\begin{aligned}
\widetilde{f}^{(0)(k+1)}_{l+1/2,i+1,j+1/2} &= \frac{p_{i+1}}{p_{i+3/2}}\left(1-\delta^{(0)}_{p,l+1/2,i+1,j+1/2}\right)\widetilde{f}^{(0)(k+1)}_{l+1/2,i+3/2,j+1/2} \\
&+\frac{p_{i+1}}{p_{i+1/2}}\delta^{(0)}_{p,l+1/2,i+1,j+1/2}\widetilde{f}^{(0)(k+1)}_{l+1/2,i+1/2,j+1/2} \\
&+\widetilde{h}^{(0)(k+1)}_{l+1/2,i+1,j+1/2}
\end{aligned} \tag{5.326}$$

where

$$\begin{aligned}
\widetilde{h}^{(0)(k+1)}_{l+1/2,i+1,j+1/2} &= p_{i+1}\frac{\xi_{0,j+1/2}I_{l+1/2}}{q_eB_{0,l+1/2}}\alpha^-_{l+1/2}\times \\
&\left(\delta^{(0)}_{p,l+1/2,i+1,j+1/2}-\delta^{(0)}_{p,l-1/2,i+1,j+1/2}\right)f^{(0)(k+1)}_{0,l-1/2,i+3/2,j+1/2} \\
&+p_{i+1}\frac{\xi_{0,j+1/2}I_{l+1/2}}{q_eB_{0,l+1/2}}\alpha^+_{l+1/2}\times \\
&\left(\delta^{(0)}_{p,l+1/2,i+1,j+1/2}-\delta^{(0)}_{p,l+3/2,i+1,j+1/2}\right)f^{(0)(k+1)}_{0,l+3/2,i+3/2,j+1/2} \\
&-p_{i+1}\frac{\xi_{0,j+1/2}I_{l+1/2}}{q_eB_{0,l+1/2}}\alpha^-_{l+1/2}\times \\
&\left(\delta^{(0)}_{p,l+1/2,i+1,j+1/2}-\delta^{(0)}_{p,l-1/2,i+1,j+1/2}\right)f^{(0)(k+1)}_{0,l-1/2,i+1/2,j+1/2} \\
&-p_{i+1}\frac{\xi_{0,j+1/2}I_{l+1/2}}{q_eB_{0,l+1/2}}\alpha^+_{l+1/2}\times \\
&\left(\delta^{(0)}_{p,l+1/2,i+1,j+1/2}-\delta^{(0)}_{p,l+3/2,i+1,j+1/2}\right)f^{(0)(k+1)}_{0,l+3/2,i+1/2,j+1/2}
\end{aligned} \tag{5.327}$$

Reordering coefficients, one obtains,

$$\begin{aligned}
\widetilde{h}^{(0)(k+1)}_{l+1/2,i+1,j+1/2} &= p_{i+1}\frac{\xi_{0,j+1/2}I_{l+1/2}}{q_eB_{0,l+1/2}}\times \\
&\Big[\alpha^-_{l+1/2}\left(\delta^{(0)}_{p,l+1/2,i+1,j+1/2}-\delta^{(0)}_{p,l-1/2,i+1,j+1/2}\right)\times \\
&\left(f^{(0)(k+1)}_{0,l-1/2,i+3/2,j+1/2}-f^{(0)(k+1)}_{0,l-1/2,i+1/2,j+1/2}\right) \\
&+\alpha^+_{l+1/2}\left(\delta^{(0)}_{p,l+1/2,i+1,j+1/2}-\delta^{(0)}_{p,l+3/2,i+1,j+1/2}\right)\times \\
&\left(f^{(0)(k+1)}_{0,l+3/2,i+3/2,j+1/2}-f^{(0)(k+1)}_{0,l+3/2,i+1/2,j+1/2}\right)\Big]
\end{aligned} \tag{5.328}$$

This double difference makes coefficient $\widetilde{h}^{(0)}_{l+1/2,i+1,j+1/2}$ is second order correction, that is almost negligible when spatial gradients are weak. However, for strong gradients, this correction must be, in principle, considered.

A similar expression is obtained for the grid point $(l+1/2,i,j+1/2)$, by replacing $i+1\rightarrow i$ in all above relations.

$$\begin{aligned}
\widetilde{f}^{(0)(k+1)}_{l+1/2,i,j+1/2} &= \frac{p_i}{p_{i+1/2}}\left(1-\delta^{(0)}_{p,l+1/2,i,j+1/2}\right)\widetilde{f}^{(0)(k+1)}_{l+1/2,i+1/2,j+1/2} \\
&+\frac{p_i}{p_{i-1/2}}\delta^{(0)}_{p,l+1/2,i,j+1/2}\widetilde{f}^{(0)(k+1)}_{l+1/2,i-1/2,j+1/2} \\
&+\widetilde{h}^{(0)}_{l+1/2,i,j+1/2}
\end{aligned} \tag{5.329}$$

where

$$\begin{aligned}\widetilde{h}^{(0)(k+1)}_{l+1/2,i,j+1/2} &= p_i\frac{\xi_{0,j+1/2}I_{l+1/2}}{q_eB_{0,l+1/2}}\times \\ &\Big[\alpha^-_{l+1/2}\left(\delta^{(0)}_{p,l+1/2,i,j+1/2}-\delta^{(0)}_{p,l-1/2,i,j+1/2}\right)\times \\ &\left(f^{(0)(k+1)}_{0,l-1/2,i+1/2,j+1/2}-f^{(0)(k+1)}_{0,l-1/2,i-1/2,j+1/2}\right) \\ &+\alpha^+_{l+1/2}\left(\delta^{(0)}_{p,l+1/2,i,j+1/2}-\delta^{(0)}_{p,l+3/2,i,j+1/2}\right)\times \\ &\left(f^{(0)(k+1)}_{0,l+3/2,i+1/2,j+1/2}-f^{(0)(k+1)}_{0,l+3/2,i-1/2,j+1/2}\right)\Big] \end{aligned} \tag{5.330}$$

Finally, a similar approach may be used for the pitch-angle grid interpolation. For grid points $(l+1/2, i+1/2, j+1)$,

$$\begin{aligned}\widetilde{f}^{(0)(k+1)}_{l+1/2,i+1/2,j+1} &= \frac{\xi_{0,j+1}}{\xi_{0,j+3/2}}\left(1-\delta^{(0)}_{\xi,l+1/2,i+1/2,j+1}\right)\widetilde{f}^{(0)(k+1)}_{l+1/2,i+1/2,j+3/2} \\ &+\frac{\xi_{0,j+1}}{\xi_{0,j+1/2}}\delta^{(0)}_{\xi,l+1/2,i+1/2,j+1}\widetilde{f}^{(0)(k+1)}_{l+1/2,i+1/2,j+1/2} \\ &+\widetilde{h}^{(0)(k+1)}_{l+1/2,i+1/2,j+1}\end{aligned} \tag{5.331}$$

where

$$\begin{aligned}\widetilde{h}^{(0)(k+1)}_{l+1/2,i+1/2,j+1} &= p_{i+1/2}\frac{\xi_{0,j+1}I_{l+1/2}}{q_eB_{0,l+1/2}}\times \\ &\Big[\alpha^-_{l+1/2}\left(\delta^{(0)}_{\xi,l+1/2,i+1/2,j+1}-\delta^{(0)}_{\xi,l-1/2,i+1/2,j+1}\right)\times \\ &\left(f^{(0)(k+1)}_{0,l-1/2,i+1/2,j+3/2}-f^{(0)(k+1)}_{0,l-1/2,i+1/2,j+1/2}\right) \\ &+\alpha^+_{l+1/2}\left(\delta^{(0)}_{\xi,l+1/2,i+1/2,j+1}-\delta^{(0)}_{\xi,l+3/2,i+1/2,j+1}\right)\times \\ &\left(f^{(0)(k+1)}_{0,l+3/2,i+1/2,j+3/2}-f^{(0)(k+1)}_{0,l+3/2,i+1/2,j+1/2}\right)\Big]\end{aligned} \tag{5.332}$$

However, since by definition, $\delta^{(0)}_{\xi,l+1/2,i+1/2,j+1}=\delta^{(0)}_{\xi,l-1/2,i+1/2,j+1}$, and $\delta^{(0)}_{\xi,l+1/2,i+1/2,j+1}=\delta^{(0)}_{\xi,l+3/2,i+1/2,j+1}$, it turns out that

$$\widetilde{h}^{(0)(k+1)}_{l+1/2,i+1/2,j+1}=0 \tag{5.333}$$

and a similar result is obtained for grid points $(l+1/2, i+1/2, j)$, expressions are

$$\begin{aligned}\widetilde{f}^{(0)(k+1)}_{l+1/2,i+1/2,j} &= \frac{\xi_{0,j}}{\xi_{0,j+1/2}}\left(1-\delta^{(0)}_{\xi,l+1/2,i+1/2,j}\right)\widetilde{f}^{(0)(k+1)}_{l+1/2,i+1/2,j+1/2} \\ &+\frac{\xi_{0,j}}{\xi_{0,j-1/2}}\delta^{(0)}_{\xi,l+1/2,i+1/2,j}\widetilde{f}^{(0)(k+1)}_{l+1/2,i+1/2,j-1/2} \\ &+\widetilde{h}^{(0)}_{l+1/2,i+1/2,j}\end{aligned} \tag{5.334}$$

where

$$\widetilde{h}^{(0)(k+1)}_{l+1/2,i+1/2,j}=0 \tag{5.335}$$

5.5.2 Momentum dynamics

The starting point of the discrete representation of the first order drift kinetic equation is the conservative relation

$$\begin{aligned}
&\left.\frac{\partial\left(p^2\mathbf{S}_p^{(0)}\right)}{\partial p}\right|_{l+1/2,i+1/2,j+1/2}^{(k)} - \frac{p_{i+1/2}}{\lambda^{l+1/2,j+1/2}} \times \\
&\left.\frac{\partial}{\partial\xi_0}\left(\sqrt{1-\xi_0^2}\lambda\mathbf{S}_\xi^{(0)}\right)\right|_{l+1/2,i+1/2,j+1/2}^{(k)} \\
= &\left.\frac{\partial\left(p^2\widetilde{\mathbf{S}}_p^{(0)}\right)}{\partial p}\right|_{l+1/2,i+1/2,j+1/2}^{(k)} - \frac{p_{i+1/2}}{\lambda^{l+1/2,j+1/2}} \times \\
&\left.\frac{\partial}{\partial\xi_0}\left(\sqrt{1-\xi_0^2}\lambda\widetilde{\mathbf{S}}_\xi^{(0)}\right)\right|_{l+1/2,i+1/2,j+1/2}^{(k)}
\end{aligned} \tag{5.336}$$

where $\mathbf{S}_p^{(0)}$ and $\mathbf{S}_\xi^{(0)}$ are fluxes related to the function $g^{(0)}$ as introduced in Sec.3.5.5, while $\widetilde{\mathbf{S}}_p^{(0)}$ and $\widetilde{\mathbf{S}}_\xi^{(0)}$ are fluxes related to the function $\widetilde{f}^{(0)}$. Since $g^{(0)}$ and $f_0^{(0)}$ have same symmetries with respect to the pitch-angle ξ_0, matrix coefficients are exactly identical for both functions (see Sec. 5.4.1). However, calculations are slightly different for $\widetilde{f}^{(0)}$, though a conservative form may still be kept. By analogy with zero order Fokker-Planck equation,

$$\begin{aligned}
\frac{\partial\left(p^2\widetilde{S}_p^{(0)}\right)}{\partial p} &= \frac{\partial}{\partial p}\left(-p^2\widetilde{D}_{pp}^{(0)}\frac{\partial\widetilde{f}^{(0)}}{\partial p} + p^2\widetilde{F}_p^{(0)}\widetilde{f}^{(0)}\right) \\
&\quad + \sqrt{1-\xi_0^2}\frac{\partial}{\partial p}\left(p\widetilde{D}_{p\xi}^{(0)}\right)\frac{\partial\widetilde{f}^{(0)}}{\partial\xi_0} \\
&\quad + \sqrt{1-\xi_0^2}p\widetilde{D}_{p\xi}^{(0)}\frac{\partial^2\widetilde{f}^{(0)}}{\partial p\partial\xi_0}
\end{aligned} \tag{5.337}$$

$$\begin{aligned}
\frac{\partial\left(\sqrt{1-\xi_0^2}\lambda\left(\psi,\xi_0\right)\widetilde{S}_\xi^{(0)}\right)}{\partial\xi_0} &= \frac{\partial}{\partial\xi_0}\left(\widetilde{D}_{\xi\xi}^{(0)}\frac{1-\xi_0^2}{p}\lambda\left(\psi,\xi_0\right)\frac{\partial\widetilde{f}^{(0)}}{\partial\xi_0}\right. \\
&\quad \left. + \sqrt{1-\xi_0^2}\lambda\left(\psi,\xi_0\right)\widetilde{F}_\xi^{(0)}\widetilde{f}^{(0)}\right) \\
&\quad - \frac{\partial}{\partial\xi_0}\left(\sqrt{1-\xi_0^2}\lambda\left(\psi,\xi_0\right)\widetilde{D}_{\xi p}^{(0)}\right)\frac{\partial\widetilde{f}^{(0)}}{\partial p} \\
&\quad - \sqrt{1-\xi_0^2}\lambda\left(\psi,\xi_0\right)\widetilde{D}_{\xi p}^{(0)}\frac{\partial^2\widetilde{f}^{(0)}}{\partial\xi_0\partial p}
\end{aligned} \tag{5.338}$$

one obtains

$$\left.\frac{\partial\left(p^2\widetilde{\mathbf{S}}_p^{(0)}\right)}{\partial p}\right|_{l+1/2,i+1/2,j+1/2}^{(k)} - \frac{p_{i+1/2}}{\lambda^{l+1/2,j+1/2}} \times \left.\frac{\partial}{\partial\xi_0}\left(\sqrt{1-\xi_0^2}\lambda\widetilde{\mathbf{S}}_\xi^{(0)}\right)\right|_{l+1/2,i+1/2,j+1/2}^{(k)} = \sum_{m=1}^{m=8}\widetilde{T}^{[m]} \tag{5.339}$$

with

$$\widetilde{T}^{[1]} = \frac{-p_{i+1}^2\widetilde{D}^{(0)}_{pp,l+1/2,i+1,j+1/2}\left.\frac{\partial\widetilde{f}^{(0)}}{\partial p}\right|_{l+1/2,i+1,j+1/2}^{(k+1)} + p_{i+1}^2\widetilde{F}^{(0)}_{p,l+1/2,i+1,j+1/2}\widetilde{f}^{(0)(k+1)}_{l+1/2,i+1,j+1/2}}{\Delta p_{i+1/2}} \tag{5.340}$$

$$\widetilde{T}^{[2]} = \frac{p_i^2\widetilde{D}^{(0)}_{pp,l+1/2,i,j+1/2}\left.\frac{\partial\widetilde{f}^{(0)}}{\partial p}\right|_{l+1/2,i,j+1/2}^{(k+1)} - p_i^2\widetilde{F}^{(0)}_{p,l+1/2,i,j+1/2}\widetilde{f}^{(0)(k+1)}_{l+1/2,i,j+1/2}}{\Delta p_{i+1/2}} \tag{5.341}$$

$$\widetilde{T}^{[3]} = +\sqrt{1-\xi_{0,j+1/2}^2}\left.\frac{\partial\left(p\widetilde{D}^{(0)}_{p\xi}\right)}{\partial p}\right|_{l+1/2,i+1/2,j+1/2}\left.\frac{\partial\widetilde{f}^{(0)}}{\partial\xi}\right|_{l+1/2,i+1/2,j+1/2}^{(k+1)} \tag{5.342}$$

$$\widetilde{T}^{[4]} = +\sqrt{1-\xi_{0,j+1/2}^2}p_{i+1/2}\widetilde{D}^{(0)}_{p\xi,l+1/2,i+1/2,j+1/2}\left.\frac{\partial^2\widetilde{f}^{(0)}}{\partial p\partial\xi}\right|_{l+1/2,i+1/2,j+1/2}^{(k+1)} \tag{5.343}$$

$$\widetilde{T}^{[5]} = -\frac{p_{i+1/2}}{\lambda^{l+1/2,j+1/2}}\left[\frac{\widetilde{D}^{(0)}_{\xi\xi,l+1/2,i+1/2,j+1}\left(1-\xi_{0,j+1}^2\right)\lambda^{l+1/2,j+1}\left.\frac{\partial\widetilde{f}^{(0)}}{\partial\xi}\right|_{l+1/2,i+1/2,j+1}^{(k+1)}}{p_{i+1/2}\Delta\xi_{j+1/2}} + \frac{p_{i+1/2}\sqrt{1-\xi_{0,j+1}^2}\lambda^{l+1/2,j+1}\widetilde{F}^{(0)}_{\xi,l+1/2,i+1/2,j+1}\widetilde{f}^{(0)(k+1)}_{l+1/2,i+1/2,j+1}}{\Delta\xi_{j+1/2}}\right] \tag{5.344}$$

$$\widetilde{T}^{[6]} = \frac{p_{i+1/2}}{\lambda^{l+1/2,j+1/2}}\left[\frac{\widetilde{D}^{(0)}_{\xi\xi,l+1/2,i+1/2,j}\left(1-\xi_{0,j}^2\right)\lambda^{l+1/2,j}\left.\frac{\partial\widetilde{f}^{(0)}}{\partial\xi}\right|_{l+1/2,i+1/2,j}^{(k+1)}}{p_{i+1/2}\Delta\xi_{j+1/2}} + \frac{p_{i+1/2}\sqrt{1-\xi_{0,j}^2}\lambda^{l+1/2,j}\widetilde{F}^{(0)}_{\xi,l+1/2,i+1/2,j}\widetilde{f}^{(0)(k+1)}_{l+1/2,i+1/2,j}}{\Delta\xi_{j+1/2}}\right] \tag{5.345}$$

$$\widetilde{T}^{[7]} = \frac{p_{i+1/2}}{\lambda^{l+1/2,j+1/2}} \frac{\partial}{\partial \xi_0} \left(\sqrt{1-\xi_0^2} \lambda \widetilde{D}^{(0)}_{\xi p} \right) \Big|_{l+1/2,i+1/2,j+1/2} \frac{\partial \widetilde{f}^{(0)}}{\partial p} \Big|^{(k+1)}_{l+1/2,i+1/2,j+1/2} \tag{5.346}$$

$$\widetilde{T}^{[8]} = \frac{p_{i+1/2}}{\lambda^{l+1/2,j+1/2}} \sqrt{1-\xi^2_{0,j+1/2}} \lambda^{l+1/2,j+1/2} \widetilde{D}^{(0)}_{\xi p,l+1/2,i+1/2,j+1/2} \frac{\partial^2 \widetilde{f}^{(0)}}{\partial \xi_0 \partial p} \Big|^{(k+1)}_{l+1/2,i+1/2,j+1/2} \tag{5.347}$$

Discrete expressions of the partial derivatives are,

$$\frac{\partial \widetilde{f}^{(0)}}{\partial p} \Big|^{(k+1)}_{l+1/2,i+1,j+1/2} = \frac{\widetilde{f}^{(0)(k+1)}_{l+1/2,i+3/2,j+1/2} - \widetilde{f}^{(0)(k+1)}_{l+1/2,i+1/2,j+1/2}}{\Delta p_{i+1}} \tag{5.348}$$

$$\frac{\partial \widetilde{f}^{(0)}}{\partial p} \Big|^{(k+1)}_{l+1/2,i+1/2,j+1/2} = \frac{\widetilde{f}^{(0)(k+1)}_{l+1/2,i+3/2,j+1/2} - \widetilde{f}^{(0)(k+1)}_{l+1/2,i-1/2,j+1/2}}{\Delta p_{i+1} + \Delta p_i} \tag{5.349}$$

$$\frac{\partial \widetilde{f}^{(0)}}{\partial p} \Big|^{(k+1)}_{l+1/2,i,j+1/2} = \frac{\widetilde{f}^{(0)(k+1)}_{l+1/2,i+1/2,j+1/2} - \widetilde{f}^{(0)(k+1)}_{l+1/2,i-1/2,j+1/2}}{\Delta p_i} \tag{5.350}$$

$$\frac{\partial \widetilde{f}^{(0)}}{\partial \xi_0} \Big|^{(k+1)}_{l+1/2,i+1/2,j+1} = \frac{\widetilde{f}^{(0)(k+1)}_{l+1/2,i+1/2,j+3/2} - \widetilde{f}^{(0)(k+1)}_{l+1/2,i+1/2,j+1/2}}{\Delta \xi_{0,j+1}} \tag{5.351}$$

$$\frac{\partial \widetilde{f}^{(0)}}{\partial \xi_0} \Big|^{(k+1)}_{l+1/2,i+1/2,j+1/2} = \frac{\widetilde{f}^{(0)(k+1)}_{l+1/2,i+1/2,j+3/2} - \widetilde{f}^{(0)(k+1)}_{l+1/2,i+1/2,j-1/2}}{\Delta \xi_{0,j+1} + \Delta \xi_{0,j}} \tag{5.352}$$

$$\frac{\partial \widetilde{f}^{(0)}}{\partial \xi_0} \Big|^{(k+1)}_{l+1/2,i+1/2,j} = \frac{\widetilde{f}^{(0)(k+1)}_{l+1/2,i+1/2,j+1/2} - \widetilde{f}^{(0)(k+1)}_{l+1/2,i+1/2,j-1/2}}{\Delta \xi_{0,j}} \tag{5.353}$$

and cross-derivatives

$$\begin{aligned} \frac{\partial^2 \widetilde{f}^{(0)}}{\partial p \partial \xi_0} \Big|^{(k+1)}_{l+1/2,i+1/2,j+1/2} &= \frac{\partial^2 \widetilde{f}^{(0)}}{\partial \xi_0 \partial p} \Big|^{(k+1)}_{l+1/2,i+1/2,j+1/2} \\ &= \frac{\widetilde{f}^{(0)(k+1)}_{l+1/2,i+3/2,j+3/2} + \widetilde{f}^{(0)(k+1)}_{l+1/2,i-1/2,j-1/2}}{(\Delta p_{i+1} + \Delta p_i)(\Delta \xi_{0,j+1} + \Delta \xi_{0,j})} \\ &\quad - \frac{\widetilde{f}^{(0)(k+1)}_{l+1/2,i+3/2,j-1/2} + \widetilde{f}^{(0)(k+1)}_{l+1/2,i-1/2,j+3/2}}{(\Delta p_{i+1} + \Delta p_i)(\Delta \xi_{0,j+1} + \Delta \xi_{0,j})} \end{aligned} \tag{5.354}$$

As for the zero-order Fokker-Planck equation, other derivatives in discrete form become

$$\frac{\partial \left(p \widetilde{D}^{(0)}_{p\xi} \right)}{\partial p} \Big|_{l+1/2,i+1/2,j+1/2} = \frac{p_{i+1} \widetilde{D}^{(0)}_{p\xi,l+1/2,i+1,j+1/2} - p_i \widetilde{D}^{(0)}_{p\xi,l+1/2,i,j+1/2}}{\Delta p_{i+1/2}} \tag{5.355}$$

$$\begin{aligned}
&\frac{\partial}{\partial\xi_0}\left(\sqrt{1-\xi_0^2}\lambda\widetilde{D}^{(0)}_{\xi p}\right)\Big|_{l+1/2,i+1/2,j+1/2}\\
=\;&\frac{\sqrt{1-\xi^2_{0,j+1}}\lambda^{l+1/2,j+1}\widetilde{D}^{(0)}_{\xi p,l+1/2,i+1/2,j+1}}{\Delta\xi_{0,j+1/2}}\\
&-\frac{\sqrt{1-\xi^2_{0,j}}\lambda^{l+1/2,j}\widetilde{D}^{(0)}_{\xi p,l+1/2,i+1/2,j}}{\Delta\xi_{0,j+1/2}}
\end{aligned}\tag{5.356}$$

Since the distribution function $\widetilde{f}^{(0)}$is defined on the half grid, while fluxes on the full grid, it is necessary to interpolate, because in some derivatives, values of are taken on the full grid. As discussed in the previous section, interpolation procedure is more complex for $\widetilde{f}^{(0)}$ than for $f_0^{(0)}$. Therefore, for terms proportional to $\widetilde{D}^{(0)}_{\xi\xi}$ and $\widetilde{F}^{(0)}_{\xi}$

$$\begin{aligned}
\widetilde{f}^{(0)(k+1)}_{l+1/2,i+1,j+1/2} &= \frac{p_{i+1}}{p_{i+3/2}}\left(1-\delta^{(0)}_{p,l+1/2,i+1,j+1/2}\right)\widetilde{f}^{(0)(k+1)}_{l+1/2,i+3/2,j+1/2}\\
&+\frac{p_{i+1}}{p_{i+1/2}}\delta^{(0)}_{p,l+1/2,i+1,j+1/2}\widetilde{f}^{(0)(k+1)}_{l+1/2,i+1/2,j+1/2}\\
&+\widetilde{h}^{(0)(k+1)}_{l+1/2,i+1,j+1/2}
\end{aligned}\tag{5.357}$$

$$\begin{aligned}
\widetilde{f}^{(0)(k+1)}_{l+1/2,i,j+1/2} &= \frac{p_{i}}{p_{i+1/2}}\left(1-\delta^{(0)}_{p,l+1/2,i,j+1/2}\right)\widetilde{f}^{(0)(k+1)}_{l+1/2,i+1/2,j+1/2}\\
&+\frac{p_{i}}{p_{i-1/2}}\delta^{(0)}_{p,l+1/2,i,j+1/2}\widetilde{f}^{(0)(k+1)}_{l+1/2,i-1/2,j+1/2}\\
&+\widetilde{h}^{(0)(k+1)}_{l+1/2,i,j+1/2}
\end{aligned}\tag{5.358}$$

and for terms proportional to $\widetilde{D}^{(0)}_{\xi\xi}$ and $\widetilde{F}^{(0)}_{\xi}$

$$\begin{aligned}
\widetilde{f}^{(0)(k+1)}_{l+1/2,i+1/2,j+1} &= \frac{\xi_{0,j+1}}{\xi_{0,j+3/2}}\left(1-\delta^{(0)}_{\xi,l+1/2,i+1/2,j+1}\right)\widetilde{f}^{(0)(k+1)}_{l+1/2,i+1/2,j+3/2}\\
&+\frac{\xi_{0,j+1}}{\xi_{0,j+1/2}}\delta^{(0)}_{\xi,l+1/2,i+1/2,j+1}\widetilde{f}^{(0)(k+1)}_{l+1/2,i+1/2,j+1/2}
\end{aligned}\tag{5.359}$$

$$\begin{aligned}
\widetilde{f}^{(0)(k+1)}_{l+1/2,i+1/2,j} &= \frac{\xi_{0,j}}{\xi_{0,j+1/2}}\left(1-\delta^{(0)}_{\xi,l+1/2,i+1/2,j}\right)\widetilde{f}^{(0)(k+1)}_{l+1/2,i+1/2,j+1/2}\\
&+\frac{\xi_{0,j}}{\xi_{0,j-1/2}}\delta^{(0)}_{\xi,l+1/2,i+1/2,j}\widetilde{f}^{(0)(k+1)}_{l+1/2,i+1/2,j-1/2}
\end{aligned}\tag{5.360}$$

since $\widetilde{h}^{(0)}_{l+1/2,i+1/2,j+1}=\widetilde{h}^{(0)}_{l+1/2,i+1/2,j}=0$.

Gathering all terms in a matrix form

$$\begin{aligned}
&\left.\frac{\partial\left(p^2\widetilde{\mathbf{S}}_p^{(0)}\right)}{\partial p}\right|_{l+1/2,i+1/2,j+1/2}^{(k)} - \frac{p_{i+1/2}}{\lambda^{l+1/2,j+1/2}} \times \\
&\left.\frac{\partial}{\partial\xi_0}\left(\sqrt{1-\xi_0^2}\lambda\widetilde{\mathbf{S}}_\xi^{(0)}\right)\right|_{l+1/2,i+1/2,j+1/2}^{(k)} \\
= &\sum_{i'=i-1}^{i'=i+1}\sum_{j'=j-1}^{j'=j+1}\widetilde{\overline{M}}^{(0)}_{p,l+1/2,i'+1/2,j'+1/2}\widetilde{f}^{(0)(k+1)}_{l+1/2,i'+1/2,j'+1/2} \\
&+\sum_{i'=i-1}^{i'=i+1}\sum_{l'=l-1}^{l'=l+1}\widetilde{\overline{H}}^{(0)}_{\psi,l'+1/2,i'+1/2,j+1/2}f^{(0)(k+1)}_{0,l'+1/2,i'+1/2,j+1/2}
\end{aligned} \tag{5.361}$$

where $\widetilde{\overline{M}}^{(0)}$ and $\overline{\overline{M}}^{(0)}$ have a very similar expressions, though slightly different because of the ratios $p_{i+1}/p_{i+3/2}, p_i/p_{i+1/2}, \xi_{0,j+1}/\xi_{0,j+3/2}$ and $\xi_{0,j}/\xi_{0,j+1/2}$ but one matrix $\widetilde{\overline{H}}^{(0)}_\psi$ that results from the spatial variation of the Chang and Cooper coefficients as shown in Sec. 5.4.3. Starting from the expression of $\overline{\overline{M}}^{(0)}$, one obtains

$$\begin{aligned}
\widetilde{\overline{M}}^{(0)}_{p,l+1/2,i+3/2,j+3/2} = &\frac{p_{i+1/2}}{\Delta p_{i+1}+\Delta p_i}\frac{\sqrt{1-\xi^2_{0,j+1/2}}}{\Delta\xi_{0,j+1}+\Delta\xi_{0,j}}\widetilde{D}^{(0)}_{p\xi,l+1/2,i+1/2,j+1/2} \\
&+\frac{p_{i+1/2}}{\Delta p_{i+1}+\Delta p_i}\frac{\sqrt{1-\xi^2_{0,j+1/2}}}{\Delta\xi_{0,j+1}+\Delta\xi_{0,j}}\widetilde{D}^{(0)}_{\xi p,l+1/2,i+1/2,j+1/2}
\end{aligned} \tag{5.362}$$

$$\begin{aligned}
\widetilde{\overline{M}}^{(0)}_{p,l+1/2,i+1/2,j+3/2} = &\frac{p_{i+1}}{\Delta p_{i+1/2}}\frac{\sqrt{1-\xi^2_{0,j+1/2}}}{\Delta\xi_{0,j+1}+\Delta\xi_{0,j}}\widetilde{D}^{(0)}_{p\xi,l+1/2,i+1,j+1/2} \\
&-\frac{p_i}{\Delta p_{i+1/2}}\frac{\sqrt{1-\xi^2_{0,j+1/2}}}{\Delta\xi_{0,j+1}+\Delta\xi_{0,j}}\widetilde{D}^{(0)}_{p\xi,l+1/2,i,j+1/2} \\
&-\frac{1-\xi^2_{0,j+1}}{\Delta\xi_{0,j+1/2}\Delta\xi_{0,j+1}}\frac{\lambda^{l+1/2,j+1}}{\lambda^{l+1/2,j+1/2}}\widetilde{D}^{(0)}_{\xi\xi,l+1/2,i+1/2,j+1} \\
&-p_{i+1/2}\frac{\sqrt{1-\xi^2_{0,j+1}}}{\Delta\xi_{0,j+1/2}}\left[\frac{\xi_{0,j+1}}{\xi_{0,j+3/2}}\right]\left(1-\delta^{(0)}_{\xi,l+1/2,i+1/2,j+1}\right)\times \\
&\frac{\lambda^{l+1/2,j+1}}{\lambda^{l+1/2,j+1/2}}\widetilde{F}^{(0)}_{\xi,l+1/2,i+1/2,j+1}
\end{aligned} \tag{5.363}$$

$$\begin{aligned}\widetilde{\widetilde{M}}^{(0)}_{p,l+1/2,i-1/2,j+3/2} &= -\frac{p_{i+1/2}}{\Delta p_{i+1}+\Delta p_i}\frac{\sqrt{1-\xi^2_{0,j+1/2}}}{\Delta\xi_{0,j+1}+\Delta\xi_{0,j}}\widetilde{D}^{(0)}_{p\xi,l+1/2,i+1/2,j+1/2} \\ &\quad -\frac{p_{i+1/2}}{\Delta p_{i+1}+\Delta p_i}\frac{\sqrt{1-\xi^2_{0,j+1/2}}}{\Delta\xi_{0,j+1}+\Delta\xi_{0,j}}\widetilde{D}^{(0)}_{\xi p,l+1/2,i+1/2,j+1/2}\end{aligned} \tag{5.364}$$

$$\begin{aligned}\widetilde{\widetilde{M}}^{(0)}_{p,l+1/2,i+3/2,j+1/2} &= -\frac{p^2_{i+1}}{\Delta p_{i+1}\Delta p_{i+1/2}}\widetilde{D}^{(0)}_{pp,l+1/2,i+1,j+1/2} \\ &\quad +\frac{p_{i+1/2}}{\Delta p_{i+1}+\Delta p_i}\frac{\sqrt{1-\xi^2_{0,j+1}}}{\Delta\xi_{0,j+1/2}}\times \\ &\quad \frac{\lambda^{l+1/2,j+1}}{\lambda^{l+1/2,j+1/2}}\widetilde{D}^{(0)}_{\xi p,l+1/2,i+1/2,j+1} \\ &\quad -\frac{p_{i+1/2}}{\Delta p_{i+1}+\Delta p_i}\frac{\sqrt{1-\xi^2_{0,j}}}{\Delta\xi_{0,j+1/2}}\times \\ &\quad \frac{\lambda^{l+1/2,j}}{\lambda^{l+1/2,j+1/2}}\widetilde{D}^{(0)}_{\xi p,l+1/2,i+1/2,j} \\ &\quad +\frac{p^2_{i+1}}{\Delta p_{i+1/2}}\left[\frac{p_{i+1}}{p_{i+3/2}}\right]\left(1-\delta^{(0)}_{p,l+1/2,i+1,j+1/2}\right)\widetilde{F}^{(0)}_{p,l+1/2,i+1,j+1/2}\end{aligned} \tag{5.365}$$

$$
\begin{aligned}
\widetilde{\widetilde{M}}^{(0)}_{p,i+1/2,j+1/2} &= \frac{p^2_{i+1}}{\Delta p_{i+1/2}\Delta p_{i+1}}\widetilde{D}^{(0)}_{pp,l+1/2,i+1,j+1/2} \\
&+\frac{p^2_{i+1}}{\Delta p_{i+1/2}}\widetilde{F}_{p,l+1/2,i+1,j+1/2}\left[\frac{p_{i+1}}{p_{i+1/2}}\right]\delta^{(0)}_{p,l+1/2,i+1,j+1/2} \\
&+\frac{p^2_i}{\Delta p_{i+1/2}\Delta p_i}\widetilde{D}^{(0)}_{pp,l+1/2,i,j+1/2} \\
&-\frac{p^2_i}{\Delta p_{i+1/2}}\left[\frac{p_i}{p_{i+1/2}}\right]\left(1-\delta^{(0)}_{p,l+1/2,i,j+1/2}\right)\widetilde{F}^{(0)}_{p,l+1/2,i,j+1/2} \\
&-\frac{1-\xi^2_{0,j+1}}{\Delta\xi_{0,j+1/2}\Delta\xi_{0,j+1}}\frac{\lambda^{l+1/2,j+1}}{\lambda^{l+1/2,j+1/2}}\widetilde{D}^{(0)}_{\xi\xi,l+1/2,i+1/2,j+1} \\
&-p_{i+1/2}\frac{\sqrt{1-\xi^2_{0,j+1}}}{\Delta\xi_{0,j+1/2}}\left[\frac{\xi_{0,j+1}}{\xi_{0,j+1/2}}\right]\delta^{(0)}_{\xi,l+1/2,i+1/2,j+1}\times \\
&\frac{\lambda^{l+1/2,j+1}}{\lambda^{l+1/2,j+1/2}}\widetilde{F}^{(0)}_{\xi,l+1/2,i+1/2,j+1} \\
&+\frac{1-\xi^2_{0,j}}{\Delta\xi_{0,j}\Delta\xi_{0,j+1/2}}\frac{\lambda^{l+1/2,j}}{\lambda^{l+1/2,j+1/2}}\widetilde{D}^{(0)}_{\xi\xi,l+1/2,i+1/2,j} \\
&+p_{i+1/2}\frac{\sqrt{1-\xi^2_{0,j}}}{\Delta\xi_{0,j+1/2}}\left[\frac{\xi_{0,j}}{\xi_{0,j+1/2}}\right]\left(1-\delta^{(0)}_{\xi,l+1/2,i+1/2,j}\right)\times \\
&\frac{\lambda^{l+1/2,j}}{\lambda^{l+1/2,j+1/2}}F^{(0)}_{\xi,l+1/2,i+1/2,j}
\end{aligned}
\tag{5.366}
$$

$$
\begin{aligned}
\widetilde{\widetilde{M}}^{(0)}_{p,l+1/2,i-1/2,j+1/2} &= -\frac{p^2_i}{\Delta p_{i+1/2}\Delta p_i}\widetilde{D}^{(0)}_{pp,l+1/2,i,j+1/2} \\
&-\frac{p_{i+1/2}}{\Delta p_{i+1}+\Delta p_i}\frac{\sqrt{1-\xi^2_{0,j+1}}}{\Delta\xi_{0,j+1/2}}\times \\
&\frac{\lambda^{l+1/2,j+1}}{\lambda^{l+1/2,j+1/2}}\widetilde{D}^{(0)}_{\xi p,l+1/2,i+1/2,j+1} \\
&+\frac{p_{i+1/2}}{\Delta p_{i+1}+\Delta p_i}\frac{\sqrt{1-\xi^2_{0,j}}}{\Delta\xi_{0,j+1/2}}\times \\
&\frac{\lambda^{l+1/2,j}}{\lambda^{l+1/2,j+1/2}}\widetilde{D}^{(0)}_{\xi p,l+1/2,i+1/2,j} \\
&-\frac{p^2_i}{\Delta p_{i+1/2}}\left[\frac{p_i}{p_{i-1/2}}\right]\delta^{(0)}_{p,i,j+1/2}\widetilde{F}^{(0)}_{p,l+1/2,i,j+1/2}
\end{aligned}
\tag{5.367}
$$

$$\widetilde{\overline{M}}^{(0)}_{p,l+1/2,i+3/2,j-1/2} = -\frac{p_{i+1/2}}{\Delta p_{i+1}+\Delta p_i}\frac{\sqrt{1-\xi^2_{0,j+1/2}}}{\Delta\xi_{0,j+1}+\Delta\xi_{0,j}}\widetilde{D}^{(0)}_{p\xi,l+1/2,i+1/2,j+1/2} - \frac{p_{i+1/2}}{\Delta p_{i+1}+\Delta p_i}\frac{\sqrt{1-\xi^2_{0,j+1/2}}}{\Delta\xi_{0,j+1}+\Delta\xi_{0,j}}\widetilde{D}^{(0)}_{\xi p,l+1/2,i+1/2,j+1/2} \tag{5.368}$$

$$\begin{aligned}\widetilde{\overline{M}}^{(0)}_{p,l+1/2,i+1/2,j-1/2} = & -\frac{p_{i+1}}{\Delta p_{i+1/2}}\frac{\sqrt{1-\xi^2_{0,j+1/2}}}{\Delta\xi_{0,j+1}+\Delta\xi_{0,j}}\widetilde{D}^{(0)}_{p\xi,l+1/2,i+1,j+1/2} \\ & +\frac{p_i}{\Delta p_{i+1/2}}\frac{\sqrt{1-\xi^2_{0,j+1/2}}}{\Delta\xi_{0,j+1}+\Delta\xi_{0,j}}\widetilde{D}^{(0)}_{p\xi,l+1/2,i,j+1/2} \\ & -\frac{1-\xi^2_{0,j}}{\Delta\xi_{0,j+1/2}\Delta\xi_{0,j}}\frac{\lambda^{l+1/2,j}}{\lambda^{l+1/2,j+1/2}}\widetilde{D}^{(0)}_{\xi\xi,l+1/2,i+1/2,j} \\ & +p_{i+1/2}\frac{\sqrt{1-\xi^2_{0,j}}}{\Delta\xi_{0,j+1/2}}\left[\frac{\xi_{0,j}}{\xi_{0,j-1/2}}\right]\delta^{(0)}_{\xi,l+1/2,i+1/2,j}\times \\ & \frac{\lambda^{l+1/2,j}}{\lambda^{l+1/2,j+1/2}}\widetilde{F}^{(0)}_{\xi,l+1/2,i+1/2,j}\end{aligned} \tag{5.369}$$

$$\begin{aligned}\widetilde{\overline{M}}^{(0)}_{p,l+1/2,i-1/2,j-1/2} = & \frac{p_{i+1/2}}{\Delta p_{i+1}+\Delta p_i}\frac{\sqrt{1-\xi^2_{0,j+1/2}}}{\Delta\xi_{0,j+1}+\Delta\xi_{0,j}}\widetilde{D}^{(0)}_{p\xi,l+1/2,i+1/2,j+1/2} \\ & +\frac{p_{i+1/2}}{\Delta p_{i+1}+\Delta p_i}\frac{\sqrt{1-\xi^2_{0,j+1/2}}}{\Delta\xi_{0,j+1}+\Delta\xi_{0,j}}\widetilde{D}^{(0)}_{\xi p,l+1/2,i+1/2,j+1/2}\end{aligned} \tag{5.370}$$

For the determination of matrix $\widetilde{\overline{H}}^{(0)}_{\psi}$, it is useful to start from terms $\widetilde{T}_1$ and $\widetilde{T}_2$ that contain $\widetilde{h}^{(0)(k+1)}_{l+1/2,i,j+1/2}$ and $\widetilde{h}^{(0)(k+1)}_{l+1/2,i+1,j+1/2}$. coefficients. Because of the grid interpolation

$$\begin{aligned}&\sum_{i'=i-1}^{i'=i+1}\sum_{l'=l-1}^{l'=l+1}\widetilde{\overline{H}}^{(0)}_{\psi,l'+1/2,i'+1/2,j+1/2}f^{(0)(k+1)}_{0,l'+1/2,i'+1/2,j+1/2} \\ = & \frac{p^2_{i+1}\widetilde{F}^{(0)}_{p,l+1/2,i+1,j+1/2}}{\Delta p_{i+1/2}}\widetilde{h}^{(0)(k+1)}_{l+1/2,i+1,j+1/2} - \frac{p^2_i\widetilde{F}^{(0)}_{p,l+1/2,i,j+1/2}}{\Delta p_{i+1/2}}\widetilde{h}^{(0)(k+1)}_{l+1/2,i,j+1/2}\end{aligned} \tag{5.371}$$

and using relations (5.328) and (5.330), it comes

$$\widetilde{\overline{H}}^{(0)}_{\psi,l-1/2,i-1/2,j+1/2} = \frac{p_i^3 \widetilde{F}^{(0)}_{p,l+1/2,i,j+1/2}}{\Delta p_{i+1/2}} \frac{\xi_{0,j+1/2} I_{l+1/2}}{q_e B_{0,l+1/2}} \times \alpha^-_{l+1/2} \left(\delta^{(0)}_{p,l+1/2,i,j+1/2} - \delta^{(0)}_{p,l-1/2,i,j+1/2} \right) \tag{5.372}$$

$$\begin{aligned} \widetilde{\overline{H}}^{(0)}_{\psi,l-1/2,i+1/2,j+1/2} = & -\frac{p_i^3 \widetilde{F}^{(0)}_{p,l+1/2,i,j+1/2}}{\Delta p_{i+1/2}} \frac{\xi_{0,j+1/2} I_{l+1/2}}{q_e B_{0,l+1/2}} \times \\ & \alpha^-_{l+1/2} \left(\delta^{(0)}_{p,l+1/2,i,j+1/2} - \delta^{(0)}_{p,l-1/2,i,j+1/2} \right) \\ & -\frac{p_{i+1}^3 \widetilde{F}^{(0)}_{p,l+1/2,i+1,j+1/2}}{\Delta p_{i+1/2}} \frac{\xi_{0,j+1/2} I_{l+1/2}}{q_e B_{0,l+1/2}} \times \\ & \alpha^-_{l+1/2} \left(\delta^{(0)}_{p,l+1/2,i+1,j+1/2} - \delta^{(0)}_{p,l-1/2,i+1,j+1/2} \right) \end{aligned} \tag{5.373}$$

$$\begin{aligned} \widetilde{\overline{H}}^{(0)}_{\psi,l-1/2,i+3/2,j+1/2} = & +\frac{p_{i+1}^3 \widetilde{F}^{(0)}_{p,l+1/2,i+1,j+1/2}}{\Delta p_{i+1/2}} \frac{\xi_{0,j+1/2} I_{l+1/2}}{q_e B_{0,l+1/2}} \times \\ & \alpha^-_{l+1/2} \left(\delta^{(0)}_{p,l+1/2,i+1,j+1/2} - \delta^{(0)}_{p,l-1/2,i+1,j+1/2} \right) \end{aligned} \tag{5.374}$$

$$\widetilde{\overline{H}}^{(0)}_{\psi,l+1/2,i-1/2,j+1/2} = 0 \tag{5.375}$$

$$\widetilde{\overline{H}}^{(0)}_{\psi,l+1/2,i+1/2,j+1/2} = 0 \tag{5.376}$$

$$\widetilde{\overline{H}}^{(0)}_{\psi,l+1/2,i+3/2,j+1/2} = 0 \tag{5.377}$$

$$\widetilde{\overline{H}}^{(0)}_{\psi,l+3/2,i-1/2,j+1/2} = \frac{p_i^3 \widetilde{F}^{(0)}_{p,l+1/2,i,j+1/2}}{\Delta p_{i+1/2}} \frac{\xi_{0,j+1/2} I_{l+1/2}}{q_e B_{0,l+1/2}} \times \alpha^+_{l+1/2} \left(\delta^{(0)}_{p,l+1/2,i,j+1/2} - \delta^{(0)}_{p,l+3/2,i,j+1/2} \right) \tag{5.378}$$

$$\begin{aligned} \widetilde{\overline{H}}^{(0)}_{\psi,l+3/2,i+1/2,j+1/2} = & -\frac{p_i^3 \widetilde{F}^{(0)}_{p,l+1/2,i,j+1/2}}{\Delta p_{i+1/2}} \frac{\xi_{0,j+1/2} I_{l+1/2}}{q_e B_{0,l+1/2}} \times \\ & \alpha^+_{l+1/2} \left(\delta^{(0)}_{p,l+1/2,i,j+1/2} - \delta^{(0)}_{p,l+3/2,i,j+1/2} \right) \\ & -\frac{p_{i+1}^3 \widetilde{F}^{(0)}_{p,l+1/2,i+1,j+1/2}}{\Delta p_{i+1/2}} \frac{\xi_{0,j+1/2} I_{l+1/2}}{q_e B_{0,l+1/2}} \times \\ & \alpha^+_{l+1/2} \left(\delta^{(0)}_{p,l+1/2,i+1,j+1/2} - \delta^{(0)}_{p,l+3/2,i+1,j+1/2} \right) \end{aligned} \tag{5.379}$$

$$\overline{\widetilde{H}}^{(0)}_{\psi,l+3/2,i+3/2,j+1/2} = \frac{p^3_{i+1}\widetilde{F}^{(0)}_{p,l+1/2,i+1,j+1/2}}{\Delta p_{i+1/2}}\frac{\xi_{0,j+1/2}I_{l+1/2}}{q_e B_{0,l+1/2}} \times \alpha^+_{l+1/2}\left(\delta^{(0)}_{p,l+1/2,i+1,j+1/2} - \delta^{(0)}_{p,l+3/2,i+1,j+1/2}\right) \quad (5.380)$$

5.5.3 Discrete description of physical processes

Collisions

Since first order drift kinetic terms may be expressed in a conservative form as for the zero order Fokker-Planck equation, the determination of the matrix elements is therefore straightforward. One obtains

$$\overline{\overline{\widetilde{D}}}^{C(0)}_p \rightarrow \begin{cases} \widetilde{D}^{C(0)}_{pp,l+1/2,i+1,j+1/2} = \left(\overline{\lambda}^{l+1/2,j+1/2}_{1,-1,0}/\lambda^{l+1/2,j+1/2}\right) A_{l+1/2,i+1} \\ \widetilde{D}^{C(0)}_{pp,l+1/2,i,j+1/2} = \left(\overline{\lambda}^{l+1/2,j+1/2}_{1,-1,0}/\lambda^{l+1/2,j+1/2}\right) A_{l+1/2,i} \\ \widetilde{D}^{C(0)}_{p\xi,l+1/2,i+1,j+1/2} = 0 \\ \widetilde{D}^{C(0)}_{\xi p,l+1/2,i+1/2,j+1} = 0 \\ \widetilde{D}^{C(0)}_{p\xi,l+1/2,i+1/2,j+1/2} = 0 \\ \widetilde{D}^{C(0)}_{\xi p,l+1/2,i+1/2,j+1/2} = 0 \\ \widetilde{D}^{C(0)}_{p\xi,l+1/2,i,j+1/2} = 0 \\ \widetilde{D}^{C(0)}_{\xi p,l+1/2,i+1/2,j} = 0 \\ \widetilde{D}^{C(0)}_{\xi\xi,l+1/2,i+1/2,j+1} = \left(\overline{\lambda}^{l+1/2,j+1}_{3,-2,0}/\lambda^{l+1/2,j+1}\right) B_{t,l+1/2,i+1/2} \\ \widetilde{D}^{C(0)}_{\xi\xi,l+1/2,i+1/2,j} = \left(\overline{\lambda}^{l+1/2,j}_{3,-2,0}/\lambda^{l+1/2,j}\right) B_{t,l+1/2,i+1/2} \end{cases} \quad (5.381)$$

and

$$\overline{\overline{\widetilde{F}}}^{C(0)}_p \rightarrow \begin{cases} \widetilde{F}^{C(0)}_{p,l+1/2,i+1,j+1/2} = -\left(\overline{\lambda}^{l+1/2,j+1/2}_{1,-1,0}/\lambda^{l+1/2,j+1/2}\right) F_{l+1/2,i+1} \\ \widetilde{F}^{C(0)}_{p,l+1/2,i,j+1/2} = -\left(\overline{\lambda}^{l+1/2,j+1/2}_{1,-1,0}/\lambda^{l+1/2,j+1/2}\right) F_{l+1/2,i} \\ \widetilde{F}^{C(0)}_{\xi,l+1/2,i+1/2,j+1} = \frac{\sqrt{1-\xi^2_{0,j+1}}}{p_{i+1/2}\xi^3_{0,j+1}}\left(\frac{\overline{\lambda}^{l+1/2,j+1}_{1,-1,0}-\overline{\lambda}^{l+1/2,j+1}_{1,-2,0}}{\lambda^{l+1/2,j+1}}\right) B_{t,l+1/2,i+1/2} \\ \widetilde{F}^{C(0)}_{\xi,l+1/2,i+1/2,j} = \frac{\sqrt{1-\xi^2_{0,j}}}{p_{i+1/2}\xi^3_{0,j}}\left(\frac{\overline{\lambda}^{l+1/2,j}_{1,-1,0}-\overline{\lambda}^{l+1/2,j}_{1,-2,0}}{\lambda^{l+1/2,j}}\right) B_{t,l+1/2,i+1/2} \end{cases} \quad (5.382)$$

where coefficients of the collision operator A, F and B_t are the same as defined for the zero order bounce averaged Fokker-Planck equation, in Sec. 5.4.4.

Concerning the first order Legendre correction for electron-electron collisions that ensures momentum conservation, one must calculate

$$\left\{C\left(f_M, \widetilde{f}\right)\right\} = -\frac{3}{2}\frac{\xi_0}{\lambda}H\left(|\xi_0| - \xi_{0T}\right)\mathcal{I}\left(f_M, \widetilde{f}^{(0)(m=1)}_0\right)$$

on the distribution function grid, where

$$\widetilde{f}_0^{(0)(m=1)}\left(\psi,p,\xi_0\right)=\int_{-1}^{+1}\xi_0\widetilde{f}_0^{(0)}\left(\psi,p,\xi_0\right)\overline{\lambda}_{2,0,0}d\xi_0 \tag{5.383}$$

as shwon in Sec. 4.1.5.

Here, the collision integral $\mathcal{I}\left(f_0,\widetilde{f}_0^{(0)(m=1)}\right)$ has a similar form as for the zero order Fokker-Planck equation except that $f_0^{(0)(m=1)}$ is just replaced by $\widetilde{f}_0^{(0)(m=1)}$ in all corresponding terms. Therefore, by definition, at the iteration number (k),

$$\begin{aligned}\left\{C\left(f_M,\widetilde{f}\right)\right\}^{(k)}_{l+1/2,i+1/2,j+1/2}&=-\frac{3}{2}\frac{\xi_{0,j+1/2}}{\lambda^{l+1/2,j+1/2}}H\left(\left|\xi_{0,j+1/2}\right|-\xi_{0T,l+1/2}\right)\\&\times\mathcal{I}\left(f_{M,},\widetilde{f}_0^{(0)(m=1)}\right)^{(k)}_{l+1/2,i+1/2,j+1/2}\end{aligned} \tag{5.384}$$

where

$$\widetilde{f}^{(0)(m=1)(k)}_{0,l+1/2,i+1/2,j+1/2}=\sum_{j'=0}^{n_{\xi_0-1}}\xi_{0,j'+1/2}\widetilde{f}^{(0)(k)}_{0,l+1/2,i+1/2,j'+1/2}\overline{\lambda}^{l+1/2,j'+1/2}_{2,0,0}\Delta\xi_{0,j'+1/2} \tag{5.385}$$

Ohmic electric field

According to the bounce averaged expression,

$$\overline{\overline{\widetilde{D}}}^{E(0)}_{p}\rightarrow\begin{cases}\widetilde{D}^{E(0)}_{pp,l+1/2,i+1,j+1/2}=0\\\widetilde{D}^{E(0)}_{pp,l+1/2,i,j+1/2}=0\\\widetilde{D}^{E(0)}_{p\xi,l+1/2,i+1,j+1/2}=0\\\widetilde{D}^{E(0)}_{\xi p,l+1/2,i+1/2,j+1}=0\\\widetilde{D}^{E(0)}_{p\xi,l+1/2,i+1/2,j+1/2}=0\\\widetilde{D}^{E(0)}_{\xi p,l+1/2,i+1/2,j+1/2}=0\\\widetilde{D}^{E(0)}_{p\xi,l+1/2,i,j+1/2}=0\\\widetilde{D}^{E(0)}_{\xi p,l+1/2,i+1/2,j}=0\\\widetilde{D}^{E(0)}_{\xi\xi,l+1/2,i+1/2,j+1}=0\\\widetilde{D}^{E(0)}_{\xi\xi,l+1/2,i+1/2,j}=0\end{cases} \tag{5.386}$$

and

$$\overline{\overline{\widetilde{F}}}^{E(0)}_{p}\rightarrow\begin{cases}\widetilde{F}^{E(0)}_{p,l+1/2,i+1,j+1/2}=\left(\overline{\lambda}^{l+1/2,j+1/2}_{2,-2,2}/\lambda^{l+1/2,j+1/2}\right)\xi_{0,j+1/2}\overline{E}_{\|0,l+1/2}\\\widetilde{F}^{E(0)}_{p,l+1/2,i,j+1/2}=\left(\overline{\lambda}^{l+1/2,j+1/2}_{2,-2,2}/\lambda^{l+1/2,j+1/2}\right)\xi_{0,j+1/2}\overline{E}_{\|0,l+1/2}\\\widetilde{F}^{E(0)}_{\xi,l+1/2,i+1/2,j+1}=-\left(\overline{\lambda}^{l+1/2,j+1}_{2,-2,2}/\lambda^{l+1/2,j+1}\right)\sqrt{1-\xi^2_{0,j+1}}\overline{E}_{\|0,l+1/2}\\\widetilde{F}^{E(0)}_{\xi,l+1/2,i+1/2,j}=-\left(\overline{\lambda}^{l+1/2,j}_{2,-2,2}/\lambda^{l+1/2,j}\right)\sqrt{1-\xi^2_{0,j}}\overline{E}_{\|0,l+1/2}\end{cases} \tag{5.387}$$

where $\overline{E}_{\|0,l+1/2}$ is the parallel component of the Ohmic electric field along the magnetic field line direction normalized to the Dreicer field taken at the poloidal position where the magnetic field $\mathbf{B}$ is minimum, as explained in Sec.4.2.

Radio-frequency waves

From the expressions given in Sec. 4.3.8, the components of the tensor $\widetilde{D}_p^{RF(0)}$ are

$$\begin{aligned}
\widetilde{D}^{\mathrm{RF}(0)}_{pp,l+1/2,i+1,j+1/2} &= \textstyle\sum_{n=-\infty}^{+\infty}\sum_b (1-\xi^2_{0,j+1/2})\widetilde{\overline{D}}^{\mathrm{RF}(0)\mathrm{D}}_{b,n,l+1/2,i+1,j+1/2}\\
\widetilde{D}^{\mathrm{RF}(0)}_{pp,l+1/2,i,j+1/2} &= \textstyle\sum_{n=-\infty}^{+\infty}\sum_b (1-\xi^2_{0,j+1/2})\widetilde{\overline{D}}^{\mathrm{RF}(0)\mathrm{D}}_{b,n,l+1/2,i,j+1/2}\\
\widetilde{D}^{\mathrm{RF}(0)}_{p\xi,l+1/2,i+1,j+1/2} &= \textstyle\sum_{n=-\infty}^{+\infty}\sum_b -\frac{\sqrt{1-\xi^2_{0,j+1/2}}}{\xi_{0,j+1/2}}\left[1-\xi^2_{0,j+1/2}-\frac{n\Omega_{0l+1/2,i+1}}{\omega_b}\right]\widetilde{\overline{D}}^{\mathrm{RF}(0)\mathrm{D}}_{b,n,l+1/2,i+1,j+1/2}\\
\widetilde{D}^{\mathrm{RF}(0)}_{\xi p,l+1/2,i+1/2,j+1} &= \textstyle\sum_{n=-\infty}^{+\infty}\sum_b -\frac{\sqrt{1-\xi^2_{0,j+1}}}{\xi_{0,j+1}}\left[1-\xi^2_{0,j+1}-\frac{n\Omega_{0l+1/2,i+1/2}}{\omega_b}\right]\widetilde{\overline{D}}^{\mathrm{RF}(0)\mathrm{D}}_{b,n,l+1/2,i+1/2,j+1}\\
\widetilde{D}^{\mathrm{RF}(0)}_{p\xi,l+1/2,i+1/2,j+1/2} &= \textstyle\sum_{n=-\infty}^{+\infty}\sum_b -\frac{\sqrt{1-\xi^2_{0,j+1/2}}}{\xi_{0,j+1/2}}\left[1-\xi^2_{0,j+1/2}-\frac{n\Omega_{0l+1/2,i+1/2}}{\omega_b}\right]\widetilde{\overline{D}}^{\mathrm{RF}(0)\mathrm{D}}_{b,n,l+1/2,i+1/2,j+1/2}\\
\widetilde{D}^{\mathrm{RF}(0)}_{\xi p,l+1/2,i+1/2,j+1/2} &= \textstyle\sum_{n=-\infty}^{+\infty}\sum_b -\frac{\sqrt{1-\xi^2_{0,j+1/2}}}{\xi_{0,j+1/2}}\left[1-\xi^2_{0,j+1/2}-\frac{n\Omega_{0l+1/2,i+1/2}}{\omega_b}\right]\widetilde{\overline{D}}^{\mathrm{RF}(0)\mathrm{D}}_{b,n,l+1/2,i+1/2,j+1/2}\\
\widetilde{D}^{\mathrm{RF}(0)}_{p\xi,l+1/2,i,j+1/2} &= \textstyle\sum_{n=-\infty}^{+\infty}\sum_b -\frac{\sqrt{1-\xi^2_{0,j+1/2}}}{\xi_{0,j+1/2}}\left[1-\xi^2_{0,j+1/2}-\frac{n\Omega_{0l+1/2,i}}{\omega_b}\right]\widetilde{\overline{D}}^{\mathrm{RF}(0)\mathrm{D}}_{b,n,l+1/2,i,j+1/2}\\
\widetilde{D}^{\mathrm{RF}(0)}_{\xi p,l+1/2,i+1/2,j} &= \textstyle\sum_{n=-\infty}^{+\infty}\sum_b -\frac{\sqrt{1-\xi^2_{0,j}}}{\xi_{0,j}}\left[1-\xi^2_{0,j}-\frac{n\Omega_{0l+1/2,i+1/2}}{\omega_b}\right]\widetilde{\overline{D}}^{\mathrm{RF}(0)\mathrm{D}}_{b,n,l+1/2,i+1/2,j}\\
\widetilde{D}^{\mathrm{RF}(0)}_{\xi\xi,l+1/2,i+1/2,j+1} &= \textstyle\sum_{n=-\infty}^{+\infty}\sum_b \frac{1}{\xi^2_{0,j+1}}\left[1-\xi^2_{0,j+1}-\frac{n\Omega_{0l+1/2,i+1/2}}{\omega_b}\right]^2\widetilde{\overline{D}}^{\mathrm{RF}(0)\mathrm{D}}_{b,n,l+1/2,i+1/2,j+1}\\
\widetilde{D}^{\mathrm{RF}(0)}_{\xi\xi,l+1/2,i+1/2,j} &= \textstyle\sum_{n=-\infty}^{+\infty}\sum_b \frac{1}{\xi^2_{0,j+1}}\left[1-\xi^2_{0,j+1}-\frac{n\Omega_{0l+1/2,i+1/2}}{\omega_b}\right]^2\widetilde{\overline{D}}^{\mathrm{RF}(0)\mathrm{D}}_{b,n,l+1/2,i+1/2,j}
\end{aligned} \tag{5.388}$$

and the components of the vector $\widetilde{F}_p^{\mathrm{RF}(0)}$ are

$$\begin{aligned}
\widetilde{F}^{\mathrm{RF}(0)}_{p,l+1/2,i+1,j+1/2} &= \frac{\sqrt{1-\xi^2_{0,j+1/2}}}{p_{i+1}\xi^3_{0,j+1/2}}\textstyle\sum_{n=-\infty}^{+\infty}\sum_b -\frac{\sqrt{1-\xi^2_{0,j+1/2}}}{\xi_{0,j+1/2}}\left[1-\xi^2_{0,j+1/2}-\frac{n\Omega_{0,l+1/2,i+1}}{\omega_b}\right]\widetilde{\overline{D}}^{\mathrm{RF}(0)\mathrm{F}}_{b,n,l+1/2,i+1,j+1/2}\\
\widetilde{F}^{\mathrm{RF}(0)}_{p,l+1/2,i,j+1/2} &= \frac{\sqrt{1-\xi^2_{0,j+1/2}}}{p_i\xi^3_{0,j+1/2}}\textstyle\sum_{n=-\infty}^{+\infty}\sum_b -\frac{\sqrt{1-\xi^2_{0,j+1/2}}}{\xi_{0,j+1/2}}\left[1-\xi^2_{0,j+1/2}-\frac{n\Omega_{0,l+1/2,i}}{\omega_b}\right]\widetilde{\overline{D}}^{\mathrm{RF}(0)\mathrm{F}}_{b,n,l+1/2,i,j+1/2}\\
\widetilde{F}^{\mathrm{RF}(0)}_{\xi,l+1/2,i+1/2,j+1} &= \frac{\sqrt{1-\xi^2_{0,j+1}}}{p_{i+1/2}\xi^3_{0,j+1}}\textstyle\sum_{n=-\infty}^{+\infty}\sum_b \frac{1}{\xi^2_{0,j+1}}\left[1-\xi^2_{0,j+1}-\frac{n\Omega_{0,l+1/2,i+1/2}}{\omega_b}\right]^2\widetilde{\overline{D}}^{\mathrm{RF}(0)\mathrm{F}}_{b,n,l+1/2,i+1/2,j+1}\\
\widetilde{F}^{\mathrm{RF}(0)}_{\xi,l+1/2,i+1/2,j} &= \frac{\sqrt{1-\xi^2_{0,j}}}{p_{i+1/2}\xi^3_{0,j}}\textstyle\sum_{n=-\infty}^{+\infty}\sum_b \frac{1}{\xi^2_{0,j}}\left[1-\xi^2_{0,j}-\frac{n\Omega_{0,l+1/2,i+1/2}}{\omega_b}\right]^2\widetilde{\overline{D}}^{\mathrm{RF}(0)\mathrm{F}}_{b,n,l+1/2,i+1/2,j}
\end{aligned} \tag{5.389}$$

where quasilinear diffusion coefficients $\widetilde{\overline{D}}^{\mathrm{RF}(0)\mathrm{D}}_{b,n,l+1/2,i+1/2,j+1/2}$ and $\widetilde{\overline{D}}^{\mathrm{RF}(0)\mathrm{F}}_{b,n,l+1/2,i+1/2,j+1/2}$ are

$$\begin{aligned}
\widetilde{\overline{D}}^{\mathrm{RF}(0)\mathrm{D}}_{b,n,l+1/2,i+1/2,j+1/2} = {}& \frac{\gamma_{i+1/2}p_{Te}}{p_{i+1/2}\left|\xi_{0,j+1/2}\right|}\frac{1}{\lambda^{l+1/2,j+1/2}\widetilde{q}_{l+1/2}}\frac{r_{\theta_{b,l+1/2}}}{R_p}\frac{B^{\theta_b}_{l+1/2}}{B^{\theta_b}_{P,l+1/2}}\frac{\xi_{0,j+12}}{\xi_{\theta_b,l+1/2,j+1/2}}\\
&\times\overline{D}^{\mathrm{RF},\theta_b}_{b,n,0,l+12}H\left(\theta_b-\theta_{\min}\right)H\left(\theta_{\max}-\theta_b\right)\\
&\times\left[\frac{1}{2}\sum_\sigma\right]_T\delta\left(N_{b\|}-N^{\theta_b}_{\|\mathrm{res},l+1/2,i+1/2,j+1/2}\right)\left|\Theta^{b,(n)}_{\mathbf{k},\theta_b,l+1/2,i+1/2,j+1/2}\right|^2
\end{aligned} \tag{5.390}$$

$$\underset{\sim}{\overline{D}}^{\mathrm{RF(0)F}}_{b,n,l+1/2,i+1/2,j+1/2} = \frac{\gamma_{i+1/2} p_{Te}}{p_{i+1/2} \left|\xi_{0,j+1/2}\right|} \frac{1}{\lambda^{l+1/2,j+1/2} \widetilde{q}_{l+1/2}} \frac{r_{\theta_{b,l+1/2}}}{R_p} \frac{B^{\theta_b}_{l+1/2}}{B^{\theta_b}_{P,l+1/2}} \frac{\xi^3_{0,j+1/2}}{\xi^3_{\theta_{bl+1/2,j+1/2}}}$$
$$\times \left(\Psi^{\theta_b}_{l+1/2} - 1\right) \overline{D}^{\mathrm{RF},\theta_b}_{b,n,0,l+12} H\left(\theta_b - \theta_{\min}\right) H\left(\theta_{\max} - \theta_b\right)$$
$$\times \left[\frac{1}{2}\sum_{\sigma}\right]_T \delta\left(N_{b\|} - N^{\theta_b}_{\|\mathrm{res},l+1/2,i+1/2,j+1/2}\right) \left|\Theta^{b,(n)}_{\mathbf{k},\theta_b,l+1/2,i+1/2,j+1/2}\right|^2 \tag{5.391}$$

Here $\overline{D}^{\mathrm{RF},\theta_b}_{b,n,0,l+12}$, $N^{\theta_b}_{\|\mathrm{res},l+1/2,i+1/2,j+1/2}$, $\Theta^{b,(n)}_{\mathbf{k},\theta_b,l+1/2,i+1/2,j+1/2}$ are similar to the case of the quasilinear diffusion coefficient for the zero-order Fokker-Planck equation, and are therefore given in Sec. 5.4.6. The definition of coefficients $\Omega_{0,l+1/2,i+1/2}$, $r_{\theta_{b,l+1/2}}$, $B^{\theta_b}_{l+1/2}$, $B^{\theta_b}_{P,l+1/2}$, $\xi^2_{\theta_b,l+1/2}$ and $\Psi_{\theta_b,l+1/2}$ are also given in the same section.

All coefficients corresponding to different indexes may be obtained readily by performing the adequate index transformation, $i+1/2 \rightarrow (i, i+1)$ and $j+1/2 \rightarrow (j, j+1)$

5.6 Initial solution

5.6.1 Zero order term: the Fokker-Planck equation

Basically, the determination of the steady-state electron distribution function is an initial value problem, where the initial guess corresponds usually to the unperturbed solution of the linearized problem. For the zero-order Fokker-Planck equation, the Maxwellian distribution function is therefore by definition an eigenfunction of the collision operator, without external perturbation. Here the weakly relativistic solution corresponding to the condition on the relativistic factor $\gamma - 1 \ll 1$ is considered at time $t = 0$,

$$f_M(\psi, p) \simeq \frac{n_e(\psi)}{\left[2\pi T_e(\psi)\right]^{3/2}} \exp\left[-\frac{p^2}{(1+\gamma) T_e(\psi)}\right] \tag{5.392}$$

where $T_e(\psi)$ and $n_e(\psi)$ are the electron temperature and density respectively. Details on the notation are given in Sec. 6.3.1. Projected on the numerical grids, as defined in Sec.5.2, the discrete form is

$$f_{M,l+1/2,i+1/2,j+1/2} \simeq \frac{n_{e,l+1/2}}{\left[2\pi T_{e,l+1/2}\right]^{3/2}} \exp\left[-\frac{p^2_{i+1/2}}{\left(1+\gamma_{i+1/2}\right) T_{e,l+1/2}}\right] \tag{5.393}$$

When the Lower Hybrid current drive problem is addressed, it is possible to start from a guess that already incorporate the existence of a plateau region, using the formulation given in Ref. [23] in the non-relativistic limit. When relativistic corrections must be considered, the effective perpendicular temperature $T_\perp$ in the resonance domain must be usualy multipled by 2. Though this elegant approach seems attractive in order to reduce the total number of iterations for reaching the steady-state solution, its effectiveness is usualy poor when large time step Δt are considered. Indeed, the total number of time steps is merely determined by the relaxation time of the most energetic part of the fast electron

tail prodiced by the wave. Since electrons are very weakly collisional, their relaxation time is very long as compared to the thermal one. Therefore, the gain for the rate of convergence is usually very small since the distribution model does not describe accurately the region above the plateau of the momentum space. Consequently, even if this method is implemented in the code, it is almost never used.

5.6.2 Up to first order term: the Drift Kinetic equation

First order distribution function The initial distribution function for the first order drift kinetic equation is determined in the non-relativistic limit using the simplified Lorentz collision model corresponding to $Z_i \gg 1$ and $T_i = 0$, as introduced in Sec. 4.1.4. In that case, the bounce-averaged collision operator reduces to

$$\left\{\nabla_{\mathbf{p}} \cdot \mathbf{S}_{\mathbf{p}}\left(f_1\right)\right\}_{\mathcal{L}} = -\frac{p}{\lambda}\frac{\partial}{\partial \xi_0}\left(\sqrt{1-\xi_0^2}\lambda \widetilde{S}^{(0)}_{\xi_0,\mathcal{L}}\right) - \frac{p}{\lambda}\frac{\partial}{\partial \xi_0}\left(\sqrt{1-\xi_0^2}\lambda S^{(0)}_{\xi_0,\mathcal{L}}\right) \tag{5.394}$$

and in the steady-state regime $\left\{\nabla_{\mathbf{p}} \cdot \mathbf{S}_{\mathbf{p}}\left(f_1\right)\right\}_{\mathcal{L}} = 0$, so that the equation to be solved is simply

$$\frac{\partial}{\partial \xi_0}\left(\sqrt{1-\xi_0^2}\lambda S^{(0)}_{\xi_0,\mathcal{L}}\right) = -\frac{\partial}{\partial \xi_0}\left(\sqrt{1-\xi_0^2}\lambda \widetilde{S}^{(0)}_{\xi_0,\mathcal{L}}\right) \tag{5.395}$$

where

$$\widetilde{S}^{(0)}_{\xi_0,\mathcal{L}} = \sigma\left\{\frac{\sigma\xi}{\sqrt{\Psi}\xi_0} S_{\xi,\mathcal{L}}\left(\widetilde{f}\right)\right\} \tag{5.396}$$

and

$$S^{(0)}_{\xi_0,\mathcal{L}} = \sigma\left\{\frac{\sigma\xi}{\sqrt{\Psi}\xi_0} S_{\xi,\mathcal{L}}\left(g\right)\right\} \tag{5.397}$$

as defined in Sec.3.5.5.

Since only pitch-angle scattering takes place in this limit, $\widetilde{S}^{(0)}_{\xi_0,\mathcal{L}}$ may be expressed in a very simple form

$$\widetilde{S}^{(0)}_{\xi_0,\mathcal{L}} = \frac{\sqrt{1-\xi_0^2}}{p}\widetilde{D}^{\mathrm{C}(0)}_{\xi\xi,\mathcal{L}}\frac{\partial \widetilde{f}^{(0)}}{\partial \xi_0} \tag{5.398}$$

since $F^C_\xi = D^C_{\xi p} = 0$ for collisions with

$$\widetilde{D}^{\mathrm{C}(0)}_{\xi\xi,\mathcal{L}} = \sigma\left\{\frac{\sigma\xi^3}{\Psi^2\xi_0^3} D^{\mathrm{C}}_{\xi\xi,\mathcal{L}}\right\} \tag{5.399}$$

while

$$S^{(0)}_{\xi_0,\mathcal{L}} = \frac{\sqrt{1-\xi_0^2}}{p} D^{\mathrm{C}(0)}_{\xi\xi,\mathcal{L}}\frac{\partial g^{(0)}}{\partial \xi_0} \tag{5.400}$$

with

$$D^{\mathrm{C}(0)}_{\xi\xi,\mathcal{L}} = \left\{\frac{\xi^2}{\Psi\xi_0^2} D^{\mathrm{C}}_{\xi\xi,\mathcal{L}}\right\} \tag{5.401}$$

where $D^{\mathrm{C}}_{\xi\xi,\mathcal{L}} = B^{\mathcal{L}}_t$ according usual notation given in Sec.4.1.4.

The differential equation to be solved is then

$$\frac{\partial}{\partial\xi_0}\left(\left(1-\xi_0^2\right)\lambda D^{\mathrm{C}(0)}_{\xi\xi,\mathcal{L}}\frac{\partial g^{(0)}}{\partial\xi_0}\right)=-\frac{\partial}{\partial\xi_0}\left(\left(1-\xi_0^2\right)\lambda \widetilde{D}^{\mathrm{C}(0)}_{\xi\xi,\mathcal{L}}\frac{\partial \widetilde{f}^{(0)}}{\partial\xi_0}\right) \tag{5.402}$$

starting from the known expression of $\partial\widetilde{f}^{(0)}/\partial\xi_0$. In the Lorentz limit, since $B_t^{\mathcal{L}}$ is simply set to 1/2, expressions of $D^{\mathrm{C}(0)}_{\xi\xi,\mathcal{L}}$ and $\widetilde{D}^{\mathrm{C}(0)}_{\xi\xi,\mathcal{L}}$ are obtained in a straightforward manner,

$$D^{\mathrm{C}(0)}_{\xi\xi,\mathcal{L}}=\frac{1}{2}\left\{\frac{\xi^2}{\Psi\xi_0^2}\right\}=\frac{1}{2}\frac{\lambda_{2,-1,0}}{\lambda} \tag{5.403}$$

and

$$\widetilde{D}^{\mathrm{C}(0)}_{\xi\xi,\mathcal{L}}=\frac{1}{2}\sigma\left\{\frac{\sigma\xi^3}{\Psi^2\xi_0^3}\right\}=\frac{1}{2}\frac{\overline{\lambda}_{3,-2,0}}{\lambda} \tag{5.404}$$

and $g^{(0)}$ is given by the simple equation

$$\frac{\partial}{\partial\xi_0}\left(\left(1-\xi_0^2\right)\lambda_{2,-1,0}\frac{\partial g^{(0)}}{\partial\xi_0}\right)=-\frac{\partial}{\partial\xi_0}\left(\left(1-\xi_0^2\right)\overline{\lambda}_{3,-2,0}\frac{\partial \widetilde{f}^{(0)}}{\partial\xi_0}\right) \tag{5.405}$$

If the solution of the zero-order Fokker-Planck equation is the Maxwellian

$$f_0^{(0)}=f_M\simeq\frac{n_e}{\left[2\pi T_e\right]^{3/2}}\exp\left[-\frac{p^2}{2T_e}\right] \tag{5.406}$$

its spatial derivative is

$$\frac{\partial f_0^{(0)}}{\partial\psi}=\left[\frac{d\ln n_e}{d\psi}+\left(\frac{p^2}{2T_e}-\frac{3}{2}\right)\frac{d\ln T_e}{d\psi}\right]f_M \tag{5.407}$$

and from the definition of $\widetilde{f}^{(0)}$ given in Sec.3.4,

$$\begin{aligned}\widetilde{f}^{(0)} &= \frac{p\xi_0 I\left(\psi\right)}{q_e B_0}\frac{\partial f_0^{(0)}(\psi,p,\xi_0)}{\partial\psi}\\ &= \frac{p\xi_0 I\left(\psi\right)}{q_e B_0}\left[\frac{d\ln n_e}{d\psi}+\left(\frac{p^2}{2T_e}-\frac{3}{2}\right)\frac{d\ln T_e}{d\psi}\right]f_M\end{aligned} \tag{5.408}$$

Projected on the numerical grids, the discrete form of $\widetilde{f}^{(0)}$ is

$$\begin{aligned}\widetilde{f}^{(0)}_{l+1/2,i+1/2,j+1/2} &= \frac{p_{i+1/2}\xi_{0,j+1/2}I_{l+1/2}}{q_e B_{0,l+1/2}}\left[\left.\frac{d\ln n_e}{d\psi}\right|_{l+1/2}\right.\\ &\quad\left.+\left(\frac{p^2_{i+1/2}}{2T_{e,l+1/2}}-\frac{3}{2}\right)\left.\frac{d\ln T_e}{d\psi}\right|_{l+1/2}\right]f_{M,l+1/2,i+1/2,j+1/2}\end{aligned} \tag{5.409}$$

where radial derivatives are performed as discussed in Sec. 5.5.1.

Since f_M is by definition independent of ξ_0,

$$\begin{aligned}\frac{\partial \widetilde{f}^{(0)}}{\partial \xi_0} &= \frac{pI(\psi)}{q_e B_0}\left[\frac{d\ln n_e}{d\psi}+\left(\frac{p^2}{2T_e}-\frac{3}{2}\right)\frac{d\ln T_e}{d\psi}\right] f_M \\ &= \Xi(\psi,p)\, f_M \end{aligned} \tag{5.410}$$

where

$$\Xi(\psi,p) = \frac{pI(\psi)}{q_e B_0}\left[\frac{d\ln n_e}{d\psi}+\left(\frac{p^2}{2T_e}-\frac{3}{2}\right)\frac{d\ln T_e}{d\psi}\right] \tag{5.411}$$

the equation becomes

$$\left(1-\xi_0^2\right)\lambda_{2,-1,0}\frac{\partial g^{(0)}}{\partial \xi_0} = -\Xi(\psi,p)\, f_M\left(1-\xi_0^2\right)\overline{\lambda}_{3,-2,0} + C \tag{5.412}$$

Assuming $\partial g^{(0)}/\partial\xi_0$ is finite at $|\xi_0|=1$, $C=0$, and

$$\begin{aligned}\frac{\partial g^{(0)}}{\partial \xi_0} &= -\Xi(\psi,p)\, f_M \frac{\overline{\lambda}_{3,-2,0}}{\lambda_{2,-1,0}} \\ &= -\Xi(\psi,p)\, f_M \frac{\lambda_{3,-2,0}}{\lambda_{2,-1,0}} H\left(|\xi_0|-\xi_{0T}\right)\end{aligned} \tag{5.413}$$

using the definition of $\overline{\lambda}_{n,m,p}$ given in Sec. 2.2.1. By definition, $\overline{\lambda}_{3,-2,0}$ is an even function of ξ_0, and therefore $g^{(0)}$ must be an odd function ξ_0. Since furthermore $g^{(0)}$ is an even function of ξ_0, $g^{(0)}=0$ in the trapped region. Integrating in the region $-\xi_0 \le \xi_{0T}$,

$$\begin{aligned}g^{(0)}(\psi,p,\xi_0) &= -\Xi(\psi,p)\, f_M \int_{-\xi_{0T}}^{\xi_0} \frac{\overline{\lambda}_{3,-2,0}}{\lambda_{2,-1,0}} d\xi_0' \\ &= \Xi(\psi,p)\, f_M \int_{\xi_{0T}}^{-\xi_0} \frac{\overline{\lambda}_{3,-2,0}}{\lambda_{2,-1,0}} d\xi_0''\end{aligned} \tag{5.414}$$

using the relation $\xi_0'' = -\xi_0'$. Performing the same operation in the region $\xi_0 \ge \xi_{0T}$, one obtains

$$g^{(0)}(\psi,p,\xi_0) = -\Xi(\psi,p)\, f_M \int_{\xi_{0T}}^{\xi_0} \frac{\overline{\lambda}_{3,-2,0}}{\lambda_{2,-1,0}} d\xi_0' \tag{5.415}$$

and gathering results

$$\begin{aligned}g^{(0)}(\psi,p,\xi_0) &= -\sigma H\left(|\xi_0|-\xi_{0T}\right)\Xi(\psi,p)\, f_M \int_{\xi_{0T}}^{|\xi_0|} \frac{\overline{\lambda}_{3,-2,0}}{\lambda_{2,-1,0}} d\xi_0' \\ &= -\sigma H\left(|\xi_0|-\xi_{0T}\right)\Xi(\psi,p)\, I_{\mathcal{L}}(\psi,|\xi_0|)\, f_M\end{aligned} \tag{5.416}$$

where

$$I_{\mathcal{L}}(\psi,|\xi_0|) = \int_{\xi_{0T}}^{|\xi_0|} \frac{\overline{\lambda}_{3,-2,0}(\psi,\xi_0')}{\lambda_{2,-1,0}(\psi,\xi_0')} d\xi_0' \tag{5.417}$$

The discrete form of $g^{(0)}(\psi,p,\xi_0)$ is

$$\begin{aligned}g^{(0)}_{l+1/2,i+1/2,j+1/2} &= -\sigma_{j+1/2} H\left(\left|\xi_{0,j+1/2}\right|-\xi_{0T,l+1/2}\right) \\ &\quad\times \Xi_{l+1/2,i+1/2} I_{\mathcal{L}}\left(\psi_{l+1/2},\left|\xi_{0,j+1/2}\right|\right) f_{M,l+1/2,i+1/2,j+1/2}\end{aligned} \tag{5.418}$$

with

$$I_{\mathcal{L}}\left(\psi_{l+1/2},\left|\xi_{0,j+1/2}\right|\right)=\sum_{j'=j_{T,l+1/2}^{+}-n_{\xi_{0T},l+1/2}}^{j'=j-n_{\xi_{0T},l+1/2}}\frac{\overline{\lambda}_{3,-2,0}^{l+1/2,j'+1/2}}{\lambda_{2,-1,0}^{l+1/2,j'+1/2}}\Delta\xi_{0,j'+1/2} \tag{5.419}$$

and $j>j_{T,l+1/2}^{+}$.

Case of circular concentric flux surfaces According to Sec. 4.1.5,

$$\overline{\lambda}_{3,-2,0}=\frac{H(|\xi_0|-\xi_{0T})}{(1+\epsilon)\,\xi_0^2}\left(\xi_0^2-\frac{\epsilon\,(1-\epsilon/2)}{(1+\epsilon)}\right) \tag{5.420}$$

and Sec. 4.1.4

$$\lambda_{2,-1,0}=\lambda\left(1-\frac{\Delta_b}{\xi_0^2}\right) \tag{5.421}$$

The integral $I_{\mathcal{L}}\left(\psi,\xi_0\right)$ then becomes

$$I_{\mathcal{L}}\left(\psi,|\xi_0|\right)=\int_{\xi_{0T}}^{|\xi_0|}\frac{\left(\xi_0'^2-\epsilon\,(1-\epsilon/2)\,/\,(1+\epsilon)\right)}{\lambda\left(1-\Delta_b/\xi_0'^2\right)(1+\epsilon)\,\xi_0'^2}d\xi_0' \tag{5.422}$$

and in the low inverse aspect ratio limit $\epsilon\ll 1$, one finds

$$I_{\mathcal{L}}\left(\psi,|\xi_0|\right)\simeq\frac{1}{1+\epsilon}\int_{\xi_{0T}}^{|\xi_0|}\frac{d\xi_0'}{\lambda\left(1-\Delta_b/\xi_0'^2\right)} \tag{5.423}$$

the expression that was first given in Ref. [3].

Flux surface averaged bootstrap current According to Sec. 3.6, the flux-averaged electron bootstrap current in the Lorentz model is given by the relation

$$\left\langle J_{\parallel,\mathcal{L}}\right\rangle(\psi)=\left\langle\widetilde{J}_{\parallel,\mathcal{L}}\right\rangle_{\phi}^{1}(\psi)+\left\langle J_{\parallel,\mathcal{L}}\right\rangle_{\phi}^{1}(\psi) \tag{5.424}$$

where

$$\left\langle\widetilde{J}_{\parallel,\mathcal{L}}\right\rangle_{\phi}^{1}(\psi)=2\pi q_e\frac{\widetilde{q}}{\overline{q}}\frac{R_p}{R_0}\frac{B_{T0}}{B_0}\int_0^{\infty}dp\;p^3\int_{-1}^{1}\lambda_{2,-2,2}\xi_0\widetilde{f}^{(0)}d\xi_0 \tag{5.425}$$

and

$$\left\langle J_{\parallel,\mathcal{L}}\right\rangle_{\phi}^{1}(\psi)=2\pi q_e\frac{q}{\overline{q}}\int_0^{\infty}dp\;p^3\int_{-1}^{1}H\left(|\xi_0|-\xi_{0T}\right)\;\xi_0 g^{(0)}d\xi_0 \tag{5.426}$$

in the non-relativistic limit $\gamma\to 1$. Therefore,

$$\begin{aligned}\left\langle\widetilde{J}_{\parallel,\mathcal{L}}\right\rangle_{\phi}^{1}(\psi) &= 2\pi\frac{\widetilde{q}}{\overline{q}}\frac{R_p}{R_0}\frac{B_{T0}}{B_0^2}I\left(\psi\right)\times\\ &\int_0^{\infty}\left[\frac{d\ln n_e}{d\psi}+\left(\frac{p^2}{2T_e}-\frac{3}{2}\right)\frac{d\ln T_e}{d\psi}\right]\;p^4 f_M dp\int_{-1}^{1}\xi_0^2\lambda_{2,-2,2}d\xi_0\end{aligned} \tag{5.427}$$

and

$$\left\langle J_{\parallel,\mathcal{L}}\right\rangle_{\phi}^{1}(\psi) = -2\pi\frac{q}{\overline{q}}\frac{I(\psi)}{B_0}\times\int_0^{\infty}\left[\frac{d\ln n_e}{d\psi}+\left(\frac{p^2}{2T_e}-\frac{3}{2}\right)\frac{d\ln T_e}{d\psi}\right]p^4 f_M dp \int_{-1}^{1}\sigma H\left(|\xi_0|-\xi_{0T}\right)\ \xi_0 I_{\mathcal{L}}\left(\psi,|\xi_0|\right)d\xi_0 \tag{5.428}$$

Using relation $R_0 B_{T0} = I(\psi)$, one obtains

$$\left\langle \widetilde{J}_{\parallel,\mathcal{L}}\right\rangle_{\phi}^{1}(\psi) = 2\pi R_p\frac{\widetilde{q}}{\overline{q}}\frac{B_{T0}^2}{B_0^2}\times \int_0^{\infty}\left[\frac{d\ln n_e}{d\psi}+\left(\frac{p^2}{2T_e}-\frac{3}{2}\right)\frac{d\ln T_e}{d\psi}\right]p^4 f_M dp\int_{-1}^{1}\xi_0^2\lambda_{2,-2,2}d\xi_0 \tag{5.429}$$

and

$$\left\langle J_{\parallel,\mathcal{L}}\right\rangle_{\phi}^{1}(\psi) = -2\pi\frac{q}{\overline{q}}R_0\frac{B_{T0}}{B_0}\times\int_0^{\infty}\left[\frac{d\ln n_e}{d\psi}+\left(\frac{p^2}{2T_e}-\frac{3}{2}\right)\frac{d\ln T_e}{d\psi}\right]p^4 f_M dp \int_{-1}^{1}\sigma H\left(|\xi_0|-\xi_{0T}\right)\ \xi_0 I_{\mathcal{L}}\left(\psi,|\xi_0|\right)d\xi_0 \tag{5.430}$$

Since

$$2\pi\int_0^{\infty}\left[\frac{d\ln n_e}{d\psi}+\left(\frac{p^2}{2T_e}-\frac{3}{2}\right)\frac{d\ln T_e}{d\psi}\right]p^4 f_M dp = \frac{3}{2}n_e T_e\left(\frac{d\ln n_e}{d\psi}+\frac{d\ln T_e}{d\psi}\right) \tag{5.431}$$

using the definite integral relation in Ref. [18],

$$\int_0^{\infty}x^{2n}\exp\left(-px^2\right) = \frac{(2n-1)!!}{2\left(2p\right)^n}\sqrt{\frac{\pi}{p}} \tag{5.432}$$

where $(2n-1)!! = 1.3.5...\times(2n-1)$,

$$\left\langle \widetilde{J}_{\parallel,\mathcal{L}}\right\rangle_{\phi}^{1}(\psi) = \frac{\widetilde{q}}{\overline{q}}R_p\frac{B_{T0}^2}{B_0^2}\frac{3}{2}n_e T_e\left(\frac{d\ln n_e}{d\psi}+\frac{d\ln T_e}{d\psi}\right)\times \int_{-1}^{1}\xi_0^2\lambda_{2,-2,2}d\xi_0 \tag{5.433}$$

and

$$\left\langle J_{\parallel,\mathcal{L}}\right\rangle_{\phi}^{1}(\psi) = -\frac{q}{\overline{q}}R_0\frac{B_{T0}}{B_0}\frac{3}{2}n_e T_e\left(\frac{d\ln n_e}{d\psi}+\frac{d\ln T_e}{d\psi}\right)\times \int_{-1}^{1}\sigma H\left(|\xi_0|-\xi_{0T}\right)\ \xi_0 I_{\mathcal{L}}\left(\psi,|\xi_0|\right)d\xi_0 \tag{5.434}$$

Finally,

$$\left\langle \widetilde{J}_{\parallel,\mathcal{L}}\right\rangle(\psi) = \mathcal{F}_t^{eff.}(\psi)\, n_e T_e R_p\left(\frac{d\ln n_e}{d\psi}+\frac{d\ln T_e}{d\psi}\right) \tag{5.435}$$

where the flux surface function usualy named "effective trapped fraction" $\mathcal{F}_t^{eff.}(\psi)$ is

$$\begin{aligned}\mathcal{F}_t^{eff.}(\psi) &= \frac{3}{2}\frac{B_{T0}}{B_0}\times \\ &\left[\frac{\widetilde{q}}{\overline{q}}\frac{B_{T0}}{B_0}\int_{-1}^{1}\xi_0^2\lambda_{2,-2,2}d\xi_0-\frac{q}{\overline{q}}\frac{R_0}{R_p}\int_{-1}^{1}\sigma H\left(|\xi_0|-\xi_{0T}\right)\ \xi_0 I_{\mathcal{L}}\left(\psi,|\xi_0|\right)d\xi_0\right]\end{aligned} \tag{5.436}$$

In the case of circular concentric flux surfaces,

$$\frac{R_0}{R_p}=1+\epsilon \tag{5.437}$$

$$\frac{\widetilde{q}}{\overline{q}}=1+\epsilon \tag{5.438}$$

and

$$\frac{q}{\overline{q}}=\frac{B_{T0}}{B_0}\sqrt{\frac{1+\epsilon}{1-\epsilon}} \tag{5.439}$$

as shown in Sec. 3.6. Therefore,

$$\left\langle\widetilde{J}_{\parallel,\mathcal{L}}\right\rangle(r)=\mathcal{F}_t^{eff.}(r)\,n_eT_e\frac{R_p}{|\nabla\psi|_0}\left(\frac{d\ln n_e}{dr}+\frac{d\ln T_e}{dr}\right) \tag{5.440}$$

and using the relations $R_0B_{P0}=|\nabla\psi|_0$, and $R_0B_{T0}=I(r)$,

$$\left\langle\widetilde{J}_{\parallel,\mathcal{L}}\right\rangle(r)=\frac{\mathcal{F}_t^{eff.}(r)}{B_T}n_eT_e\frac{B_{T0}}{B_{P0}}\left(\frac{d\ln n_e}{dr}+\frac{d\ln T_e}{dr}\right) \tag{5.441}$$

where $R_pB_T=I(r)$. Hence,

$$\begin{aligned}&\mathcal{F}_t^{eff.}(r)=\frac{3}{2}(1+\epsilon)\left(\frac{B_{T0}}{B_0}\right)^2 \\ &\left[\int_{-1}^{1}\xi_0^2\lambda_{2,0,0}d\xi_0-\sqrt{\frac{1+\epsilon}{1-\epsilon}}\int_{-1}^{1}\sigma H\left(|\xi_0|-\xi_{0T}\right)\ \xi_0 I_{\mathcal{L}}\left(r,|\xi_0|\right)d\xi_0\right]\end{aligned} \tag{5.442}$$

and since $R_0/R=\Psi$, $\lambda_{2,-2,2}=\lambda_{2,0,0}$, as shown in Sec. 3.6. In the limit $B_p\ll B_T$, further simplifications may be carried out and

$$\lim_{\epsilon\to 0}\mathcal{F}_t^{eff.}(r)\simeq\frac{3}{2}(1+\epsilon)\left[\int_{-1}^{1}\xi_0^2\lambda_{2,0,0}d\xi_0-\sqrt{\frac{1+\epsilon}{1-\epsilon}}\int_{-1}^{1}\sigma H\left(|\xi_0|-\xi_{0T}\right)\ \xi_0 I_{\mathcal{L}}\left(r,|\xi_0|\right)d\xi_0\right] \tag{5.443}$$

The first term in the square bracket may be evaluated analyticaly. Indeed

$$\begin{aligned}\int_{-1}^{1}\xi_0^2\lambda_{2,0,0}d\xi_0 &= \frac{1}{\widetilde{q}}\int_{-1}^{1}\xi_0^2d\xi_0\left[\frac{1}{2}\sum_{\sigma}\right]_T\int_0^{2\pi}\frac{d\theta}{2\pi}\epsilon\frac{B}{B_P}\frac{\xi_0}{\xi}\frac{\xi^2}{\xi_0^2} \\ &= \int_{-1}^{1}d\xi_0\left[\frac{1}{2}\sum_{\sigma}\right]_T\int_0^{2\pi}\frac{d\theta}{2\pi}\xi_0\xi\end{aligned} \tag{5.444}$$

since B/B_P is only function of r and $\widetilde{q} = \epsilon B/B_P$. The sum over trapped electrons may be dropped, since $\xi_0\xi$ is independent of σ. Therefore,

$$\begin{aligned}\int_{-1}^{1} \xi_0^2 \lambda_{2,0,0} d\xi_0 &= \int_{-1}^{1} d\xi_0 \int_0^{2\pi} \frac{d\theta}{2\pi} \xi_0 \xi \\ &= \int_0^{2\pi} \frac{d\theta}{2\pi} \int_{-1}^{1} \xi_0 \xi H\left(|\xi_0| - \sqrt{1 - \frac{1}{\Psi}}\right) d\xi_0 \end{aligned} \tag{5.445}$$

which means that only particles who reach the position θ must be considered. Since

$$\begin{aligned}\int_{-1}^{1} \xi_0 \xi H\left(|\xi_0| - \sqrt{1 - \frac{1}{\Psi}}\right) d\xi_0 &= 2\int_{\sqrt{1-\frac{1}{\Psi}}}^{1} \xi_0 \xi d\xi_0 \\ &= 2\int_{\sqrt{1-\frac{1}{\Psi}}}^{1} \xi_0 \sqrt{1 - \Psi\left(1 - \xi_0^2\right)} d\xi_0 \\ &= \frac{2}{3}\frac{1}{\Psi} \end{aligned} \tag{5.446}$$

and

$$\begin{aligned}\int_0^{2\pi} \frac{d\theta}{2\pi} \frac{2}{3} \frac{1}{\Psi} &= \frac{2}{3} \int_0^{2\pi} \frac{d\theta}{2\pi} \frac{2}{3} \frac{1 + \epsilon\cos\theta}{1 + \epsilon} \\ &= \frac{2}{3} \frac{1}{1 + \epsilon} \end{aligned} \tag{5.447}$$

Consequently,

$$\int_{-1}^{1} \xi_0^2 \lambda_{2,0,0} d\xi_0 = \frac{2}{3} \frac{1}{1 + \epsilon} \tag{5.448}$$

and using the

$$\begin{aligned}\lim_{\epsilon \to 0} \mathcal{F}_t^{eff.}(r) &\simeq 1 - \frac{3}{2}\sqrt{\frac{1}{1 - \epsilon^2}} \int_{-1}^{1} \sigma H\left(|\xi_0| - \xi_{0T}\right) \xi_0 I_{\mathcal{L}}\left(r, |\xi_0|\right) d\xi_0 \\ &\simeq 1 - \frac{3}{2}\int_{-1}^{1} \sigma H\left(|\xi_0| - \xi_{0T}\right) \xi_0 I_{\mathcal{L}}\left(r, |\xi_0|\right) d\xi_0 \end{aligned} \tag{5.449}$$

It can be shown in Appendix C after lengthly calculations, that

$$\lim_{\epsilon \to 0} \mathcal{F}_t^{eff.}(r) \simeq K\sqrt{\epsilon} + \mathcal{O}(\epsilon) \tag{5.450}$$

where

$$K = \frac{3\sqrt{2}}{2}\left[1 - \sum_{m}^{\infty}\sum_{i_1}^{\infty}\sum_{i_2}^{\infty} ... \sum_{i_m}^{\infty} \frac{C_{i_1} C_{i_2} ... C_{i_m}}{2^{i_1 + i_2 + ... + i_m}\left[2\left(i_1 + i_2 + ... + i_m\right) - 1\right]}\right] \tag{5.451}$$

with

$$C_n = \frac{\left[(2n)!\right]^2}{(2n - 1)\, 2^{3n}\, (n!)^4} \tag{5.452}$$

A rather fast convergence is obtained with m, and for $m = n = 6$, $K \simeq 1.467$, the usual value found in the litterature on neoclassical theory.

5.7 Boundary conditions

5.7.1 Zero order term: the Fokker-Planck equation

Momentum dynamics

Internal boundaries Momentum dynamics is described in spherical coordinates, because collisions is the dominant physical process for current drive and matrices are therefore expected to be well conditionned. Consequently, internal boundaries must be specified at $p = 0$ and $|\xi_0| = 1$ which correspond to the condition

$$f_0^{(0)}(\psi, -p, \xi_0) = f_0^{(0)}(\psi, p, -\xi_0) \tag{5.453}$$

Here Neumann type boundary conditions are used, and therefore only gradients must be specified at the internal boundaries[4]. One must thus determine $(\Delta p, \Delta\xi_0)$ at $p = 0$ and $|\xi_0| = 1$ for the flux grid only, since the distribution and flux grids are interlaced by definition. Therefore, starting from grids definition given in Sec. 5.2,

$$\Delta\xi_{0,0} = \frac{\Delta\xi_{0,1/2} + \Delta\xi_{0,-1/2}}{2} = \Delta\xi_{0,1/2} = \xi_{0,1} - \xi_{0,0} = 2\left(\xi_{0,1/2} + 1\right) \tag{5.454}$$

as $\Delta\xi_{0,1/2} = \Delta\xi_{0,-1/2}$, $\xi_{0,1/2} = \frac{\xi_{0,1}+\xi_{0,0}}{2}$et $\xi_{0,0} = -1$.

Much in the same way,

$$\Delta\xi_{0,n_\xi} = \frac{\Delta\xi_{0,n_\xi+1/2} + \Delta\xi_{0,n_\xi-1/2}}{2} = \Delta\xi_{0,n_\xi-1/2} = \xi_{0,n_\xi} - \xi_{0,n_\xi-1} = 1 - \xi_{0,n_\xi-1} \tag{5.455}$$

since $\Delta\xi_{0,n_\xi+1/2} = \Delta\xi_{0,n_\xi-1/2}$. Furthermore, since by definition,

$$\xi_{0,n_\xi-1/2} = \frac{\xi_{0,n_\xi} + \xi_{0,n_\xi-1}}{2} = \frac{1 + \xi_{0,n_\xi-1}}{2} \tag{5.456}$$

one obtains finally

$$\Delta\xi_{0,n_\xi} = 2\left(1 - \xi_{0,n_\xi-1/2}\right) \tag{5.457}$$

A similar technique may be used for the momentum grid p. Hence

$$\Delta p_0 = \frac{1}{2}\left(\Delta p_{1/2} + \Delta p_{-1/2}\right) = \Delta p_{1/2} \tag{5.458}$$

using $\Delta p_{-1/2} = \Delta p_{1/2}$. Since $\Delta p_{1/2} = p_1 - p_0$, and $p_{1/2} = \frac{p_1+p_0}{2}$ one obtains finally,

$$\Delta p_0 = 2p_{1/2} \tag{5.459}$$

because $p_0 = 0$.

[4]In some specific cases, it is possible to consider Dirichlet type boundary conditions, espcially at $p = 0$. In that case, the Maxwellian distribution function is enforced. However, in most cases, this type of condition must avoided, to keep the most general approach, and in particular to cross-check that the conservative nature of the code is well satisfied

It is important to note that internal boundary conditions are only needed in the evaluation of the cross-derivative terms, since in the discrete form of the Fokker-Planck equation using two grids, as shown, in Sec. 5.4.1, they are automatically fullfiled for other terms. Indeed, at fixed $\psi_{l+1/2}$,

$$\begin{aligned}\frac{\widetilde{q}\left(\psi\right)}{B_0\left(\psi\right)}p^2\nabla_{\mathbf{p}}\cdot\mathbf{S}_{\mathbf{p}}^{(0)}\Big|_{l+1/2,1/2,j+1/2}^{(k+1)} &= \frac{\widetilde{q}_{l+1/2}}{B_{0,l+1/2}}\left.\frac{\partial\left(p^2\mathbf{S}_p^{(0)}\right)}{\partial p}\right|_{l+1/2,1/2,j+1/2}^{(k+1)} \\ &\quad -\frac{\widetilde{q}_{l+1/2}}{B_{0,l+1/2}}\frac{p_{1/2}}{\lambda^{l+1/2,j+1/2}}\times \\ &\quad \left.\frac{\partial}{\partial\xi_0}\left(\sqrt{1-\xi_0^2}\lambda\left(\psi,\xi_0\right)\mathbf{S}_{\xi}^{(0)}\right)\right|_{l+1/2,1/2,j+1/2}^{(k+1)} \qquad (5.460)\end{aligned}$$

gives

$$\begin{aligned}\frac{\widetilde{q}\left(\psi\right)}{B_0\left(\psi\right)}p^2\nabla_{\mathbf{p}}\cdot\mathbf{S}_{\mathbf{p}}^{(0)}\Big|_{l+1/2,1/2,j+1/2}^{(k+1)} &= \frac{\widetilde{q}_{l+1/2}}{B_{0,l+1/2}}\frac{p_1^2\mathbf{S}_{p,l+1/2,1,j+1/2}^{(0)(k+1)}}{\Delta p_{1/2}} \\ &\quad -\frac{\widetilde{q}_{l+1/2}}{B_{0,l+1/2}}\frac{p_{1/2}}{\lambda^{l+1/2,j+1/2}}\times \\ &\quad \left.\frac{\partial}{\partial\xi_0}\left(\sqrt{1-\xi_0^2}\lambda\left(\psi,\xi_0\right)\mathbf{S}_{\xi}^{(0)}\right)\right|_{l+1/2,1/2,j+1/2}^{(k+1)} \qquad (5.461)\end{aligned}$$

since $p_0^2\mathbf{S}_{p,l+1/2,0,j+1/2}^{(0)(k+1)}=0$ with the flux grid here considered, at $p_0=0$. In a similar way,

$$\begin{aligned}&\frac{\widetilde{q}\left(\psi\right)}{B_0\left(\psi\right)}p^2\nabla_{\mathbf{p}}\cdot\mathbf{S}_{\mathbf{p}}^{(0)}\Big|_{l+1/2,i+1/2,1/2}^{(k+1)} \\ &= \frac{\widetilde{q}_{l+1/2}}{B_{0,l+1/2}}\left.\frac{\partial\left(p^2\mathbf{S}_p^{(0)}\right)}{\partial p}\right|_{l+1/2,i+1/2,1/2}^{(k+1)} \qquad (5.462) \\ &\quad -\frac{\widetilde{q}_{l+1/2}}{B_{0,l+1/2}}\frac{p_{i+1/2}}{\lambda^{l+1/2,j+1/2}}\times \\ &\quad \frac{\sqrt{1-\xi_{0,1}^2}\lambda\left(\psi,\xi_{0,1}\right)\mathbf{S}_{\xi,l+1/2,i+1/2,1}^{(0)(k+1)}}{\Delta\xi_{0,1/2}} \qquad (5.463)\end{aligned}$$

and

$$\begin{aligned}
&\frac{\widetilde{q}\left(\psi\right)}{B_0\left(\psi\right)}p^2\nabla_{\mathbf{p}}\cdot\mathbf{S}_{\mathbf{p}}^{(0)}\Big|_{l+1/2,i+1/2,n_{\xi_0}-1/2}^{(k+1)}\\
=\;&\frac{\widetilde{q}_{l+1/2}}{B_{0,l+1/2}}\frac{\partial\left(p^2\mathbf{S}_p^{(0)}\right)}{\partial p}\Big|_{l+1/2,i+1/2,n_{\xi_0}-1/2}^{(k+1)}\\
&+\frac{\widetilde{q}_{l+1/2}}{B_{0,l+1/2}}\frac{p_{i+1/2}}{\lambda^{l+1/2,j+1/2}}\times\\
&\frac{\sqrt{1-\xi_{0,n_{\xi_0}-1}^2}\lambda^{l+1/2,n_{\xi_0}-1}\mathbf{S}_{\xi,l+1/2,i+1/2,n_{\xi_0}-1}^{(0)(k+1)}}{\Delta\xi_{0,n_{\xi_0}-1/2}}
\end{aligned}\tag{5.464}$$

as

$$\begin{cases}\sqrt{1-\xi_{0,0}^2}\lambda^{l+1/2,0}\mathbf{S}_{\xi,l+1/2,i+1/2,0}^{(0)}=0\\ \sqrt{1-\xi_{0,n_{\xi_0}}^2}\lambda^{l+1/2,n_{\xi_0}}\mathbf{S}_{\xi,l+1/2,i+1/2,n_{\xi_0}}^{(0)}=0\end{cases}\tag{5.465}$$

with $\xi_{0,0}^2=\xi_{0,n_{\xi_0}}^2=1$

External boundaries The other boundaries are inserted into the problem in violation of the true physical picture, mainly because the momentum domain extends off to infinity, while only a subspace is considered in computations. The upper limit of the domain is therefore chosen so that the interesting physics may be accurately described, i.e. $p_{\max}\gg p_{th}$ for studying the Maxwellian distribution function, $p_{\max}\gg\gamma\left(\omega/k\right)_{\max}$ for the RF waves and $p_{\max}\gg p_{Dreicer}$ for the runaway electrons. These conditions must ensure the conservative nature of the problem here addressed, i.e. that plasma cannot enter or leave the domain of integration. This corresponds to the local condition

$$\mathbf{S}_{\mathbf{p}}\cdot\widehat{n}=0\tag{5.466}$$

where $\widehat{n}$ is the normal to the external boundary. Because of the symmetry of the collision operator, the subspace considered for computations is a sphere of radius $p_{\max}$, $\widehat{n}=\widehat{p}$. When the condition (5.466) is fullfiled, external boundary conditions have almost a negligible influence, and the numerical solution in the subspace is usually close to the theoretical one. It is usually the case for most RF problems except for the Lower Hybrid wave in very hot plasmas, since the range of resonant interaction between the wave and the electrons is well localized in momentum space, far enough from the boundary so that no electron can leave the domain of integration.

The Fokker-Planck equation reduces to an hyperbolic equation in the vicinity of $p_{\max}$ (high velocity limit), and therefore no boundary condition must be specified. In this condition, the standard upstream differencing applies. Since for collisions, $D_{pp}^{C(0)}/v\sim 1/v^4$ and $F_p^{C(0)}\sim 1/v^2$, one can consider that $D_{pp}^{C(0)}\approx 0$ at $p=p_{\max}$. Here, the pitch-angle scattering term $D_{\xi\xi}^{C(0)}$requires no special handling, because it causes diffusion in a direction which is parallel to the boundary.

Nevertheless, since cross-derivative terms potentially involves points outside the computational domain, the following rule is used, even if the exact value of $\Delta p_{\max}$ has no specific importance,

$$\Delta p_{n_p} = \Delta p_{\max} = \frac{1}{2}\left(\Delta p_{n_p+1/2} + \Delta p_{n_p-1/2}\right) = \Delta p_{n_p-1/2} = p_{n_p} - p_{n_p-1} \tag{5.467}$$

As by definition $p_{n_p+1/2} = \frac{p_{n_p}+p_{n_p-1}}{2} = \frac{p_{\max}+p_{n_p-1}}{2}$, it results

$$\Delta p_{n_p} = 2\left(p_{n_p} - p_{n_p-1/2}\right) \tag{5.468}$$

or in equivalent manner,

$$\Delta p_{\max} = 2\left(p_{\max} - p_{n_p-1/2}\right) \tag{5.469}$$

Runaway electron problem If an electric field is present, then in the real problem, some electrons will runaway and leave the domain of integration. In that case, the condition $\mathbf{S_p} \cdot \widehat{p} = 0$ is no more fullfiled, leading to an effective loss of electrons. Since the Fokker-planck differential equation is of hyperbolic type, no specific modification must be applied to the limit of the integration domain. However, one must ensure that the total number of electrons is kept constant. Several techniques may be used to avoid a decay of the number of electrons at the runaway rate $\Gamma_R^{(0)}$, as defined in Sec. 3.6.

A possibility is to perform the following substitution

$$f_0^{(0)}(t,\psi,p,\xi_0) \rightarrow f_0^{(0)}(\psi,p,\xi_0)\exp\left[-\int_0^t \frac{\Gamma_R^{(0)}(\psi,t')}{n_e(\psi)}dt'\right] \tag{5.470}$$

in the Fokker-Planck equation, so that $f_0^{(0)}(t\rightarrow\infty)$ is independent of t. In that case, the momentum matrix coefficients $\overline{\overline{M}}^{(0)}_{p,l+1/2,i+1/2,j+1/2}$ must be modified according to the prescription

$$\overline{\overline{M}}^{(0)(k)}_{p,l+1/2,i+1/2,j+1/2} \rightarrow \overline{\overline{M}}^{(0)}_{p,l+1/2,i+1/2,j+1/2} - \Gamma^{(0)(k)}_{R,l+1/2} \tag{5.471}$$

where $\Gamma^{(0)(k)}_{R,l+1/2}$ is the runaway rate calculated at $\psi_{l+1/2}$ and time step k as defined in Sec. 5.2. As a consequence, the Fokker-Planck equation becomes slightly non-linear, since $\Gamma^{(0)(k)}_{R,l+1/2}$ is an integral over the distribution function $f_0^{(0)(k)}$ determined at time step k. However, since the runaway population is usually very small as compared to the bulk, the non-linearity remains fairly weak. Nevertheless, this approach has two major drawbacks: the Fokker-Planck equation has no more an intrinsic conservative form, and in addition matrix $\overline{\overline{M}}^{(0)}_p$ must be recalculated at each time step, since it is time dependent. All the advantages of the numerical implicit time scheme for a fast and stable rate of convergence are therefore lost. For this reason, this method is not considered in the code.

Another technique is to inject cold electrons at $p = 0$, in order to compensate runaway losses and keep the electron density constant at $\psi_{l+1/2}$. Such an approach has the main advantage to have a clear physical meaning. Indeed, the loss of electrons will generate locally an electric field which in turn will force a flux of particles to compensate this local

depletion. By definition, the number of electrons leaving the integration domain is simply $\Gamma_R^{(0)}$. In principle, without particle losses, $p_0^2 S^{(0)}_{p,l+1/2,0,j+1/2} = 0$, though $S^{(0)}_{p,l+1/2,0,j+1/2}$ is infinite at $p = 0$, since, by definition, the Maxwellian distribution is an exact eigenfunction of the Fokker-Planck operator. Compensation of hot electron losses by cold ones leads to the relation

$$2\pi \sum_{j=0}^{n_{\xi_0}-1} p_0^2 S^{(0)(k+1)}_{p,l+1/2,0,j+1/2} \Delta\xi_{0,j+1/2} = \Gamma^{(0)(k+1)}_{R,l+1/2} \tag{5.472}$$

By definition, $S^{(0)(k+1)}_{p,l+1/2,0,j+1/2}$ is assumed uniform in pitch-angle, since no specific direction can be physicaly priviledged. Therefore,

$$2\pi p_0^2 S^{(0)(k+1)}_{p,l+1/2,0,j+1/2} \sum_{j=0}^{n_{\xi_0}-1} \Delta\xi_{0,j+1/2} = 4\pi p_0^2 S^{(0)(k+1)}_{p,l+1/2,0,j+1/2} = \Gamma^{(0)(k+1)}_{R,l+1/2} \tag{5.473}$$

and

$$p_0^2 S^{(0)(k+1)}_{p,l+1/2,0,j+1/2} = \frac{\Gamma^{(0)(k+1)}_{R,l+1/2}}{4\pi} \tag{5.474}$$

for all j values.

Expression (5.461) is then modified according to the relation

$$\begin{aligned}\frac{\widetilde{q}}{B_0} p^2 \nabla_{\mathbf{p}} \cdot \mathbf{S}^{(0)}_{\mathbf{p}} \Big|^{(k+1)}_{l+1/2,1/2,j+1/2} &= \frac{\widetilde{q}_{l+1/2}}{B_{0,l+1/2}} \left(\frac{p_1^2 \mathbf{S}^{(0)(k+1)}_{p,l+1/2,1,j+1/2}}{\Delta p_{1/2}} - \frac{p_0^2 \mathbf{S}^{(0)(k+1)}_{p,l+1/2,0,j+1/2}}{\Delta p_{1/2}} \right) \\ &\quad - \frac{\widetilde{q}_{l+1/2}}{B_{0,l+1/2}} \frac{p_{1/2}}{\lambda^{l+1/2,j+1/2}} \times \\ &\quad \frac{\partial}{\partial \xi_0} \left(\sqrt{1-\xi_0^2} \lambda \mathbf{S}^{(0)}_{\xi} \right) \Big|^{(k+1)}_{l+1/2,1/2,j+1/2}\end{aligned} \tag{5.475}$$

or

$$\begin{aligned}\frac{\widetilde{q}}{B_0} p^2 \nabla_{\mathbf{p}} \cdot \mathbf{S}^{(0)}_{\mathbf{p}} \Big|^{(k+1)}_{l+1/2,1/2,j+1/2} &= \frac{\widetilde{q}_{l+1/2}}{B_{0,l+1/2}} \left(\frac{p_1^2 \mathbf{S}^{(0)(k+1)}_{p,l+1/2,1,j+1/2}}{\Delta p_{1/2}} - \frac{\Gamma^{(0)(k+1)}_{R,l+1/2}}{4\pi \Delta p_{1/2}} \right) \\ &\quad - \frac{\widetilde{q}_{l+1/2}}{B_{0,l+1/2}} \frac{p_{1/2}}{\lambda^{l+1/2,j+1/2}} \times \\ &\quad \frac{\partial}{\partial \xi_0} \left(\sqrt{1-\xi_0^2} \lambda \mathbf{S}^{(0)}_{\xi} \right) \Big|^{(k+1)}_{l+1/2,1/2,j+1/2}\end{aligned} \tag{5.476}$$

Since $\Gamma^{(0)(k+1)}_{R,l+1/2}$ is a weak function of $f_0^{(0)}$, it is possible to replace $\Gamma^{(0)(k+1)}_{R,l+1/2}$ by its explicit form $\Gamma^{(0)(k)}_{R,l+1/2}$, so that one may avoid to recalculate matrix $\overline{\overline{M}}^{(0)}_{p,l+1/2,i+1/2,j+1/2}$ at each iteration, an extremely time consuming procedure. Consequently, with this scheme,

the zero order Fokker-Planck equation becomes simply

$$\begin{aligned}
&\frac{\widetilde{q}_{l+1/2}}{B_{0,l+1/2}} p_{i+1/2}^2 \frac{f_{0,l+1/2,i+1/2,j+1/2}^{(0)(k+1)} - f_{0,l+1/2,i+1/2,j+1/2}^{(0)(k)}}{\Delta t} \\
&+ \frac{\widetilde{q}}{B_0} p^2 \nabla_{\mathbf{p}} \cdot \mathbf{S}_{\mathbf{p}}^{(0)} \Big|_{l+1/2,i+1/2,j+1/2}^{(k+1)} \\
&+ \frac{\widetilde{q}}{B_0} p^2 \nabla_{\psi} \cdot \mathbf{S}_{\psi}^{(0)} \Big|_{l+1/2,i+1/2,j+1/2}^{(k+1)} \\
&- \frac{\widetilde{q}_{l+1/2}}{B_{0,l+1/2}} \frac{\Gamma_{R,l+1/2}^{(0)(k)}}{4\pi \Delta p_{1/2}} \\
= \;& 0
\end{aligned} \tag{5.477}$$

The condition to maintain density constant at each radial location $\psi_{l+1/2}$ leads therefore to an additional term, that adds to the operator which describes damping of Maxwellian electrons on suprathermal ones. With this approach, the Fokker-Planck equation is slightly non-linear, provided the fraction of runaway electrons remain small as compared to the bulk one.

Furthermore, the electron distribution function is not a Maxwellian in the vicinity of $p = 0$, since an ad-hoc source term of particle with no velocity is added. This approach is therefore questionable for its validity, owing to the basic assumptions that are used to derive the linearized Fokker-Planck equation around a Maxwellian bulk. Therefore, in order to avoid this singularity, an alternative approach may be to add a source term normalized to $\Gamma_{R,l+1/2}^{(0)(k)}$ but, whose distribution function is an exact Maxwellian corresponding to the electron temperature at $\psi_{l+1/2}$.

In that case, in steady-state regime, the flux divergence $\nabla_{\mathbf{p}} \cdot \mathbf{S}_{\mathbf{p}}^{(0)}$ is no more null at each plasma location, but is given by the relation

$$p^2 \nabla_{\mathbf{p}} \cdot \mathbf{S}_{\mathbf{p}}^{(0)} \Big|_{l+1/2,i+1/2,j+1/2}^{(k+1)} = p_{i+1/2}^2 \frac{\Gamma_{R,l+1/2}^{(0)(k)}}{\left[2\pi T_{e,l+1/2}\right]^{3/2}} \exp\left[- \frac{p_{i+1/2}^2}{\left(1 + \gamma_{l+1/2,i+1/2}\right) T_{e,l+1/2}} \right] \tag{5.478}$$

where $T_e\left(\psi_{l+1/2}\right) = T_{e,l+1/2}$, which corresponds to the existence of an external Maxwellian source term. By definition,

$$\begin{aligned}
&2\pi \sum_{j=0}^{n_{\xi_0}-1} \sum_{i=0}^{n_p-1} \frac{\Gamma_{R,l+1/2}^{(0)(k)}}{\left[2\pi T_{e,l+1/2}\right]^{3/2}} \exp\left[- \frac{p_{i+1/2}^2}{\left(1 + \gamma_{l+1/2,i+1/2}\right) T_{e,l+1/2}} \right] \\
&\times p_{i+1/2}^2 \Delta p_{i+1/2} \Delta \xi_{0,j+1/2} = \Gamma_{R,l+1/2}^{(0)(k)}
\end{aligned} \tag{5.479}$$

and the Fokker-Planck equation becomes simply

$$\begin{aligned}
&\frac{\widetilde{q}_{l+1/2}}{B_{0,l+1/2}} p_{i+1/2}^2 \frac{f_{0,l+1/2,i+1/2,j+1/2}^{(0)(k+1)} - f_{0,l+1/2,i+1/2,j+1/2}^{(0)(k)}}{\Delta t} \\
&+ \frac{\widetilde{q}}{B_0} p^2 \nabla_{\mathbf{p}} \cdot \mathbf{S}_{\mathbf{p}}^{(0)} \Big|_{l+1/2,i+1/2,j+1/2}^{(k+1)} \\
&+ \frac{\widetilde{q}}{B_0} p^2 \nabla_{\psi} \cdot \mathbf{S}_{\psi}^{(0)} \Big|_{l+1/2,i+1/2,j+1/2}^{(k+1)} \\
&- \frac{\widetilde{q}_{l+1/2}}{B_{0,l+1/2}} \frac{p_{i+1/2}^2 \Gamma_{R,l+1/2}^{(0)(k)}}{\left[2\pi T_{e,l+1/2}\right]^{3/2}} \exp\left[- \frac{p_{i+1/2}^2}{\left(1+\gamma_{l+1/2,i+1/2}\right) T_{e,l+1/2}} \right] \\
= \; & 0
\end{aligned} \tag{5.480}$$

Though this technique is in principle the most consistent with the underlying physics, it has also still some numerical drawbacks, because of the forward time differencing. It is well known that such terms put strong limitations on the time step value Δt, in order to preserve numerical stability. A coarse estimate of its level can be deduced from the condition

$$\frac{\Gamma_{R,l+1/2}^{(0)(k)}}{\left[2\pi T_{e,l+1/2}\right]^{3/2}} \exp\left[- \frac{p_{i+1/2}^2}{\left(1+\gamma_{l+1/2,i+1/2}\right) T_{e,l+1/2}} \right] \ll \frac{f_{0,l+1/2,i+1/2,j+1/2}^{(0)(k)}}{\Delta t} \tag{5.481}$$

Assuming $f_{0,l+1/2,i+1/2,j+1/2}^{(0)(k)} \simeq f_{0M,l+1/2,i+1/2,j+1/2}^{(0)}$, it turns out that

$$\frac{\Delta t \Gamma_{R,l+1/2}^{(0)(k)}}{n_{e,l+1/2}} \ll 1 \tag{5.482}$$

where $n_{e,l+1/2} = n_e\left(\psi_{l+1/2}\right)$ is the local electron density. In normalized units, as defined in Sec.6.3, time step of the order of $\Delta t \sim 10^{+3} - 10^{+4}$ are used to reach in few iterations the steady-state solution. Therefore, $\Gamma_{R,l+1/2}^{(0)(k)} / n_{e,l+1/2}$ must be lower than $10^{-5} - 10^{-6}$ in order to avoid onset of numerical instabilities, which corresponds usually to normalized Ohmic electric field less than 0.05.

Finally, the ultimate and most simple approach to deal with the loss of runaway electrons is to enforce the electron distribution function at each time step. Defining a numerical density $n_{e,l+1/2}^{(k)}$ at time step k ,

$$2\pi \sum_{j=0}^{n_{\xi_0}-1} \sum_{i=0}^{n_p-1} f_{0,l+1/2,i+1/2,j+1/2}^{(0)(k)} p_{i+1/2}^2 \Delta p_{i+1/2} \Delta \xi_{0,j+1/2} = n_{e,l+1/2}^{(k)} \tag{5.483}$$

this procedure corresponds to the following replacement

$$f_{0,l+1/2,i+1/2,j+1/2}^{(0)(k)} \rightarrow \frac{n_{e,l+1/2}}{n_{e,l+1/2}^{(k)}} f_{0,l+1/2,i+1/2,j+1/2}^{(0)(k)} \tag{5.484}$$

This procedure is equivalent to reinject electrons in the plasma so that local density is steadily maintained. The main advantage of this method is that it preserves the implicit or backward numerical time advancing. Furthermore, it avoids flux calculations in order to determine the runaway rate at ech time step, a procedure which slows down the rate of convergence. Finally, the normalization procedure is general and may be applied for any process that leads to local electron losses, like radial transport, magnetic ripple losses. For this reason, this method is chosen, if needed, for the code. However, even if this technique is numericaly very powerful, and physicaly justified, it may hinder some artificial numerical electron losses resulting from an improper numerical flux balance in each cell. Consequently, it is crucial to benchmark the Fokker-Planck code without this option, in order to verify that the conservative scheme is well satisfied and that electron losses remain always small.

Lower hybrid wave and very high temperature plasmas For the Lower Hybrid current drive problem, difficulties similar to the runaway problem may take place in the core region of the plasma, when the electron temperature is very high. For this quasi-electrostatic wave, the resonant interaction with the plasma takes place along the magnetic field line, as discussed in Sec. 4.3.2, and therefore, a tail of very energetic electrons is pulled out from the bulk in the parallel direction $p_\parallel$ as for the Ohmic electric field. Unlike the Ohmic case, the domain of interaction for the Lower Hybrid wave is bounded in momentum space, and is given by the well known wave-particle resonance condition

$$v_{\parallel\,\min}^{LH} \leq \frac{p_\parallel}{\gamma} \leq v_{\parallel\,\max}^{LH} \tag{5.485}$$

where the relativistic factor $\gamma = \sqrt{1+(\beta_{th}p)^2}$, $\beta_{th} = v_{th}/c$ and $p^2 = p_\parallel^2 + p_\perp^2$. On the axis $p_\perp = 0$, the resonance domain is given by the relation

$$p_{\parallel\,\min}^{LH,0} \leq p_\parallel^0 \leq p_{\parallel\,\max}^{LH,0} \tag{5.486}$$

where

$$p_{\parallel\,\min}^{LH,0} = \frac{v_{\parallel\,\min}^{LH}}{\sqrt{1-\left(\beta_{th}v_{\parallel\,\min}^{LH}\right)^2}} \tag{5.487}$$

and

$$p_{\parallel\,\max}^{LH,0} = \frac{v_{\parallel\,\max}^{LH}}{\sqrt{1-\left(\beta_{th}v_{\parallel\,\max}^{LH}\right)^2}} \tag{5.488}$$

When $p_\perp \neq 0$, the lower bound of the resonance condition becomes

$$\left(\frac{p_{\parallel\,\min}^{LH}}{p_{\parallel\,\min}^{LH,0}}\right)^2 - \beta_{th}^2 p_\perp^2 = 1 \tag{5.489}$$

while the upper limit is

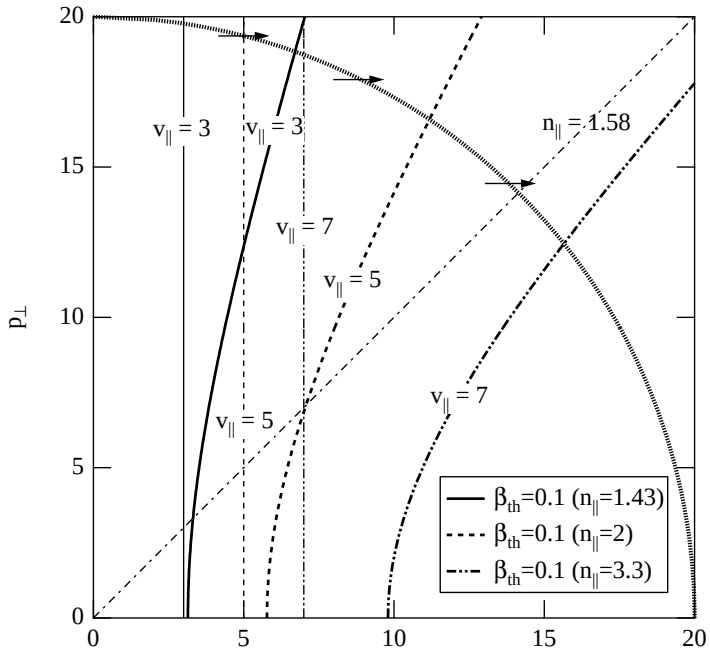

cmcm

Figure 5.3: Lower Hybrid boundary problem

$$\left(\frac{p_{\parallel\max}^{LH}}{p_{\parallel\max}^{LH,0}}\right)^2 - \beta_{th}^2 p_\perp^2 = 1 \tag{5.490}$$

For very cold plasmas, i.e. when $\beta_{th}^2 p_{\max}^2 \ll 1$ since $p_\perp \leq p_{\max}$,

$$\begin{cases} p_{\parallel\min}^{LH} \simeq p_{\parallel\min}^{LH,0} \\ p_{\parallel\max}^{LH} \simeq p_{\parallel\max}^{LH,0} \end{cases} \tag{5.491}$$

and resonance domain boundaries are straight lines parallel to $p_\parallel = 0$ axis. In that case, electron losses are naturally very weak, since at the intersection of the resonance and integration domains, the wave-induced flux is nearly tangent to the boundary of the integration domain. Since $p_{\max}$ ranges usualy between $20-30$, β_{th} must be much less than 0.01, which corresponds to electron temperatures less than $0.06keV$. Such a condition is never encountered in tokamak plasmas, except close to the very edge.

Because of relativistic corrections, lower and upper boundaries of the Lower Hybrid resonance domain are hyperbolic functions of $p_\perp$, which indicates that the wave induced particle flux always crosses the integration domain. The curvature of the resonance domain boundaries as a function of $p_\perp$ depends directly of β_{th} as shown in Fig. 5.3 and therefore, one may expect that particle flux induced by the wave may be nearly perpendicular to the integration domain boundary. This is the worst situation, for which important losses of

electrons may take place if the quasilinear diffusion is very large between $p_{\parallel\min}^{LH}$ and $p_{\parallel\max}^{LH}$, as for the runaway problem. In such a regime, a tail of very energetic electrons is pulled out from the bulk up to the integration domain, and the accuracy of the current driven by the wave as calculated by the code is highly questionable, when a significant fraction of this population leaves the integration domain.

This difficulty becomes rapidly important when β_{th} increases as a consequence of the forward peaking of the electron dynamic because of the relativistic corrections. In that case, the total kinetic energy comes into play, and therefore electrons with a high $p_\perp$ component will interact resonantly with the wave at larger p values because of their increasing mass.

It is difficult to introduce an unambiguous criterion which defines limits beyond which electron losses become important, since there is an interplay between the shape of the resonant domain, and also the absolute level of the quasilinear diffusion rate. As discussed in Sec. 4.3.2, its value is given by the relation

$$\begin{aligned}\overline{D}_{b,n}^{\mathrm{RF}(0)}(p,\xi_0) &= \frac{\gamma p_{Te}}{p\,|\xi_0|}\frac{1}{\lambda\widetilde{q}}\frac{r_{\theta_b}}{R_0}\frac{B^{\theta_b}}{B_P^{\theta_b}}\frac{\xi_0^2}{\xi_{\theta_b}^2}\Psi_{\theta_b}\overline{D}_{b,n,0}^{\mathrm{RF},\theta_b}\left|\Theta_{\mathbf{k},\theta_b}^{b,n}\left(\mathbf{k}_b\right)\right|^2\times \\ &\quad H\left(\theta_b-\theta_{\min}\right)H\left(\theta_{\max}-\theta_b\right)\left[\frac{1}{2}\sum_\sigma\right]_T\delta\left(N_{\parallel b}-N_{\parallel\mathrm{res}}^{\theta_b}\right) \quad (5.492)\end{aligned}$$

which roughly decreases as $p_\parallel^{-1}$. This dependence, usually neglected since the shape of the plateau in the distribution function is independent of the value of $\overline{D}_{b,n}^{\mathrm{RF}(0)}$ when the quasilinear diffusion rate is very large, is however very important when the $2-D$ momentum dynamics is fully taken into account. This is in fact the only way to avoid unacceptable electrons losses, and $p_{\max}$ must determined so that $\overline{D}_{b,n}^{\mathrm{RF}(0)} \ll 1$ at the boundary of the integration domain. Indeed, curvatures of the resonance domain boundaries as $p_\parallel$ increases are not favorable for a reduction of the losses, since at high energy, the flux of particles induced by the Lower Hybrid wave becomes more and more perpendicular to the integration domain.

As shown in Fig. 5.3, the only possibility for particle losses to remain at an acceptable small level whatever the quasilinear diffusion level, is that the upper boundary of the Lower Hybrid resonance domain crosses the integration domain at $p_\perp/p_{\max} > 1/\sqrt{2}$. This purely geometrical effect put very strong limitations on the lowest level of the parallel refractive index $n_{\parallel\min}^{LH}$ that can be studied. Indeed, , $p_{\parallel\max}^{LH,0}\,(p_\perp=0)$ is therefore given by the relation,

$$p_{\parallel\max}^{LH,0} = 1/\sqrt{\frac{2}{p_{\max}^2}+\beta_{th}^2} \quad (5.493)$$

or

$$v_{\parallel\max}^{LH} = \frac{1}{\sqrt{2}}\frac{p_{\max}}{\sqrt{1+\beta_{th}^2 p_{\max}^2}} \quad (5.494)$$

In term of parallel refractive wave index, the previous condition is equivalent to the

simple relation

$$n_{\parallel\,\min}^{LH} = \sqrt{2}\frac{\sqrt{1+\beta_{th}^2 p_{\max}^2}}{\beta_{th} p_{\max}} \tag{5.495}$$

where the usual resonance relation

$$v_{\parallel\,\max}^{LH} = \frac{1}{\beta_{th}}\frac{1}{n_{\parallel\,\min}^{LH}} \tag{5.496}$$

is used. In the limit $\beta_{th}^2 p_{\max}^2 \gg 1$, $v_{\parallel\,\max}^{LH}$ becomes independent of $p_{\max}$

$$v_{\parallel\,\max}^{LH} \simeq \frac{1}{\sqrt{2}}\frac{1}{\beta_{th}} \tag{5.497}$$

which equivalent to

$$n_{\parallel\,\min}^{LH} \gtrsim \sqrt{2} \simeq 1.4 \tag{5.498}$$

This result confirms that increasing $p_{\max}$ is useless in order to reduce particle losses, if the quasilinear diffusion coefficient $\overline{D}_{b,n}^{\mathrm{LH}(0)}$ remains very large over all the quasilinear resonance domain, except if the parallel refractive index is small. In most calculations, $p_{\max} \simeq 20 - 30$, and since in the core of the plasma β_{th} ranges between 0.14 and 0.17, $\beta_{th}^2 p_{\max}^2 \simeq 7.8 - 26$, which fully justify this approximation.

As discussed for the runaway problem, particle losses are compensated by the normalization of the electron distribution function at each time step. However, when $n_{\parallel\,\min}^{LH}$ exceeds $\sqrt{2}$, a warning is send by the code, in order to indicate that strong particle losses may take place if the quasilinear diffusion coefficient is large at the boundary of the integration domain.

Treatment of the trapped region Since characteristic times for collision, RF quasilinear diffusion and Ohmic electric field acceleration are all much larger than the bounce time in the weak collision "banana" regime, $f_0^{(0)}(\psi, p, \xi_0) = f_0^{(0)}(\psi, p, -\xi_0)$ when $|\xi_0| \leq \xi_{0T}$. Therefore, symmetrically place points around $\xi_0 = 0$ are equivalent in the trapped region, a physical property that is described by the term $\left[\frac{1}{2}\sum_\sigma\right]_T$ in the bounce averaging procedure in Sec. 2.2.1. This effect introduces a new internal boundary corresponding to the trapped-passing transition, and an external one at $\xi_0 = 0$, since by symmetry,

$$\frac{\partial f_0^{(0)}}{\partial \xi_0}(\xi_0 = 0) = 0 \tag{5.499}$$

The Fokker-Planck equation is then solved in a reduced domain of integration, where the momentum phase space corresponding to $-\xi_{0T} \leq \xi_0 \leq 0$ is removed. Once determined in this reduced domain, the distribution function is recovered on the whole space, by enforcing the condition $f_0^{(0)}(\psi, p, -\xi_0) = f_0^{(0)}(\psi, p, \xi_0)$ in the interval $|\xi_0| \leq \xi_{0T}$.

A specific treatment of the new internal boundary must be considered, so that flux continuity is correctly described between co- and counter-passing regions, despite the

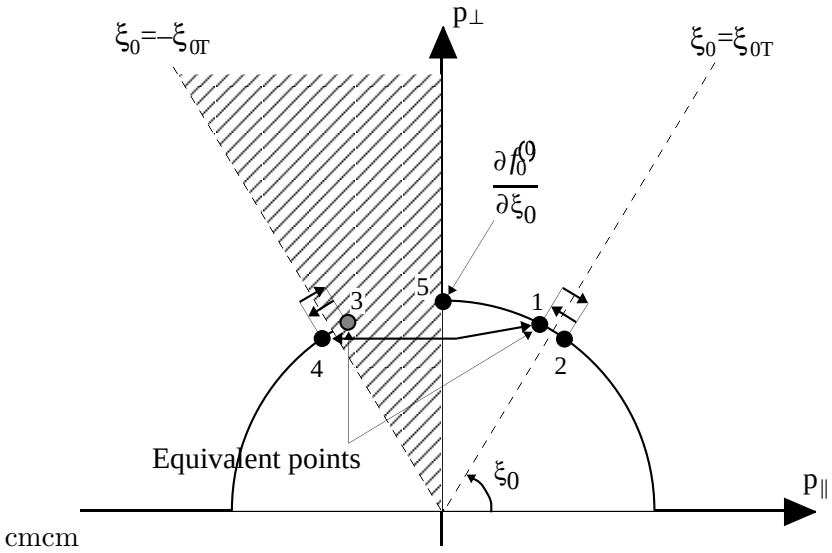

Figure 5.4: Trapped domain and related flux connections

reduction of the phase space domain. Let define grid points

$$\begin{cases} 1:\left(l+1/2,i+1/2,j^{+}_{T,l+1/2}-1/2\right) \\ 2:\left(l+1/2,i+1/2,j^{+}_{T,l+1/2}+1/2\right) \\ 3:\left(l+1/2,i+1/2,j^{-}_{T,l+1/2}+1/2\right) \\ 4:\left(l+1/2,i+1/2,j^{-}_{T,l+1/2}-1/2\right) \\ 5:\left(l+1/2,i+1/2,j_{T_0}+1/2\right) \end{cases} \tag{5.500}$$

where $j_{T_0}=\left(n_{\xi_0}+1\right)/2=\left(j^{+}_{T,l+1/2}+j^{-}_{T,l+1/2}\right)/2$, as indicated in Fig.5.4. Here $j^{-}_{T,l+1/2}$ is the index that corresponds to the trapped/passing boundary $\xi_0=-\xi_{0T}$, while $j^{+}_{T,l+1/2}$ corresponds to the symmetric boundary with respect to the axis $\xi_0=0$, i.e. $\xi_0=\xi_{0T}$.

By definition, grid points 1 and 3 are in the trapped region, just placed below and above co- and counter-passing boundaries respectively at opposite sides of the axis $\xi_0=0$ and with the same distance to this axis, while grid points 2 and 4 have a similar arrangement but are placed in the co- and counter-passing regions respectively right after the trapped-passing boundary. The grid point 5 is placed on the right side of the axis $\xi_0=0$, in the trapped sub-domain $0\leq\xi_0\leq\xi_{0T}$.

Before performing the reduction of the domain of integration, the symmetry inside the trapped region must be enforced according to the relation

$$\overline{\overline{M}}^{(0)}_{p,l+1/2,i+1/2,j^{+}+1/2}=\left(\overline{\overline{M}}^{(0)}_{p,l+1/2,i+1/2,j^{+}+1/2}+\overline{\overline{M}}^{(0)}_{p,l+1/2,i+1/2,j^{-}+1/2}\right)/2 \tag{5.501}$$

where $j_{T_0}=\left(j^{+}+j^{-}\right)/2$, with $j^{-}_{T,l+1/2}<j^{-}<j_{T_0}$ or an in equivalent manner $j_{T_0}<$

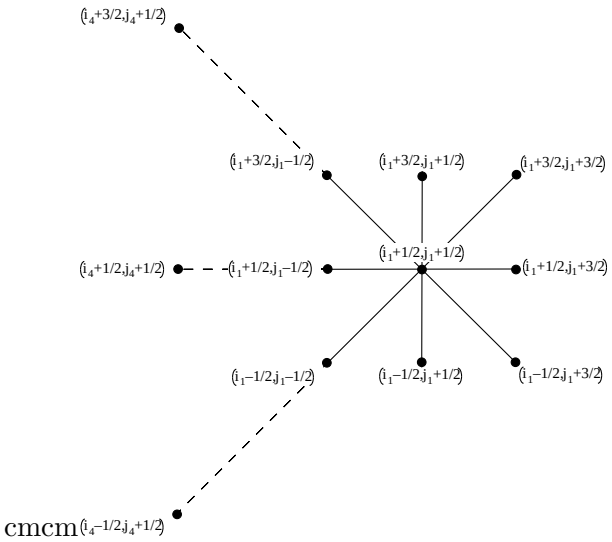

Figure 5.5: Momentum flux connections for grid point 1 in the trapped region

$j^+ < j^+_{T,l+1/2}$. This procedure allows to correctly account for some processes that are not symmetric in $p_\parallel$, like wave-particle interaction.

The reduction of the domain of integration in the momentum phase space leads to introduce a new matrix, $\widehat{\overline{M}}^{(0)}_p$ whose coefficients are defined as follows

$$\widehat{\overline{M}}^{(0)}_{p,l+1/2,i+1/2,j'+1/2} = \overline{\overline{M}}^{(0)}_{p,l+1/2,i+1/2,j+1/2} \tag{5.502}$$

with $j' = j$, when $0 \leq j < j^-_{T,l+1/2}$, and $j' = j - n_{\xi_{0T,l+1/2}}$, when $j_{T_0} \leq j \leq n_{\xi_0} - 1$. Here, $n_{\xi_{0T,l+1/2}} = \left(j^+_{T,l+1/2} - j^-_{T,l+1/2}\right)/2$ corresponds to the number of grid points removed in the pitch-angle direction, and with this definition, it can be easily cross-checked that $j_{T_0} - n_{\xi_{0T,l+1/2}} = j^-_{T,l+1/2}$.

Furthermore, since grid point 3 is no more considered in the calculations while grid points 3 and 1 are equivalent, flux relations between neighboring grid points 4 and 3 must then be replaced by new relations wich link grid points 4 and 1. Much in the same way, flux relations between grid points 2 and 3 no more exist, and therefore, the flux relation between grid points 2 and 1 must be modified accordingly. This procedure leads to add six new set of coefficients to the matrix $\widehat{\overline{M}}^{(0)}_p$, namely

$$\begin{cases} \widehat{\overline{M}}^{(0)}_{p,l+1/2,i-1/2,\left[j'^-_{T,l+1/2}-1/2\right]+n_{\xi_{0T,l+1/2}}} \\ \widehat{\overline{M}}^{(0)}_{p,l+1/2,i+1/2,\left[j'^-_{T,l+1/2}-1/2\right]+n_{\xi_{0T,l+1/2}}} \\ \widehat{\overline{M}}^{(0)}_{p,l+1/2,i+3/2,\left[j'^-_{T,l+1/2}-1/2\right]+n_{\xi_{0T,l+1/2}}} \end{cases} \tag{5.503}$$

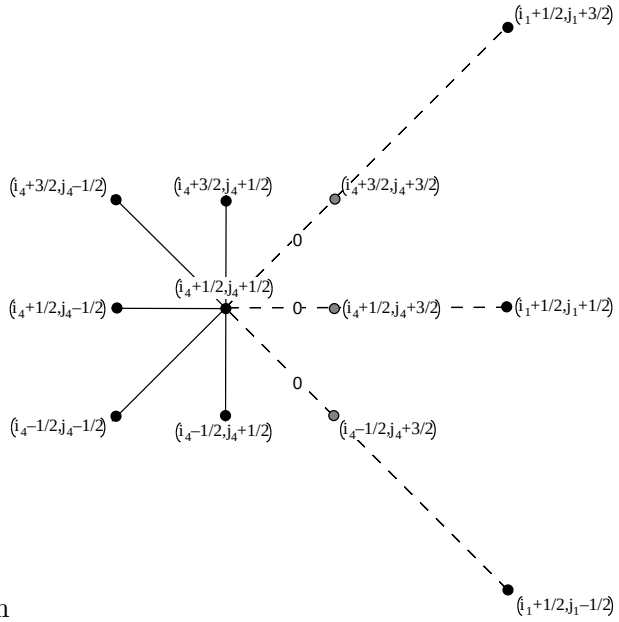

cmcm

Figure 5.6: Momentum flux connections for grid point 4 in the counter-passing region

and

$$\begin{cases} \widehat{\overline{M}}^{(0)}_{p,l+1/2,i-1/2,\left[j'^{+}_{T,l+1/2}-1/2\right]-n_{\xi_{0T,l+1/2}}} \\ \widehat{\overline{M}}^{(0)}_{p,l+1/2,i+1/2,\left[j'^{+}_{T,l+1/2}-1/2\right]-n_{\xi_{0T,l+1/2}}} \\ \widehat{\overline{M}}^{(0)}_{p,l+1/2,i+3/2,\left[j'^{+}_{T,l+1/2}-1/2\right]-n_{\xi_{0T,l+1/2}}} \end{cases} \tag{5.504}$$

while matrix coefficients

$$\begin{cases} \widehat{\overline{M}}^{(0)}_{p,l+1/2,i-1/2,\left[j'^{-}_{T,l+1/2}-1/2\right]+1} \\ \widehat{\overline{M}}^{(0)}_{p,l+1/2,i+1/2,\left[j'^{-}_{T,l+1/2}-1/2\right]+1} \\ \widehat{\overline{M}}^{(0)}_{p,l+1/2,i+3/2,\left[j'^{-}_{T,l+1/2}-1/2\right]+1} \end{cases} \tag{5.505}$$

and

$$\begin{cases} \widehat{\overline{M}}^{(0)}_{p,l+1/2,i-1/2,\left[j'^{+}_{T,l+1/2}-1/2\right]+1} \\ \widehat{\overline{M}}^{(0)}_{p,l+1/2,i+1/2,\left[j'^{+}_{T,l+1/2}-1/2\right]+1} \\ \widehat{\overline{M}}^{(0)}_{p,l+1/2,i+3/2,\left[j'^{+}_{T,l+1/2}-1/2\right]+1} \end{cases} \tag{5.506}$$

where $j'^{-}_{T,l+1/2} = j^{-}_{T,l+1/2}$ and $j'^{+}_{T,l+1/2} = j^{+}_{T,l+1/2} - n_{\xi_{0T,l+1/2}}$ must be modified accordingly.

As shown in a graphic form in Figs. 5.5 and 5.6,

$$\begin{cases} \widehat{\overline{M}}^{(0)}_{p,l+1/2,i-1/2,\left[j'^{-}_{T,l+1/2}-1/2\right]+1} = 0 \\ \widehat{\overline{M}}^{(0)}_{p,l+1/2,i+1/2,\left[j'^{-}_{T,l+1/2}-1/2\right]+1} = 0 \\ \widehat{\overline{M}}^{(0)}_{p,l+1/2,i+3/2,\left[j'^{-}_{T,l+1/2}-1/2\right]+1} = 0 \end{cases} \tag{5.507}$$

since the distribution function at grid 4 is no more connected with the one at grid point 3 or 5, but to the grid point 1 only. Furthermore, since grid points 1 and 3 are equivalent, their clockwise flux links with grid point 2 are only half in order to avoid counting them twice. Therefore,

$$\begin{aligned} \widehat{\overline{M}}^{(0)}_{p,l+1/2,i-1/2,\left[j'^{+}_{T,l+1/2}-1/2\right]+1} &= \overline{\overline{M}}^{(0)}_{p,l+1/2,i-1/2,\left[j'^{+}_{T,l+1/2}-1/2\right]+1+n_{\xi_{0T},l+1/2}}/2 \\ \widehat{\overline{M}}^{(0)}_{p,l+1/2,i+1/2,\left[j'^{+}_{T,l+1/2}-1/2\right]+1} &= \overline{\overline{M}}^{(0)}_{p,l+1/2,i+1/2,\left[j^{+}_{T,l+1/2}-1/2\right]+1+n_{\xi_{0T},l+1/2}}/2 \\ \widehat{\overline{M}}^{(0)}_{p,l+1/2,i+3/2,\left[j'^{+}_{T,l+1/2}-1/2\right]+1} &= \overline{\overline{M}}^{(0)}_{p,l+1/2,i+3/2,\left[j^{+}_{T,l+1/2}-1/2\right]+1+n_{\xi_{0T},l+1/2}}/2 \end{aligned} \tag{5.508}$$

Moreover, since counterclockwise flux that links grid points 3 and 4 is equivalent by symmetry with clockwise flux that links grid points 1 and 2 , one obtains,

$$\begin{aligned} \widehat{\overline{M}}^{(0)}_{p,l+1/2,i-1/2,\left[j'^{-}_{T,l+1/2}-1/2\right]+n_{\xi_{0T},l+1/2}} &= \overline{\overline{M}}^{(0)}_{p,l+1/2,i-1/2,\left[j'^{+}_{T,l+1/2}-1/2\right]+1+n_{\xi_{0T},l+1/2}} \\ \widehat{\overline{M}}^{(0)}_{p,l+1/2,i+1/2,\left[j'^{-}_{T,l+1/2}-1/2\right]+n_{\xi_{0T},l+1/2}} &= \overline{\overline{M}}^{(0)}_{p,l+1/2,i+1/2,\left[j'^{+}_{T,l+1/2}-1/2\right]+1+n_{\xi_{0T},l+1/2}} \\ \widehat{\overline{M}}^{(0)}_{p,l+1/2,i+3/2,\left[j'^{-}_{T,l+1/2}-1/2\right]+n_{\xi_{0T},l+1/2}} &= \overline{\overline{M}}^{(0)}_{p,l+1/2,i+3/2,\left[j'^{+}_{T,l+1/2}-1/2\right]+1+n_{\xi_{0T},l+1/2}} \end{aligned} \tag{5.509}$$

and

$$\begin{aligned} \widehat{\overline{M}}^{(0)}_{p,l+1/2,i-1/2,\left[j'^{+}_{T,l+1/2}-1/2\right]-n_{\xi_{0T},l+1/2}} &= \overline{\overline{M}}^{(0)}_{p,l+1/2,i-1/2,\left[j'^{+}_{T,l+1/2}-1/2\right]+1+n_{\xi_{0T},l+1/2}}/2 \\ \widehat{\overline{M}}^{(0)}_{p,l+1/2,i+1/2,\left[j'^{+}_{T,l+1/2}-1/2\right]-n_{\xi_{0T},l+1/2}} &= \overline{\overline{M}}^{(0)}_{p,l+1/2,i+1/2,\left[j'^{+}_{T,l+1/2}-1/2\right]+1+n_{\xi_{0T},l+1/2}}/2 \\ \widehat{\overline{M}}^{(0)}_{p,l+1/2,i+3/2,\left[j'^{+}_{T,l+1/2}-1/2\right]-n_{\xi_{0T},l+1/2}} &= \overline{\overline{M}}^{(0)}_{p,l+1/2,i+3/2,\left[j'^{+}_{T,l+1/2}-1/2\right]+1+n_{\xi_{0T},l+1/2}}/2 \end{aligned} \tag{5.510}$$

Finally, for the external boundary at $\xi_0 = 0$, all matrix coefficients at grid point $j_{T_0} + 1/2$ are forced to zero, except two,

$$\begin{aligned} \widehat{\overline{M}}^{(0)}_{p,l+1/2,i-1/2,\left[j'^{-}_{T,l+1/2}+1/2\right]+n_{\xi_{0T},l+1/2}} &= 1 \\ \widehat{\overline{M}}^{(0)}_{p,l+1/2,i-1/2,\left[j'^{-}_{T,l+1/2}+3/2\right]+n_{\xi_{0T},l+1/2}} &= -1 \end{aligned} \tag{5.511}$$

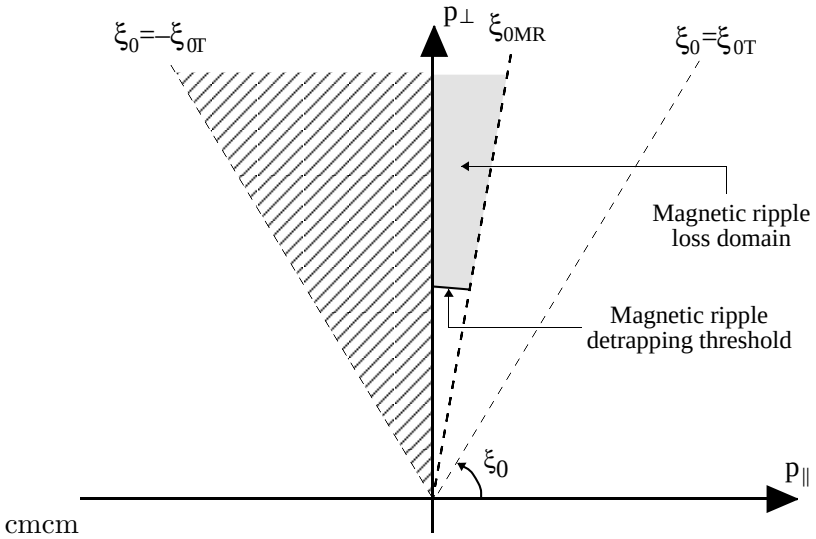

Figure 5.7: Heuristic magnetic ripple modeling. The trapped/supertrapped boundary varies as well as the collision detrapping threshold are both functions of the radial location

since $j'^{-}_{T,l+1/2} = j_{T_0} - n_{\xi_{0T,l+1/2}} = j'_{T_0}$.

Magnetic ripple losses Super-trapped electrons with $p_\parallel/p_\perp \ll 1$ are very sensitive to all the details of the magnetic configuration, and may be lossed in the local magnetic wells because of the finite number of toroidal magnetic field coils. This effect requires in principle a full $3-D$ spatial calculation, that is beyond the present theoretical frame here described, as for the stellarator magnetic configuration. Nevertheless, some interesting results may be obtained, by considering that super-trapped electrons whose banana tips fall in the magnetic well drift vertically in an irreversible manner and leave therefore the plasma. This process takes place provided their kinetic energy is large enough so that the detrapping probability by collisions remain negligible.

Describing this effect is consequently equivalent to introduce new external boundaries in the trapped region, in order to describe in an ad-hoc manner this physical effect. This approach is justified because the drifting time across the plasma is short enough for the locally trapped electrons in the magnetic ripple to neglect their contributions to the overall momentum dynamics.

For this purpose, an Krook term is introduced in the Fokker-Planck equation

$$\left.\frac{\partial f_0^{(0)}}{\partial t}\right|^{(k+1)}_{l+1/2,i+1/2,j+1/2} = \nu_{MR,l+1/2,i+1/2,j'+1/2} f^{(0)(k+1)}_{0,l+1/2,i+1/2,j'+1/2} \tag{5.512}$$

where $\nu_{MR,l+1/2,i+1/2,j'+1/2}$ is an effective loss frequency, whose value is a function of the super-trapped domain as shown in Fig. 5.7. This loss frequency varies therefore with the radial location $\psi_{l+1/2}$, but also with momentum $p_{i+1/2}$ and pitch-angle $\xi_{0,j'+1/2}$. Outside

this domain, $\nu_{MR,l+1/2,i+1/2,j'+1/2}$ is set to a zero so that losses are always negligible on the time scale for the steady-state distribution function to build-up. Conversely, inside the domain characterized by the pitch-angle boundary $0 \leq \xi_{0,j'+1/2} \leq \xi_{0,j'^{+}_{MR,l+1/2}+1/2}$ and $p_{i+1/2} \geq p_{MR,l+1/2}$, where $j'^{+}_{MR,l+1/2}$ is the index below which particle are lossed in the magnetic ripple, and $p_{MR,l+1/2}$ is the momentum detrapping threshold by collisions, $\nu_{MR,l+1/2,i+1/2,j'+1/2}$ is usually taken constant and much larger than τ_t^{-1} which is the smallest time scale here considered, namely the transit time. The matrix is then simply modified according to the following rule

$$\widehat{\overline{M}}^{(0)}_{p,l+1/2,i+1/2,j'+1/2} \rightarrow \widehat{\overline{M}}^{(0)}_{p,l+1/2,i+1/2,j'+1/2} - \nu_{MR,l+1/2,i+1/2,j'+1/2} \tag{5.513}$$

With this method, it is not necessary to introduce additional specific conditions and moreover the implicit time scheme is fully preserved. By definition, the Fokker-Planck equation is no more conservative, but particle losses are compensated by the normalization technique at each time step, as for the runaway problem. This is an acceptable technique, provided level of losses due to magnetic ripple is small as compared to the electron bulk density.

Spatial dynamics

Internal boundary For the dynamics in configuration space, since the problem has only one dimension, the internal boundary must be only specified at $\psi = \psi_0 = 0$, which corresponds to the condition

$$f_0^{(0)}(\psi, p, \xi_0) = f_0^{(0)}(-\psi, p, \xi_0) \tag{5.514}$$

Using the same approach as for the momentum dynamics, $\Delta\psi$ must be defined at this location. Hence

$$\Delta\psi_0 = \frac{1}{2}\left(\Delta\psi_{1/2} + \Delta\psi_{-1/2}\right) = \Delta\psi_{1/2} \tag{5.515}$$

using $\Delta\psi_{-1/2} = \Delta\psi_{1/2}$. Since $\Delta\psi_{1/2} = \psi_1 - \psi_0$, and $\psi_{1/2} = \frac{\psi_1+\psi_0}{2}$ one obtains finally,

$$\Delta\psi_0 = 2\psi_{1/2} \tag{5.516}$$

because $\psi_0 = 0$.

It is important to note that internal boundary conditions are also only needed for the evaluation of cross-derivative terms, since in the discrete form of the Fokker-Planck equation using two grids, as shown, in Sec. 5.4.2, it is automatically fullfiled for other terms. Indeed, at fixed $p_{i+1/2}, \xi_{0,j+1/2}$,

$$\begin{aligned} &\frac{\widetilde{q}}{B_0} p^2 \nabla_\psi \cdot \mathbf{S}^{(0)}_\psi \Big|^{(k+1)}_{1/2,i+1/2,j+1/2} \\ = \frac{p^2_{i+1/2}}{\lambda^{1/2,j+1/2}} \times &\quad \frac{\partial}{\partial\psi}\left(R_0 \widetilde{q} \frac{B_{P0}}{B_0} \lambda \mathbf{S}^{(0)}_\psi\right)\Big|^{(k+1)}_{1/2,i+1/2,j+1/2} \end{aligned} \tag{5.517}$$

or

$$\begin{aligned} & \frac{\widetilde{q}}{B_0}p^2\nabla_\psi\cdot\mathbf{S}_\psi^{(0)}\Big|_{1/2,i+1/2,j+1/2}^{(k+1)} \\ = \frac{p_{i+1/2}^2}{\lambda^{1/2,j+1/2}}\times & \quad R_{0,1}\widetilde{q}_1\frac{B_{P0,1}}{B_{0,1}}\lambda^{1,j+1/2}\mathbf{S}_{\psi_{1,i+1/2,j+1/2}}^{(0)(k+1)} \end{aligned} \tag{5.518}$$

since $R_{0,0}B_{P0,0}\mathbf{S}_{\psi_{0,i+1/2,j+1/2}}^{(0)(k+1)}=0$. Indeed, $B_{P0,0}=0$ on the magnetic axis.

External boundary As discussed for the momentum dynamics, a primary condition of the code is that electron density profile is preserved. As for the particle losses in momentum space, this can be performed by injecting an equivalent number of particles at $p=0$, in order to compensate the particle flux leaving the integration domain because of diffusion across magnetic flux surfaces. It corresponds to a reaction of the bulk, because of the occurence of a small electric field, generated by the electron transport so that the overall electron density profile is kept constant. By this method, a steady state regime may be achieved, and it is not necessary to specify which type of mechanism is at play, diffusion or convection.

Let define the local variation of the electron density $\Delta n_{e,l+1/2}^{(k)}$ at time step k because of spatial transport by the simple relation

$$\Delta n_e^{(k)}(\psi)=\iint\left[f_0^{(0)(k)}(\psi,p,\xi_0)-f_0^{(0)(k-1)}(\psi,p,\xi_0)\right]\lambda(\psi,\xi_0)\,p^2dpd\xi_0 \tag{5.519}$$

It can be expressed in term of a loss rate

$$\Gamma_T^{(0)(k)}(\psi)=\Delta n_e^{(k)}(\psi)/\Delta t$$

by introducing the integration time step Δt and the flux balance gives on the discrete mesh is

$$2\pi p_0^2 S_{p,l+1/2,0,j+1/2}^{(0)}\sum_{j=0}^{n_{\xi_0}-1}\Delta\xi_{0,j+1/2}=4\pi p_0^2 S_{p,l+1/2,0,j+1/2}^{(0)}=\Gamma_{T,l+1/2}^{(0)} \tag{5.520}$$

assuming like for losses in momentum space that the flux has no pitch-angle dependence at p_0. The zero order Fokker-Planck equation becomes simply

$$\begin{aligned} & \frac{\widetilde{q}_{l+1/2}}{B_{0,l+1/2}}p_{i+1/2}^2\frac{f_{0,l+1/2,i+1/2,j+1/2}^{(0)(k+1)}-f_{0,l+1/2,i+1/2,j+1/2}^{(0)(k)}}{\Delta t} \\ & +\frac{\widetilde{q}}{B_0}p^2\nabla_{\mathbf{p}}\cdot\mathbf{S}_{\mathbf{p}}^{(0)}\Big|_{l+1/2,i+1/2,j+1/2}^{(k+1)} \\ & +\frac{\widetilde{q}}{B_0}p^2\nabla_\psi\cdot\mathbf{S}_\psi^{(0)}\Big|_{l+1/2,i+1/2,j+1/2}^{(k+1)} \\ & -\frac{\widetilde{q}_{l+1/2}}{B_{0,l+1/2}}\frac{\Gamma_{R,l+1/2}^{(0)(k)}+\Gamma_{T,l+1/2}^{(0)(k)}}{4\pi\Delta p_{1/2}} \\ = & \ 0 \end{aligned} \tag{5.521}$$

in order to maintain electron density at each time step. By definition, radial transport or runaway play a similar role, and as a result their respective contributions are equivalent in the Fokker-Planck equation. If the electrons that are reinjected have a Maxwellian distribution function corresponding to the electron temperature at $\psi_{l+1/2}$, one may obtain, as for the runaway problem,

$$\begin{aligned}
&\frac{\widetilde{q}_{l+1/2}}{B_{0,l+1/2}} p_{i+1/2}^2 \frac{f^{(0)(k+1)}_{0,l+1/2,i+1/2,j+1/2} - f^{(0)(k)}_{0,l+1/2,i+1/2,j+1/2}}{\Delta t} \\
&+ \frac{\widetilde{q}}{B_0} p^2 \nabla_{\mathbf{p}} \cdot \mathbf{S}^{(0)}_{\mathbf{p}} \Big|^{(k+1)}_{l+1/2,i+1/2,j+1/2} \\
&+ \frac{\widetilde{q}}{B_0} p^2 \nabla_{\psi} \cdot \mathbf{S}^{(0)}_{\psi} \Big|^{(k+1)}_{l+1/2,i+1/2,j+1/2} \\
&- \frac{\widetilde{q}_{l+1/2}}{B_{0,l+1/2}} p_{i+1/2}^2 \frac{\Gamma^{(0)(k)}_{R,l+1/2} + \Gamma^{(0)(k)}_{T,l+1/2}}{\left[2\pi T_{e,l+1/2}\right]^{3/2}} \exp\left[- \frac{p^2_{i+1/2}}{\left(1+\gamma_{l+1/2,i+1/2}\right) T_{e,l+1/2}} \right] \\
= \;& 0
\end{aligned} \tag{5.522}$$

Finally, for cross-derivative terms, one have to determine $\Delta\psi_{n_\psi}$ at the boundary of the integration domain. It is readily given by relation,

$$\Delta\psi_{n_\psi} = 2\left(\psi_{n_\psi} - \psi_{n_\psi - 1/2}\right) = 2\left(\psi_a - \psi_{n_\psi - 1/2}\right) \tag{5.523}$$

as done for p, since $\psi_{n_\psi} = \psi_a$.

Treatment of the trapped region The radial transport equation is greatly complicated by the presence of trapped electrons, since the diffusion across magnetic field lines may contribute to trap or detrap particles who are in the close vicinity of the trapped/passing boundary, because of the radial dependence of this boundary, as shown in Fig. 5.8. By definition, this process takes place intrinsically at fixed magnetic moment, a fundamental assumption of the flux conservative form of the bounce averaged Fokker-Planck equation, as shown in Sec.3.5.1.

The matrix build-up is therefore quite complex, since one has to take into account that counter-passing electrons may be trapped when they diffuse towards lower magnetic regions of the plasma, while conversely, trapped electrons may be detrapped by crossing magnetic flux surfaces in the high magnetic field side direction.

Let define three neighboring grid points at radial locations $\psi_{l-1/2}$, $\psi_{l+1/2}$ and $\psi_{l+3/2}$ and corresponding trapped/passing boundaries $\xi_{0T,j^{\pm}_{T,l-1/2}}$, $\xi_{0T,j^{\pm}_{T,l+1/2}}$, and $\xi_{0T,j^{\pm}_{T,l+3/2}}$, since non-uniform pitch-angle grid mesh is designed so that each boundary is exactly placed on the flux grid. By definition, since

$$-\xi_{0T,j^{-}_{T,l+3/2}} < -\xi_{0T,j^{-}_{T,l+1/2}} < -\xi_{0T,j^{-}_{T,l-1/2}} < \xi_{0T,j^{+}_{T,l-1/2}} < \xi_{0T,j^{+}_{T,l+1/2}} < \xi_{0T,j^{+}_{T,l+3/2}} \tag{5.524}$$

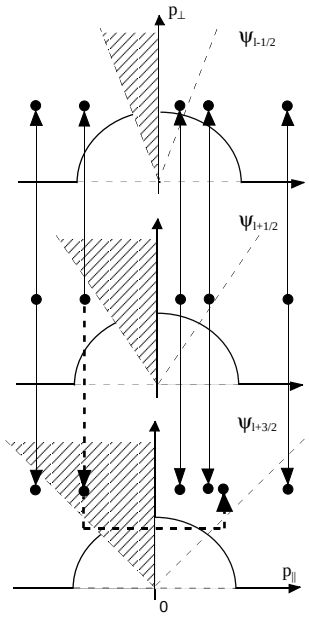

cmcm

Figure 5.8: Trapping and detrapping process induced by radial transport

the following relation holds

$$j^-_{T,l+3/2} < j^-_{T,l+1/2} < j^-_{T,l-1/2} < j_{T_0} < j^+_{T,l-1/2} < j^+_{T,l+1/2} < j^+_{T,l+3/2} \tag{5.525}$$

Here j_{T_0} is the index of the grid point corresponding to the axis $\xi_0 = 0$ in the trapped region at $\psi_{l+1/2}$. This defines naturaly eight different regions in momentum space at $\psi_{l+1/2}$, where spatial fluxes must be considered. Since matrix is reduced in momentum space, because the region $j^-_{l+1/2} < j^-_{l-1/2} < j_{T_{0,l+1/2}}$ is not considered in the calculations, one has therefore to consider effectively only six regions, namely corresponding to

$$j^-_{T,l+3/2} < j^-_{T,l+1/2} \tag{5.526}$$

and

$$j_{T_0} < j^+_{T,l-1/2} < j^+_{T,l+1/2} < j^+_{T,l+3/2} \tag{5.527}$$

or using relations $j'^-_{T,l+1/2} = j^-_{T,l+1/2}$ and $j'^+_{T,l+1/2} = j^+_{T,l+1/2} - n_{\xi_{0T,l+1/2}}$

$$j'^-_{T,l+3/2} < j'^-_{T,l+1/2} < j'^+_{T,l-1/2} < j'^+_{T,l+1/2} < j'^+_{T,l+3/2} \tag{5.528}$$

As for the momentum dynamics, the reduction of the domain of integration in the momentum phase space leads to introduce a new matrix, $\widehat{\overline{M}}^{(0)}_{\psi}$. Obviously, the main diagonal is fully preserved, and therefore

$$\widehat{\overline{M}}^{(0)}_{\psi,l+1/2,i+1/2,j'+1/2} = \overline{\overline{M}}^{(0)}_{\psi,l+1/2,i+1/2,j'+1/2} \tag{5.529}$$

provided $j' < j'^{-}_{T,l+1/2}$, while

$$\widehat{\overline{M}}^{(0)}_{\psi,l+1/2,i+1/2,j'+1/2} = \overline{\overline{M}}^{(0)}_{\psi,l+1/2,i+1/2,[j'+1/2]+n_{\xi_{0T,l+1/2}}} \tag{5.530}$$

when for $j' > j'^{+}_{T,l+1/2}$. Only off-diagonal matrix coefficients have to be modified, because of the presence of trapped and circulating electrons. Indeed, these coefficients reflect the particle flux transfer between different location.

If $j' < j'^{-}_{T,l+3/2}$, matrix coefficients are given by

$$\begin{cases} \widehat{\overline{M}}^{(0)}_{\psi,l-1/2,i+1/2,j'+1/2} = \overline{\overline{M}}^{(0)}_{\psi,l-1/2,i+1/2,j'+1/2} \\ \widehat{\overline{M}}^{(0)}_{\psi,l+3/2,i+1/2,j'+1/2} = \overline{\overline{M}}^{(0)}_{\psi,l+3/2,i+1/2,j'+1/2} \end{cases} \tag{5.531}$$

and for $j'^{-}_{T,l+3/2} < j' < j'^{-}_{T,l+1/2}$, the simple relation still holds for one matrix coefficient only

$$\widehat{\overline{M}}^{(0)}_{\psi,l-1/2,i+1/2,j'+1/2} = \overline{\overline{M}}^{(0)}_{\psi,l-1/2,i+1/2,j'+1/2} \tag{5.532}$$

since the trapped region is narrower at $\psi_{l-1/2}$ as compared to $\psi_{l+1/2}$. But since counter-circulating electrons become trapped by diffusion from $\psi_{l+1/2} \rightarrow \psi_{l+3/2}$ and electron dynamics in the domain $j^{-}_{T,l+3/2} < j < j_{T_0}$ is removed and replaced by its counterpart in the positive pitch-angle region $j_{T_0} < j < j^{+}_{T,l+3/2}$, it turns out that

$$\widehat{\overline{M}}^{(0)}_{\psi,l+3/2,i+1/2,j'+1/2} = 0 \tag{5.533}$$

and the flux link must be replaced by

$$\widehat{\overline{M}}^{(0)}_{\psi,l+3/2,i+1/2,[j'+1/2]+2\left(j_{T_0}-(j'+1/2)\right)-n_{\xi_{0T,l+3/2}}} = \overline{\overline{M}}^{(0)}_{\psi,l+3/2,i+1/2,j'+1/2} \tag{5.534}$$

taking into account of the mirror indexing around the axis $\xi_0 = 0$, and the fact that matrix blocks corresponding to different radii have different sizes.

In a general way, when $j' > j'^{-}_{T,l+1/2}$, the following rule applies

$$\begin{cases} \widehat{\overline{M}}^{(0)}_{\psi,l-1/2,i+1/2,j'+1/2} = 0 \\ \widehat{\overline{M}}^{(0)}_{\psi,l+3/2,i+1/2,j'+1/2} = 0 \end{cases} \tag{5.535}$$

all corresponding matrix coefficients being replaced by new ones according to the relations

$$\begin{cases} \widehat{\overline{M}}^{(0)}_{\psi,l-1/2,i+1/2,[j'+1/2]+\left(n_{\xi_{0T,l+1/2}}-n_{\xi_{0T,l-1/2}}\right)} = \overline{\overline{M}}^{(0)}_{\psi,l-1/2,i+1/2,[j'+1/2]+n_{\xi_{0T,l+1/2}}} \\ \widehat{\overline{M}}^{(0)}_{\psi,l+3/2,i+1/2,[j'+1/2]+\left(n_{\xi_{0T,l+1/2}}-n_{\xi_{0T,l+3/2}}\right)} = \overline{\overline{M}}^{(0)}_{\psi,l+3/2,i+1/2,[j'+1/2]+n_{\xi_{0T,l+1/2}}} \end{cases} \tag{5.536}$$

wether electrons remains trapped or co-passing, or become trapped by the outward radial transport or detrapped by the inward cross-field diffusion. Since $n_{\xi_{0T,l+1/2}} - n_{\xi_{0T,l-1/2}} > 0$ and $n_{\xi_{0T,l+1/2}} - n_{\xi_{0T,l+3/2}} < 0$,

$$\begin{cases} [j'+1/2] + \left(n_{\xi_{0T,l+1/2}} - n_{\xi_{0T,l-1/2}}\right) > j'+1/2 \\ [j'+1/2] + \left(n_{\xi_{0T,l+1/2}} - n_{\xi_{0T,l+3/2}}\right) < j'+1/2 \end{cases} \tag{5.537}$$

which indicates that diagonals shrink when trapped/passing boundary is crossed, i.e. $j' > j'^{-}_{T,l+1/2}$. Therefore, matrix $\widehat{\overline{M}}^{(0)}_{\psi}$ contains much more diagonals than $\overline{\overline{M}}^{(0)}_{\psi}$ which has only three ones.

At $\psi = 0$, there is no need to specify the spatial flux $S^{(0)}_{\psi}$, with the two grids technique. Since by construction $R_{\min,0} B_{P\min,0} \mathbf{S}^{(0)(k+1)}_{\psi_{0,i+1/2,j+1/2}} = 0$, no particle accumulation occurs naturaly at ψ , and at this singular point $f^{(0)(k+1)}_{0,1/2,i+1/2,j+1/2} = f^{(0)(k+1)}_{0,-1/2,i+1/2,j+1/2}$ is well fullfiled.

At the plasma edge ψ_a, i.e. at the boundary of the integration domain, there is also no need to specify any condition on the flux of fast particles are leaving the plasma definitively, as for the runaway problem. Consequently, even without any external perturbation, the fact that radial transport of fast transport leads to strong departure from the Maxwellian momentum dependence at all radius.

As for the dynamics in momentum space, $\Delta\psi$ must be specified at the boundaries of the domain of integration. One finds that

$$\Delta\psi_0 = 2\psi_{1/2} \tag{5.538}$$

since $\psi_0 = 0$, and

$$\Delta\psi_{n_\psi} = 2\left(\psi_{n_\psi} - \psi_{n_\psi - 1/2}\right) = 2\left(\psi_a - \psi_{n_\psi - 1/2}\right) \tag{5.539}$$

noting that $\psi_{n_\psi} = \psi_a$.

5.7.2 Up to first order term: the Drift Kinetic equation

Since the first order bounce-averaged drift kinetic equation may be expressed in the same conservative form as for zero order Fokker-Planck bounce-averaged equation, most of the boundary conditions apply in a natural way without additional specifications, in particular at $p = 0$ and $|\xi_0| = 1$, as a consequence of the two grids technique, one for the fluxes and the other for the distribution function.

In matrix form, the general expression of the first order bounce averaged drift kinetic equation

$$\{\mathcal{C}(g)\} + \{\mathcal{Q}(g)\} + \{\mathcal{E}(g)\} = -\left\{\mathcal{C}\left(\widetilde{f}\right)\right\} - \left\{\mathcal{Q}\left(\widetilde{f}\right)\right\} - \left\{\mathcal{E}\left(\widetilde{f}\right)\right\} \tag{5.540}$$

becomes

$$\begin{aligned}
&\sum_{i'=i-1}^{i'=i+1}\sum_{j''=j-1}^{j''=j+1}\overline{\overline{M}}^{(0)}_{p,l+1/2,i'+1/2,j''+1/2}g^{(0)(k)}_{0,l+1/2,i'+1/2,j''+1/2}\\
&+p^2_{i+1/2}C^{(0)}\left(f_{M,l+1/2,i+1/2,j+1/2},\frac{3}{2}\xi_{0,j+1/2}g^{(0)(m=1)(k)}_{l+1/2,i+1/2,j+1/2}\right)\\
=\;&-\sum_{i'=i-1}^{i'=i+1}\sum_{j''=j-1}^{j''=j+1}\widetilde{\overline{M}}^{(0)}_{p,l+1/2,i'+1/2,j''+1/2}\widetilde{f}^{(0)}_{l+1/2,i'+1/2,j''+1/2}\\
&-\sum_{i'=i-1}^{i'=i+1}\sum_{l'=l-1}^{l'=l+1}\widetilde{\overline{H}}^{(0)}_{\psi,l'+1/2,i'+1/2,j+1/2}f^{(0)}_{0,l'+1/2,i'+1/2,j+1/2}\\
&-p^2_{i+1/2}\widetilde{C}^{(0)}\left(f_{M,l+1/2,i+1/2,j+1/2},\frac{3}{2}\xi_{0,j+1/2}\widetilde{f}^{(0)(m=1)}_{l+1/2,i+1/2,j+1/2}\right)
\end{aligned}\tag{5.541}$$

or

$$\begin{aligned}
&\sum_{i'=i-1}^{i'=i+1}\sum_{j''=j-1}^{j''=j+1}\overline{\overline{M}}^{(0)}_{p,l+1/2,i'+1/2,j''+1/2}g^{(0)(k)}_{0,l+1/2,i'+1/2,j''+1/2}\\
&+p^2_{i+1/2}C^{(0)}\left(f_{M,l+1/2,i+1/2,j+1/2},\frac{3}{2}\xi_{0,j+1/2}g^{(0)(m=1)(k)}_{l+1/2,i+1/2,j+1/2}\right)\\
=\;&\widetilde{W}^{(0)}_{l+1/2,i+1/2,j+1/2}
\end{aligned}\tag{5.542}$$

where

$$\begin{aligned}
\widetilde{W}^{(0)}_{l+1/2,i+1/2,j+1/2} =\;&-\sum_{i'=i-1}^{i'=i+1}\sum_{j''=j-1}^{j''=j+1}\widetilde{\overline{M}}^{(0)}_{p,l+1/2,i'+1/2,j''+1/2}\widetilde{f}^{(0)(k)}_{l+1/2,i'+1/2,j''+1/2}\\
&-\sum_{i'=i-1}^{i'=i+1}\sum_{l'=l-1}^{l'=l+1}\widetilde{\overline{H}}^{(0)}_{\psi,l'+1/2,i'+1/2,j+1/2}f^{(0)(k)}_{0,l'+1/2,i'+1/2,j+1/2}\\
&-p^2_{i+1/2}\widetilde{C}^{(0)}\left(f_{M,l+1/2,i+1/2,j+1/2},\frac{3}{2}\xi_{0,j+1/2}\widetilde{f}^{(0)(m=1)}_{l+1/2,i+1/2,j+1/2}\right)
\end{aligned}\tag{5.543}$$

Here, (k) is the iteration index number, while $C^{(0)}$ and $\widetilde{C}^{(0)}$ are the electron-electron self-collision operators that make the equation non-linear.

Internal boundaries for function $\mathbf{g}^{(0)}$

In the weak collision "banana" regime, it is shown in Sec.3.4 that $g^{(0)}(\psi,p,\xi_0)=0$ for trapped electrons. Therefore, the drift kinetic equation must be solved in a reduced domain of integration, as for $f_0^{(0)}(\psi,p,\xi_0)$, but with different and more simple internal boundary conditions. Indeed, the only constraint is to enforce the condition $g^{(0)}(\psi,p,\xi_0)=0$ for $|\xi_0|\leq\xi_{0T}$.

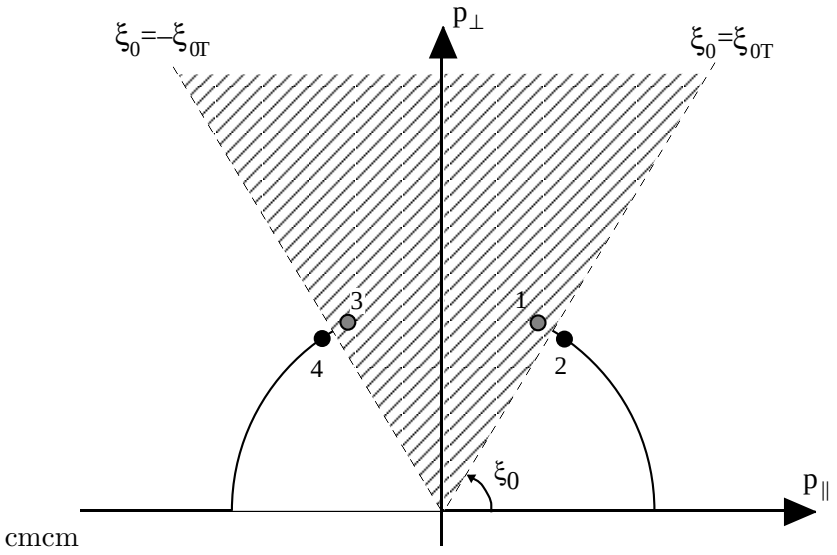

Figure 5.9: Trapped domain for the first order distribution g

Let define grid points

$$\begin{cases} 1 : \left(l+1/2, i+1/2, j^{+}_{T,l+1/2} - 1/2\right) \\ 2 : \left(l+1/2, i+1/2, j^{+}_{T,l+1/2} + 1/2\right) \\ 3 : \left(l+1/2, i+1/2, j^{-}_{T,l+1/2} + 1/2\right) \\ 4 : \left(l+1/2, i+1/2, j^{-}_{T,l+1/2} - 1/2\right) \end{cases} \tag{5.544}$$

as indicated in Fig.5.9. Here $j^{-}_{T,l+1/2}$ is the index that corresponds to the trapped/passing boundary $\xi_0 = -\xi_{0T}$, while $j^{+}_{T,l+1/2}$ corresponds to the symmetric boundary with respect to the axis $\xi_0 = 0$, i.e. $\xi_0 = \xi_{0T}$.

Since $g^{(0)}$ is prescribed in the trapped domain, all the region may be removed from the calculations, and the reduction of the domain of integration in the momentum phase space leads to introduce a new matrix $\widehat{\widehat{M}}^{(0)}_{p}$ whose coefficients are defined as follows

$$\widehat{\widehat{M}}^{(0)}_{p,l+1/2,i+1/2,j'+1/2} = \overline{\overline{M}}^{(0)}_{p,l+1/2,i+1/2,j+1/2} \tag{5.545}$$

with $j' = j$, when $0 \leq j < j^{-}_{T,l+1/2}$, and $j' = j - m_{\xi_{0T},l+1/2}$, when $j^{+}_{T,l+1/2} < j \leq n_{\xi_0}$. Here, $m_{\xi_{0T},l+1/2} = j^{+}_{T,l+1/2} - j^{-}_{T,l+1/2}$ corresponds to the number of grid points removed in the pitch-angle direction, and with this definition, it is easy to cross-check that $j'^{+}_{T,l+1/2} - j'^{-}_{T,l+1/2} = j^{+}_{T,l+1/2} - j^{-}_{T,l+1/2} - m_{\xi_{0T},l+1/2} = 0$. Since grid points 2 and 4 are not connected,

the following condition applies

$$\begin{cases} \widehat{\widehat{M}}^{(0)}_{p,l+1/2,i-1/2,\left[j'_{T,l+1/2}-1/2\right]+1} = 0 \\ \widehat{\widehat{M}}^{(0)}_{p,l+1/2,i+1/2,\left[j'_{T,l+1/2}-1/2\right]+1} = 0 \\ \widehat{\widehat{M}}^{(0)}_{p,l+1/2,i+3/2,\left[j'_{T,l+1/2}-1/2\right]+1} = 0 \end{cases} \tag{5.546}$$

and conversely

$$\begin{cases} \widehat{\widehat{M}}^{(0)}_{p,l+1/2,i-1/2,\left[j'_{T,l+1/2}+1/2\right]-1} = 0 \\ \widehat{\widehat{M}}^{(0)}_{p,l+1/2,i+1/2,\left[j'_{T,l+1/2}+1/2\right]-1} = 0 \\ \widehat{\widehat{M}}^{(0)}_{p,l+1/2,i+3/2,\left[j'_{T,l+1/2}+1/2\right]-1} = 0 \end{cases} \tag{5.547}$$

where $j'^{-}_{T,l+1/2} = j'^{+}_{T,l+1/2} = j'_{T,l+1/2}$. As internal boundaries match already existing diagonals of the matrix $\overline{\overline{M}}^{(0)}_{p,l+1/2,i+1/2,j+1/2}$, $\widehat{\widehat{M}}^{(0)}_{p,l+1/2,i+1/2,j'+1/2}$ remains a simple nine diagonal matrix, and is therefore less complex than the 15 diagonals matrix $\widehat{\overline{M}}^{(0)}_{p,l+1/2,i+1/2,j'+1/2}$ corresponding to the Fokker-Planck equation.

Internal boundaries for $\widetilde{f}$

Since no inversion is required for calculating the vector $\widetilde{W}^{(0)}_{l+1/2,i+1/2,j+1/2}$, it is consequently evaluated at all grid points, including those corresponding to trapped electron domain. Consequently, the reduction along the pitch-angle direction that results from the condition $g^{(0)}(\psi, p, \xi_0) = 0$ is only performed after the calculation of $\widetilde{W}_{l+1/2,i+1/2,j+1/2}$ over the full ξ_0 grid. Once done, the prescription on the index number j' that holds for the matrix conversion

$$\overline{\overline{M}}^{(0)}_{p,l+1/2,i+1/2,j+1/2} \rightarrow \widehat{\widehat{M}}^{(0)}_{l+1/2,i+1/2,j+1/2p,l+1/2,i+1/2,j'+1/2} \tag{5.548}$$

may be then applied in a similar way for $\widetilde{W}_{l+1/2,i+1/2,j+1/2}$, which leads to define a new vector $\widehat{\widehat{W}}^{(0)}_{p,l+1/2,i+1/2,j'+1/2}$ whose size is reduced

$$\widetilde{W}^{(0)}_{l+1/2,i+1/2,j+1/2} \rightarrow \widehat{\widehat{W}}^{(0)}_{p,l+1/2,i+1/2,j'+1/2} \tag{5.549}$$

and finally the drift kinetic equation on the reduced grid is simply given by the relation

$$\sum_{i'=i-1}^{i'=i+1} \sum_{j''=j'-1}^{j''=j'+1} \widehat{\widehat{M}}^{(0)}_{p,l+1/2,i+1/2,j''+1/2} g^{(0)(k)}_{0,l+1/2,i'+1/2,j''+1/2} = \widehat{\widehat{W}}^{(0)}_{p,l+1/2,i+1/2,j'+1/2} \tag{5.550}$$

where all the trapped electron domain is removed.

External boundaries

The problem of external boundaries discussed in Sec. 5.7.1 for the zero-order Fokker-Planck equation may be applied in a straightforward manner to the first-order drift kinetic ones, since it may be expressed in a similar conservative form. Consequently, if the zero-order Fokker-Planck equation conserves the total number of particles without specific conditions, the solution g may be found without additional constraints at the boundaries of the integration domain. Conversely, if Dirichlet conditions are considered for the Fokker-Planck equation, like enforcing the Maxwellian solution at $p = 0$, similar and consistent conditions must be also applied for the drift kinetic equation.

5.8 Moments of the Distribution Function

5.8.1 Flux discretization for moment calculations

The calculation of momentum-space moments of the distribution function, such as the density of power absorbed or the stream function, requires to calculate the bounce-averaged momentum space fluxes $\mathbf{S}_{\mathbf{p}}^{(0)}$ associated with a distribution function. Considering a given distribution function $f^{(0)}$ (which could be $f_0^{(0)}$, $\widetilde{f}^{(0)}$ or $g^{(0)}$) and given momentum-space diffusion $\mathbb{D}_{\mathbf{p}}^{(0)\mathcal{O}}$ and convection $\mathbf{F}_{\mathbf{p}}^{(0)\mathcal{O}}$coefficients, associated with a particular physical mechanism $\mathcal{O}$ (such as collisions, RF waves and DC electric field) and calculated in chapter 4, these fluxes are given by (3.187) or equivalently (3.216) and their components are

$$S_p^{(0)} = -D_{pp}^{(0)\mathcal{O}} \frac{\partial f^{(0)}}{\partial p} + \frac{\sqrt{1-\xi_0^2}}{p} D_{p\xi}^{(0)\mathcal{O}} \frac{\partial f^{(0)}}{\partial \xi_0} + F_p^{(0)\mathcal{O}} f^{(0)} \tag{5.551}$$

$$S_{\xi_0}^{(0)} = -D_{\xi p}^{(0)\mathcal{O}} \frac{\partial f^{(0)}}{\partial p} + \frac{\sqrt{1-\xi_0^2}}{p} D_{\xi\xi}^{(0)\mathcal{O}} \frac{\partial f^{(0)}}{\partial \xi_0} + F_\xi^{(0)\mathcal{O}} f^{(0)} \tag{5.552}$$

- First, both for power density (5.574) and stream function calculations (5.577), we need to calculate the discretized flux $S_p^{(0)}$ at the flux grid point $(l+1/2, i, j+1/2)$

$$\begin{aligned} S_{p,l+1/2,i,j+1/2}^{(0)\mathcal{O}} = & -D_{pp,l+1/2,i,j+1/2}^{(0)\mathcal{O}} \left.\frac{\partial f^{(0)}}{\partial p}\right|_{l+1/2,i,j+1/2} \\ & + \frac{\sqrt{1-\xi_{0,j+1/2}^2}}{p_i} D_{p\xi,l+1/2,i,j+1/2}^{(0)\mathcal{O}} \left.\frac{\partial f^{(0)}}{\partial \xi_0}\right|_{l+1/2,i,j+1/2} \\ & + F_{p,l+1/2,i,j+1/2}^{(0)\mathcal{O}} f_{l+1/2,i,j+1/2}^{(0)} \end{aligned} \tag{5.553}$$

  The first derivative is straightforward (5.58)

$$\left.\frac{\partial f^{(0)}}{\partial p}\right|_{l+1/2,i,j+1/2} = \frac{f_{l+1/2,i+1/2,j+1/2}^{(0)} - f_{l+1/2,i-1/2,j+1/2}^{(0)}}{\Delta p_i} \tag{5.554}$$

while the second derivative, similar to (5.60)

$$\left.\frac{\partial f^{(0)}}{\partial \xi_0}\right|_{l+1/2,i,j+1/2} = \frac{f^{(0)}_{l+1/2,i,j+3/2} - f^{(0)}_{l+1/2,i,j-1/2}}{\Delta\xi_{0,j+1} + \Delta\xi_{0,j}} \tag{5.555}$$

and the convective term both requires further interpolation (5.67)

$$f^{(0)}_{l+1/2,i,j+3/2} = \left(1 - \delta^{(0)}_{p,l+1/2,i,j+3/2}\right) f^{(0)}_{l+1/2,i+1/2,j+3/2} + \delta^{(0)}_{p,l+1/2,i,j+3/2} f^{(0)}_{l+1/2,i-1/2,j+3/2} \tag{5.556}$$

$$f^{(0)}_{l+1/2,i,j+1/2} = \left(1 - \delta^{(0)}_{p,l+1/2,i,j+1/2}\right) f^{(0)}_{l+1/2,i+1/2,j+1/2} + \delta^{(0)}_{p,l+1/2,i,j+3/2} f^{(0)}_{l+1/2,i-1/2,j+1/2} \tag{5.557}$$

$$f^{(0)}_{l+1/2,i,j-1/2} = \left(1 - \delta^{(0)}_{p,l+1/2,i,j-1/2}\right) f^{(0)}_{l+1/2,i+1/2,j-1/2} + \delta^{(0)}_{p,l+1/2,i,j-1/2} f^{(0)}_{l+1/2,i-1/2,j-1/2} \tag{5.558}$$

The expanded expression is then

$$\begin{aligned}
S^{(0)\mathcal{O}}_{p,l+1/2,i,j+1/2} = &\left[-\frac{D^{(0)\mathcal{O}}_{pp,l+1/2,i,j+1/2}}{\Delta p_i} \right. \\
&\left. + F^{(0)\mathcal{O}}_{p,l+1/2,i,j+1/2} \left(1 - \delta^{(0)}_{p,l+1/2,i,j+1/2}\right) \right] f^{(0)}_{l+1/2,i+1/2,j+1/2} \\
&+ \left[\frac{D^{(0)\mathcal{O}}_{pp,l+1/2,i,j+1/2}}{\Delta p_i} + F^{(0)\mathcal{O}}_{p,l+1/2,i,j+1/2} \delta^{(0)}_{p,l+1/2,i,j+3/2} \right] f^{(0)}_{l+1/2,i-1/2,j+1/2} \\
&+ \frac{\sqrt{1-\xi^2_{0,j+1/2}}}{p_i} \frac{D^{(0)\mathcal{O}}_{p\xi,l+1/2,i,j+1/2}}{\Delta\xi_{0,j+1} + \Delta\xi_{0,j}} \left(1 - \delta^{(0)}_{p,l+1/2,i,j+3/2}\right) f^{(0)}_{l+1/2,i+1/2,j+3/2} \\
&+ \frac{\sqrt{1-\xi^2_{0,j+1/2}}}{p_i} \frac{D^{(0)\mathcal{O}}_{p\xi,l+1/2,i,j+1/2}}{\Delta\xi_{0,j+1} + \Delta\xi_{0,j}} \delta^{(0)}_{p,l+1/2,i,j+3/2} f^{(0)}_{l+1/2,i-1/2,j+3/2} \\
&- \frac{\sqrt{1-\xi^2_{0,j+1/2}}}{p_i} \frac{D^{(0)\mathcal{O}}_{p\xi,l+1/2,i,j+1/2}}{\Delta\xi_{0,j+1} + \Delta\xi_{0,j}} \left(1 - \delta^{(0)}_{p,l+1/2,i,j-1/2}\right) f^{(0)}_{l+1/2,i+1/2,j-1/2} \\
&- \frac{\sqrt{1-\xi^2_{0,j+1/2}}}{p_i} \frac{D^{(0)\mathcal{O}}_{p\xi,l+1/2,i,j+1/2}}{\Delta\xi_{0,j+1} + \Delta\xi_{0,j}} \delta^{(0)}_{p,l+1/2,i,j-1/2} f^{(0)}_{l+1/2,i-1/2,j-1/2}
\end{aligned} \tag{5.559}$$

- For Stream function calculations (5.579), we also need to calculate the discretized

flux $S_{\xi}^{(0)}$ at the flux grid point $(l+1/2, i+1/2, j)$

$$\begin{aligned} S^{(0)\mathcal{O}}_{\xi,l+1/2,i+1/2,j} = &-D^{(0)\mathcal{O}}_{\xi p,l+1/2,i+1/2,j} \left.\frac{\partial f^{(0)}}{\partial p}\right|_{l+1/2,i+1/2,j} \\ &+ \frac{\sqrt{1-\xi_{0,j}^2}}{p_{i+1/2}} D^{(0)\mathcal{O}}_{\xi\xi,l+1/2,i+1/2,j} \left.\frac{\partial f^{(0)}}{\partial \xi_0}\right|_{l+1/2,i+1/2,j} \\ &+ F^{(0)\mathcal{O}}_{\xi,l+1/2,i+1/2,j} f^{(0)}_{l+1/2,i+1/2,j} \end{aligned} \tag{5.560}$$

The first derivative is similar to (5.57)

$$\left.\frac{\partial f^{(0)}}{\partial p}\right|_{l+1/2,i+1/2,j} = \frac{f^{(0)}_{l+1/2,i+3/2,j} - f^{(0)}_{l+1/2,i-1/2,j}}{\Delta p_{i+1} + \Delta p_i} \tag{5.561}$$

while the second is given by (5.61)

$$\left.\frac{\partial f^{(0)}}{\partial \xi_0}\right|_{l+1/2,i+1/2,j} = \frac{f^{(0)}_{l+1/2,i+1/2,j+1/2} - f^{(0)}_{l+1/2,i+1/2,j-1/2}}{\Delta \xi_{0,j}} \tag{5.562}$$

The first diffusion term and the convective term both requires further interpolation (5.69)

$$f^{(0)}_{l+1/2,i+3/2,j} = \left(1 - \delta^{(0)}_{\xi,l+1/2,i+3/2,j}\right) f^{(0)}_{l+1/2,i+3/2,j+1/2} + \delta^{(0)}_{\xi,l+1/2,i+3/2,j} f^{(0)}_{l+1/2,i+3/2,j-1/2} \tag{5.563}$$

$$f^{(0)}_{l+1/2,i+1/2,j} = \left(1 - \delta^{(0)}_{\xi,l+1/2,i+1/2,j}\right) f^{(0)}_{l+1/2,i+1/2,j+1/2} + \delta^{(0)}_{\xi,l+1/2,i+1/2,j} f^{(0)}_{l+1/2,i+1/2,j-1/2} \tag{5.564}$$

$$f^{(0)}_{l+1/2,i-1/2,j} = \left(1 - \delta^{(0)}_{\xi,l+1/2,i-1/2,j}\right) f^{(0)}_{l+1/2,i-1/2,j+1/2} + \delta^{(0)}_{\xi,l+1/2,i-1/2,j} f^{(0)}_{l+1/2,i-1/2,j-1/2} \tag{5.565}$$

The expanded expression is then

$$
\begin{aligned}
S^{(0)\mathcal{O}}_{\xi,l+1/2,i+1/2,j} = & \left[\frac{\sqrt{1-\xi^2_{0,j}}}{p_{i+1/2}} \frac{D^{(0)\mathcal{O}}_{\xi\xi,l+1/2,i+1/2,j}}{\Delta\xi_{0,j}} \right. \\
& \left. + F^{(0)\mathcal{O}}_{\xi,l+1/2,i+1/2,j} \left(1 - \delta^{(0)}_{\xi,l+1/2,i+1/2,j}\right) \right] f^{(0)}_{l+1/2,i+1/2,j+1/2} \\
& + \left[-\frac{\sqrt{1-\xi^2_{0,j}}}{p_{i+1/2}} \frac{D^{(0)\mathcal{O}}_{\xi\xi,l+1/2,i+1/2,j}}{\Delta\xi_{0,j}} \right. \\
& \left. + F^{(0)\mathcal{O}}_{\xi,l+1/2,i+1/2,j} \delta^{(0)}_{\xi,l+1/2,i+1/2,j} \right] f^{(0)}_{l+1/2,i+1/2,j-1/2} \\
& - \frac{D^{(0)\mathcal{O}}_{\xi p,l+1/2,i+1/2,j}}{\Delta p_{i+1} + \Delta p_i} \left(1 - \delta^{(0)}_{\xi,l+1/2,i+3/2,j}\right) f^{(0)}_{l+1/2,i+3/2,j+1/2} \\
& - \frac{D^{(0)\mathcal{O}}_{\xi p,l+1/2,i+1/2,j}}{\Delta p_{i+1} + \Delta p_i} \delta^{(0)}_{\xi,l+1/2,i+3/2,j} f^{(0)}_{l+1/2,i+3/2,j-1/2} \\
& + \frac{D^{(0)\mathcal{O}}_{\xi p,l+1/2,i+1/2,j}}{\Delta p_{i+1} + \Delta p_i} \left(1 - \delta^{(0)}_{\xi,l+1/2,i-1/2,j}\right) f^{(0)}_{l+1/2,i-1/2,j+1/2} \\
& + \frac{D^{(0)\mathcal{O}}_{\xi p,l+1/2,i+1/2,j}}{\Delta p_{i+1} + \Delta p_i} \delta^{(0)}_{\xi,l+1/2,i-1/2,j} f^{(0)}_{l+1/2,i-1/2,j-1/2}
\end{aligned}
\tag{5.566}
$$

5.8.2 Numerical integrals for moment calculations

Density

From calculations in Sec.3.6, the flux surface averaged density $\langle n_e \rangle_{V,l+1/2}$ at $\psi_{l+1/2}$ may be expressed as a sum of three terms

$$
\langle n_e \rangle_{V,l+1/2} = \langle n_e \rangle^0_{V,l+1/2} + \langle n_e \rangle^1_{V,l+1/2} + \langle \widetilde{n}_e \rangle^1_{V,l+1/2}
$$

the first one corresponding to the zero order Fokker-Planck equation

$$
\langle n_e \rangle^0_{V,l+1/2} = 2\pi \frac{\widetilde{q}_{l+1/2}}{\widehat{q}_{l+1/2}} \sum_{i=0}^{n_p-1} \sum_{j=0}^{n_{\xi_0}-1} p^2_{i+1/2} \lambda^{l+1/2,j+1/2} f^{(0)}_{0,l+1/2,i+1/2,j+1/2} \Delta p_{i+1/2} \Delta\xi_{0,j+1/2}
\tag{5.567}
$$

while the two others result from the solution of the electron drift kinetic equation

$$
\langle n_e \rangle^1_{V,l+1/2} = 2\pi \frac{\widetilde{q}_{l+1/2}}{\widehat{q}_{l+1/2}} \sum_{i=0}^{n_p-1} \sum_{j=0}^{n_{\xi_0}-1} p^2_{i+1/2} \lambda^{l+1/2,j+1/2} g^{(0)}_{l+1/2,i+1/2,j+1/2} \Delta p_{i+1/2} \Delta\xi_{0,j+1/2}
\tag{5.568}
$$

and

$$\langle \widetilde{n}_e \rangle^1_{V,l+1/2} = 2\pi \frac{\widetilde{q}_{l+1/2}}{\widehat{q}_{l+1/2}} \sum_{i=0}^{n_p-1} \sum_{j=0}^{n_{\xi_0}-1} p^2_{i+1/2} \overline{\lambda}^{l+1/2,j+1/2}_{1,-1,0} \widetilde{f}^{(0)}_{l+1/2,i+1/2,j+1/2} \Delta p_{i+1/2} \Delta \xi_{0,j+1/2} \tag{5.569}$$

Current Density

In a similar way, the flux surface averaged parallel current $\langle J_\parallel \rangle_{\phi,l+1/2}$ at $\psi_{l+1/2}$ may be expressed as a sum of three terms

$$\langle J_\parallel \rangle_{\phi,l+1/2} = \langle J_\parallel \rangle^0_{\phi,l+1/2} + \langle J_\parallel \rangle^1_{\phi,l+1/2} + \left\langle \widetilde{J}_\parallel \right\rangle^1_{\phi,l+1/2} \tag{5.570}$$

where the zero order term is

$$\begin{aligned} \langle J_\parallel \rangle^0_{\phi,l+1/2} = {} & \frac{2\pi q_e}{m_e} \frac{q_{l+1/2}}{\overline{q}_{l+1/2}} \sum_{i=0}^{n_p-1} \sum_{j=0}^{n_{\xi_0}-1} \frac{p^3_{i+1/2}}{\gamma_{i+1/2}} H\left(\left|\xi_{0,j+1/2}\right| - \xi_{0T,l+1/2}\right) \\ & \times \xi_{0,j+1/2} f^{(0)}_{0,l+1/2,i+1/2,j+1/2} \Delta p_{i+1/2} \Delta \xi_{0,j+1/2} \end{aligned} \tag{5.571}$$

The first order term arising from function g is

$$\begin{aligned} \langle J_\parallel \rangle^1_{\phi,l+1/2} = {} & \frac{2\pi q_e}{m_e} \frac{q_{l+1/2}}{\overline{q}_{l+1/2}} \sum_{i=0}^{n_p-1} \sum_{j=0}^{n_{\xi_0}-1} \frac{p^3_{i+1/2}}{\gamma_{i+1/2}} H\left(\left|\xi_{0,j+1/2}\right| - \xi_{0T,l+1/2}\right) \\ & \times \xi_{0,j+1/2} g^{(0)}_{l+1/2,i+1/2,j+1/2} \Delta p_{i+1/2} \Delta \xi_{0,j+1/2} \end{aligned} \tag{5.572}$$

while the other one which results from $\widetilde{f}$ is more complex and

$$\begin{aligned} \left\langle \widetilde{J}_\parallel \right\rangle^1_{\phi,l+1/2} = {} & \frac{2\pi q_e}{m_e} \frac{\widetilde{q}_{l+1/2}}{\overline{q}_{l+1/2}} \frac{R_p}{R_{0,l+1/2}} \frac{B_{T0,l+1/2}}{B_{0,l+1/2}} \sum_{i=0}^{n_p-1} \sum_{j=0}^{n_{\xi_0}-1} \frac{p^3_{i+1/2}}{\gamma_{i+1/2}} \lambda^{l+1/2,j+1/2}_{2,-2,2} \\ & \times \xi_{0,j+1/2} \widetilde{f}^{(0)}_{l+1/2,i+1/2,j+1/2} \Delta p_{i+1/2} \Delta \xi_{0,j+1/2}. \end{aligned} \tag{5.573}$$

Power Density Associated with a Flux

The density of power absorbed by the plasma through a particular mechanism is the sum

$$\langle P^{\mathcal{O}}_{abs} \rangle^0_{V,l+1/2} = \langle P^{\mathcal{O}}_{abs} \rangle^0_{V,l+1/2} + \langle P^{\mathcal{O}}_{abs} \rangle^1_{V,l+1/2} + \left\langle \widetilde{P}^{\mathcal{O}}_{abs} \right\rangle^1_{V,l+1/2}$$

where the respective contributions are given by the equations (3.322) and (3.324-3.325) and discretized as

$$\left\langle P_{abs}^{\mathcal{O}}\right\rangle_{V,l+1/2}^{0}=\frac{2\pi}{m_e}\frac{\widetilde{q}_{l+1/2}}{\widehat{q}_{l+1/2}}\sum_{i=1}^{n_p}\sum_{j=0}^{n_{\xi_0}-1}\frac{p_i^3}{\gamma_i}\lambda^{l+1/2,j+1/2}S_{p,l+1/2,i,j+1/2}^{(0)\mathcal{O}}\left(f_0^{(0)}\right)\Delta p_i\Delta\xi_{0,j+1/2} \tag{5.574}$$

$$\left\langle P_{abs}^{\mathcal{O}}\right\rangle_{V,l+1/2}^{1}=\frac{2\pi}{m_e}\frac{\widetilde{q}_{l+1/2}}{\widehat{q}_{l+1/2}}\sum_{i=1}^{n_p}\sum_{j=0}^{n_{\xi_0}-1}\frac{p_i^3}{\gamma_i}\lambda^{l+1/2,j+1/2}S_{p,l+1/2,i,j+1/2}^{(0)\mathcal{O}}\left(g^{(0)}\right)\Delta p_i\Delta\xi_{0,j+1/2} \tag{5.575}$$

$$\left\langle \widetilde{P}_{abs}^{\mathcal{O}}\right\rangle_{V,l+1/2}^{1}=\frac{2\pi}{m_e}\frac{\widetilde{q}_{l+1/2}}{\widehat{q}_{l+1/2}}\sum_{i=1}^{n_p}\sum_{j=0}^{n_{\xi_0}-1}\frac{p_i^3}{\gamma_i}\lambda^{l+1/2,j+1/2}\widetilde{S}_{p,l+1/2,i,j+1/2}^{(0)\mathcal{O}}\left(\widetilde{f}^{(0)}\right)\Delta p_i\Delta\xi_{0,j+1/2} \tag{5.576}$$

The discretization of the momentum-space flux components $S_{p,l+1/2,i,j+1/2}^{(0)\mathcal{O}}$ and $\widetilde{S}_{p,l+1/2,i,j+1/2}^{(0)\mathcal{O}}$ is done in (5.559).

Stream Function for Momentum Space fluxes

The stream function gives the local direction of the momentum-space fluxes, and its gradient is an indication of the flux intensity. Because it is a flux function, it is naturally defined on the momentum-space flux grid. According to the three equivalent expressions for the stream function (3.352-3.353), we have the following discretizations, for $1\leq i\leq n_p$ and $1\leq j\leq n_\xi-1$

$$A_{l+1/2,i,j}^{(0)}=\frac{2\pi p_i^2}{n_{e,l+1/2}}\sum_{m=0}^{j-1}\Delta\xi_{0,m+1/2}\;S_{p,l+1/2,i,m+1/2}^{(0)} \tag{5.577}$$

$$A_{l+1/2,i,j}^{(0)}=\frac{2\pi p_i^2}{n_{e,l+1/2}}\sum_{m=j}^{n_\xi-1}\Delta\xi_{0,m+1/2}\;S_{p,l+1/2,i,m+1/2}^{(0)} \tag{5.578}$$

and

$$A_{l+1/2,i,j}^{(0)}=\frac{2\pi\sqrt{1-\xi_{0,j}^2}}{n_{e,l+1/2}}\sum_{m=0}^{i-1}p_{m+1/2}\Delta p_{m+1/2}\;S_{\xi,l+1/2,m+1/2,j}^{(0)} \tag{5.579}$$

where the boundary conditions are

$$A_{l+1/2,0,j}^{(0)}=A_{l+1/2,i,0}^{(0)}=A_{l+1/2,i,n_\xi}^{(0)}=0 \tag{5.580}$$

The discretization of the momentum-space flux components $S_{p,l+1/2,i,j+1/2}^{(0)\mathcal{O}}$ and $S_{\xi,l+1/2,i+1/2,j}^{(0)\mathcal{O}}$ is done in (5.559) and (5.566).

Ohmic electric field

As shown in Sec. 4.2, the flux surface averaged parallel Ohmic electrid field $\langle E_\parallel \rangle_\phi (\psi)$ may be expressed as a function of its local value $E_{\parallel 0}(\psi)$ taken at the poloidal position where the magnetic field $\mathbf{B}$ is minimum, and

$$\langle E_\parallel \rangle_{\phi,l+1/2} = E_{\parallel 0,l+1/2} \frac{\widetilde{q}_{l+1/2}}{\overline{q}_{l+1/2}} \frac{R_p}{R_{0,l+1/2}} \frac{B_{T0,l+1/2}}{B_{0,l+1/2}} \overline{\lambda}^{l+1/2,j+1/2}_{1,-3,4} \tag{5.581}$$

Exact and effective fractions of trapped electrons

The exact fraction of trapped electrons is given by relation,

$$\begin{aligned}
\mathcal{F}_{t,l+1/2} = & \left[\sum_{i=0}^{n_p-1} \sum_{j=0}^{n_{\xi_0}-1} p^2_{i+1/2} H\left(\left| \xi_{0,j+1/2} \right| - \xi_{0T,l+1/2} \right) \lambda^{l+1/2,j+1/2} \right. \\
& \left. \times \left(\widetilde{f}^{(0)}_{l+1/2,i+1/2,j+1/2} + g^{(0)}_{l+1/2,i+1/2,j+1/2} \right) \Delta p_{i+1/2} \Delta \xi_{0,j+1/2} \right] \\
& \times \left[\sum_{i=0}^{n_p-1} \sum_{j=0}^{n_{\xi_0}-1} p^2_{i+1/2} \lambda^{l+1/2,j+1/2} \right. \\
& \left. \times \left(f^{(0)}_{0,l+1/2,i+1/2,j+1/2} + \widetilde{f}^{(0)}_{l+1/2,i+1/2,j+1/2} + g^{(0)}_{l+1/2,i+1/2,j+1/2} \right) \Delta p_{i+1/2} \Delta \xi_{0,j+1/2} \right]^{-1}
\end{aligned} \tag{5.582}$$

according to calculations given in Sec. 3.6.

The effective fraction of trapped electrons, as deduced from the Lorentz model in Sec. 5.6.2 is

$$\begin{aligned}
\mathcal{F}^{eff.}_{t,l+1/2} = & \frac{3}{2} \frac{B_{T0,l+1/2}}{B_{0,l+1/2}} \times \\
& \left[\frac{\widetilde{q}_{l+1/2}}{\overline{q}_{l+1/2}} \frac{B_{T0,l+1/2}}{B_{0,l+1/2}} \sum_{j=0}^{n_{\xi_0}-1} \xi^2_{0,j+1/2} \lambda^{l+1/2,j+1/2}_{2,-2,2} \Delta \xi_{0,j+1/2} \right. \\
& - \frac{q_{l+1/2}}{\overline{q}_{l+1/2}} \frac{R_{0,l+1/2}}{R_p} \sum_{j=0}^{n_{\xi_0}-1} \sigma_{j+1/2} H\left(\left| \xi_{0,j+1/2} \right| - \xi_{0T,l+1/2} \right) \\
& \left. \times \ \xi_{0,j+1/2} I_{\mathcal{L}} \left(\psi_{l+1/2}, \left| \xi_{0,j+1/2} \right| \right) \Delta \xi_{0,j+1/2} \right]
\end{aligned} \tag{5.583}$$

Runaway loss rate

As shown in Sec. 3.6, the runaway loss rate $\langle \Gamma_R \rangle_V (\psi)$ is given

$$\langle \Gamma_R \rangle_{V,l+1/2} = \frac{\widetilde{q}_{l+1/2}}{\widehat{q}_{l+1/2}} 2\pi p^2_{n_p-1} \sum_{j=0}^{n_{\xi_0}-1} \lambda^{l+1/2,j+1/2} S^{(0)}_{p,l+1/2,n_p-1,j+1/2} \Delta \xi_{0,j+1/2} \tag{5.584}$$

Magnetic ripple losses

In a similar way, the magnetic ripple loss rate $\Gamma^{(0)}_{ST}(\psi)$ is given by

$$\Gamma^{(0)}_{ST,l+1/2} = 2\pi p_{i_c}^2 \sum_{j=0}^{n_{\xi_0}-1} \lambda^{l+1/2,j+1/2} \left(1 - H\left(\left|\xi_{0,j+1/2}\right| - \xi_{0ST,l+1/2}\right)\right) S^{(0)}_{p,l+1/2,i_c,j+1/2} \Delta\xi_{0,j+1/2} + 4\pi\lambda^{l+1/2,j_{ST}} \sqrt{1-\xi^2_{0ST,j}} \sum_{i=0}^{n_p-1} p_{i+1/2} H\left(p_{i+1/2} - p_{i_c+1/2}\right) S^{(0)}_{\xi_0,l+1/2,i+1/2,j_{ST}} \Delta p_{i+1/2} \tag{5.585}$$

and the second formulation given in Sec.3.6 is

$$\Gamma^{(0)}_{ST,l+1/2} = 2\pi \sum_{i=0}^{n_p-1} \sum_{j=0}^{n_{\xi_0}-1} \left(1 - H\left(\left|\xi_{0,j+1/2}\right| - \xi_{0ST,l+1/2}\right)\right) H\left(p_{i+1/2} - p_{i_c+1/2}\right) \times \nu_{d_{ST,l+1/2,i+1/2,j+1/2}} f^{(0)}_{0,l+1/2,i+1/2,j+1/2} \Delta\xi_{0,j+1/2} \Delta p_{i+1/2} \tag{5.586}$$

where i_c is the index number that corresponds to the detrapping threshold by collisions, and $\xi_{0ST,l+1/2}$ is the picth-angle boundary value between super-trapped and trapped electrons.

Non-thermal bremsstrahlung

For the bremsstrahlung emission, it is necessary to calculate numericaly all coefficients of the Legendre series. Since Legendre polynomials P_m strongly oscillate between -1 and $+1$, as their order m increases, it is not possible to evaluate accurately integrals of the type

$$h^{(m)} = \int_{-1}^{+1} h(x) P_m(x) dx \tag{5.587}$$

by standard integration techniques, like trapezoidal or Simpson rules. The only possibility is to replace integral (5.587) by a discrete sum, namely a Gaussian quadrature,

$$h^{(m)} = \sum_{n=1}^{N} w_n h(x_n) P_m(x_n) \tag{5.588}$$

where weights w_n and abscissas x_n are determined independently. Here, the use of Legendre polynomials lead to consider the fast ans accurate Gauss-Legendre algorithm as derived by G. B. Ribicki in Ref. [24], where x_n are N zeros of the Legendre polynomial of degree N, the weights being given by the relation

$$w_n = \frac{2}{\left(1-x_n^2\right)\left[P'_N(x_n)\right]^2} \tag{5.589}$$

Very accurate determination of $h^{(m)}$ may be obtained by this method, which requires a value of $N = 50$.

Chapter 6

Algorithm

6.1 Matrix representation

6.1.1 Zero order term: the Fokker-Planck equation

Implicit time scheme

Projected on the numerical distribution function grid, and taking into account of the internal and external boundaries, the $3-D$ electron Fokker-Planck equation may be expressed as

$$\begin{aligned}
&\frac{\widetilde{q}_{l+1/2}}{B_{0,l+1/2}} p_{i+1/2}^2 \frac{f_{0,l+1/2,i+1/2,j'+1/2}^{(0)(k+1)} - f_{0,l+1/2,i+1/2,j'+1/2}^{(0)(k)}}{\Delta t} \\
&+ \frac{\widetilde{q}_{l+1/2}}{B_{0,l+1/2}} \sum_{i'=i-1}^{i'=i+1} \sum_{j''=j'-1}^{j''=j'+1} \widehat{\overline{M}}_{p,l+1/2,i'+1/2,j''+1/2}^{(0)} f_{0,l+1/2,i'+1/2,j''+1/2}^{(0)(k+1)} \\
&+ \frac{p_{i+1/2}^2}{\lambda^{l+1/2,j'+1/2}} \sum_{l'=l-1}^{l'=l+1} \widehat{\overline{M}}_{\psi,l'+1/2,i+1/2,j'+1/2}^{(0)} f_{0,l'+1/2,i+1/2,j'+1/2}^{(0)(k+1)} \\
&+ \frac{\widetilde{q}_{l+1/2}}{B_{0,l+1/2}} p_{i+1/2}^2 C^{(0)} \left(f_{M,l+1/2,i+1/2,j'+1/2}, \frac{3}{2} \xi_{0,j+1/2} f_{0,l+1/2,i+1/2,j'+1/2}^{(0)(m=1)(k)} \right) \\
= \; & 0
\end{aligned} \tag{6.1}$$

where $C^{(0)}$ is the first order Legendre electron-electron self-collision term that ensures momentum conservation, as discussed in Sec. 4.1, a contribution that introduces a weak non-linear dependence. Here, the Fokker-Planck equation (6.1) is evaluated on the reduced pitch-angle grid which is described by the index number j'.

Upwind differencing corresponding to the fully implicit time scheme is used, since it is usually numerically stable for arbitrary values of Δt. Therefore, with this method, a fast rate of convergence towards the steady-state solution $\lim_{k\to\infty} f_{0,l+1/2,i+1/2,j'+1/2}^{(0)(k+1)} = f_{0,l+1/2,i+1/2,j'+1/2}^{(0)(\infty)}$ may be achieved, using extremely large time step Δt, with respect to the usual collision reference time $\tau_c^\dagger$ as discussed in Sec. 6.3. The fact that both momentum

and spatial dynamics are considered simultaneously represents a considerable progress as compared to the standard operator splitting technique[1], where alternatively, dynamics in each space are considered explicitely, a procedure which puts strong limitations on the time step $\Delta t/\tau_c^\dagger \approx 1$.

In compact matrix form, the differential equation in the reduced momentum phase space has the following symbolic form

$$\left(\frac{\widehat{\mathbb{A}}}{\Delta t}+\widehat{\mathbb{B}}\right)X^{(k+1)}=\left(\frac{\widehat{\mathbb{A}}}{\Delta t}\right)X^{(k)}+\widehat{C}\left(X_M,X^{(k)}\right) \tag{6.2}$$

where $\widehat{\mathbb{A}}$ is a single diagonal matrix associated to time differencing, $\widehat{\mathbb{B}}$ corresponds to the flux divergence and $\widehat{C}$ is the first order Legendre correction. Here $X^{(k)}$ is a vector whose components are the discrete values of the distribution function $f_0^{(0)}$ at time step (k), organized as follows

$$X^{(k)}\rightarrow\left\{\begin{array}{l} l=0\rightarrow\left\{\begin{array}{l} i=0\rightarrow\left\{\begin{array}{l} j'=0\\ j'=\ldots\\ j'=n_{\xi_0}-n_{\xi_{0T,l+1/2}}-1\end{array}\right.\\ i=\ldots\\ i=n_p-1\end{array}\right.\\ l=\ldots\\ l=n_\psi-1\end{array}\right. \tag{6.3}$$

while X_M corresponds to the Maxwellian distribution function.

Without radial transport, $\widehat{\mathbb{B}}$ is a block diagonal matrix. Each block, which describes the momentum dynamics at location $\psi_{l+1/2}$, is a square matrice of 15 diagonals whose size $\left(n_{\xi_0}-n_{\xi_{0T,l+1/2}}\right)n_p\times\left(n_{\xi_0}-n_{\xi_{0T,l+1/2}}\right)n_p$ progressively decreases from $\psi_{1/2}$ to $\psi_{n_{\xi_0}-1/2}$ because of the trapped/passing boundary enlarges from the center to the plasma edge, as shown in Fig. 6.1. The main diagonal of $\widehat{\mathbb{B}}$ is dominant because collisions predominate over other physical processes at each plasma radius.

The introduction of the radial dynamics adds several extra off-diagonals, which connect neighboring blocks corresponding to different radial positions, in addition to the main diagonal which is also modified accordingly. The complexity arises from the fact that trapped electrons may become passing as a result of the radial transport process, and conversely. However, matrix $\widehat{\mathbb{B}}$ keeps a global banded structure and is still highly sparce, a property that is extensively used for reducing memory storage requirement. Indeed, size of $\widehat{\mathbb{B}}$ is roughly given by relation

$$size\left(\widehat{\mathbb{B}}\right)=n_p^2\left[\sum_{l=0}^{l=n_\psi-1}\left(n_{\xi_0}-n_{\xi_{0T,l+1/2}}\right)\right]^2\leq n_\psi^2n_p^2n_{\xi_0}^2 \tag{6.4}$$

For tokamak with very large aspect ratio, $size\left(\widehat{\mathbb{B}}\right)\approx n_\psi^2n_p^2n_{\xi_0}^2$ since trapped particle contribution is fairly negligible. In this limit, an upper boundary of the memory size

[1]The Alternative Direction Implicit (ADI) belongs also to the operator splitting method, but with a slightly different twist. The limitation on the time step is therefore similar

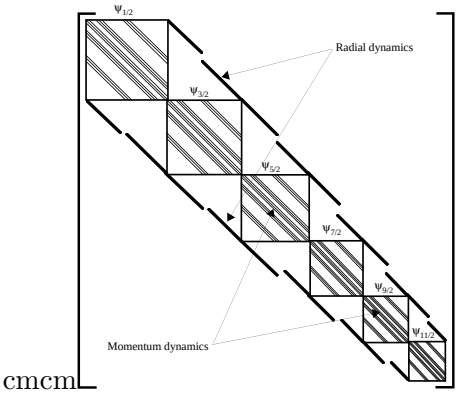

Figure 6.1: Qualitative shape of matrix $\widehat{\mathbb{B}}$ for the Fokker-Planck equation

requirement may be estimated. For the reference case, $n_\psi = 20$, $n_p = 200$ and $n_{\xi_0} = 200$, the total number of coefficients reaches $64 \times 10^{+10}$, and the needed memory capacity[2] is $5.12 TBytes$! Hopefully, this huge number may be drastically reduced down to $11 \times n_\psi n_p n_{\xi_0}$, since $\widehat{\mathbb{A}}$ becomes in that limit a simple banded matrix with exactly 11 diagonals. The required memory falls down therefore to $70.4 MBytes$[3], a level which can be easily handled by most computers today.

Crank-Nicholson time scheme

The Crank-Nicholson time scheme is used for time evolution studies of the distribution function $f_0^{(0)}$. It is second order accurate in time, but this scheme requires usualy $\Delta t/\tau_c^\dagger \approx 1$, in order to avoid spurious numerical oscillations towards the steady-state solution $f_0^{(0)(\infty)}$. From Eq.6.2, it is straightforward to derive the new matrix form of the Fokker-Planck equation

$$\left(\frac{\widehat{\mathbb{A}}}{\Delta t} + \frac{\widehat{\mathbb{B}}}{2}\right) X^{(k+1)} = \left(\frac{\widehat{\mathbb{A}}}{\Delta t} - \frac{\widehat{\mathbb{B}}}{2}\right) X^{(k)} + \widehat{C}\left(X_M, X^{(k)}\right) \tag{6.5}$$

by just replacing

$$\widehat{\mathbb{B}} X^{(k+1)} \rightarrow \widehat{\mathbb{B}}\left(\frac{X^{(k)} + X^{(k+1)}}{2}\right) \tag{6.6}$$

since $\widehat{\mathbb{B}}$ is a linear operator.

6.1.2 Up to first order term: the Drift Kinetic equation

Projected on the numerical distribution function grid, and taking into account of the internal and external boundaries, the $3-D$ electron drift kinetic equation may be expressed

[2] On a basis that a double precision real number is described by 8 Bytes.

[3] This number is usualy slightly larger, in order to store index values of all non-zero coefficients. However, the order of magnitude is not modified

as

$$\sum_{i'=i-1}^{i'=i+1}\sum_{j''=j'-1}^{j''=j'+1}\widehat{\overline{M}}^{(0)}_{p,l+1/2,i'+1/2,j'+1/2}g^{(0)(k)}_{l+1/2,i'+1/2,j''+1/2} = \widehat{\widetilde{W}}^{(0)}_{p,l+1/2,i+1/2,j'+1/2} - p^2_{i+1/2}C^{(0)}\left(f_{M,l+1/2,i+1/2,j'+1/2}, \frac{3}{2}\xi_{0,j+1/2}g^{(0)(m=1)(k)}_{l+1/2,i+1/2,j'+1/2}\right) \tag{6.7}$$

where

$$\begin{aligned}\widehat{\widetilde{W}}^{(0)}_{p,l+1/2,i+1/2,j+1/2} &= -\sum_{i'=i-1}^{i'=i+1}\sum_{j''=j-1}^{j''=j+1}\widetilde{\overline{M}}^{(0)}_{p,l+1/2,i'+1/2,j''+1/2}\widetilde{f}^{(0)}_{l+1/2,i'+1/2,j''+1/2} \\ &\quad -\sum_{i'=i-1}^{i'=i+1}\sum_{j''=j-1}^{j''=j+1}\widetilde{\overline{H}}^{(0)}_{\psi,l+1/2,i'+1/2,j''+1/2}\widetilde{f}^{(0)}_{l+1/2,i'+1/2,j''+1/2} \\ &\quad -p^2_{i+1/2}\widetilde{C}^{(0)}\left(f_{M,l+1/2,i+1/2,j+1/2}, \frac{3}{2}\xi_{0,j+1/2}\widetilde{f}^{(0)(m=1)}_{l+1/2,i+1/2,j+1/2}\right)\end{aligned} \tag{6.8}$$

As mentioned in Sec.5.7.2, $j \rightarrow \{0, n_{\xi_0}-1\}$, while $j' \rightarrow \left\{0, n_{\xi_0} - m_{\xi_{0T,l+1/2}} - 1\right\}$ corresponds to the reduced pitch-angle grid which depends of the radial position $\psi_{l+1/2}$, since all the trapped region has been removed. In Eq.6.7, time evolution is not considered, since function $g^{(0)}$ is only determined for steady-state value of $\widetilde{f}^{(0)}$. Therefore, iterations to reach the solution only result from the non-linear electron self-collision operator $C^{(0)}$, that ensures momentum conservation, in order to find a self-consistent solution.

In compact matrix form, the differential equation in the reduced momentum phase space has the following symbolic form

$$\widehat{\mathbb{G}}Y^{(k+1)} = \widehat{\mathbb{G}}Y^{(k)} + \widehat{C}\left(X_M, Y^{(k)}\right) + \widehat{\widetilde{W}} \tag{6.9}$$

where $\widehat{\mathbb{G}}$ corresponds to the flux divergence, $\widehat{C}$ is the first order Legendre correction and $\widehat{\widetilde{W}}$ to the contribution of the radial gradient of the distribution function $f_0^{(0)}$. Here $Y^{(k)}$ is a vector whose components are the discrete values of the distribution function $g^{(0)(k)}$ at iteration step (k), organized as follows

$$Y^{(k)} \rightarrow \left\{\begin{array}{l} l=0 \rightarrow \left\{\begin{array}{l} i=0 \rightarrow \left\{\begin{array}{l} j'=0 \\ j'=\ldots \\ j'=n_{\xi_0}-m_{\xi_{0T,l+1/2}}-1 \end{array}\right. \\ i=\ldots \\ i=n_p-1 \end{array}\right. \\ l=\ldots \\ l=n_\psi-1 \end{array}\right. \tag{6.10}$$

and vector X_M is corresponding to the Maxwellian distribution function, as defined in Sec. 6.1.1.

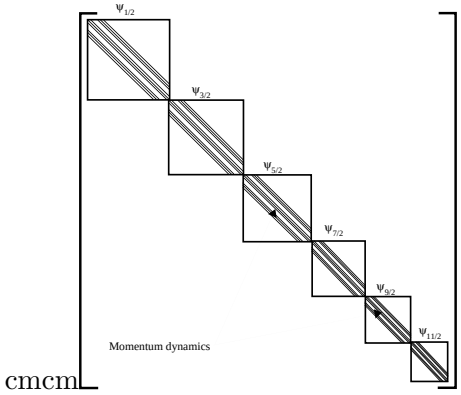

Figure 6.2: Qualitative shape of matrix $\widehat{\mathbb{G}}$ for the drift kinetic equation

By construction, $\widehat{\mathbb{G}}$ is simply a block diagonal matrix. Each block, which describes the momentum dynamics at location $\psi_{l+1/2}$, is a square matrice of 9 diagonals whose size $\left(n_{\xi_0} - m_{\xi_{0T,l+1/2}}\right) n_p \times \left(n_{\xi_0} - m_{\xi_{0T,l+1/2}}\right) n_p$ progressively decreases from $\psi_{1/2}$ to $\psi_{n_{\xi_0}-1/2}$ because of the trapped/passing boundary enlarges from the center to the plasma edge, as shown in Fig. 6.2. The main diagonal of $\widehat{\mathbb{G}}$ is also dominant because collisions predominate over other physical processes at each plasma radius.

The matrix $\widehat{\mathbb{G}}$ has a global banded structure with an extremely high sparcity, a property that is also extensively used for memory storage, like for the Fokker-Planck equation (see Sec. 6.1.1). Indeed, the size of $\widehat{\mathbb{G}}$ is roughlu given by relation

$$size\left(\widehat{\mathbb{G}}\right) = n_p^2 \left[\sum_{l=0}^{l=n_\psi-1} \left(n_{\xi_0} - m_{\xi_{0T,l+1/2}}\right)\right]^2 \leq n_\psi^2 n_p^2 n_{\xi_0}^2 \tag{6.11}$$

For tokamak with very large aspect ratio, $size\left(\widehat{\mathbb{G}}\right) \approx n_\psi^2 n_p^2 n_{\xi_0}^2$ since trapped particle contribution is fairly negligible. In this limit, $size\left(\widehat{\mathbb{G}}\right) \simeq size\left(\widehat{\mathbb{B}}\right)$, where $\widehat{\mathbb{B}}$ is the flux matrix of the Fokker-Planck equation. For the values of n_ψ, n_p and n_{ξ_0} taken in Sec. 6.1.1, the required memory is approximately $57.6 MBytes$, a lower level than for the Fokker-Planck equation, since the trapped region is completely removed in the calculations.

6.2 Inversion procedure

6.2.1 Incomplete matrix factorization

According to Sec. 6.1.1, the electron Fokker-Planck equation may be expressed in a general symbolic matrix form

$$\widehat{\mathbb{N}} Z^{(k+1)} = \Upsilon^{(k)} \tag{6.12}$$

where $Z = X$ with

$$\widehat{\mathbb{N}} = \frac{\widehat{\mathbb{A}}}{\Delta t} + \widehat{\mathbb{B}} \tag{6.13}$$

$$\Upsilon^{(k)} = \left(\frac{\widehat{\mathbb{A}}}{\Delta t}\right) X^{(k)} + \widehat{C}\left(X_M, X^{(k)}\right) \tag{6.14}$$

for the fully implicit time difference scheme, and

$$\widehat{\mathbb{N}} = \frac{\widehat{\mathbb{A}}}{\Delta t} + \frac{\widehat{\mathbb{B}}}{2} \tag{6.15}$$

$$\Upsilon^{(k)} = \left(\frac{\widehat{\mathbb{A}}}{\Delta t} - \frac{\widehat{\mathbb{B}}}{2}\right) X^{(k)} + \widehat{C}\left(X_M, X^{(k)}\right) \tag{6.16}$$

for the the Crank-Nicholson time scheme.

The formal expression (6.12) may be also used for the electron drift kinetic equation as shown in Sec. 6.1.2, and in this case, $Z = Y$ with

$$\widehat{\mathbb{N}} = \widehat{\mathbb{G}} \tag{6.17}$$

$$\Upsilon^{(k)} = \widehat{\mathbb{G}} Y^{(k)} + \widehat{C}\left(X_M, Y^{(k)}\right) + \widehat{\widetilde{W}} \tag{6.18}$$

In all cases, matrices are square with similar structures, i.e. non-zero elements are aligned along a reduced number of diagonals which are roughly symmetricaly placed around the main one[4], as shown in Fig.6.3. Consequently, the method for determining the asymptotic solution

$$Z^{(\infty)} = \lim_{k \to \infty} Z^{(k)} \tag{6.19}$$

of the system of equations (6.12) will be the same, either for the Fokker-Planck or the drift kinetic equations.

In order to avoid manipulation of large matrix coefficients that may reduce the numerical accuracy and also leads often to numerical instabilities, main diagonal matrix preconditioning is first performed. The modified system of equation to solve is then

$$\left(\widehat{\mathbb{P}}_N^{-1} \widehat{\mathbb{N}}\right) Z^{(k+1)} = \widehat{\mathbb{P}}_N^{-1} \Upsilon^{(k)} \tag{6.20}$$

where all the coefficients of the main diagonal of matrix $\widehat{\mathbb{N}}'$

$$\widehat{\mathbb{N}}' = \widehat{\mathbb{P}}_N^{-1} \widehat{\mathbb{N}} \tag{6.21}$$

are one by definition. Here $\widehat{\mathbb{P}}_N$ is a diagonal matrix whose coefficients are those of the main diagonal of $\widehat{\mathbb{N}}$. Since collision is the dominant physics process, all off-diagonal coefficients are usualy less than one, as shown in Fig.6.4, except when specific internal boundary conditions apply, like at $\xi_0 = 0$ in the trapped region.

[4]The lack of symmetry between upper and lower diagonals arises usually from boundary conditions.

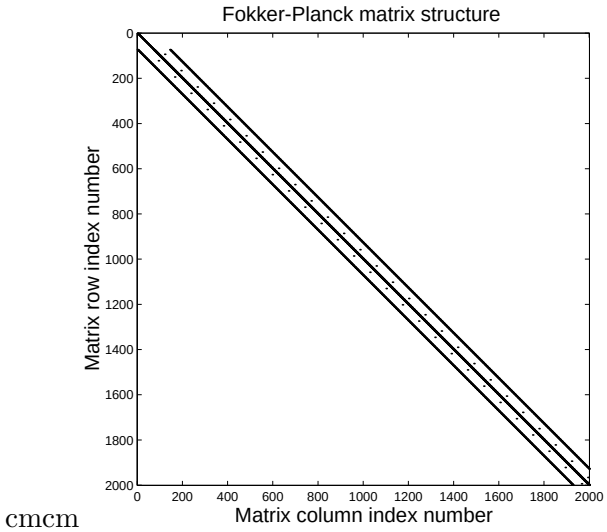

cmcm

Figure 6.3: Typical arrangement of non-zero matrix coefficients in the first 2000 columns and rows in matrix $\widehat{\mathbb{N}}$ corresponding to the Fokker-Planck equation

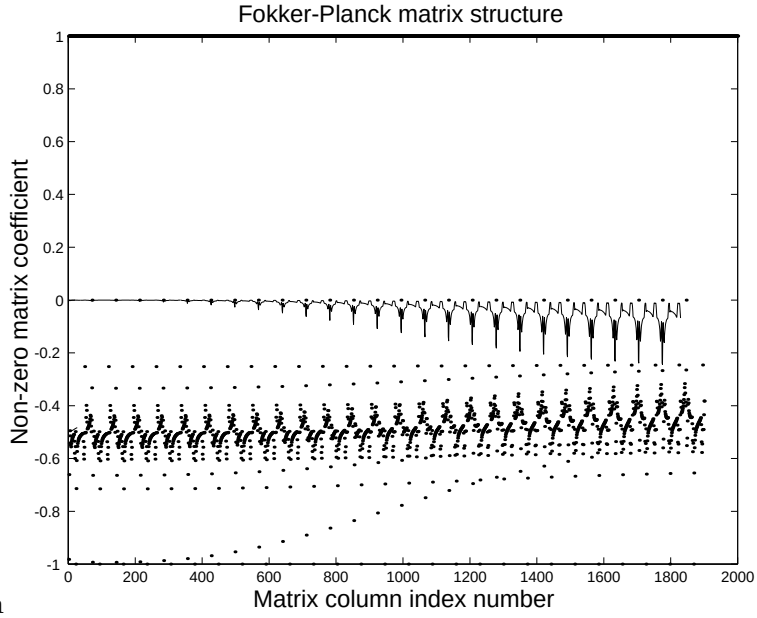

cmcm

Figure 6.4: Values of the non-zero matrix coefficients after diagonal preconditionning for matrix $\widehat{\mathbb{N}}'$ corresponding to the Fokker-Planck equation. Dot points correspond to pitch-angle process at constant p, while full line for slowing-down process at constant ξ_0. By definition values of all coefficients on the main diagonal are one

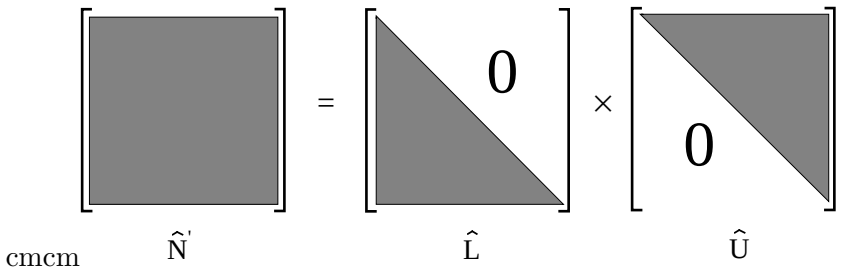

Figure 6.5: Matrix factorization principle. Dashed areas correspond to non-zero coefficients.

The determination of $Z^{(k+1)}$ requires to invert the system of equation (6.12). The usual method based on a direct inversion by the well known Gaussian elimination is immediately ruled out, since the number of operations for each direction is $\mathcal{O}\left(N^3\right)$, where N is the number of rows (or columns) of matrix $\widehat{\mathbb{N}}$. For the example $n_\psi = 20$, $n_p = 200$ and $n_{\xi_0} = 200$ discussed in Sec. 6.1.1, $N = n_\psi n_p n_{\xi_0} = 800000$, $\mathcal{O}\left(N^3\right) \simeq 10^{+17}$, corresponding to a prohibitive number of operations. In addition, since memory requirements grow as $\mathcal{O}\left(N^2\right)$ unacceptable storage constraints take also place.

Consequently, alternative methods must be used, in order to perform a fast matrix inversion without the need of a large memory storage requirement. The basic principle is to factorize $\widehat{\mathbb{N}}'$ into upper and lower triangular matrices $\widehat{\mathbb{U}}$ and $\widehat{\mathbb{L}}$ respectively

$$\widehat{\mathbb{N}}' = \widehat{\mathbb{L}}\widehat{\mathbb{U}} \tag{6.22}$$

as shown in Fig. 6.5, that are themselves highly sparse matrices. A strong reduction of the computational effort may then be foreseen, since the number of coefficients that are considered in the calculations is considerably lower. Indeed, aside from the time required to perform the matrix factorization itself which represents a computational effort equivalent to a direct matrix inversion, each further inversion needs only $\mathcal{O}\left(N^2\right)$ operations for each triangular system of equations as shown in the next sections. Therefore, for large values of N, a substantial gain may be expected, as soon as the number of iterations for an accurate estimate of the solution $Z^{(\infty)}$ is greater than unity. This is usually the case for the time dependent problem where all time steps must be evaluated, but also when only the steady-state solution $Z^{(\infty)}$ is seeked, since the non-linearity resulting form self-collision operators $\widehat{C}$ requires several iterations either for the Fokker-Planck or the drift kinetic equations. This elegant approach has been first considered for Fokker-Planck calculations for a five diagonals operator as presented in Ref. [25], since in that case $\widehat{\mathbb{U}}$ and $\widehat{\mathbb{L}}$ are both triangular and tridiagonal matrices. However, as discussed in Ref. [9], the fact that cross-derivatives are considered explicitely with respect to the time differencing scheme puts strong limitations. Indeed, the integration time step Δt must be much lower than one for an accurate determination of the solution of the set of linear equations. Consequently, the overall time duration for calculating the steady-state solution is very long, an important drawback when the kinetic solver must be incorporated in a chain of codes for realistic tokamak simulations.

For this purpose, this method has been succesfully extended to the nine diagonals operator case, allowing the use of much larger Δt values while the numerical scheme remains stable, as shown in Ref. [9]. However, this approach is only useful for local kinetic calculations, where trapped particle contribution is negligible, i.e. close to the plasma center. When off-axis electron dynamics must be described, one must in that case fully consider both circulating and trapped electron dynamics which leads to a number of diagonals with non-zero elements that is much larger, fifteen diagonals at each radial location as shown in Fig. 6.1. Therefore, the method developped for nine diagonal operators may no more be used, since the number of operations to determine $\widehat{\mathbb{U}}$ and $\widehat{\mathbb{L}}$ increases dramaticaly. The fully $3-D$ approach with radial transport makes also this method unusable, since the matrix that must be inverted has no more the nine diagonal structure.

However, an equivalent form of the approximate matrix factorization may still be employed, noting that exact $\widehat{\mathbb{U}}$ and $\widehat{\mathbb{L}}$ matrices are made of a large number of very small coefficients, close to zero. This indicates that information on the electron dynamics is fully contained in a few set of coefficients, whose number is several order of magnitude lower than the total one. Such a structure results in fact from the well conditionning of the matrix $\widehat{\mathbb{N}}'$, a physical consequence that collisions predominate over all other physical processes. Consequently, the general approach is to introduce a non-negative scalar named as the drop tolerance parameter δ_{lu}, below which small coefficients of exact $\widehat{\mathbb{U}}$ and $\widehat{\mathbb{L}}$ matrices are forced to zero. By this way, an approximation of the exact matrix factorization is performed. The only exception to the dropping rule is the diagonal of the upper triangular matrix which is preserved even if coefficients are too small, in order to avoid singular factors. Since coefficients of $\widehat{\mathbb{N}}'$ lie between 0 and 1 in the limit where the model holds, because of the main diagonal preconditioning, the drop tolerance parameter δ_{lu} may be arbitrarily chosen in the same interval, i.e.

$$0 \leq \delta_{lu} \leq 1 \tag{6.23}$$

and when δ_{lu} is close to 0, approximate and exact matrices $\widehat{\mathbb{U}}$ and $\widehat{\mathbb{L}}$ are roughly equivalent, while they differ strongly when δ_{lu} tends to one. In the latter case, considerable saving may be foreseen for the memory requirement, as well as a significant reduction of the computer time consumption, since less non-zero coefficients must be considered. An example is shown in Fig. 6.6, where δ_{lu} varies from zero to 10^{-2}. Consequently, from the exact matrix factorization to the approximate one, the number of non-zero elements drops by a factor around 30.

The rule is therefore to find the largest δ_{lu} value that is compatible with a stable inversion procedure, even in presence of a large Ohmic electric field or a high RF power. However too large δ_{lu} values will remove important physical informations, leading to spurious solutions. However, it turns out that margins are usually considerable, making the method very effective. An example is given in Fig. 6.7, which illustrates the effectiveness of the method, for the Lower Hybrid current drive local problem. For $\delta_{lu} \simeq 2\times10^{-3}$, memory size requirement to store matrices $\widehat{\mathbb{U}}$ and $\widehat{\mathbb{L}}$ does not exceed $2.2MBytes$, while it reaches $66MBytes$ when $\delta_{lu} = 0$. It is interesting to observe that the convergence rate towards the steady-state solution $Z^{(\infty)}$ is reduced by 50%, and that the result is moreover independent of δ_{lu}. For larger δ_{lu} values, the inversion scheme becomes progressively unstable, and the benefit gains on the memory storage requirement is therefore cancelled by a reduced rate

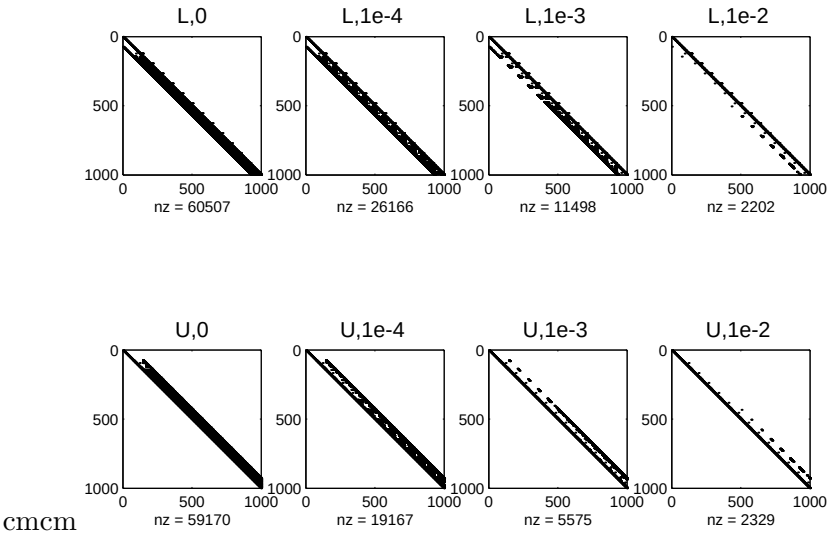

Figure 6.6: Reduction of the non-zero elements for the $\widehat{\mathbb{L}}$ and $\widehat{\mathbb{U}}$ matrices, by increasing δ_{lu}. Values of δ_{lu} are indicated on the top of each subfigure. For $\delta_{lu} = 10^{-2}$, the inversion becomes instable.

of convergence. For this reason, the upper value used in the code is usually $\delta_{lu} \simeq 2 \times 10^{-3}$. More refined methods may be used to optimized the choice of δ_{lu}. The trade-off that must be found between memory saving and stability of the inversion procedure requires extensive investigations that are beyond the scope of this document. Hopefully, it turns out that the domain $1 \times 10^{-4} \leq \delta_{lu} \leq 2 \times 10^{-3}$ covers must of the parameter range for the current drive problem in tokamaks, even in presence of radial transport. Since the local problems needs only $2.2 MBytes$, it is therefore possible to extrapolate that the full $3-D$ problem with 20 radial positions will only require approximately $44 MBytes$. This result has justified the development of this new approach.

6.2.2 Zero order term: the Fokker-Planck equation

The matrix inversion procedure is based on the possibility of matrix factorization as discussed in Sec.6.2.1. Formally, the iterative method may be expressed in the simple form

$$\widehat{\mathbb{N}}' Z^{(k+1)} = \widehat{\mathbb{N}}' Z^{(k)} - \beta_C \left(\widehat{\mathbb{N}}' Z^{(k)} - \widehat{\mathbb{P}}_N^{-1} \Upsilon^{(k)} \right) \tag{6.24}$$

where β_C is the iteration parameter that may be adjusted for an improvement of the rate of convergence, using a Chebyshev acceleration technique as shown in Ref. [16]. Here $\widehat{\mathbb{P}}$ is used for the main diagonal precondiotiong as explained in Sec.6.2.1 . However, it has been shown that values of β_C other than unity do not give much better results in general for implicit methods ([9]), and therefore, only the case $\beta_C = 1$ is considered. Then Eq. 6.24 is equivalent to Eq. 6.12 given in Sec. 6.2.1. Replacing $\widehat{\mathbb{N}}'$ by $\widehat{\mathbb{L}}\widehat{\mathbb{U}}$, one obtains

$$\widehat{\mathbb{L}}\widehat{\mathbb{U}} Z^{(k+1)} = \widehat{\mathbb{P}}_N^{-1} \Upsilon^{(k)} \tag{6.25}$$

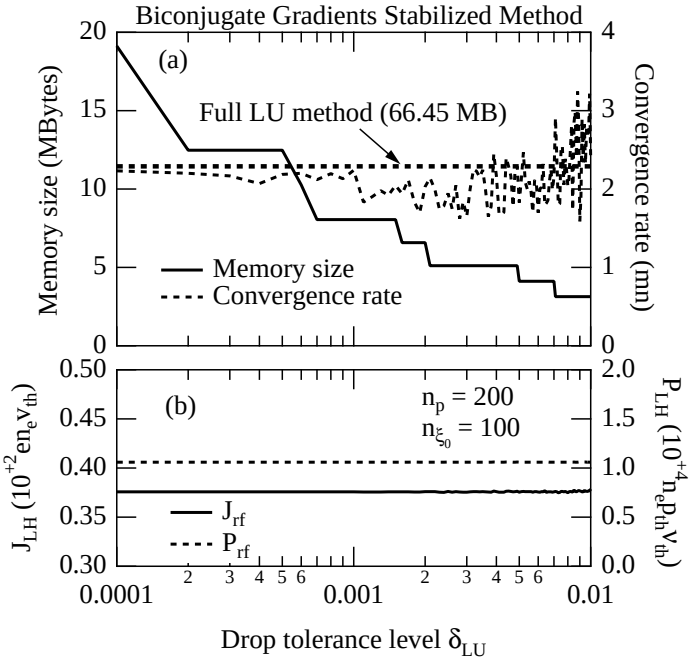

cmcm

Figure 6.7: Memory storage requirement reduction by increasing the δ_{lu} parameter, for the Lower Hybrid current drive problem. The rate of convergence towards the steady state solution is given, using the biconjugate gradients stabilized method to solve the system of linear equations. Here only a local analysis is considered at a given radial position

If we introduce the increment $\Delta_Z^{(k+1)}$

$$\Delta_Z^{(k+1)} = Z^{(k+1)} - Z^{(k)} \tag{6.26}$$

and the residual $R_Z^{(k)}$

$$R_Z^{(k)} = \widehat{\mathbb{P}}_N^{-1}\Upsilon^{(k)} - \widehat{\mathbb{N}}' Z^{(k)} \tag{6.27}$$

Eq.6.25 becomes simply

$$\widehat{\mathbb{L}}\widehat{\mathbb{U}}\Delta_Z^{(k+1)} = R_Z^{(k)} \tag{6.28}$$

which can be solved by two successive inversion steps, evaluating respectively forward and backward solutions from triangular systems of equations

$$\widehat{\mathbb{L}} V_Z^{(k+1)} = R_Z^{(k)} \tag{6.29}$$

$$\widehat{\mathbb{U}}\Delta_Z^{(k+1)} = V_Z^{(k+1)} \tag{6.30}$$

For achieving convergence towards the steady state solution $Z^{(\infty)}$, various iterative methods may be used, like the Conjugate Gradient Squared (CGS), the BiConjigate Gradient (BICG) or the Quasi-Minimal Residual (QMR) methods. These methods, which both give equivalent results in term of convergence rate, are preferred to the BiConjigate Gradient Stabilized (BICGSTAB) method, since the conservative scheme is nearly always well fullfiled even for marginaly well-conditionned matrices, like in presence of RF waves whose intensity is large. All methods here considered are build-in MatLab functions whose principle may be found in Refs. [24] or [26] for more detailed insights.

After numerous tests, it has been found that the drop tolerance parameter δ_{lu} has a close link with the maximum number of iterations $MAXIT$ allowed inside the function that performs the iterative matrix inversion, in order to avoid cumulative numerical errors that lead usually to violation of the conservative nature of the code. Even if this problem may be cured by forcing the Maxwellian solution close to $p = 0$ and normalizing the solution at each iteration, this approach has not been considered, because it may hinder more serious problems regarding the overall numerical conservative scheme. So far, a very robust and fully conservative scheme is achieved with the following rule of thumb

$$\begin{cases} \delta_{lu} = 10^{-5} : MAXIT < 2-3 \\ \delta_{lu} = 10^{-4} : MAXIT < 4-5 \\ \delta_{lu} = 10^{-3} : MAXIT < 9-10 \\ \delta_{lu} = 10^{-2} : MAXIT < 19-20 \end{cases} \tag{6.31}$$

for all cases addressed by the code, including the in presence of RF waves. More detailed studied are necessary to clarify this point.

At each iteration, $Z^{(k+1)}$ is evaluated from the knowledge of $\Delta_Z^{(k+1)}$, and the electron distribution function $f^{(0)}_{0,l+1/2,i+1/2,j+1/2}$ is reconstructed in order to evaluate the non-linear term $\widehat{C}\left(X_M, Z^{(k)}\right)$ that arises from self-collisions. Though this procedure is quite time consuming, its incidence on the overall time for converging is fairly marginal, since the number of iterations never exceeds 10 in most cases.

According to Ref. [22], convergence towards $Z^{(\infty)}$ is considered to be achieved and the iteration is stopped when the following criterion is fullfiled

$$\sqrt{\frac{2\pi \iint \left[\partial f_0^{(0)}/\partial t\right]^2 f_0^{(0)} J_p J_{\xi_0} dp d\xi_0}{2\pi \iint f_0^{(0)} J_p J_{\xi_0} dp d\xi_0}} < \mathcal{R}_{\mathcal{C}}^f \tag{6.32}$$

for an arbitrarily small $\mathcal{R}_{\mathcal{C}}^f$, at all plasma locations ψ, where J_p and J_{ξ_0} are the partial Jacobians as introduced in Sec. 3.5.1[5].

Projected on the numerical grid, the criterion (6.32) becomes

$$\begin{aligned}
&\left[\sum_{i=0}^{i=n_p-1}\sum_{j=0}^{j=n_{\xi_0}-1}\left[f^{(0)(k+1)}_{0,l+1/2,i+1/2,j+1/2} - f^{(0)(k)}_{0,l+1/2,i+1/2,j+1/2}\right]^2\right.\\
&\quad\left.\times f^{(0)(k)}_{0,l+1/2,i+1/2,j+1/2} p^2_{i+1/2}\Delta p_{i+1/2}\Delta\xi_{0,j+1/2}\right]^{1/2}\\
&\quad\times\left[\Delta t^2\sum_{i=0}^{i=n_p-1}\sum_{j=0}^{j=n_{\xi_0}-12} f^{(0)(k)}_{0,l+1/2,i+1/2,j+1/2} p^2_{i+1/2}\Delta p_{i+1/2}\Delta\xi_{0,j+1/2}\right]^{-1/2}\\
&< \mathcal{R}_{\mathcal{C}}^f
\end{aligned} \tag{6.33}$$

The criterion introduced in Ref. [16] has the main advantage to ensure that convergence is achieved not for electrons whose energy is close to the thermal one, but also for the fastest when a tail is driven by an external source. Usually, $\mathcal{R}_{\mathcal{C}}^f$ ranges between 10^{-10} and 10^{-12}, and in the code the standard value is 10^{-11}. The quantity (6.32) may be viewed as a norm, and its definition is consequently independent of the level of current which results from the the lack of symmetry of $f_0^{(0)}$ in momentum space. It may therefore be used for strong deformations of the electron distribution function, even if the net current is close to zero.

In practice, the total number of iteration $\mathcal{N}_{\mathcal{C}}^f$ is a free choice. It is usually set to 50, so that inversion procedure stops when (6.32) is fullfiled in quite all cases. If the number of iterations reaches $\mathcal{N}_{\mathcal{C}}^f$, the program warns that convergence is not achieved and that something is going wrong in the calculations. This may occur sometimes when too large quasilinear RF diffusion coefficient are used, leading to inconsistent and non physical solutions. This point is extensively discussed in Sec.7.3. Conversely, when time step is very large, i.e. $\Delta\bar{t} \geq 1000$, the convergence may be achieved for a given value $\mathcal{R}_{\mathcal{C}}^f$ before the current level is fully established. Such an event may arise because there is a too reduced number of iterations which involves the 1^{st} order Legendre non-linear correction term for momentum conservation. Consequently, to avoid this problem, a minimum number of iterations has been set to 6, which turns out to be enough for giving reliable results, owing to the weakness of the non-linearity.

[5]The possibility to define a fully $3-D$ criterion has been foreseen. However, since collision rates may change drasticaly from plasma center to the edge, this choice ensures that convergence is well achieved at the right level at all plasma locations.

6.2.3 Up to first order term: the Drift Kinetic equation

The inversion procedure for solving the first order drift kinetic equation is exactly similar to the one described in Sec. 6.2.2. Indeed, the linear system of equation to be solved may be cast in a similar form. Usually, the convergence coefficient $\mathcal{R}_{\mathcal{C}}^{g}$ is set to similar values than for the Fokker-Planck problem, while the maximum number of iterations allowed $\mathcal{N}_{\mathcal{C}}^{g}$ is slightly larger [6], since the convergence requires more iterations, around $20-30$. Since the function $g_0^{(0)}$ may be negative and that dt has no sense here, as the solution is determined once the steady-state regime is achieved, the convergence criterion is modified accordingly

$$\sqrt{\left|\frac{2\pi\iint \Delta g_0^{(0)2} g_0^{(0)} J_p J_{\xi_0} dp d\xi_0}{2\pi\iint g_0^{(0)} J_p J_{\xi_0} dp d\xi_0}\right|} < \mathcal{R}_{\mathcal{C}}^{g} \tag{6.34}$$

at all plasma locations ψ. Here again J_p and J_{ξ_0} are the partial Jacobians introduced in Sec. 3.5.1[7].

Projected on the numerical grid, the criterion (6.34) becomes

$$\begin{aligned}&\left|\sum_{i=0}^{i=n_p-1}\sum_{j=0}^{j=n_{\xi_0}-1}\left[g^{(0)(k+1)}_{0,l+1/2,i+1/2,j+1/2} - g^{(0)(k)}_{0,l+1/2,i+1/2,j+1/2}\right]^2\right.\\ &\left.\times g^{(0)(k)}_{0,l+1/2,i+1/2,j+1/2} p^2_{i+1/2}\Delta p_{i+1/2}\Delta\xi_{0,j+1/2}\right|^{1/2}\\ &\times\left|\sum_{i=0}^{i=n_p-1}\sum_{j=0}^{j=n_{\xi_0}-12} g^{(0)(k)}_{0,l+1/2,i+1/2,j+1/2} p^2_{i+1/2}\Delta p_{i+1/2}\Delta\xi_{0,j+1/2}\right|^{-1/2} < \mathcal{R}_{\mathcal{C}}^{g}\end{aligned} \tag{6.35}$$

where (k) is the iteration step number. Since all quantities are normalized, this definition is fully acceptable. If the number of iterations reaches $\mathcal{N}_{\mathcal{C}}^{g}$, the program warns that convergence is not achieved and that something is going wrong in the calculations, as for the Fokker-Planck part.

6.3 Normalization and definitions

6.3.1 Temperature and density

In order to use parameters without dimensions in the calculations, all of them are normalized to reference values. Here temperature and densities correspond to flux surface-averaged values, though the usual bracket notation is not introduce, for sake on simplicity.

Normalized temperatures, are defined by the relations

$$\begin{aligned}\overline{T}_e(\psi) &= T_e(\psi)/T_e^{\dagger}\\ \overline{T}_{ss'}(\psi) &= T_{ss'}(\psi)/T_e^{\dagger}\end{aligned} \tag{6.36}$$

[6] Usually twice $\mathcal{N}_{\mathcal{C}}^{f}$

[7] The possibility to define a fully $3-D$ criterion has been foreseen. However, since collision rates may change drasticaly from plasma center to the edge, this choice ensures that convergence is well achieved at the right level at all plasma locations.

where the subscripts e stands for electrons and ss' for ion species s in the ionization state s', whose charge is $Z_{ss'}$. Here, both $T_e(\psi)$ and $T_e^\dagger$ have defined units, while $T_e^\dagger$ is the reference value for the normalization. According to this rule, the normalized densities are defined in the same way

$$\begin{cases} \overline{n}_e(\psi) = n_e(\psi)/n_e^\dagger \\ \overline{n}_{ss'}(\psi) = n_{ss'}(\psi)/n_e^\dagger \end{cases} \tag{6.37}$$

and in order to ensure that all quantities are less than unity from the plasma center to the edge, references values are given by the condition

$$\begin{cases} T_e^\dagger = \max\left(T_e(\psi), T_{ss'}(\psi)\right) \\ n_e^\dagger = \max\left(n_e(\psi), n_{ss'}(\psi)\right) \end{cases} \tag{6.38}$$

for $0 \leq \psi \leq \psi_{\max}$.

In principle, ion densities $n_{ss'}(\psi)$ are obtained from a particle transport code transport code. However, when the plasma is made of two types of ions which are fully ionized (low Z limit), a simple model may be used in order to determine densities $n_s(\psi)$ with $s = \{1, 2\}$, knowing electron density $n_e(\psi)$ and effective charge $Z_{eff}(\psi)$ profiles. Indeed, since by definition,

$$\begin{aligned} Z_{eff}(\psi) &= \sum_s \sum_{s'} \frac{n_{ss'}(\psi) Z_{ss'}^2}{n_{ss'}(\psi) Z_{ss'}} \\ &= \frac{1}{n_e(\psi)} \sum_s \sum_{s'} n_{ss'}(\psi) Z_{ss'}^2 \end{aligned} \tag{6.39}$$

taking into account of the local electro-neutrality, $n_e(\psi) = \sum_s \sum_{s'} n_{ss'}(\psi) Z_{ss'}$, one obtains in this simple case a system of two equations with two unknowns,

$$\begin{cases} n_1(\psi) Z_1^2 + n_2(\psi) Z_2^2 = n_e(\psi) Z_{eff}(\psi) \\ n_1(\psi) Z_1 + n_2(\psi) Z_2 = n_e(\psi) \end{cases} \tag{6.40}$$

Therefore,

$$n_1(\psi) = n_e(\psi) \frac{(Z_{eff}(\psi) - Z_2)}{Z_1(Z_1 - Z_2)} \tag{6.41}$$

$$n_2(\psi) = n_e(\psi) \frac{(Z_1 - Z_{eff}(\psi))}{Z_2(Z_1 - Z_2)} \tag{6.42}$$

and using the normalization rule,

$$\overline{n}_1(\psi) = \overline{n}_e(\psi) \frac{(Z_{eff}(\psi) - Z_2)}{Z_1(Z_1 - Z_2)} \tag{6.43}$$

$$\overline{n}_2(\psi) = \overline{n}_e(\psi) \frac{(Z_1 - Z_{eff}(\psi))}{Z_2(Z_1 - Z_2)} \tag{6.44}$$

since by definition $Z_{eff}(\psi)$ has no units.

In the calculations, one may also consider several isotopes, since ion inertia play a significant role for the collision operator. Hence,

$$n_{ss'}(\psi) = \sum_m n^m_{ss'}(\psi) \tag{6.45}$$

or

$$\overline{n}_{ss'}(\psi) = \sum_m \overline{n}^m_{ss'}(\psi) \tag{6.46}$$

where the masses of isotope m of ion species ss' are $m^m_{ss'}$. In the calculations

$$\overline{m}^k_{ss'} = m^m_{ss'}/m_e \tag{6.47}$$

where m_e is the electron rest mass.

6.3.2 Time

Regarding time ordering which is considered in the derivation of the drift kinetic equation and the dominant role played by collisions for the electron momentum distribution function build-up, it is natural to scale time evolution to the reference electron thermal collision frequency $\nu^\dagger_e$ according to the relation

$$\bar{t} = t/\tau^\dagger_c = t\nu^\dagger_e \tag{6.48}$$

where

$$\nu^\dagger_e = \frac{q^4_e n^\dagger_e \ln\Lambda^\dagger}{4\pi\varepsilon_0 m^2_e c^3 \beta^{\dagger 3}_{th}} \tag{6.49}$$

Here $\varepsilon_0 = 8.854187818 \times 10^{-12}$ (F/m) is the free space permeability, $c = 299792458$ (km/s) the speed of light, $q_e = -1.60217733 \times 10^{-19}$ (C) the electric charge of the electron, $m_e = 9.1093897 \times 10^{-31}$ (Kg) the electron rest mass, and

$$\ln\Lambda^\dagger = 25.2 - 0.5 * \log(n^*_e) + \log(T^*_e) \tag{6.50}$$

is the usual reference Coulomb logarithm, with

$$\beta^\dagger_{th} = \sqrt{\frac{T^\dagger_e}{m_e c^2}} = \sqrt{\Theta^\dagger} \tag{6.51}$$

where $m_e c^2 = 510.99905$ $(keV)$is the electron rest mass energy.

6.3.3 Momentum, velocity, and kinetic energy

In the calculations, the momentum p in relativistic units $(m_e c)$ is normalized to the thermal reference value $p^\dagger_{th} = m_e v^\dagger_{th}$,

$$\overline{p} = p/p^\dagger_{th} \tag{6.52}$$

and consequently

$$p^\dagger_{th}/m_e c \approx v^\dagger_{th}/c = \beta^\dagger_{th} \tag{6.53}$$

since thermal electrons are only weakly relativistic. The well known relativistic Lorentz correction factor γ is then simply given by the relation

$$\gamma = \sqrt{p^2 + 1} = \sqrt{\overline{p}^2 \beta_{th}^{\dagger 2} + 1} \tag{6.54}$$

and in the non-relativistic limit, i.e. when $\overline{p}^2 \beta_{th}^{\dagger 2} \ll 1$, $\gamma \approx 1$.

Since in relativistic units, the total energy is linked to the relativistic momentum according to the expression,

$$(E_c + 1)^2 = \gamma \tag{6.55}$$

it is straightforward to expression the kinetic energy E_c as a function of $\overline{p}$ in units of electron rest mass energy $m_e c^2$

$$E_c = m_e c^2 \left(\sqrt{\overline{p}^2 \beta_{th}^{\dagger 2} + 1} - 1 \right) \tag{6.56}$$

Finally, concerning the normalization of the electron velocity v, one has

$$\begin{aligned} v/c &= p/\left(\gamma m_e c\right) \\ &= \overline{p} p_{th}^{\dagger}/\left(\gamma m_e c\right) \\ &= \overline{p} \beta_{th}^{\dagger}/\gamma \end{aligned} \tag{6.57}$$

and using $\overline{v} = v/v_{th}^{\dagger}$, it comes

$$\overline{v} v_{th}^{\dagger}/c = \overline{p} \beta_{th}^{\dagger}/\gamma \tag{6.58}$$

or

$$\overline{v} = \overline{p}/\gamma \tag{6.59}$$

with

$$v_{th}^{\dagger}/c = \beta_{th}^{\dagger} \tag{6.60}$$

6.3.4 Maxwellian electron momentum distribution

With the definition of $\overline{p}$, the approximate relativistic Maxwellian electron momentum distribution function $f_M(\psi, p)$ up to first order γ correction used in the code is given by

$$f_M(\psi, p) \simeq \frac{n_e(\psi)}{\left[2\pi T_e(\psi)\right]^{3/2}} \exp\left[-\frac{p^2}{(1+\gamma) T_e(\psi)} \right] \tag{6.61}$$

where $T_e(\psi)$ is expressed in electron rest mass energy $m_e c^2$ unit, and providing that $\gamma - 1 \ll 1$. Therefore, the condition

$$\overline{p}^2 \beta_{th}^{\dagger 2} \ll 1 \tag{6.62}$$

must be fulfiled. Since $\overline{p}$ may be as large as 30 in calculations, in order to correctly describe momentum dynamics of the fastest electrons, it results that

$$\beta_{th}^{\dagger} = \Theta^{\dagger 2} \ll 1/30 \tag{6.63}$$

or

$$T_e^\dagger \ll 511\sqrt{1/30} \approx 100keV \tag{6.64}$$

Usually, this condition is well satisfied even in the core of tokamak plasmas, where $T_e^\dagger$ never exceeds $20keV$. In normalized units,

$$f_M(\psi,p) = \alpha \frac{\overline{n}_e(\psi)\, n_e^\dagger}{\left[2\pi \overline{T}_e(\psi)\, T_e^\dagger\right]^{3/2}} \exp\left[-\frac{\overline{p}^2 \beta_{th}^{\dagger 2}}{(1+\gamma)\, T_e(\psi)}\right] \tag{6.65}$$

and since $\beta_{th}^\dagger = \sqrt{T_e^\dagger / m_e c^2}$, it turns out that

$$f_M(\psi,p) = \frac{n_e^\dagger}{\beta_{th}^{\dagger 3}} \overline{f}_M(\psi,p) = \frac{n_e^\dagger}{p_{th}^{\dagger 3}} \overline{f}_M(\psi,p) \tag{6.66}$$

where

$$\overline{f}_M(\psi,p) \approx \alpha \frac{\overline{n}_e(\psi)}{\left[2\pi \overline{T}_e(\psi)\right]^{3/2}} \exp\left[-\frac{\overline{p}^2}{(1+\gamma)\, \overline{T}_e(\psi)}\right] \tag{6.67}$$

With this definition one can cross-check that

$$2\pi \int_{-1}^{+1} d\xi_0 \int_0^{+\infty} p^2 f_M(\psi,p)\, dp = 2\pi p_{th}^{\dagger 3} \frac{n_e^\dagger}{\beta_{th}^{\dagger 3}} \int_{-1}^{+1} d\xi_0 \int_0^{+\infty} \overline{p}^2 \overline{f}_M(\psi,p)\, d\overline{p} = n_e^\dagger \overline{n}_e = n_e \tag{6.68}$$

since $p_{th}^\dagger = \beta_{th}^\dagger$ and the normalisation coefficient α is defined by the relation

$$\alpha = \frac{\overline{n}_e(\psi)}{4\pi \frac{\overline{n}_e(\psi)}{\left[2\pi \overline{T}_e(\psi)\right]^{3/2}} \int_0^{+\infty} \overline{p}^2 \exp\left[-\frac{\overline{p}^2}{(1+\gamma)\overline{T}_e(\psi)}\right] d\overline{p}} \tag{6.69}$$

with $\alpha = 1$ for $\beta_{th}^\dagger \ll 1$. Usually, no simple analytical expression of α may be obtained, and its value is only determined numerically. A good criterion upon the validity of the condition (6.62) is that the value of α must always remain close to unity.

6.3.5 Poloidal flux coordinate

For the poloidal flux coordinate, the normalized value is

$$\overline{\psi} = \psi / \psi_a \tag{6.70}$$

where ψ_a is the value at the plasma edge, corresponding usually to the last closed magnetic flux surface, as given by the equilibrium code. Usually, it is taken so that $0 \leq \overline{\psi} \leq 1$ from the center to the plasma edge. For

6.3.6 Drift kinetic coefficient

The first order drift kinetic equation requires to calculate $\widetilde{f}^{(0)}$ defined as

$$\widetilde{f}^{(0)} = \frac{v_{\|0} I_0(\psi)}{\Omega_{e0}} \frac{\partial f_0^{(0)}}{\partial \psi} \tag{6.71}$$

where by definition $B_{T0}(\psi) = |I_0(\psi)|/R_0$ and $\Omega_{e0} = -\frac{|e|B_0}{\gamma m_e}$ is the electron Larmor frequency, all quantities being determined at the poloidal location where the magnetic field B is minimum, as discussed in Sec. 3.5.5. Since

$$\overline{v} v_{th}^{\dagger}/c = \overline{p}\beta_{th}^{\dagger}/\gamma \tag{6.72}$$

one obtains in normalized units

$$\begin{aligned} \overline{\widetilde{f}}^{(0)} &= v\xi_0 \frac{\gamma m_e}{q_e} R_0 \frac{B_{T0}}{B_0} \frac{\partial \overline{f}_0^{(0)}}{\partial \psi} \\ &= \overline{v} v_{th}^{\dagger} \xi_0 \frac{\gamma m_e}{q_e} \frac{B_{T0}}{B_0} \frac{R_0}{\psi_a} \frac{\partial \overline{f}_0^{(0)}}{\partial \overline{\psi}} \\ &= \overline{p}\xi_0 \frac{c m_e}{q_e} \beta_{th}^{\dagger} \frac{B_{T0}}{B_0} \frac{R_0}{\psi_a} \frac{\partial \overline{f}_0^{(0)}}{\partial \overline{\psi}} \end{aligned} \tag{6.73}$$

Therefore,

$$\overline{\widetilde{f}}^{(0)} = \overline{p}\xi_0 \widetilde{C}_0 \frac{\partial \overline{f}_0^{(0)}}{\partial \overline{\psi}} \tag{6.74}$$

where

$$\widetilde{C}_0 = \frac{c m_e}{q_e} \beta_{th}^{\dagger} \frac{B_{T0}}{B_0} \frac{R_0}{\psi_a} \tag{6.75}$$

For circular concentric flux surfaces, since $\partial/\partial\psi = (1/\nabla\psi)\,\partial/\partial r$ and $\nabla\psi = RB_P$, it turns out that

$$\widetilde{f}^{(0)} = v\xi \frac{\gamma m_e}{q_e} \frac{B_{T0}}{B_{P0}} \frac{1}{B_0} \frac{\partial f_0^{(0)}}{\partial r} \tag{6.76}$$

and naturaly

$$\widetilde{C}_{(0)} \approx \frac{c m_e}{q_e} \beta_{th}^{\dagger} \frac{q}{a_p \epsilon} \frac{1}{B_0} \tag{6.77}$$

where the safety factor q is approximated by its cylindrical expression $q = \frac{rB_T}{RB_P}$, a_p the plasma minor radius, and $\epsilon = r/R_p$ the inverse aspect ratio.

6.3.7 Momentum convection and diffusion

From the conservative form of the Fokker-Planck equation in momentum space

$$\frac{\partial f_0^{(0)}}{\partial t} \propto \frac{\partial}{\partial p}\left(S_{\mathbf{p}}^{(0)}\right) \tag{6.78}$$

where

$$S_{\mathbf{p}}^{(0)} \propto -\mathbb{D}_{\mathbf{p}}^{(0)} \frac{\partial f_0^{(0)}}{\partial p} + \mathbf{F}_{\mathbf{p}}^{(0)} f_0^{(0)} \tag{6.79}$$

Introducing normalized coordinates, it turns out that

$$\begin{aligned} \frac{\partial \overline{f}_0^{(0)}}{\partial \overline{t}} &\propto \frac{1}{\nu_e^\dagger p_{th}^\dagger} \frac{\partial}{\partial \overline{p}} \left(-\frac{\mathbb{D}_{\mathbf{p}}^{(0)}}{p_{th}^\dagger} \frac{\partial \overline{f}_0^{(0)}}{\partial \overline{p}} + \mathbf{F}_{\mathbf{p}}^{(0)} \overline{f}_0^{(0)} \right) \\ &= \frac{\partial}{\partial \overline{p}} \left(-\frac{\mathbb{D}_{\mathbf{p}}^{(0)}}{\nu_e^\dagger p_{th}^{\dagger 2}} \frac{\partial \overline{f}_0^{(0)}}{\partial \overline{p}} + \frac{\mathbf{F}_{\mathbf{p}}^{(0)}}{\nu_e^\dagger p_{th}^\dagger} \overline{f}_0^{(0)} \right) \\ &= \frac{\partial}{\partial \overline{p}} \left(-\overline{\mathbb{D}}_{\mathbf{p}}^{(0)} \frac{\partial \overline{f}_0^{(0)}}{\partial \overline{p}} + \overline{\mathbf{F}}_{\mathbf{p}}^{(0)} \overline{f}_0^{(0)} \right) \end{aligned} \tag{6.80}$$

where normalized diffusive and convective coefficients are

$$\overline{\mathbb{D}}_{\mathbf{p}}^{(0)} = \mathbb{D}_{\mathbf{p}}^{(0)} / \mathbb{D}_{\mathbf{p}}^\dagger \tag{6.81}$$

$$\overline{\mathbf{F}}_{\mathbf{p}}^{(0)} = \mathbf{F}_{\mathbf{p}}^{(0)} / \mathbf{F}_{\mathbf{p}}^\dagger \tag{6.82}$$

with

$$\mathbb{D}_{\mathbf{p}}^\dagger = \nu_e^\dagger p_{th}^{\dagger 2} \tag{6.83}$$

$$\mathbf{F}_{\mathbf{p}}^\dagger = \nu_e^\dagger p_{th}^\dagger \tag{6.84}$$

For the case of the Ohmic electric field, this normalization leads to introduce naturaly the Dreicer field

$$E^\dagger = \nu_e^\dagger p_{th}^\dagger / q_e \tag{6.85}$$

the electric field being normalized according to the relation

$$\overline{E}_{\|0} = E_{\|0} / E^\dagger \tag{6.86}$$

6.3.8 Radial convection and diffusion

From the conservative form of the Fokker-Planck equation in configuration space

$$\frac{\partial f_0^{(0)}}{\partial t} \propto \frac{\partial}{\partial \psi} \left(|\nabla \psi|_0 \, S_\psi^{(0)} \right) \tag{6.87}$$

where

$$S_\psi^{(0)} \propto -\mathbb{D}_\psi^{(0)} \, |\nabla \psi|_0 \, \frac{\partial f_0^{(0)}}{\partial \psi} + \mathbf{F}_\psi^{(0)} f_0^{(0)} \tag{6.88}$$

Introducing normalized coordinates, it turns out that

$$\begin{aligned}\frac{\partial \overline{f}_0^{(0)}}{\partial \overline{t}} &\propto \frac{1}{\nu_e^\dagger \psi_a}\frac{\partial}{\partial \overline{\psi}}\left(|\nabla\psi|_0 S_\psi^{(0)}\right)\\ &= \frac{1}{\nu_e^\dagger \psi_a}\frac{\partial}{\partial \overline{\psi}}\left(\frac{\mathbb{D}_\psi^{(0)}}{\psi_a}|\nabla\psi|_0^2\frac{\partial \overline{f}_0^{(0)}}{\partial \overline{\psi}} + |\nabla\psi|_0 \mathbf{F}_\psi^{(0)}\overline{f}_0^{(0)}\right)\\ &= \frac{\partial}{\partial \overline{\psi}}\left(\frac{\mathbb{D}_\psi^{(0)}}{\nu_e^\dagger \psi_a^2}|\nabla\psi|_0^2\frac{\partial \overline{f}_0^{(0)}}{\partial \overline{\psi}} + |\nabla\psi|_0\frac{\mathbf{F}_\psi^{(0)}}{\nu_e^\dagger\psi_a}\overline{f}_0^{(0)}\right) \end{aligned} \tag{6.89}$$

with

$$\overline{\mathbb{D}}_\psi^{(0)} = \mathbb{D}_\psi^{(0)}/\mathbb{D}_\psi^\dagger \tag{6.90}$$

$$\overline{\mathbf{F}}_\psi^{(0)} = \mathbf{F}_\psi^{(0)}/\mathbf{F}_\psi^\dagger \tag{6.91}$$

with

$$\mathbb{D}_\psi^\dagger = \nu_e^\dagger \psi_a^2 \tag{6.92}$$

$$\mathbf{F}_\psi^\dagger = \nu_e^\dagger \psi_a \tag{6.93}$$

However, since it is more convenient to handle diffusion and convection coefficients that scale in m^2/s and m/s respectively, one must introduce new reference values for the diffusion and convection coefficients. Let

$$\mathbb{D}_\psi^{\dagger *} = \nu_e^\dagger a_p^2 \tag{6.94}$$

$$\mathbf{F}_\psi^{\dagger *} = \nu_e^\dagger a_p \tag{6.95}$$

the reference diffusion and convection, where a_p is the plasma minor radius as defined in Sec.2.1. The relation is

$$\overline{\mathbb{D}}_\psi^{(0)} = \alpha_{\mathbb{D}}\mathbb{D}_\psi^{(0)}/\mathbb{D}_\psi^{\dagger *} \tag{6.96}$$

$$\overline{\mathbf{F}}_\psi^{(0)} = \alpha_{\mathbf{F}}\mathbf{F}_\psi^{(0)}/\mathbf{F}_\psi^{\dagger *} \tag{6.97}$$

where

$$\alpha_{\mathbb{D}} = \mathbb{D}_\psi^{\dagger *}/\mathbb{D}_\psi^\dagger = a_p^2/\psi_a^2 \tag{6.98}$$

$$\alpha_{\mathbf{F}} = \mathbf{F}_\psi^{\dagger *}/\mathbf{F}_\psi^\dagger = a_p/\psi_a \tag{6.99}$$

6.3.9 Fluxes

In momentum space,

$$\begin{aligned} S_{\mathbf{p}}^{(0)} &\propto -\mathbb{D}_{\mathbf{p}}^{(0)}\frac{\partial f_0^{(0)}}{\partial p} + \mathbf{F}_{\mathbf{p}}^{(0)} f_0^{(0)} \\ &= -\overline{\mathbb{D}}_{\mathbf{p}}^{(0)}\mathbb{D}_{\mathbf{p}}^{\dagger}\frac{n_e^{\dagger}}{p_{th}^{\dagger 3}}\frac{\partial \overline{f}_0^{(0)}}{p_{th}^{\dagger}\partial \overline{p}} + \overline{\mathbf{F}}_{\mathbf{p}}^{(0)}\mathbf{F}_{\mathbf{p}}^{\dagger}\frac{n_e^{\dagger}}{p_{th}^{\dagger 3}}\overline{f}_0^{(0)} \\ &= -\overline{\mathbb{D}}_{\mathbf{p}}^{(0)}\left(\frac{\nu_e^{\dagger}n_e^{\dagger}}{p_{th}^{\dagger 2}}\right)\frac{\partial \overline{f}_0^{(0)}}{\partial \overline{p}} + \overline{\mathbf{F}}_{\mathbf{p}}^{(0)}\left(\frac{\nu_e^{\dagger}n_e^{\dagger}}{p_{th}^{\dagger 2}}\right)\overline{f}_0^{(0)} \\ &= \left(\frac{\nu_e^{\dagger}n_e^{\dagger}}{p_{th}^{\dagger 2}}\right)\left(-\overline{\mathbb{D}}_{\mathbf{p}}^{(0)}\frac{\partial \overline{f}_0^{(0)}}{\partial \overline{p}} + \overline{\mathbf{F}}_{\mathbf{p}}^{(0)}\overline{f}_0^{(0)}\right) \end{aligned} \tag{6.100}$$

and

$$S_{\mathbf{p}}^{(0)} = \overline{S}_{\mathbf{p}}^{(0)} S_{\mathbf{p}}^{\dagger} \tag{6.101}$$

where

$$S_{\mathbf{p}}^{\dagger} = \frac{\nu_e^{\dagger}n_e^{\dagger}}{p_{th}^{\dagger 2}} \tag{6.102}$$

and with these definitions,

$$\overline{S}_{\mathbf{p}}^{(0)} \propto -\overline{\mathbb{D}}_{\mathbf{p}}^{(0)}\frac{\partial \overline{f}_0^{(0)}}{\partial \overline{p}} + \overline{\mathbf{F}}_{\mathbf{p}}^{(0)}\overline{f}_0^{(0)}$$

A similar procedure is applied for dynamics in configuration space,

$$\begin{aligned} S_{\psi}^{(0)} &\propto -\mathbb{D}_{\psi\psi}^{(0)}\left|\nabla\psi\right|_0\frac{\partial f_0^{(0)}}{\partial \psi} + \mathbf{F}_{\psi}^{(0)} f_0^{(0)} \\ &= -\overline{\mathbb{D}}_{\psi\psi}^{(0)}\mathbb{D}_{\psi\psi}^{\dagger}\frac{n_e^{\dagger}}{p_{th}^{\dagger 3}}\left|\nabla\psi\right|_0\frac{\partial \overline{f}_0^{(0)}}{\psi_a\partial \overline{\psi}} + \mathbf{F}_{\psi}^{(0)}\mathbf{F}_{\psi}^{\dagger}\frac{n_e^{\dagger}}{p_{th}^{\dagger 3}}\overline{f}_0^{(0)} \\ &= -\overline{\mathbb{D}}_{\psi\psi}^{(0)}\left(\frac{n_e^{\dagger}}{p_{th}^{\dagger 3}}\nu_e^{\dagger}\psi_a\right)\left|\nabla\psi\right|_0\frac{\partial \overline{f}_0^{(0)}}{\partial \overline{\psi}} + \mathbf{F}_{\psi}^{(0)}\left(\frac{n_e^{\dagger}}{p_{th}^{\dagger 3}}\nu_e^{\dagger}\psi_a\right)\overline{f}_0^{(0)} \\ &= \left(\frac{n_e^{\dagger}}{p_{th}^{\dagger 3}}\nu_e^{\dagger}\psi_a\right)\left(-\overline{\mathbb{D}}_{\psi\psi}^{(0)}\left|\nabla\psi\right|_0\frac{\partial \overline{f}_0^{(0)}}{\partial \overline{\psi}} + \mathbf{F}_{\psi}^{(0)}\overline{f}_0^{(0)}\right) \end{aligned} \tag{6.103}$$

and

$$S_{\psi}^{(0)} = \overline{S}_{\psi}^{(0)} S_{\psi}^{\dagger} \tag{6.104}$$

with

$$S_{\psi}^{\dagger} = \frac{n_e^{\dagger}}{p_{th}^{\dagger 3}}\nu_e^{\dagger}\psi_a \tag{6.105}$$

and with these definitions,

$$\overline{S}_{\psi}^{(0)} \propto -\overline{\mathbb{D}}_{\psi\psi}^{(0)}\left|\nabla\psi\right|_0\frac{\partial \overline{f}_0^{(0)}}{\partial \overline{\psi}} + \overline{\mathbf{F}}_{\psi}^{(0)}\overline{f}_0^{(0)} \tag{6.106}$$

6.3.10 Current density

The local current density at the minimum **B** value on the flux surface is given by the relation

$$\begin{aligned} J^{(0)} &\propto 2\pi q_e \int p^2 dp \int_{-1}^{+1} \xi_0 v f_0^{(0)} d\xi_0 \\ &= 2\pi q_e \int \frac{p^3}{\gamma m_e} dp \int_{-1}^{+1} \xi_0 f_0^{(0)} d\xi_0 \\ &= 2\pi \frac{q_e}{m_e} p_{th}^{\dagger 4} \frac{n_e^\dagger}{\beta_{th}^{\dagger 3}} \int \frac{\overline{p}^3}{\gamma} d\overline{p} \int_{-1}^{+1} \xi_0 \overline{f}_0^{(0)} d\xi_0 \end{aligned} \tag{6.107}$$

Therefore,

$$\overline{J}^{(0)} = J^{(0)}/J^\dagger \tag{6.108}$$

where

$$J^\dagger = \frac{q_e}{m_e} p_{th}^\dagger n_e^\dagger \tag{6.109}$$

With this definition

$$\overline{J}^{(0)} \propto 2\pi \int \frac{\overline{p}^3}{\gamma} d\overline{p} \int_{-1}^{+1} \xi_0 \overline{f}_0^{(0)} d\xi_0 \tag{6.110}$$

6.3.11 Power density

The power density is deduced from the integral

$$\begin{aligned} P^{(0)} &\propto 2\pi \int_{-1}^{+1} d\xi_0 \int_0^\infty \frac{p^3}{\gamma m_e} S_{\mathbf{p}}^{(0)} dp \\ &= 2\pi \frac{p_{th}^{\dagger 4}}{m_e} \frac{\nu_e^\dagger n_e^\dagger}{p_{th}^{\dagger 2}} \int_{-1}^{+1} d\xi_0 \int_0^\infty \frac{\overline{p}^3}{\gamma} \overline{S}_{\mathbf{p}}^{(0)} d\overline{p} \end{aligned} \tag{6.111}$$

and defining

$$\overline{P}^{(0)} = P^{(0)}/P^\dagger \tag{6.112}$$

one has

$$P^\dagger = \frac{\nu_e^\dagger p_{th}^{\dagger 3} n_e^\dagger}{m_e} \tag{6.113}$$

With this definition

$$\overline{P}^{(0)} \propto 2\pi \int_{-1}^{+1} d\xi_0 \int_0^\infty \frac{\overline{p}^3}{\gamma} \overline{S}_{\mathbf{p}}^{(0)} d\overline{p} \tag{6.114}$$

6.3.12 Electron runaway rate

The electron runaway rate $\Gamma_R^{(0)}$ is given by the relation

$$\begin{aligned} \Gamma_R^{(0)} &\propto 2\pi p^2 \int_{-1}^{+1} S_{\mathbf{p}}^{(0)} d\xi_0 \\ &= 2\pi \overline{p}^2 p_{th}^{\dagger 2} \frac{\nu_e^\dagger n_e^\dagger}{p_{th}^{\dagger 2}} \int_{-1}^{+1} \overline{S}_{\mathbf{p}}^{(0)} d\xi_0 \end{aligned} \tag{6.115}$$

Therefore, normalized expression is

$$\overline{\Gamma}_R^{(0)} = \Gamma_R^{(0)} / \Gamma_R^{\dagger} \tag{6.116}$$

with

$$\Gamma_R^{\dagger} = \nu_e^{\dagger} n_e^{\dagger} \tag{6.117}$$

so that

$$\overline{\Gamma}_R^{(0)} \propto 2\pi \overline{p}^2 \int_{-1}^{+1} \overline{S}_{\mathbf{p}}^{(0)} d\xi_0 \tag{6.118}$$

The consistency of the normalized units may be benchmarked by the approximate relation between the total current and the bulk current, the difference coming from the electron runaway tail. For small Γ_R, the runaway distribution is independent of $v_{\parallel}$, so that it may be approximated by the simple expression $f_0^{(0)}\left(v_{\parallel} \gg v_{th}\right) \approx (\gamma/E)\,\delta\left(p_{\perp}\right)$. By integrating the current integral $v_{\parallel} f_0^{(0)}$ out to $p_{\max}$, one obtains

$$J^{(0)}\left(v_{\max}\right) \approx J_{bulk}^{(0)} + \frac{1}{2m_e}\left(\frac{\Gamma_R^{(0)}}{E_{\parallel 0}}\right) p_{\max}^2 \tag{6.119}$$

and in normalized units,

$$\overline{J}^{(0)}\left(v_{\max}\right) J^{\dagger} \approx \overline{J}_{bulk}^{(0)} J^{\dagger} + \frac{1}{2m_e}\left(\frac{\overline{\Gamma}_R^{(0)} \Gamma_R^{\dagger}}{\overline{E}_{\parallel 0} E^{\dagger}}\right) p_{th}^{\dagger 2} \overline{p}_{\max}^2 \tag{6.120}$$

so that

$$\overline{J}^{(0)}\left(v_{\max}\right) \approx \overline{J}_{bulk}^{(0)} + \frac{1}{2m_e} \frac{p_{th}^{\dagger 2} \Gamma_R^{\dagger}}{E^{\dagger} J^{\dagger}} \left(\frac{\overline{\Gamma}_R^{(0)}}{\overline{E}_{\parallel 0}}\right) \overline{p}_{\max}^2 \tag{6.121}$$

According to their respective expression,

$$\frac{p_{th}^{\dagger 2} \Gamma_R^{\dagger}}{m_e E^{\dagger} J_{th}^{\dagger}} = \frac{p_{th}^{\dagger 2} \nu_e^{\dagger} n_e^{\dagger}}{m_e \frac{q_e}{m_e} p_{th}^{\dagger} n_e^{\dagger} \nu_e^{\dagger} p_{th}^{\dagger} / q_e} = 1 \tag{6.122}$$

which demonstrates the overall consistency of the normalization of the different quantities calculated by the code.

6.3.13 Electron magnetic ripple loss rate

By definition, the electron magnetic ripple loss rate $\Gamma_{ST}^{(0)}$ is given by a relation relation similar to $\Gamma_R^{(0)}$, except that integrals of fluxes are calculated for different boundaries. Therefore, the normalized expression is simply given by the relation

$$\overline{\Gamma}_{ST}^{(0)} = \Gamma_{ST}^{(0)} / \Gamma_{ST}^{\dagger} \tag{6.123}$$

where

$$\Gamma_{ST}^{\dagger} = \Gamma_R^{\dagger} = \nu_e^{\dagger} n_e^{\dagger} \tag{6.124}$$

6.3.14 Units

In the code, the following units are used

Quantity	Units
Temperature	keV
Density	m^{-3}
Time	s
Frequency	s^{-1}

Chapter 7

Examples

This chapter is dedicated to the code performances. Since numerous combinations are possible, it is not the purpose to give an exhaustive list of results, but to select different problems that have been addressed by existing codes in simplified magnetic configuration, a condition that allows interesting benchmarks. Moreover, in some cases, analytical expressions are available, and consequently accurate comparisons may be performed.

It is well known that all codes contain numerous hidden bugs, that are difficult to track, even if a careful attention as been paid to avoid as much as possible such problems. The only way to reduce them is to run extensively the code for different purposes. It is the reason why both the documentation and the code have been made as transparent as possible, so that its robustness may be continuously improved. When some difficulties have been encountered, they are reported in the different sections dedicated to benchmarking. However, none of them have made the code so far unable to determine the correct solution, providing input parameters corresponds to assumptions used to derive the equations and their numerical counterpart. It is well known that such kind of codes are often missused, using input parameters well beyond the acceptable range. In some cases, warnings are indicated by the code, but it is the duty of users to take care of this problem before considering that the code gives a wrong answer.

The kernel of the kinetic calculations is contained by the MatLab routine "dke_1_4yp.m", whish contains both the $3-D$ zero-order Fokker-Planck solver, and the first-order neo-classical corrections. Only this routine and all related subroutines must be used in a chain of codes like in CRONOS simulation package ([2]). In order to help how to make this link, and to benchmark the code, a test routine "testdke_1yp.m" has been written. Main global input parameters can be modified in the subroutine "psim_dke_1yp.m" that is called by "testdke_1yp.m", while parameter that are specific to a machine (Tore Supra, JET, ITER, C-MOD,...) are gathered in the subroutine "ptok_dke_1yp.m". The machine may be virtual, for benchmarking purposes. The input parameters for the RF wave physics problem have be put in separate files, sinces they are quite independent of the global input parameters. The corresponding file names for simplified RF wave physics are called "psim_idealhcd_jd.m" or "psim_coldlhcd_jd.m" for the Lower Hybrid wave, or "psim_ideaeccd_jd.m" or "psim_coldeccd_jd.m" for the Electron Cyclotron wave. Other types of waves are also available as well as input parameter files for more realistic ray-tracing calculations.

Once input parameters have been set, one runs the code by executing the MatLab script "script_dke_1yp.m". This structure allows to run several cases in a single run, for systematic studies of the influence of one given parameter on the final result. For example, the role played by the Ohmic electric field may be investigated for a single value "epsi0= 0.01 and epsia= 0.01", or multiple ones "epsi0= [0.01:0.01:0.05] and epsia= [0.01:0.01:0.05]". In that case, all the results are saved in different .mat binary MatLab files, in the directory that contains "dke_1_4yp.m", under the generic name "RESULTS_X_SY.mat" where X is the machine name, and Y the index number of the simulation. The magnetic equilibrium calculated by HELENA is stored in an separate file named "EQUIL_X.mat", so that it may be used independently by another program for calculating various moments of the electron distribution function like the non-thermal bremsstrahlung emission.

All the results may be displayed using the MatLab routine "display_dke_1yp.m", with or without graphical outputs. A special interface has been also written for an easy transfer of selected binary data to IGOR scientific display program for final reports.

The full list of routines is given in Appendix F. Except for arbitrary equilibrium cases that require the use of the FORTRAN F77 mexfiles "helmex77.f" and "separatrix.f" which both must be compiled[1], all files are standard MatLab scripts. No external functions are used, and once MatLab path is correctly set-up to load text files in the "Project_DKE" directory, the code can be run immediatly on any computer without additional needs.

All benchmark results discussed in the text are gathered in the file "Benchmark.txt", with the corresponding input parameters.

7.1 Ohmic conductivity

The determination of the Ohmic electrical conductivity

$$\sigma = \frac{\overline{J}}{\overline{E}} \tag{7.1}$$

is a fundamental test for such kinetic codes. Extensive analysis have been performed to investigate code capabilities. To avoid the runaway problem, $\overline{E} = 0.01$, and $\overline{p}_{\max} = 15$. Machine parameters are corresponding to non-relativistic limit $T_e^\dagger = 0.1keV$, and a rather low density $n_e^\dagger = 10^{+19}m^{-3}$ at the plasma center. Here, $T_i^\dagger = n_i^\dagger = 0$. Except if it is specified, all profiles are flat. The dominant ion species is usually hydrogen, though some simulations have been done for deuterium. No impurities are considered, except for investigating the role of the effective charge. In order to investigate the effect of trapped particle, a simplified tokamak geometry is considered, with circular plasma cross-sections and neglecting any Shafranov shift. Except if it is mentionned, bounce integrals are performed analytically, according to the expressions given throughout the text. The minor radius is set to $a_p = 2.3899m$ and the major one is $R_p = 2.39m$ so that the normalized radius ρ

[1]The code may use a simplified magnetic equilibrium with circular plasma cross-sections, that is valid in the large aspect ration limit $\epsilon \ll 1$. More realistic equilibria are determined numericaly. First, the external shape of the plasma equilibrium is evaluated by specifying positions of X-points and derivatives at this point. Then the full magnetic equilibrium is calculated using pressure and current density profiles, in agreemnt with the shape required at the plasma boundary. This procedure avoids numerical instabilities that may arise from coarse estimate of the plasma shape.

Collision operator	σ [DKE code]	σ [Karney]
Maxwellian	3.7655	3.773
High velocity	3.0158	2.837
Exact	7.4406	7.429

Table 7.1: Ohmic conductivity as function of the e-e collision model

Z_{eff}	σ [DKE code]	σ [Karney]
1	7.4353	7.429
2	4.3697	4.377
5	2.0619	2.078
10	1.1147	1.133

Table 7.2: Ohmic conductivity as function of the effective charge using the linearized e-e collision model

is very close to ϵ value from 0 to 1. In the tokamak parameter M-file "ptok_dke_1yp.m", the corresponding section for these simulations is named "CQL3D_OHM", since it corresponds to conditions that have been used for code comparison with the well know CQL3D program [27]. For all cases, except when notified, the drop tolerance level is set to 2×10^{-3}. It has been also verified that the results are independent of this parameter, providing the convergence is achieved.

First local analysis have been performed, without considering bounce averaging. The role played by the collision operator is crucial on the driven current as shown in Table 7.1

An excellent agreement is found with Karney's results [16], even with a coarse numerical grid corresponding to $n_p = 88$ and $n_{\xi_0} = 120$. Some slight differences may arise from the different form of the collision operators, and the number of grid points. In that case, the code is running in a fully conservative mode, namely without normalization of the density at each time step $\left(\Delta\bar{t} = 10000\right)$, nor by forcing the Maxwellian solution at $i = 1/2$ for the momentum grid. When a more refined grid is used, slight evolutions are observed, and the conductivity decreases from $\sigma = 7.4406$ down to $\sigma = 7.4343$, less than 0.1% for the exact collision operator when $n_p = 165$, while n_{ξ_0} is kept constant. The role of the mass is also fairly weak, since for the deuterium case, $\sigma = 7.4471$ for $n_p = 88$. Finally, by increasing the integration domain up to $\overline{p}_{\max} = 20$, $\sigma = 7.4387$. The very small variation confirms that no particle are leaving the domain of integration. which confirms that 7.4387.

As far as Z_{eff} is increased, the Lorentz limit is progressively reached, since the pitch-angle predominates. This is clearly shown in Table 7.2

and in the limit $Z_{eff} \gg 1$, the result is well independent of the electron-electron collision model [16]. Its value is roughly given by expression

$$\sigma \simeq 16\sqrt{\frac{2}{\pi}}\frac{1}{Z_{eff}} \simeq \frac{12.766}{Z_{eff}} \tag{7.2}$$

and the analytical limit is recovered by the code with $Z_{eff} \simeq 20$.

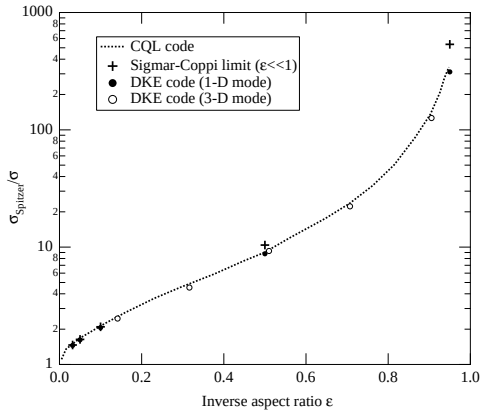

cmcm

Figure 7.1: Normalized Ohmic resistivity as function of the inverse aspect ratio ϵ

A full $3-D$ calculation has been performed with flat profiles at normalized radial positions on the spatial flux grid $[0.2, 0.4, 0.6, 0.8]$, giving the following radial positions $\rho = [0.14142, 0.31623, 0.5099, 0.70711, 0.90554]$. In that case, the code calculates itself the pitch-angle grid and the number of step is $n_{\xi_0} = 168$, while $n_p = 125$.The conductivity is found to be independent of the method of calculations, and the value $\sigma = 7.4353$ is well recovered. It is found that the code remains fully conservative without forcing the Maxwellian solution at $i = 1/2$ and without normalizing the density at each iteration.

Bounce averaged calculations have be performed first locally. As shown in Fig. 7.1, an excellent agreement is found with CQL code from Ref. [19] over a broad range for the inverse aspect ratio, and also its more recent version CQL3D [27]. At the limit $\epsilon \ll 1$, the approximate Sigmar-Coppi expression

$$\sigma/\sigma_{Spitzer} = 1 - 1.95\sqrt{\epsilon} + 0.95\epsilon \tag{7.3}$$

is well recovered. When $\epsilon \simeq 1$, the value found by the code is very close to the asymptoytic limit given by the expression of Connor, as discussed in Ref. [19].

As shown in Fig. 7.1, in $3-D$ mode, the agreement with theory and CQL(3D) codes remains fully very good, whatever the normalization reference of the electric field, at the plasma center, or at the local position. This result gives strong confidence to the code when kinetic calculations are simultaneously performed at various radial positions. Moreover, it has been cross-checked that the conductivity level is independent of the sign of the electric field, but also of the method used for calculating the bounce integrals. This latter point is crucial and demonstrates that numerical calculations of the bounce integrals is very accurate, even for finite inverse aspect ratio. The drop tolerance has been lowered in that case to 10^{-4} for ensuring a stable convergence, leading to a modest increase of the matrix sizes. However the rate of convergence is not affected, and the final result is obtained usually after $11-13$ iterations, even when several radial positions are considered.

Z_{eff}	$\overline{\Gamma}_R$ [DKE code]	$\overline{\Gamma}_R$ [Kulsrud et al.]
1	2.8487×10^{-4}	3.177×10^{-4}
2	1.5904×10^{-4}	1.735×10^{-4}
5	9.6565×10^{-5}	1.047×10^{-4}
10	8.1878×10^{-6}	9.0×10^{-6}

Table 7.3: Runaway rate as function of the effective charge using the Maxwellian e-e collision model

7.2 Runaway losses

The runaway loss rate $\overline{\Gamma}_R$ is also an important physical quantity that can be determined by the code. It becomes significant when the Ohmic electric field is large. For the benchmarking procedure, the Ohmic electric field is then set to $\overline{E} = 0.08$, which corresponds to a standard value for such studies. Usually, runaway losses become significant above $\overline{E} = 0.03$. All other parameters are kept constant as compared to the benchmarking procedure done for the Ohmic conductivity in Sec. 7.1. In the tokamak parameter M-file "ptok_dke_1yp.m", the corresponding section for these simulations is named "CQL3D_RUNAWAY", since it corresponds to conditions that have been used for code comparison with the well know CQL3D program ([27]). By definition, the code is no more conservative since runaway electrons are leaving the domain of integration. Consequently, the particle losses must be compensated in order to keep constant the total number of particle. Consequently, the same the Maxwellian solution is enforced at $i = 1/2$ while the density is normalized at each iteration. It has been cross-checked that the compensation of losses has no influence on the final solution and therefore the runaway rate. Indeed, results normalized to the final numerical electron density found by the code, or normalized at each time step are similar.

In a first step, a local analysis is performed, without considering bounce averaging. Here, only the Maxwellian electron-electron collision operator is considered, for allowing comparisons with analytical solutions, as shown in 7.3

The agreement between numerical results obtained with the drift kinetic code and the code written by Kulsrud and coauthors is reasonably good [28], a modest systematic difference of -15% being observed for all Z_{eff} values. For $Z_{eff} = 1$, the agreement is slightly better with the model of Kruskal-Bernstein [28], and the relative difference is now positive and less than 7%. The role played by the numerical grid is marginal, less than 1%. when n_p is varying from 88 to 125 or 165 while n_{ξ_0} is kept constant at 120.

A full $3 - D$ calculation has been performed with flat profiles at normalized radial positions on the spatial flux grid $[0.2, 0.4, 0.6, 0.8]$, giving the following radial positions $\rho = [0.14142, 0.31623, 0.5099, 0.70711, 0.90554]$. In that case, the code calculates itself the pitch-angle grid and the number of step is now $n_{\xi_0} = 168$, while $n_p = 125$.The runaway rate is found to be independent of the method of calculations, and the Kruskal-Bernstein is well recovered when $Z_{eff} = 1$ at all plasma radii. In Fig.7.2 , and example of a runaway distribution at Bmin is given, for $\rho = 0.31623$. The trapped domain is large, and the region where the electric field may accelerate fast electrons above the Dreicer limit is quite narrow

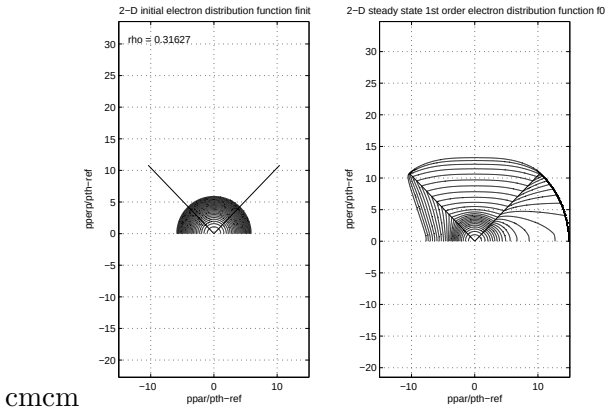

Figure 7.2: Contour plot of the electron distribution function at $\epsilon = 0.31623$

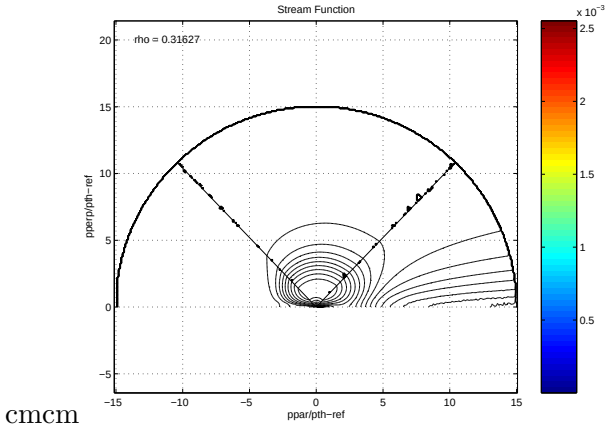

Figure 7.3: Contour plot of the stream lines at $\epsilon = 0.31623$

in pitch-angle. The stream lines given in Fig.7.3 along with electrons are moving in the momentum space show the clear boundary between close loops for regular electrons that remain in the integration domain because of collisions, and the open loops, for runaways that continuously accelerated by the Ohmic electric field up to the integration domain.

In Fig. 7.4, the parallel component of the electron distribution function

$$F_{\|0}^{(0)}\left(\psi, p_{\|}\right) = 2\pi \int_0^{\infty} f_0^{(0)}\left(\psi, p_{\|}, p_{\perp}\right) p_{\perp} dp_{\perp} \tag{7.4}$$

the normalized perpendicular temperature $\overline{T}_{\perp}\left(\psi, p_{\|}\right) = T_{\perp}\left(\psi, p_{\|}\right)/T_e^{\dagger}$ where

$$T_{\perp}\left(\psi, p_{\|}\right) = \frac{1}{2} \frac{\int_0^{\infty} f_0^{(0)}\left(p_{\|}, p_{\perp}\right) p_{\perp}^3 dp_{\perp}}{\int_0^{\infty} f_0^{(0)}\left(p_{\|}, p_{\perp}\right) p_{\perp} dp_{\perp}} \tag{7.5}$$

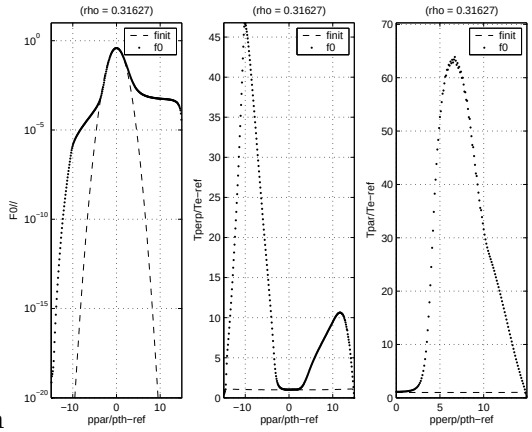

cmcm

Figure 7.4: Electron distribution function averaged over the perpendicular momentum direction at $\epsilon = 0.31623$. Parallel and perpendicular temperatures of the electron distribution function are also shown

and the parallel one $\overline{T}_{\parallel}(\psi, p_\perp) = T_{\parallel}(\psi, p_\perp)/T_e^\dagger$ defined as

$$T_{\parallel}(\psi, p_\perp) = \frac{\int_{-\infty}^{\infty} f_0^{(0)}\left(p_{\parallel}, p_\perp\right) p_{\parallel}^2 dp_{\parallel}}{\int_{-\infty}^{\infty} f_0^{(0)}\left(p_{\parallel}, p_\perp\right) dp_{\parallel}} \tag{7.6}$$

are also given to illustrate the deformations of the electron distribution function with respect to the Maxwellian shape.

Bounce averaged calculations have be performed first locally. As shown in Fig. 7.5, it is observed $\overline{\Gamma}_R$ decreases with the inverse aspect ratio ϵ. The influence of toroidicity on Dreicer generation, which is not predicted by the theory of Gurevitch [29], is in good agreement with never published calculations using the CQL3D code. The explanation for such an effect is quite complex, since it arises from the combination of the poloidal dependence of the electric field value and the fact that trapped electrons do not contribute to the runaway generation process. As shown in Sec. 3.6, the electric field on the low magnetic field side is lower than the flux surface value, while it is larger on the high field side, by a ratio R_0/R for circular concentric magnetic flux surfaces. So we could expect that these electrons are more efficiently accelerated along bthe magnetic field line. But since they are close to trapped/passing boundary, their probability to be trapped before reaching the Dreicer limit is fairly high, and therefore, the density close to the Dreicer boundary is likely significantly lowered. Consequently, the relative reduction of the runaway rate

$$\Delta\overline{\Gamma}_R = \frac{\overline{\Gamma}_R(\epsilon) - \overline{\Gamma}_R(\epsilon = 0)}{\overline{\Gamma}_R(\epsilon = 0)} \tag{7.7}$$

must be roughly given by a factor proportional to the effective fraction of trapped electron $\mathcal{F}_t^{eff.}$, since not only trapped but also barely trapped electron dynamics are concerned. A

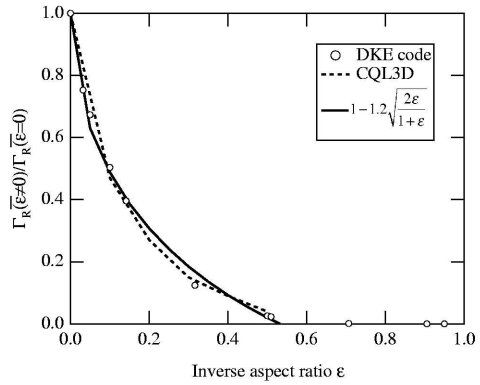

cmcm

Figure 7.5: Normalized Ohmic runaway rate as function of the inverse aspect ratio ϵ

fit of the numerical results confirms this coarse analysis, since

$$\Delta\overline{\Gamma}_R \simeq -1.2\sqrt{\frac{2\epsilon}{1+\epsilon}} \tag{7.8}$$

for $\epsilon \lesssim 0.53$ and $\lim_{\epsilon\to 0}\Delta\overline{\Gamma}_R(\epsilon) \simeq 1.7\sqrt{\epsilon} \simeq -1.16\mathcal{F}_t^{eff.}$[2]. This result is important, since it indicates that runaway generation is nearly cancelled when the inverse aspect ratio is larger than $\epsilon \simeq 0.5$. The trapped particles have therefore a beneficial effect by preventing runaways, that may cause severe damages to machine walls in case of disruptions.

Similar results are obtained in $3-D$ mode, whatever the normalization reference of the electric field, at the plasma center, or at the local position. As expected, the runaway rate $\overline{\Gamma}_R$ is nearly independent of the sign of the electric field, and moreover, but also of the method (analytical or numerical) for calculating the bounce integrals. The relative accuracy which is less than 1% close to the plasma center, tends to decrease down to 50% at the plasma edge, but since $\overline{\Gamma}_R$ is very small the error has only a weak influence[3].

Once more, this demonstrates that numerical calculations of the bounce integrals is very accurate, even for finite inverse aspect ratio. The drop tolerance has been lowered in that case to 10^{-4} for ensuring a stable convergence, leading to a modest increase of the matrix sizes. However the rate of convergence is not affected, and the final result is obtained usually after $11-13$ iterations, even when several radial positions are considered.

7.3 Lower Hybrid Current drive

The Lower Hybrid current drive problem is one the more important addressed by Fokker-Planck calculations in the field of fusion by magnetic confinement. It is also certainly one of the most demanding case regarding the numerical constraints that must be satisfied

[2]The reduction factor of the runaway losses as predicted by the drift kinetic code is much larger than calculations done using Monte-Carlo technique, as shown in Ref. [30], since the reduction factor that scales like $\Delta\overline{\Gamma}_R \simeq -0.5\sqrt{2\epsilon}$. This discrepancy has not been resolved so far.

[3]It is important to note that the order of magnitude is always correct.

simultaneously such as possible discontinuities and large values of the quasilinear diffusion coefficient, presence of cross-derivatives $D_{p\xi} = D_{\xi p} \neq 0$. In that conditions, the matrix conditionning may be significantly reduced, leading to possible onset of numerical instabilities, lack of convergence or possible convergence towards a solution that has no physical sense. In these conditions, the demonstration that the code remains fully conservative and gives a physical solution for a domain of parameters that is relevant for magnetic fusion simulations is a stringent test for the validity of the projection technique of the kinetic equations on the numerical grids as well as the correct description of both the internal and external boundary conditions.

For the test procedure, a simplified expression of the quasilinear diffusion operator is considered, as described in Appendix D.2.8, using the familiar boxcar shape in momentum space $\overline{D}^{LH}_{0,new} = 1$ for $v_1 \leq v_\parallel \leq v_2$, and $\overline{D}^{LH}_{0,new} = 0$ otherwise, neglecting the factor $v^\dagger_{th}/v_\parallel$, as done usually in the litterature which only acceptable in principle when $\overline{D}^{LH}_{0,new} \gg 1$ (see Refs. [31],[16],[25],[9]). For comparison with existing results, simulations are performed for the couples of values $(v_1 = 3.5, v_2 = 6)$ and $(v_1 = 4, v_2 = 7)$. Except it is specified, the default upper bound of the integration domain is taken at $p_{\max} = 20$. Plasma parameters are similar to those used in Sec.7.1 dedicated to the the Ohmic conductivity problem, except that the reference electron temperature may take two different values $T^\dagger_e = 5.11 \times 10^{-4} keV$ and $T^\dagger_e = 5.11 keV$ corresponding to non-relativistic to relativistic limits respectively. The choice of these electron temperatures allows comparaison with already published results at $\beta^\dagger_{th} = 0.01\,(\approx 0)$ and $\beta^\dagger_{th} = 0.1$. All corresponding plasma parameters are gathered in section "CQL3D_LH" of the M-file "ptok_dke_1yp.m", since it corresponds to conditions that have been used for code comparison with the well known CQL3D code [27].

Concerning the numerical parameters, the code is running by default in the fully implicit mode $\Delta\bar{t} = 10000$, with the linearized electron-electron Belaiev-Budker collision operator that conserve momentum. The drop tolerance for incomplete LU matrix factorization is 10^{-4}, while no Maxwellian solution is imposed at $i = 1/2$. The momentum and pitch-angle grids are taken uniform with $n_p = n_{\xi_0} \simeq 200$ except when simulations with different numbers of grid points or non-uniform meshes are studied. Furthermore, no bounce averaging is considered, expect if specified.

The first problem that is addressed is the numerical accuracy with the number of grid points. For a pure hydrogen plasma $(Z_s = 1)$, $n_p = n_{\xi_0}$ are varying from 50 to 250. Here a very simple case is considered, with $(v_1 = 3, v_2 = 5)$, using the relativistic Maxwellian collision operator, but at $\beta^\dagger_{th} = 0.001$ (non-relativistic limit). This allows easy comparison with previously published results [16]. As shown in Fig.7.6, significant oscillations of the absorbed RF $\langle P_{LH} \rangle$ power density arises when $(n_p, n_{\xi_0}) \leq 150$ which correspond to the relative position of the lower bound of the Lower Hybrid resonance domain with respect to the nearest grid point. The exponential decrease makes the solution very sensitive to this parameter. For this domain of parameter, the power density absorbed by collisions $\langle P_{coll} \rangle$ is not exactly equivalent to $\langle P_{LH} \rangle$, though close to unity within 5%, leading to oscillations of the ratio $\langle P_{coll} \rangle / \langle P_{LH} \rangle$. The current density is clearly less sensitive to the grid size, since it is mainly driven by the upper part of the tail. Nevertheless, small oscillations are observed for a coarse grid. Consequently, the current drive efficiency is varying significantly when $(n_p, n_{\xi_0}) \leq 150$, as shown in Fig. 7.6, and a reltive accuracy lower than 0.5% is

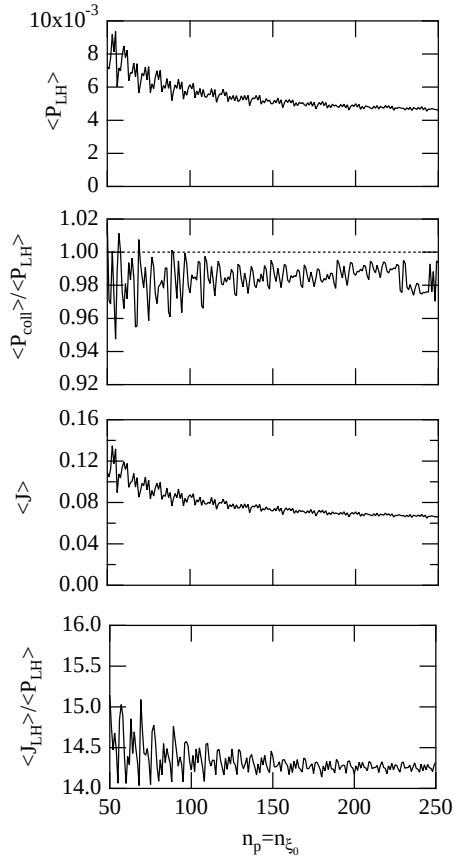

cmcm

Figure 7.6: Variations of the Lower Hybrid current and power densities, ratio between the RF and collision absorbed power density, and the current drive efficiency with the grid size. Here uniform pitch-angle and momentum grids are considered. Detailed aspect of the simulation are given in the text

only found when $(n_p, n_{\xi_0}) \geq 150$. From this systematic study, is turns out that accurate calculations with uniform pitch-angle and momentum grids require discrete steps lower than $(\Delta p, \Delta\xi_0) \lesssim 0.13$. The asymptotic value of the current drive efficiency is found to reach 14.26, very close to the value 14.35 given in Ref. [16], despite the fact that $\langle P_{LH} \rangle$ and $\langle j_{LH} \rangle$ found by the code are larger by more than 10%. The difference arises likely from the collision operator that may exhibit some differences.

The effect of the grid size of memory storage requirements and the full elapsed time for kinetic calculations. A shown in Fig.7.7 the memory used for data storage of $\widehat{\mathbb{L}}$ and $\widehat{\mathbb{U}}$ grows quadratically as expected from a $2-D$ problem. The dashed line is a parabolic fit that confirms this dependence. However, even if the scaling is quadratic, memory requirement remains reasonable, because of the small coefficients pruning in the matric factorization procedure. In the case here considered, the drop tolerance is fairly low, 10^{-4}, but large values may drastically reduce this size as discussed in Sec.6.2.1. Much in the

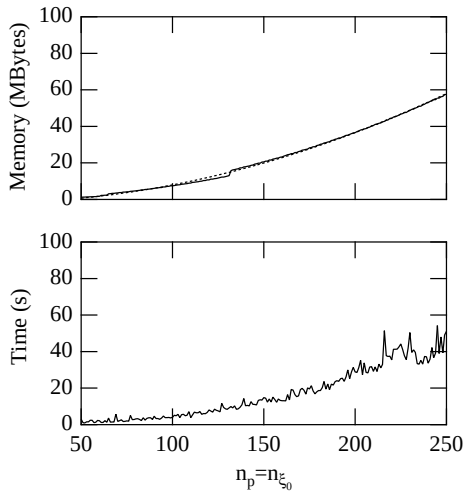

cmcm

Figure 7.7: Variations of the memory storage requirement and the time elapsed for kinetic calculations with the grid size. Here uniform pitch-angle and momentum grids are considered. Detailed aspect of the simulation are given in the text

same way, the full elapsed time for kinetic calculations increases also quadratically, but since time step is very large, is remains nevertheless lower than one minute. This confirms the effectiveness of the code, which is fast, accurate and robust, therefore fully designed for self-consistent realistic calculations that involve a chain of codes.

For a fixed number of grid points, the upper limit of the integration domain may have a crucial role, especially when entering relativistic regimes at $\beta_{th}^{\dagger} = 0.1$ and when the resonance domain involves large values of $v_{\parallel}$. As shown in Fig. 7.8 for a pure hydrogen plasma $(Z_s = 1)$, $p_{\max}$ must be larger than 25 for $(v_1 = 4, v_2 = 7)$ so that η_{LH} becomes independent of $p_{\max}$, while $p_{\max} \simeq 15$ is acceptable for $(v_1 = 3.5, v_2 = 6)$. The ratio between the power absorbed by the Lower Hybrid wave and by collisions is also a good estimate of the robustness of the calculations regarding this parameter. In principle, this ratio must be close to unity, but significant departures are observed when the upper limit of the integration domain in momentum space is too low. Consequently, for robust estimate of the current drive efficiency in realistic tokamak simulations, $p_{\max} = 30$ must be considered as a reference value for relativistic calculations, providing the lower bound of the resonance domain is larger than $n_{\parallel} \simeq 1.4$. As shown in Sec. 5.7.1, values of $n_{\parallel}$ lower than 1.4 becomes rapidly highly questionable when $T_e^{\dagger}$ exceeds $1keV$, because of the relativistic curvature of the resonance domain that makes the code fondamentaly non conservative, like in a runaway regime. Considering that in most plasma conditions encountered in tokamaks, $n_{\parallel} \geq 1.4$, the choice of $p_{\max} = 30$ makes the code fairly insensitive to the characteristics of the Lower Hybrid wave spectrum. This is an important aspect for the robustness of self-consistent simulations. Since the upper value of the momentum domain of integration is fairly large, the main consequence is that the number of mometum or pitch-angle grid points must exceed 230.

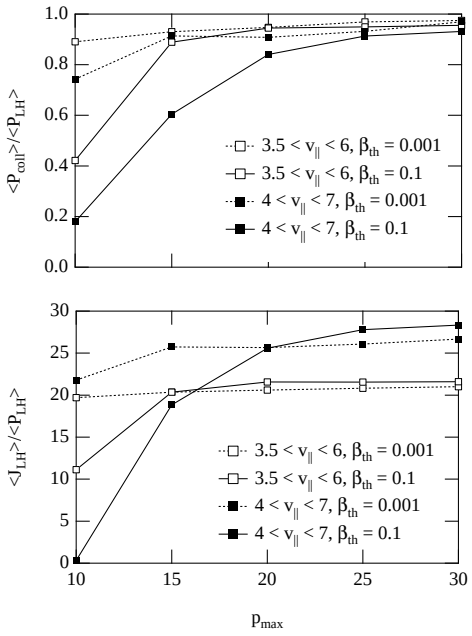

cmcm

Figure 7.8: Variation of the current drive efficiency with the upper mometum limit of the integration domain

The physical benchmark of the code is performed by investigating the role played by increasingly large values of Z_s. Though this corresponds to unrealistic situations, it allows interesting comparisons with theoretical results. As shown in Fig. 7.9, the current drive efficiency defined as the ratio

$$\eta_{LH} = \frac{\langle j_{LH} \rangle}{\langle P_{LH} \rangle} \tag{7.9}$$

is decreasing as Z_s rises as expected because of enhanced pitch-angle scattering, either for $(v_1 = 3.5, v_2 = 6)$ or $(v_1 = 4, v_2 = 7)$. Relativistic effects are almost negligible for the case $(v_1 = 3.5, v_2 = 6)$ but also for $(v_1 = 4, v_2 = 7)$ when the upper limit of the momentum integration domain is $p_{\max} = 30$. For $p_{\max} = 20$, the current drive efficiency is significantly underestimated, as discussed above, when large values of $v_{\|}$ are considered, and when relativistic effects become significant, i.e. when $\beta_{th}^{\dagger} = 0.1$ in the case here considered. The current drive efficiency scales roughly with the $1 - D$ non-relativistic model given in Ref. [16]

$$\eta_{LH}^{1-D} \simeq 0.7 \frac{4}{5 + Z_s} \frac{v_2^2 - v_1^2}{\ln\left(v_2/v_1\right)} \tag{7.10}$$

where the dependence $4/\left(5 + Z_s\right)$ with Z_s is deduced from Langevin analysis. It is found that the coefficient 0.7 is independent of (v_1, v_2). This factor could arise from that fact that the $1 - D$ expression is obtained in the saturated limit corresponding to $\overline{D}_{0,new}^{LH} = +\infty$, while numerical calculations are obtained with $\overline{D}_{0,new}^{LH} = 1$. This result confirms on one side the role played by pitch-angle scattering that make the kinetic problem a $2 - D$

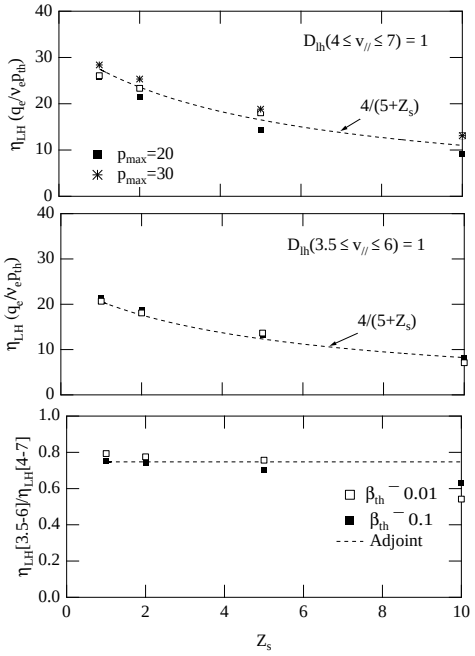

cmcm

Figure 7.9: Variation of the current drive efficiency with the main ion charge in the plasma

one, and that on the other side, important aspects of the $1-D$ description remains still valid. The $1-D$ aspect of the Lower Hybrid physics is supported by the ratio $\eta_{LH}\left[v_1=3.5, v_2=6\right]/\eta_{LH}\left[v_1=4, v_2=7\right]$ which is close to the expected theoretical value 0.75 when Z_s is not too large. In this regime, electron-electron interactions deeply contribute to the current drive process that is fundamentaly 1-D in momentum space, since resonace acceleration takes place along the magnetic field line. When $Z_s \gg 1$, the ratio of current drive efficiencies drop much faster, since $2-D$ effects start to become important. From these tests, it is clear that the code captures most of the features of the Lower Hybrid current drive. The parametric dependence with Z_s indicates that $1-D$ physics predominates over the $2-D$ one provided Z_s is not too large. The $2-D$ effects are just corrections that may be incorporated in a single reduction factor. It is important to mention that this result is independent of the model for describing electron-ion collisions, considering an ion Maxwellian background, or the high-velocity limit.

Successful comparisons between different Fokker-Planck codes have been performed. Results are given in Table 7.4 for a uniform grid,

considering the current efficiency in normalized units, but also an excellent agreement is found in absolute units, as shown in Table 7.5 taking the same value for the Coulomb logarithm, $\ln\Lambda \approx 15$.

An important question is the code reliability owing to the increase of $\overline{D}^{LH}_{0,new}$. Indeed, in weak absorption regime, as often encountered in Lower Hybrid current drive regime in present day tokamaks, $\overline{D}^{LH}_{0,new}$ may exceed significantly unity. In principle, there is

(v_1, v_2)	η_{LH} [DKE code]	η_{LH} [25]	η_{LH} [16]
$(3.5, 6)$	21.4	22.3	–
$(4, 7)$	28.38	28.8	29.7

Table 7.4: Lower Hybrid current drive efficiencies η_{LH} in a pure hydrogen plasma from various $2-D$ relativistic Fokker-Planck codes

(v_1, v_2)	η_{LH} [DKE code]	η_{LH} [32]	[CQL3D code] [27]
$(4, 7)$	32	31.96	31.34

Table 7.5: Lower Hybrid current drive efficiencies $(A \cdot m/W)$ in a pure hydrogen plasma from various $2-D$ relativistic Fokker-Planck codes

no limitation on the value of $\overline{D}^{LH}_{0,new}$, and numerous analytical results corresponds to the asymptotic solution $\overline{D}^{LH}_{0,new} = +\infty$. However, limitations do exist in numerical simulations, and it is important to qualify the robustness of the code regarding this problem. A systematic study has been performed for $(v_1 = 3.5, v_2 = 6)$ and $(v_1 = 4, v_2 = 7)$, with $\beta^{\dagger}_{th} = 0.001$ and $\beta^{\dagger}_{th} = 0.1$. In these simulations, $p_{\max} = 30$, and uniform momentum and pitch-angle grids are taken, with a size $n_p = n_{\xi_0} \simeq 200$ except when specified.

As shown in Fig.7.10, for all simulations with $\overline{D}^{LH}_{0,new}$ ranging from 1 to 10, the conservative scheme is preserved, which clearly indicates the robustness of the discrete projection of the Fokker-Planck equation on the numerical grid. Furthermore, from the non-relativistic regime to the relativistic one, the ratio $\langle P_{coll} \rangle / \langle P_{LH} \rangle$ is close to 1, as expected when the solution has a physical sense, i.e. when $\overline{D}^{LH}_{0,new} \leq 2$ only. It is interesting to observe that the current drive efficiency does not vary significantly from $\overline{D}^{LH}_{0,new} = 1$ to $\overline{D}^{LH}_{0,new} = 2$, which indicates that the saturated regime with a flat plateau is almost reached when $\overline{D}^{LH}_{0,new} = 1$.

When $\overline{D}^{LH}_{0,new}$ exceeds 5, numerous numerical problems occur. For $\beta^{\dagger}_{th} = 0.001$, the value of the driven current has no sense, and may have also the wrong direction, while the ratio $\langle P_{coll} \rangle / \langle P_{LH} \rangle$ is always far from unity. This situation can never be recovered by increasing the grid size up to $n_p = n_{\xi_0} \simeq 300$. The difference between distribution functions given by the code with $\overline{D}^{LH}_{0,new} = 2$ and $\overline{D}^{LH}_{0,new} = 10$ is clearly visible between contour plots in Figs.7.11 and 7.12, for the case $(v_1 = 3.5, v_2 = 6)$. Spurious shapes appear for $\overline{D}^{LH}_{0,new} = 10$ whose weight in the current drive efficiency calculation is dramatic. Conversely, for $\overline{D}^{LH}_{0,new} = 2$, the distribution function is well behaved, and the stream countours given in Fig.7.13 clearly have the expected physical shape.

Attempt to reduce this problem by smoothing the momentum variation of $\overline{D}^{LH}_{0,new}$, in particular the sharp transition at the resonance domain boundaries, turns out to be absolutely useless. With a 5 points smoothing, the onset of numerical instabilities remains similar to the one with sharp variations.

For the relativistic regime $\beta^{\dagger}_{th} = 0.1$, the effect of increasing $\overline{D}^{LH}_{0,new}$ above 5 is more sub-

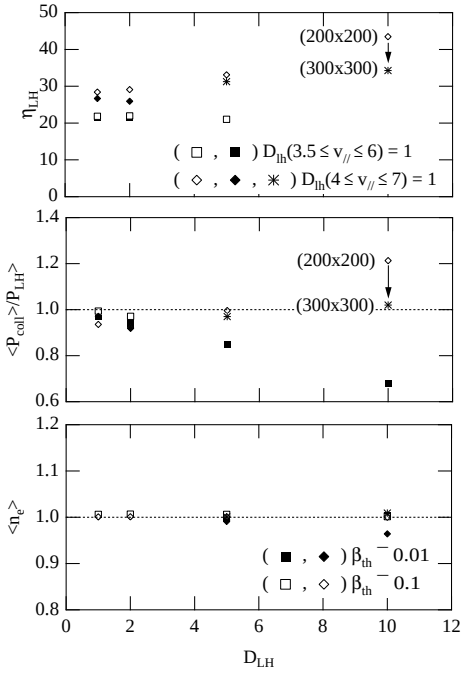

cmcm

Figure 7.10: Variation of the current drive efficiency with the amplitude of the quasilinear diffusion coefficient for the Lower Hybrid current drive problem

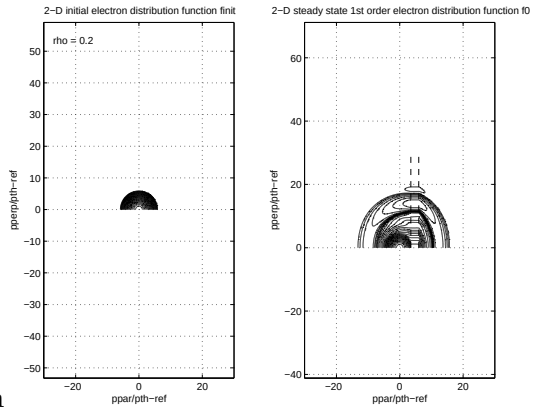

cmcm

Figure 7.11: Contour plot of the electron distribution function for $D_{LH} = 10$

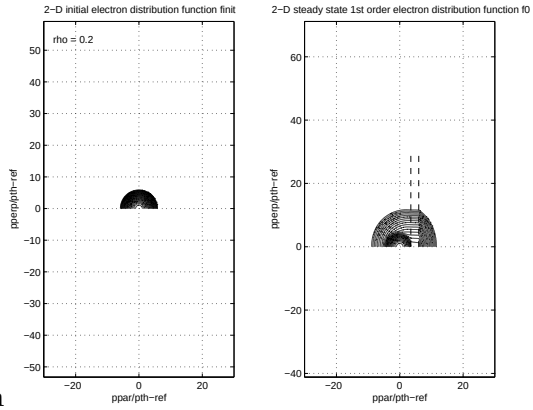

cmcm

Figure 7.12: Contour plot of the electron distribution function for $D_{LH} = 2$

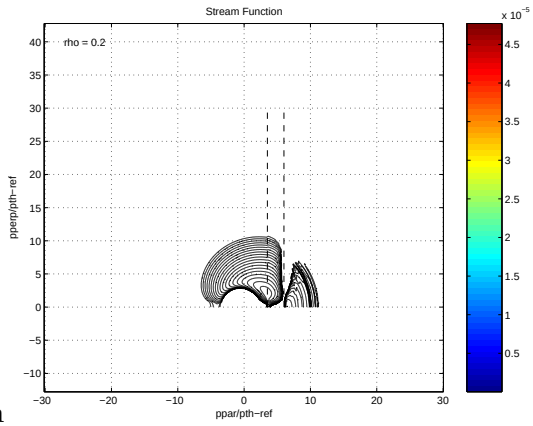

cmcm

Figure 7.13: Contour plot of the electron stream function for $D_{LH} = 2$

tile since in that case the current drive efficiency increases significantly, while $\langle P_{coll} \rangle / \langle P_{LH} \rangle$ remains close to 1 within 20%. It is therefore very difficult to identify unambiguously that the solution has no physical sense. In order to cross-check that the solution is wrong, the grid size has been increased up to $n_p = n_{\xi_0} \simeq 300$. In that case, the effect is spectacular, and the current drive efficient drops down to an acceptable level, while $\langle P_{coll} \rangle / \langle P_{LH} \rangle$ is very close to unity for $\overline{D}^{LH}_{0,new} = 10$ as shown, in Fig. 7.10. Still visible, this effect is weaker for $\overline{D}^{LH}_{0,new} = 5$.

From this analysis, it is clear that a too coarse grid leads to strong limitations on the upper value of $\overline{D}^{LH}_{0,new}$ that may be used for accurate estimate of the current drive level with sharp variation of the Lower Hybrid quasilinear diffusion coefficient. It is clear that this problem is enhanced in the non-relativistic regime, for an unknown reason yet. Finally, a smooth transition from a solution that has a physical sense to a solution that has no physical sense is clearly observed by increasing $\overline{D}^{LH}_{0,new}$. There is no evidence that this problem corresponds always to an increase of the current drive efficiency. This difficulty is particularly difficult to handle, since no clear criterion may help to reject the solution. Consequently, it is highly recommended to avoid the use of the code with $\overline{D}^{LH}_{0,new}$ larger 2 to be free from numerical problems for almost all situations. In any case, forcing the Maxwellian solution close to $p = 0$ and normalizing the density at each iteration when numerical problems occur is usualy useless, since the solution given by the code remain in general fully non physical, though convergence can be ensured. In that case, the overall absorption process fails, and the result has no meaning. A possible way to overcome this problem is to perform calculations with the upper acceptable $\overline{D}^{LH}_{0,new} = 2$ value, while using an adhoc correcting factor, in order to recover the solution corresponding asymptotic limit at $\overline{D}^{LH}_{0,new} = +\infty$.

From the physical point of view, it is not surprizing that the use of very large $\overline{D}^{LH}_{0,new}$ values leads to numerical instabilities. Indeed, in that case, the characteristic quasilinear time in the resonance domain is close to zero, with respect to the collision time. Consequently, there is some degeneracy in the corresponding part of the matrix, since different regions of the momentum space are instantaneoulsy connected at the collision scale. Therefore, parts of the matrix do not provide additionnal information, but the numerical errors related to the projection of the differential equations on the numerical grids act like a reservoir of numerical instabilities in that case. There are some similarities with the implicit description of the trapped electrons, when bounce-averaged Fokker-Planck equation must be solved. The only and consistent way to solve this problem is to remove the domain where the time ordering fails, and establish correct internal boundary conditions so that the density of electron at v_1 is exactly equal to the one at v_2 at all pich-angles ξ_0 grid points. Obviously, this process adds new off-diagonal coefficients in the matrix, but in that case, the conditionning of the matrix is preserved even for $\overline{D}^{LH}_{0,new} = +\infty$. With the new general method of partial matrix factorization discussed in Sec.6.2.1, such an approach may be in principle easily tractable, without prohibitive computational efforts.

The role played by a non-uniform pitch-angle grid is critical, since in realistic simulations, bounce-averaging must be considered with trapped-passing boundaries that moves in mometum space with the radial position. In that region, the pitch-angle gris step

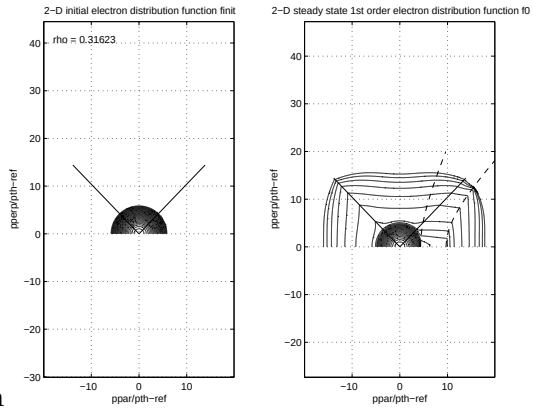

Figure 7.14: Contour plot of the electron distribution function at $\epsilon = 0.31623$

must be lower, for more accurate results. Concerning the momentum grid, as discussed in Sec.5.4.3 the domain where the grid is non-uniform, is by construction far from the region where the quasilinear diffusion coefficient is different from zero, and consequently all the results obtain for the uniform grid are valid. It is found that a non-uniform pitch-angle grid has no effect for $\overline{D}^{LH}_{0,new} \leq 2$, $n_p = n_{\xi_0} \simeq 200$ and $p_{\max} = 30$ on the solution found by the code, within less than 1%, which is an important result for $3-D$ operation, even when Z_s increases, and $2-D$ broadening by pitch-angle scattering plays progressively a dominant role over the parallel direction along the magnetic field line direction.

Ultimate benchmarks have been performed to validate the implementation of the Lower Hybrid current drive in the code in $3-D$ configuration and relativistic regime, in presence of bounce-averaging. The same radial grid introduced for the electrical conductivity calculations in Sec. 7.1 is used, and flat profiles are considered, so that only the role of trapped electrons comes into play. In Fig.7.14 , a typical case for $\overline{D}^{LH}_{0,new} = 1$, $n_p = n_{\xi_0} \simeq 200$ and $p_{\max} = 20$ with $(v_1 = 4, v_2 = 7)$ at $\rho = 0.31623$ is shown. This corresponds to a similar inverse aspect ratio ϵ, since in this calculation $a_p \simeq R_p$. Only a part of the quasilinear domain at large $p_\perp$ intercepts the trapped-passing boundary, leading therefore to a modest reduction of the current drive efficiency, by 6% in this case. The contour plot of the corresponding quasilinear domain is shown in Fig. 7.15, and in Fig.7.16 the $1-D$ like distribution function $F^{(0)}_{\|0}\left(\psi, p_\|\right)$ averaged over the direction perpendicular to the magnetic field line direction, as well as the parallel and perpendicular temperatures $T_\|$ and $T_\perp$. defined in Sec. No anomalous numerical behaviour is observed. An important results is that the current drive efficiency does not vary when the resonance domain is replaced by $(v_1 = -7, v_2 = -4)$. Only the sign of the current is reversed. Moreover, when a compound spectrum is launched, with $(v_1 = 4, v_2 = 7)$ and $(v_1 = -7, v_2 = -4)$, the current level given by the code is zero within the numerical accuracy, at least 3 orders of magnitude lower than for the case $(v_1 = 4, v_2 = 7)$ or $(v_1 = -7, v_2 = -4)$ alone. This results confirm the robustness of the numerical scheme, for complex and realistic modeling of the Lower Hybrid current drive problem.

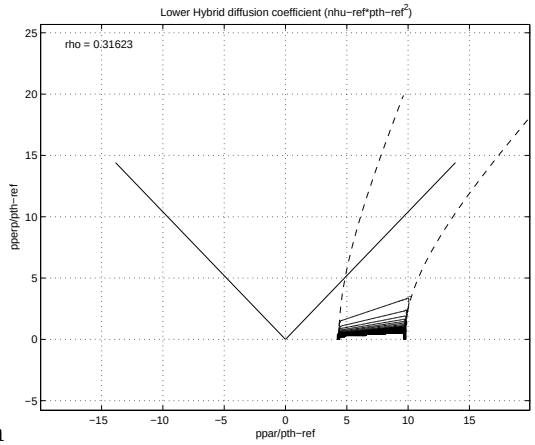

cmcm

Figure 7.15: Contour plot of the Lower Hybrid quasilinear diffusion coefficient at $\epsilon = 0.31623$

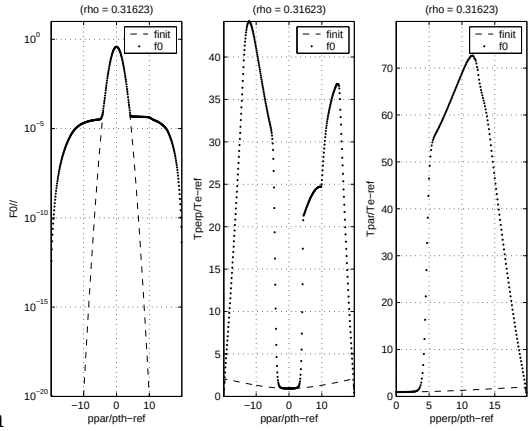

cmcm

Figure 7.16: Electron distribution function averaged over the perpendicular momentum direction at $\epsilon = 0.31623$. The perpendicular and parallel temperatures are also shown

7.4 Electron Cyclotron Current drive

7.4.1 Introduction

Fast and accurate kinetic calculations of electron cyclotron current drive (ECCD) are of great importance given that ECCD provides the most controllable and adjustable known source of CD in tokamaks, and is used in a wide range of advanced tokamak experiments, including to achieve fully non-inductive steady state operation and stabilize neoclassical tearing modes . The calculation of ECCD requires to use all the features and power of the the DKE code, including the fast implicit treatment of trapped particles and momentum space fluxes at the trapped/passing boundary. Indeed, wave-induced trapping and momentum exchange with trapped particles are a dominant aspect of off-axis ECCD as they explain the Ohkawa effect.

We illustrate ECCD calculations using an idealized DIII-D scenario with $R_p = 1.67$ m, $a_p = 0.67$ m, $B_t = 2$ T, $Z_{\text{eff}} = 2$, $T_{e0} = 4$ keV and $n_{e0} = 3{\times}10^{19}$ m^{-3}. The temperature and density profiles are either parabolic or constant, as specified for each following simulation. The poloidal magnetic field is assumed to be negligible. For simplicity, the plasma is assumed to be circular without Shafranov shift. The primary ECCD parameters are X-mode polarization, $N_{\|} = 0.3$, $f_{\text{EC}} = 110$ MHz $P_{0\text{EC}} = 1.0$ MW and Gaussian spectrum width $\Delta N_{\|} = 0.02$. For these parameters, an ideal EC beam propagating from the low field side on the outboard midplane ($\theta_b = 0$) would be absorbed at second harmonic near the plasma center, and the peak in the power deposition profile would be located at a normalized radius $\rho = 0.1$. At this location, the frequency ratio $y_2 = 2\omega_{ce}/\omega$, which defines the position of the resonance curve in momentum space (along with $N_{\|}$), is $y_2 = 0.98$. The normalized diffusion coefficient is $D_{0\text{EC}}^{\text{new}} = 0.15$. In the following sets of calculation, the relaxation is let to evolve completely freely: no normalization between time steps and no forced Maxwellian at $p = 0$.

7.4.2 Grid size effects

In the first set of calculations, we consider the primary ECCD case ($\rho = 0.1$, $\theta_b = 0$, $N_{\|} = 0.3$, $\Delta N_{\|} = 0.02$, $y_2 = 0.98$, $D_{0\text{EC}}^{\text{new}} = 0.15$) and vary the size of the momentum grid (n_p, n_ξ), which is taken to be uniform (Fig 7.17). The maximum momentum grid point is set at $p_{\max} = 10$. The computed electron density increases slightly then stabilizes during the relaxation and reaches an output value $n_{e\text{out}}$ with $((n_{e\text{out}} - n_e)/n_e \leq 6\%)$. This difference is quite small given that a EC diffusion coefficient of $D_{0\text{EC}}^{\text{new}} = 0.15$ is rather large. The output density does not rapidly converge to 1 when the grid size in increased (graph a) which indicates that the primary reason for the density increase is not the precision of the discretization scheme. The the flux-surface averaged driven current densiry (graph b) converges towards a normalized asymptotic value $j_\infty^{\text{EC}} = 2.4 \times 10^{-2}$ $(en_e v_{Te})$. However, there are oscillations in the evolution of j^{EC} with (n_p, n_ξ) which account for most of the disparity with j_∞. These oscillations can be attributed to the sharp Gaussian-like evolution of the diffusion coefficient in momentum space, with a characteristic variation size that is smaller than a grid step. The gaussian shape of the spectrum being somewhat

(a)

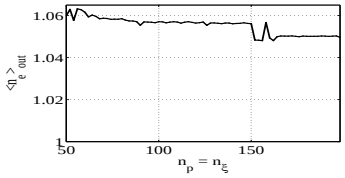

(b)

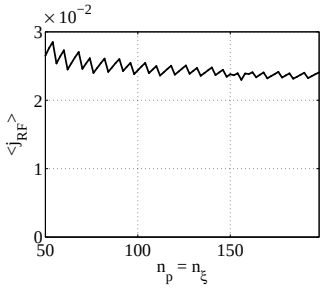

(c)

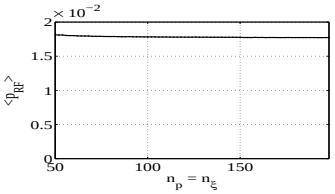

(d)

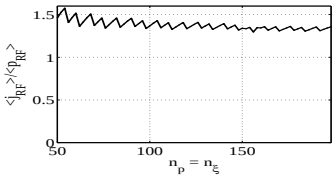

(e)

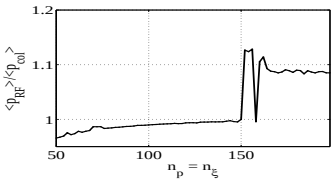

Figure 7.17: ECCD in DIII-D ($\rho = 0.1,\ D_{\mathrm{EC}} = 0.15,\ N_{\|} = 0.3,\ Y = 0.98$). Output density (a), normalized current density (b), normalized absorbed power density (c), normalized current drive efficiency (d), ratio of power absorbed to power lost on collisions (e), as a function of grid size ($n_p = n_\xi$).

smoother than the LH square spectrum, the variations in j^{EC} are less important than for the previous LH case. The calculation of the the flux-surface averaged density of power absorbed (graph c) is however quite robust and does not depend much on the grid size. It rapidly converges to a value $p_{\infty}^{\mathrm{EC}} = 1.8 \times 10^{-2}$ $(n_e m_e \nu_e v_{Te}^2)$. The evolution of the normalized figure of merit $\eta^{\mathrm{EC}} \equiv j^{\mathrm{EC}}/p^{\mathrm{EC}}$ mostly follows the variations of j^{EC} (graph d). It converges to a value of $\eta_{\infty}^{\mathrm{EC}} = 1.3$ $(e/m_e \nu_e v_{Te})$. For a 100×100 grid, the mean error on j^{EC} and η^{EC} is about 10%. It reduces to less than 5% for a 200×200 grid. The ratio of the power absorbed from ECW to the power lost on collisions expectedly tends to 1 as the grid size increases (graph e), until the grid size reaches about 150×150, where it undergoes an unexplained jump to about 1.1.

The requirements of ECCD calculations on the maximum momentum $p_{\max}$ are far more easily satisfied than for LHCD. To illustrate this, we consider the same case ($\rho = 0.1$, $\theta_b = 0$, $N_{\parallel} = 0.3$, $\Delta N_{\parallel} = 0.02$, $y_2 = 0.98$, $D_{0\mathrm{EC}}^{\mathrm{new}} = 0.15$) and fix $n_{\xi} = 100$. The maximum momentum $p_{\max}$ and the momentum grid size n_p are varied proportionally so that the momentum step size remains unchanged and the discretization effects are therefore removed. The results are shown on Fig. 7.18. None of the relevant integral quantities ($n_{e\mathrm{out}}$, j^{EC}, p^{EC}, $p^{\mathrm{EC}}/p^{\mathrm{col.}}$, η^{EC}) varies significantly for $p_{\max}/p_{Te} \geq 7$. For comparison, the maximum value of $p_{\perp}$ on the resonance curve is $p_{\perp,\max}^{\mathrm{res}} = 2.7 p_{Te}$ and the maximum value of p is $p_{\max}^{\mathrm{res}} = 6.4 p_{Te}$.

7.4.3 Electron trapping effects

In the next set of calculation (Fig. 7.19), we keep the same ECCD parameters ($\theta_b = 0$, $N_{\parallel} = 0.3$, $\Delta N_{\parallel} = 0.02$, $y_2 = 0.98$, $D_{0\mathrm{EC}}^{\mathrm{new}} = 0.15$) but vary the radial location of ECCD. The density and temperature profiles are kept constant such that the only effect to consider is the increasing number of trapped particles as $\epsilon = r/R_p$ increases. The output density increases slightly with ϵ (graph a) but remains acceptable. The density of driven current steadily decreases and reverses signs for $\epsilon \geq 0.16$ (graph b). This evolution indicates that the Ohkawa effect, which is due to ECW-induced trapping and drives a counter-current, eventually compensates and even dominates the Fisch-Boozer effect. In fact, the Ohkawa current density peaks at $\epsilon \simeq 0.25$ and then $\left|j^{\mathrm{EC}}\right|$ goes back to 0 as ϵ further increases. The ohkawa effect is maximum where the EC resonance curve in momentum space is tangent to the trapped passing boundary, so that wave-induced trapping is maximum. For larger ϵ - or wider trapping region - most of the EC power is transferred directly to trapped electrons, which do not drive current. This explains why $\left|j^{\mathrm{EC}}\right| \to 0$ as $\epsilon \geq 0.25$ increases. The density of power absorbed slowly increases with ϵ (graph c). The increases is faster for $\epsilon \geq 0.25$, which can be expected since at these location, increasing coupling with trapped particles occur. Indeed, because of the fast bounce motion, this coupling is effectively distributed between trapped electrons travelling in both directions. This distribution divides the effective magnitude of the diffusion coefficient by two but also doubles the amount of resonant particles in the trapped region. As a result, quasilinear effects on ECCD with trapped particles are reduced, which explains the larger density of power absorbed. The evolution of the normalized figure of merit is similar as that of $\left|j^{\mathrm{EC}}\right|$ (graph d) and the ratio of he power absorbed from ECW to the power lost on collisions is quite stable, and very close to 1.

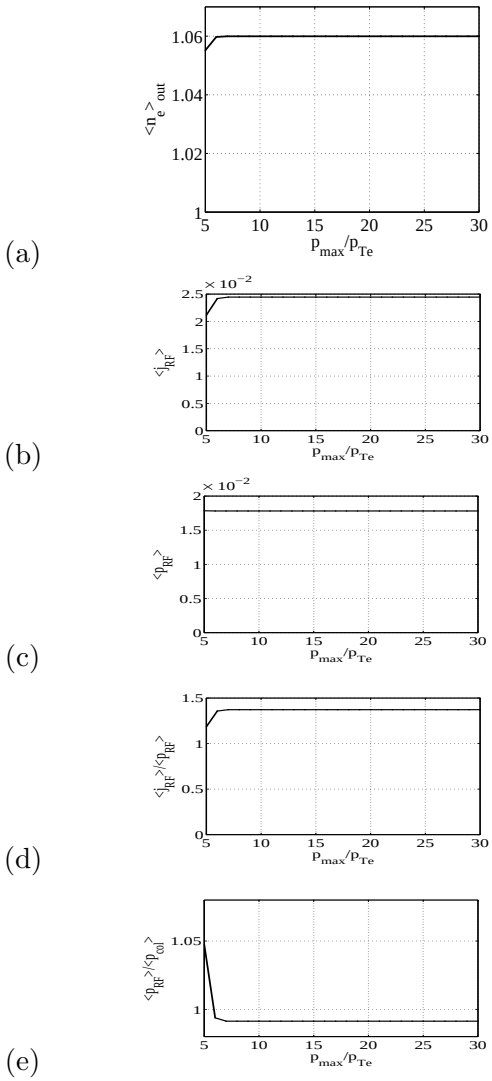

Figure 7.18: ECCD in DIII-D ($\rho = 0.1,\ D_{\mathrm{EC}} = 0.15,\ N_{\|} = 0.3,\ Y = 0.98$). Output density (a), normalized current density (b), normalized absorbed power density (c), normalized current drive efficiency (d), ratio of power absorbed to power lost on collisions (e), as a function of momentum grid limit $p_{\max}$ ($n_p = 10p_{\max},\ n_\xi = 100$).

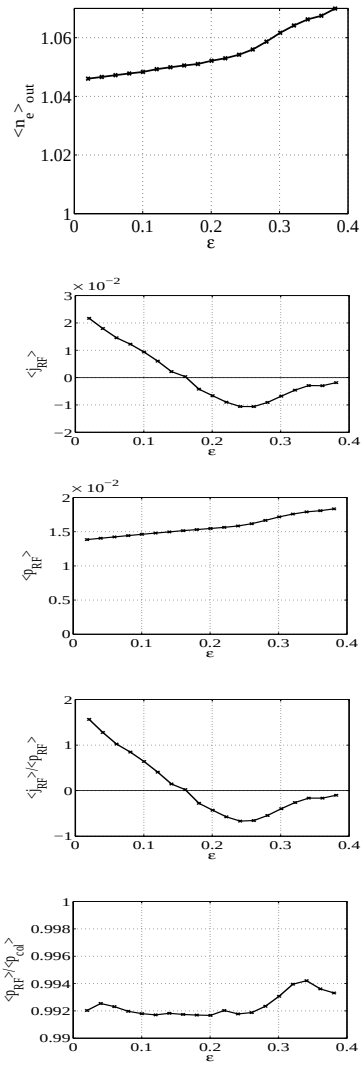

Figure 7.19: ECCD in DIII-D ($D_{\mathrm{EC}} = 0.15,\ N_{\|} = 0.3,\ Y = 0.98$). Output density (a), normalized current density (b), normalized absorbed power density (c), normalized current drive efficiency (d), ratio of power absorbed to power lost on collisions (e), as a function of the inverse aspect ratio $\epsilon = r/R_p$; temperatures, densities and Z_{eff} are kept constant across the plasma.

7.4.4 Momentum-space dynamics

In order to illustrate the momentum-space dynamics of ECCD, the 2D distribution function is plotted in the $\left(p_{\|}, p_{\perp}\right)$ space (Fig. 7.20). The case considered here is again our primary example ($\rho = 0.1$, $\theta_b = 0$, $N_{\|} = 0.3$, $\Delta N_{\|} = 0.02$, $y_2 = 0.98$, $D_{0\mathrm{EC}}^{\mathrm{new}} = 0.15$). On graph a, the initial Maxwellian (thin blue contours) and the steady-state ECCD distribution (thick red contours) are displayed, as well as contour of the magnitude of the EC diffusion coefficient (green dashed contours). The distortion of the distribution from a Maxwellian in the vicinity of the resonant region is clearly visible. Collisions are trying to restore the Maxwellian and induce momentum-space fluxes that affect the entire momentum space. By integrating over $p_{\perp}$, we obtain the parallel distribution

$$F_{\|}\left(p_{\|}\right) = 2\pi \int_0^{\infty} p_{\perp} dp_{\perp}\; f\left(p_{\|}, p_{\perp}\right) \tag{7.11}$$

shown on graph b. In the non-relativistic limit, the integration of $\left(ep_{\|}/m_e\right) F_{\|}\left(p_{\|}\right)$ over $p_{\|}$ gives the driven current density. The Fisch-Boozer effect, resulting in an accumulation of particles with large, positive $p_{\|}$, appears clearly. This effect - understood as an asymmetric resistivity due to EC heating - is also illustrated on graph c, where the perpendicular temperature is plotted as a function of $p_{\|}$; the difference in temperature, due to asymmetric EC heating, induces the asymmetric resistivity and driven current. Note that EC induced diffusion in momentum space is mostly in the perpendicular direction, and therefore does not directly drive any current. It is always the collisional response to this diffusion which drives a current.

7.4.5 Coupling to propagation models

The code can be coupled to ray-tracing calculations. Iterations on the 3D ECCD calculations ensure that the power absorbed from the EC wave is consistent with the power travelling in the EC beam. Such calculations are very fast, thanks to the fully-implicit 3D algorithm. To illustrate this, we consider a simplified ECCD scenario with X-mode polarization, $N_{\|} = 0.3$, $f_{\mathrm{EC}} = 110$ MHz, $P_{0\mathrm{EC}} = 1.0$ MW and Gaussian spectrum width $\Delta N_{\|} = 0.02$. The EC beam propagates from the low field side on the outboard midplane ($\theta_b = 0$). The evolution of $N_{\|}$ due to toroidicity is neglected, and the cold plasma model is used to solve the dispersion relation. The DKE calculations are performed on a $n\psi \times n_p \times n_\xi = 26 \times 100 \times 100$ grid, and consistency between travelling and absorbed power is reached after 4 iterations. The resultant current density and absorbed power density profiles are shown on Fig. 7.21. The current profile appears to be shifted slightly to the right compared to te power profile. This shift results from the fact that at $\rho \geq 0.1$, resonant electrons are further in the tail of the distribution - meaning that they are less collisional - than at $\rho \leq 0.1$, and therefore the local efficiency is higher for $\rho \geq 0.1$. The location $\rho = 0.1$ corresponds to the peak in the absorbed power profile, which justifies taking this value for the previous simulations.

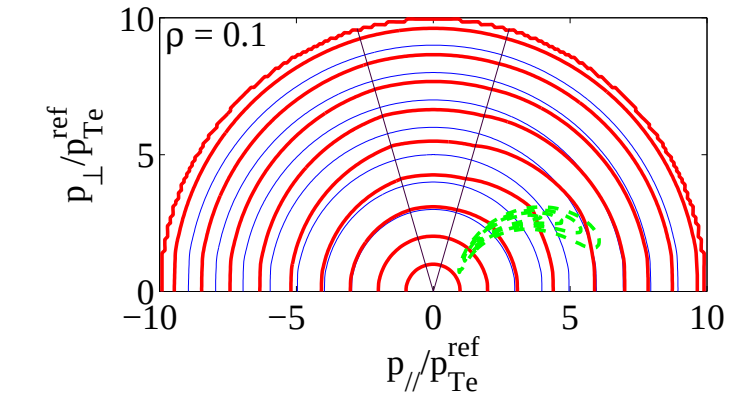

(a)

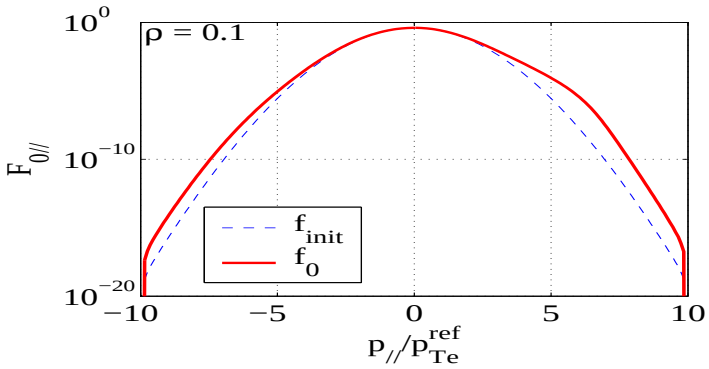

(b)

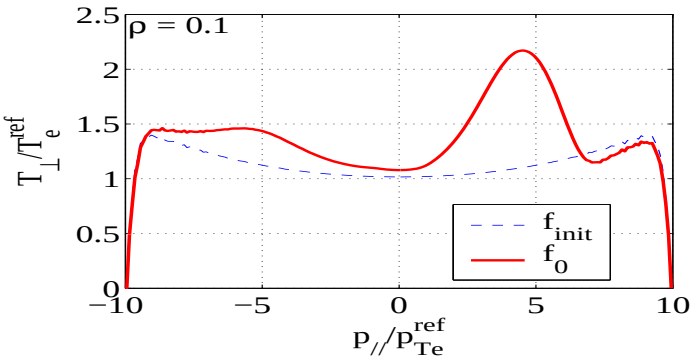

(c)

Figure 7.20: ECCD in DIII-D ($\rho = 0.1$, $D_{\mathrm{EC}} = 0.15$, $N_{\|} = 0.3$, $Y = 0.98$). 2D electron distribution function (a), parallel distribution function (b) and perpendicular temperature (c); blue thin lines represent f_{init}, red thick lines represent f_0, and green dashed contours represent D_{EC}.

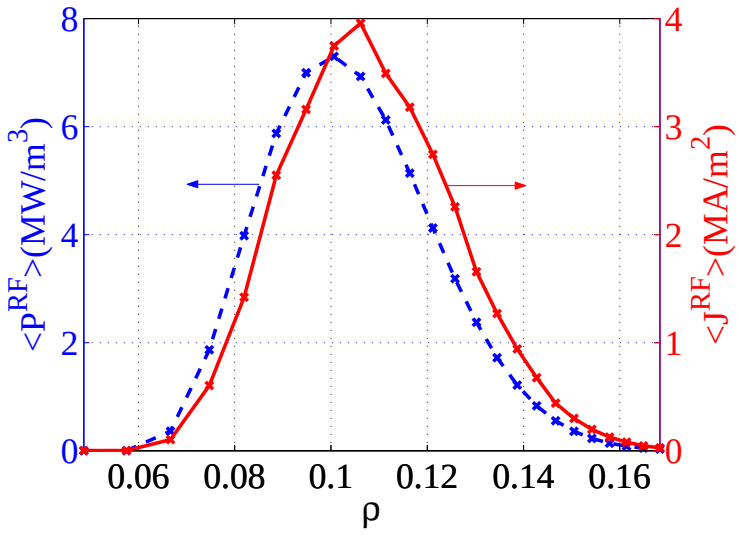

Figure 7.21: ECCD in DIII-D ($\theta_b = 0$, $P_{\rm EC} = 1$ MW, $N_{||} = 0.3$, $f_{\rm EC} = 110$ MHz). Current and power densities deposition profiles. 3D calculation with $n_p = n_\xi = 100, n_\psi = 26$.

7.4.6 Conclusion

To sum up, we have shown that the DKE code accurately describes and calculates ECCD. It runs robustly in the free conservative mode. Grid parametric requirements are somewhat less restrictive than for LHCD, because the EC diffusion coefficient variations are somewhat smoother. It accounts correctly for trapped electron effects, such as the Ohkawa current. It can be used to simulate actual ECCD scenarios, including coupling and consistency with ray-tracing calculations.

7.5 Fast electron radial transport

This simulation is here presented to illustrate code capabilities for a realistic magnetic configuration and a hot deuterium plasma. It corresponds to a typical JET Lower Hybrid current drive discharge, where both bounce-averaging and fast electron particle transport are considered. Global parameters of the discharge are gathered in section "JET" of the tokamak parameter M-file "ptok_dke_1yp.m".

As shown in Fig.7.22 , the spatial ψ half-grid, on which the electron distribution function is calculated, is non-uniform, though grid steps $\Delta\rho$ for the normalized radius defined in Sec. 2.1 are constant for this example. The spatial mesh size for $f_0^{(0)}$ has $n_\psi - 1 = 14$ points, which is the typical number of spatial grid points considered in most of the current drive simulations. The corresponding pitch-angle grid is strongly non uniform, as indicated in Fig.7.23, since trapped/passing boundaries corresponding to all radial positions are exactly placed on the flux grid in momentum space. The total number

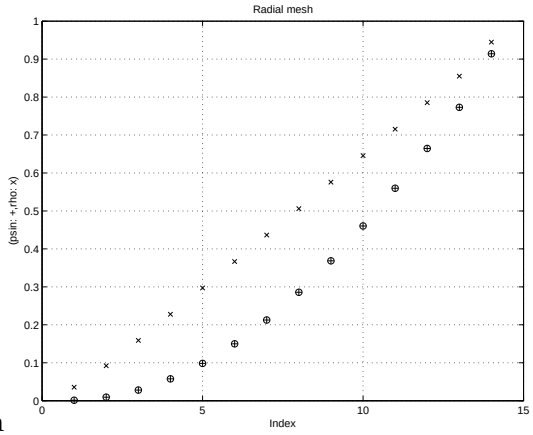

cmcm

Figure 7.22: Radial grid for 3-D JET current drive simulation. Circles correspond to the normalized poloidal flux coordinate ψ, while crosses correspond to normalized radius ρ

of pitch-angle points for $f_0^{(0)}$ is $n_{\xi_0} - 1 = 206$. Finally the momentum grid is also taken no uniform with $n_p - 1 = 210$ points. As shown in Fig.7.24 the momentum grid is first nearly uniform in the vicinity of $p = 0$ for the first twenty points, with a small step $\Delta p \simeq 0.07$, as indicated in Fig. 7.25. For $p \gtrsim 1.5$, the grid is also uniform, but with larger momentum step $\Delta p \simeq 0.15$. The smooth transition between the two grids involves 7 grid points.

Temperature and density profiles used as input for the magnetic equilibrium calculations done by HELENA code are presented in Fig. 7.26. As usual in current drive regime at low density, the electron temperature profile is peaked, and its value is much larger than ion temperature. The dominant ion (deuterium) profile is determined selfconsistently from the electron density and effective charge profiles, the latter being taken flat at a level of $Z_{eff} = 1.5$. In the calculations which are based on electroneutrality, only one fully stripped impurity is considered, i.e. carbon $Z_s = 6$, in order to avoid the use of an impurity transport code. The resulting $2 - D$ contour plot of the magnetic poloidal flux surfaces is given in Fig. 7.27, for a configuration with a bottom X-point close to the divertor. Here, calculations are performed for a monotonic safety factor profile.

In the calculations, fully relativistic corrections are considered. In Fig.7.28, the deviation from the relation $v = p$ clearly indicates that relativistic corrections come into play when $p \gtrsim 4$[4]. Consequently, since a simplified expression for the Lower Hybrid quasilinear diffusion operator is considered, as described in Appendix D.2.8 and used in Sec. 7.3, boundary values of the resonance domain which correspond to $(v_1 = 3.5, v_2 = 6)$ exhibit strong curvature as a function of p, as shown in Fig. 7.29. In order to simulate a spatialy localized off-axis absorption of the RF power, the quasilinear diffusion coefficient

[4]Here v and p are normalized respectively to p_{th}/m_e and p_{th}, where m_e is the electron rest mass and p_{th} the thermal momentum.All reference values in the calculations are taken at the plasma center, including p_{th} as discussed in Sec.6.3.

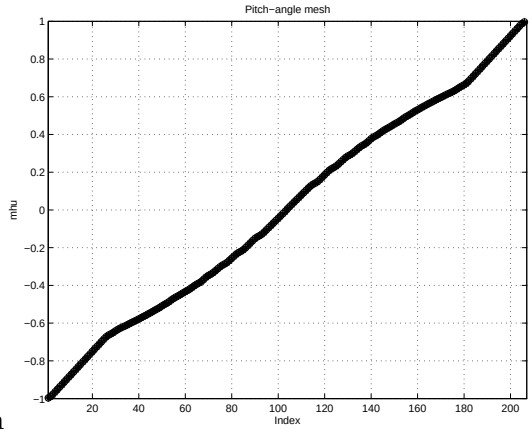

cmcm

Figure 7.23: Pitch-angle grid for 3-D JET current drive simulation.

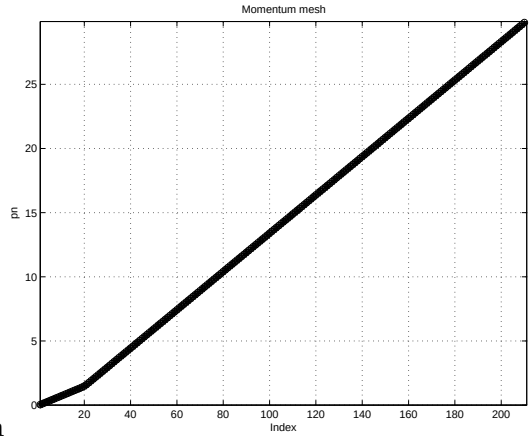

cmcm

Figure 7.24: Momentum grid for 3-D JET current drive simulation.

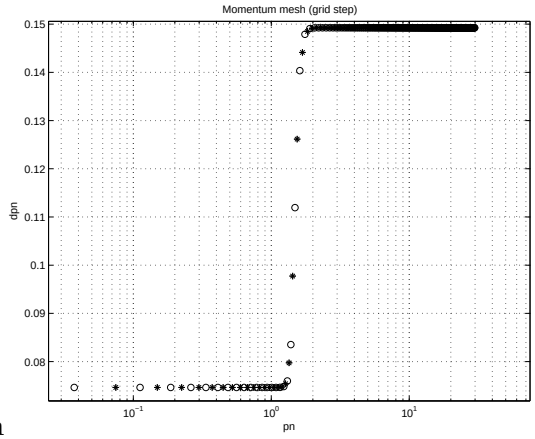

cmcm

Figure 7.25: Momentum grid step for 3-D JET current drive simulation. Circles correspond to the flux grid, while stars to the distribution function half-grid

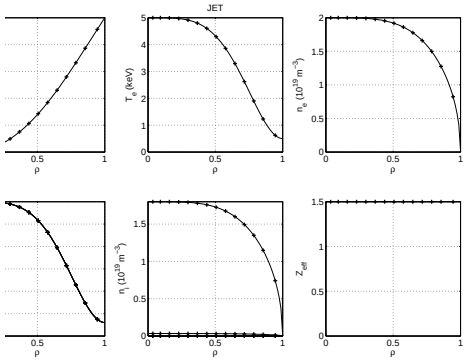

cmcm

Figure 7.26: Ion and electron temperature and density profiles, and effective charge profile used for calculating the JET magnetic equilibrium with HELENA. Here hydrogen and tritium densities are zero (pure deuterium plasma) . The poloidal flux coordinate ψ as function of the normalized radius ρ in the equatorial mid-plane corresponds to the magnetic equilibrium code output

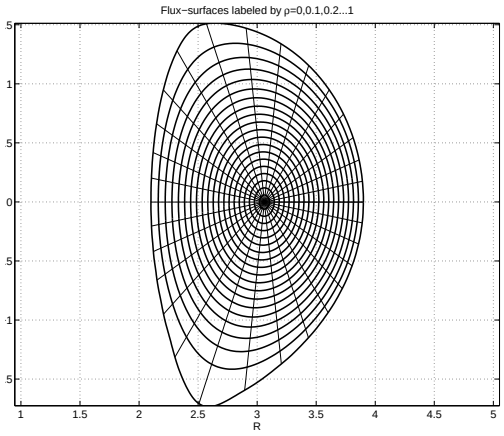

cmcm

Figure 7.27: $2-D$ contour plot of the poloidal magnetic flux surfaces as calculated for JET tokamak by the code HELENA

$\overline{D}^{LH}_{0,new}(\psi,p)$is defined as

$$\overline{D}^{LH}_{0,new}(\psi,p)=\overline{D}^{LH}_{0,new}(0,p)\,\frac{2\sqrt{\ln 2}}{\sqrt{\pi}}\exp\left[-\frac{\left(\rho-\rho^{peak}_{LH}\right)^2}{\left(\frac{\Delta\rho_{LH}}{2\sqrt{\ln 2}}\right)^2}\right] \tag{7.12}$$

where $\overline{D}^{LH}_{0,new}(0,p)=1$ in the interval $v_1\leq v_{\|}\leq v_2$, and $\rho^{peak}_{LH}=0.5$ is the radial position at which absorption is maximum, and $\Delta\rho_{LH}=0.2$ the half-width. For $\rho\leq 0.2$ and $\rho\geq 0.65$, power absorption is null.

Fast electron radial transport that could result from magnetic turbulence is expressed in the usual form

$$D^{(0)}_{\psi}(\psi,p)=D^{(0)}_{\psi}(0,p)\,H\left(\left|v_{\|}\right|-v_{\|c}\right)\left(\left|v_{\|}\right|-v_{\|c}\right)/v_{\|c} \tag{7.13}$$

where $D^{(0)}_{\psi}$ is the radial diffusion coefficient as defined in Sec.6.3. Here, $D^{(0)}_{\psi}$ scales like $\left|v_{\|}\right|$ as expected from theory [5], with a velocity threshold which is set to 3.5. The simulation is performed with $D^{(0)}_{\psi}=5m^2/s$, its value and the threshold level being uniform throughout the plasma, while any convection is neglected. The $2-D$ contour plot of the $D^{(0)}_{\psi}$ is shown in Fig. 7.30

The $3-D$ simulation is performed in the fully implicit mode with usual parameters, i.e. $\Delta\bar{t}=10000$, using the linearized electron-electron Belaiev-Budker collision operator for momentum conservation. While the time taken to calculate all matrix coefficients associated to momentum dynamics is extremely fast, of the order of $120s$[5], since calculations may be performed in a vectorial form that is very convenient for MatLab, coefficients for radial transport needs a much longer computer time is this version of the code, typically

[5]Absolute computer time values may depend significantly from the charge of the computers. A reduction by 50% is likely for a workstation with few jobs.

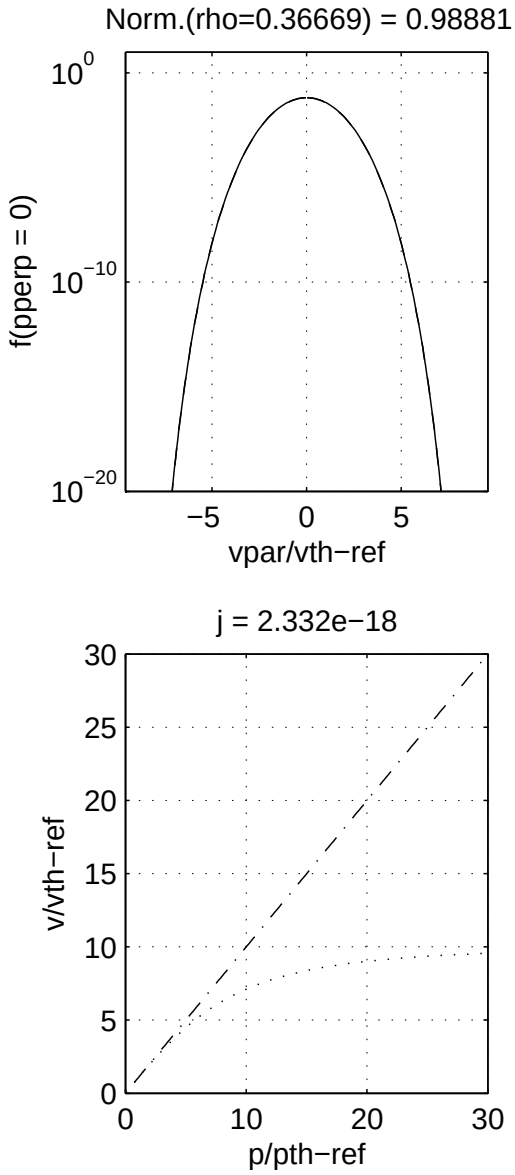

Figure 7.28: Momentum dependence of the relativistic Maxwellian distribution function at $\rho \simeq 0.36$, and relation between velocity v and momentum p. The deviation from the main diagonal indicates that above $p = 4$, relativistic effects become important

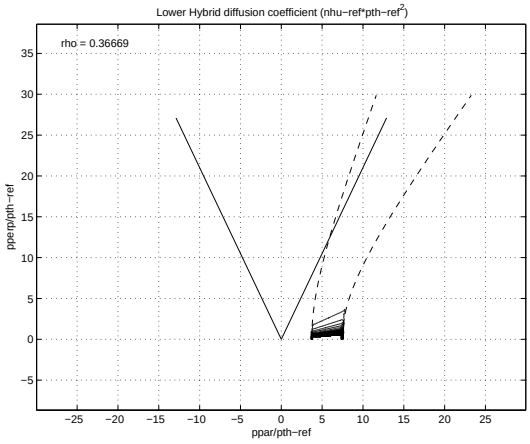

cmcm

Figure 7.29: $2-D$ contour plot in momentum space of the Lower Hybrid quasilinear diffusion cofficient at $\rho \simeq 0.36$. The relativistic curvature of the lower bound of the resonance domain avoid intersection with the region of trapped electrons. The two full straight lines correspond to trapped/passing boundaries at that radial position

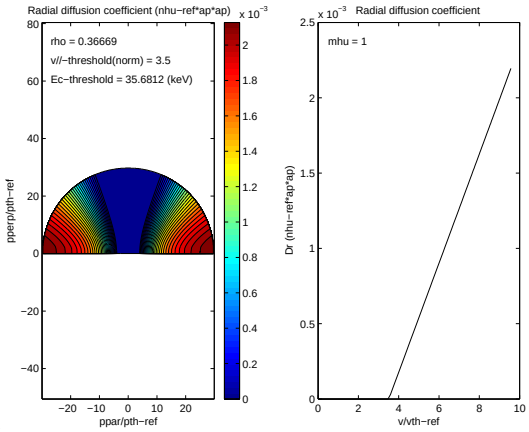

cmcm

Figure 7.30: On the left side, $2-D$ contour plot of the radial diffusion rate at $\rho \simeq 0.36$. The velocity threshold corresponds to a kinetic energy of 35 keV approximately in the $MKSA$ units. On the right side, the velocity dependence of $D_{\psi}^{(0)}$ at $\xi_0 = 1$

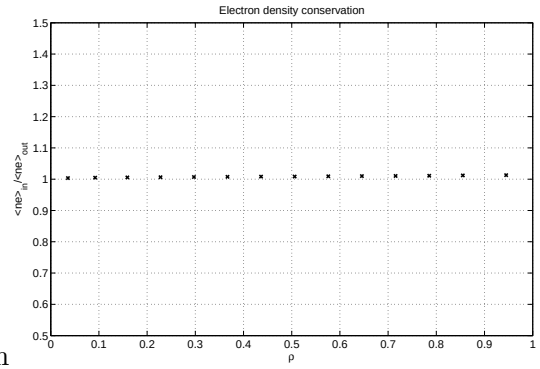

cmcm

Figure 7.31: Relative particle conservation of the drift kinetic code for the $3-D$ JET Lower Hybrid current drive simulation

an order of magnitude more. This limitation results from the fact that loops have been used in MatLab as a consequence of the complexity of the coefficients arrangement in the matrix related to the change of the trapped/passing boundary with radial position. In that case, a specific MEX-file written in C or FORTRAN should considerably reduce time consumption, at a level comparable to the one needed for calculating the coefficients which result from momentum dynamics.

In the case of full $3-D$ calculation, the Maxwellian solution is imposed at $i = 1/2$. Though this condition is not necessary in principle, it turns out to increase matrix conditionning, and reduce significantly the memory required to store LU matrices. However, no normalization of the density at each time step is performed. Consequently, the drop tolerance for incomplete LU matrix factorization may be increased from 10^{-4} to 10^{-3} as compared to the case without radial transport, a important advantage since it reduces considerably computer time consumption for performing the incomplete factorization[6]. On a Compaq workstation, the characteristic time used for this calculation is around $1500s$, and the memory required to store LU matrices is $214MBytes$ in the example here studied.

Once LU matrices are calculated, the convergence is very fast. it is achieved after 6 iterations, corresponding to the minimum value required for a correct convergence with the explicit momentum conservation term (first Legendre truncated term) as discussed in Sec.6.2.2. As shown in Fig.7.31, the code is fully conservative, within less than 1%.

While the absorbed RF power density profile given in Fig.7.32 shows a localized peak around $\rho = 0.5$, the current density profile is much broader, as indicated in Fig.7.33. In the direction of the plasma center, the broadening effect is weak, since collisional slowing down prevails over radial transport when density is high. Towards plasma edge, the effect of radial transport is much more visible, and for $\rho \geq 0.6$, all the fast electrons are driven by this mechanism instead of direct kinetic resonance. The effect of plasma magnetic equibrium on radial transport is fully considered in the calculations.

[6]It is interesting to note that the presence of a radial transport contributes also to use larger drop tolerance parameter, by smoothing out the momentum dynamics. It acts like a regularization process which increases the matrix conditionning.

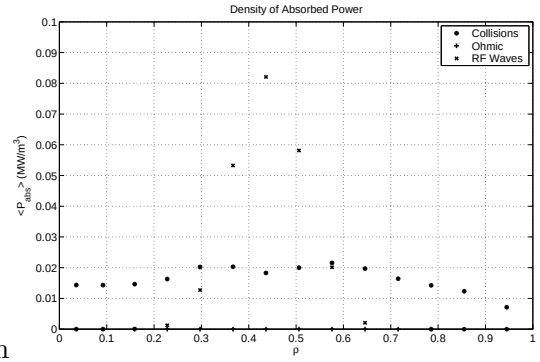

cmcm

Figure 7.32: Flux surface averaged power density profiles for collision, RF and Ohmic electric field absorption for the $3-D$ JET Lower Hybrid current drive simulation.

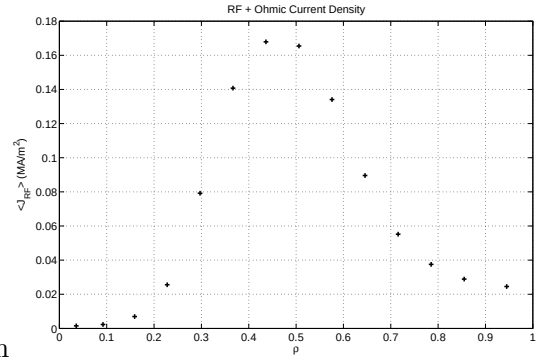

cmcm

Figure 7.33: Flux surface averaged current density profiles for the $3-D$ JET Lower Hybrid current drive simulation.

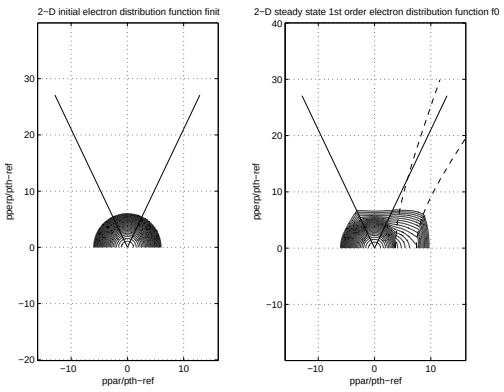

cmcm

Figure 7.34: $2-D$ contour plot of the electron distribution function at $\rho \simeq 0.36$ for JET Lower Hybrid current drive

Comparison between distributions at radial positions where RF absorption peaks (Figs.7.34 and 7.35) and in the region where radial transport predominates (Figs.7.36 and 7.37) clearly shows the difference of dynamics in momentum space. While a plateau is clearly formed at $\rho \simeq 0.36$, the distribution exibits a bump at $\rho \simeq 0.78$. There are nevertheless some reminiscence of the Lower Hybrid quasilinear resonance boundaries. In all figures, the output of the code is clean from numerical instabilities, even far from the resonance domain, which confirms the robustness of the numerical scheme here employed for $3-D$ calculations.

Finally, it is important to mention that the power density absorbed by collisions is much broader than the RF contribution, as shown in Fig. 7.32. Since radial fast electron transport makes the current response non-local, in that case the current drive efficiency may be only defined as the ratio of the total current driven by the wave and the total RF absorbed power in the plasma.

7.6 Fast electron magnetic ripple losses

This simulation is here again presented to illustrate code capabilities for a realistic magnetic configuration and a hot plasma. The problem addressed corresponds to fast electron losses in magnetic ripple, between two consecutive toroidal magnetic field coils. The case studied correponds only for the Tore Supra tokamak, which exhibits a very large magnetic ripple on the outer plasma edge, of the order of 7% [7]. Though the description of the physical process is not fully consistent with the basic assumptions of the code, and the bounce-averaged theory especially, calculations are expected to give valuable informations of the loss rate profile.

Simulations parameters are exactly those used in Sec.7.5 for fast electron transport studies, except that the magnetic configuration corresponds to the tokamak Tore Supra which has a circular plasma cross-section, and that fast electron radial transport is here neglected. Moreover, the magnetic ripple losses are modelized by a characteristic loss

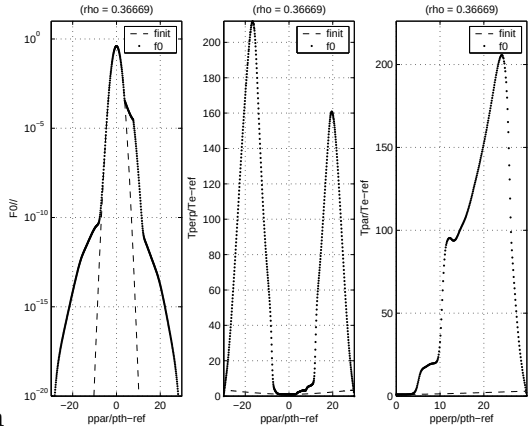

cmcm

Figure 7.35: Electron distribution function averaged over the perpendicular momentum direction at $\rho \simeq 0.36$ for JET Lower Hybrid current drive. The perpendicular and parallel temperatures are also shown

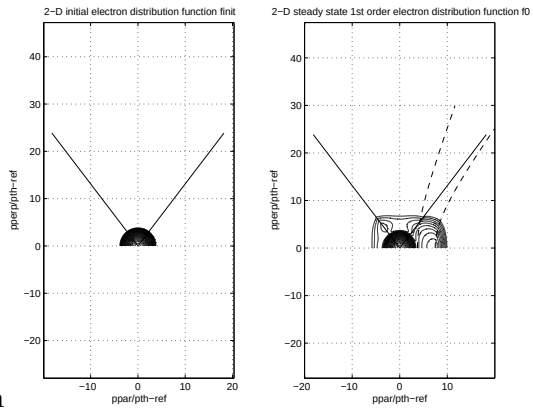

cmcm

Figure 7.36: $2-D$ contour plot of the electron distribution function at $\rho \simeq 0.78$ for JET Lower Hybrid current drive

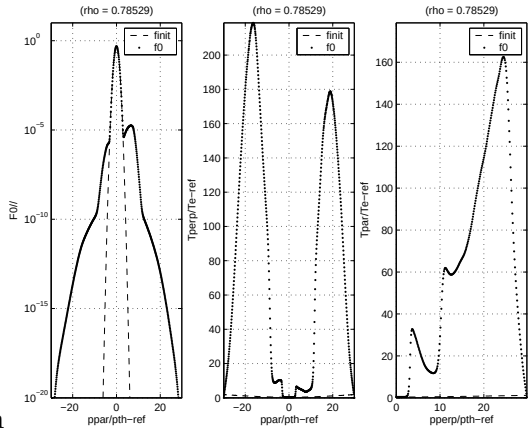

cmcm

Figure 7.37: Electron distribution function averaged over the perpendicular momentum direction at $\rho \simeq 0.78$ for JET Lower Hybrid current drive. The perpendicular and parallel temperatures are also shown

(drift) time $\nu_{d_{ST}}^{-1} = 1000$ inside the supertrapped domain bounded by $|\xi_0| \leq \xi_{0ST}$ and $p \gtrsim p_c$ as discussed in Sec.3.6.

Temperature and density profiles used as input for the magnetic equilibrium calculations done by HELENA code are presented in Fig. 7.38. As usual in current drive regime at low density, the electron temperature profile is peaked, and its value is much larger than ion temperature. The dominant ion (deuterium) profile is determined selfconsistently from the electron density and effective charge profiles, the latter being taken flat at a level of $Z_{eff} = 1.5$. In the calculations which are based on electroneutrality, only one fully stripped impurity is considered, i.e. carbon $Z_s = 6$, in order to avoid the use of an impurity transport code. The resulting $2 - D$ contour plot of the magnetic poloidal flux surfaces is given in Fig. 7.39, where the Shafranov shift is clearly visible. Here, calculations are performed for a monotonic safety factor profile, like for the JET case discussed in the previous section.

In order to be concerned by more energetic electrons in this simulation, the Lower Hybrid quasilinear resonance domain is slightly at higher energy, i.e. $(v_1 = 4, v_2 = 7)$, with the same radial profile dependence of $\overline{D}_{0,new}^{LH}(\psi, p)$ as discussed in Sec. 7.5. The RF power absorption takes place close to $\rho \simeq 0.4$ as shown in Fig.7.40. In this case, the current density and RF power absorption profiles are aligned, since the physics is basically local (slowing-down).

As shown in Fig. 7.41, the fact electron loss rate exhibits a clear peak at $\rho \simeq 0.7$, as observed experimentaly. The $3 - D$ calculations reproduce therefore correctly the profiles given by previous studies with a $2 - D$ Fokker-Planck code [7]. In addition, the two methods used to evaluate the magnetic ripple loss rate profile, as discussed in Sec.3.6 gives very similar quantitative results, that makes the code very reliable concerning this problem.

The detailed dynamics in momentum space is given by the $2 - D$ contour plot. As

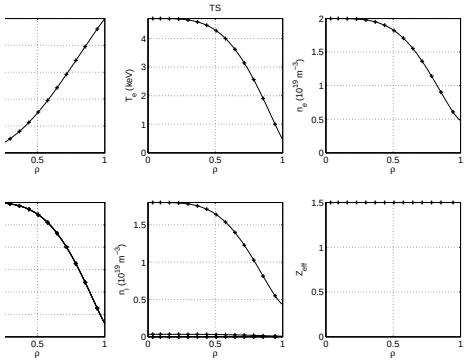

cmcm

Figure 7.38: Ion and electron temperature and density profiles, and effective charge profile used for calculating the Tore Supra magnetic equilibrium with HELENA. Here hydrogen and tritium densities are zero (pure deuterium plasma) . The poloidal flux coordinate ψ as function of the normalized radius ρ in the equatorial mid-plane corresponds to the magnetic equilibrium code output

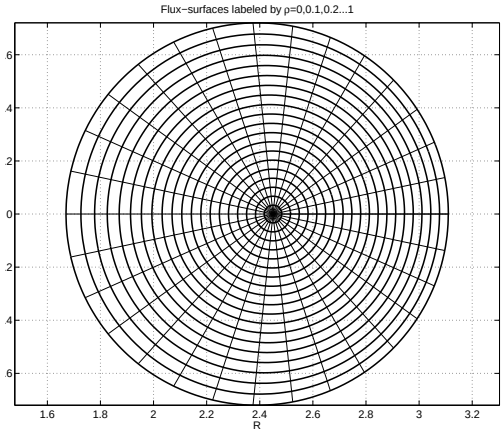

cmcm

Figure 7.39: $2-D$ contour plot of the poloidal magnetic flux surfaces as calculated for Tore Supra tokamak by the code HELENA

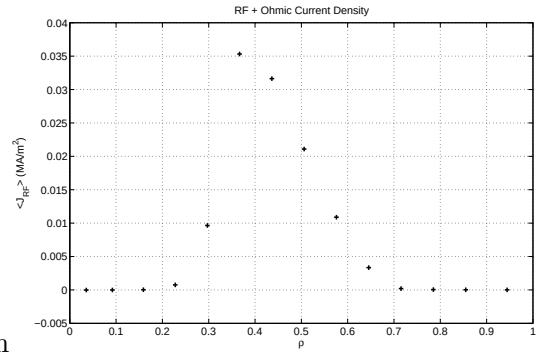

cmcm

Figure 7.40: Flux surface averaged current density profiles for the $3-D$ Tore Supra Lower Hybrid current drive simulation.

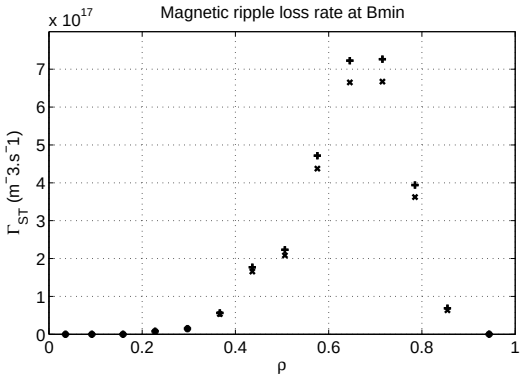

cmcm

Figure 7.41: Magnetic ripple loss rate profile for Tore Supra tokamak in Lower Hybridcurrent drive regime, as calculated by two different methods (see the text for more details)

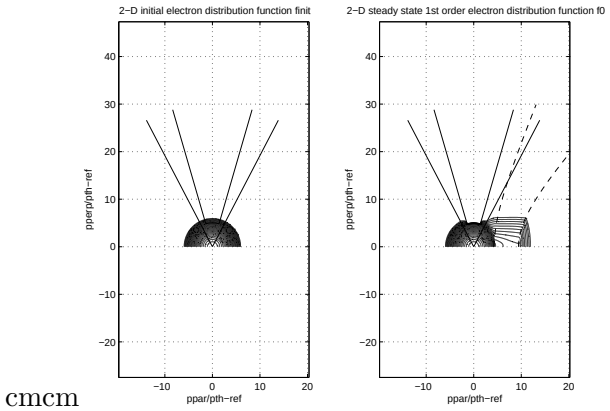

Figure 7.42: $2-D$ contour plot of the electron distribution function at $\rho \simeq 0.44$ for Tore Supra Lower Hybrid current drive

shown in Fig.7.42 at the radial position $\rho \simeq 0.44$, the supertrapped domain defined by $|\xi_0| \leq \xi_{0ST}$ in which electrons are considered as lost lies well inside the domain where electrons are trapped $|\xi_0| \leq \xi_{0T}$. The collisional detrapping threshold is approximately $p_c = 5$ at the local density here presented. The effect of the magnetic ripple losses may be clearly seen on the distribution function $f_0^{(0)}$ which drops dramatically above p_c provided $|\xi_0| \leq \xi_{0ST}$. It is important to show that outside from this domain, the electron distribution function is nearly similar to the one without magnetic ripple losses. This is particularly clear in Fig.7.43. This confirms that losses are very small, and this is the reason why the code remains globally conservative at each radial location.

7.7 Maxwellian bootstrap current

The $3-D$ relativistic and bounce-averaged electron drift kinetic solver allows kinetic calculations of the bootstrap current for arbitrary tokamak magnetic configuration and in principle any type of electron velocity distribution function. Consequently, it offers for the first time the possibility to evaluate accurately potential synergistic effects due to external perturbations like application of RF waves. Indeed, so far, in all current drive simulations, the bootstrap current due to plasma pressure gradient is determined in the Maxwellian limit, while plasma may be locally far from the thermal regime during non inductive current drive. With this code, a self-consistent description of all current sources may be performed.

At this stage, this section is only given to demonstrate code performances in simple limits, like using the simplified Lorentz model, or for a Maxwellian plasma. Indeed, since there is no possibility to perform any benchmark in presence of RF current drive, this problem is not addressed here.

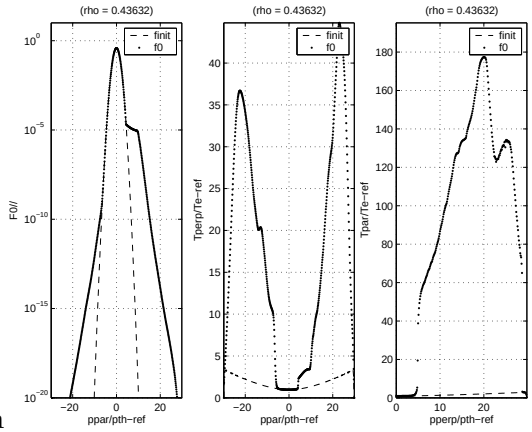

cmcm

Figure 7.43: Electron distribution function averaged over the perpendicular momentum direction at $\rho \simeq 0.44$ for Tore Supra Lower Hybrid current drive. The perpendicular and parallel temperatures are also shown

Lorentz model

As shown in Sec.5.6.2, the Lorentz model applied to thermal plasma represents a unique opportunity for benchmarking the $3-D$ drift kinetic code against simple analytical results. Here, comparisons are presented for a circular magnetic equilibrium, using numerical bounce integrals[7]. As for the electrical conductivity problem addressed in Sec.7.1, the minor radius is set to $a_p = 2.3899m$ and the major one is $R_p = 2.39m$ so that the normalized radius ρ is very close to ϵ value from 0 to 1. Global parameters of the discharge are gathered in section "TEST_LORENTZ" of the tokamak parameter M-file "ptok_dke_1yp.m". In order to simplify calculations, and identify clearly the pitch-angle dynamics that plays a major role in the bootstrap current calculation, all temperatures profiles are taken flat, and consequently the pressure profile arises only from density gradient. Its radial dependence is

$$n_e(\rho) = (n_{e0} - n_{ea})\left(1-\rho^2\right)^2 + n_{ea} \tag{7.14}$$

where the central electron density is $n_{e0} = 2 \times 10^{+19} m^{-3}$, and $n_{ea}/n_{e0} = 10^{-3}$. Electron temperature is taken low enough to neglect relativistic corrections, while $T_s/T_e = 10^{-2}$, to simulate that ion background is fully cold. The dominant ion charge is taken $Z_s = 30$, in agreement with basic assumptions of the Lorentz model.

In the simulation, the spatial ψ half-grid, on which the electron distribution function is calculated, is highly non-uniform. Indeed, the effective spatial mesh size where bootstrap current is determined has $n_\psi - 1 = 14$ points, but the distribution function $f_0^{(0)}$ must be evaluated on $14 \times 3 = 42$ values of ψ for spatial gradients calculation by the parabolic interpolation technique discussed in Sec.5.5.1 which requires 2 additional neighboring points. Their distances to an effective point never exceed $\Delta\psi \leq 0.01$. The fact

[7]It has been cross-checked that results are similar when analytical forms of the bounce integrals given throughout the text are used.

that calculations may be easily performed with so close radial points is a good indication of code capabilities for describing bootstrap current in presence of strong pressure gradients. The pitch-angle grid is therefore also strongly non uniform, like in Fig.7.23 for the Lower current drive problem, since trapped/passing boundaries corresponding to all radial positions are exactly placed on the flux grid in momentum space. Despite the number of ψ values is three times larger, the total number of pitch-angle points for $f_0^{(0)}$ may be maintained to $n_{\xi_0} - 1 = 206$, in order to avoid computer memory limitations. The program that generates the pitch-angle grid may optimize automaticaly the shape of the mesh, in order to achieve this goal. Finally, the electron distribution is Maxwellian for this study and the momentum grid is also non-uniform. The number of points is reduced as compared to the Lower Hybrid current drive problem down to $n_p - 1 = 110$ points, so that memory storage requirements may be reduced.

As discussed in Sec.6.2.2, the drop tolerance parameter δ_{lu} for incomplete LU matrix factorization plays a crucial role in the calculations. For very large matrix sizes[8], its value is a trade-off between the time to perform this factorization, the memory required to store the matrices $\widehat{\mathbb{L}}$ and $\widehat{\mathbb{U}}$, and finally the fact that the convergence towards a physical solution may be effectively achieved. Indeed, if δ_{lu} is to large, $\widehat{\mathbb{L}}$ and $\widehat{\mathbb{U}}$ are badly conditionned and no result may be obtained. It turns out that forcing the Maxwellian solution in the vicinity of $p = 0$ strongly contributes to improve matrix conditionning, though it has been tested with a reduced number of radial grid points that the code is naturaly fully conservative and does not require this condition as a major prescription. Hence in the case here discussed, the Maxwellian solution is enforced on the forced 5 first points of the momentum grid from $i = 1/2$ to $i = 11/2$. Consequently, δ_{lu} may be lowered down to 10^{-4}, while time step in maintained to $\Delta\bar{t} = 10000$.

It is important to note that these constraints are not applied to the matrix used for determining the first order corrections. In that case, the matrix size is much lower (by a factor 3), and consequently, no solution is enforced in the vicinity of $p = 0$.

A comparison between results given by the drift kinetic code and well known analytical expressions that may be found in Refs. [33][34][35][36][37][38] is performe. For Maxwellian plasmas circular magnetic flux surfaces, in the low aspect ratio limit $\epsilon \to 0$ and low collisionality limit $\nu^* \to 0$, flux surface-averaged parallel current may be expressed in the general simple form

$$\left\langle J_{\parallel} \right\rangle_{\phi} (\rho) \propto -p_e (\rho) \frac{B_T (\rho)}{B_P (\rho)} \left(L_{31} A_1 + L_{32} A_2 + L_{34} A_4 \right) \tag{7.15}$$

where

$$A_1 = \frac{d \ln p_e}{d\rho} + \frac{T_i (\rho)}{Z_i T_e (\rho)} \frac{d \ln p_e}{d\rho} \tag{7.16}$$

$$A_2 = \frac{d \ln T_e}{d\rho} \tag{7.17}$$

$$A_3 = \alpha_i \frac{T_i (\rho)}{Z_i T_e (\rho)} \frac{d \ln T_i}{d\rho} \tag{7.18}$$

[8]For the case here discussed, the matrix size is of the order of (900000×900000).

p_e being the electron pressure. Neoclassical transport coefficients L_{31}, L_{32} and L_{34} and the parameter α_i depends of the model. For the non-relativistic Lorentz model, with flat temperature gradients, $A_2 = A_3 = 0$, and consequently only the coefficient L_{31} plays a role. Therefore both models [35] and [37] are expected to give equivalent results. Moreover since $Z_i \gg 1$ and $T_i/T_e \ll 1$,

$$A_1 \simeq \frac{d\ln p_e}{d\rho} = \frac{d\ln n_e}{d\rho} \tag{7.19}$$

In the low collisionality limit but for arbitrary inverse aspect ratio between 0 and 1, the expression of L_{31} given by Hirshman [35] may be used

$$\begin{aligned} L_{31} &= x\left[0.754 + 2.21Z_i + Z_i^2 \right. \\ &\quad \left. + x\left(0.348 + 1.243Z_i + Z_i^2\right)\right]/D\left(x\right) \end{aligned} \tag{7.20}$$

where

$$\begin{aligned} D\left(x\right) &= 1.414Z_i + Z_i^2 + x\left(0.754 + 2.657Z_i + 2Z_i^2\right) \\ &\quad + x^2\left(0.348 + 1.243Z_i + Z_i^2\right) \end{aligned} \tag{7.21}$$

and

$$x \simeq \frac{1.46\sqrt{\epsilon} + 2.4\epsilon}{\left(1-\epsilon\right)^{3/2}} \tag{7.22}$$

In the limit $Z_i \gg 1$,

$$\lim_{Z_i \to +\infty} L_{31} = \frac{x}{1+x} \tag{7.23}$$

L_{31} is independent of Z_i. Therefore, the flux-surface averaged bootstrap current scales as

$$\lim_{Z_i \to +\infty} \left\langle J_{\parallel,\mathcal{L}} \right\rangle_\phi \left(\rho\right) \propto -\frac{1.46\sqrt{\epsilon} + 2.4\epsilon}{1.46\sqrt{\epsilon} + 2.4\epsilon + \left(1-\epsilon\right)^{3/2}} n_e\left(\rho\right) T_e \frac{B_T\left(\rho\right)}{B_P\left(\rho\right)} \frac{d\ln n_e}{d\rho} \tag{7.24}$$

with

$$\rho = \epsilon \frac{R_p}{a_p} \tag{7.25}$$

and using the definition $p_e \equiv n_e T_e$. For the case here studied, $R_p \approx a_p$ and consequently $\rho = \epsilon$. With the expression (7.24), the well known limit $\epsilon \ll 1$

$$\lim_{Z_i \to +\infty} \left\langle J_{\parallel,\mathcal{L}} \right\rangle_\phi \left(\rho\right) \propto -1.46\sqrt{\epsilon} n_e\left(\rho\right) T_e \frac{B_T\left(\rho\right)}{B_P\left(\rho\right)} \frac{d\ln n_e}{d\rho} \tag{7.26}$$

is recovered, while

$$\lim_{Z_i \to +\infty} \left\langle J_{\parallel,\mathcal{L}} \right\rangle_\phi \left(\rho\right) \propto -n_e\left(\rho\right) T_e \frac{B_T\left(\rho\right)}{B_P\left(\rho\right)} \frac{d\ln n_e}{d\rho} \tag{7.27}$$

when $\epsilon \to 1$.[9]

[9] It is important toi note that replacing $B_T\left(\rho\right)/B_P\left(\rho\right)$ by q/ϵ leads to strong errors in the bootstrap current profile, especially when $\epsilon \to 1$. In particular, the radial localtion where the bootstrap current peak is significantly shifted outward.

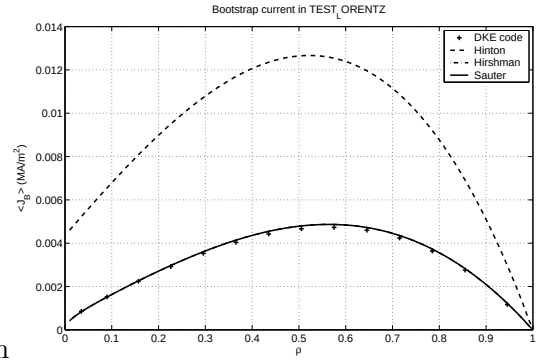

cmcm

Figure 7.44: Bootstrap current profile given in the Lorentz model limit by the drift kinetic code and different analytical formulaes

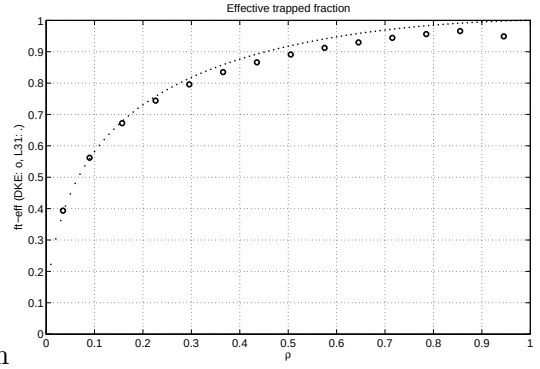

cmcm

Figure 7.45: Effective trapped fraction as given by the by the drift kinetic code in the Lorentz limit and by coefficient L_{31} from analytical expression (see the text for more details)

As shown in Fig.7.44, the agreement between the bootstrap current calculated by the code and determined by the Hirshman or Sauter models is excellent for all ρ values [10]. The model given in Ref. [33] strongly fails, since it corresponds only to the case $Z_i = 1$. A confirmation of the robustness of the code is the very good agreement between numerical caclualtions and analytical expressions of the effective trapped fraction $\mathcal{F}_t^{eff.}(\rho)$ at all plasma radii, as shown in Fig. 7.45, despite the fact that the integral $\int_{-1}^{1} \sigma H\left(|\xi_0| - \xi_{0T}\right) \xi_0 I_{\mathcal{L}}\left(\psi, |\xi_0|\right) d\xi_0$ is fairly difficult to evaluate numerically, since $I_{\mathcal{L}}\left(\psi, |\xi_0|\right)$ is itself an integral, as discussed in Sec. 5.6.2. A small departure is observed for the largest ϵ value, since in that case $\int_{-1}^{1} \sigma H\left(|\xi_0| - \xi_{0T}\right) \xi_0 I_{\mathcal{L}}\left(\psi, |\xi_0|\right) d\xi_0 \simeq 0$, and its numerical evaluation may have a large error on the chosen numerical grid.

The exact trapped fraction $\mathcal{F}_t$ calculated by the code is increasing smoothly from 0 to 1 with a radial dependence that is very different from $\mathcal{F}_t^{eff.}(\rho)$ which should scale

[10] Both models use the same parameter L_{31} in this limit.

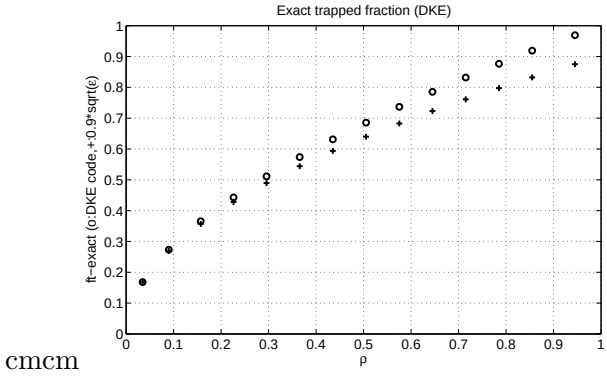

cmcm

Figure 7.46: Exact trapped fraction as given by the by the drift kinetic code in the Lorentz limit and by analytical expression (see the text for more details)

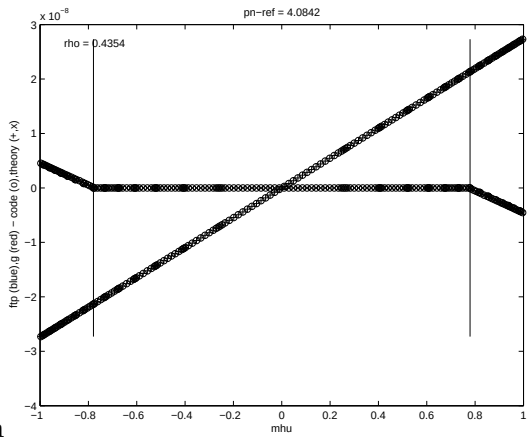

cmcm

Figure 7.47: Pitch-angle dependence of $\widetilde{f}^{(0)}$ and $g^{(0)}$ at $\rho \simeq 0.4354$, as given by the drift kinetic code and analytical expressions, for the Lorentz model limit

as L_{31} in the simulation here studied. At the lowest $\epsilon \approx 0.034$ value determined by the code, the ratio $\mathcal{F}_t^{eff.}(\rho)/\mathcal{F}_t \approx 2$ is larger than the expected value $1.46/0.9 \approx 1.62$, which indicates that the well known limit value $\mathcal{F}_t^{eff.}(\rho) \simeq 1.46\sqrt{\epsilon}$ is only only valid for very small inverse aspect ratio ϵ. Indeed, $\mathcal{F}_t$ is very well reproduced by the asymptotic expression $\mathcal{F}_t(\rho) \simeq 0.9\sqrt{\epsilon}$ quite far from the limit $\epsilon \ll 1$, as presented in Fig.7.46. There is also very good confidence in the simulation results since $\mathcal{F}_t^{eff.}(\rho) \simeq L_{31}$ is well verified numericaly, as expected from Hirshman theory.

At $\rho \simeq \epsilon \leq 0.4354$, and for $p = 4.08$, the agreement for $\widetilde{f}^{(0)}$ and $g^{(0)}$ is excellent for all ξ_0 values, as seen in Fig 7.47. The difference is so small between the code and the analytical expressions given in Sec. 5.6.2, that it cannot be identify on the figure.

This excellent agreement is confirmed for first order distribution $F_{\|0}^{(1)}$ averaged over

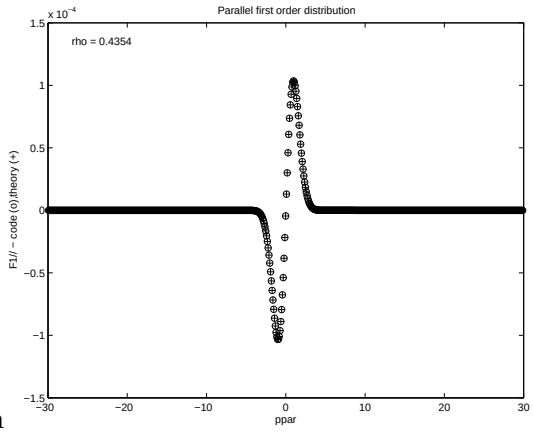

cmcm

Figure 7.48: First order distribution $F_{\|0}^{(1)}$ averaged over the perpendicular momentum direction $p_\perp$ as fonction of $p_\|$ at $\rho \simeq 0.4354$, as given by the drift kinetic code and analytical expressions, for the Lorentz model limit

the perpendicular momentum direction $p_\perp$

$$F_{\|0}^{(1)}\left(p_\|\right) = 2\pi \int_0^\infty \left(\widetilde{f}^{(0)} + g^{(0)}\right) p_\perp dp_\perp \tag{7.28}$$

as shown in Fig. 7.48.

In Figs. 7.49 and 7.50, the 2-D contour plot of $\widetilde{f}^{(0)}$ and $g^{(0)}$ are represented. As expected for a Maxwellian distribution function, $g^{(0)} = 0$ in the trapped region while $\widetilde{f}^{(0)}$ is clearly antisymmetric.

The overall results confirm that the drift kinetic solver gives the correct dependences and level of the first order neoclaissicla corrections. The robustness of the code is remarkable, since no specific boundary conditions have to be imposed at the limits of the domain to ensure the determination of the correct solution.

Full simulation

The Maxwellian bootstrap current for a realistic tokamak magnetic configuration has been calculated. Here the Tore Supra tokamak is studied, with numerical parameters that are similar to the case of the discussed in the previous section, while physical parameters, in particular pressure profiles, are those taken for magnetic ripple losses studies (see Sec. 7.6). The full first order Legendre collision term for momentum conservation is now considered, which is crucial to estimate the right current level.

As shown in Fig. 7.51, an excellent agreement with both Hirschman and Sauter models given in Refs. [35] and [37] is found at plasma radii. In that case the maximum inverse aspect ratio reaches approximately 0.3. The Hinton model fails also, since an effective charge $Z_{eff} = 1.5$ is considered, the major light impurity being fully strip carbon.

The exact $\mathcal{F}_t(\psi)$ and effective $\mathcal{F}_t^{eff.}(\psi)$ trapped fraction are given respectively in Figs. 7.52 and 7.53. In that case, the exact trapped fraction reaches $\mathcal{F}_t(\psi) \simeq 0.5$ at the edge,

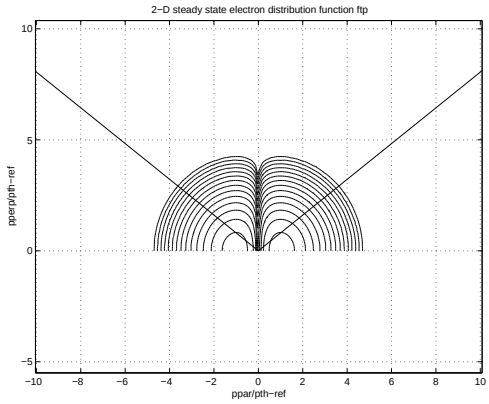

cmcm

Figure 7.49: Contour plot of $\widetilde{f}^{(0)}$ at $\rho \simeq 0.4354$, as given by the drift kinetic code for the Lorentz model limit

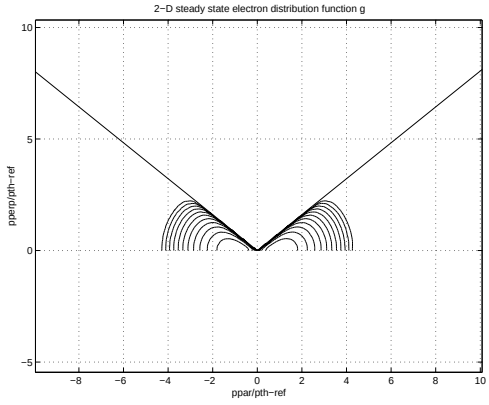

cmcm

Figure 7.50: Contour plot of $g^{(0)}$ at $\rho \simeq 0.4354$, as given by the drift kinetic code for the Lorentz model limit

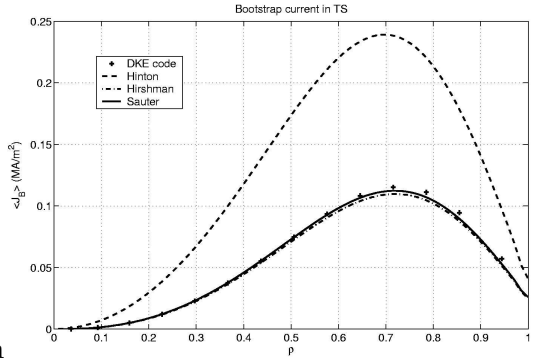

cmcm

Figure 7.51: Bootstrap current profile given by the drift kinetic code for the Tore Supra magnetic configuration and different corresponding analytical formulas (see the text for more details)

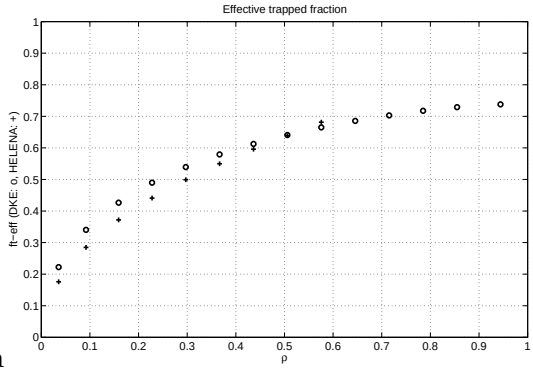

cmcm

Figure 7.52: Effective trapped fraction as given by the by the drift kinetic code and the HELENA magnetic equilbrium code for the tokamak Tore Supra

while the effective one $\mathcal{F}_t^{eff.}(\psi) \simeq 0.7$. This difference may be easily understood, since in the calculation of the effective trapped fraction, the time spend on the banana orbit is considered, while it is not for the exact trapped fraction.

For the exact trapped fraction, the level at the limit $\epsilon \ll 1$ is very consistent with the analytical expression given in Sec.3.6. A very good agreement is also found for $\mathcal{F}_t^{eff.}(\psi)$ given by the HELENA equlibrium code using the analytical formula (see also Sec.3.6).

As for the case of the Lorentz model, the pitch-angle dependence at $\rho = 0.435$ and for $p = 4.08$ of first order distribution functions $\widetilde{f}^{(0)}$ and $g^{(0)}$ is given as function of ξ_0. Similar dependences are observed in Fig 7.54 as well as for the first order distribution $F_{\|0}^{(1)}$ averaged over the perpendicular momentum direction $p_\perp$ shown in Fig. 7.55

In Figs. 7.56 and 7.57, the 2-D contour plot of $\widetilde{f}^{(0)}$ and $g^{(0)}$ are represented. As expected for a Maxwellian distribution function, $g^{(0)} = 0$ in the trapped region while $\widetilde{f}^{(0)}$ is clearly antisymmetric.

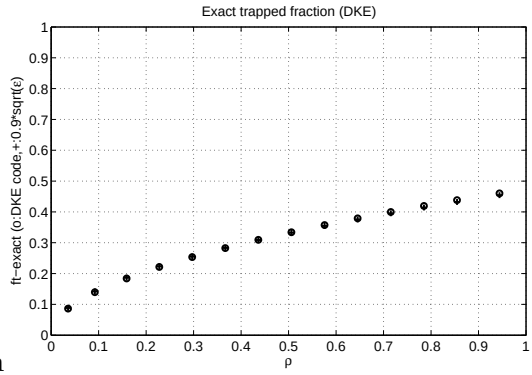

cmcm

Figure 7.53: Exact trapped fraction as given by the by the drift kinetic code for the tokamak Tore Supra

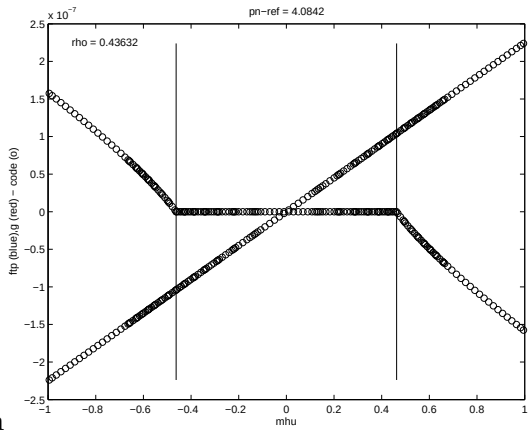

cmcm

Figure 7.54: Pitch-angle dependence of $\widetilde{f}^{(0)}$ and $g^{(0)}$ at $\rho \simeq 0.4354$, as given by the drift kinetic code for the tokamak Tore Supra

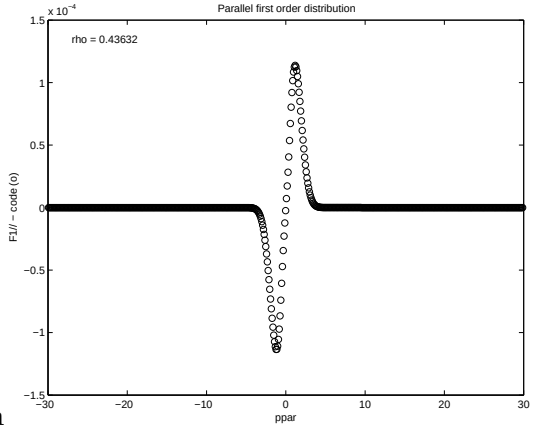

cmcm

Figure 7.55: First order distribution $F_{\|0}^{(1)}$ averaged over the perpendicular momentum direction $p_\perp$ as fonction of $p_\|$ at $\rho \simeq 0.4354$, as given by the drift kinetic code for the tokamak Tore Supra

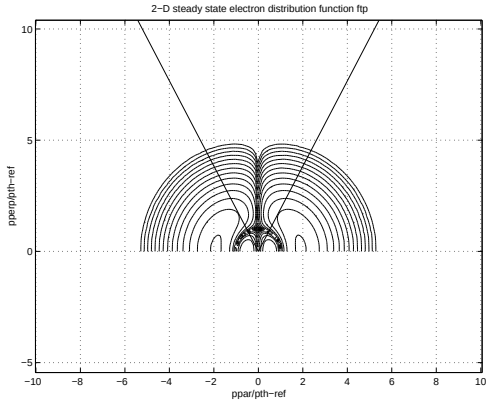

cmcm

Figure 7.56: Contour plot of $\widetilde{f}^{(0)}$ at $\rho \simeq 0.4354$, as given by the drift kinetic code for the tokamak Tore Supra

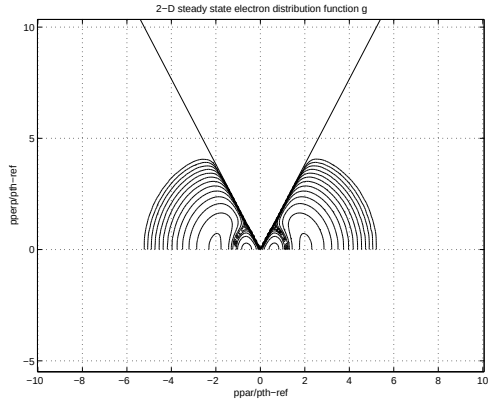

cmcm

Figure 7.57: Contour plot of $g^{(0)}$ at $\rho \simeq 0.4354$, as given by the drift kinetic code for the tokamak Tore Supra

These results illustrate that the drift kientic code is able to determine accurately the boostrap current level. For the ion contribution, the expression given in the fluid limit as given in Ref. [35] is taken. This is the same value taken in Ref. [37], only the coefficent L_{32} being different. However, for this case, results are very similar, though the drift kinetic code results seem more closer to the one given by the Sauter formula [37][38].

Chapter 8

Conclusion

The determination of the current density profile is a crucial issue for next step tokamaks like ITER, since it may directly modify plasma performances. Up to now, most of the tools where designed for simplified magnetic configuration, or using crude physical assumptions that consequently reduce considerably the confidence in the results. Accurate and realistic kinetic calculations for the electron population in magnetized plasmas where therefore an important step towards a consistent modeling of the current drive process.

For this purpose, a completely new numerical solver has been designed which contains most of the salient features of the physics in hot plasmas, where the weak collision regime holds: relativistic collision operator, bounce-averaging for trapped and passing particles, arbitrary magnetic configuration, first order neoclassical corrections. A special attention has been paid to derive in a rigorous and consistent manner all the equations, in particular for the interplay between inductive, non-inductive and bootstrap currents. The conservative nature of the equations has been the guideline in this work, especially to have a clear derivation of radial transport equation for the fast electron population in arbitrary magnetic configuration when bounce averaging is concerned.

The numerical part has been derived with the same spirit, keeping a systematic approach for all types of operators in the discretization technique. This point is especially important for a consistent evaluation of the current drive efficiency, a key parameter in order to evaluate performances of the method used for driving current. In particular, the formalism is general so that arbitrary type of mechanismes may be incorporated for possible synergistic effect. As for the analytical part, a detail analysis of the conservative nature of the numerical code has been performed. A clear and comprehensive discussion of all the aspects is presented, which is crucial for a reliable numerical tool. It is shown that the both for the zero- and first-order equations, the numerical solver is naturally conservative, in the sense that no need of arbitrary external source or normalization factor is necessary in order to compensate possible hidden numerical particle leaks which are the consequence of an incorrect discrete projection of the equations on the numerical grids. This reference work is critical in order to make the code transparent for possible further evolutions.

Advanced numerical matrix factorization techniques have shown that considerable savings may be expected, not only for storage purposes but also for the time duration needed in determining the steady-state current drive solution on the collision and fast electron

transport time scales. The pionneering work performed initially for the $2-D$ problem in velocity space in a fully implicit manner (reverse time scheme that is inconditionnaly stable with respect to the integration time step)([25],[17] and [9]) has been fully extended to the $3-D$ case ([39]), including the complexity arising from the radial dependence of the trapped-passing boundary for bounce-averaged equations. With the incomplete LU technique ([10]), it has been possible to converge in few iterations towards the steady-state current drive solution on standard computers, taking advantage of the high sparcity of the Fokker-Planck and electron drift kinetic equation matrices. This tool is therefore fully designed to be incorporated in a chain of codes, for realistic self-consistent calculations, in which plasma magnetic equilibrium, wave propagation and absorption, energy and particle transport must be evaluating as a function of time and space ([2]). In is important to notice that special attention has been paid to the delicate problem of coupling the kinetic solver with ray-tracing. This amazing feat has been made easily possible with the use of the compact MatLab numerical environment for solving the huge linear system of equations ([40]).

Furthermore, numerous moments of the electron distribution function are evaluated like the RF power, magnetic ripple and runaway losses, fast electron bremsstrahlung and trapped fraction. Moreover, the code may also be used for specific physical studies which imply time evolution, and a standard Crank-Nicholson time-scheme has been also incorporated. In the same spirit, simplified collision models may be used, like the Lorentz operator, for which analytical expressions may be easily derived. This point is crucial for an effective benchmarking, even in a complex magnetic topology, like for ITER.

At this stage, the code may be considered as mature for the initial goal that was considered. Several additional benchmarking must be certainly done in order to enhance the realibility on several quantities, but most of the resultats obtained by the code are already robust. The domain of stabitility related to the drop tolerance parameter for the approximate matrix factorization technique needs also refined estimates for optimizing the numerical method.

Several enhancement of the code may be easily foreseen in a near future. In the framework, one of the most important issue is to use a correct quasilinear diffusion operator for the wave-particle interaction. Indeed, like for most kinetic solvers available today, the code use the well known Kennel-Engelman-Lerche expression that is derived for plane waves in homogenous plasmas. Regarding the assumptions, it is necessary to use a more precise quasilinear diffusion operator that is decuded from the Hamiltonian theory in toroidal configuration ([41]). This requires further analytical developments, using the appropriate coordinate system, where the effective banana width of the particle is fully taken into account. In this framework, the description of the wave-induced particle transport becomes natural, and the code in its present conservative form fully allows this kind of description that may play a fundamental role for the RF power absorption, but also for thermal particle pinch in steady-state conditions ([42]). Furthermore, once the bounce-averaging is replaced by trajectory-averaging, it is natural to extend the code for multiple ion dynamics. In that case, parallel processing may be foreseen for each species, in order to optimize calculations.

Finally, an ultimate though important evolution for the code may concern non-linear problems. So far, the collision operator is linearized for a Maxwellian bulk, that is a

reasonable assumption in most tokamak conditions today. However, some experimental evidences that the bulk could be non-Maxwellian in presence of strong electron cyclotron heating and current drive suggest that non-linear effects could take place. This may be also the case in reactor conditions when α-particle population is damping on the electrons. In that case, the neoclassical theory for non-Maxwellian distribution must be previously revisited before any numerical implementation.

Besides the development of modern tools that is effectively described in this document and will be useful for a detailed understanding of the current drive in tokamak, this work has allowed to highlight the subtile interplay between physics and numerics. This is an good example of what should be performed for advanced realistic simulations of complex dynamical systems. It enables to draw in a very clear manner paths for refined studies, based on robust formalisms that takes into account in a rigorous way the physics principles. The method here presented has therefore broad potential applications for other challenging physics domains, like for the numerical determination of the full-wave problem when very short wavelengths must be considered as compared to the machine size and the gradient lengths.

Chapter 9

Acknowledgements

The authors are particularly grateful to Pr. A. Bers (MIT/USA) for having motivated the present work, by pointing out the interest in calculating selfconsistently the RF current drive with the bootstrap current in high-β_p plasmas, for arbitrary type of waves. His constant support during this works is warmely acknowledged. The authors are also grateful to Pr. A. Ram (MIT/USA) for interesting suggestions concerning this work, Dr. R. W. Harvey (CompX, USA) for his interest concerning the design of the fully implicit $3-D$ bounce-averaged Fokker-Planck solver as a part of the kinetic calculation tool, and especially fast electron transport physics.

They would like also to acknowledge Dr. L. -G. Eriksson (CEA/France) for enlightening discussions on fundamental aspects of the kinetic physics in tokamaks, Dr. G. Huysmans (CEA/France) for providing his kind help concerning informations on magnetic equilibrium code reconstruction HELENA, Dr. V. Basiuk for a continuous support concerning some interface aspects in the development of the kinetic code, and Dr. R. Dumont for fruitful discussions.

One of the author (Y.P.) would like to express his thanks for Dr. M. Shoucri (Hydro-Québec, Canada) and Dr. I. P. Shkarofsky (Canada) who both started in the pionneering work on fast relativistic Fokker-Planck calculations, ten years ago. The present results are based on a similar approach which extends this type of calculation tool for realistic applications in reactor relevant fusion devices like ITER.

Appendix A

Curvilinear Coordinate Systems

In the following, we note $\mathbf{X} = (x, y, z)$ the vector position in the space under consideration. In general, vectors are written in bold characters, except unit vectors, noted with a hat. We consider the following curvilinear coordinate systems

A.1 General Case (u^1, u^2, u^3)

We consider the curvilinear coordinate system (u^1, u^2, u^3).

A.1.1 Vector Algebra

Covariant (Tangent) Basis

The covariant, or tangent vector basis $(\mathbf{e}_1, \mathbf{e}_2, \mathbf{e}_3)$is defined as

$$\mathbf{e}_i = \frac{\partial \mathbf{X}}{\partial u^i} \tag{A.1}$$

where the $\mathbf{e}_i$ are tangent to the curvilinear lines. They can be normalized by

$$\widehat{e}_i = \frac{\mathbf{e}_i}{h_i} \tag{A.2}$$

where we introduce the scale factors

$$h_i = \left| \frac{\partial \mathbf{X}}{\partial u^i} \right| \tag{A.3}$$

Contravariant (reciprocal) Basis

The gradient ∇f of a function f being defined by the differential

$$df = \nabla f \cdot d\mathbf{X} \tag{A.4}$$

we apply to u^i which gives

$$du^i = \nabla u^i \cdot d\mathbf{X} \tag{A.5}$$

By chain rule, we have

$$d\mathbf{X} = \frac{\partial \mathbf{X}}{\partial u^j} du^j = \mathbf{e}_j du^j \tag{A.6}$$

so that

$$du^i = \nabla u^i \cdot \mathbf{e}_j du^j \tag{A.7}$$

which implies

$$\nabla u^i \cdot \mathbf{e}_j = \delta^i_j \tag{A.8}$$

thus defining two reciprocal basis $\left(\nabla u^i, \mathbf{e}_j\right)$ of vectors. The reciprocal basis vectors are also called contravariant, and noted

$$\mathbf{e}^i \equiv \nabla u^i \tag{A.9}$$

These vectors are perpendicular to the surfaces of constant u^i.

From the properties of reciprocal basis, we can calculate a vector from the three vectors of the reciprocal basis, such that

$$\mathbf{e}^i = \nabla u^i = \frac{\mathbf{e}_j \times \mathbf{e}_k}{\mathbf{e}_i \cdot \mathbf{e}_j \times \mathbf{e}_k} \tag{A.10}$$

$$\mathbf{e}_i = \frac{\partial \mathbf{X}}{\partial u^i} = \frac{\mathbf{e}^j \times \mathbf{e}^k}{\mathbf{e}^i \cdot \mathbf{e}^j \times \mathbf{e}^k} \tag{A.11}$$

Metric Coefficients

They are defined as

$$\begin{aligned} g_{ij} &= \mathbf{e}_i \cdot \mathbf{e}_j \\ g^{ij} &= \mathbf{e}^i \cdot \mathbf{e}^j \end{aligned} \tag{A.12}$$

With the differential vector given in (A.6), we show that the differential arc length along a curve is

$$dl = |d\mathbf{X}| = \sqrt{d\mathbf{X} \cdot d\mathbf{X}} = \sqrt{g_{ij} du^i du^j} \tag{A.13}$$

In addition, we have the relations

$$\begin{aligned} \mathbf{e}_i &= g_{ij} \mathbf{e}^j \\ \mathbf{e}^i &= g^{ij} \mathbf{e}_j \end{aligned} \tag{A.14}$$

We also show that

$$\left[g_{ij}\right] = \left[g^{ij}\right]^{-1} \tag{A.15}$$

$$\left[g^{ij}\right] = \left[g_{ij}\right]^{-1} \tag{A.16}$$

so that, defining

$$g = \det\left[g_{ij}\right] \tag{A.17}$$

we find

$$g^{-1} = \det\left[g^{ij}\right] \tag{A.18}$$

Jacobian

We define the Jacobian

$$J \equiv \frac{\partial(x,y,z)}{\partial(u^1,u^2,u^3)} = \det \begin{pmatrix} \partial x/\partial u^1 & \partial x/\partial u^2 & \partial x/\partial u^3 \\ \partial y/\partial u^1 & \partial y/\partial u^2 & \partial y/\partial u^3 \\ \partial z/\partial u^1 & \partial z/\partial u^2 & \partial z/\partial u^3 \end{pmatrix} \tag{A.19}$$

which gives

$$J = \frac{\partial \mathbf{X}}{\partial u^1} \cdot \frac{\partial \mathbf{X}}{\partial u^2} \times \frac{\partial \mathbf{X}}{\partial u^3} = \mathbf{e}_1 \cdot \mathbf{e}_2 \times \mathbf{e}_3 \tag{A.20}$$

and the reciprocal Jacobian

$$\mathcal{J} \equiv \frac{\partial(u^1,u^2,u^3)}{\partial(x,y,z)} = \det \begin{pmatrix} \partial u^1/\partial x & \partial u^1/\partial y & \partial u^1/\partial z \\ \partial u^2/\partial x & \partial u^2/\partial y & \partial u^2/\partial z \\ \partial u^3/\partial x & \partial u^3/\partial y & \partial u^3/\partial z \end{pmatrix} \tag{A.21}$$

which gives

$$\mathcal{J} = \nabla u^1 \cdot \nabla u^2 \times \nabla u^3 = \mathbf{e}^1 \cdot \mathbf{e}^2 \times \mathbf{e}^3 \tag{A.22}$$

We can show that

$$\mathcal{J} = J^{-1} \tag{A.23}$$

and the relations (A.10-A.11) become

$$\mathbf{e}^i = \frac{1}{J}\left(\mathbf{e}_j \times \mathbf{e}_k\right) \tag{A.24}$$

$$\mathbf{e}_i = J\left(\mathbf{e}^j \times \mathbf{e}^k\right) \tag{A.25}$$

Also,

$$g = J^2 \tag{A.26}$$

Vector Identities

With

$$\mathbf{A} = \left(\mathbf{A} \cdot \mathbf{e}_i\right)\mathbf{e}^i = A_i \mathbf{e}^i \tag{A.27}$$

$$\mathbf{A} = \left(\mathbf{A} \cdot \mathbf{e}^i\right)\mathbf{e}_i = A^i \mathbf{e}_i \tag{A.28}$$

we find

$$\mathbf{A} \cdot \mathbf{B} = g_{ij} A^i B^j = g^{ij} A_i B_j \tag{A.29}$$

so that

$$A = |\mathbf{A}| = \sqrt{g_{ij} A^i A^j} = \sqrt{g^{ij} A_i A_j} \tag{A.30}$$

We also find

$$\mathbf{A} \times \mathbf{B} = A^i B^j \mathbf{e}_i \times \mathbf{e}_j = A_i B_j \mathbf{e}^i \times \mathbf{e}^j \tag{A.31}$$

which gives

$$\left(\mathbf{A} \times \mathbf{B}\right)_k = \varepsilon_{ijk} J A^i B^j = \frac{\varepsilon^{ijk}}{J} A_i B_j \tag{A.32}$$

Note that from (A.14),

$$A_i = g_{ij} A^j \tag{A.33}$$

$$A^i = g^{ij} A_j \tag{A.34}$$

Differential elements

differential length along u^i

$$dl\,(i) = |d\mathbf{X}\,(i)| = h_i du^i = \sqrt{g_{ii}} du^i \tag{A.35}$$

Equivalently,

$$dl\,(i) = J \left| \nabla u^j \times \nabla u^k \right| du^i \tag{A.36}$$

differential area in surface of constant u^i Using

$$dS\,(i) = |d\mathbf{X}\,(j) \times d\mathbf{X}\,(k)| = |\mathbf{e}_j \times \mathbf{e}_k|\, du^j du^k \tag{A.37}$$

which becomes

$$dS\,(i) = \sqrt{g_{jj} g_{kk} - g_{jk}^2} du^j du^k \tag{A.38}$$

Equivalently

$$dS\,(i) = J \left| \nabla u^i \right| du^j du^k \tag{A.39}$$

so that

$$d\mathbf{S}\,(i) = \pm J du^j du^k \nabla u^i \tag{A.40}$$

differential volume element

$$d^3\mathbf{X} = d\mathbf{X}\,(1) \cdot d\mathbf{X}\,(2) \times d\mathbf{X}\,(3) = J du^1 du^2 du^3 \tag{A.41}$$

Vector Differentiation

$$d\mathbf{A} = \frac{\partial \mathbf{A}}{\partial u^k} du^k \tag{A.42}$$

$$\frac{\partial \mathbf{A}}{\partial u^k} = \left(\frac{\partial \mathbf{A}}{\partial u^k} \right)^j \mathbf{e}_j \equiv \mathbf{A}_k^j \mathbf{e}_j \tag{A.43}$$

$$= \left(\frac{\partial \mathbf{A}}{\partial u^k} \right)_j \mathbf{e}^j \equiv \mathbf{A}_{j,k} \mathbf{e}^j \tag{A.44}$$

with

$$\mathbf{A}_k^j = \frac{\partial A^j}{\partial u^k} + A^i \left\{ \frac{\partial \mathbf{e}_i}{\partial u^k} \cdot \mathbf{e}^j \right\} \tag{A.45}$$

$$\mathbf{A}_{j,k} = \frac{\partial A_j}{\partial u^k} + A_i \left\{ \frac{\partial \mathbf{e}^i}{\partial u^k} \cdot \mathbf{e}_j \right\} \tag{A.46}$$

Then,

$$\delta \mathbf{A}^j = (d\mathbf{A})^j = \frac{\partial A^j}{\partial u^k} du^k + A^i \left\{ \frac{\partial \mathbf{e}_i}{\partial u^k} \cdot \mathbf{e}^j \right\} du^k \tag{A.47}$$

$$= dA^j + \left\{ \frac{\partial \mathbf{e}_i}{\partial u^k} \cdot \mathbf{e}^j \right\} A^i du^k \tag{A.48}$$

It can be shown that the Christoffel Symbol of the second kind is

$$\left\{ \frac{\partial \mathbf{e}_i}{\partial u^k} \cdot \mathbf{e}^j \right\} \equiv \left\{ \begin{array}{cc} j & \\ i & k \end{array} \right\} = \frac{1}{2} g^{jn} \left[\frac{\partial g_{ni}}{\partial u^k} + \frac{\partial g_{nk}}{\partial u^i} - \frac{\partial g_{ik}}{\partial u^n} \right] \tag{A.49}$$

so that

$$\mathbf{A}^j_k = \frac{\partial A^j}{\partial u^k} + \left\{ \begin{array}{cc} j & \\ i & k \end{array} \right\} A^i \tag{A.50}$$

$$\mathbf{A}_{j,k} = \frac{\partial A_j}{\partial u^k} - \left\{ \begin{array}{cc} i & \\ j & k \end{array} \right\} A_i \tag{A.51}$$

Note that since

$$\frac{\partial \mathbf{e}_i}{\partial u^k} = \frac{\partial \mathbf{e}_k}{\partial u^i} \tag{A.52}$$

we have

$$\left\{ \begin{array}{cc} j & \\ i & k \end{array} \right\} = \left\{ \begin{array}{cc} j & \\ k & i \end{array} \right\} \tag{A.53}$$

Operator ∇

The operator ∇ can be decomposed in the curvilinear coordinates as

$$\nabla = \nabla u^i \frac{\partial}{\partial u^i} = \mathbf{e}^i \frac{\partial}{\partial u^i} \tag{A.54}$$

We then find the following differential operations:

Gradient It follows simply that

$$\nabla f = \nabla u^i \frac{\partial f}{\partial u^i} = \frac{\partial f}{\partial u^i} \mathbf{e}^i \tag{A.55}$$

so that

$$(\nabla f)_i = (\nabla f \cdot \mathbf{e}_i) = \frac{\partial f}{\partial u^i} \tag{A.56}$$

Divergence It can be shown that the divergence is expressed as

$$\nabla \cdot \mathbf{A} = \frac{1}{J} \frac{\partial}{\partial u^i} \left(J A^i \right) \tag{A.57}$$

Curl It becomes, a compact notations,

$$\nabla \times \mathbf{A} = \frac{\varepsilon^{ijk}}{J} \frac{\partial A_j}{\partial u^i} \mathbf{e}_k \tag{A.58}$$

or is extended as

$$(\nabla \times \mathbf{A})^k = \frac{1}{J} \left(\frac{\partial A_j}{\partial u^i} - \frac{\partial A_i}{\partial u^j} \right) \tag{A.59}$$

A.1.2 Tensor Algebra

A.2 Configuration space

A.2.1 System (R, Z, ϕ)

Definition

The coordinates (R, Z, ϕ) are defined on the space

$$\begin{aligned} 0 \leq R < \infty \\ -\infty \leq Z < \infty \\ 0 \leq \phi < 2\pi \end{aligned} \tag{A.60}$$

and is related to (x, y, z) by

$$\begin{aligned} R &= \sqrt{x^2 + y^2} \\ Z &= -z \\ \phi &= \arctan(y/x) + \pi H(-x) \quad [2\pi] \end{aligned} \tag{A.61}$$

which is inverted to

$$\begin{aligned} x &= R\cos\phi \\ y &= R\sin\phi \\ z &= -Z \end{aligned} \tag{A.62}$$

Position Vector

The position vector then becomes

$$\mathbf{X} = R\widehat{R} + Z\widehat{Z} \tag{A.63}$$

where we define a local orthonormal basis $\left(\widehat{R}, \widehat{Z}, \widehat{\phi}\right)$ as

$$\widehat{R} = \cos\phi\, \widehat{x} + \sin\phi\, \widehat{y} \tag{A.64}$$

$$\widehat{Z} = -\widehat{z} \tag{A.65}$$

$$\widehat{\phi} = \widehat{R} \times \widehat{Z} = -\sin\phi\, \widehat{x} + \cos\phi\, \widehat{y} \tag{A.66}$$

Covariant Basis

The covariant vector basis is defined in (A.1), which becomes here

$$\mathbf{e}_R = \frac{\partial \mathbf{X}}{\partial R} = \widehat{R} \tag{A.67}$$

$$\mathbf{e}_Z = \frac{\partial \mathbf{X}}{\partial Z} = \widehat{Z} \tag{A.68}$$

$$\mathbf{e}_\phi = \frac{\partial \mathbf{X}}{\partial \phi} = R\frac{\partial \widehat{R}}{\partial \phi} = R\widehat{\phi} \tag{A.69}$$

so that we have the covariant basis

$$(\mathbf{e}_R, \mathbf{e}_Z, \mathbf{e}_\phi) = \left(\widehat{R}, \widehat{Z}, R\widehat{\phi}\right) \tag{A.70}$$

the scaling factors

$$(h_R, h_Z, h_\phi) = (1, 1, R) \tag{A.71}$$

and the normalized tangent basis

$$(\widehat{e}_R, \widehat{e}_Z, \widehat{e}_\phi) = \left(\widehat{R}, \widehat{Z}, \widehat{\phi}\right) \tag{A.72}$$

Contravariant Basis

The Contravariant vector basis is defined in (A.9), which becomes here

$$\mathbf{e}^R = \nabla R = \widehat{R} \tag{A.73}$$

$$\mathbf{e}^Z = \nabla Z = \widehat{Z} \tag{A.74}$$

$$\mathbf{e}^\phi = \nabla \phi = \frac{\widehat{\phi}}{R} \tag{A.75}$$

The relations (A.10-A.11) are here readily verified. The normalized reciprocal basis is

$$\left(\widehat{e}^R, \widehat{e}^Z, \widehat{e}^\phi\right) = \left(\widehat{R}, \widehat{Z}, \widehat{\phi}\right) \tag{A.76}$$

which here coincides with the normalized tangent basis, since both bases are orthogonal.

Metric Coefficients

They are defined in (A.12) and become here

$$g_{ij} = \begin{pmatrix} 1 & 0 & 0 \\ 0 & 1 & 0 \\ 0 & 0 & R^2 \end{pmatrix} \tag{A.77}$$

$$g^{ij} = \begin{pmatrix} 1 & 0 & 0 \\ 0 & 1 & 0 \\ 0 & 0 & 1/R^2 \end{pmatrix}$$

As a result

$$g = R^2 \tag{A.78}$$

and the Jacobian is

$$J = R \tag{A.79}$$

Differential elements

$$dl\left(R\right) = dR \tag{A.80}$$
$$dl\left(Z\right) = dZ \tag{A.81}$$
$$dl\left(\phi\right) = Rd\phi \tag{A.82}$$

$$d\mathbf{S}\left(R\right) = RdZd\phi\widehat{R} \tag{A.83}$$
$$d\mathbf{S}\left(Z\right) = RdRd\phi\widehat{Z} \tag{A.84}$$
$$d\mathbf{S}\left(\phi\right) = dRdZ\widehat{\phi} \tag{A.85}$$

$$d^3\mathbf{X} = RdRdZd\phi \tag{A.86}$$

Christoffel Symbols

They are defined in (A.49) and are all zero here except

$$\left\{ \begin{array}{cc} \phi & \\ \phi & R \end{array} \right\} = \left\{ \begin{array}{cc} \phi & \\ R & \phi \end{array} \right\} = \frac{1}{2}g^{\phi\phi}\frac{\partial g_{\phi\phi}}{\partial R} = \frac{1}{R}$$
$$\left\{ \begin{array}{cc} R & \\ \phi & \phi \end{array} \right\} = -\frac{1}{2}g^{RR}\frac{\partial g_{\phi\phi}}{\partial R} = -R \tag{A.87}$$

Differential Operations

Gradient

$$\nabla f = \frac{\partial f}{\partial R}\widehat{R} + \frac{\partial f}{\partial Z}\widehat{Z} + \frac{1}{R}\frac{\partial f}{\partial \phi}\widehat{\phi} \tag{A.88}$$

Divergence

$$\nabla \cdot \mathbf{A} = \frac{1}{R}\frac{\partial}{\partial R}\left(R\mathbf{A}\cdot\widehat{R}\right) + \frac{\partial}{\partial Z}\left(\mathbf{A}\cdot\widehat{Z}\right) + \frac{1}{R}\frac{\partial}{\partial \phi}\left(\mathbf{A}\cdot\widehat{\phi}\right) \tag{A.89}$$

Curl

$$\left(\nabla\times\mathbf{A}\right)\cdot\widehat{R} = \frac{\partial}{\partial Z}\left(\mathbf{A}\cdot\widehat{\phi}\right) - \frac{1}{R}\frac{\partial}{\partial \phi}\left(\mathbf{A}\cdot\widehat{Z}\right) \tag{A.90}$$
$$\left(\nabla\times\mathbf{A}\right)\cdot\widehat{Z} = \frac{1}{R}\frac{\partial}{\partial \phi}\left(\mathbf{A}\cdot\widehat{R}\right) - \frac{1}{R}\frac{\partial}{\partial R}\left(R\mathbf{A}\cdot\widehat{\phi}\right) \tag{A.91}$$
$$\left(\nabla\times\mathbf{A}\right)\cdot\widehat{\phi} = \frac{\partial}{\partial R}\left(\mathbf{A}\cdot\widehat{Z}\right) - \frac{\partial}{\partial Z}\left(\mathbf{A}\cdot\widehat{R}\right) \tag{A.92}$$

A.2.2 System (r, θ, ϕ)

Definition

The coordinates (r, θ, ϕ) are defined from the origin (R_p, Z_p) on the space

$$\begin{aligned} 0 \leq r < \infty \\ 0 \leq \theta < 2\pi \end{aligned} \tag{A.93}$$

and is related to (R, Z, ϕ) by

$$\begin{aligned} r &= \sqrt{(R - R_p)^2 + (Z - Z_p)^2} \\ \theta &= \arctan\left((Z - Z_p) / (R - R_p)\right) + \pi H(R_p - R) \quad [2\pi] \end{aligned} \tag{A.94}$$

which is inverted to

$$R = R_p + r\cos\theta \tag{A.95}$$

$$Z = Z_p + r\cos\theta \tag{A.96}$$

Position Vector

The position vector then becomes

$$\mathbf{X} = R_p\widehat{R} + Z_p\widehat{Z} + r\widehat{r} \tag{A.97}$$

where we define a local orthonormal basis $\left(\widehat{r}, \widehat{\theta}, \widehat{\phi}\right)$ as

$$\widehat{r} = \cos\theta\ \widehat{R} + \sin\theta\ \widehat{Z} \tag{A.98}$$

$$\widehat{\theta} = \widehat{\phi} \times \widehat{r} = -\sin\theta\ \widehat{R} + \cos\theta\ \widehat{Z} \tag{A.99}$$

since

$$\widehat{\phi} \times \widehat{r} = \left(\widehat{R} \times \widehat{Z}\right) \times \left(\cos\theta\ \widehat{R} + \sin\theta\ \widehat{Z}\right) \tag{A.100}$$

$$= \left[\left(\cos\theta\ \widehat{R} + \sin\theta\ \widehat{Z}\right) \cdot \widehat{R}\right] \widehat{Z} - \left[\left(\cos\theta\ \widehat{R} + \sin\theta\ \widehat{Z}\right) \cdot \widehat{Z}\right] \widehat{R} \tag{A.101}$$

$$= \cos\theta\widehat{Z} - \sin\theta\ \widehat{R} \tag{A.102}$$

Covariant Basis

The covariant vector basis is defined in (A.1), which becomes here

$$\mathbf{e}_r = \frac{\partial \mathbf{X}}{\partial r} = \widehat{r} \tag{A.103}$$

$$\mathbf{e}_\theta = \frac{\partial \mathbf{X}}{\partial \theta} = r\frac{\partial \widehat{r}}{\partial \theta} = r\widehat{\theta} \tag{A.104}$$

$$\mathbf{e}_\phi = \frac{\partial \mathbf{X}}{\partial \phi} = R_p\frac{\partial \widehat{R}}{\partial \phi} + r\frac{\partial \widehat{r}}{\partial \phi} = (R_p + r\cos\theta)\frac{\partial \widehat{R}}{\partial \phi} = R\widehat{\phi} \tag{A.105}$$

so that we have the covariant basis

$$(\mathbf{e}_r, \mathbf{e}_\theta, \mathbf{e}_\phi) = \left(\widehat{r}, r\widehat{\theta}, R\widehat{\phi}\right) \tag{A.106}$$

the scaling factors

$$(h_r, h_\theta, h_\phi) = (1, r, R) \tag{A.107}$$

and the normalized tangent basis

$$(\widehat{e}_r, \widehat{e}_\theta, \widehat{e}_\phi) = \left(\widehat{r}, \widehat{\theta}, \widehat{\phi}\right) \tag{A.108}$$

Contravariant Basis

The Contravariant vector basis is defined in (A.9), which becomes here

$$\mathbf{e}^r = \nabla r = \widehat{r} \tag{A.109}$$

$$\mathbf{e}^\theta = \nabla\theta = \frac{1}{r}\widehat{\theta} \tag{A.110}$$

$$\mathbf{e}^\phi = \nabla\phi = \frac{\widehat{\phi}}{R} \tag{A.111}$$

The relations (A.10-A.11) are here readily verified. The normalized reciprocal basis is

$$\left(\widehat{e}^r, \widehat{e}^\theta, \widehat{e}^\phi\right) = \left(\widehat{r}, \widehat{\theta}, \widehat{\phi}\right) \tag{A.112}$$

which here coincides with the normalized tangent basis, since both bases are orthogonal.

Metric Coefficients

They are defined in (A.12) and become here

$$g_{ij} = \begin{pmatrix} 1 & 0 & 0 \\ 0 & r^2 & 0 \\ 0 & 0 & R^2 \end{pmatrix} \tag{A.113}$$

$$g^{ij} = \begin{pmatrix} 1 & 0 & 0 \\ 0 & 1/r^2 & 0 \\ 0 & 0 & 1/R^2 \end{pmatrix}$$

As a result

$$g = r^2 R^2 \tag{A.114}$$

and the Jacobian is

$$J = rR \tag{A.115}$$

Differential elements

$$dl\left(r\right) = dr \tag{A.116}$$
$$dl\left(\theta\right) = d\theta \tag{A.117}$$
$$dl\left(\phi\right) = Rd\phi \tag{A.118}$$

$$d\mathbf{S}\left(r\right) = rRd\theta d\phi\widehat{r} \tag{A.119}$$
$$d\mathbf{S}\left(\theta\right) = Rdrd\phi\widehat{\theta} \tag{A.120}$$
$$d\mathbf{S}\left(\phi\right) = rdrd\theta\widehat{\phi} \tag{A.121}$$

$$d^3\mathbf{X} = rRdrd\theta d\phi \tag{A.122}$$

Christoffel Symbols

They are defined in (A.49) and are all zero here except

$$\left\{ \begin{array}{cc} \theta & \\ \theta & r \end{array} \right\} = \left\{ \begin{array}{cc} \theta & \\ r & \theta \end{array} \right\} = \frac{1}{2}g^{\theta\theta}\frac{\partial g_{\theta\theta}}{\partial r} = \frac{1}{r} \tag{A.123}$$

$$\left\{ \begin{array}{cc} r & \\ \theta & \theta \end{array} \right\} = -\frac{1}{2}g^{rr}\frac{\partial g_{\theta\theta}}{\partial r} = -r \tag{A.124}$$

$$\left\{ \begin{array}{cc} \phi & \\ \phi & r \end{array} \right\} = \left\{ \begin{array}{cc} \phi & \\ r & \phi \end{array} \right\} = \frac{1}{2}g^{\phi\phi}\frac{\partial g_{\phi\phi}}{\partial r} = \frac{1}{R}\cos\theta \tag{A.125}$$

$$\left\{ \begin{array}{cc} r & \\ \phi & \phi \end{array} \right\} = -\frac{1}{2}g^{rr}\frac{\partial g_{\phi\phi}}{\partial r} = -R\cos\theta \tag{A.126}$$

$$\left\{ \begin{array}{cc} \phi & \\ \phi & \theta \end{array} \right\} = \left\{ \begin{array}{cc} \phi & \\ \theta & \phi \end{array} \right\} = \frac{1}{2}g^{\phi\phi}\frac{\partial g_{\phi\phi}}{\partial\theta} = -\frac{r}{R}\sin\theta \tag{A.127}$$

$$\left\{ \begin{array}{cc} \theta & \\ \phi & \phi \end{array} \right\} = -\frac{1}{2}g^{\theta\theta}\frac{\partial g_{\phi\phi}}{\partial\theta} = \frac{R}{r}\sin\theta \tag{A.128}$$

Differential Operations

Gradient

$$\nabla f = \frac{\partial f}{\partial r}\widehat{r} + \frac{1}{r}\frac{\partial f}{\partial\theta}\widehat{\theta} + \frac{1}{R}\frac{\partial f}{\partial\phi}\widehat{\phi} \tag{A.129}$$

Divergence

$$\nabla\cdot\mathbf{A} = \frac{1}{rR}\frac{\partial}{\partial r}\left(rR\mathbf{A}\cdot\widehat{r}\right) + \frac{1}{rR}\frac{\partial}{\partial\theta}\left(R\mathbf{A}\cdot\widehat{\theta}\right) + \frac{1}{R}\frac{\partial}{\partial\phi}\left(\mathbf{A}\cdot\widehat{\phi}\right) \tag{A.130}$$

Curl

$$(\nabla \times \mathbf{A}) \cdot \widehat{r} = \frac{1}{rR}\frac{\partial}{\partial \theta}\left(R\mathbf{A} \cdot \widehat{\phi}\right) - \frac{1}{R}\frac{\partial}{\partial \phi}\left(\mathbf{A} \cdot \widehat{\theta}\right) \tag{A.131}$$

$$(\nabla \times \mathbf{A}) \cdot \widehat{\theta} = \frac{1}{R}\frac{\partial}{\partial \phi}\left(\mathbf{A} \cdot \widehat{r}\right) - \frac{1}{R}\frac{\partial}{\partial r}\left(R\mathbf{A} \cdot \widehat{\phi}\right) \tag{A.132}$$

$$(\nabla \times \mathbf{A}) \cdot \widehat{\phi} = \frac{1}{r}\frac{\partial}{\partial r}\left(r\mathbf{A} \cdot \widehat{\theta}\right) - \frac{1}{r}\frac{\partial}{\partial \theta}\left(\mathbf{A} \cdot \widehat{r}\right) \tag{A.133}$$

A.2.3 System (ψ, s, ϕ)

Definition

The coordinates (ψ, s, ϕ), used to parametrize closed flux-surfaces, are defined from the origin (R_p, Z_p) on the (closed) space

$$\min\left(\psi_0, \psi_a\right) \leq \psi \leq \max\left(\psi_0, \psi_a\right) \tag{A.134}$$

$$0 \leq s \leq s_{\max} \tag{A.135}$$

and is related to (r, θ, ϕ) by

$$\begin{aligned} \psi &= \psi\left(r, \theta\right) \\ s &= s\left(r, \theta\right) \end{aligned} \tag{A.136}$$

which is inverted to

$$\begin{aligned} r &= r\left(\psi, s\right) \\ \theta &= \theta\left(\psi, s\right) \end{aligned}$$

Note that $\psi\left(r, \theta\right)$ must be a monotonic function of r from ψ_0 at the center (R_p, Z_p) to ψ_a at the edge. It is the case for nested flux-surfaces.

We define a local orthonormal basis $\left(\widehat{\psi}, \widehat{s}, \widehat{\phi}\right)$ as

$$\begin{aligned} \widehat{\psi} &= \frac{\nabla\psi}{|\nabla\psi|} \\ \widehat{s} &= \widehat{\phi} \times \widehat{\psi} \end{aligned} \tag{A.137}$$

The transformation from $\left(\widehat{r}, \widehat{\theta}\right)$ to $\left(\widehat{\psi}, \widehat{s}\right)$ is a rotation of angle α such that

$$\begin{pmatrix} \widehat{\psi} \\ \widehat{s} \end{pmatrix} = \begin{pmatrix} \cos\alpha & -\sin\alpha \\ \sin\alpha & \cos\alpha \end{pmatrix} \cdot \begin{pmatrix} \widehat{r} \\ \widehat{\theta} \end{pmatrix} \tag{A.138}$$

Position Vector

The position vector remains

$$\mathbf{X} = R_p\widehat{R} + Z_p\widehat{Z} + r\widehat{r} \tag{A.139}$$

Covariant Basis

The covariant vector basis is defined in (A.1), which becomes here

$$\mathbf{e}_\psi = \frac{\partial \mathbf{X}}{\partial \psi} = \left.\frac{\partial r}{\partial \psi}\right|_s \widehat{r} + r \left.\frac{\partial \widehat{r}}{\partial \psi}\right|_s = \left.\frac{\partial r}{\partial \psi}\right|_s \widehat{r} + r \left.\frac{\partial \theta}{\partial \psi}\right|_s \widehat{\theta} \tag{A.140}$$

$$\mathbf{e}_s = \frac{\partial \mathbf{X}}{\partial s} = \left.\frac{\partial r}{\partial s}\right|_\psi \widehat{r} + r \left.\frac{\partial \widehat{r}}{\partial s}\right|_\psi = \left.\frac{\partial r}{\partial s}\right|_\psi \widehat{r} + r \left.\frac{\partial \theta}{\partial s}\right|_\psi \widehat{\theta} \tag{A.141}$$

$$\mathbf{e}_\phi = \frac{\partial \mathbf{X}}{\partial \phi} = R_p \frac{\partial \widehat{R}}{\partial \phi} + r \frac{\partial \widehat{r}}{\partial \phi} = (R_p + r\cos\theta) \frac{\partial \widehat{R}}{\partial \phi} = R\widehat{\phi} \tag{A.142}$$

so that we have the covariant basis

$$(\mathbf{e}_\psi, \mathbf{e}_s, \mathbf{e}_\phi) = \left(\left.\frac{\partial r}{\partial \psi}\right|_s \widehat{r} + r \left.\frac{\partial \theta}{\partial \psi}\right|_s \widehat{\theta}, \left.\frac{\partial r}{\partial s}\right|_\psi \widehat{r} + r \left.\frac{\partial \theta}{\partial s}\right|_\psi \widehat{\theta}, R\widehat{\phi} \right) \tag{A.143}$$

the scaling factors

$$(h_\psi, h_s, h_\phi) = \left(\sqrt{\left.\frac{\partial r}{\partial \psi}\right|_s^2 + r^2 \left.\frac{\partial \theta}{\partial \psi}\right|_s^2}, \sqrt{\left.\frac{\partial r}{\partial s}\right|_\psi^2 + r^2 \left.\frac{\partial \theta}{\partial s}\right|_\psi^2}, R \right) \tag{A.144}$$

and the normalized tangent basis

$$(\widehat{e}_\psi, \widehat{e}_s, \widehat{e}_\phi) = \left(\frac{1}{h_\psi} \left[\left.\frac{\partial r}{\partial \psi}\right|_s \widehat{r} + r \left.\frac{\partial \theta}{\partial \psi}\right|_s \widehat{\theta} \right], \frac{1}{h_s} \left[\left.\frac{\partial r}{\partial s}\right|_\psi \widehat{r} + r \left.\frac{\partial \theta}{\partial s}\right|_\psi \widehat{\theta} \right], \widehat{\phi} \right) \tag{A.145}$$

Contravariant Basis

The Contravariant vector basis is defined in (A.9), which becomes here

$$\mathbf{e}^\psi = \nabla\psi = |\nabla\psi|\, \widehat{\psi} \tag{A.146}$$

$$\mathbf{e}^s = \nabla s = \widehat{s} \tag{A.147}$$

$$\mathbf{e}^\phi = \nabla\phi = \frac{\widehat{\phi}}{R} \tag{A.148}$$

The relations (A.11) then give

$$\mathbf{e}_\psi = \frac{\mathbf{e}^s \times \mathbf{e}^\phi}{\mathbf{e}^\psi \cdot \mathbf{e}^s \times \mathbf{e}^\phi} = \frac{\widehat{\psi}}{|\nabla\psi|} \tag{A.149}$$

$$\mathbf{e}_s = \frac{\mathbf{e}^\phi \times \mathbf{e}^\psi}{\mathbf{e}^s \cdot \mathbf{e}^\phi \times \mathbf{e}^\psi} = \widehat{s}$$

$$\mathbf{e}_\phi = \frac{\mathbf{e}^\psi \times \mathbf{e}^s}{\mathbf{e}^\phi \cdot \mathbf{e}^\psi \times \mathbf{e}^s} = R\widehat{\phi}$$

so that we have the following tangent basis

$$(\mathbf{e}_\psi, \mathbf{e}_s, \mathbf{e}_\phi) = \left(\frac{\widehat{\psi}}{|\nabla\psi|}, \widehat{s}, R\widehat{\phi} \right) \tag{A.150}$$

the scaling factors

$$(h_\psi, h_s, h_\phi) = \left(\frac{1}{|\nabla\psi|}, 1, R\right) \tag{A.151}$$

the normalized tangent basis

$$(\widehat{e}_\psi, \widehat{e}_s, \widehat{e}_\phi) = \left(\widehat{\psi}, \widehat{s}, \widehat{\phi}\right) \tag{A.152}$$

the reciprocal basis

$$\left(\mathbf{e}^\psi, \mathbf{e}^s, \mathbf{e}^\phi\right) = \left(|\nabla\psi|\,\widehat{\psi}, \widehat{s}, \frac{\widehat{\phi}}{R}\right) \tag{A.153}$$

and the normalized reciprocal basis

$$\left(\widehat{e}^\psi, \widehat{e}^s, \widehat{e}^\phi\right) = \left(\widehat{\psi}, \widehat{s}, \widehat{\phi}\right) \tag{A.154}$$

which here coincides with the normalized tangent basis, since both bases are orthogonal.

By comparing (A.143) with (A.149), we also find that

$$\left.\frac{\partial r}{\partial \psi}\right|_s = \frac{\cos\alpha}{|\nabla\psi|} \tag{A.155}$$

$$\left.\frac{\partial \theta}{\partial \psi}\right|_s = \frac{-\sin\alpha}{r\,|\nabla\psi|} \tag{A.156}$$

$$\left.\frac{\partial r}{\partial s}\right|_\psi = (\widehat{s}\cdot\widehat{r}) = \sin\alpha \tag{A.157}$$

$$\left.\frac{\partial \theta}{\partial s}\right|_\psi = \frac{\left(\widehat{s}\cdot\widehat{\theta}\right)}{r} = \frac{\cos\alpha}{r} \tag{A.158}$$

Metric Coefficients

They are defined in (A.12) and become here

$$g_{ij} = \begin{pmatrix} 1/|\nabla\psi|^2 & 0 & 0 \\ 0 & 1 & 0 \\ 0 & 0 & R^2 \end{pmatrix} \tag{A.159}$$

$$g^{ij} = \begin{pmatrix} |\nabla\psi|^2 & 0 & 0 \\ 0 & 1 & 0 \\ 0 & 0 & 1/R^2 \end{pmatrix}$$

As a result

$$g = \frac{R^2}{|\nabla\psi|^2} \tag{A.160}$$

and the Jacobian is

$$J = \frac{R}{|\nabla\psi|} \tag{A.161}$$

Differential elements

$$dl\left(\psi\right) = \frac{d\psi}{|\nabla\psi|} \tag{A.162}$$
$$dl\left(s\right) = ds \tag{A.163}$$
$$dl\left(\phi\right) = Rd\phi \tag{A.164}$$

$$d\mathbf{S}\left(\psi\right) = Rdsd\phi\widehat{\psi} \tag{A.165}$$
$$d\mathbf{S}\left(s\right) = \frac{R}{|\nabla\psi|}d\psi d\phi\widehat{s} \tag{A.166}$$
$$d\mathbf{S}\left(\phi\right) = \frac{1}{|\nabla\psi|}d\psi ds\widehat{\phi} \tag{A.167}$$

$$d^3\mathbf{X} = \frac{R}{|\nabla\psi|}d\psi dsd\phi \tag{A.168}$$

Christoffel Symbols

They are defined in (A.49) and are here

Differential Operations

Gradient

$$\nabla f = |\nabla\psi|\frac{\partial f}{\partial\psi}\widehat{\psi} + \frac{\partial f}{\partial s}\widehat{s} + \frac{1}{R}\frac{\partial f}{\partial\phi}\widehat{\phi} \tag{A.169}$$

Divergence

$$\nabla\cdot\mathbf{A} = \frac{|\nabla\psi|}{R}\frac{\partial}{\partial\psi}\left(R\mathbf{A}\cdot\widehat{\psi}\right) + \frac{|\nabla\psi|}{R}\frac{\partial}{\partial s}\left(\frac{R}{|\nabla\psi|}\mathbf{A}\cdot\widehat{s}\right) + \frac{1}{R}\frac{\partial}{\partial\phi}\left(\mathbf{A}\cdot\widehat{\phi}\right) \tag{A.170}$$

Curl

$$\left(\nabla\times\mathbf{A}\right)\cdot\widehat{\psi} = \frac{1}{R}\frac{\partial}{\partial s}\left(R\mathbf{A}\cdot\widehat{\phi}\right) - \frac{1}{R}\frac{\partial}{\partial\phi}\left(\mathbf{A}\cdot\widehat{s}\right) \tag{A.171}$$
$$\left(\nabla\times\mathbf{A}\right)\cdot\widehat{s} = \frac{1}{R}\frac{\partial}{\partial\phi}\left(\mathbf{A}\cdot\widehat{\psi}\right) - \frac{|\nabla\psi|}{R}\frac{\partial}{\partial\psi}\left(R\mathbf{A}\cdot\widehat{\phi}\right)$$
$$\left(\nabla\times\mathbf{A}\right)\cdot\widehat{\phi} = |\nabla\psi|\frac{\partial}{\partial\psi}\left(\mathbf{A}\cdot\widehat{s}\right) - |\nabla\psi|\frac{\partial}{\partial s}\left(\frac{\mathbf{A}\cdot\widehat{\psi}}{|\nabla\psi|}\right)$$

A.2.4 System (ψ, θ, ϕ)

Definition

The coordinates (ψ, θ, ϕ) are defined from the origin (R_p, Z_p) on the space

$$\min(\psi_0, \psi_a) \leq \psi < \max(\psi_0, \psi_a)$$

and is related to (r, θ, ϕ) by

$$\psi = \psi(r, \theta)$$

which is inverted to

$$r = r(\psi, \theta)$$

Note that $\psi(r, \theta)$ must be a monotonic function of r from ψ_0 at the center (R_p, Z_p) to ψ_a at the edge. It is the case for nested flux-surfaces.

Position Vector

The position vector then becomes

$$\mathbf{X} = R_p \widehat{R} + Z_p \widehat{Z} + r(\psi, \theta)\, \widehat{r} \tag{A.172}$$

Covariant Basis

The covariant vector basis is defined in (A.1), which becomes here

$$\mathbf{e}_\psi = \frac{\partial \mathbf{X}}{\partial \psi} = \left.\frac{\partial r}{\partial \psi}\right|_\theta \widehat{r} \tag{A.173}$$

$$\mathbf{e}_\theta = \frac{\partial \mathbf{X}}{\partial \theta} = \left.\frac{\partial r}{\partial \theta}\right|_\psi \widehat{r} + r\frac{\partial \widehat{r}}{\partial \theta} = \left.\frac{\partial r}{\partial \theta}\right|_\psi \widehat{r} + r\widehat{\theta} \tag{A.174}$$

$$\mathbf{e}_\phi = \frac{\partial \mathbf{X}}{\partial \phi} = R_p \frac{\partial \widehat{R}}{\partial \phi} + r\frac{\partial \widehat{r}}{\partial \phi} = (R_p + r\cos\theta)\frac{\partial \widehat{R}}{\partial \phi} = R\widehat{\phi} \tag{A.175}$$

so that we have the covariant basis

$$(\mathbf{e}_\psi, \mathbf{e}_\theta, \mathbf{e}_\phi) = \left(\left.\frac{\partial r}{\partial \psi}\right|_\theta \widehat{r},\ \left.\frac{\partial r}{\partial \theta}\right|_\psi \widehat{r} + r\widehat{\theta},\ R\widehat{\phi} \right) \tag{A.176}$$

the scaling factors

$$(h_\psi, h_\theta, h_\phi) = \left(\left| \left.\frac{\partial r}{\partial \psi}\right|_\theta \right|,\ \sqrt{\left|\left.\frac{\partial r}{\partial \theta}\right|_\psi\right|^2 + r^2},\ R \right) \tag{A.177}$$

and the normalized tangent basis

$$(\widehat{e}_\psi, \widehat{e}_\theta, \widehat{e}_\phi) = \left(\widehat{r},\ \frac{1}{h_\theta}\left[\left.\frac{\partial r}{\partial \theta}\right|_\psi \widehat{r} + r\widehat{\theta} \right],\ \widehat{\phi} \right) \tag{A.178}$$

Contravariant Basis

The Contravariant vector basis is defined in (A.9), which becomes here

$$\mathbf{e}^{\psi} = \nabla\psi = |\nabla\psi|\,\widehat{\psi} \tag{A.179}$$

$$\mathbf{e}^{\theta} = \nabla\theta = \frac{\widehat{\theta}}{r} \tag{A.180}$$

$$\mathbf{e}^{\phi} = \nabla\phi = \frac{\widehat{\phi}}{R} \tag{A.181}$$

The relations (A.11) then give

$$\mathbf{e}_{\psi} = \frac{\mathbf{e}^{\theta}\times\mathbf{e}^{\phi}}{\mathbf{e}^{\psi}\cdot\mathbf{e}^{\theta}\times\mathbf{e}^{\phi}} = \frac{\widehat{r}}{|\nabla\psi|\cos\alpha} \tag{A.182}$$

$$\mathbf{e}_{\theta} = \frac{\mathbf{e}^{\phi}\times\mathbf{e}^{\psi}}{\mathbf{e}^{\theta}\cdot\mathbf{e}^{\phi}\times\mathbf{e}^{\psi}} = \frac{r\widehat{s}}{\left(\widehat{\theta}\cdot\widehat{s}\right)} = \frac{r\widehat{s}}{\cos\alpha} \tag{A.183}$$

$$\mathbf{e}_{\phi} = \frac{\mathbf{e}^{\psi}\times\mathbf{e}^{\theta}}{\mathbf{e}^{\phi}\cdot\mathbf{e}^{\psi}\times\mathbf{e}^{\theta}} = R\widehat{\phi} \tag{A.184}$$

so that we have the following tangent basis

$$(\mathbf{e}_{\psi},\mathbf{e}_{\theta},\mathbf{e}_{\phi}) = \left(\frac{\widehat{r}}{|\nabla\psi|\cos\alpha},\frac{r\widehat{s}}{\cos\alpha},R\widehat{\phi}\right) \tag{A.185}$$

the scaling factors

$$(h_{\psi},h_{\theta},h_{\phi}) = \left(\frac{1}{|\nabla\psi|\cos\alpha},\frac{r}{\cos\alpha},R\right) \tag{A.186}$$

the normalized tangent basis

$$(\widehat{e}_{\psi},\widehat{e}_{\theta},\widehat{e}_{\phi}) = \left(\widehat{r},\widehat{s},\widehat{\phi}\right) \tag{A.187}$$

the reciprocal basis

$$\left(\mathbf{e}^{\psi},\mathbf{e}^{\theta},\mathbf{e}^{\phi}\right) = \left(|\nabla\psi|\,\widehat{\psi},\frac{\widehat{\theta}}{r},\frac{\widehat{\phi}}{R}\right) \tag{A.188}$$

and the normalized reciprocal basis

$$\left(\widehat{e}^{\psi},\widehat{e}^{\theta},\widehat{e}^{\phi}\right) = \left(\widehat{\psi},\widehat{\theta},\widehat{\phi}\right) \tag{A.189}$$

which here does not coincide with the normalized tangent basis, since both bases are not orthogonal.

By comparing (A.176) with (A.185), we also find that

$$\left.\frac{\partial r}{\partial\psi}\right|_{\theta} = \frac{1}{|\nabla\psi|\cos\alpha} \tag{A.190}$$

$$\left.\frac{\partial r}{\partial\theta}\right|_{\psi} = r\sqrt{\frac{1}{\left(\widehat{\theta}\cdot\widehat{s}\right)^2}-1} = r\tan\alpha \tag{A.191}$$

Metric Coefficients

They are defined in (A.12) and become here

$$g_{ij} = \begin{pmatrix} 1/\left[|\nabla\psi|\cos\alpha\right]^2 & r\tan\alpha/\left[|\nabla\psi|\cos\alpha\right] & 0 \\ r\tan\alpha/\left[|\nabla\psi|\cos\alpha\right] & r^2/\cos^2\alpha & 0 \\ 0 & 0 & R^2 \end{pmatrix} \tag{A.192}$$

or equivalently

$$g_{ij} = \begin{pmatrix} \partial r/\partial\psi|_\theta^2 & \partial r/\partial\psi|_\theta\,\partial r/\partial\theta|_\psi & 0 \\ \partial r/\partial\psi|_\theta\,\partial r/\partial\theta|_\psi & \partial r/\partial\theta|_\psi^2 + r^2 & 0 \\ 0 & 0 & R^2 \end{pmatrix}$$

and

$$g^{ij} = \begin{pmatrix} |\nabla\psi|^2 & -|\nabla\psi|\sin\alpha/r & 0 \\ -|\nabla\psi|\sin\alpha/r & 1/r^2 & 0 \\ 0 & 0 & 1/R^2 \end{pmatrix} \tag{A.193}$$

As a result

$$g = \frac{R^2 r^2}{|\nabla\psi|^2\cos^2\alpha} \tag{A.194}$$

and the Jacobian is

$$J = \frac{Rr}{|\nabla\psi|\cos\alpha} \tag{A.195}$$

Differential elements

$$dl\left(\psi\right) = \frac{d\psi}{|\nabla\psi|\cos\alpha} \tag{A.196}$$

$$dl\left(\theta\right) = \frac{r}{\cos\alpha}d\theta \tag{A.197}$$

$$dl\left(\phi\right) = Rd\phi \tag{A.198}$$

$$d\mathbf{S}\left(\psi\right) = \frac{Rr}{\cos\alpha}d\theta d\phi\widehat{\psi} \tag{A.199}$$

$$d\mathbf{S}\left(\theta\right) = \frac{R}{|\nabla\psi|\cos\alpha}d\psi d\phi\widehat{s} \tag{A.200}$$

$$d\mathbf{S}\left(\phi\right) = \frac{r}{|\nabla\psi|\cos\alpha}d\psi d\theta\widehat{\phi} \tag{A.201}$$

$$d^3\mathbf{X} = \frac{Rr}{|\nabla\psi|\cos\alpha}d\psi d\theta d\phi \tag{A.202}$$

Christoffel Symbols

They are defined in (A.49) and are here

Differential Operations

Gradient

$$\nabla f = |\nabla\psi| \frac{\partial f}{\partial \psi}\widehat{\psi} + \frac{1}{r}\frac{\partial f}{\partial \theta}\widehat{\theta} + \frac{1}{R}\frac{\partial f}{\partial \phi}\widehat{\phi} \tag{A.203}$$

Divergence

$$\nabla \cdot \mathbf{A} = \frac{|\nabla\psi|\cos\alpha}{Rr}\frac{\partial}{\partial\psi}\left(\frac{Rr}{\cos\alpha}\mathbf{A}\cdot\widehat{\psi}\right) + \frac{|\nabla\psi|\cos\alpha}{Rr}\frac{\partial}{\partial\theta}\left(\frac{R}{|\nabla\psi|\cos\alpha}\mathbf{A}\cdot\widehat{\theta}\right) + \frac{1}{R}\frac{\partial}{\partial\phi}\left(\mathbf{A}\cdot\widehat{\phi}\right) \tag{A.204}$$

Curl

$$(\nabla\times\mathbf{A})\cdot\widehat{\psi} = \frac{\cos\alpha}{Rr}\frac{\partial}{\partial\theta}\left(R\mathbf{A}\cdot\widehat{\phi}\right) - \frac{1}{R}\frac{\partial}{\partial\phi}\left(\mathbf{A}\cdot\widehat{s}\right) \tag{A.205}$$

$$(\nabla\times\mathbf{A})\cdot\widehat{\theta} = \frac{1}{R}\frac{\partial}{\partial\phi}\left(\mathbf{A}\cdot\widehat{r}\right) - \frac{|\nabla\psi|\cos\alpha}{R}\frac{\partial}{\partial\psi}\left(R\mathbf{A}\cdot\widehat{\phi}\right) \tag{A.206}$$

$$(\nabla\times\mathbf{A})\cdot\widehat{\phi} = \frac{|\nabla\psi|\cos\alpha}{r}\frac{\partial}{\partial\psi}\left(\frac{r\mathbf{A}\cdot\widehat{s}}{\cos\alpha}\right) - \frac{|\nabla\psi|\cos\alpha}{r}\frac{\partial}{\partial\theta}\left(\frac{\mathbf{A}\cdot\widehat{r}}{|\nabla\psi|\cos\alpha}\right) \tag{A.207}$$

A.3 Momentum Space

We consider a cartesian momentum space in coordinates (p_x, p_y, p_z) along axes $(\widehat{x}, \widehat{y}, \widehat{z})$. The vector position is momentum space is written

$$\mathbf{P} = p_x\widehat{x} + p_y\widehat{y} + p_z\widehat{z} \tag{A.208}$$

We consider the two following curvilinear systems:

A.3.1 System $\left(p_\parallel, p_\perp, \varphi\right)$

Definition

The coordinates $\left(p_\parallel, p_\perp, \varphi\right)$ are defined on the space

$$-\infty \leq p_\parallel < \infty \tag{A.209}$$

$$0 \leq p_\perp < \infty \tag{A.210}$$

$$0 \leq \varphi < 2\pi \tag{A.211}$$

and is related to (p_x, p_y, p_z) by

$$\begin{aligned} p_\parallel &= p_z \\ p_\perp &= \sqrt{p_x^2 + p_y^2} \\ \varphi &= \arctan\left(p_y/p_x\right) + \pi H\left(-p_x\right) \quad [2\pi] \end{aligned} \tag{A.212}$$

which is inverted to

$$\begin{aligned} p_x &= p_\perp \cos\varphi \\ p_y &= p_\perp \sin\varphi \\ p_z &= p_\parallel \end{aligned} \tag{A.213}$$

Position Vector

The position vector in momentum space then becomes

$$\mathbf{P} = p_\perp \widehat{\perp} + p_\parallel \widehat{\parallel} \tag{A.214}$$

where we define a local orthonormal basis $\left(\widehat{\parallel}, \widehat{\perp}, \widehat{\varphi}\right)$ as

$$\widehat{\parallel} = \widehat{z} \tag{A.215}$$

$$\widehat{\perp} = \cos\varphi\, \widehat{x} + \sin\varphi\, \widehat{y} \tag{A.216}$$

$$\widehat{\varphi} = \widehat{p}_\parallel \times \widehat{p}_\perp = -\sin\varphi\, \widehat{x} + \cos\varphi\, \widehat{y} \tag{A.217}$$

Covariant Basis

The covariant vector basis is defined in (A.1), which becomes here

$$\mathbf{e}_\parallel = \frac{\partial \mathbf{P}}{\partial p_\parallel} = \widehat{\parallel} \tag{A.218}$$

$$\mathbf{e}_\perp = \frac{\partial \mathbf{P}}{\partial p_\perp} = \widehat{\perp} \tag{A.219}$$

$$\mathbf{e}_\varphi = \frac{\partial \mathbf{P}}{\partial \varphi} = p_\perp \frac{\partial \widehat{\perp}}{\partial \varphi} = p_\perp \widehat{\varphi} \tag{A.220}$$

so that we have the covariant basis

$$\left(\mathbf{e}_\parallel, \mathbf{e}_\perp, \mathbf{e}_\varphi\right) = \left(\widehat{\parallel}, \widehat{\perp}, p_\perp \widehat{\varphi}\right) \tag{A.221}$$

the scaling factors

$$\left(h_\parallel, h_\perp, h_\varphi\right) = (1, 1, p_\perp) \tag{A.222}$$

and the normalized tangent basis

$$\left(\widehat{e}_\parallel, \widehat{e}_\perp, \widehat{e}_\varphi\right) = \left(\widehat{\parallel}, \widehat{\perp}, \widehat{\varphi}\right) \tag{A.223}$$

Contravariant Basis

The Contravariant vector basis is defined in (A.9), which becomes here

$$\mathbf{e}^\parallel = \nabla p_\parallel = \widehat{\parallel} \tag{A.224}$$

$$\mathbf{e}^\perp = \nabla p_\perp = \widehat{\perp} \tag{A.225}$$

$$\mathbf{e}^\varphi = \nabla \varphi = \frac{\widehat{\varphi}}{p_\perp} \tag{A.226}$$

The relations (A.10-A.11) are here readily verified. The normalized reciprocal basis is

$$\left(\widehat{e}^{\parallel}, \widehat{e}^{\perp}, \widehat{e}^{\varphi}\right) = \left(\widehat{\parallel}, \widehat{\perp}, \widehat{\varphi}\right) \tag{A.227}$$

which here coincides with the normalized tangent basis, since both bases are orthogonal.

Metric Coefficients

They are defined in (A.12) and become here

$$g_{ij} = \begin{pmatrix} 1 & 0 & 0 \\ 0 & 1 & 0 \\ 0 & 0 & p_\perp^2 \end{pmatrix} \tag{A.228}$$
$$g^{ij} = \begin{pmatrix} 1 & 0 & 0 \\ 0 & 1 & 0 \\ 0 & 0 & 1/p_\perp^2 \end{pmatrix}$$

As a result

$$g = p_\perp^2 \tag{A.229}$$

and the Jacobian is

$$J = p_\perp \tag{A.230}$$

Differential elements

$$dl\left(p_\parallel\right) = dp_\parallel \tag{A.231}$$
$$dl\left(p_\perp\right) = dp_\perp \tag{A.232}$$
$$dl\left(\varphi\right) = p_\perp d\varphi \tag{A.233}$$

$$d\mathbf{S}\left(p_\parallel\right) = p_\perp dp_\perp d\varphi \widehat{\parallel} \tag{A.234}$$
$$d\mathbf{S}\left(p_\perp\right) = p_\perp dp_\parallel d\varphi \widehat{\perp} \tag{A.235}$$
$$d\mathbf{S}\left(\varphi\right) = dp_\parallel dp_\perp \widehat{\varphi} \tag{A.236}$$

$$d^3\mathbf{X} = p_\perp dp_\parallel dp_\perp d\varphi \tag{A.237}$$

Christoffel Symbols

They are defined in (A.49) and are all zero here except

$$\left\{ \begin{array}{cc} \varphi & \\ p_\perp & R \end{array} \right\} = \left\{ \begin{array}{cc} \varphi & \\ R & p_\perp \end{array} \right\} = \frac{1}{2} g^{\varphi\varphi} \frac{\partial g_{\varphi\varphi}}{\partial p_\perp} = \frac{1}{p_\perp}$$
$$\left\{ \begin{array}{cc} p_\perp & \\ \varphi & \varphi \end{array} \right\} = -\frac{1}{2} g^{RR} \frac{\partial g_{\varphi\varphi}}{\partial p_\perp} = -p_\perp \tag{A.238}$$

Differential Operations

Gradient

$$\nabla_{\mathbf{p}} f = \frac{\partial f}{\partial p_{\parallel}} \widehat{\parallel} + \frac{\partial f}{\partial p_{\perp}} \widehat{\perp} + \frac{1}{p_{\perp}} \frac{\partial f}{\partial \varphi} \widehat{\varphi} \tag{A.239}$$

Divergence

$$\nabla_{\mathbf{p}} \cdot \mathbf{A} = \frac{\partial}{\partial p_{\parallel}} \left(\mathbf{A} \cdot \widehat{\parallel} \right) + \frac{1}{p_{\perp}} \frac{\partial}{\partial p_{\perp}} \left(p_{\perp} \mathbf{A} \cdot \widehat{\perp} \right) + \frac{1}{p_{\perp}} \frac{\partial}{\partial \varphi} \left(\mathbf{A} \cdot \widehat{\varphi} \right) \tag{A.240}$$

Curl

$$(\nabla_{\mathbf{p}} \times \mathbf{A}) \cdot \widehat{\parallel} = \frac{1}{p_{\perp}} \frac{\partial}{\partial p_{\perp}} \left(p_{\perp} \mathbf{A} \cdot \widehat{\varphi} \right) - \frac{1}{p_{\perp}} \frac{\partial}{\partial \varphi} \left(\mathbf{A} \cdot \widehat{\perp} \right) \tag{A.241}$$

$$(\nabla_{\mathbf{p}} \times \mathbf{A}) \cdot \widehat{\perp} = \frac{1}{p_{\perp}} \frac{\partial}{\partial \varphi} \left(\mathbf{A} \cdot \widehat{\parallel} \right) - \frac{\partial}{\partial p_{\parallel}} \left(\mathbf{A} \cdot \widehat{\varphi} \right) \tag{A.242}$$

$$(\nabla_{\mathbf{p}} \times \mathbf{A}) \cdot \widehat{\varphi} = \frac{\partial}{\partial p_{\parallel}} \left(\mathbf{A} \cdot \widehat{\perp} \right) - \frac{\partial}{\partial p_{\perp}} \left(\mathbf{A} \cdot \widehat{\parallel} \right) \tag{A.243}$$

A.3.2 System (p, ξ, φ)

Definition

The coordinates (p, ξ, φ) are defined on the space

$$0 \leq p < \infty \tag{A.244}$$

$$-1 \leq \xi < 1 \tag{A.245}$$

$$0 \leq \varphi < 2\pi \tag{A.246}$$

and is related to (p_x, p_y, p_z) by

$$p = \sqrt{p_x^2 + p_y^2 + p_z^2} \tag{A.247}$$

$$\xi = \frac{p_z}{\sqrt{p_x^2 + p_y^2 + p_z^2}} \tag{A.248}$$

$$\varphi = \arctan\left(p_y / p_x\right) + \pi H\left(-p_x\right) \quad [2\pi]$$

which is inverted to

$$\begin{aligned} p_x &= p\sqrt{1-\xi^2}\cos\varphi \\ p_y &= p\sqrt{1-\xi^2}\sin\varphi \\ p_z &= p\xi \end{aligned} \tag{A.249}$$

Note that we have the following transformation from $\left(p_{\parallel}, p_{\perp}\right)$ to (p, ξ)

$$\begin{aligned} p &= \sqrt{p_{\parallel}^2 + p_{\perp}^2} \\ \xi &= \frac{p_{\parallel}}{\sqrt{p_{\parallel}^2 + p_{\perp}^2}} \end{aligned} \tag{A.250}$$

which is inverted to

$$\begin{aligned} p_{\parallel} &= p\xi \\ p_{\perp} &= p\sqrt{1-\xi^2} \end{aligned} \tag{A.251}$$

Position Vector

The position vector in momentum space then becomes

$$\mathbf{P} = p\widehat{p} \tag{A.252}$$

where we define a local orthonormal basis $\left(\widehat{p}, \widehat{\xi}, \widehat{\varphi}\right)$ as

$$\widehat{p} = \sqrt{1-\xi^2}\left(\cos\varphi\,\widehat{x} + \sin\varphi\,\widehat{y}\right) + \xi\,\widehat{z} \tag{A.253}$$

$$\widehat{\xi} = \widehat{\varphi} \times \widehat{p} = \xi\left(\cos\varphi\,\widehat{x} + \sin\varphi\,\widehat{y}\right) - \sqrt{1-\xi^2}\,\widehat{z} \tag{A.254}$$

$$\widehat{\varphi} = -\sin\varphi\,\widehat{x} + \cos\varphi\,\widehat{y} \tag{A.255}$$

Covariant Basis

The covariant vector basis is defined in (A.1), which becomes here

$$\mathbf{e}_p = \frac{\partial \mathbf{P}}{\partial p} = \widehat{p} \tag{A.256}$$

$$\mathbf{e}_{\xi} = \frac{\partial \mathbf{P}}{\partial \xi} = p\frac{\partial \widehat{p}}{\partial \xi} = -\frac{p}{\sqrt{1-\xi^2}}\widehat{\xi} \tag{A.257}$$

$$\mathbf{e}_{\varphi} = \frac{\partial \mathbf{P}}{\partial \varphi} = p\frac{\partial \widehat{p}}{\partial \varphi} = p\sqrt{1-\xi^2}\widehat{\varphi} \tag{A.258}$$

so that we have the covariant basis

$$\left(\mathbf{e}_p, \mathbf{e}_{\xi}, \mathbf{e}_{\varphi}\right) = \left(\widehat{p}, -\frac{p}{\sqrt{1-\xi^2}}\widehat{\xi}, p\sqrt{1-\xi^2}\widehat{\varphi}\right) \tag{A.259}$$

the scaling factors

$$\left(h_p, h_{\xi}, h_{\varphi}\right) = \left(1, -\frac{p}{\sqrt{1-\xi^2}}, p\sqrt{1-\xi^2}\right) \tag{A.260}$$

and the normalized tangent basis

$$\left(\widehat{e}_p, \widehat{e}_{\xi}, \widehat{e}_{\varphi}\right) = \left(\widehat{p}, \widehat{\xi}, \widehat{\varphi}\right) \tag{A.261}$$

Contravariant Basis

The Contravariant vector basis is defined in (A.9), which becomes here

$$\mathbf{e}^p = \nabla p = \frac{\partial p}{\partial \mathbf{P}} = \widehat{p} \tag{A.262}$$

$$\mathbf{e}^\xi = \nabla \xi = \frac{\partial \xi}{\partial \mathbf{P}} = -\frac{\sqrt{1-\xi^2}}{p}\widehat{\xi} \tag{A.263}$$

$$\mathbf{e}^\varphi = \nabla \varphi = \frac{\partial \varphi}{\partial \mathbf{P}} = \frac{1}{p\sqrt{1-\xi^2}}\widehat{\varphi} \tag{A.264}$$

The relations (A.10-A.11) are here readily verified. The reciprocal basis is

$$\left(\mathbf{e}^p, \mathbf{e}^\xi, \mathbf{e}^\varphi\right) = \left(\widehat{p}, -\frac{\sqrt{1-\xi^2}}{p}\widehat{\xi}, \frac{1}{p\sqrt{1-\xi^2}}\widehat{\varphi}\right) \tag{A.265}$$

and the normalized reciprocal basis is

$$\left(\widehat{e}^p, \widehat{e}^\xi, \widehat{e}^\varphi\right) = \left(\widehat{p}, \widehat{\xi}, \widehat{\varphi}\right) \tag{A.266}$$

which here coincides with the normalized tangent basis, since both bases are orthogonal.

Metric Coefficients

They are defined in (A.12) and become here

$$g_{ij} = \begin{pmatrix} 1 & 0 & 0 \\ 0 & p^2/\left(1-\xi^2\right) & 0 \\ 0 & 0 & p^2\left(1-\xi^2\right) \end{pmatrix} \tag{A.267}$$

$$g^{ij} = \begin{pmatrix} 1 & 0 & 0 \\ 0 & \left(1-\xi^2\right)/p^2 & 0 \\ 0 & 0 & 1/\left[p^2\left(1-\xi^2\right)\right] \end{pmatrix}$$

As a result

$$g = p^4 \tag{A.268}$$

and the Jacobian is

$$J = p^2 \tag{A.269}$$

Differential elements

$$dl\left(p\right) = dp \tag{A.270}$$

$$dl\left(\xi\right) = \frac{p}{\sqrt{1-\xi^2}}d\xi \tag{A.271}$$

$$dl\left(\varphi\right) = p\sqrt{1-\xi^2}d\varphi \tag{A.272}$$

$$d\mathbf{S}(p) = p^2 d\xi d\varphi \widehat{p} \tag{A.273}$$
$$d\mathbf{S}(\xi) = -p\sqrt{1-\xi^2} dp d\varphi \widehat{\xi} \tag{A.274}$$
$$d\mathbf{S}(\varphi) = \frac{p}{\sqrt{1-\xi^2}} dp d\xi \widehat{\varphi} \tag{A.275}$$

$$d^3\mathbf{X} = p^2 dp d\xi d\varphi \tag{A.276}$$

Christoffel Symbols

They are defined in (A.49) and are all zero here except

Differential Operations

Gradient

$$\nabla_{\mathbf{p}} f = \frac{\partial f}{\partial p}\widehat{p} - \frac{\sqrt{1-\xi^2}}{p}\frac{\partial f}{\partial \xi}\widehat{\xi} + \frac{1}{p\sqrt{1-\xi^2}}\frac{\partial f}{\partial \varphi}\widehat{\varphi} \tag{A.277}$$

Divergence

$$\nabla_{\mathbf{p}} \cdot \mathbf{A} = \frac{1}{p^2}\frac{\partial}{\partial p}\left(p^2 \mathbf{A}\cdot\widehat{p}\right) - \frac{1}{p}\frac{\partial}{\partial \xi}\left(\sqrt{1-\xi^2}\mathbf{A}\cdot\widehat{\xi}\right) + \frac{1}{p\sqrt{1-\xi^2}}\frac{\partial}{\partial \varphi}\left(\mathbf{A}\cdot\widehat{\varphi}\right) \tag{A.278}$$

Curl

$$(\nabla\times\mathbf{A})\cdot\widehat{p} = \frac{1}{p}\frac{\partial}{\partial \xi}\left(\sqrt{1-\xi^2}\mathbf{A}\cdot\widehat{\varphi}\right) + \frac{1}{p\sqrt{1-\xi^2}}\frac{\partial}{\partial \varphi}\left(\mathbf{A}\cdot\widehat{\xi}\right) \tag{A.279}$$
$$(\nabla\times\mathbf{A})\cdot\widehat{\xi} = \frac{1}{p}\frac{\partial}{\partial p}\left(p\mathbf{A}\cdot\widehat{\varphi}\right) - \frac{1}{p\sqrt{1-\xi^2}}\frac{\partial}{\partial \varphi}\left(\mathbf{A}\cdot\widehat{p}\right)$$
$$(\nabla\times\mathbf{A})\cdot\widehat{\varphi} = -\frac{1}{p}\frac{\partial}{\partial p}\left(p\mathbf{A}\cdot\widehat{\xi}\right) - \frac{\sqrt{1-\xi^2}}{p}\frac{\partial\left(\mathbf{A}\cdot\widehat{p}\right)}{\partial \xi}$$

Appendix B

Calculation of Bounce Coefficients for Circular Concentric FS

B.1 Calculation of $\lambda(\xi_0)$

B.1.1 Series Expansion

The bounce-averaging normalization coefficient is defined in the case of circular concentric flux-surfaces as (2.100)

$$\lambda(\xi_0) = \int_{-\theta_c}^{\theta_c} \frac{d\theta}{2\pi} \frac{\xi_0}{\xi} \tag{B.1}$$

with

$$\theta_c = \begin{cases} \pi & \text{for circulating particles} \\ \theta_T = \cos^{-1}\left(1 - 2\xi_0^2/\xi_{0T}^2\right) & \text{for trapped particles} \end{cases} \tag{B.2}$$

We use the expression of ξ from (2.22):

$$\xi = \sigma\sqrt{1 - \Psi(1 - \xi_0^2)} \tag{B.3}$$

where Ψ has a simple expression for the case of circular flux-surface, given in (2.79):

$$\Psi(r,\theta) = \frac{1+\epsilon}{1+\epsilon\cos(\theta)} \tag{B.4}$$

Defining $\alpha = \theta/2$, we have $\cos(\theta) = 1 - 2\sin^2(\alpha)$ and then (B.4) becomes

$$\begin{aligned} \Psi(r,\theta) &= \frac{1+\epsilon}{1+\epsilon-2\epsilon\sin^2(\alpha)} \\ &= \frac{1}{1-\xi_{0T}^2\sin^2(\alpha)} \end{aligned} \tag{B.5}$$

where ξ_{0T} is the pitch-angle at the trapped passing boundary, defined in (2.24) and $\epsilon = r/R_p$ is the inverse aspect ratio.

Then, with $\alpha_c = \theta_c/2$, (B.1) becomes

$$\begin{aligned}\lambda(\xi_0) &= \int_{-\theta_c}^{\theta_c} \frac{d\theta}{2\pi} \frac{\xi_0}{\sigma\sqrt{1-\Psi(r,\theta)(1-\xi_0^2)}} \\ &= \frac{1}{\pi}\int_0^{\theta_c} d\theta \frac{|\xi_0|}{\sqrt{1-(1-\xi_0^2)/(1-\xi_{0T}^2\sin^2(\alpha))}} \\ &= \frac{2}{\pi}\int_0^{\alpha_c} d\alpha \frac{\sqrt{1-\xi_{0T}^2\sin^2(\alpha)}}{\sqrt{1-\xi_{0T}^2/\xi_0^2\ \sin^2(\alpha)}} \end{aligned} \tag{B.6}$$

We have the following series expansion, valid for $|x| < 1$:

$$\sqrt{1-x} = \sum_{m=0}^{\infty} \chi_m x^m \tag{B.7}$$

with

$$\chi_0 = 1, \qquad \chi_m = \frac{2m-3}{2m}\chi_{m-1} \tag{B.8}$$

Applying (B.7) to $\sqrt{1-\xi_{0T}^2\sin^2(\alpha)}$, (B.6) becomes:

$$\lambda(\xi_0) = \frac{2}{\pi}\sum_{m=0}^{\infty} \chi_m \xi_{0T}^{2m} J_{2m} \tag{B.9}$$

with

$$J_{2m} = \int_0^{\alpha_c} d\alpha \frac{\sin^{2m}(\alpha)}{\sqrt{1-\xi_{0T}^2/\xi_0^2\ \sin^2(\alpha)}} \tag{B.10}$$

B.1.2 Calculation of the Integrals J_{2m}

The integrals J_{2m} can be expressed in terms of complete ellipstic integrals of the first and second kind ([18],[19]):

$$\begin{aligned} K(k^2) &= \int_0^{\pi/2} \frac{d\alpha}{\sqrt{1-k^2\sin^2(\alpha)}} = \int_0^1 \frac{dx}{\sqrt{(1-x^2)(1-k^2x^2)}} \\ E(k^2) &= \int_0^{\pi/2} d\alpha\ \sqrt{1-k^2\sin^2(\alpha)} = \int_0^1 dx\ \frac{\sqrt{(1-k^2x^2)}}{\sqrt{(1-x^2)}} \end{aligned} \tag{B.11}$$

- **For Trapped particles ($|\xi_0| < \xi_{0T}$)**, we have from (B.2):

$$\sin(\alpha_c) = \sin(\theta_T/2) = \sqrt{\frac{1-\cos(\theta_T)}{2}} = \frac{|\xi_0|}{\xi_{0T}} \tag{B.12}$$

so that

$$\begin{aligned} J_0 &= \int_0^{\alpha_c} \frac{d\alpha}{\sqrt{1-\xi_{0T}^2/\xi_0^2\ \sin^2(\alpha)}} \\ &= \int_0^{\sin(\alpha_c)} \frac{dx}{\sqrt{1-x^2}\sqrt{1-\xi_{0T}^2/\xi_0^2\ x^2}} \\ &= \frac{|\xi_0|}{\xi_{0T}} \int_0^1 \frac{dx}{\sqrt{1-\xi_0^2/\xi_{0T}^2\ x^2}\sqrt{1-x^2}} \\ &= \frac{|\xi_0|}{\xi_{0T}} K\left(\frac{\xi_0^2}{\xi_{0T}^2}\right) \end{aligned} \tag{B.13}$$

and

$$\begin{aligned} J_2 &= \int_0^{\alpha_c} d\alpha\ \frac{\sin^2(\alpha)}{\sqrt{1-\xi_{0T}^2/\xi_0^2\ \sin^2(\alpha)}} \\ &= \int_0^{\sin(\alpha_c)} dx\ \frac{x^2}{\sqrt{1-x^2}\sqrt{1-\xi_{0T}^2/\xi_0^2\ x^2}} \\ &= \frac{|\xi_0|}{\xi_{0T}} \int_0^1 dx\ \frac{\xi_0^2/\xi_{0T}^2\ x^2}{\sqrt{1-\xi_0^2/\xi_{0T}^2\ x^2}\sqrt{1-x^2}} \\ &= \frac{|\xi_0|}{\xi_{0T}} \left(\int_0^1 dx\ \frac{1}{\sqrt{1-\xi_0^2/\xi_{0T}^2\ x^2}\sqrt{1-x^2}} - \int_0^1 dx \frac{1-\xi_0^2/\xi_{0T}^2\ x^2}{\sqrt{1-\xi_0^2/\xi_{0T}^2\ x^2}\sqrt{1-x^2}} \right) \\ &= \frac{|\xi_0|}{\xi_{0T}} \left[K\left(\frac{\xi_0^2}{\xi_{0T}^2}\right) - E\left(\frac{\xi_0^2}{\xi_{0T}^2}\right) \right] \end{aligned} \tag{B.14}$$

- **For Circulating particles** ($|\xi_0| > \xi_{0T}$), we have

$$\alpha_c = \frac{\theta_c}{2} = \frac{\pi}{2} \tag{B.15}$$

so that

$$\begin{aligned} J_0 &= \int_0^{\pi/2} \frac{d\alpha}{\sqrt{1-\xi_{0T}^2/\xi_0^2\ \sin^2(\alpha)}} \\ &= \int_0^1 \frac{dx}{\sqrt{1-x^2}\sqrt{1-\xi_{0T}^2/\xi_0^2\ x^2}} \\ &= K\left(\frac{\xi_{0T}^2}{\xi_0^2}\right) \end{aligned} \tag{B.16}$$

and

$$\begin{aligned} J_2 &= \int_0^{\pi/2} d\alpha \, \frac{\sin^2(\alpha)}{\sqrt{1-\xi_{0T}^2/\xi_0^2 \, \sin^2(\alpha)}} \\ &= \int_0^1 dx \, \frac{x^2}{\sqrt{1-x^2}\sqrt{1-\xi_{0T}^2/\xi_0^2 \, x^2}} \\ &= \frac{\xi_0^2}{\xi_{0T}^2}\int_0^1 dx \, \frac{\xi_{0T}^2/\xi_0^2 \, x^2}{\sqrt{1-x^2}\sqrt{1-\xi_{0T}^2/\xi_0^2 \, x^2}} \\ &= \frac{\xi_0^2}{\xi_{0T}^2}\left(\int_0^1 dx \, \frac{1}{\sqrt{1-x^2}\sqrt{1-\xi_{0T}^2/\xi_0^2 \, x^2}} - \int_0^1 dx \frac{1-\xi_{0T}^2/\xi_0^2 \, x^2}{\sqrt{1-x^2}\sqrt{1-\xi_{0T}^2/\xi_0^2 \, x^2}}\right) \\ &= \frac{\xi_0^2}{\xi_{0T}^2}\left[K\left(\frac{\xi_{0T}^2}{\xi_0^2}\right) - E\left(\frac{\xi_{0T}^2}{\xi_0^2}\right)\right] \end{aligned} \tag{B.17}$$

- **For all particles**, the integrals $J_{2m}, m > 1$ can be derived from J_0 and J_2 from the following recursive relation [19]:

$$J_{2m} = \frac{(2m-2)}{(2m-1)}\left(1+\frac{\xi_0^2}{\xi_{0T}^2}\right)J_{2m-2} - \frac{(2m-3)}{(2m-1)}\frac{\xi_0^2}{\xi_{0T}^2}J_{2m-4} \tag{B.18}$$

B.1.3 Truncated Expression

It can be shown in Fig. B.1 that keeping only the two first terms in the expansion is sufficient. Therefore $\lambda(\xi_0)$ can be evaluated with an excellent accuracy using:

$$\lambda(\xi_0) = \frac{2}{\pi}\left(J_0 - \frac{1}{2}\xi_{0T}^2 J_2\right) \tag{B.19}$$

with J_0 and J_2 calculated above.

B.2 Calculation of s^*

The coefficient s^* is defined for circular concentric flux-surfaces as

$$s^* = \int_{-\pi}^{\pi}\frac{d\theta}{2\pi}\frac{R\,(r,0)}{R\,(r,\theta)} = \int_{-\pi}^{\pi}\frac{d\theta}{2\pi}\frac{1+\epsilon}{1+\epsilon\cos(\theta)} \tag{B.20}$$

Defining

$$z = e^{i\theta} \tag{B.21}$$

we get

$$d\theta = \frac{1}{iz}dz, \qquad cos(\theta) = \frac{1}{2}(z+1/z) \tag{B.22}$$

and (B.20) becomes

$$s^* = \frac{2}{\epsilon}\frac{(1+\epsilon)}{2\pi i}\int_\gamma \frac{dz}{z^2+2z/\epsilon+1} \tag{B.23}$$

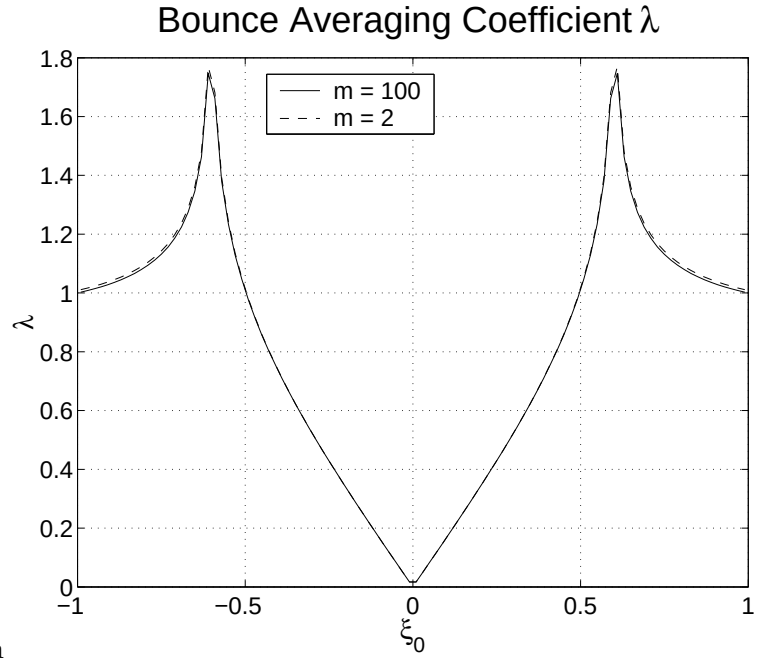

cmcm

Figure B.1: Bounce averaging coefficient λ

where the contour γ is the unity circle in the complex plane.

The two roots of the denominator in (B.23) are

$$z_{\pm} = -\frac{1}{\epsilon}(1 \mp \sqrt{1-\epsilon^2}) \tag{B.24}$$

Only the greater root z_+ lies inside the contour γ, so that (B.23) becomes

$$s^* = \frac{2}{\epsilon}\frac{(1+\epsilon)}{2\pi i}(2\pi i)\mathrm{Res}\left(\frac{1}{z^2+2z/\epsilon+1}, z=z_+\right) \tag{B.25}$$

where

$$\mathrm{Res}\left(\frac{1}{z^2+2z/\epsilon+1}, z=z_+\right) = \frac{1}{z_+ - z_-} = \frac{1}{2/\epsilon\ \sqrt{1-\epsilon^2}} \tag{B.26}$$

is the residue of the integral in (B.23) at $z = z_+$.

Finally, inserting (B.26) in (B.25), we find

$$s^* = H(|\xi_0| > \xi_{0T})\ \sqrt{\frac{1+\epsilon}{1-\epsilon}} \tag{B.27}$$

B.3 Calculation of $\{\Psi\}$

Following the same derivation as forcoefficient λ,

$$\begin{aligned}\{\Psi\} &= \frac{1}{\lambda}\int_{-\theta_c}^{\theta_c}\frac{d\theta}{2\pi}\frac{\xi_0}{\xi}\Psi\left(r,\theta\right)\\ &= \frac{1}{\lambda}\frac{2}{\pi}\int_0^{\pi/2}d\alpha\frac{\sqrt{1-\xi_{0T}^2\sin^2(\alpha)}}{\sqrt{1-\xi_{0T}^2/\xi_0^2\ \sin^2(\alpha)}}\frac{1}{1-\xi_{0T}^2\sin^2(\alpha)}\\ &= \frac{1}{\lambda}\frac{2}{\pi}\int_0^{\pi/2}d\alpha\frac{1}{\sqrt{1-\xi_{0T}^2/\xi_0^2\ \sin^2(\alpha)}\sqrt{1-\xi_{0T}^2\sin^2(\alpha)}}\end{aligned} \tag{B.28}$$

We have teh following series expansion, valid for $|x|<1$,

$$\frac{1}{\sqrt{1-x}}=\sum_{m=0}^{\infty}\widetilde{\chi}_m x^m \tag{B.29}$$

with the recurrence relation

$$\widetilde{\chi}_0=1,\widetilde{\chi}_m=\frac{2m-1}{2m}\widetilde{\chi}_{m-1} \tag{B.30}$$

Applying (B.29) to $1/\sqrt{1-\xi_{0T}^2\sin^2(\alpha)}$, relation (B.28) becomes

$$\{\Psi\}=\frac{1}{\lambda}\frac{2}{\pi}\sum_{m=0}^{\infty}\widetilde{\chi}_m\xi_{0T}^{2m}J_{2m} \tag{B.31}$$

where the integrals J_{2m} is defined in (B.18)

B.4 Calculation of Δ_b

The coefficient Δ_b results from the bounce averaging of the collision operator, as shown in Sec. 4.1.4. Using relation

$$1-\frac{1}{\Psi\left(r,\theta\right)}=\frac{\epsilon}{1+\epsilon}\left(1-\cos\theta\right)=\xi_{0T}^2\frac{1-\cos\theta}{2} \tag{B.32}$$

one obtains

$$\Delta_b=\frac{1}{\lambda}\left[\frac{1}{2}\sum_{\sigma=\pm1}\right]\int_{-\theta_c}^{\theta_c}\frac{d\theta}{2\pi}\frac{\xi_0}{\xi}\xi_{0T}^2\frac{1-\cos\theta}{2} \tag{B.33}$$

The sum over σ, which holds for trapped particles, can be removed since the function to be integrated is independent of σ. Therefore, this integral is very similar to the integral

λ. Noting that $1-\cos\theta = 2\sin^2\alpha$ with $\alpha = \theta/2$, and following the same derivation as for the bounce coefficient λ, we get readily from expression (B.9),

$$\begin{aligned}
\Delta_b &= \frac{1}{\lambda}\int_{-\theta_c}^{\theta_c}\frac{d\theta}{2\pi}\frac{\xi_0}{\xi}\xi_{0T}^2\frac{1-\cos\theta}{2} \\
&= \frac{1}{\lambda}\frac{2}{\pi}\int_0^{\alpha_c} d\alpha \frac{\xi_{0T}^2\sin^2(\alpha)\sqrt{1-\xi_{0T}^2\sin^2(\alpha)}}{\sqrt{1-\xi_{0T}^2/\xi_0^2\ \sin^2(\alpha)}} \\
&= \frac{1}{\lambda}\frac{2}{\pi}\sum_{m=0}^{\infty}\chi_m\xi_{0T}^{2m+2}J_{2m+2}
\end{aligned} \tag{B.34}$$

As for λ, only the two first terms of the expansion need to be kept. The truncated form of Δ_b is therefore

$$\Delta_b \simeq \frac{1}{\lambda}\frac{2}{\pi}\left(\xi_{0T}^2 J_2 + \frac{1}{2}\xi_{0T}^4 J_4\right) \tag{B.35}$$

Appendix C

Effective trapped fraction for Circular Concentric FS

Evaluation of $K(\epsilon)$ if the small ϵ approximation

We can rewrite

$$I(\xi_0) = \frac{1}{(1+\epsilon)} \int_{\xi_{0T}}^{\xi_0} \frac{d\xi_0'}{\lambda_{2,-1,0}(\xi_0')} \tag{C.1}$$

with, for $\xi_0' > \xi_{0T}$,

$$\lambda_{2,-1,0}(\xi_0') = \int_0^{2\pi} \frac{d\theta}{2\pi} \frac{\xi'}{\Psi \xi_0'} \tag{C.2}$$

where

$$\xi' = \sqrt{1 - \Psi\left(1 - \xi_0'^2\right)} \tag{C.3}$$

In the limit $\epsilon \ll 1$, we have

$$\begin{aligned} \Psi &\equiv \frac{1+\epsilon}{1+\epsilon\cos\theta} \\ &= (1+\epsilon)\left[1 - \epsilon\cos\theta + \mathcal{O}\left(\epsilon^2\right)\right] \\ &= 1 + \epsilon(1-\cos\theta) + \mathcal{O}\left(\epsilon^3\right) \end{aligned} \tag{C.4}$$

so that

$$\begin{aligned} \xi' &= \sqrt{1 - \left[1 + \epsilon(1-\cos\theta) + \mathcal{O}(\epsilon^2)\right]\left(1 - \xi_0'^2\right)} \\ &= \xi_0' \sqrt{1 - \epsilon \frac{(1-\cos\theta)\left(1-\xi_0'^2\right)}{\xi_0'^2} + \mathcal{O}(\epsilon^2)} \end{aligned}$$

In fact, the series expansion of the square root must be kept to all orders for the term in ϵ, because the ratio $\epsilon/\xi_0'^2 \to 1$ for $\xi_0' \to \xi_{0T}$. This gives

$$\xi' = \xi_0' \left\{ 1 - \sum_{n=1}^{\infty} \frac{(2n-2)!}{2^{2n-1}(n-1)!n!} \left[\frac{\epsilon(1-\cos\theta)\left(1-\xi_0'^2\right)}{\xi_0'^2} \right]^n + \mathcal{O}\left(\epsilon^2\right) \right\}$$

where we used

$$(1+x)^{\alpha} = 1 + \sum_{n=1}^{\infty} \frac{\alpha\,(\alpha-1)\cdots(\alpha-n+1)}{n!} x^n \tag{C.5}$$

$$(1+x)^{1/2} = 1 + \sum_{n=1}^{\infty} \frac{1}{2}\left(\frac{1}{2}-1\right)\cdots\left(\frac{1}{2}-n+1\right)\frac{x^n}{n!} \tag{C.6}$$

$$= 1 + \frac{1}{2}x + \sum_{n=2}^{\infty} \frac{(-1)^{n-1}}{2^n}\,(1)\,(3)\cdots(2n-3)\,\frac{x^n}{n!} \tag{C.7}$$

$$= 1 + \frac{1}{2}x + \sum_{n=2}^{\infty} \frac{(-1)^{n-1}\,(2n-3)!}{2^{2(n-1)}\,(n-2)!n!} x^n \tag{C.8}$$

$$= 1 + \sum_{n=2}^{\infty} \frac{(-1)^{n-1}\,(2n-2)!}{2^{2n-1}\,(n-1)!n!} x^n \tag{C.9}$$

In addition,

$$\frac{1}{\Psi} = \frac{1}{1+\epsilon\,(1-\cos\theta)+\mathcal{O}\left(\epsilon^2\right)}$$
$$= 1-\epsilon\,(1-\cos\theta)+\mathcal{O}\left(\epsilon^2\right) \tag{C.10}$$

We get

$$\lambda_{2,-1,0}\left(\xi_0'\right) = \int_0^{2\pi}\frac{d\theta}{2\pi}\left\{1-\epsilon\,(1-\cos\theta)-\sum_{n=1}^{\infty}\frac{(2n-2)!}{2^{2n-1}\,(n-1)!n!}\left[\frac{\epsilon\,(1-\cos\theta)\left(1-\xi_0'^2\right)}{\xi_0'^2}\right]^n\right\} \tag{C.11}$$

$$= \int_0^{2\pi}\frac{d\theta}{2\pi}\left\{1-\frac{1}{2}\frac{\epsilon\,(1-\cos\theta)\left(1+\xi_0'^2\right)}{\xi_0'^2}\right.$$
$$\left.-\sum_{n=2}^{\infty}\frac{(2n-2)!}{2^{2n-1}\,(n-1)!n!}\left[\frac{\epsilon\,(1-\cos\theta)\left(1-\xi_0'^2\right)}{\xi_0'^2}\right]^n\right\} \tag{C.12}$$

$$= 1-\sum_{n=1}^{\infty}\lambda_{2,-1,0}^{(n)}\left(\xi_0'\right)+\mathcal{O}\left(\epsilon^2\right) \tag{C.13}$$

with

$$\lambda_{2,-1,0}^{(1)}\left(\xi_0'\right) = \int_0^{2\pi}\frac{d\theta}{2\pi}\frac{\epsilon}{2}\frac{(1-\cos\theta)\left(1+\xi_0'^2\right)}{\xi_0'^2} \tag{C.14}$$

$$= \frac{\epsilon}{2\xi_0'^2}\left(1+\xi_0'^2\right) \tag{C.15}$$

and, for $n \geq 2$,

$$\lambda_{2,-1,0}^{(n\geq 2)}\left(\xi_0'\right) = \int_0^{2\pi} \frac{d\theta}{2\pi} \frac{(2n-2)!\epsilon^n}{2^{2n-1}\,(n-1)!n!} \left[\frac{(1-\cos\theta)\left(1-\xi_0'^2\right)}{\xi_0'^2}\right]^n \tag{C.16}$$

$$= \frac{(2n-2)!\epsilon^n}{2^{2n-1}\,(n-1)!n!} \left[\frac{\left(1-\xi_0'^2\right)}{\xi_0'^2}\right]^n \int_0^{2\pi} \frac{d\theta}{2\pi} (1-\cos\theta)^n \tag{C.17}$$

$$= \frac{(2n-2)!\epsilon^n}{2^{2n-1}\,(n-1)!n!} \left[\frac{\left(1-\xi_0'^2\right)}{\xi_0'^2}\right]^n \int_0^{2\pi} \frac{d\theta}{2\pi} \left[2\sin^2\left(\frac{\theta}{2}\right)\right]^n \tag{C.18}$$

$$= \frac{(2n-2)!\epsilon^n}{2^{n-1}\,(n-1)!n!} \left[\frac{\left(1-\xi_0'^2\right)}{\xi_0'^2}\right]^n \int_0^{\pi} \frac{d\theta}{\pi} \sin^{2n}\theta \tag{C.19}$$

We can transform, for $n \geq 2$,

$$\begin{aligned} Y^n &= \int_0^{\pi} \frac{d\theta}{\pi} \sin^{2n}\theta \\ &= \int_0^{\pi} \frac{d\theta}{\pi} \sin\theta \sin^{2n-1}\theta \\ &= (2n-1)\int_0^{\pi} \frac{d\theta}{\pi} \cos^2\theta \sin^{2(n-1)}\theta \\ &= (2n-1)\left[\int_0^{\pi} \frac{d\theta}{\pi} \sin^{2(n-1)}\theta - \int_0^{\pi} \frac{d\theta}{\pi} \sin^2\theta\right] \\ &= (2n-1)\left[Y^{n-1} - Y^n\right] \end{aligned}$$

so that

$$Y^n = \frac{(2n-1)}{2n} Y^{n-1}$$

with

$$Y^1 = \frac{1}{2}$$

so that

$$\begin{aligned} Y^n &= \frac{(2n-1)}{2n} \frac{(2\,(n-1)-1)}{2\,(n-1)} \cdots \frac{(6-1)}{6} \frac{(4-1)}{4} \frac{1}{2} \\ &= \frac{(2n)!}{\left[2n\,(2n-2)\cdots 2\right]^2} \\ &= \frac{(2n)!}{2^{2n}\,(n!)^2} \end{aligned}$$

and we find

$$\lambda_{2,-1,0}^{(n\geq 2)}\left(\xi_0'\right) = \frac{(2n)!\,(2n-2)!\epsilon^n}{2^{3n-1}\,(n-1)!\,(n!)^3} \left[\frac{\left(1-\xi_0'^2\right)}{\xi_0'^2}\right]^n \tag{C.20}$$

$$= \frac{\left[(2n)!\right]^2\epsilon^n}{(2n-1)\,2^{3n}\,(n!)^4} \left[\frac{\left(1-\xi_0'^2\right)}{\xi_0'^2}\right]^n \tag{C.21}$$

We obtain

$$\begin{aligned} I(\xi_0) &= \frac{1}{(1+\epsilon)} \int_{\xi_{0T}}^{\xi_0} \frac{d\xi_0'}{\lambda_{2,-1,0}(\xi_0')} \\ &= \frac{1}{(1+\epsilon)} \int_{\xi_{0T}}^{\xi_0} d\xi_0' \left[1 + \sum_{m=1}^{\infty} \left[\sum_{n=1}^{\infty} \lambda_{2,-1,0}^{(n)}(\xi_0') \right]^m + \mathcal{O}(\epsilon^2) \right] \\ &= \int_{\xi_{0T}}^{\xi_0} d\xi_0' \left[1 - \epsilon + \sum_{m=1}^{\infty} \left[\sum_{n=1}^{\infty} \lambda_{2,-1,0}^{(n)}(\xi_0') \right]^m + \mathcal{O}(\epsilon^2) \right] \\ &= \xi_0 - \sqrt{2}\epsilon^{1/2} + \sum_{m=1}^{\infty} I_{(m)}(\xi_0) + \mathcal{O}(\epsilon) \end{aligned}$$

with

$$I_{(m)}(\xi_0) = \int_{\xi_{0T}}^{\xi_0} d\xi_0' \left[\sum_{n=1}^{\infty} \lambda_{2,-1,0}^{(n)}(\xi_0') \right]^m$$

where we used

$$\frac{1}{1-x} = 1 + \sum_{m=1}^{\infty} x^m \tag{C.22}$$

$$\xi_{0T} = \sqrt{\frac{2\epsilon}{1+\epsilon}} = \sqrt{2\epsilon} \left[1 - \frac{\epsilon}{2} + \mathcal{O}(\epsilon^2) \right] \tag{C.23}$$

$$\frac{1}{\xi_{0T}} = \frac{1}{\sqrt{2\epsilon}} \left[1 + \frac{\epsilon}{2} + \mathcal{O}(\epsilon^2) \right] \tag{C.24}$$

We have

$$I_{(m)}(\xi_0) = \int_{\xi_{0T}}^{\xi_0} d\xi_0' \left[\frac{\epsilon}{2\xi_0'^2} \left(1 + \xi_0'^2 \right) + \sum_{n=2}^{\infty} \frac{\left[(2n)! \right]^2 \epsilon^n}{(2n-1)\, 2^{3n} (n!)^4} \left[\frac{\left(1 - \xi_0'^2 \right)}{\xi_0'^2} \right]^n \right]^m$$

Clearly, the only term of order $\epsilon^{-1/2}$ comes from the $\xi_0'^{-2}$ contribution integrated and

taken on ξ_{0T}. We need to keep only

$$\begin{aligned}
I_{(m)}(\xi_0) &= \int_{\xi_{0T}}^{\xi_0} d\xi_0' \left[\sum_{n=1}^{\infty} \frac{[(2n)!]^2 \epsilon^n}{(2n-1)\, 2^{3n}\, (n!)^4} \left[\frac{1}{\xi_0'^2}\right]^n\right]^m + \mathcal{O}(\epsilon) \\
&= \int_{\xi_{0T}}^{\xi_0} d\xi_0' \left[\sum_{n=1}^{\infty} \epsilon^n C_n \left[\frac{1}{\xi_0'^2}\right]^n\right]^m + \mathcal{O}(\epsilon) \\
&= \int_{\xi_{0T}}^{\xi_0} d\xi_0' \sum_{i_1=1}^{\infty}\sum_{i_2=1}^{\infty}\cdots\sum_{i_m=1}^{\infty} C_{i_1} C_{i_2} \cdots C_{i_m} \epsilon^{i_1+i_2+\cdots+i_m} \left[\frac{1}{\xi_0'^2}\right]^{i_1+i_2+\cdots+i_m} + \mathcal{O}(\epsilon) \\
&= \sum_{i_1=1}^{\infty}\sum_{i_2=1}^{\infty}\cdots\sum_{i_m=1}^{\infty} C_{i_1} C_{i_2} \cdots C_{i_m} \epsilon^{i_1+i_2+\cdots+i_m} \int_{\xi_{0T}}^{\xi_0} d\xi_0' \left[\frac{1}{\xi_0'^2}\right]^{i_1+i_2+\cdots+i_m} + \mathcal{O}(\epsilon) \\
&= \sum_{i_1=1}^{\infty}\sum_{i_2=1}^{\infty}\cdots\sum_{i_m=1}^{\infty} \frac{C_{i_1} C_{i_2} \cdots C_{i_m} \epsilon^{i_1+i_2+\cdots+i_m}}{2(i_1+i_2+\cdots+i_m)-1} \left[\frac{-1}{\xi_0'^{2(i_1+i_2+\cdots+i_m)-1}}\right]_{\xi_{0T}}^{\xi_0} + \mathcal{O}(\epsilon) \\
&= \sqrt{2}\epsilon^{1/2} \sum_{i_1=1}^{\infty}\sum_{i_2=1}^{\infty}\cdots\sum_{i_m=1}^{\infty} \frac{C_{i_1} C_{i_2} \cdots C_{i_m}}{2^{i_1+i_2+\cdots+i_m}\left[2(i_1+i_2+\cdots+i_m)-1\right]} + \mathcal{O}(\epsilon)
\end{aligned}$$

with

$$C_n = \frac{[(2n)!]^2}{(2n-1)\, 2^{3n}\, (n!)^4}$$

and finally we get

$$I(\xi_0) = \xi_0 - \sqrt{2}\epsilon^{1/2}\left[1 - \sum_{m=1}^{\infty}\sum_{i_1=1}^{\infty}\sum_{i_2=1}^{\infty}\cdots\sum_{i_m=1}^{\infty} \frac{C_{i_1} C_{i_2} \cdots C_{i_m}}{2^{i_1+i_2+\cdots+i_m}\left[2(i_1+i_2+\cdots+i_m)-1\right]}\right] + \mathcal{O}(\epsilon)$$

$$\begin{aligned}
&\int_{-1}^{1} d\xi_0\, \sigma\xi_0 H(|\xi_0| - \xi_{0T})\, I(|\xi_0|) \\
&= 2\int_{\xi_{0T}}^{1} d\xi_0\, \xi_0^2 - \xi_0 \epsilon^{1/2}\sqrt{2} \\
&\quad \times \left[1 - \sum_{m=1}^{\infty}\sum_{i_1=1}^{\infty}\sum_{i_2=1}^{\infty}\cdots\sum_{i_m=1}^{\infty} \frac{C_{i_1} C_{i_2} \cdots C_{i_m}}{2^{i_1+i_2+\cdots+i_m}\left[2(i_1+i_2+\cdots+i_m)-1\right]}\right] + \mathcal{O}(\epsilon) \\
&= \frac{2}{3} - \epsilon^{1/2}\sqrt{2}\left[1 - \sum_{m=1}^{\infty}\sum_{i_1=1}^{\infty}\sum_{i_2=1}^{\infty}\cdots\sum_{i_m=1}^{\infty} \frac{C_{i_1} C_{i_2} \cdots C_{i_m}}{2^{i_1+i_2+\cdots+i_m}\left[2(i_1+i_2+\cdots+i_m)-1\right]}\right] + \mathcal{O}(\epsilon)
\end{aligned}$$

and therefore

$$\boxed{K(\epsilon) = \frac{3\sqrt{2}}{2}\left[1 - \sum_{m=1}^{\infty}\sum_{i_1=1}^{\infty}\sum_{i_2=1}^{\infty}\cdots\sum_{i_m=1}^{\infty} \frac{C_{i_1} C_{i_2} \cdots C_{i_m}}{2^{i_1+i_2+\cdots+i_m}\left[2(i_1+i_2+\cdots+i_m)-1\right]}\right] + \mathcal{O}\left(\epsilon^{1/2}\right)} \tag{C.25}$$

with

$$\boxed{C_n = \frac{[(2n)!]^2}{(2n-1)\,2^{3n}\,(n!)^4}}$$

For example, $C_1 = 1/2$, $C_2 = 3/16$, $C_3 = 5/32$, $\cdots$

m	i_1	i_2	correction
1	1	–	1/4
1	2	–	1/64
1	3	–	1/256
1	4	–	25/16384
1	5	–	17/22737
2	1	1	1/48
2	1	2	$3/1280 \times 2$
2	2	2	9/28672
2	1	3	$5/7168 \times 2$
2	2	3	$5/49152 \times 2$
2	3	3	6/173015

The sum of all these coefficient gives $K = 1.486$, which is already much better that $9\sqrt{2}/8 = 1.591$

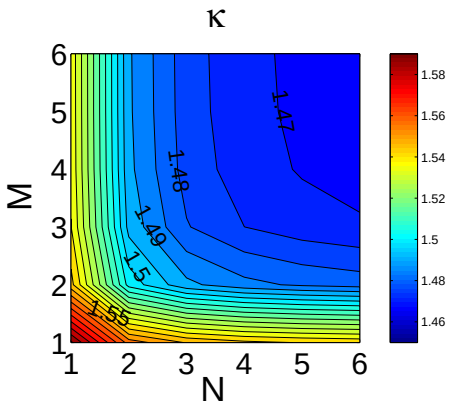

Figure C.1: Bootstrap current coefficient κ as a function of the highest terms M and N kept in the series.

We compute the coefficient K for several values of the highest terms M and N in the series (C.25). The results are shown on Fig. C.1. We first see that K converges for high M and N, towards a value that seems close to 1.46. The best combination seems to be for $M = N$, as both high M and high N are needed for convergence. Therefore, we take $M = N$ and calculate K as a function of M. Results are shown on Fig. C.2. We can see that K indeed converges, and that the asymptotic limit is about $K = 1.46$. For $M = N = 6$, we find $K = 1.467$.

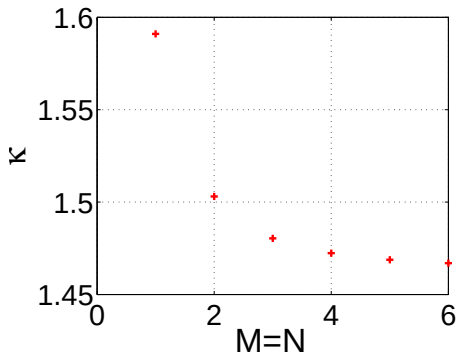

Figure C.2: Bootstrap current coefficient κ as a function of the highest terms M and N kept in the series, for $M = N$

Appendix D

Cold Plasma Model for RF Waves

D.1 Cold Plasma Model

In this section, we use the cold plasma model to calculate the wave properties. This approximation is valid only if the following conditions are satisfied:

- The wave must exist in the cold plasma model, which is not the case of electrons Bernstein waves (EBW). The description of EBW requires a hot plasma model.
- The wave remains far from resonances, where $k_\perp \to \infty$. Near resonances, mode conversion to electrostatic waves (IBW, EBW) occur, which are not described by cold plasma wave theory. LHCD and ECCD usually take place far enough from the LH and UH resonances, respectively, so that the cold plasma description is valid.
- Hot plasma effects, such as the energy flow carried by the coherent motion of particles $\mathbf{\Phi}_{bT}$, must be negligible.
- FLR effects must be small, that is, we must have

$$|z| = \left| \frac{k_\perp v_\perp}{\Omega} \right| \ll 1 \tag{D.1}$$

  This condition generally holds for LHW and ECW as long as the temperature is not too high ($T \leq 10$ keV) and the resonance harmonic is low ($n = 0, 1, 2$).

In the first subsection, we discuss the modeling of RF $k_\parallel$ spectrum. In the second subsection, we use the cold plasma model to calculate wave properties. In the third and fourth subsections, we use further approximations to give analytical formulas for the properties of LHW and ECW. This leads to a simplified description of LHCD and ECCD and allows us to compare our models and results with other codes.

D.1.1 Wave Equation and Dispersion Tensor

We consider the two-fluids description of a non relativistic plasma in a constant magnetic field $\mathbf{B}_0 = B_0 \widehat{z}$. In a continuous homogeneous linear medium, a Fourier component $\mathbf{E}_b\left(\mathbf{k}_b, \omega_b\right)$ verifies the wave equation [43]

$$\mathbf{N}_b \times (\mathbf{N}_b \times \mathbf{E}_b) + \mathbb{K} \cdot \mathbf{E}_b = 0 \tag{D.2}$$

or equivalently

$$(\mathbf{N}_b \cdot \mathbf{E}_b)\mathbf{N}_b - N_b^2 \mathbf{E}_b + \mathbb{K} \cdot \mathbf{E}_b = 0 \tag{D.3}$$

where $\mathbf{N}_b = c\mathbf{k}_b/\omega_b$ is the wave refractive index and $\mathbb{K}$ is the dielectric tensor. This equation can be expressed in tensorial form as

$$\mathbb{D} \cdot \mathbf{E}_b = 0 \tag{D.4}$$

where the dispersion tensor is

$$\mathbb{D} = \mathbf{N}_b \mathbf{N}_b - N_b^2 \mathbb{I} + \mathbb{K} \tag{D.5}$$

By evaluating the susceptibilities in the cold plasma limit, the following dielectric tensor is obtained [44] in the frame (x, y, z):

$$\mathbb{K} = \begin{pmatrix} K_\perp & -iK_{xy} & 0 \\ iK_{xy} & K_\perp & 0 \\ 0 & 0 & K_\parallel \end{pmatrix} \tag{D.6}$$

whose elements in a plasma made of species s are given by

$$\begin{aligned} K_\perp &= 1 - \sum_s \frac{\omega_{ps}^2}{\omega^2 - \omega_{cs}^2} \\ K_\parallel &= 1 - \sum_s \frac{\omega_{ps}^2}{\omega^2} \\ K_{xy} &= -\sum_s \frac{\omega_{ps}^2 \omega_{cs}}{\omega(\omega^2 - \omega_{cs}^2)} \end{aligned} \tag{D.7}$$

where

$$\omega_{ps} = \sqrt{\frac{n_s q_s^2}{\varepsilon_0 m_s}} \tag{D.8}$$

is the plasma frequency and

$$\omega_{cs} = \frac{|q_s|\, B_0}{m_s} \tag{D.9}$$

the cyclotron frequency for the species s.

D.1.2 Dispersion Relation

In order to have a non-trivial solution to the wave equation, the dispersion relation must therefore be satisfied:

$$D(\mathbf{k}_b, \omega_b) = |\mathbb{D}| = 0 \tag{D.10}$$

The axis $\widehat{x}$ is chosen such that

$$\mathbf{N}_b = N_{b\perp}\widehat{x} + N_{b\parallel}\widehat{z} \tag{D.11}$$

Taking the parallel component $N_{b\parallel}$ as given, (D.10) lead to the following equation for $N_{b\perp}$

$$AN_{b\perp}^4 + BN_{b\perp}^2 + C = 0 \tag{D.12}$$

with

$$A = K_\perp \tag{D.13}$$
$$B = \left(N_{b\parallel}^2 - K_\perp\right)\left(K_\perp + K_\parallel\right) + K_{xy}^2 \tag{D.14}$$
$$C = K_\parallel\left[\left(N_{b\parallel}^2 - K_\perp\right)^2 - K_{xy}^2\right] \tag{D.15}$$

or equivalently

$$A = K_\perp \tag{D.16}$$
$$B = \left(K_\perp + K_\parallel\right)N_{b\parallel}^2 - \left(K_R K_L + K_\perp K_\parallel\right) \tag{D.17}$$
$$C = K_{b\parallel}\left(N_{b\parallel}^2 - K_R\right)\left(N_{b\parallel}^2 - K_L\right) \tag{D.18}$$

with

$$K_R = K_\perp + K_{xy} \tag{D.19}$$
$$K_L = K_\perp - K_{xy} \tag{D.20}$$

We find the expression for $N_{b\perp}$ as a function of $N_{b\parallel}$ and ω:

$$N_{b\perp}^2 = \frac{-B \pm \sqrt{B^2 - 4AC}}{2A} \tag{D.21}$$

We see immediately that the resonances occur for $A = 0$, that is,

$$K_\perp = 0 \tag{D.22}$$

and that cut-offs occur for $C = 0$, that is,

$$K_R = N_{b\parallel}^2 \tag{D.23}$$

$$K_L = N_{b\parallel}^2 \tag{D.24}$$

or

$$K_\parallel = 0 \tag{D.25}$$

D.1.3 Polarization components

Once $N_{b\perp}$ has been evaluated, the components of the polarization of the electric field are simply given as the eigenvector of the wave equation (D.4)

$$\mathbb{D} \cdot \mathbf{E}_b = 0 \tag{D.26}$$

D.1.4 Power flow

The relation between power flux and electric field was described using the vector $\mathbf{\Phi}_b$ defined in (4.266)

$$\mathbf{\Phi}_b = \mathbf{\Phi}_{bP} + \mathbf{\Phi}_{bT} \tag{D.27}$$

with (4.269)

$$\mathbf{\Phi}_{bP} = \mathrm{Re}\left[\mathbf{N}_b - (\mathbf{N}_b \cdot \mathbf{e}_b)\,\mathbf{e}_b^*\right] \tag{D.28}$$

and (4.268)

$$\mathbf{\Phi}_{bT} = -\frac{1}{2}\mathbf{e}_b^* \cdot \frac{\partial \mathbb{K}^H}{\partial \mathbf{N}_b} \cdot \mathbf{e}_b \tag{D.29}$$

In the cold plasma model, the dielectric tensor $\mathbb{K}$ is independent of $\mathbf{N}_b$ and the contribution $\mathbf{\Phi}_{bT}$, from the coherent motion of particles, vanishes.

$$\mathbf{\Phi}_{bT} = 0 \tag{D.30}$$

It is usually a very good approximation to neglect this kinetic power flux, even for quasi-electrostatic waves like Lower-Hybrid waves (See D.2.7).

D.1.5 Conclusion

The cold plasma model gives expressions (D.21), (D.26) and (D.28) for the calculation of $N_\perp$, e_b and $\mathbf{\Phi}_b$ respectively. These formulas can be generally used for the calculation of the diffusion coefficient in LHCD and ECCD.

D.2 Lower Hybrid Current Drive

Analytic expression for the properties of LH waves can be obtained in the cold plasma description if further approximations are made. Then, an analytical expression can be obtained for the LH diffusion coefficient.

D.2.1 Electrostatic Dispersion Relation

We consider the wave equation (D.4)

$$(\mathbf{N}_b \cdot \mathbf{E}_b)\mathbf{N}_b - N_b^2\mathbf{E}_b + \mathbb{K} \cdot \mathbf{E}_b = 0 \tag{D.31}$$

The electric field can be separated into its longitudinal and transverse components with respect to the normalized wave vector $\mathbf{N}_b$:

$$\mathbf{E}_b = \mathbf{E}_{bL} + \mathbf{E}_{bT} \tag{D.32}$$

so that the wave equation (D.31) becomes

$$(N_b^2 - \mathbb{K})\mathbf{E}_{bT} - \mathbb{K} \cdot \mathbf{E}_{bL} = 0 \tag{D.33}$$

Electrostatic waves, and also electromagnetic waves approaching resonances, such as LHW, can satisfy the condition

$$N_b^2 \gg |K_{ij}| \tag{D.34}$$

and therefore (D.33) reduces to

$$N_b^2 \mathbf{E}_{bT} - \mathbb{K} \cdot \mathbf{E}_{bL} \simeq 0 \tag{D.35}$$

Dot-multiplying (D.35) by $\widehat{N}_b = \mathbf{N}_b / N_b$ leads to the electrostatic dispersion relation

$$D_L \equiv \widehat{N}_b \cdot \mathbb{K} \cdot \widehat{N}_b = 0 \tag{D.36}$$

and the transverse electric field is given by

$$\mathbf{E}_{bT} = \frac{1}{N_b^2} \mathbb{K} \cdot \mathbf{E}_{bL} \tag{D.37}$$

We note from (D.37) and (D.34) that $|\mathbf{E}_{bT}| \ll |\mathbf{E}_{bL}|$. The electric field is quasi longitudinal, which justify the term electrostatic approximation given to the condition (D.34).

D.2.2 Cold Plasma Limit

Using (D.6), the electrostatic dispersion relation (D.36) in the cold plasma limit is then given by

$$D_L = N_{b\perp}^2 K_\perp + N_{b\parallel}^2 K_\parallel = 0 \tag{D.38}$$

which gives an expression for $N_{b\perp}$ as a function of $N_{b\parallel}$ and ω_b:

$$N_{b\perp}^2 = \frac{-K_\parallel}{K_\perp} N_{b\parallel}^2 \tag{D.39}$$

D.2.3 Lower Hybrid Waves

We consider the lower-hybrid range of frequency in a electron-ion plasma, where the following ordering applies

$$\omega_{ci} \ll \omega_b \ll \omega_{ce} \tag{D.40}$$

Assuming in addition that

$$\omega_b \ll \omega_{pe} \tag{D.41}$$

leads to approximate expressions of the dielectric tensor components given by:

$$K_\perp \simeq 1 + \frac{\omega_{pe}^2}{\omega_{ce}^2} - \frac{\omega_{pi}^2}{\omega_b^2}$$

$$K_\parallel \simeq -\frac{\omega_{pe}^2}{\omega_b^2} \tag{D.42}$$

$$K_{xy} \simeq \frac{\omega_{pe}^2}{\omega_b \omega_{ce}} \tag{D.43}$$

where $K_\perp$ can be rewritten as

$$K_\perp = \left(1 + \frac{\omega_{pe}^2}{\omega_{ce}^2}\right)\left(1 - \frac{\omega_{pi}^2/\omega_b^2}{1 + \omega_{pe}^2/\omega_{ce}^2}\right) \tag{D.44}$$

$$= \left(1 + \frac{\omega_{pe}^2}{\omega_{ce}^2}\right)\left(1 - \frac{\omega_{\mathrm{LH}}^2}{\omega_b^2}\right) \tag{D.45}$$

$$= \frac{\omega_{pi}^2}{\omega_b^2}\left(\frac{\omega_b^2}{\omega_{\mathrm{LH}}^2} - 1\right) \tag{D.46}$$

where

$$\omega_{\mathrm{LH}}^2 = \frac{\omega_{pi}^2}{1 + \omega_{pe}^2/\omega_{ce}^2} \tag{D.47}$$

is the lower hybrid frequency.

The perpendicular index of refraction becomes

$$N_{b\perp}^2 = \frac{\omega_{pe}^2/\omega_{pi}^2}{\left(\omega_b^2/\omega_{\mathrm{LH}}^2 - 1\right)} N_{b\parallel}^2 \tag{D.48}$$

We recognize that $N_{b\perp} \to \infty$ as the the lower-hybrid frequency approaches the wave frequency. However, in most LHCD scenarios, wave frequency are sensibly higher than the lower-hybrid frequency in order to avoid conversion to IBW. Typically, in Alcator C-Mod, we have

$$\frac{\omega_b}{\omega_{\mathrm{LH}}} \sim 2 \text{ or } 3 \tag{D.49}$$

In that case, and as shown in D.2.7, the contribution of $\mathbf{\Phi}_{bT}$ to the power flow can be neglected. The cold plasma description therefore remains valid.

D.2.4 Polarization

The LH Waves of concern for LHCD are quasi-electrostatic, and therefore the electric field is quasi-longitudinal ($\mathbf{E}_b \parallel \mathbf{N}_b$) and we have

$$e_{b,i} = \frac{E_{b,i}}{|\mathbf{E}_b|} \simeq \frac{k_{b,i}}{|\mathbf{k}_b|} \tag{D.50}$$

for any component i, so that the polarization elements become

$$e_{b,+} \equiv \frac{E_{b,x} + iE_{b,y}}{\sqrt{2}\,|\mathbf{E}_b|} = \frac{k_{b\perp}}{\sqrt{2}k_b}\left(\cos\alpha + i\sin\alpha\right) = \frac{k_{b\perp}}{\sqrt{2}k_b}e^{+i\alpha} \tag{D.51}$$

$$e_{b,-} \equiv \frac{E_{b,x} - iE_{b,y}}{\sqrt{2}\,|\mathbf{E}_b|} = \frac{k_{b\perp}}{\sqrt{2}k_b}\left(\cos\alpha - i\sin\alpha\right) = \frac{k_{b\perp}}{\sqrt{2}k_b}e^{-i\alpha}$$

$$e_{b,\parallel} \equiv \frac{E_{b,z}}{|\mathbf{E}_b|} = \frac{k_{b\parallel}}{k_b}$$

D.2.5 Determination of $\Theta_{\mathbf{k}}^{b,\mathbf{LH}}$

Lower Hybrid Current Drive (LHCD) results from momentum exchange from the LH wave to the plasma through Landau damping (harmonic $n = 0$). In this case, the coefficient (4.290) becomes

$$\Theta_{\mathbf{k}}^{b,0} = \frac{1}{\sqrt{2}} e_{b,+} e^{-i\alpha} J_{-1}\left(\frac{k_{b\perp} v_\perp}{\Omega}\right) + \frac{1}{\sqrt{2}} e_{b,-} e^{+i\alpha} J_1\left(\frac{k_{b\perp} v_\perp}{\Omega}\right) + \frac{p_\parallel}{p_\perp} e_{b,\parallel} J_0\left(\frac{k_{b\perp} v_\perp}{\Omega}\right) \tag{D.52}$$

$$= \frac{1}{\sqrt{2}} \left(e_{b,-} e^{+i\alpha} - e_{b,+} e^{-i\alpha}\right) J_1\left(\frac{k_{b\perp} v_\perp}{\Omega}\right) + \frac{p_\parallel}{p_\perp} e_{b,\parallel} J_0\left(\frac{k_{b\perp} v_\perp}{\Omega}\right) \tag{D.53}$$

Using (D.51), we see that the perpendicular components cancel and we are left with

$$\Theta_{\mathbf{k}}^{b,\mathrm{LH}} = \frac{p_\parallel}{p_\perp} \frac{k_{b\parallel}}{k_b} J_0\left(\frac{k_{b\perp} v_\perp}{\Omega}\right) \tag{D.54}$$

The argument of the Bessel function in (D.54) is

$$\frac{k_{b\perp} v_\perp}{\Omega} = N_{b\perp} \frac{v_\perp}{c} \frac{\omega_b}{\Omega} \tag{D.55}$$

where an expression for $N_\perp$ is given by (D.48). The argument of the Bessel function becomes

$$\frac{k_{b\perp} v_\perp}{\Omega} = \frac{1}{\sqrt{\omega_b^2/\omega_{\mathrm{LH}}^2 - 1}} \frac{\omega_{pe}}{\omega_{pi}} \frac{\omega_b}{\omega_{ce}} N_{b\parallel} \frac{p_\perp}{p_{Te}} \beta_{Te} \tag{D.56}$$

and we see that for $\omega_{pe} \sim \omega_{ce}$ and $\omega_b \sim 2\omega_{\mathrm{LH}}$, we get

$$\left|\frac{k_{b\perp} v_\perp}{\Omega}\right| \sim \beta_{Te} N_{b\parallel} \frac{p_\perp}{p_{Te}} \tag{D.57}$$

Given that most electrons concerned with LHCD have $p_\perp \sim p_{Te}$, and that for LHCD we have typically $N_{b\parallel} \sim 2$, we see that it is reasonable to take the limit

$$\left|\frac{k_{b\perp} v_\perp}{\Omega}\right| \ll 1 \tag{D.58}$$

as long as the plasma is not too relativistic ($\beta_{Te} \ll 1$). This limit is consistent with the validity condition of the cold plasma description. In this limit, valid for most LHCD scenarios, we have

$$\Theta_{\mathbf{k}}^{b,\mathrm{LH}} \simeq \frac{p_\parallel}{p_\perp} \frac{k_{b\parallel}}{k_b} \tag{D.59}$$

D.2.6 Determination of $\mathbf{\Phi}_{bP}^{\mathbf{LH}}$

The vector $\mathbf{\Phi}_b^{\mathrm{LH}}$ describes the relation between the energy flux and the electric field. Although LHW are almost electrostatic, the dominant contribution to the power flux is the wave Poynting flux $\mathbf{\Phi}_{bP}^{\mathrm{LH}}$, assuming that the wave frequency remains sensibly higher

than the LH frequency. The contribution of the Kinetic power flux is calculated in D.2.7. In most LHCD scenarios, this contribution is not more than a few percents of the total flux and can therefore be neglected. We have (D.28).

$$\mathbf{\Phi}_{bP} = \mathrm{Re}\left[|e_{bT}|^2 \mathbf{N}_b - N_b e_{bL} \mathbf{e}_{bT}^*\right] \tag{D.60}$$

LH waves are quasi-electrostatic, so that the longitudinal and transverse components are given by (D.37)

$$e_{bL} \simeq 1 \tag{D.61}$$

$$\mathbf{e}_{bT} = \frac{1}{N_b^2} \mathbb{K} \cdot \mathbf{e}_{bL} \tag{D.62}$$

so that the first term in (D.60) can be neglected, and

$$\begin{aligned} \mathbf{\Phi}_{bP}^{\mathrm{LH}} &\simeq \mathrm{Re}\left(-e_{bL} \frac{1}{N_b} \mathbb{K}^* \cdot \mathbf{e}_{bL}^*\right) \\ &= \mathrm{Re}\left(-\frac{1}{N_b} \mathbb{K}^* \cdot \widehat{N}\right) \end{aligned} \tag{D.63}$$

Note from (D.63) and (D.36) that the Poynting flux is in the direction perpendicular to the wave vector:

$$\mathbf{\Phi}_{bP}^{\mathrm{LH}} \cdot \widehat{N} = 0 \tag{D.64}$$

We finally find, using (D.6),

$$\mathbf{\Phi}_{bP}^{\mathrm{LH}} = -\frac{1}{N_b^2} \left(K_\perp \mathbf{N}_{b\perp} + K_\parallel N_{b\parallel} \widehat{z}\right) \tag{D.65}$$

D.2.7 Determination of $\mathbf{\Phi}_{bT}^{\mathrm{LH}}$

In the analysis above the kinetic part of the power flux, due to the coherent motion of charge carriers, has been neglected. This approximation must be justified by comparing the Poynting and the kinetic fluxes.

The normalized expression for the kinetic power flux associated with an electromagnetic wave in a kinetic plasma is given by (4.268)

$$\mathbf{\Phi}_{bT} = -\frac{\omega_b}{2c} \mathbf{e}_b^* \cdot \frac{\partial \mathbb{K}^H}{\partial \mathbf{k}} \cdot \mathbf{e}_b \tag{D.66}$$

Electrostatic Waves

In the electrostatic approximation, the electric field is quasi-longitudinal (D.37)

$$|\mathbf{e}_{bT}| \ll e_{bL} \simeq 1 \tag{D.67}$$

and (D.66) becomes

$$\mathbf{\Phi}_{bT} = -\frac{\omega_b}{2c} \widehat{k}_b \cdot \frac{\partial \mathbb{K}^H}{\partial \mathbf{k}} \cdot \widehat{k}_b \tag{D.68}$$

In the frame of the wave vector $\widehat{k}_b$, (D.68) can then be expressed as

$$\mathbf{\Phi}_{bT} = -\frac{\omega_b}{2c}\frac{\partial K_L^H}{\partial k}\widehat{k}_b \tag{D.69}$$

where

$$K_L = \widehat{k}_b \cdot \mathbb{K} \cdot \widehat{k}_b \tag{D.70}$$

is the longitudinal (electrostatic) component of the dielectric tensor.

Lower Hybrid Waves

An expression of the electrostatic dispersion relation for LH waves that includes the first-order thermal corrections is given by [45]:

$$K_L^{\mathrm{LH}}(\omega, k_b) \simeq 1 + \frac{k_{b\perp}^2}{k_b^2}\frac{\omega_{pe}^2}{\omega_{ce}^2}\left(1 - \frac{3b_e}{4}\right) - \frac{k_{b\perp}^2}{k_b^2}\frac{\omega_{pi}^2}{\omega_b^2}\left(1 + \frac{3b_i\omega_{ci}^2}{\omega_b^2}\right) - \frac{k_{b\parallel}^2}{k_b^2}\frac{\omega_{pe}^2}{\omega_b^2} \tag{D.71}$$

where the finite Larmor radius (FRL) effects are scaled by the parameters

$$b_e = \frac{k_{b\perp}^2 v_{Te}^2}{\omega_{ce}^2}, \qquad b_i = \frac{k_{b\perp}^2 v_{Ti}^2}{\omega_{ci}^2} \tag{D.72}$$

with $v_T^2 = T/m$.

The k-dependence of the dispersion relation is found in the thermal correction terms so that

$$\frac{\partial K_L^{\mathrm{LH}}}{\partial k} = -\frac{3}{4}\frac{k_{b\perp}^4}{k_b^4}\frac{\omega_{pe}^2}{\omega_{ce}^2}\frac{2k_b v_{Te}^2}{\omega_{ce}^2} - \frac{k_{b\perp}^4}{k_b^4}\frac{\omega_{pi}^2}{\omega_b^2}\frac{3\omega_{ci}^2}{\omega_b^2}\frac{2k_b v_{Ti}^2}{\omega_{ci}^2} \tag{D.73}$$

Inside the plasma, we have $k_{b\parallel}^2 \ll k_{b\perp}^2$ and therefore $k_{b\perp}^2/k_b^2 \simeq 1$. We finally get the following expression for the kinetic flux associated with quasi-electrostatic LH waves:

$$\mathbf{\Phi}_{bT}^{\mathrm{LH}} = \frac{1}{N_b}\left(\frac{1}{4}\frac{\omega_{pe}^2 k_b^2 v_{Te}^2}{\omega_{ce}^4} + \frac{\omega_{pi}^2 k_b^2 v_{Ti}^2}{\omega_b^4}\right)\widehat{k}_b \tag{D.74}$$

The kinetic flux is oriented in the direction of the wave vector, and the incident flux on the flux surface

$$\left|\mathbf{\Phi}_{bT}^{\mathrm{LH}} \cdot \widehat{\psi}\right| = \frac{1}{N_b}\left(\frac{1}{4}\frac{\omega_{pe}^2 k_b^2 v_{Te}^2}{\omega_{ce}^4} + \frac{\omega_{pi}^2 k_b^2 v_{Ti}^2}{\omega_b^4}\right)\left|\widehat{k}_b \cdot \widehat{\psi}\right| \tag{D.75}$$

This incident kinetic flux must be compared to the incident Poynting flux taken in the cold plasma limit from (D.65)

$$\left|\mathbf{\Phi}_{bP}^{\mathrm{LH}} \cdot \widehat{\psi}\right| = \frac{K_\perp}{N_b^2}\left|\mathbf{N}_{b\perp} \cdot \widehat{\psi}\right| \simeq \frac{K_\perp}{N_b}\left|\widehat{k}_b \cdot \widehat{\psi}\right| \tag{D.76}$$

The ratio of the incident kinetic power flux to the Poynting flux is given by

$$\frac{\left|\mathbf{\Phi}_{bT}^{\mathrm{LH}} \cdot \widehat{\psi}\right|}{\left|\mathbf{\Phi}_{bP}^{\mathrm{LH}} \cdot \widehat{\psi}\right|} = \frac{1}{K_\perp}\left(\frac{3}{4}\frac{\omega_{pe}^2 v_{Te}^2 k_b^2}{\omega_{ce}^4} + 3\frac{\omega_{pi}^2 v_{Ti}^2 k_b^2}{\omega_b^4}\right) \tag{D.77}$$

Using (D.39) we have

$$k_b^2 \simeq \frac{\omega_b^2}{c^2} N_{b\perp}^2 \simeq \frac{\omega_b^2}{c^2} \frac{\left(-K_\parallel\right)}{K_\perp} N_{b\parallel}^2 \simeq \frac{1}{K_\perp} \frac{\omega_{pe}^2}{c^2} N_{b\parallel}^2 \tag{D.78}$$

so that

$$\frac{\mathbf{\Phi}_{bT\perp}^{\mathrm{LH}}}{\mathbf{\Phi}_{bP\perp}^{\mathrm{LH}}} = \frac{3\beta_{Te}^2 N_{b\parallel}^2}{(1+\omega_{pe}^2/\omega_{ce}^2)(1-\omega_{\mathrm{LH}}^2/\omega_b^2)} \left(\frac{1}{4} \frac{\omega_{pe}^4}{\omega_{ce}^4} + \frac{\omega_{pi}^4}{\omega_b^4} \frac{T_i}{T_e} \right) \tag{D.79}$$

where $\beta_{Te}^2 = T_e/mc^2$.

It can be seen from (D.79) that the kinetic part of the power flux becomes significant only as the wave approaches the lower-hybrid resonance very closely. In a typical LHCD context (for instance Alcator C-Mod, [46]), we have

$$\omega_b \sim 2\omega_{\mathrm{LH}},\ \omega_{pe} \sim \Omega_e,\ \omega_{pi} \sim \omega,\ T_e \sim T_i \text{ and } \beta_{Te} \sim 0.1 \tag{D.80}$$

so that the kinetic part of the power flux is not more than a few percents.

D.2.8 LH Diffusion Coefficient

General expression in small FLR limit and ES approximation

The normalized bounce-averaged diffusion coefficient for the Fokker-Planck equation is given by (4.313)

$$\begin{aligned} \overline{D}_b^{\mathrm{LH}(0)}(p,\xi_0) = {} & \frac{\gamma p_{Te}}{p\left|\xi_0\right|} \frac{1}{\lambda \widetilde{q}} \frac{r_{\theta_b}}{R_p} \frac{B^{\theta_b}}{B_P^{\theta_b}} \frac{\xi_0^2}{\xi_{\theta_b}^2} \Psi_{\theta_b} \overline{D}_{b,0}^{\mathrm{LH},\theta_b} \times \\ & H\left(\theta_b - \theta_{\min}\right) H\left(\theta_{\max} - \theta_b\right) \left[\frac{1}{2}\sum_\sigma\right]_T \delta\left(N_{b\parallel} - N_{\parallel\mathrm{res}}^{\theta_b \mathrm{LH}}\right) \left|\Theta_{\mathbf{k},\theta_b}^{b,\mathrm{LH}}\right|^2 \end{aligned} \tag{D.81}$$

with

$$\overline{D}_{b,0}^{\mathrm{LH},\theta_b} = \frac{1}{r_{\theta_b} R_{\theta_b}} \frac{1}{m_e \ln\Lambda} \frac{1}{\omega_b \omega_{pe}^2} \frac{f_{\mathrm{inc},b}^{l+1/2}}{\left|\mathbf{\Phi}_b^{\mathrm{LH}}\right|} P_{b,\mathrm{inc}} \tag{D.82}$$

$$N_{\parallel\mathrm{res}}^{\theta_b \mathrm{LH}} = \frac{1}{\beta_{Te}} \frac{\gamma p_{Te}}{p \xi_{\theta_b}} \tag{D.83}$$

Within the electrostatic approximation and in the small FLR limit, we have obtained the following expressions for the LHW properties (D.59), (D.39), (D.65)

$$\Theta_{\mathbf{k},\theta_b}^{b,\mathrm{LH}} = \frac{\xi_{\theta_b}}{\sqrt{\Psi_{\theta_b}\left(1-\xi_0^2\right)}} \frac{N_{b\parallel}}{N_b} \tag{D.84}$$

$$N_{b\perp} = \sqrt{\frac{-K_\parallel}{K_\perp}} N_{b\parallel} \tag{D.85}$$

$$\mathbf{\Phi}_b^{\mathrm{LH}} = -\frac{1}{N_b^2}\left(K_\perp \mathbf{N}_{b\perp} + K_\parallel N_{b\parallel} \widehat{z}\right) \tag{D.86}$$

so that

$$\left|\mathbf{\Phi}_b^{\mathrm{LH}}\right| = \frac{1}{N_b^2}\sqrt{K_\perp^2 N_{b\perp}^2 + K_\parallel^2 N_{b\parallel}^2} \tag{D.87}$$

$$\simeq \frac{N_{b\parallel}}{N_b^2}\left|K_\parallel\right| \tag{D.88}$$

$$= \frac{K_\perp}{N_{b\parallel}} \tag{D.89}$$

and where $K_\perp$ and $K_\parallel$ are given by (D.44) and (D.42) respectively

Simplified expression for LHCD

We consider the limit of a large aspect ratio tokamak with circular flux-surfaces (limit of a cylindrical plasma). In that case, $r_{\theta_b}/R_p \to 0$ and the effects of magnetic trapping disppear. We can use the following asymptotic expressions

$$\Psi_{\theta_b} \to 1 \tag{D.90}$$

$$\lambda\left(\psi, \xi_0\right) \to 1 \tag{D.91}$$

$$\frac{1}{\widetilde{q}}\frac{r_{\theta_b}}{R_p}\frac{B^{\theta_b}}{B_P^{\theta_b}} \to 1 \tag{D.92}$$

$$\frac{\xi_{\theta_b}}{\xi_0} \to 1 \tag{D.93}$$

Because of cylindrical symmetry, the dependence θ_b on disappears.

The QL diffusion coefficient for LHCD (D.81) can therefore be written as

$$\overline{D}_b^{\mathrm{LH}(0)}(p,\xi_0) = \frac{\gamma p_{Te}}{p\left|\xi_0\right|}\frac{\xi_0^2}{\left(1-\xi_0^2\right)}\frac{K_\perp}{\left(-K_\parallel\right)}\overline{D}_{b,0}^{\mathrm{LH}}\frac{1}{\Delta N_{b\parallel}}H\left(N_{\parallel\mathrm{res}}^{\mathrm{LH}} - N_{b\parallel\,\min}\right)H\left(N_{b\parallel\,\max} - N_{\parallel\mathrm{res}}^{\mathrm{LH}}\right) \tag{D.94}$$

with

$$\overline{D}_{b,0}^{\mathrm{LH}} = \frac{1}{rR_p}\frac{1}{m_e\ln\Lambda}\frac{1}{\omega_b\omega_{pe}^2}\frac{N_{b\parallel,0}}{K_\perp}f_{\mathrm{inc},b}^{l+1/2}P_{b,\mathrm{inc}} \tag{D.95}$$

$$N_{\parallel\mathrm{res}}^{\mathrm{LH}} = \frac{1}{\beta_{Te}}\frac{\gamma p_{Te}}{p\xi_0} \tag{D.96}$$

and where we used $N_b \simeq N_{b\perp}$ and assume a square power spectrum as in (4.333).

In order to compare with LHCD operators found in the litterature, we redefine the LH constant factor such that

$$\overline{D}_b^{\mathrm{LH}(0)}(p,\xi_0) = \frac{\gamma p_{Te}}{p\left|\xi_0\right|}\frac{\xi_0^2}{\left(1-\xi_0^2\right)}\overline{D}_{b,0,\mathrm{new}}^{\mathrm{LH}}H\left(N_{\parallel\mathrm{res}}^{\mathrm{LH}} - N_{b\parallel\,\min}\right)H\left(N_{b\parallel\,\max} - N_{\parallel\mathrm{res}}^{\mathrm{LH}}\right) \tag{D.97}$$

with

$$\overline{D}_{b,0,\mathrm{new}}^{\mathrm{LH}} = \frac{N_{b\parallel,0}^2}{N_{b\perp,0}^2}\frac{1}{\Delta N_{b\parallel}}\overline{D}_{b,0}^{\mathrm{LH}} \tag{D.98}$$

$$= \frac{1}{rR_p}\frac{1}{m_e\ln\Lambda}\frac{\omega_b}{\omega_{pe}^4}\frac{N_{b\parallel,0}}{\Delta N_{b\parallel}}f_{\mathrm{inc},b}^{l+1/2}P_{b,\mathrm{inc}} \tag{D.99}$$

A familiar expression for the LH QL operator is obtained in cylindrical geometry. From (4.221) and (4.224-4.227) we see that for LHCD, the QL operator can be rewritten as

$$\begin{aligned} Q^{\mathrm{LH}}(f) &= \frac{\partial}{\partial p_\parallel} D_{\parallel\parallel}^{\mathrm{RF}} \frac{\partial f}{\partial p_\parallel} \\ &= \sum_b \frac{\partial}{\partial p_\parallel} \overline{D}_{b,0,\mathrm{new}}^{\mathrm{LH}} \frac{v_{Te}}{|v_\parallel|} H\left(\frac{c}{v_\parallel} - N_{b\parallel\,\min}\right) H\left(N_{b\parallel\,\max} - \frac{c}{v_\parallel}\right) \frac{\partial f}{\partial p_\parallel} \end{aligned} \tag{D.100}$$

Although it is better to keep the exact formula (D.100), the factor $v_{Te}/|v_\parallel|$ has often been neglected in the litterature, which is an acceptable approximation when $\overline{D}_{b,0,\mathrm{new}}^{\mathrm{LH}} \gg \nu_e p_{Te}^2$ and $\Delta N_{b\parallel} \ll N_{b\parallel\,\min}$. In this case, considering only one ray b, the LH Operator reduces to

$$Q^{\mathrm{LH}}(f) \simeq \begin{cases} \dfrac{\partial}{\partial p_\parallel} \overline{D}_{0,\mathrm{new}}^{\mathrm{LH}} \dfrac{\partial f}{\partial p_\parallel} & \text{for } v_1 < \dfrac{v_\parallel}{v_{Te}} < v_2 \\ 0 & \text{otherwise} \end{cases} \tag{D.101}$$

with

$$v_1 = \frac{1}{\beta_{Te} N_{\parallel\,\max}} \tag{D.102}$$

$$v_2 = \frac{1}{\beta_{Te} N_{\parallel\,\min}} \tag{D.103}$$

$$\overline{D}_{0,\mathrm{new}}^{\mathrm{LH}} = \overline{\left[\frac{v_{Te}}{|v_\parallel|}\right]} \overline{D}_{b,0,\mathrm{new}}^{\mathrm{LH}} \tag{D.104}$$

$$= \frac{1}{rR_p} \frac{1}{|(v_1+v_2)/2|} \frac{1}{m_e \ln\Lambda} \frac{\omega}{\omega_{pe}^4} \frac{N_{\parallel,0}}{\Delta N_\parallel} f_{\mathrm{inc}}^{l+1/2} P_{\mathrm{inc}} \tag{D.105}$$

where $\overline{\left[\frac{v_{Te}}{|v_\parallel|}\right]}$ is an averaged value of $\frac{v_{Te}}{|v_\parallel|}$ which can be taken to be $\frac{1}{\beta_{Te} N_{\parallel,0}}$ and then

$$\overline{D}_{0,\mathrm{new}}^{\mathrm{LH}} = \frac{1}{rR_p} \frac{1}{\beta_{Te}} \frac{1}{m_e \ln\Lambda} \frac{\omega}{\omega_{pe}^4} \frac{1}{\Delta N_\parallel} f_{\mathrm{inc}}^{l+1/2} P_{\mathrm{inc}} \tag{D.106}$$

D.3 Electron Cyclotron Current Drive

The cold plasma description is usually a good approximation to determine the ECW properties, as long as we stay away from the upper-hybrid resonance, where mode-conversion to EBW occurs. However, even in the cold plasma model, the polarizations are usually mixed for oblique propagation, and no simple analytical formulation is possible. Still, it is possible to find limit cases (small FLR effects, small $N_\parallel$) for which a simple analytical derivation is possible.

D.3.1 Polarization

In the case of mostly perpendicular propagation, where $|N_\parallel| \ll 1$, the two modes are the quasi-X and quasi-O modes.

The polarization is mostly right-hand circular for X and parallel linear for O. The only exception is for the X mode near the first harmonic $n = 1$ where $e^{\mathrm{X}}_{b,-} \simeq 0$. For this reason, the first-harmonic is almost transparent to the X-mode and this resonance is usually not considered. Moreover, this harmonic can only be reached from the high field side, because of the right-hand cut-off. From now, we consider only the X mode with $n \geq 2$.

D.3.2 Determination of $\Theta^{b,\mathbf{EC}}_{\mathbf{k}}$

Small FLR limit

Electron Cyclotron Current Drive (ECCD) results from momentum exchange from the EC wave to the plasma through electron cyclotron damping at some harmonic n. For a ray b, considering a given harmonic n, the coefficient (4.290) is

$$\Theta^{b,n}_{\mathbf{k}} = \frac{1}{\sqrt{2}} e_{b,+} e^{-i\alpha} J_{n-1}(z_b) + \frac{1}{\sqrt{2}} e_{b,-} e^{+i\alpha} J_{n+1}(z_b) + \frac{p_\parallel}{p_\perp} e_{b,\parallel} J_n(z_b) \tag{D.107}$$

where $z_b = k_{b\perp} v_\perp / \Omega$.

Since the resonance condition is $\omega_b - k_{b\parallel} v_\parallel - n\Omega = 0$ and

$$\Omega = \frac{q_e B}{\gamma m_e} = -\frac{\omega_{ce}}{\gamma} < 0 \tag{D.108}$$

the only harmonics to be considered for electrons are for

$$n \leq -1 \tag{D.109}$$

Applying the substitution

$$n' = -n \geq 1 \tag{D.110}$$

and renaming $n' \to n \geq 0$, we get

$$\begin{aligned}
\Theta^{b,\mathrm{EC}n}_{\mathbf{k}} &= \frac{1}{\sqrt{2}} e_{b,+} e^{-i\alpha} J_{-n-1}(z_b) + \frac{1}{\sqrt{2}} e_{b,-} e^{+i\alpha} J_{-n+1}(z_b) + \frac{p_\parallel}{p_\perp} e_{b,\parallel} J_{-n}(z_b) \\
&= \frac{1}{\sqrt{2}} e_{b,+} e^{-i\alpha} (-1)^{n+1} J_{n+1}(z_b) + \frac{1}{\sqrt{2}} e_{b,-} e^{+i\alpha} (-1)^{n-1} J_{n-1}(z_b) \\
&\quad + \frac{p_\parallel}{p_\perp} e_{b,\parallel} (-1)^n J_n(z_b)
\end{aligned} \tag{D.111}$$

We have

$$z_b = \frac{k_{b\perp} v_\perp}{\Omega} = -N_{b\perp} \frac{p_\perp}{m_e c} \frac{\omega_b}{\omega_{ce}} \tag{D.112}$$

Using $\omega_b \sim n\omega_{ce}$, we get an estimation for $|z_b|$

$$|z_b| \sim n N_{b\perp} \frac{p_\perp}{p_{Te}} \beta_{Te} \tag{D.113}$$

Typically, for ECCD in tokamaks, we have

$$N_{b\perp} \lesssim 1, \ \beta_{Te} \lesssim 0.1 \tag{D.114}$$

and most electrons of concern have

$$\frac{p_\perp}{p_{Te}} \leq 3 \tag{D.115}$$

so that for low harmonics, the condition $|z_b| \ll 1$ is satisfied. In other words, the Larmor radius remains small compared to the perpendicular wavelength. This condition is consistent with the conditions of the cold plasma description of the EC waves. From now on, we assume $|z_b| \ll 1$, which is the : limit of small FLR effects.

In this case, for $n \geq 0$, the following approximate expression can be used

$$J_n(z) \simeq \frac{1}{n!}\left(\frac{z}{2}\right)^n \tag{D.116}$$

and we have

$$\begin{aligned}\Theta_{\mathbf{k}}^{b,\mathrm{EC}n} \simeq & \frac{e_{b,+}}{\sqrt{2}} e^{-i\alpha}(-1)^{n+1}\frac{1}{(n+1)!}\left(\frac{z_b}{2}\right)^{n+1} + \frac{e_{b,-}}{\sqrt{2}} e^{+i\alpha}(-1)^{n-1}\frac{1}{(n-1)!}\left(\frac{z_b}{2}\right)^{n-1} \\ & + \frac{p_\parallel}{p_\perp} e_{b,\parallel}\frac{1}{n!}\left(\frac{z_b}{2}\right)^n \end{aligned} \tag{D.117}$$

X-mode, $n \geq 2$

Because $e_{b,-}$ is the dominant polarization component and $|z_b| \ll 1$, the second term in the sum in (D.117) is largely dominant. We obtain

$$\Theta_{\mathbf{k}}^{b,\text{EC-Xn}} \simeq e^{+i\alpha}\frac{e_{b,-}}{\sqrt{2}}\frac{1}{(n-1)!}\left(\frac{1}{2}N_{b\perp}\frac{p_\perp}{m_e c}\frac{\omega_b}{\omega_{ce}}\right)^{n-1} \tag{D.118}$$

O-mode, $n \geq 1$

For the O-mode, things are more complicated. However, if $\left|N_\parallel\right| \ll 1$, $e_{b,\parallel}$ is much larger than $e_{b,-}$. The last term in (D.117) is dominant if

$$\left|\frac{e_{b,-}}{e_{b,\parallel}}\right| \ll \frac{1}{\sqrt{2}}\frac{\left|p_\parallel\right|}{m_e c} \tag{D.119}$$

which is satisfied for resonant electrons as long as the temperature is not too low. In that case, we have

$$\Theta_{\mathbf{k}}^{b,\text{EC-On}} \simeq \frac{p_\parallel}{p_\perp} e_{b,\parallel}\frac{1}{n!}\left(\frac{1}{2}N_{b\perp}\frac{p_\perp}{m_e c}\frac{\omega_b}{\omega_{ce}}\right)^n \tag{D.120}$$

D.3.3 Determination of $\mathbf{\Phi}_b^{\mathbf{EC}}$ in the low density limit.

The vector $\mathbf{\Phi}_b$ describes the relation between the energy flux and the electric field. In the cold plasma description, it is given by (4.269).

$$\mathbf{\Phi}_{bP} = \mathrm{Re}\left[\mathbf{N}_b - (\mathbf{N}_b \cdot \mathbf{e}_b)\,\mathbf{e}_b^*\right] \tag{D.121}$$

In general, both terms must be kept. However, where the density is low

$$\omega_{pe} \ll \omega_b \tag{D.122}$$

the ECW is mostly electromagnetic and mostly keeps its free-space characteristics. In that case,

$$N_b \simeq 1 \tag{D.123}$$

$$\frac{\mathbf{N}_b \cdot \mathbf{e}_b}{N_b} \ll 1 \tag{D.124}$$

so that

$$\mathbf{\Phi}_b^{\mathrm{EC}} \simeq \widehat{N}_b \tag{D.125}$$

D.3.4 EC Diffusion Coefficient

General expression with small FLR, $\left|N_\parallel\right| \ll 1$ and $\omega_{pe} \ll \omega_b$ - or EM - approximations

The normalized bounce-averaged diffusion coefficient for the Fokker-Planck equation is given by (4.313)

$$\overline{D}_{b,n}^{\mathrm{EC}(0)}(p,\xi_0) = \frac{\gamma p_{Te}}{p\left|\xi_0\right|}\frac{1}{\lambda\widetilde{q}}\frac{r_{\theta_b}}{R_p}\frac{B^{\theta_b}}{B_P^{\theta_b}}\frac{\xi_0^2}{\xi_{\theta_b}^2}\Psi_{\theta_b}\overline{D}_{b,n,0}^{\mathrm{EC},\theta_b}\times$$
$$H\left(\theta_b-\theta_{\min}\right)H\left(\theta_{\max}-\theta_b\right)\left[\frac{1}{2}\sum_\sigma\right]_T\delta\left(N_{b\parallel}-N_{\parallel\mathrm{res}}^{\theta_b}\right)\left|\Theta_{\mathbf{k},\theta_b}^{b,(n)}\right|^2 \tag{D.126}$$

with

$$\overline{D}_{b,n,0}^{\mathrm{EC},\theta_b} = \frac{1}{r_{\theta_b}R_{\theta_b}}\frac{1}{m_e\ln\Lambda}\frac{1}{\omega_b\omega_{pe}^2}\frac{f_{\mathrm{inc},b}^{l+1/2}}{\left|\mathbf{\Phi}_b\right|}P_{b,\mathrm{inc}} \tag{D.127}$$

$$N_{\parallel\mathrm{res}}^{\theta_b} = \frac{1}{\beta_{Te}}\frac{p_{Te}}{p\xi_{\theta_b}}\left(\gamma-\frac{n\Psi_{\theta_b}\omega_{ce,0}}{\omega_b}\right) \tag{D.128}$$

where we used the substitution $n' \to n$ as in (D.111).

Within the small FLR, $\left|N_\parallel\right| \ll 1$ and $\omega_{pe} \ll \omega_b$ - or electromagnetic - approximations, we have obtained the following expressions for the ECW properties (D.118), (D.120), (D.125)

$$\Theta_{\mathbf{k}}^{b,\text{EC-Xn}} \simeq e^{+i\alpha}\frac{e_{b,-}}{\sqrt{2}}\frac{1}{(n-1)!}\left(\frac{1}{2}N_{b\perp}\frac{p\sqrt{\Psi_{\theta_b}\left(1-\xi_0^2\right)}}{m_e c}\frac{\omega_b}{\Psi_{\theta_b}\omega_{ce,0}}\right)^{n-1} \tag{D.129}$$

$$\Theta_{\mathbf{k}}^{b,\text{EC-On}} \simeq \frac{\xi_{\theta_b}}{\sqrt{\Psi_{\theta_b}\left(1-\xi_0^2\right)}}e_{b,\parallel}\frac{1}{n!}\left(\frac{1}{2}N_{b\perp}\frac{p\sqrt{\Psi_{\theta_b}\left(1-\xi_0^2\right)}}{m_e c}\frac{\omega_b}{\Psi_{\theta_b}\omega_{ce,0}}\right)^{n} \tag{D.130}$$

$$\mathbf{\Phi}_b^{\mathrm{EC}} \simeq \widehat{N}_b \tag{D.131}$$

so that

$$\left|\mathbf{\Phi}_b^{\mathrm{EC}}\right| \simeq 1$$

In addition, within these approximations, the polarizations take the following limit expressions:

$$|e_{b,-}| \simeq \frac{\sqrt{2}}{2} \text{ for the X mode } (n \geq 2) \tag{D.132}$$

$$\left|e_{b,\parallel}\right| \simeq 1 \text{ for the O mode} \tag{D.133}$$

Simplified expression for ECCD in the case of circular concentric flux-surfaces

We consider the limit of a tokamak with circular flux-surfaces. In that case, we have the following identities

$$\left|\widehat{\psi} \cdot \widehat{r}\right| = 1 \tag{D.134}$$

$$\widetilde{q} = \frac{r}{R_p}\frac{B}{B_P} = \frac{r_{\theta_b}}{R_p}\frac{B^{\theta_b}}{B_P^{\theta_b}} \tag{D.135}$$

and the QL diffusion coefficients for ECCD (D.126) can therefore be written as

$$\begin{aligned}\overline{D}_b^{\text{EC-Xn(0)}}(p,\xi_0) = & \frac{\gamma p_{Te}}{p\left|\xi_0\right|}\frac{1}{\lambda}\frac{\xi_0^2}{\xi_{\theta_b}^2}\Psi_{\theta_b}\overline{D}_{b,n,0}^{\mathrm{EC},\theta_b}\frac{1}{4\left[(n-1)!\right]^2} \\ \times & \left(\frac{p}{p_{Te}}\right)^{2(n-1)}\left(\frac{1-\xi_0^2}{\Psi_{\theta_b}}\right)^{(n-1)}\left(\frac{1}{2}N_{b\perp}\beta_{Te}\frac{\omega_b}{\omega_{ce,0}}\right)^{2(n-1)} \\ \times & H\left(\theta_b-\theta_{\min}\right)H\left(\theta_{\max}-\theta_b\right)\frac{1}{\sqrt{\pi}\Delta N_\parallel}\left[\frac{1}{2}\sum_\sigma\right]_T \exp\left[\frac{-\left(N_{\parallel\mathrm{res}}-N_{b\parallel,0}\right)^2}{\Delta N_\parallel^2}\right]\end{aligned} \tag{D.136}$$

$$\begin{aligned}\overline{D}_b^{\text{EC-On(0)}}(p,\xi_0) = & \frac{\gamma p_{Te}}{p\left|\xi_0\right|}\frac{1}{\lambda}\frac{\xi_0^2}{\left(1-\xi_0^2\right)}\overline{D}_{b,n,0}^{\mathrm{EC},\theta_b}\frac{1}{[n!]^2} \\ \times & \left(\frac{p}{p_{Te}}\right)^{2n}\left(\frac{1-\xi_0^2}{\Psi_{\theta_b}}\right)^{n}\left(\frac{1}{2}N_{b\perp}\beta_{Te}\frac{\omega_b}{\omega_{ce,0}}\right)^{2n} \\ \times & H\left(\theta_b-\theta_{\min}\right)H\left(\theta_{\max}-\theta_b\right)\frac{1}{\sqrt{\pi}\Delta N_\parallel}\left[\frac{1}{2}\sum_\sigma\right]_T \exp\left[\frac{-\left(N_{\parallel\mathrm{res}}-N_{b\parallel,0}\right)^2}{\Delta N_\parallel^2}\right]\end{aligned} \tag{D.137}$$

with

$$\overline{D}_{b,n,0}^{\mathrm{EC},\theta_b} = \frac{1}{rR_{\theta_b}}\frac{1}{m_e\ln\Lambda}\frac{1}{\omega_b\omega_{pe}^2}f_{\mathrm{inc},b}^{l+1/2}P_{b,\mathrm{inc}} \tag{D.138}$$

$$N_{\parallel\mathrm{res}}^{\theta_b} = \frac{1}{\beta_{Te}}\frac{p_{Te}}{p\xi_{\theta_b}}\left(\gamma - \frac{n\Psi_{\theta_b}\omega_{ce,0}}{\omega_b}\right) \tag{D.139}$$

and where we assume a gaussian power spectrum as in (4.337).

In order to compare with ECCD operators found in the litterature, we redefine the EC constant factors such that

$$\overline{D}_b^{\text{EC-Xn(0)}}(p,\xi_0) = \frac{\gamma p_{Te}}{p\,|\xi_0|}\left(\frac{p}{p_{Te}}\right)^{2(n-1)} \frac{\xi_0^2}{\xi_{\theta_b}^2}\overline{D}_{b,0,\text{new}}^{\text{EC-Xn},\theta_b}\frac{\left(1-\xi_0^2\right)^{(n-1)}}{\Psi_{\theta_b}^{(n-2)}}\frac{1}{\lambda}$$
$$H\left(\theta_b-\theta_{\min}\right)H\left(\theta_{\max}-\theta_b\right)\left[\frac{1}{2}\sum_{\sigma}\right]_T \exp\left[\frac{-\left(N_{\parallel\text{res}}-N_{b\parallel,0}\right)^2}{\Delta N_\parallel^2}\right] \quad \text{(D.140)}$$

with

$$\overline{D}_{b,0,\text{new}}^{\text{EC-Xn},\theta_b} = \frac{1}{\sqrt{\pi}\Delta N_\parallel}\frac{1}{4\left[(n-1)!\right]^2}\left(\frac{1}{2}N_{b\perp}\beta_{Te}\frac{\omega_b}{\omega_{ce,0}}\right)^{2(n-1)}\overline{D}_{b,n,0}^{\text{EC},\theta_b} \quad \text{(D.141)}$$
$$= \frac{1}{rR_{\theta_b}}\frac{1}{m_e\ln\Lambda}\frac{1}{\omega_b\omega_{pe}^2}\frac{1}{\sqrt{\pi}\Delta N_\parallel}\frac{1}{4\left[(n-1)!\right]^2}\left(\frac{1}{2}N_{b\perp}\beta_{Te}\frac{\omega_b}{\omega_{ce,0}}\right)^{2(n-1)} f_{\text{inc},b}^{l+1/2}P_{b,\text{inc}} \quad \text{(D.142)}$$

and

$$\overline{D}_b^{\text{EC-On(0)}}(p,\xi_0) = \frac{\gamma p_{Te}}{p\,|\xi_0|}\left(\frac{p}{p_{Te}}\right)^{2n}\frac{\xi_0^2\left(1-\xi_0^2\right)^{n-1}}{\Psi_{\theta_b}^n}\overline{D}_{b,0,\text{new}}^{\text{EC-On},\theta_b}\frac{1}{\lambda}$$
$$H\left(\theta_b-\theta_{\min}\right)H\left(\theta_{\max}-\theta_b\right)\left[\frac{1}{2}\sum_{\sigma}\right]_T \exp\left[\frac{-\left(N_{\parallel\text{res}}-N_{b\parallel,0}\right)^2}{\Delta N_\parallel^2}\right] \quad \text{(D.143)}$$

with

$$\overline{D}_{b,0,\text{new}}^{\text{EC-On},\theta_b} = \frac{1}{\sqrt{\pi}\Delta N_\parallel}\frac{1}{[n!]^2}\left(\frac{1}{2}N_{b\perp}\beta_{Te}\frac{\omega_b}{\omega_{ce,0}}\right)^{2n}\overline{D}_{b,n,0}^{\text{EC},\theta_b} \quad \text{(D.144)}$$
$$= \frac{1}{rR_{\theta_b}}\frac{1}{m_e\ln\Lambda}\frac{1}{\omega_b\omega_{pe}^2}\frac{1}{\sqrt{\pi}\Delta N_\parallel}\frac{1}{[n!]^2}\left(\frac{1}{2}N_{b\perp}\beta_{Te}\frac{\omega_b}{\omega_{ce,0}}\right)^{2n} f_{\text{inc},b}^{l+1/2}P_{b,\text{inc}} \quad \text{(D.145)}$$

The two most common ECCD scenarios in experiments are the ones with the largest diffusion coefficient: X2 and O1. For these case, we find

$$\overline{D}_b^{\text{EC-X2(0)}}(p,\xi_0) = \frac{\gamma p_{Te}}{p\,|\xi_0|}\left(\frac{p}{p_{Te}}\right)^{2}\frac{\xi_0^2\left(1-\xi_0^2\right)}{\xi_{\theta_b}^2}\overline{D}_{b,0,\text{new}}^{\text{EC-X2},\theta_b}\frac{1}{\lambda}$$
$$H\left(\theta_b-\theta_{\min}\right)H\left(\theta_{\max}-\theta_b\right)\left[\frac{1}{2}\sum_{\sigma}\right]_T \exp\left[\frac{-\left(N_{\parallel\text{res}}-N_{b\parallel,0}\right)^2}{\Delta N_\parallel^2}\right] \quad \text{(D.146)}$$

with

$$\overline{D}_{b,0,\text{new}}^{\text{EC-X2},\theta_b} = \frac{1}{rR_{\theta_b}}\frac{1}{m_e\ln\Lambda}\frac{1}{\omega_b\omega_{pe}^2}\frac{1}{\sqrt{\pi}\Delta N_\parallel}\frac{1}{4}\left(\frac{1}{2}N_{b\perp}\beta_{Te}\frac{\omega_b}{\omega_{ce,0}}\right)^{2} f_{\text{inc},b}^{l+1/2}P_{b,\text{inc}} \quad \text{(D.147)}$$

and

$$\overline{D}_b^{\text{EC-O1(0)}}(p,\xi_0) = \frac{\gamma p_{Te}}{p\,|\xi_0|}\left(\frac{p}{p_{Te}}\right)^2 \frac{\xi_0^2}{\Psi_{\theta_b}} \overline{D}_{b,0,\text{new}}^{\text{EC-O1},\theta_b} \frac{1}{\lambda} \\ H\left(\theta_b - \theta_{\min}\right) H\left(\theta_{\max} - \theta_b\right) \left[\frac{1}{2}\sum_{\sigma}\right]_T \exp\left[\frac{-\left(N_{\parallel\text{res}} - N_{b\parallel,0}\right)^2}{\Delta N_{\parallel}^2}\right] \quad \text{(D.148)}$$

with

$$\overline{D}_{b,0,\text{new}}^{\text{EC-O1},\theta_b} = \frac{1}{rR_{\theta_b}} \frac{1}{m_e \ln\Lambda} \frac{1}{\omega_b \omega_{pe}^2} \frac{1}{\sqrt{\pi}\Delta N_{\parallel}} \left(\frac{1}{2} N_{b\perp} \beta_{Te} \frac{\omega_b}{\omega_{ce,0}}\right)^2 f_{\text{inc},b}^{l+1/2} P_{b,\text{inc}} \quad \text{(D.149)}$$

Appendix E

Alternative discrete cross-derivatives coefficients

In the approach here considered, $D^{(0)}_{p\xi}$ and $D^{(0)}_{\xi p}$ are not separated from the derivatives of the distribution function. Therefore $\frac{\partial}{\partial p}\left(pD^{(0)}_{p\xi}\frac{\partial f_0^{(0)}}{\partial \xi_0}\right)$ and $\frac{\partial}{\partial \xi_0}\left(\sqrt{1-\xi_0^2}\lambda D^{(0)}_{\xi p}\frac{\partial f_0^{(0)}}{\partial p}\right)$ are directly discretized on the flux grid, and coefficients may be expressed as

$$\frac{\widetilde{q}}{B_0}p^2\nabla_{\mathbf{p}}\cdot\mathbf{S}^{(0)}_p\Big|^{(k+1)}_{l+1/2,i+1/2,j+1/2} = \frac{\widetilde{q}_{l+1/2}}{B_{0,l+1/2}}\sum_{m=1}^{m=8}T^{[m]} \tag{E.1}$$

with

$$T^{[1]} = \frac{-p^2_{i+1}D^{(0)}_{pp,l+1/2,i+1,j+1/2}\left.\frac{\partial f_0^{(0)}}{\partial p}\right|^{(k+1)}_{l+1/2,i+1,j+1/2} + p^2_{i+1}F^{(0)}_{p,l+1/2,i+1,j+1/2}f^{(0)(k+1)}_{0,l+1/2,i+1,j+1/2}}{\Delta p_{i+1/2}} \tag{E.2}$$

$$T^{[2]} = \frac{p^2_i D^{(0)}_{pp,l+1/2,i,j+1/2}\left.\frac{\partial f_0^{(0)}}{\partial p}\right|^{(k+1)}_{l+1/2,i,j+1/2} - p^2_i F^{(0)}_{p,l+1/2,i,j+1/2}f^{(0)(k+1)}_{0,l+1/2,i,j+1/2}}{\Delta p_{i+1/2}} \tag{E.3}$$

$$T^{[3]} = +\frac{\sqrt{1-\xi^2_{0,j+1/2}}}{\Delta p_{i+1/2}}p_{i+1}D^{(0)}_{p\xi,l+1/2,i+1,j+1/2}\left.\frac{\partial f_0^{(0)}}{\partial \xi_0}\right|^{(k+1)}_{l+1/2,i+1,j+1/2} \tag{E.4}$$

$$T^{[4]} = -\frac{\sqrt{1-\xi^2_{0,j+1/2}}}{\Delta p_{i+1/2}}p_{i}D^{(0)}_{p\xi,l+1/2,i,j+1/2}\left.\frac{\partial f_0^{(0)}}{\partial \xi_0}\right|^{(k+1)}_{l+1/2,i,j+1/2} \tag{E.5}$$

$$T^{[5]} = -\frac{p_{i+1/2}}{\lambda^{l+1/2,j+1/2}}\left[\frac{D^{(0)}_{\xi\xi,l+1/2,i+1/2,j+1}\left(1-\xi^2_{0,j+1}\right)\lambda^{l+1/2,j+1}\left.\frac{\partial f_0^{(0)}}{\partial\xi_0}\right|^{(k+1)}_{l+1/2,i+1/2,j+1}}{\cdot p_{i+1/2}\Delta\xi_{0,j+1/2}}\right.$$
$$\left.+\frac{p_{i+1/2}\sqrt{1-\xi^2_{0,j+1}}\lambda^{l+1/2,j+1}F^{(0)}_{\xi,l+1/2,i+1/2,j+1}f^{(0)(k+1)}_{0,l+1/2,i+1/2,j+1}}{\Delta\xi_{0,j+1/2}}\right] \tag{E.6}$$

$$T^{[6]} = \frac{p_{i+1/2}}{\lambda^{l+1/2,j+1/2}}\left[\frac{D^{(0)}_{\xi\xi,l+1/2,i+1/2,j}\left(1-\xi^2_{0,j}\right)\lambda^{l+1/2,j}\left.\frac{\partial f_0^{(0)}}{\partial\xi_0}\right|^{(k+1)}_{l+1/2,i+1/2,j}}{p_{i+1/2}\Delta\xi_{0,j+1/2}}\right.$$
$$\left.+\frac{p_{i+1/2}\sqrt{1-\xi^2_{0,j}}\lambda^{l+1/2,j}F^{(0)}_{\xi,l+1/2,i+1/2,j}f^{(0)(k+1)}_{0,l+1/2,i+1/2,j}}{\Delta\xi_{0,j+1/2}}\right] \tag{E.7}$$

$$T^{[7]} = \frac{p_{i+1/2}}{\lambda^{l+1/2,j+1/2}}\frac{\sqrt{1-\xi^2_{0,j+1}}}{\Delta\xi_{0,j+1/2}}\lambda^{l+1/2,j+1}D^{(0)}_{\xi p,l+1/2,i+1/2,j+1}\left.\frac{\partial f_0^{(0)}}{\partial p}\right|^{(k+1)}_{l+1/2,i+1/2,j+1} \tag{E.8}$$

$$T^{[8]} = -\frac{p_{i+1/2}}{\lambda^{l+1/2,j+1/2}}\frac{\sqrt{1-\xi^2_{0,j}}}{\Delta\xi_{0,j+1/2}}\lambda^{l+1/2,j}D^{(0)}_{\xi p,l+1/2,i+1/2,j}\left.\frac{\partial f_0^{(0)}}{\partial p}\right|^{(k+1)}_{l+1/2,i+1/2,j} \tag{E.9}$$

Here discrete expressions of the partial derivatives are those given in Sec. 5.4.1, with new ones

$$\left.\frac{\partial f_0^{(0)}}{\partial p}\right|^{(k+1)}_{l+1/2,i+1/2,j+1} = \frac{f^{(0)(k+1)}_{0,l+1/2,i+1,j+1} - f^{(0)(k+1)}_{0,l+1/2,i,j+1}}{\Delta p_{i+1/2}} \tag{E.10}$$

$$\left.\frac{\partial f_0^{(0)}}{\partial p}\right|^{(k+1)}_{l+1/2,i+1/2,j} = \frac{f^{(0)(k+1)}_{0,l+1/2,i+1,j} - f^{(0)(k+1)}_{0,l+1/2,i,j}}{\Delta p_{i+1/2}} \tag{E.11}$$

$$\left.\frac{\partial f_0^{(0)}}{\partial \xi_0}\right|^{(k+1)}_{l+1/2,i+1,j+1/2} = \frac{f^{(0)(k+1)}_{0,l+1/2,i+1,j+1} - f^{(0)(k+1)}_{0,l+1/2,i+1,j}}{\Delta\xi_{0,j+1/2}} \tag{E.12}$$

$$\left.\frac{\partial f_0^{(0)}}{\partial \xi_0}\right|^{(k+1)}_{l+1/2,i,j+1/2} = \frac{f^{(0)(k+1)}_{0,l+1/2,i,j+1} - f^{(0)(k+1)}_{0,l+1/2,i,j}}{\Delta\xi_{0,j+1/2}} \tag{E.13}$$

Since the distribution function is defined on the half grid, while fluxes on the full grid, it is necessary to interpolate, because in derivatives E.10-E.13, values of $f_0^{(0)}$ are taken on the full grid. In a general way, whatever the detailed value of the weighting factor $\delta^{(0)}$

which will be discussed in the Sec. 5.4.3, one may write for the terms proportional to $D^{(0)}_{pp}$, $F^{(0)}_{p}$, $D^{(0)}_{\xi\xi}$ and $F^{(0)}_{\xi}$ as in Sec. 5.4.1

For terms involving $D^{(0)}_{p\xi}$ and $D^{(0)}_{\xi p}$, expressions are more complicated.

$$\begin{aligned} f^{(0)(k+1)}_{0,l+1/2,i+1,j+1} &= \left(1-\delta^{(0)}_{p,l+1/2,i+1,j+1}\right) f^{(0)(k+1)}_{0,l+1/2,i+3/2,j+1} \\ &\quad +\delta^{(0)}_{p,l+1/2,i+1,j+1} f^{(0)(k+1)}_{0,l+1/2,i+1/2,j+1} \end{aligned} \tag{E.14}$$

and using relations

$$\begin{aligned} f^{(0)(k+1)}_{0,l+1/2,i+3/2,j+1} &= \left(1-\delta^{(0)}_{\xi,l+1/2,i+3/2,j+1}\right) f^{(0)(k+1)}_{0,l+1/2,i+3/2,j+3/2} \\ &\quad +\delta^{(0)}_{\xi,l+1/2,i+3/2,j+1} f^{(0)(k+1)}_{0,l+1/2,i+3/2,j+1/2} \end{aligned} \tag{E.15}$$

and

$$\begin{aligned} f^{(0)(k+1)}_{0,l+1/2,i+1/2,j+1} &= \left(1-\delta^{(0)}_{\xi,l+1/2,i+1/2,j+1}\right) f^{(0)(k+1)}_{0,l+1/2,i+1/2,j+3/2} \\ &\quad +\delta^{(0)}_{\xi,l+1/2,i+1/2,j+1} f^{(0)(k+1)}_{0,l+1/2,i+1/2,j+1/2} \end{aligned} \tag{E.16}$$

one obtains

$$\begin{aligned} f^{(0)(k+1)}_{0,l+1/2,i+1,j+1} &= \left(1-\delta^{(0)}_{p,l+1/2,i+1,j+1}\right)\left(1-\delta^{(0)}_{\xi,l+1/2,i+3/2,j+1}\right) f^{(0)(k+1)}_{0,l+1/2,i+3/2,j+3/2} \\ &\quad +\left(1-\delta^{(0)}_{p,l+1/2,i+1,j+1}\right)\delta^{(0)}_{\xi,l+1/2,i+3/2,j+1} f^{(0)(k+1)}_{0,l+1/2,i+3/2,j+1/2} \\ &\quad +\delta^{(0)}_{p,l+1/2,i+1,j+1}\left(1-\delta^{(0)}_{\xi,l+1/2,i+1/2,j+1}\right) f^{(0)(k+1)}_{0,l+1/2,i+1/2,j+3/2} \\ &\quad +\delta^{(0)}_{p,l+1/2,i+1,j+1}\delta^{(0)}_{\xi,l+1/2,i+1/2,j+1} f^{(0)(k+1)}_{0,l+1/2,i+1/2,j+1/2} \end{aligned} \tag{E.17}$$

By performing the appropriate index number transformations $(i+1 \to i)$ and $(j+1 \to j)$ other interpolations are

$$\begin{aligned} f^{(0)(k+1)}_{0,l+1/2,i,j+1} &= \left(1-\delta^{(0)}_{p,l+1/2,i,j+1}\right)\left(1-\delta^{(0)}_{\xi,l+1/2,i+1/2,j+1}\right) f^{(0)(k+1)}_{0,l+1/2,i+1/2,j+3/2} \\ &\quad +\left(1-\delta^{(0)}_{p,l+1/2,i,j+1}\right)\delta^{(0)}_{\xi,l+1/2,i+1/2,j+1} f^{(0)(k+1)}_{0,l+1/2,i+1/2,j+1/2} \\ &\quad +\delta^{(0)}_{p,l+1/2,i,j+1}\left(1-\delta^{(0)}_{\xi,l+1/2,i-1/2,j+1}\right) f^{(0)(k+1)}_{0,l+1/2,i-1/2,j+3/2} \\ &\quad +\delta^{(0)}_{p,l+1/2,i,j+1}\delta^{(0)}_{\xi,l+1/2,i-1/2,j+1} f^{(0)(k+1)}_{0,l+1/2,i-1/2,j+1/2} \end{aligned} \tag{E.18}$$

$$\begin{aligned} f^{(0)(k+1)}_{0,l+1/2,i+1,j} &= \left(1-\delta^{(0)}_{p,l+1/2,i+1,j}\right)\left(1-\delta^{(0)}_{\xi,l+1/2,i+3/2,j}\right) f^{(0)(k+1)}_{0,l+1/2,i+3/2,j+1/2} \\ &\quad +\left(1-\delta^{(0)}_{p,l+1/2,i+1,j}\right)\delta^{(0)}_{\xi,l+1/2,i+3/2,j} f^{(0)(k+1)}_{0,l+1/2,i+3/2,j-1/2} \\ &\quad +\delta^{(0)}_{p,l+1/2,i+1,j}\left(1-\delta^{(0)}_{\xi,l+1/2,i+1/2,j}\right) f^{(0)(k+1)}_{0,l+1/2,i+1/2,j+1/2} \\ &\quad +\delta^{(0)}_{p,l+1/2,i+1,j}\delta^{(0)}_{\xi,l+1/2,i+1/2,j} f^{(0)(k+1)}_{0,l+1/2,i+1/2,j-1/2} \end{aligned} \tag{E.19}$$

$$
\begin{aligned}
f^{(0)(k+1)}_{0,l+1/2,i,j} &= \left(1-\delta^{(0)}_{p,l+1/2,i,j}\right)\left(1-\delta^{(0)}_{\xi,l+1/2,i+1/2,j}\right) f^{(0)(k+1)}_{0,l+1/2,i+1/2,j+1/2} \\
&+ \left(1-\delta^{(0)}_{p,l+1/2,i,j}\right)\delta^{(0)}_{\xi,l+1/2,i+1/2,j} f^{(0)(k+1)}_{0,l+1/2,i+1/2,j-1/2} \\
&+ \delta^{(0)}_{p,l+1/2,i,j}\left(1-\delta^{(0)}_{\xi,l+1/2,i-1/2,j}\right) f^{(0)(k+1)}_{0,l+1/2,i-1/2,j+1/2} \\
&+ \delta^{(0)}_{p,l+1/2,i,j}\delta^{(0)}_{\xi,l+1/2,i-1/2,j} f^{(0)(k+1)}_{0,l+1/2,i-1/2,j-1/2}
\end{aligned} \tag{E.20}
$$

Gathering all terms, corresponding matrix coefficients for the zero order Fokker-Planck equation may be expressed as

$$
\begin{aligned}
&\frac{\widetilde{q}}{B_0} p^2 \nabla_{\mathbf{p}} \cdot \mathbf{S}^{(0)}_p \Big|^{(k+1)}_{l+1/2,i+1/2,j+1/2} \\
&\quad = \frac{\widetilde{q}_{l+1/2}}{B_{0,l+1/2}} \sum_{i'=i-1}^{i'=i+1} \sum_{j'=j-1}^{j'=j+1} \overline{\overline{M}}^{(0)}_{p,l+1/2,i'+1/2,j'+1/2} f^{(0)(k+1)}_{0,l+1/2,i'+1/2,j'+1/2}
\end{aligned} \tag{E.21}
$$

where

$$
\overline{\overline{M}}^{(0)}_{p,l+1/2,i'+1/2,j'+1/2} = \overline{\overline{M}}^{(0)[1]}_{p,l+1/2,i'+1/2,j'+1/2} + \overline{\overline{M}}^{(0)[2]}_{p,l+1/2,i'+1/2,j'+1/2}
$$

Terms proportional to $D^{(0)}_{\xi\xi}$, $F^{(0)}_{\xi}$ and $D^{(0)}_{pp}$, $F^{(0)}_{p}$ are all gathered in matrix $\overline{\overline{M}}^{(0)[1]}_{p}$ and may be easily obtained from $\overline{\overline{M}}^{(0)}_{p}$ given in Sec. 5.4.1 by taking $D^{(0)}_{p\xi} = D^{(0)}_{\xi p} = 0$.

The other terms proportional to $D^{(0)}_{p\xi}$ and $D^{(0)}_{\xi p}$ are

$$
\begin{aligned}
\overline{\overline{M}}^{(0)[2]}_{p,l+1/2,i+3/2,j+3/2} &= + \frac{\sqrt{1-\xi^2_{0,j+1/2}}}{\Delta p_{i+1/2}\Delta\xi_{0,j+1/2}} p_{i+1} D^{(0)}_{p\xi,l+1/2,i+1,j+1/2} \\
&\times \left(1-\delta^{(0)}_{p,l+1/2,i+1,j+1}\right)\left(1-\delta^{(0)}_{\xi,l+1/2,i+3/2,j+1}\right) \\
&+ \frac{p_{i+1/2}}{\lambda^{l+1/2,j+1/2}} \frac{\sqrt{1-\xi^2_{0,j+1}}}{\Delta\xi_{0,j+1/2}\Delta p_{i+1/2}} \lambda^{l+1/2,j+1} D^{(0)}_{\xi p,l+1/2,i+1/2,j+1} \\
&\times \left(1-\delta^{(0)}_{p,l+1/2,i+1,j+1}\right)\left(1-\delta^{(0)}_{\xi,l+1/2,i+3/2,j+1}\right)
\end{aligned} \tag{E.22}
$$

$$
\begin{aligned}
\overline{\overline{M}}^{(0)[2]}_{p,l+1/2,i+1/2,j+3/2} &= +\frac{\sqrt{1-\xi^2_{0,j+1/2}}}{\Delta p_{i+1/2}\Delta\xi_{0,j+1/2}} p_{i+1} D^{(0)}_{p\xi,l+1/2,i+1,j+1/2} \\
&\quad \times\delta^{(0)}_{p,l+1/2,i+1,j+1}\left(1-\delta^{(0)}_{\xi,l+1/2,i+1/2,j+1}\right) \\
&\quad -\frac{\sqrt{1-\xi^2_{0,j+1/2}}}{\Delta p_{i+1/2}\Delta\xi_{0,j+1/2}} p_{i} D^{(0)}_{p\xi,l+1/2,i,j+1/2} \\
&\quad \times\left(1-\delta^{(0)}_{p,l+1/2,i,j+1}\right)\left(1-\delta^{(0)}_{\xi,l+1/2,i+1/2,j+1}\right) \\
&\quad +\frac{p_{i+1/2}}{\lambda^{l+1/2,j+1/2}}\frac{\sqrt{1-\xi^2_{0,j+1}}}{\Delta\xi_{0,j+1/2}\Delta p_{i+1/2}}\lambda^{l+1/2,j+1} D^{(0)}_{\xi p,l+1/2,i+1/2,j+1} \\
&\quad \times\delta^{(0)}_{p,l+1/2,i+1,j+1}\left(1-\delta^{(0)}_{\xi,l+1/2,i+1/2,j+1}\right) \\
&\quad -\frac{p_{i+1/2}}{\lambda^{l+1/2,j+1/2}}\frac{\sqrt{1-\xi^2_{0,j+1}}}{\Delta\xi_{0,j+1/2}\Delta p_{i+1/2}}\lambda^{l+1/2,j+1} D^{(0)}_{\xi p,l+1/2,i+1/2,j+1} \\
&\quad \times\left(1-\delta^{(0)}_{p,l+1/2,i,j+1}\right)\left(1-\delta^{(0)}_{\xi,l+1/2,i+1/2,j+1}\right)
\end{aligned}
\tag{E.23}
$$

$$
\begin{aligned}
\overline{\overline{M}}^{(0)[2]}_{p,l+1/2,i-1/2,j+3/2} &= -\frac{\sqrt{1-\xi^2_{0,j+1/2}}}{\Delta p_{i+1/2}\Delta\xi_{0,j+1/2}} p_{i} D^{(0)}_{p\xi,l+1/2,i,j+1/2} \\
&\quad \times\delta^{(0)}_{p,l+1/2,i,j+1}\left(1-\delta^{(0)}_{\xi,l+1/2,i-1/2,j+1}\right) \\
&\quad -\frac{p_{i+1/2}}{\lambda^{l+1/2,j+1/2}}\frac{\sqrt{1-\xi^2_{0,j+1}}}{\Delta\xi_{0,j+1/2}\Delta p_{i+1/2}}\lambda^{l+1/2,j+1} D^{(0)}_{\xi p,l+1/2,i+1/2,j+1} \\
&\quad \times\delta^{(0)}_{p,l+1/2,i,j+1}\left(1-\delta^{(0)}_{\xi,l+1/2,i-1/2,j+1}\right)
\end{aligned}
\tag{E.24}
$$

$$
\begin{aligned}
\overline{\overline{M}}^{(0)[2]}_{p,l+1/2,i+3/2,j+1/2} \;=\;& +\frac{\sqrt{1-\xi^2_{0,j+1/2}}}{\Delta p_{i+1/2}\Delta\xi_{0,j+1/2}} p_{i+1} D^{(0)}_{p\xi,l+1/2,i+1,j+1/2} \\
& \times \left(1-\delta^{(0)}_{p,l+1/2,i+1,j+1}\right)\delta^{(0)}_{\xi,l+1/2,i+3/2,j+1} \\
& -\frac{\sqrt{1-\xi^2_{0,j+1/2}}}{\Delta p_{i+1/2}\Delta\xi_{0,j+1/2}} p_{i+1} D^{(0)}_{p\xi,l+1/2,i+1,j+1/2} \\
& \times \left(1-\delta^{(0)}_{p,l+1/2,i+1,j}\right)\left(1-\delta^{(0)}_{\xi,l+1/2,i+3/2,j}\right) \\
& +\frac{p_{i+1/2}}{\lambda^{l+1/2,j+1/2}} \frac{\sqrt{1-\xi^2_{0,j+1}}}{\Delta\xi_{0,j+1/2}\Delta p_{i+1/2}} \lambda^{l+1/2,j+1} D^{(0)}_{\xi p,l+1/2,i+1/2,j+1} \\
& \times \left(1-\delta^{(0)}_{p,l+1/2,i+1,j+1}\right)\delta^{(0)}_{\xi,l+1/2,i+3/2,j+1} \\
& -\frac{p_{i+1/2}}{\lambda^{l+1/2,j+1/2}} \frac{\sqrt{1-\xi^2_{0,j}}}{\Delta\xi_{0,j+1/2}\Delta p_{i+1/2}} \lambda^{l+1/2,j} D^{(0)}_{\xi p,l+1/2,i+1/2,j} \\
& \times \left(1-\delta^{(0)}_{p,l+1/2,i+1,j}\right)\left(1-\delta^{(0)}_{\xi,l+1/2,i+3/2,j}\right)
\end{aligned}
\tag{E.25}
$$

$$
\begin{aligned}
\overline{\overline{M}}^{(0)[2]}_{p,i+1/2,j+1/2} \quad = \quad & +\frac{\sqrt{1-\xi^2_{0,j+1/2}}}{\Delta p_{i+1/2}\Delta\xi_{0,j+1/2}} p_{i+1} D^{(0)}_{p\xi,l+1/2,i+1,j+1/2} \\
& \times\delta^{(0)}_{p,l+1/2,i+1,j+1}\delta^{(0)}_{\xi,l+1/2,i+1/2,j+1} \\
& -\frac{\sqrt{1-\xi^2_{0,j+1/2}}}{\Delta p_{i+1/2}\Delta\xi_{0,j+1/2}} p_{i+1} D^{(0)}_{p\xi,l+1/2,i+1,j+1/2} \\
& \times\delta^{(0)}_{p,l+1/2,i+1,j}\left(1-\delta^{(0)}_{\xi,l+1/2,i+1/2,j}\right) \\
& -\frac{\sqrt{1-\xi^2_{0,j+1/2}}}{\Delta p_{i+1/2}\Delta\xi_{0,j+1/2}} p_{i} D^{(0)}_{p\xi,l+1/2,i,j+1/2} \\
& \times\left(1-\delta^{(0)}_{p,l+1/2,i,j+1}\right)\delta^{(0)}_{\xi,l+1/2,i+1/2,j+1} \\
& +\frac{\sqrt{1-\xi^2_{0,j+1/2}}}{\Delta p_{i+1/2}\Delta\xi_{0,j+1/2}} p_{i} D^{(0)}_{p\xi,l+1/2,i,j+1/2} \\
& \times\left(1-\delta^{(0)}_{p,l+1/2,i,j}\right)\left(1-\delta^{(0)}_{\xi,l+1/2,i+1/2,j}\right) \\
& +\frac{p_{i+1/2}}{\lambda^{l+1/2,j+1/2}}\frac{\sqrt{1-\xi^2_{0,j+1}}}{\Delta\xi_{0,j+1/2}\Delta p_{i+1/2}}\lambda^{l+1/2,j+1} D^{(0)}_{\xi p,l+1/2,i+1/2,j+1} \\
& \times\delta^{(0)}_{p,l+1/2,i+1,j+1}\delta^{(0)}_{\xi,l+1/2,i+1/2,j+1} \\
& -\frac{p_{i+1/2}}{\lambda^{l+1/2,j+1/2}}\frac{\sqrt{1-\xi^2_{0,j+1}}}{\Delta\xi_{0,j+1/2}\Delta p_{i+1/2}}\lambda^{l+1/2,j+1} D^{(0)}_{\xi p,l+1/2,i+1/2,j+1} \\
& \times\left(1-\delta^{(0)}_{p,l+1/2,i,j+1}\right)\delta^{(0)}_{\xi,l+1/2,i+1/2,j+1} \\
& -\frac{p_{i+1/2}}{\lambda^{l+1/2,j+1/2}}\frac{\sqrt{1-\xi^2_{0,j}}}{\Delta\xi_{0,j+1/2}\Delta p_{i+1/2}}\lambda^{l+1/2,j} D^{(0)}_{\xi p,l+1/2,i+1/2,j} \\
& \times\delta^{(0)}_{p,l+1/2,i+1,j}\left(1-\delta^{(0)}_{\xi,l+1/2,i+1/2,j}\right) \\
& +\frac{p_{i+1/2}}{\lambda^{l+1/2,j+1/2}}\frac{\sqrt{1-\xi^2_{0,j}}}{\Delta\xi_{0,j+1/2}\Delta p_{i+1/2}}\lambda^{l+1/2,j} D^{(0)}_{\xi p,l+1/2,i+1/2,j} \\
& \times\left(1-\delta^{(0)}_{p,l+1/2,i,j}\right)\left(1-\delta^{(0)}_{\xi,l+1/2,i+1/2,j}\right)
\end{aligned}
\tag{E.26}
$$

$$
\begin{aligned}
\overline{\overline{M}}^{(0)[2]}_{p,l+1/2,i-1/2,j+1/2} &= -\frac{\sqrt{1-\xi^2_{0,j+1/2}}}{\Delta p_{i+1/2}\Delta\xi_{0,j+1/2}} p_i D^{(0)}_{p\xi,l+1/2,i,j+1/2} \\
&\quad \times\delta^{(0)}_{p,l+1/2,i,j+1}\delta^{(0)}_{\xi,l+1/2,i-1/2,j+1} \\
&\quad + \frac{\sqrt{1-\xi^2_{0,j+1/2}}}{\Delta p_{i+1/2}\Delta\xi_{0,j+1/2}} p_i D^{(0)}_{p\xi,l+1/2,i,j+1/2} \\
&\quad \times\delta^{(0)}_{p,l+1/2,i,j}\left(1-\delta^{(0)}_{\xi,l+1/2,i-1/2,j}\right) \\
&\quad - \frac{p_{i+1/2}}{\lambda^{l+1/2,j+1/2}} \frac{\sqrt{1-\xi^2_{0,j+1}}}{\Delta\xi_{0,j+1/2}\Delta p_{i+1/2}} \lambda^{l+1/2,j+1} D^{(0)}_{\xi p,l+1/2,i+1/2,j+1} \\
&\quad \times\delta^{(0)}_{p,l+1/2,i,j+1}\delta^{(0)}_{\xi,l+1/2,i-1/2,j+1} \\
&\quad + \frac{p_{i+1/2}}{\lambda^{l+1/2,j+1/2}} \frac{\sqrt{1-\xi^2_{0,j}}}{\Delta\xi_{0,j+1/2}\Delta p_{i+1/2}} \lambda^{l+1/2,j} D^{(0)}_{\xi p,l+1/2,i+1/2,j} \\
&\quad \times\delta^{(0)}_{p,l+1/2,i,j}\left(1-\delta^{(0)}_{\xi,l+1/2,i-1/2,j}\right)
\end{aligned}
\tag{E.27}
$$

$$
\begin{aligned}
\overline{\overline{M}}^{(0)[2]}_{p,l+1/2,i+3/2,j-1/2} &= -\frac{\sqrt{1-\xi^2_{0,j+1/2}}}{\Delta p_{i+1/2}\Delta\xi_{0,j+1/2}} p_{i+1} D^{(0)}_{p\xi,l+1/2,i+1,j+1/2} \\
&\quad \times\left(1-\delta^{(0)}_{p,l+1/2,i+1,j}\right)\delta^{(0)}_{\xi,l+1/2,i+3/2,j} \\
&\quad - \frac{p_{i+1/2}}{\lambda^{l+1/2,j+1/2}} \frac{\sqrt{1-\xi^2_{0,j}}}{\Delta\xi_{0,j+1/2}\Delta p_{i+1/2}} \lambda^{l+1/2,j} D^{(0)}_{\xi p,l+1/2,i+1/2,j} \\
&\quad \times\left(1-\delta^{(0)}_{p,l+1/2,i+1,j}\right)\delta^{(0)}_{\xi,l+1/2,i+3/2,j}
\end{aligned}
\tag{E.28}
$$

$$
\begin{aligned}
\overline{\overline{M}}^{(0)[2]}_{p,l+1/2,i+1/2,j-1/2} &= -\frac{\sqrt{1-\xi^2_{0,j+1/2}}}{\Delta p_{i+1/2}\Delta\xi_{0,j+1/2}} p_{i+1} D^{(0)}_{p\xi,l+1/2,i+1,j+1/2} \\
&\quad \times \delta^{(0)}_{p,l+1/2,i+1,j}\delta^{(0)}_{\xi,l+1/2,i+1/2,j} \\
&\quad + \frac{\sqrt{1-\xi^2_{0,j+1/2}}}{\Delta p_{i+1/2}\Delta\xi_{0,j+1/2}} p_i D^{(0)}_{p\xi,l+1/2,i,j+1/2} \\
&\quad \times \left(1-\delta^{(0)}_{p,l+1/2,i,j}\right)\delta^{(0)}_{\xi,l+1/2,i+1/2,j} \\
&\quad - \frac{p_{i+1/2}}{\lambda^{l+1/2,j+1/2}} \frac{\sqrt{1-\xi^2_{0,j}}}{\Delta\xi_{0,j+1/2}\Delta p_{i+1/2}} \lambda^{l+1/2,j} D^{(0)}_{\xi p,l+1/2,i+1/2,j} \\
&\quad \times \delta^{(0)}_{p,l+1/2,i+1,j}\delta^{(0)}_{\xi,l+1/2,i+1/2,j} \\
&\quad + \frac{p_{i+1/2}}{\lambda^{l+1/2,j+1/2}} \frac{\sqrt{1-\xi^2_{0,j}}}{\Delta\xi_{0,j+1/2}\Delta p_{i+1/2}} \lambda^{l+1/2,j} D^{(0)}_{\xi p,l+1/2,i+1/2,j} \\
&\quad \times \left(1-\delta^{(0)}_{p,l+1/2,i,j}\right)\delta^{(0)}_{\xi,l+1/2,i+1/2,j}
\end{aligned}
\tag{E.29}
$$

$$
\begin{aligned}
\overline{\overline{M}}^{(0)[2]}_{p,l+1/2,i-1/2,j-1/2} &= + \frac{\sqrt{1-\xi^2_{0,j+1/2}}}{\Delta p_{i+1/2}\Delta\xi_{0,j+1/2}} p_i D^{(0)}_{p\xi,l+1/2,i,j+1/2} \\
&\quad \times \delta^{(0)}_{p,l+1/2,i,j}\delta^{(0)}_{\xi,l+1/2,i-1/2,j} \\
&\quad + \frac{p_{i+1/2}}{\lambda^{l+1/2,j+1/2}} \frac{\sqrt{1-\xi^2_{0,j}}}{\Delta\xi_{0,j+1/2}\Delta p_{i+1/2}} \lambda^{l+1/2,j} D^{(0)}_{\xi p,l+1/2,i+1/2,j} \\
&\quad \times \delta^{(0)}_{p,l+1/2,i,j}\delta^{(0)}_{\xi,l+1/2,i-1/2,j}
\end{aligned}
\tag{E.30}
$$

Considerable simplifications occur for uniform momentum and pitch-angle grids. In that case, $\delta^{(0)}_{\xi} = \delta^{(0)}_{p} = 1/2$, and

$$
\begin{aligned}
\overline{\overline{M}}^{(0)[2u]}_{p,l+1/2,i+3/2,j+3/2} &= + \frac{\sqrt{1-\xi^2_{0,j+1/2}}}{4\Delta p_{i+1/2}\Delta\xi_{0,j+1/2}} p_{i+1} D^{(0)}_{p\xi,l+1/2,i+1,j+1/2} \\
&\quad + \frac{p_{i+1/2}}{\lambda^{l+1/2,j+1/2}} \frac{\sqrt{1-\xi^2_{0,j+1}}}{4\Delta\xi_{0,j+1/2}\Delta p_{i+1/2}} \lambda^{l+1/2,j+1} D^{(0)}_{\xi p,l+1/2,i+1/2,j+1}
\end{aligned}
\tag{E.31}
$$

$$\begin{aligned}\overline{\overline{M}}^{(0)[2u]}_{p,l+1/2,i+1/2,j+3/2} &= +\frac{\sqrt{1-\xi^2_{0,j+1/2}}}{4\Delta p_{i+1/2}\Delta\xi_{0,j+1/2}}p_{i+1}D^{(0)}_{p\xi,l+1/2,i+1,j+1/2}\\ &\quad -\frac{\sqrt{1-\xi^2_{0,j+1/2}}}{4\Delta p_{i+1/2}\Delta\xi_{0,j+1/2}}p_{i}D^{(0)}_{p\xi,l+1/2,i,j+1/2}\end{aligned} \tag{E.32}$$

$$\begin{aligned}\overline{\overline{M}}^{(0)[2u]}_{p,l+1/2,i-1/2,j+3/2} &= -\frac{\sqrt{1-\xi^2_{0,j+1/2}}}{4\Delta p_{i+1/2}\Delta\xi_{0,j+1/2}}p_{i}D^{(0)}_{p\xi,l+1/2,i,j+1/2}\\ &\quad -\frac{p_{i+1/2}}{\lambda^{l+1/2,j+1/2}}\frac{\sqrt{1-\xi^2_{0,j+1}}}{4\Delta\xi_{0,j+1/2}\Delta p_{i+1/2}}\lambda^{l+1/2,j+1}D^{(0)}_{\xi p,l+1/2,i+1/2,j+1}\end{aligned} \tag{E.33}$$

$$\begin{aligned}\overline{\overline{M}}^{(0)[2u]}_{p,l+1/2,i+3/2,j+1/2} &= +\frac{\sqrt{1-\xi^2_{0,j+1/2}}}{4\Delta p_{i+1/2}\Delta\xi_{0,j+1/2}}p_{i+1}D^{(0)}_{p\xi,l+1/2,i+1,j+1/2}\\ &\quad -\frac{\sqrt{1-\xi^2_{0,j+1/2}}}{4\Delta p_{i+1/2}\Delta\xi_{0,j+1/2}}p_{i+1}D^{(0)}_{p\xi,l+1/2,i+1,j+1/2}\\ &\quad +\frac{p_{i+1/2}}{\lambda^{l+1/2,j+1/2}}\frac{\sqrt{1-\xi^2_{0,j+1}}}{4\Delta\xi_{0,j+1/2}\Delta p_{i+1/2}}\lambda^{l+1/2,j+1}D^{(0)}_{\xi p,l+1/2,i+1/2,j+1}\\ &\quad -\frac{p_{i+1/2}}{\lambda^{l+1/2,j+1/2}}\frac{\sqrt{1-\xi^2_{0,j}}}{4\Delta\xi_{0,j+1/2}\Delta p_{i+1/2}}\lambda^{l+1/2,j}D^{(0)}_{\xi p,l+1/2,i+1/2,j}\end{aligned} \tag{E.34}$$

$$\overline{\overline{M}}^{(0)[2u]}_{p,i+1/2,j+1/2} = 0$$

$$\begin{aligned}\overline{\overline{M}}^{(0)[2u]}_{p,l+1/2,i-1/2,j+1/2} &= -\frac{p_{i+1/2}}{\lambda^{l+1/2,j+1/2}}\frac{\sqrt{1-\xi^2_{0,j+1}}}{4\Delta\xi_{0,j+1/2}\Delta p_{i+1/2}}\lambda^{l+1/2,j+1}D^{(0)}_{\xi p,l+1/2,i+1/2,j+1}\\ &\quad +\frac{p_{i+1/2}}{\lambda^{l+1/2,j+1/2}}\frac{\sqrt{1-\xi^2_{0,j}}}{4\Delta\xi_{0,j+1/2}\Delta p_{i+1/2}}\lambda^{l+1/2,j}D^{(0)}_{\xi p,l+1/2,i+1/2,j}\end{aligned} \tag{E.35}$$

$$\begin{aligned}\overline{\overline{M}}^{(0)[2u]}_{p,l+1/2,i+3/2,j-1/2} &= -\frac{\sqrt{1-\xi^2_{0,j+1/2}}}{4\Delta p_{i+1/2}\Delta\xi_{0,j+1/2}}p_{i+1}D^{(0)}_{p\xi,l+1/2,i+1,j+1/2}\\ &\quad -\frac{p_{i+1/2}}{\lambda^{l+1/2,j+1/2}}\frac{\sqrt{1-\xi^2_{0,j}}}{4\Delta\xi_{0,j+1/2}\Delta p_{i+1/2}}\lambda^{l+1/2,j}D^{(0)}_{\xi p,l+1/2,i+1/2,j}\end{aligned} \tag{E.36}$$

$$\begin{aligned}\overline{\overline{M}}^{(0)[2u]}_{p,l+1/2,i+1/2,j-1/2} &= -\frac{\sqrt{1-\xi^2_{0,j+1/2}}}{4\Delta p_{i+1/2}\Delta\xi_{0,j+1/2}}p_{i+1}D^{(0)}_{p\xi,l+1/2,i+1,j+1/2} \\ &\quad +\frac{\sqrt{1-\xi^2_{0,j+1/2}}}{4\Delta p_{i+1/2}\Delta\xi_{0,j+1/2}}p_i D^{(0)}_{p\xi,l+1/2,i,j+1/2}\end{aligned} \tag{E.37}$$

$$\begin{aligned}\overline{\overline{M}}^{(0)[2u]}_{p,l+1/2,i-1/2,j-1/2} &= +\frac{\sqrt{1-\xi^2_{0,j+1/2}}}{4\Delta p_{i+1/2}\Delta\xi_{0,j+1/2}}p_i D^{(0)}_{p\xi,l+1/2,i,j+1/2} \\ &\quad +\frac{p_{i+1/2}}{\lambda^{l+1/2,j+1/2}}\frac{\sqrt{1-\xi^2_{0,j}}}{4\Delta\xi_{0,j+1/2}\Delta p_{i+1/2}}\lambda^{l+1/2,j}D^{(0)}_{\xi p,l+1/2,i+1/2,j}\end{aligned} \tag{E.38}$$

Appendix F

MatLab File List

File list in ../Project_DKE/

Notice_DKE (directory that contains the TeX documentation)

- *Equilibrium files that are automaticaly generated by the test program (here given as examples)*

  EQUIL_CMOD.mat

  EQUIL_CQL3D_LH.mat

  EQUIL_CQL3D_OHM.mat

  EQUIL_NSTX.mat

  EQUIL_TEST_LORENTZ.mat

  EQUIL_TS.mat

- *Output files that contain results (here given as examples)*

  RESULTS_CMOD_S1.mat

  RESULTS_CMOD_S2.mat

- *Program files*

  banana_dke_jd.m

  besselj_dke_jd.m

  bhe_dke_yp.m

  bounce_dke_jd.m

  bounceparam_dke_yp.m

  bremsstrahlung_dke_yp.m

  colddisp_OX_jd.m

  colddisp_dke_jd.m

  coldeccd_dke_jd.m

  coldlhcd_dke_jd.m

comput_dke_yp.m

createwaveparam_dke_yp.m

deriv_dke_yp.m

disp_ebw_jd.m

disp_jd.m

display_dke_1yp.m

display_time_dke_1yp.m

dke_1_4yp.m

ebw_dke_jd.m

eh_dke_yp.c

equilibrium_jd.m

execute_jd.m

fact_dke_jd.m

firstordercollop_dke_yp.m

fluxes_dke_jd.m

fpengine_dke_yp.m

fppgridweights_dke_yp.m

ft_llm_dke_yp.m

g_dke_yp.m

gauleg_dke_yp.m

gradient_dke_jd.m

graph1D_jd.m

grid_dke_yp.m

haug_dke_yp.m

helena/ (directory that contains files for magnetic equilibrium calculations) helena/helena12a.f

helena/helmex77

helena/helmex77.f

helena/helmex77.mexaxp

helena/ppplib.f

helena/runhel

helena/separatrice.f

helena/separatrice.mexaxp

helena/separatriceITER.m

helenaequil_f_jd.m
hsneomodels_dke_jd.m
idealeccd_dke_jd.m
idealequil_f_jd.m
ideallhcd_dke_jd.m
info_dke_yp.m
input_dke_yp.m
integral_dke_jd.m
jseries_dke_jd.m
leg_dke_yp.m
makecircequil_jd.m
makedisp_simparam_jd.m
makedisp_tokparam_jd.m
makedisp_waveparam_jd.m
makegrid_dke_jd.m
makeraytracing.m
mg_interp_jd.m
momentumgrid_dke_jd.m
pc_dke_yp.m
powerdiff_dke_jd.m
propagation_jd.m
psi2rho_jd.m
psim_coldeccd_jd.m
psim_coldlhcd_jd.m
psim_dke_1yp.m
psim_idealeccd_jd.m
psim_ideallhcd_jd.m
psim_straightray_jd.m
ptok_dke_1yp.m
qfactors_dke_yp.m
qtilde_dke_jd.m
radialgrid_dke_jd.m
raypath_prop_jd.m
resizejd.m

rfdiff_dke_jd.m

rfprop_dke_jd.m

rfwave_dke_jd.m

rho2psi_jd.m

rippleTS/ (directory that contains files for magnetic ripple losses. Specific to tokamak Tore Supra) rippleTS/bmaxcalcmj3.m

rippleTS/deltacalmj3.m

rippleTS/detrapmj3.m

rippleTS/fracmircalcmj3.m

rippleTS/rhocalcmj3.m

rippleTS/sigmacalcmj3.m

rippleTS/thetaconemj3.m

s2c_dke_yp.m

safetyf_dke_jd.m

script_dke_1yp.m

smat2f_jd.m

smooth_dke_yp.m

species_dke_yp.m

straightray_jd.m

stream_dke_jd.m

test_dke_1yp.m

test_grid_dke_yp.m

testboot.m

testlambda.m

tilefigs_dke_yp.m

timescale_dke_1yp.m

tokparamf_jd.m

trapeze_dke_jd.m

trapt.m

trapz_dke_yp.m

warmeccd_dke_jd.m

weights_dke_jd.m

Bibliography

[1] Y. Peysson et al. Towards steady-state sustainment of electron transport barrier in tore supra. In *Advances in Plasma Physics Research, Vol.4, Francois Gerard, Nova*, pages 1–29, 2003.

[2] V. Basiuk et al. Simulations of steady-state scenarios for tore supra using the cronos code. *Nucl. Fusion*, 43:822–830, 2003.

[3] S. Schultz. *Lower Hybrid and Electron Cyclotron Current Drive With Bootstrap Current in Tokamaks*. PhD thesis, MIT, 1999.

[4] E. Westerhof and A. G. Peeters. A model for bootstrap current calculations with bounce averaged fokker-planck codes. *Comp. Phys. Comm.*, 95:131, 1996.

[5] Y. Peysson. Transport of fast electrons during lhcd in ts, jet and asdex. *Plasma Phys. Control. Fusion*, 35(12B):253–262, 1993.

[6] B.J. Braams and C.F.F Karney. Conductivity of a relativistic plasma. *Phys. Fluids B*, 1(7):1355–1368, 1989.

[7] M. Ju et al. Collisionless fast electron losses in magnetic toroidal ripple during lower hybrid current drive in tore supra. *Phys. Plasma*, 9(11):4615–4622, 2002.

[8] Y. Peysson and F. Imbeaux. Tomography of the fast electron bremsstrahlung emission during lower hubrid current drive on tore supra. *Rev. Phys. Instruments*, 70(10):3987–4007, 1999.

[9] Y. Peysson and M Schoucri. An approximate factorization procedure for solving nine-point elliptic difference equations. application for a fast 2-D relativistic Fokker-Planck solver. *Comp. Phys. Comm.*, 109:55–80, 1998.

[10] Y. Saad. *Iterative Methods for Sparse Linear Systems, 2nd Edition*. Society for Industrial and Applied Mathematics, 2003.

[11] K. Kupfer and A. Bers. Fast electron transport in lower-hybrid current drive. *Phys. Fluids*, 3(10):2783–2795, 1991.

[12] G. T. A. Huysmans et al. To be found. In *CP90 Conf. on Comp. Physics (Singapore:Word Scientific)*, page 371, 1991.

[13] W.D. D'haeseleer et al. *Flux Coordinates and Magnetic Field Structure*. Springer-Verlag, 1990.

[14] I. S. Gradshteyn and I. M. Ryzhik. *Table of Integrals, Series and Products, 1st Edition*. Academic Press (New York, USA), 1965.

[15] R. Balescu. *Transport Processes in Plasmas, Vol. 2*. Elsevier Science Publishing Compny, Inc. (New York, USA), 1988.

[16] C.F.F. Karney. Fokker-Planck and quasilinear codes. *Comp. Phys. Rep*, 4:183–244, 1986.

[17] I.P. Shkarofsky and M.M. Shoucri. Modelling of lower hybrid current drive in the presence of spatial diffusion. *Nuclear Fusion*, 37(4):539–547, 1997.

[18] M. Abramowitz and I. A. Stegun. *Handbook of Mathmatical functions, 9th Edition*. Dover Publication (New York, USA), 1970.

[19] J. Killeen et al. *Computational Methods for Kinetic Models of Magnetically Confined Plasmas*. Springer-Verlag, 1986.

[20] C.F. Kennel and F. Engelmann. Velocity space diffusion from weak plasma turbulence in a magnetic field. *Phys. Fluids*, 9(12):2377–2387, 1966.

[21] I. Lerche. Quasilinear theory of resonant diffusion in a magneto-active relativistic plasma. *Phys. Fluids*, 11(8):1720–1726, 1968.

[22] J.P.S Bizarro and P. Rodrigues. Fast and accurate two dimentional Fokker-Planck calculations in velocity space for RF heating and current drive. *Nuclear Fusion*, 37(11):1509–1513, 1997.

[23] V. Fuchs et al. A one-dimensional model for lower-hybrid current drive including perpendicular dynamics. *Phys. Fluids*, 28(12):3619–3628, 1985.

[24] W.H. Press et al. *Numerical Recipes in C, 2th Edition*. Cambridge University Press, 1992.

[25] M. Shoucri and I. Shkarofsky. A fast 2D Fokker-Planck solver with synergistic effects. *Comp. Phys. Comm.*, 82:287–305, 1994.

[26] O. Axelsson. *Iterative solution methods*. Cambridge University Press, 1994.

[27] R.W. Harvey and M.G. McCoy. The cql3d fokker-planck code. In *IAEA Technical Committee on Advances in Simulation and Modeling of Thermonuclear Plasmas*, pages 489–526, 1993.

[28] R. M. Kulsrud et al. Runaway electrons in a plasma. *Phys. rev. Letters*, 31:690–693, 1973.

[29] A. V. Gurevitch and Ya. S. Dimant. Kinetic theory of runaway production in toroidal magnetic devices. *Nucl. Fusion*, 18:629–645, 1978.

[30] L. G. Eriksson and P. Helander. Simulation of runaway electrons during tokamak disruptions. *Comp. Phys. Comm.*, 154:175–196, 2003.

[31] C.F.F. Karney and N.J. Fisch. Efficiency of current drive by fast waves. *Phys. Fluids*, 28(1):116–126, 1985.

[32] C.F.F. Karney and N.J. Fisch. Numerical studies of current generation by radio-frequency traveling waves. *Phys. Fluids*, 22(9):1817–1824, 1979.

[33] F.L. Hinton and R. D. Hazeltine. *Review of Modern Physics*, 48:239, 1976.

[34] S. P. Hirshman and D. J. Sigmar. *Nucl. Fusion*, 21:1079, 1981.

[35] S. P. Hirshman. Finite aspect ratio effects on the bootstrap current in tokamaks. *Phys. Fluids*, 31(10):3150–3152, 1988.

[36] C. E. Kessel. *Nucl. Fusion*, 34:1221, 1994.

[37] O. Sauter et al. Neoclassical conductivity and bootstrap current formulas for general axisymmetric equilibria and arbitrary collisionality regime. *Phys. Plasma*, 6(7):2834–2839, 1999.

[38] O. Sauter et al. Erratum:neoclassical conductivity and bootstrap current formulas for general axisymmetric equilibria and arbitrary collisionality regime. *Phys. Plasma*, 9(12):5140, 2002.

[39] Y. Peysson, J. Decker, and R.W. Harvey. Advanced 3-D electron Fokker-Planck transport calculations. In *15th Conference on Radio Frequency Power in Plasmas, AIP Conference Proceedings*, volume 694, pages 495–498, 2003.

[40] Inc. The MathWorks. *MatLab, The Language of Technical Computing, Version 6.* The MathWorks, Inc., (Natick, USA), 2002.

[41] L.-G. Eriksson and P. Helander. Monte-carlo operators for orbit-averaged fokker-planck equations. *Phys. Plasmas*, 1(2):308–314, 1994.

[42] G. T. Hoang et al. Particle pinch with fully noninductive lower hybrid current drive in tore supra. *Rev. Phys. Instruments*, 90(15):155002–155006, 1999.

[43] T.H. Stix. *Waves in Plasmas.* American Institute of Physics, 1992.

[44] P.T. Bonoli. Linear theory of lower hybrid heating. *IEEE Trans. on Plasma Sci.*, PS-12(2):95–107, 1984.

[45] M. Porkolab. Plasma waves. MIT Course 8.624 Notes, 2002.

[46] P.T. Bonoli et al. Modelling of advanced tokamak scenarios with LHCD in Alcator C-Mod. *Nuclear Fusion*, 40(6):1251–1256, 2000.